TABLE OF CONTENTS

TABLE OF CONTENTS

LIST OF TABLES

LIST OF FIGURES

LIST OF PLATES

LIST OF APPENDICES

Reservoir Pressurization (Washita-Fredericksburg Injection Interval)

SWIFT Model Run **Chemours WF Prs** – End of Operations Pressure Buildup
Chemours WF Prs models reservoir pressure buildup associated with the injection of an average density injection fluid into the Washita-Fredericksburg Injection Interval. Model includes historical injection from October 1979 to December 31, 2015 and future injection at 2,200 gpm (550 gpm into Well Nos. 2, 3, 4 and 5) from January 1, 2016 to December 31, 2050. Chemours WF Prs.dat is the input file for the model run and Chemours WF Prs.out is the output file for the model run.

SWIFT Model Run **Chemours WF Prs(2)** – End of Operations Pressure Buildup
Chemours WF Prs(2) models reservoir pressure buildup associated with the injection of an average density injection fluid into the Washita-Fredericksburg Injection Interval. Model includes historical injection from October 1979 to December 31, 2015 and future injection at 2,200 gpm (400 gpm into Well Nos. 2, 3 and 4 and 1,000 gpm into Well No. 5) from January 1, 2016 to December 31, 2050. Chemours WF Prs(2).dat is the input file for the model run and Chemours WF Prs(2).out is the output file for the model run.

SWIFT Model Run **Chemours WF Prs(3)** – End of Operations Pressure Buildup
Chemours WF Prs(3) models reservoir pressure buildup associated with the injection of an average density injection fluid into the Washita-Fredericksburg Injection Interval. Model includes historical injection from October 1979 to December 31, 2015 and future injection at 2,200 gpm (250 gpm into Well Nos. 2, 3, 4 and 5 and 1,200 gpm into Well No. 6) from January 1, 2016 to December 31, 2050. Chemours WF Prs(3).dat is the input file for the model run and Chemours WF Prs(3).out is the output file for the model run.

LIST OF APPENDICES (Continued)

Reservoir Pressurization (Tuscaloosa Massive Sand)

SWIFT Model Run **Chemours TMS Prs** – End of Operations Pressure Buildup
Chemours TMS Prs models reservoir pressure buildup associated with the injection of an average density injection fluid into the Tuscaloosa Massive Sand. Model includes future injection at 2,200 gpm (550 gpm into Well Nos. 2, 3, 4 and 5) from January 1, 2020 to December 31, 2050. Chemours TMS Prs.dat is the input file for the model run and Chemours TMS Prs.out is the output file for the model run.

SWIFT Model Run **Chemours TMS Prs(2)** – End of Operations Pressure Buildup
Chemours TMS Prs(2) models reservoir pressure buildup associated with the injection of an average density injection fluid into the Tuscaloosa Massive Sand. Model includes future injection at 2,200 gpm (400 gpm into Well Nos. 2, 3 and 4 and 1,000 gpm into Well No. 5) from January 1, 2020 to December 31, 2050. Chemours TMS Prs(2).dat is the input file for the model run and Chemours TMS Prs(2).out is the output file for the model run.

SWIFT Model Run **Chemours TMS Prs(3)** – End of Operations Pressure Buildup
Chemours TMS Prs(3) models reservoir pressure buildup associated with the injection of an average density injection fluid into the Tuscaloosa Massive Sand. Model includes future injection at 2,200 gpm (250 gpm into Well Nos. 2, 3, 4 and 5 and 1,200 gpm into Well No. 6) from January 1, 2020 to December 31, 2050. Chemours TMS Prs(3).dat is the input file for the model run and Chemours TMS Prs(3).out is the output file for the model run.

Lateral Migration – Light Density Injection Fluid - (Washita-Fredericksburg Injection Interval)

Chemours WF-LD considers injection of a light density injection fluid into the Washita-Fredericksburg Injection Interval. Model includes historical injection from October 1979 to December 31, 2015 and future injection at 2,200 gpm (550 gpm into Well Nos. 2, 3, 4 and 5) from January 1, 2016 to December 31, 2050. Chemours WF-LD Lat.dat is the input file for the model run and Chemours WF-LD Lat.out is the output file for the model run.

Lateral Migration – Light Density Injection Fluid (Tuscaloosa Massive Sand)

Chemours TMS-LD considers injection of a light density injection fluid into the Tuscaloosa Massive Sand. Model includes future injection at 2,200 gpm (550 gpm into Well Nos. 2, 3, 4 and 5) from January 1, 2020 to December 31, 2050. Chemours TMS-LD Lat.dat is the input file for the model run and Chemours TMS-LD Lat.out is the output file for the model run.

Lateral Migration – High Density Injection Fluid - (Washita-Fredericksburg Injection Interval)

Chemours WF-HD considers injection of a high density injection fluid into the Washita-Fredericksburg Injection Interval. Model includes historical injection from October 1979 to December 31, 2015 and future injection at 2,200 gpm (550 gpm into Well Nos. 2, 3, 4 and 5) from January 1, 2016 to December 31, 2050. Chemours WF-HD Lat.dat is the input file for the model run and Chemours WF-HD Lat.out is the output file for the model run.

Lateral Migration – High Density Injection Fluid (Tuscaloosa Massive Sand)

Chemours TMS-HD considers injection of a high density injection fluid into the Tuscaloosa Massive Sand. Model includes future injection at 2,200 gpm (550 gpm into Well Nos. 2, 3, 4 and 5) from January 1, 2020 to December 31, 2050. Chemours TMS-HD Lat.dat is the input file for the model run and Chemours TMS-HD Lat.out is the output file for the model run.

3.0 MODELING

Information regarding the geologic, hydrogeologic and geochemical data of site conditions, and the waste stream characteristics at Chemours DeLisle Plant are presented in earlier sections. That information is used in this section to provide a demonstration, via model simulation, that injected wastes will not migrate to a point outside the permitted Injection Zone within a period of 10,000 years. A discussion of the modeling approach and methodology is presented below.

3.1 Model Objectives and Approach

The modeling performed herein specifically addresses three considerations to demonstrate no-migration:

1. Injection Interval pressurization during the operational period;
2. Lateral waste transport and containment within the Injection Zone during the 10,000-year post-operational period; and,
3. Vertical waste transport and containment within the Injection Zone during the 10,000-year post-operational period.

To meet these objectives, three separate models were constructed using different approaches. Each model addresses specific considerations for a demonstration of no migration. The descriptions and approaches of the three models are shown in the table below.

General Model Description	*General Modeling Approach*
Lateral Injection Interval Pressurization	Numerical Model (SWIFT)
Lateral Plume Transport for Low and High Density Injectate	Numerical Model (SWIFT)
Vertical Transport of Injectate	1-D Analytical Model

The Sandia Waste Isolation Flow and Transport (SWIFT) code was employed in the lateral (numerical) models. The lateral models are three-dimensional in the sense that the Injection Interval is modeled based on approximate geologic structure, as defined in Section 2.0. There is, however, no vertical transport allowed, thereby maximizing the Injection Interval pressurization and lateral waste transport.

Analytical techniques were used in the vertical transport model. In accordance with 40 CFR §148.21(a)(3) and (5), the numerical and analytical models used to demonstrate no migration have been verified and validated. The models are available to the public and are based on sound engineering and hydrogeologic principles.

3.1.1 SWIFT for Windows Computer Code

The computer simulation code used for modeling the pressure buildup and lateral migration of injected waste at the Chemours facility is SWIFT for Windows (HSI Geotrans, 2000). SWIFT for Windows is a version of the SWIFT code (Reeves and others, 1986; Finley and Reeves, 1982; Ward and others, 1987; Reeves and Ward, 1986; Intercomp, 1976). SWIFT was originally called SWIP (Survey Waste Injection Program) and was developed under contract to the U.S. Geological Survey (Intercomp, 1976). Tetra Tech, Inc. is the current custodian of the SWIFT code. The code was developed to model waste injection in deep brine aquifers under conditions of variable fluid density, viscosity and temperature.

SWIFT is a three-dimensional finite difference code that can be used to simulate ground water flow, contaminant transport and heat transport in single or dual porosity media. Steady state or transient conditions can be simulated. In SWIFT, the equations governing ground water flow and solute transport are coupled through: 1) the pore fluid velocity; 2) the dependence of the fluid density on pressure, solute mass fraction and temperature; and 3) the dependence of fluid viscosity on solute mass fraction and temperature.

SWIFT has been extensively verified and validated. Ward and others (1984) documented the benchmarking of SWIFT against eleven analytical solutions and field problems. These problems explore a wide range of SWIFT's capabilities including variable density flow and disposal well injection. Illustrative problems using the SWIFT code have been published in two reports (Finley and Reeves, 1982; Reeves and others, 1987).

3.1.2 Analytical Model

The vertical transport of waste and dissolved waste constituents was calculated using analytical models. These models incorporated the effects due to both advection and molecular diffusion. The advective transport arises from the Injection Interval pressure buildup during the operational period, and the buoyant gradient resulting from the density contrast between the injectate and formation fluid. The molecular diffusion component of transport results from the concentration gradient between the Injection Interval and the overlying strata. Additionally, the diffusive transport through a mud-filled borehole is calculated to address the possibility of a mud-filled artificial penetration intersecting the Injection Interval and waste plume.

The analytical solutions are derived from published materials and employ sound hydrologic principles. Derivations and discussions of the mathematical models used in the vertical transport of waste are presented in Section 3.6.

3.2 General Modeling Methodology and Assumptions

In this modeling, a "conservative approach" methodology was applied. Model input parameters, initial conditions and boundary conditions were employed to ensure that the simulated Injection Interval pressurization and waste transport distance are overestimated. The general methods employed to ensure conservative modeling results are discussed below. Information regarding the specifics of each model are presented in the appropriate model discussions.

The Chemours site has five wells permitted by MDEQ Permit No. MSI1001. Four wells are active and inject into the same injection interval (Washita-Fredericksburg Sand) as Well Nos. 2, 3, 4 and 5. Well No. 6 has not been constructed as of the date of this demonstration (October 2016). Monitor Well No. 1 was originally intended to be used as an injection well. However, the location of manufacturing process within the DeLisle Plant was moved, and sometime between 1974 and 1978 it was decided that Monitor Well No. 1 was located too far from the process areas to be used as an injection well. A seventh well (Well No. 7) is considered in this demonstration, should Chemours opt to permit and construct an additional well at the Chemours DeLisle Plant.

The Confining Zone, Injection Zone and Injection Interval are present at the following depths in each well:

Regulatory Units in Well No. 1

Regulatory Unit	Geologic Formation	Depth (feet)
Confining Zone*	Midway Group and Selma Formation	6,200 – 8,035
Injection Zone*	Eutaw, Tuscaloosa, Washita-Fredericksburg	8,035 – 10,043
Injection Interval*	Tuscaloosa Massive Sand	9,282 – 9,610
Injection Interval*	Washita-Fredericksburg	9,820 – 10,043

* all depths are approximate and are referenced to Well No. 1 Dual Induction/Laterolog geophysical well log

Regulatory Units in Well No. 2

Regulatory Unit	Geologic Formation	Depth (feet)
Confining Zone*	Midway Group and Selma Formation	6,200 – 8,035
Injection Zone*	Eutaw, Tuscaloosa, Washita-Fredericksburg	8,035 – 10,043
Injection Interval*	Tuscaloosa Massive Sand	9,282 – 9,610
Injection Interval*	Washita-Fredericksburg	9,820 – 10,043

* all depths are approximate and are referenced to Well No. 2 (MSI1001) Dual Induction/Laterolog geophysical well log

Regulatory Units in Well No. 3

Regulatory Unit	Geologic Formation	Depth (feet)
Confining Zone*	Midway Group and Selma Formation	6,200 – 8,045
Injection Zone*	Eutaw, Tuscaloosa, Washita-Fredericksburg	8,045 – 10,035
Injection Interval*	Tuscaloosa Massive Sand	9,282 – 9,610
Injection Interval*	Washita-Fredericksburg	9,799 – 10,035

* all depths are approximate and are referenced to Well No. 3 (MSI1001) Dual Induction/Laterolog geophysical well log

Regulatory Units in Well No. 4

Regulatory Unit	Geologic Formation	Depth (feet)
Confining Zone*	Midway Group and Selma Formation	6,158 – 7,998
Injection Zone*	Eutaw, Tuscaloosa, Washita-Fredericksburg	7,998 – 9,982
Injection Interval*	Tuscaloosa Massive Sand	9,282 – 9,610
Injection Interval*	Washita-Fredericksburg	9,752 – 9,982

* all depths are approximate and are referenced to Well No. 4 (MSI1001) Dual Induction/Laterolog geophysical well log

Regulatory Units in Well No. 5

Regulatory Unit	Geologic Formation	Depth (feet)
Confining Zone*	Midway Group and Selma Formation	6,130 – 8,003
Injection Zone*	Eutaw, Tuscaloosa, Washita-Fredericksburg	8,003 – 10,043
Injection Interval*	Tuscaloosa Massive Sand	9,282 – 9,610
Injection Interval*	Washita-Fredericksburg	9,744 – 9,995

* all depths are approximate and are referenced to Well No. 5 (MSI1001) Dual Induction/Density-Neutron geophysical well log

Regulatory Units in Well No. 6 (Construction Pending)

Regulatory Unit	Geologic Formation	Depth (feet)
Confining Zone*	Midway Group and Selma Formation	6,130 – 8,003
Injection Zone*	Eutaw, Tuscaloosa, Washita-Fredericksburg	8,003 – 10,043
Injection Interval*	Tuscaloosa Massive Sand	9,282 – 9,610
Injection Interval*	Washita-Fredericksburg	9,744 – 9,995

* all depths are approximate are referenced to Well No. 5 (MSI1001) Dual Induction/Density-Neutron geophysical well log

Regulatory Units at Proposed Location of Well No. 7

Regulatory Unit	Geologic Formation	Depth (feet)
Confining Zone*	Midway Group and Selma Formation	6,130 – 8,003
Injection Zone*	Eutaw, Tuscaloosa, Washita-Fredericksburg	8,003 – 10,043
Injection Interval*	Tuscaloosa Massive Sand	9,282 – 9,610
Injection Interval*	Washita-Fredericksburg	9,744 – 9,995

* all depths are approximate are referenced to Well No. 5 (MSI1001) Dual Induction/Density-Neutron geophysical well log

Although the Chemours well(s) may inject into varying sand horizons within each Injection Interval, the modeling scenario employed in this demonstration was designed to conservatively represent waste migration and reservoir pressurization for the **collective** net sand within each Injection Interval. The lateral migration models (light density and heavy density waste) and pressurization model assumes a reservoir with a conservative reservoir thickness, and an appropriate reservoir permeability for the given scenario.

This demonstration considers disposal into the authorized Injection Interval at a cumulative injection rate (future) of 2,200 gallons per minute (gpm). The historical volume injected into each individual well was input at each individual well location for each year of operation from the time each well was originally placed in service until December 31, 2015. Future injection at the maximum cumulative injection rate (Washita-Fredericksburg Injection Interval) commences on January 1, 2016 and ceases on December 31, 2050.

Regional structural information was incorporated into the lateral transport models (variable structure, variable net sand thickness) to address the possibility of "up-dip" or "down-dip" movement of injected wastes. The transport models include the effects of advection, dispersion and molecular diffusion. The average historical injectate density was incorporated into the Injection Interval pressurization model. The minimum injectate density was incorporated into the low-density injectate lateral transport model and the vertical transport model to maximize up-dip and vertical movement during a 10,000-year operational period. The maximum injectate density was incorporated into the high-density injectate lateral transport model to maximize down-dip movement during a 10,000-year post operational period. Formation structural information was not incorporated into the vertical transport model, thereby maximizing the upward driving forces of pressure buildup and buoyancy at the point of maximum concentration (wellbore).

3.2.1 Geologic and Hydrologic Model Assumptions

Several hydrologic and geologic assumptions were made in the modeling portion of this petition. General assumptions required for both the lateral SWIFT and vertical models are: 1) Darcy's law is valid, i.e. ground water flow is laminar; 2) the porous medium is fully saturated and confined; 3) hydrodynamic dispersion can be described as a Fickian process; 4) the initial model concentration is zero; 5) the injected and formation fluids are miscible and no reactions between waste constituents or between waste and formation or formation fluids occur; and 6) the waste movement is modeled by considering the movement of a single conservative species, i.e., no sorption or decay of the waste occurs. Specific assumptions pertaining to each model is detailed in the appropriate following section.

3.2.2 Modeled Concentration Reduction

In Section 3.2 of the petition approved in May 2000, the fractional concentration reductions required for the various "Appendix VIII" constituents in the injection waste to meet health-based standards were determined. These fractional concentration reductions (also referred to in the present text as concentration reduction factor or C/C_o) are defined simply as the health-based standard values (or detection limits) (expressed as C in this discussion) divided by the concentrations in the waste stream (expressed as C_o in this discussion). The calculated concentration reduction factor for constituents requiring great reductions were chromium (Cr) and lead (Pb). The largest calculated concentration factor necessary to reach the health-based limit or detection limit is for lead (based on the maximum assumed concentration in the injected waste stream) and is **1.0×10^{-8}**. As a further conservative approach, a theoretical "worst-case" constituent was modeled to represent yet unidentified constituents. Use of a more conservative concentration reduction factor of **1.0×10^{-9}** was employed for a theoretical "worst-case" constituent to ensure that maximum diffusion distances where calculated for the waste stream at the DeLisle Plant. This demonstration utilizes a concentration reduction factor of **1.0×10^{-9}** for 1) all lateral migration models for the Washita-Fredericksburg Injection Interval and the Tuscaloosa Massive Sand; 2) all vertical migration calculations of movement through formation matrix above the Washita-Fredericksburg Injection Interval and the Tuscaloosa Massive Sand and 3) vertical migration calculations of movement through mud-filled boreholes which penetrate the Washita-Fredericksburg Injection Interval. Vertical migration calculations of movement through mud-filled boreholes which penetrate the Tuscaloosa Massive Sand employ the actual concentration reduction factor of **1.0×10^{-8}**.

3.2.3 Boundary Conditions

For lateral migration modeling, the Injection Interval is assumed to be open on all sides to maximize plume dimensions. This is accomplished by imposing transmissive Carter-Tracy boundaries on the lateral sides using the same transmissivities and porosity-thickness values that are used along the side grid blocks of the model.

The "top" and "bottom" of the Injection Interval in the lateral model are non-transmissive with the assignment of zero hydraulic conductivity in the z-direction, thus confining waste movement and Injection Interval pressurization within the modeled Injection Interval layer. This is a conservative condition since no waste transmission or pressure leakoff to the remaining injection reservoir can occur, thereby maximizing waste movement and pressure buildup within the Injection Interval.

The top of the vertical model is placed at the top of the Injection Zone at 7,998 feet KB in Well No. 4. The transport model is 1-dimensional with no transverse component of movement (hydraulic conductivity or dispersivity), thereby maximizing vertical movement. Boundary conditions are not relevant for the vertical model calculations.

3.3 Model Input Parameters

The key parameters used in the lateral, pressure and vertical models are summarized in Table 3-1. The parameters employed in these models have been selected to result in maximum Injection Interval pressurization and waste transport distances. Some additional discussion is given below for parameters of particular importance.

3.3.1 Injection Interval Depth, Structure and Thickness

For purposes of the following discussion, and within various other sections of this document, it is necessary to establish a reference depth for various model input parameters. Well No. 4 is located in the approximate center of the group of the DeLisle injection wells and depths of interest (reference depth) are stated relative to this well.

The top of the Washita-Fredericksburg Injection Interval is present at a depth of about 9,810 feet subsea in Well No. 4. A depth of **9,888.6 feet subsea** (approximate depth to top of Injection Interval plus 50 percent of NET sand thickness [160 feet/2] at well location) was chosen as the reference depth for the depth specific SWIFT model parameters for the Washita-Fredericksburg.

The top of the Tuscaloosa Massive Sand is present at a depth of about 9,413 feet subsea in Well No. 4. A depth of **9,511.6 feet subsea** (approximate depth to top of Tuscaloosa Massive Sand plus 50 percent of the approximate NET sand thickness [200 feet/2] at well location) was chosen as the reference depth for the depth specific SWIFT model parameters for the Tuscaloosa Massive Sand.

Figure 3-1 is portion of a composite electric log that illustrates the electric log signature across this portion of the Injection Interval at the Chemours facility location. Both the Washita-Fredericksburg Injection Interval and Tuscaloosa Massive Sand are highlighted on Figure 3-1.

Each light-density waste and high-density waste lateral migration model and each reservoir pressurization model incorporates the structure on top of the Injection Interval (Washita-Fredericksburg and Tuscaloosa Massive Sand). Collectively, the lateral migration models and reservoir pressurization models are referred to as SWIFT models. The structural information used in the modeling is based on the regional and local geologic area of review at the Chemours facility, as discussed in Section 2.0.

Each SWIFT model also incorporates the variable NET SAND thickness of the modeled sand interval. Plate 3-2 is an isopach map of the Washita-Fredericksburg. The NET SAND thickness is about 80 percent of the total isopach thickness. As an example, the isopach thickness at Well No. 2 is about 190 feet and net sand thickness at Well No. 2 is about 152 feet.

Plate 3-4 is an isopach map of the Tuscaloosa Massive Sand. The NET SAND thickness is about 77 percent of the total isopach thickness of the Tuscaloosa Massive Sand. The isopach thickness of the Tuscaloosa Massive Sand at Well No. 2 is about 255 feet and net sand thickness at Well No. 2 is about 196 feet.

For the vertical migration model, all transport is directed upward from the top of the Injection Zone at depth of 7,998 feet KB (7,968 feet MSL) in Well 4. This depth serves as a reference depth, and upward vertical migration distances can be applied to each individual well location. The transport model is 1-dimensional with no transverse component of movement, thereby maximizing vertical movement.

Reference Depth: The SWIFT model requires the input of an arbitrary depth for setting up initial conditions measured relative to the reference plane. The depth to the center of the permitted Injection Interval (Washita-Fredericksburg) in the reservoir modeling is placed at **9,888.6 feet** MSL (Well No. 4). The depth to the center of the Tuscaloosa Massive Sand in the reservoir modeling is placed at **9,511.6 feet** MSL (Well No. 4).

3.3.2 SWIFT Hydraulic Conductivity and Permeability

The hydraulic conductivity and permeability employed in the SWIFT models was selected based on analyses of fall-off testing performed on Chemours injection wells. Core data derived from analyzing cores collected from the Injection Interval were also considered when deriving conductivity and permeability values of the Injection Interval.

Washita-Fredericksburg Injection Interval: Whole and sidewall cores of the Washita-Fredericksburg injection sand were taken in Monitoring Well No. 1 (Appendix 2-28). Whole cores were obtained from Well No. 2 (Appendix 2-29), but only side-wall cores were obtained from Well No. 4 (Appendix 2-33), and Well No. 5 (Appendix 2-34). The average air permeability of the cores from Monitoring Well No. 1 was 405 milliDarcies (mD), with a range from a low of 22.8 mD to a high of 953 mD. The range of permeability from Well No. 2 was from 36 to 1,152 mD, with 86 samples analyzed. The average permeability of all samples was 336mD. The range of permeability for samples from Well No. 4 is 12 to 810 mD, with 34 samples analyzed. The average permeability of all samples is 363 mD. The cores from Well No. 5 offered additional corroboration of the permeability values. The range of permeability in the samples was from 50 mD to 1,000 mD, with an average value of 350 mD.

In December 1992, comprehensive interference and step rate/pulse tests were conducted over a 14-day period on Well Nos. 2, 3, and 4, with Monitor Well No. 1 used as the observing well. Evidence of pressure communication among the injection wells and Monitor Well No. 1 was indicated by observing the correspondence between downhole pressure and injection well flow rate changes as a function of time. A direct correlation exists with the injection rate changes in the wells and observed downhole pressure changes at all of the injection wells and at Monitor Well No. 1. When injection into one well is initiated, its pressure and rate effects are quickly observed at the adjacent offset wells, and conversely, the effect of turning one well off can be directly indicated in the response at the offset wells. Results of the testing indicate that all of the individual wells tested are in pressure communication, with Monitor Well No. 1 directly observing the pressure effects from the injection well field injection rate changes. This conclusion confirms that all wells are in communication, with the formation open throughout all of the downhole well completions. The effective permeability, as derived from inter-well transmissivity analysis and type curve solutions from the comprehensive testing, averages 330 mD (Appendix 3-1).

In addition to the comprehensive well-to-well testing in December 1992, annual injection and falloff testing has been performed on the injection wells. Well No. 3 was tested in April 2015. Transient analysis of the April 2015 test in Well No. 3 results in a calculated transmissibility of 161,029 mD-feet/centiPoise, which is equivalent to an effective permeability of 423 mD in the Washita-Fredericksburg Injection Interval. Since 1997, the annual testing has rotated sequentially through the injection well field. Prior to 1997, either Well No. 4 or Well No. 5 was the tested well, with exceptions when those wells were undergoing repair. Table 3-2 is a summary of the Washita-Fredericksburg reservoir test results. Based on the results of single well reservoir tests, inter-well transmissivity analysis, type curve solutions and core data, the average permeability of the Washita-Fredericksburg Injection Interval is approximately 210 mD.

To estimate pressure buildup, a permeability of **210 mD** is used in the SWIFT pressurization model for the Washita-Fredericksburg Injection Interval. To be conservative in the prediction of waste plume migration, a permeability of **500 mD** is used in the SWIFT lateral migration models.

Using model inputs of 160 feet for thickness, 0.405 centiPoise (cP) for fluid viscosity in the Injection Interval, and a permeability value of 210 mD, the derived transmissibility is **82,963 mD-ft/cP**. This value of transmissibility is utilized in calculating the reservoir pressure buildup in the Washita-Fredericksburg Injection Interval to estimate pressure buildup during the operational timeframe of the wells. Using model inputs of 160 feet for thickness, 0.405 cP for fluid viscosity in the Washita-Fredericksburg Injection Interval, and a permeability value of 500 mD, the derived transmissibility is **197,531 mD-ft/cP**. This value of transmissibility is utilized in calculating the post-operational plume migration in the Washita-Fredericksburg Injection Interval to maximize transport during the 10,000-year modeling timeframe.

The formation hydraulic conductivity used in the **SWIFT pressurization model** of the Washita-Fredericksburg Injection Interval was **1.561 ft/day**, based on a flow capacity of 33,600 mD-ft, formation fluid density of 68.49 lb/ft^3, formation fluid viscosity of 0.405 cP and a receiving interval thickness of 160 feet.

The formation hydraulic conductivity used in the **SWIFT lateral transport model** for the Washita-Fredericksburg Injection Interval was **3.716 ft/day**, based on a flow capacity of 80,000 mD-ft, formation fluid density of 68.49 lb/ft^3, formation fluid viscosity of 0.405 cP and a receiving interval thickness of 160 feet.

Tuscaloosa Massive Sand: Whole and sidewall cores of the Tuscaloosa Massive Sand injection sand were taken in Monitoring Well No. 1 (Appendix 2-28). Whole cores were also obtained from Well No. 2 (Appendix 2-29). Only sidewall cores were obtained from Well No. 4 (Appendix 2-33) and Well No. 5 (Appendix 2-34). The average permeability of the cores from Monitoring Well No. 1 was 139.4 mD, with a range from a low of 13.7 mD to a high of 339 mD. A total of 21 samples were analyzed. The core results from Well No. 2 show an average permeability of approximately 419 mD. The range of permeability from Well No. 2 was from 95.6 to 782 mD, with 10 samples analyzed. The range of permeability for samples from Well No. 4 is 153 to 395 mD, with 5 samples analyzed. The average permeability of all samples is 272 mD. The cores from Well No. 5 offered additional corroboration of the permeability values. The range of air permeability in the samples was from 81.1 mD to 6,665 mD, with an average value of 2,100 mD. As a rule of thumb, liquid permeability is about 65 percent of air permeability from 100 mD to 500 mD. Applying this approximate correction suggests the average liquid permeability for core samples from Well No. 5 is about 1,365 mD.

To calculate pressure buildup, a permeability of **450 mD** is used in the SWIFT pressurization model for the Tuscaloosa Massive Sand. To be conservative in the prediction of waste plume migration, a permeability of **750 mD** is used in the SWIFT lateral migration models.

Using model inputs of 200 feet for thickness, 0.418 cP for fluid viscosity in the Injection Interval, and a permeability value of 450 mD, the derived transmissibility is **215,311 mD-ft/cP**. This value of transmissibility is utilized in calculating the reservoir pressure buildup in the Tuscaloosa Massive Sand to estimate pressure buildup during the operational timeframe of the wells. Using model inputs of 200 feet for thickness, 0.418 cP for fluid viscosity in the Tuscaloosa Massive Sand, and a permeability value of 750 mD, the derived transmissibility is **358,852 mD-ft/cP**. This value of transmissibility is utilized in calculating the post-operational plume migration in the Tuscaloosa Massive Sand to maximize transport during the 10,000-year modeling timeframe.

The formation hydraulic conductivity used in the **SWIFT pressurization model** of the Tuscaloosa Massive Sand was **3.243 ft/day**, based on a flow capacity of 90,000 mD-ft, formation fluid density of 68.55 lb/ft^3, formation fluid viscosity of 0.418 cP and a receiving interval thickness of 200 feet.

The formation hydraulic conductivity used in the **SWIFT lateral transport model** for the Tuscaloosa Massive Sand was **5.405 ft/day**, based on a flow capacity of 150,000 mD-ft, formation fluid density of 68.55 lb/ft^3, formation fluid viscosity of 0.418 cP and a receiving interval thickness of 200 feet.

Vertical Model Hydraulic Conductivity

The values of shale layer permeabilities specified as inputs in the vertical modeling calculations were determined from direct measurements on core samples obtained in Monitor Well No. 1, and from a correlation developed by Porter and Newsom (1987) giving the upper limits of shale permeabilities for the Gulf Coast region. The Porter and Newsom (1987) study is included in Appendix 3-2.

Porter and Newsom (1987) conducted a literature investigation to evaluate information available on the permeability and porosity of Gulf Coast clays and shales. In this study, they developed a relationship for determining a reasonable worst-case upper bound to shale permeability as a function of depth below ground level for use in conservatively predicting vertical waste permeation into the shale aquitard layer overlying an injection interval. The Porter/Newsom relationship is consistent with the body of experimental data on shale permeabilities discussed above for the region in proximity to the DeLisle Plant.

The shale permeabilities of the layers involved in containment of waste were determined from vertical permeability tests performed on shale cores obtained in Monitor Well No. 1. Permeability was measured from samples of Tuscaloosa and Washita-Fredericksburg shales. The highest permeability measured was approximately 6.2 x 10^{-8} Darcies (Vesic, 1974). Additional permeability measurements were made from samples recovered from Injection Well No. 5, and corroborate this value.

In the vertical migration model the shale overlying and underlying the Washita-Fredericksburg Injection Interval is assigned a conservative upper bound permeability of 6.2 x 10^{-8} Darcies (6.2 x 10^{-5} mD). This permeability value is equal to the upper bound value from the site-specific whole core data. Therefore, its use in the vertical transport modeling will result in an overestimate of vertical permeation of injectate and formation brine during the operational and post-operational period.

Based on the data included in the previous paragraphs, the value of 6.2 x 10^{-5} mD is assigned as the vertical shale intrinsic permeability in the containment interval. This value was converted to a hydraulic conductivity using the light density injectate at reservoir conditions in the Washita-Fredericksburg Injection Interval (viscosity of 0.231 and a density of 62.43 lb/ft^3.

$$K_z = \frac{k\rho g}{\mu}$$

ρg = injectate fluid specific weight (density) = 62.43 lb/ft^3
μ = injectate fluid viscosity = 0.231 cP (at reservoir temperature)
k = shale intrinsic permeability = 6.2 x 10^{-5} mD

Therefore:

$$K_z = \frac{(6.2\,x\,10^{-5}\ \text{mD})(62.43\,\text{lb/ft}^3)(1.062\,x\,10^{-11}\ \text{ft}^2/\text{Darcy})(86{,}400\,\text{sec/day})}{(0.231\,\text{cP})(2.088\,\text{x}\,10^{-5}\ \text{lb-sec/ft}^2\text{-cP})(1{,}000\,\text{mD/Darcy})}$$

$K_z = 7.36 \text{ x } 10^{-7}$ ft/day

The formation hydraulic conductivity used in the **vertical migration model** is **$7.36 \text{ x } 10^{-7}$ ft/day.** The vertical hydraulic conductivity of the containment interval is assumed homogeneous (no variation in permeability along the vertical path). Additionally, since the vertical model is one-dimensional (vertically upward), the hydraulic conductivity is assumed to be isotropic.

3.3.3 SWIFT Model Reference Pressure and Fluid Gradients

An initial formation pressure at a specific reference depth is used as the reference point for the operational period pressure models. As such, they only indirectly affect the post-operational modeling performed in this application. Pressures used in this document have been referenced to mean sea level. Often, the zero-measurement reference is listed on the historic static gradient survey reports, which make corrections to ground level straightforward. Many times, however, there is no reported zero value for the measurement (report sections left blank). Uncertainty in the zero-measurement reference introduces error in the overall computed static bottom-hole value at the sand reference depth. This is on the order of 4 to 6 pounds per square inch (psi) for the range of fluid gradients and known zero reference elevations above ground level used for the wells. Maximum uncertainty is likely less than 10 psi, which is relatively small in comparison to the measured bottom-hole pressures.

The original formation pressure of the injection sand is not a direct input to the models, but is necessary for model pressure calibration and evaluation. During pressure calibration, historical measured formation pressures are compared with model predicted formation pressures. The modeled formation pressures are expressed only as the incremental increase in pressure over original formation pressure. Therefore, a valid approximation of the original formation pressure for the injection sand is essential. A record of historical wellhead pressures from Monitoring Well No. 1 is present in Table 3-3, which were also used to survey the integrity of the original and historical formation pressure measurements (pre-injection period).

The initial estimate of the original formation pressure for the Washita-Fredericksburg Injection Interval is derived from a 1974 drill stem test measurement in Monitoring Well No. 1 (Halliburton, 1974d). The measured final shut in pressure was 4,626 psi at a depth of 9,893 feet BGL, which is equal to a gradient of 0.467 psi/ft. Correcting this value to the midpoint of the Washita-Fredericksburg Injection Interval (9,850 feet BGL), using the above gradient, the original formation pressure based on the drill stem test is equal to 4,606 psi (see Table 3-3). However, based on subsequent well testing and static bottom-hole pressure measurements, it appears that this value may be too high. Figure 3-2 presents the historically calculated bottom-hole shut-in pressures in Monitor Well No. 1 and the injection wells with time.

Testing from the comprehensive reservoir testing program in 1992 yielded a stabilized bottom-hole pressure value of 4,516 psi at a depth of 9,760 feet, which when referenced to the sand midpoint at 9,850 feet, is equal to a pressure of 4,558 psi. This offers documentation that the true original formation pressure is nearer to this value than indicated from the drill stem test data. Recent bottom-hole pressure measurements and reservoir tests conducted on Well Nos. 2, 3, 4, and 5 also demonstrate that the measured original formation pressure from the 1974 drill stem test is probably inappropriate. The measured pressure in Well No. 4 (while Well No. 2 was shut-in) was 4,537 psia or 4,523 psi at a depth of 9,750 feet BGL (Gulf Coast Well Analysis, 1989). This equates to a pressure gradient of 0.4639 psi/ft. The pressure corrected to the midpoint of the injection sand (9,850 feet) is equal to 4,568 psi. Since this measured pressure, after years of injection (4,568 psi), is lower than the estimated original formation pressure from the 1974 drill stem test, it can be concluded that the drill stem test pressure is incorrect.

Tables 3-4, 3-5, and 3-6 present historical bottom-hole pressure measurements recorded from all the wells on site. Figure 3-3 is a graph of formation pressures measured from historical pressure tests with depth obtained during drilling or recompletion of the site wells. Figure 3-4 presents this data as gradients plotted versus depth. Slightly different slopes are apparent within the scatter trend of the distributed data. The data indicates a common trend between the overlying Tuscaloosa Formation and the Washita-Fredericksburg Injection Interval. From these relationships, a detailed evaluation/screening of the data indicates that the estimated original formation pressure of the Washita-Fredericksburg Injection Interval used in the model should be approximately 4,555 psi at a depth of 9,850 feet BGL, which is equal to a gradient of **0.4624 psi/ft**. This formation pressure is supported by the data and derived from the calibration of the pressure model with the recent pressure measurements in the wells. This represents a reasonable value based on site specific DeLisle Plant data, which has been evaluated for its integrity.

Reference Pressure: The SWIFT model requires a reference pressure at which the densities (reservoir fluid and injected fluid) are to be entered. The SWIFT model reference pressures where calculated at the approximate grid block center of Well No. 4. The SWIFT model reference pressure for the Washita-Fredericksburg Injection Interval is **4,580.7 psi** at the grid block center depth of 9,888.6 feet MSL. The SWIFT model reference pressure for the Tuscaloosa Massive Sand is **4,406.4 psi** at the grid block center depth of 9,511.6 feet MSL. NOTE: The reference pressure estimated for the Tuscaloosa Massive Sand was calculated using the original formation pressure of the Washita-Fredericksburg (4,555 psi at 9,850 feet BGL) and correcting for depth using a fluid gradient of 0.4624 psi/ft.

Reference Pressure: The SWIFT model requires an initial pressure at depth in the model. The SWIFT model initial pressure (approximate Well No. 4 grid block center) for the Washita-Fredericksburg Injection Interval is **4,580.7 psi** at the grid block center depth of 9,888.6 feet MSL. The SWIFT model initial pressure (approximate Well No. 4 grid block center) for the Tuscaloosa Massive Sand is **4,406.4 psi** at the grid block center depth of 9,511.6 feet MSL.

Bottom-Hole Pressure (Grid Block Center): For the SWIFT models included in this demonstration, the bottom-hole pressure at the center of the grid block in which each well is located was calculated and input in the model.

3.3.4 Bottom-Hole Temperature

Knowledge of formation temperature and total dissolved solids (TDS) concentrations is necessary to predict fluid viscosities and densities at depth. Figure 3-5 shows a plot and distribution of measured bottom-hole logging temperatures at the DeLisle Plant as a function of depth. This data was obtained from the five geophysical well logs of the injection wells and Monitor Well No. 1 (all wells present within the Area of Review). Recorded bottom-hole temperature data, and information from drill stem testing of the Washita-Fredericksburg and other overlying and shallower formations were also compiled from Monitor Well No. 1. These data have been used in the present calculations to establish temperatures at depth.

Figure 3-5 also shows a plot of measured temperatures, obtained from drill stem tests in Monitoring Well No. 1 (Halliburton, 1974a, 1974b, 1974c, and 1974d) as a function of depth. The average mean surface temperature was estimated to be 70°F, and the maximum recorded temperature was observed in Monitoring Well No. 1, where a value of 215°F was indicated in 1974. Table 3-7 lists the values used to derive this temperature versus depth plot. The depth interval from approximately 9,000 to 9,600 feet represents the Tuscaloosa Formation (Upper, Middle, and Massive Tuscaloosa Sands), while the interval from 9,750 to 10,050 feet corresponds to the Washita-Fredericksburg Injection Interval.

In 2005, 2012 and 2016, differential temperature survey logs were run in Monitor Well No. 1. These temperature data are accepted as being the best measurement of bottom-hole temperature and wellbore temperature gradients. Figure 3-6 is a plot which shows the historical temperature data (Table 3-7) and the temperature data collected from the subject temperature logs. Based on these data, the SWIFT model reference temperatures at depth and for the grid block centers were determined.

<u>*Reference Temperatures:*</u> The SWIFT model requires a reference temperature for the resident-fluid (formation fluid) viscosity and injection fluid viscosity. The SWIFT model reference temperature (Well No. 4 grid block center) for the resident-fluid (formation fluid) viscosity and injection fluid viscosity for the Washita-Fredericksburg Injection Interval is assumed to be **243.6°F**. The SWIFT model reference temperature (Well No. 4 grid block center) for the resident-fluid (formation fluid) viscosity and injection fluid viscosity for the Tuscaloosa Massive Sand is **236.4°F**.

<u>*Initial Temperatures (Reference Depth)*</u>: The SWIFT model requires initial temperatures to be input relative to the SWIFT model reference plane. The SWIFT model reference temperatures for Washita-Fredericksburg Injection Interval are **228.5°F** at **9,100 feet subsea** and **278.2°F** at **11,700 feet subsea.** The SWIFT model reference temperatures for Tuscaloosa Massive Sand are **222.8°F** at **8,800 feet subsea** and **274.4°F** at **11,500 feet subsea.**

<u>*Initial Temperatures (Grid Block Center)*</u>: The SWIFT model hydraulic conductivity and density reference temperature (at Well No. 4 grid block center) for the Washita-Fredericksburg Injection Interval is assumed to be **243.6°F**. The SWIFT model hydraulic conductivity and density reference temperature (at Well No. 4 grid block center) for the Tuscaloosa Massive Sand is **236.4°F**.

<u>*Injection Fluid Temperature*</u>: For the SWIFT models included in this demonstration, it is assumed that the injection fluid temperature is equivalent to the initial formation temperature prior to injection. This is reasonable given the SWIFT modeling timeframe of up to 10,000 years. The SWIFT model injection fluid temperature for the Washita-Fredericksburg Injection Interval is assumed to be **243.6°F**. The SWIFT model injection fluid temperature for the Tuscaloosa Massive Sand is **236.4°F**.

3.3.5 Porosity

Porosity is defined as the ratio of void space in a given volume of rock to the total bulk volume of rock expressed as a percentage (Amyx et al., 1960). The more porous a rock, the more fluid can be stored in a given rock volume.

Average values of reservoir porosities for the various sand layers in the stratigraphic column have been derived from core data obtained from Monitoring Well No. 1 and Well Nos. 2, 4, and 5. Average porosities for sand layers with no core data available were estimated from nearby sands which have core data analyzed.

The porosity of the Washita-Fredericksburg Injection Interval was determined from the average of all core measurements from Monitoring Well No. 1 and Well Nos. 2, 4, and 5. The calculated average porosity of the Washita-Fredericksburg Injection Interval in all of the wells is **24 percent**. The average porosities from cores from each well are 23.6, 23.9, 22.3, and 23.9 percent, respectively, for Monitoring Well No. 1 and Well Nos. 2, 4, and 5. These data are corroborated from the open hole geophysical well logs in each of the wells.

The porosity of the Tuscaloosa Massive Sand was also determined from the average of all core measurements from Monitoring Well No. 1 and Well Nos. 2, 4, and 5. The calculated average porosity of the Tuscaloosa in all of the wells is **25 percent**. The average porosities from cores from each well are 23.6, 24.1, 26.0, and 24.0 percent, respectively, for Monitoring Well No. 1 and Well Nos. 2, 4, and 5. These data were corroborated from the open hole geophysical well logs in each of the wells.

The results derived from the flow and containment modeling calculations are, to a large degree, not particularly sensitive to the values employed for the sand layer porosities. Only the results from the lateral waste transport models (i.e., the *SWIFT lateral migration model* for operational injection period and the *SWIFT 10,000-Year Waste Plume Model* for long-term post-injection) show mild sensitivities to assigned injection interval sand porosities. The predicted lateral extent of a waste plume during active injection varies roughly in inverse proportion to the square root of sand porosity. Therefore, a decrease in porosity from 0.30 to 0.25 would result in an increase in the extent of a one-mile plume (radius) by about 0.1 mile. The extent of lateral waste drift during the 10,000-year period following injection is inversely proportional to the porosity. Therefore, the long term model is somewhat more sensitive to the assigned porosity value.

Predictions of injection sand pressure buildup from the *SWIFT Pressure Models* are only slightly influenced by the value employed for the porosity of the injection interval. Predictions of vertical waste permeation into the shale layer overlying the injection interval from the *Vertical Permeation Model* and predictions of the extent of molecular diffusion into the overlying shale layer are completely independent of injection sand porosities.

The porosity used in the **SWIFT pressurization model** and **SWIFT lateral transport model** of the Tuscaloosa Massive Sand was **24 percent**.

The porosity used in the **SWIFT lateral transport model** and **SWIFT lateral transport model** for the Tuscaloosa Massive Sand was **25 percent**.

Porosities of Shale Layers: The shale or aquiclude layer porosities were determined from the correlations developed for Gulf Coast shales presented in Porter and Newsome (1987) and Amyx et al. (1960). In performing modeling calculations to predict an upper bound to the vertical distance of formation fluid and waste permeation due to pressure buildup, it is conservative to employ a lower bound to the aquiclude layer porosity, as the extent of permeation is inversely proportional to the aquiclude layer porosity. The "effective" shale porosity, which discounts the bound water within the clay structure as well as water contained in dead-end pores, represents an appropriate choice of a porosity value for such a calculation. The data contained in Porter and Newsome (1987) (see Appendix 3-2) indicate that an effective porosity of **five (5) percent** represents a conservative lower bound value for operational vertical transport modeling. This value is employed in the *Vertical Permeation Model*.

In contrast to the vertical permeation calculation, the extent of vertical molecular diffusion of a contaminant species through the aquiclude layers overlying the Injection Interval is proportional to the aquiclude layer porosity, increasing roughly in direct proportion to the layer porosity. Therefore, in calculations to predict a conservative upper bound to vertical diffusion distance, a reasonable upper limit to porosity, such as total shale porosity, should be used. The total porosity of the shale overlying the injection interval at the DeLisle Plant was established using a relationship for Louisiana sediments developed by Dickinson (1953) (see Appendix 3-2). This relationship is based on a considerable body of observational data and provides an upper bound to the total porosity of onshore Louisiana shales as a function of depth. Conditions at the DeLisle site are similar to those of coastal Louisiana, and the same relationship is expected. The Dickinson porosity-depth relationship predicts higher porosity values than other similar correlations derived for Louisiana sediments by various investigators (Schmidt, 1973). Based on the Dickinson relationship, the value of total porosity employed in the present predictions of molecular diffusion into the shale layer overlying the Injection Interval is **20 percent**.

3.3.6 Tortuosity (τ) and Geometric Correction Factor (G)

The tortuosity factor (τ) is expressed as the square of the actual length of a flow path (which is sinuous in nature) divided by the straight-line distance between the ends of the flow path. Daniel & Shackleford (1988) report tortuosities varying from 0.01 in a clay matrix to 0.84 in a 100 percent sand matrix. These data suggest that τ (dimensionless) is approximately equal to the porosity value of the given matrix. Therefore, for the Washita-Fredericksburg Injection Interval sand porosity of 24 percent (0.24), the tortuosity is estimated to be 0.24 (dimensionless). For the Tuscaloosa Massive Sand porosity of 25 percent (0.25), the tortuosity is estimated to be 0.25 (dimensionless). The Confining Zone and Containment Interval shale porosity is estimated to be no more than 20 percent (0.20) and the tortuosity is estimated to be 0.20 (dimensionless).

Miller (1989) indicates that tortuosity is the reciprocal of the geometric correction factor (G) which itself is equal to $(\text{shale porosity})^2$ or $(\text{consolidated sandstone porosity})^{0.3}$ or $(\text{unconsolidated sandstone porosity})^{0.8}$ as upper bounds. The Washita-Fredericksburg Injection Interval sand porosity is estimated to be 24 percent as determined from whole and sidewall core collected the DeLisle Plant monitoring and injection wells. The Tuscaloosa Massive Sand porosity is estimated to be 25 percent as determined from whole and sidewall core collected the DeLisle Plant monitoring and injection wells. The Confining Zone and Containment Interval shale porosity is estimated to be no more than 20 percent. The geometric correction factor (G) was calculated to be **0.320** for the Washita-

Fredericksburg Injection Interval sands, and **0.330** for the Tuscaloosa Massive Sand. In the vertical transport model, G was estimated to be **0.003** for confining interval shale with a porosity of five (5) percent and **0.040** for a confining interval shale with a porosity of 20 percent.

3.3.7 Reservoir Dip Angle

The SWIFT models used to simulate lateral plume movement for the light density waste plume movement, heavy density waste plume movement and reservoir pressure buildup employ a variable structure concept. Each grid block is set at a depth within the SWIFT model to closely match the mapped geologic structure on the subject structure map (top of Washita-Fredericksburg formation or top of Tuscaloosa Massive Sand formation). The structure depth mapped on the top of the subject formation was then adjusted to the appropriate depth to simulate lateral migration within either the Washita-Fredericksburg Injection Interval or Tuscaloosa Massive Sand.

3.3.8 Longitudinal and Transverse Dispersivity

In general, increasing plume migration distance equates to greater dispersion and, therefore, higher dispersivities. However, higher dispersivities allow the moving plume to spread out more (becoming more diffuse), which results in less transport. The longitudinal and transverse dispersivities used in the Chemours facility models are given in Table 3-1. In the SWIFT lateral migration and reservoir pressurization models, the two separate component axes that control plume movement are the longitudinal and transverse dispersivity values. The value specified for the field scale longitudinal dispersivity α_L within the injection sand is **50 feet**. This selection was based on information on longitudinal (lateral) dispersivities for similar sand layers as presented in Walton (1985) and Anderson (1984). According to Walton (1985), the transverse dispersivity α_T is commonly five to 10 times smaller than the longitudinal or lateral dispersivity. In the subject SWIFT models, a value of **five (5)** feet has been employed as the value of the lateral dispersivity to maintain this conservative relationship derived from the literature.

Dispersivity was not considered in the vertical model for two reasons. First, the vertical transport is modeled conservatively as one-dimensional; no transverse component of advection or diffusion was allowed (these would dilute the waste as it moves upward). The result is that the waste movement is maximized. Second, at the end of the operational period when the Injection Interval pressurization has subsided, it is assumed that there is no additional potential for fluid flow in any direction; diffusion is the only transport mechanism. The result is a zero-fluid velocity and therefore, no dispersion, since dispersion is the product of the fluid velocity and dispersivity.

3.3.9 Molecular Diffusivity

The diffusivities in free aqueous solution of these constituents have been determined at a maximum temperature of 243.6°F, which would more than cover the temperature of the Washita-Fredericksburg Injection Interval sand and shale layer overlying the injection sand. The bulk diffusion coefficient for chromium and lead (key constituents) were determined using the Stokes-Einstein equation (Daniel and Shackleford, 1988). For chromium, using the Stokes-Einstein equation:

$$D_m = \frac{RT}{6\pi N \mu r}$$

where,

D_m = bulk molecular diffusion coefficient
R = ideal gas constant = 8.314 J-mol / K = 8.314×10^7 cm^2-g / (sec^2-mol-K)
N = Avagadro's number = 6.022×10^{23} / mol
T = absolute temperature = 243.6°F = 390.7°K (Washita-Fredericksburg Injection Interval)
μ = absolute viscosity = 0.405 cP (formation brine at 243.6°F) = 0.00405 g / (cm-sec)
r = ionic radius for chromium valence +6 = 4.4×10^{-9} cm (CRC Handbook of Chemistry and Physics, 88th Ed.)

Substituting the values and solving:

$$D_m = 1.61 \times 10^{-4} \text{ cm}^2/\text{sec} = 1.49 \times 10^{-2} \text{ ft}^2/\text{day}$$

The free-water diffusivity for chromium is **1.49×10^{-2} ft^2/day** in the Washita-Fredericksburg Injection Interval. Similarly calculated, the free-water diffusivity for lead is **6.99×10^{-3} ft^2/day**.

Similarly, the free-water diffusivity for chromium is **1.43×10^{-2} ft^2/day** in the Massive Tuscaloosa Sand. Similarly, the free-water diffusivity for lead is **7.21×10^{-3} ft^2/day** in the Tuscaloosa Massive Sand.

Effective Molecular Diffusivity (Lateral Migration)

Molecular diffusion is included in SWIFT models to account for transport facilitated by the concentration gradient of injected waste. Molecular diffusion is modeled by considering the movement of a conservative electrolyte species in a porous medium. In

SWIFT, the relationship between the effective and free solution (in water) molecular diffusivity is:

$$D_{eff} = D_0 n \tau$$

where D_{eff} is the effective molecular diffusivity in a porous medium, D_0 is the molecular diffusivity in water, n is the porosity, and τ is the tortuosity.

Effective Molecular Diffusivity (Vertical Migration)

The effective diffusion coefficient within a water-saturated shale aquitard layer is always lower than in free aqueous solution. This is the result of microscopic geometric complexities in the pore channels, which make it more difficult for diffusing molecules to wind their way through the pores. Such complexities include pore constrictions, tortuosities in diffusion path, and dead-end pores.

For the vertical migration model (analytical, the effective diffusion coefficient in shale layer can be predicted (see Appendix 3-3) by multiplying the diffusive value in free aqueous solution by a Geometric Correction Factor, **G**, to account for complexities in the pore channel geometry. As discussed in Section 7.3.6, the Geometric Correction Factor **G** is primarily a function of lithology and porosity.

The lithology of the aquitard layer overlying the injection interval has been established from the driller's log, from wireline logs run by well service companies, and from cores taken specifically for laboratory analysis. These techniques all indicate that a great preponderance of shale exists within the overlying Washita-Fredericksburg Sand layer (and Tuscaloosa Massive Sand layer). From geophysical logs, the total porosity of the shale was determined to be 20 percent, which is a very conservative representation of the formation. Therefore, an upper bound to the Geometric Correction Factor at DeLisle can be established as:

$$D_{eff} = D_0\mathbf{G}$$

These values apply to the rather extensive portion of the overlying aquitard containing shale; and, for consistency, only net shale is included in the present predictions of vertical diffusion distance. This approach provides an additional margin of safety since the thin sand stringers and lenses present within the overall very thick shale aquitard also serve to retard molecular diffusion.

Molecular Diffusion Through Injection Interval (Lateral Migration)

The SWIFT model requires that bulk molecular diffusion be input as effective molecular diffusion coefficient (D_{eff}). D_{eff} is derived by multiplying the bulk molecular diffusion coefficient (of the waste constituent having the highest bulk molecular diffusion coefficient (chromium)) by the Injection Interval porosity and the tortuosity. The Washita-Fredericksburg Injection Interval sand porosity is 24 percent. The tortuosity coefficient is estimated to be 0.24.

Therefore:

$$D_{eff} = 1.49 \text{ x } 10^{-4} \text{ ft}^2\text{/day x } 0.24 \text{ x } 0.24 = \mathbf{8.60 \text{ x } 10^{-4} \text{ ft}^2\text{/day}}$$

The effective diffusivity for chromium is **$8.60 \text{ x } 10^{-4}$ ft^2/day** in the Washita-Fredericksburg Injection Interval. The effective diffusivity for chromium is **$8.95 \text{ x } 10^{-4}$ ft^2/day** in the Tuscaloosa Massive Sand (porosity of 25 percent and tortuosity of 0.25).

Molecular Diffusion Through Containment Interval (Vertical Migration)

In the vertical transport model (analytical solution), the effective molecular diffusion coefficient (D_{eff}) for transport of waste constituents through the overlying containment interval (Eutaw, Tuscaloosa Shale) was determined by multiplying the free water diffusion coefficient by Containment Interval porosity (0.20) and a geometric correction factory (**G**) of 0.04. In the vertical transport model, the worst-case constituent movement is associated with arsenic.

Therefore:

$$D_{eff} = 1.49 \text{ x } 10^{-2} \text{ ft}^2\text{/day x } 0.20 \text{ x } 0.04 = \mathbf{1.19 \text{ x } 10^{-4} \text{ ft}^2\text{/day}}$$

Molecular diffusion through the containment interval for each of the waste constituents of concern was calculated and is presented on Table 3-8. As stated previously, the waste constituent having the farthest vertical movement through the containment interval is chromium.

Molecular Diffusion Through a Mud Filled Borehole (Vertical Migration)

The effective molecular diffusion coefficient (D_{eff}) employed to calculate the movement of the waste constituents through a mud-filled borehole was determined by multiplying the free water diffusivity for chromium, by a tortuosity value of 0.5 and porosity of 0.9 for the drilling mud. This tortuosity value is chosen to reflect the tortuosity of the mud column, where the clay particles provide a substantial tortuosity effect.

Therefore:

$$D_{eff} = 1.49 \times 10^{-2}\ ft^2/day \times 0.50 \times 0.90 = \mathbf{6.70 \times 10^{-3}\ ft^2/day}$$

Molecular diffusion through a mud filled borehole for each of the waste constituents of concern were calculated and are presented on Table 3-8. The waste constituent having the farthest vertical movement in a mud filled borehole is chromium.

3.3.10 Modeled Injection Rates

Currently, four waste disposal wells are present at the DuPont DeLisle Plant. These wells are Well Nos. 2, 3, 4, and 5. All the wells are completed in the Washita-Fredericksburg Injection Interval. Monitoring Well No. 1 is also completed in the Washita-Fredericksburg Injection Interval, but has never been used as an injection well; its only use has been as a monitor well (pressure monitoring). This application is seeking approval to convert Well No. 1 to an injection well. Figure 3-7 presents the injection volumes for the facility monthly through year end 2015. Figure 3-8 shows the cumulative volume per well. The facility has permitted the construction and operation of a new waste disposal well, Well No. 6, which will also be completed into the Washita-Fredericksburg Injection Interval. This application is seeking showing the future construction of another well identical to Well No. 6 that has not yet been permitted. Both of these wells will add redundancy to the existing well field and each will be built as a high-capacity well, with a maximum anticipated rate of 1,200 gpm. However, the site injection limit will remain as 2,200 gpm cumulative between all wells (per Condition No. 2 of the May 5, 2000 exemption). Operational model cases considered the following injection rates:

Model Case	Modeled Rate	Well Nos.
Base Rate Case	550 gpm (each well)	2, 3, 4 and 5
High-Capacity Sensitivity	1,000 gpm 400 gpm	5 2, 3 and 4
Maximum-Capacity Sensitivity	1,200 gpm 250 gpm	6 2, 3, 4 and 5

In each model case, the remaining cumulative volume of 2,200 gpm is distributed to the other injection wells. The operating parameters necessary for modeling the site are the monthly and yearly injection history for each well which have been recorded and reported to the Mississippi Department of Environmental Quality. These data are updated through year-end 2015, and are presented in Tables 3-9 and 3-10. Note that the data is presented as equivalent injection rates in gallons per minute. The record of monitoring well pressures is used in the pressure comparison of the model and is updated through year end 2015, in Table 3-11. The plant records were the main source of information for the monitoring well pressures and injection history.

For all SWIFT modeling for the Washita-Fredericksburg Injection Interval, historical injection as it occurred at each well location is input into the model on an average annual injection rate value. For all future injection into the Washita-Fredericksburg Injection Interval, injection is at the maximum requested cumulative injection rate (2,200 gpm).

This demonstration also considers injection into an alternative Injection Interval. The alternative Injection Interval is the Tuscaloosa Massive Sand. For all future injection into the Tuscaloosa Massive Sand, injection is at the maximum requested cumulative injection rate (2,200 gpm). Injection operations are assumed to commence on January 1, 2020 and cease on December 31, 2050.

3.3.11 Modeled Brine and Injectate Fluid Densities

Table 3-12 compiles the formation fluid TDS values at the DeLisle Plant. The TDS value at ground level is assumed to be zero, and the value at 2,700 feet below ground level (BGL), estimated to be the base of the lowermost USDW, is 10,000 parts per million (ppm). Additional data points on the table were derived from drill stem testing and recovery of fluids from Monitoring Well No. 1 in 1974, as well as research literature data from the Wilcox Formation at 5,900 feet and calculated data from 9,855 feet.

Included in Figure 3-9 are TDS values recovered from Monitoring Well No. 1 taken during drill stem tests (Halliburton, 1974a, 1974c). The analyzed samples contained approximately 57,000 and 114,000 ppm TDS at approximately 3,900 and 9,400 feet, respectively (Bishop, 1974). Formation fluids obtained from a drill stem test in the Washita-Fredericksburg Injection Interval were estimated to contain 102,500 ppm NaCl based on resistivity (Halliburton, 1974d). TDS for one sample was estimated to be 155,000 ppm based on the NaCl to TDS ratio of the other two formation fluid samples (3,900 and 9,400 feet), and the NaCl content of the sample from the injection sand. In 1994, a formation fluid sample was recovered from the Washita-Fredericksburg Sand during construction of Well 5. Subsequent laboratory analysis indicated a value of 105,000 ppm TDS.

Based on the information plotted and presented on Figure 3-9, the Washita-Fredericksburg Injection Interval formation fluid TDS is estimated to be 188,000 mg/L. This is also accepted as a representative value of the TDS of the Tuscaloosa Massive Sand formation fluid. Reservoir brine and injected fluid density were calculated for input into the SWIFT model. The SWIFT model requires that the fluid densities be entered in pounds per cubic foot (lb/ft^3). Density data was calculated at reservoir conditions of temperature and pressure.

Reservoir Brine Density

The Washita-Fredericksburg Injection Interval formation fluid has an estimated TDS concentration of 188,000 mg/L. Using interpolation data developed by Potter, R.W., and Brown, D. L., 1977, a formation brine density of 1.097 gm/cm^3 (**68.49 lb/ft^3**) was derived at reservoir conditions (243.6°F and 4,581 psi).

The Tuscaloosa Massive Sand also has an estimated TDS concentration of 188,000 mg/L. Again, using interpolation data developed by Potter, R.W., and Brown, D. L., 1977, a formation brine density of 1.098 gm/cm^3 (**68.55 lb/ft^3**) was derived at reservoir conditions (236.4°F and 4,406 psi).

Light Injectate Fluid Densities

The low-density injectate (up-dip) waste transport model uses an injectate fluid density of **62.43 lb/ft^3** at reservoir conditions in the Washita-Fredericksburg Injection Interval. This is equivalent to a density of 1.00 g/cm^3 at reservoir depth, and a specific gravity of 1.00 at reservoir depth. This is approximately equivalent to a density of 1.04 g/cm^3 at SATP, and a specific gravity of 1.04 at SATP.

The low-density injectate (up-dip) waste transport model also uses an injectate fluid density of **62.43 lb/ft^3** at reservoir conditions in the Tuscaloosa Massive Sand. This is equivalent to a density of 1.00 g/cm^3 at reservoir depth, and a specific gravity of 1.00 at reservoir depth. This is approximately equivalent to a density of 1.04 g/cm^3 at SATP, and a specific gravity of 1.04 at SATP.

Heavy Injectate Fluid Densities

The heavy-injectate (down-dip) waste transport model uses an injection fluid density of **81.16 lb/ft^3** at reservoir conditions in the Tuscaloosa Massive Sand. This is equivalent to a density of 1.30 g/cm^3 at reservoir depth, and a specific gravity of 1.30 at reservoir depth. This is approximately equivalent to a density of 1.36 g/cm^3 at SATP, and a specific gravity of 1.36 at SATP.

The heavy-density injectate down-dip) waste transport model also uses an injectate fluid density of **81.16 lb/ft^3** at reservoir conditions in the Tuscaloosa Massive Sand. This is equivalent to a density of 1.30 g/cm^3 at reservoir depth, and a specific gravity of 1.30 at reservoir depth. This is approximately equivalent to a density of 1.35 g/cm^3 at SATP, and a specific gravity of 1.35 at SATP.

Pressure Model Injectate Fluid Densities

The Washita-Fredericksburg Injection Interval pressurization model uses an injection fluid density 1.20 g/cm^3 at SATP, and a specific gravity of 1.20 at SATP. This is the average historical value of specific gravity of the injection fluid. At reservoir conditions (corrected for pressure and temperature) the injection fluid density is **71.80 lb/ft^3**.

The Tuscaloosa Massive Sand pressurization model also uses an injection fluid density 1.20 g/cm^3 at SATP, and a specific gravity of 1.20 at SATP. At reservoir conditions (corrected for pressure and temperature of the Tuscaloosa Massive Sand) the injection fluid density is **71.92 lb/ft^3**.

3.3.12 Modeled Brine and Injectate Fluid Viscosities

The formation brine viscosities used in the SWIFT lateral transport and pressurization models are assigned to be that of an 18.8 percent sodium chloride solution in both the Washita-Fredericksburg Injection Interval and Tuscaloosa Massive Sand. The low density injectate is expected to be approximately equivalent to that of fresh water. The high density waste stream is best described as a ferrous chloride ($FeCl_2$) solution. Each of the subject fluid viscosities are temperature-dependent, as discussed in following paragraphs.

Formation Brine Viscosities

The formation brine viscosities used in the SWIFT lateral transport and pressurization models are assigned to be that of an 18.8 percent sodium chloride solution in both the Washita-Fredericksburg Injection Interval and Tuscaloosa Massive Sand. These viscosities are temperature-dependent. This selection maximizes waste movement in the models. The viscosities shown below were determined using a concentration of 18.8 percent sodium chloride, as available in the Fig. D.35 NaCl nomograph provided in Earlougher (Appendix 3-4). The Washita-Fredericksburg Injection Interval brine viscosity at 243.6 °F was determined to be **0.405 cP**. The Tuscaloosa Massive Sand formation brine viscosity at 236.4 °F was determined to be **0.418 cP**

18.8% NaCl Brine Viscosity

Temperature (ºF)	Formation Brine Viscosity (cP)
200	0.51
220	0.45
240	0.42
260	0.38
280	0.35

Light Injectate Viscosities

The low density injectate is expected to be approximately equivalent to that of fresh water at reservoir conditions. Therefore, the low density injectate fluid viscosities used in the lateral migration plume model were estimated, based on the equivalent salinity of a fluid having a density of 62.43 lb/ft^3. This selection maximizes waste movement in the model. The viscosities shown below were determined using a concentration of 0.00 percent sodium chloride, as available in the Fig. D.35 NaCl nomograph provided in Earlougher (1977, Appendix 3-4). The low density injectate viscosity at 243.6 °F (Washita-Fredericksburg Injection Interval) was determined to be **0.231 cP**. The low density injectate viscosity at 236.4 °F (Tuscaloosa Massive Sand) was determined to be **0.240 cP**.

Light Density Injectate (Fresh Water) Viscosity

Temperature (ºF)	Freshwater Viscosity (cP)
200	0.30
220	0.26
240	0.24
260	0.21
280	0.19

Average Injectate Viscosities

The normally injected waste stream is best described as a $FeCl_2$ solution. The historical average specific gravity of the normally injected waste stream in 1.20. This is assumed to be equal to a density of 1.20 g/cm^3. Viscosity data for $FeCl_2$ solutions at this concentration were not readily available. Chemours obtained a normally injected waste stream sample to obtain a viscosity value. The derived viscosity was 0.972 centistokes (0.972 cP) in a sample with specific gravity 1.213 at 70 °C (158 °F). containing 15.83 weight percent TDS.

The derived viscosity was 0.739 cP in a sample with a specific gravity of 1.19 at 80 °C (176 °F) and 0.621 cP in a sample with a specific gravity of 1.18 at 95 °C (203 °F).

Given the limited viscosity data for $FeCl_2$ solutions, for purposes of this demonstration, the viscosity of a 1.20 g/cm^3 $FeCl_2$ solution is assumed to be 25% greater than the reservoir brine (18.8% NaCl solution) at reservoir conditions. Given this assumption, at 200 °F, a 1.20 g/cm^3 $FeCl_2$ solution would have a viscosity of 0.64 cP. This is in close agreement with the Chemours data which suggests a viscosity of 0.621 cP in a FeCl2 sample with a specific gravity of 1.18 at 203 °F. The average density injectate viscosity at 243.6 °F (Washita-Fredericksburg Injection Interval) was estimated to be **0.506 cP**. The averaged density injectate viscosity at 236.4 °F (Tuscaloosa Massive Sand) was estimated to be **0.523 cP**.

Average Density Injectate (1.20 g/cm^3 $FeCl_2$) Viscosity*

Temperature (ºF)	Heavy Injectate Viscosity (cP)
200	0.64
220	0.56
240	0.53
260	0.48
280	0.44

Heavy Injectate Viscosities

The high density waste stream is best described as a saturated $FeCl_2$ solution. The high density injectate fluid viscosities used in the Injection Intervals' heavy-injectate lateral models are assigned to be that of the maximum density injectate of a 1.30 g/cm^3 (at reservoir conditions). This selection maximizes post-operational plume movement in the models. As discussed in the previous paragraph, the viscosity data for $FeCl_2$ solutions is limited. For purposes of this demonstration, the viscosity of a 1.30 g/cm^3 $FeCl_2$ solution is assumed to be 50% greater than the reservoir brine (18.8% NaCl solution) at reservoir conditions. The average density injectate viscosity at 243.6 °F (Washita-Fredericksburg Injection Interval) was estimated to be **0.608 cP**. The averaged density injectate viscosity at 236.4 °F (Tuscaloosa Massive Sand) was estimated to be **0.627 cP**.

High Density Injectate (1.30 g/cm^3 $FeCl_2$) Viscosity*

Temperature (ºF)	Heavy Injectate Viscosity (cP)
200	0.77
220	0.68
240	0.63
260	0.57
280	0.53

3.3.13 Regional Ground Water Flow

Natural regional hydraulic gradients of deep saline aquifers in the coastal Gulf of Mexico were ascertained during the geology study to be gulfward. Studies reviewed and referenced for compilation of the information on area geology conclude that water movement in many regional deep saline aquifers in the Gulf Coast is extremely slow due to the lack of discharge pathways because of burial and enclosure of sand bodies by fine-grained muds. These studies show sluggish circulation to nearly static conditions in the deep subsurface. Flow rates in the deep saline aquifers (Clark, 1988) from the studies presented in Appendix 3-5 were found generally to be on the order of inches per year. A south-southeasterly (downdip) direction of regional flow established for the Washita-Fredericksburg Injection Interval and Tuscaloosa Massive Sand is consistent with the theory of deep basin flows and the physical mechanisms (topographic relief near outcrops and deep basin compaction) identified as contributing to natural formation drift (Bethke et al, 1988; Clark, 1988; Kreitler, 1986).

Chemours believes that a formation fluid velocity of 0.5 ft/yr is *very* conservative, since lateral facies changes that result in sand pinch-outs and formation fluid flow-path interruptions are known to occur in the direction of the recharge area of the Washita-Fredericksburg Injection Interval and Tuscaloosa Massive Sand.

For the “light-density” plume migration models, the ground water flow velocity was set at **0.0 ft/year**. This was done to ensure that the maximum up-dip injectate plume movement would be realized, since regional ground water (down-dip) flow would act to counter the up-dip force of buoyancy.

For the “high-density” plume movement demonstration, the ground water flow velocity was set at **0.5 ft/year**. This was done to ensure that the maximum down-dip injectate plume movement would be realized. The background velocity was implemented in the “high-density” plume models by: (1) running the lateral migration model with a 0 ft/yr ground water gradient to account for plume drift due to buoyancy; and (2) shifting the center of mass for the 10,000-year waste plume in the downdip direction by 5,000 feet (10,000 years x 0.5 ft/yr).

3.3.14 Rock and Fluid Compressibilities

The compressibility values were chosen conservatively to maximize the pressure increases in the models. The compressibility value affects the magnitude of the storativity, which has a relationship with the amount of model pressure increase. The smaller the storativity, the greater the pressure increase. Smaller compressibilities also maximize the plume extents. This is accomplished via the coupling equations for porosity and density in SWIFT (Reeves and others, 1986, p. 6). The porosity and fluid density are minimized with decreasing rock and water compressibility. The total compressibility is equal to the compressibility of the formation rock plus the compressibility of the formation fluid. Compressibility values are small (on the order of 10^{-6} psi^{-1}) and the values lie within a relatively small range. Total system compressibility (fluid and rock compressibility) was chosen for water and rock in order to maximize the pressure increases and the plume sizes in the models.

Fluid Compressibility

The brine compressibility for the Injection Interval was calculated using a method provided in Hewlett Packard (1982, p. 94):

$$\text{Compressibility of water} = Cw = \frac{A + BT + CT^2}{1x10^6}$$

$A = 3.8546 - (0.000134)(P)$
$B = -0.01052 + (4.77 \times 10^{-7})(P)$
$C = 3.9267 \times 10^{-5} - (8.8 \times 10^{-10})(P)$
T = temperature in °F
P = pressure in psi

Compressibility brine =

$$Cb = Cw\{[-0.052 + 2.7 \times 10^{-4}(T) - 1.14 \times 10^{-6}(T^2) + 1.121 \times 10^{-9}(T^3)]\%NACL^{0.7} + 1\}$$

For the Washita-Fredericksburg Injection Interval, the compressibility of reservoir brine is calculated as follows:

A = 3.4570154
B = -0.009151487
C = 3.67423E-05
%NaCl = 18.8
T = 243.6 °F
P = 4,580.7 psi

$Cb = 2.33 \times 10^{-6}/psi^{-1}$

For the Tuscaloosa Massive Sand, the compressibility of reservoir brine is calculated as follows:

A = 3.4570154
B = -0.009151487
C = 3.67423E-05
%NaCl = 18.8
T = 236.4 °F
P = 4,406.4 psi

Cb = 2.31 x 10^{-6}/psi^{-1}

Rock Compressibility

For the formation compressibilities, a value of **3.2 x 10^{-6} psi^{-1}** was approximated for the Washita-Fredericksburg Injection Interval and Tuscaloosa Massive Sand, based on a porosity of 24 percent and 25 percent porosity, respectively. This value was obtained from Hall's correlation for unconsolidated sandstones in Earlougher (1977, p. 229, Fig. D.12) (see Appendix 3-6).

Total System Compressibility

The total system compressibility for the Washita-Fredericksburg Injection Interval is the sum of the fluid compressibility (2.33 x 10^{-6}/psi^{-1}) and rock compressibility (3.2 x 10^{-6} psi^{-1}), which is **5.53 x 10^{-6} psi^{-1}**. The total system compressibility for the Tuscaloosa Massive Sand is the sum of the fluid compressibility (2.31 x 10^{-6}/psi^{-1}) and rock compressibility (3.2 x 10^{-6} psi^{-1}), which is **5.51 x 10^{-6} psi^{-1}**.

3.3.15 Well Index Value

The well index is calculated using the following equation (Reeves and others, 1986, equation 4-3):

$$WI = 2\pi K_s \sum_k \frac{\Delta z_k}{\ell n\left(r_1 / r_w \right)}$$

where: K_s = hydraulic conductivity of the wellbore skin
$\Sigma\Delta z$ = sum of the thickness for the model layers
$r| = r_1 = [(\Delta x \Delta y)/\pi]^{0.5}$
$\Delta x \Delta y$ = product of x and y grid dimensions at the well location
r_w = the well radius
$\ell n(r_1/r_w) = r_w \{1+(r_|/r_w)[\ell n(r_|/r_w)-1]\}/(r_|-r_w)$

For all the models, wellbore skin was ignored and the sand hydraulic conductivity was used.

Washita-Fredericksburg Injection Interval

For the Washita-Fredericksburg Injection Interval low-density plume, high-density plume and reservoir pressure models, the well index was calculated for each injection well at its specific grid location. The reservoir thickness, grid cell dimensions and wellbore radius varies slightly for each well. Following are well index values for the Washita-Fredericksburg Injection Interval low-density, high density and reservoir pressure SWIFT models:

Washita-Fredericksburg Well Index Values

Well Nos.	Light Density Plume Migration Model (ft^2/day)	High Density Plume Migration Model (ft^2/day)	Reservoir Pressure Model (ft^2/day)
Monitoring Well No. 1	867.1	873.6	367.0
Well No. 2	922.1	922.1	387.4
Well No. 3	971.1	971.1	410.6
Well No. 4	916.0	916.0	387.4
Well No. 5	1076.1	1082.8	454.9
Well No. 6	1013.7	1013.7	425.8
Well No. 7	952.6	922.1	402.7

Tuscaloosa Massive Sand

For the Tuscaloosa Massive Sand low-density plume, high-density plume and reservoir pressure models, the well index was calculated for each injection well at its specific grid location. The reservoir thickness, grid cell dimensions and wellbore radius varies slightly for each well. Following are well index values for the Tuscaloosa Massive Sand low-density, high density and reservoir pressure SWIFT models:

Well Index Values

Well Nos.	Light Density Plume Migration Model (ft^2/day)	High Density Plume Migration Model (ft^2/day)	Reservoir Pressure Model (ft^2/day)
Monitoring Well No. 1	1778.9	1788.3	1078.6
Well No. 2	1776.5	1820.9	1092.5
Well No. 3	1846.4	1864.9	1118.9
Well No. 4	1776.5	1785.3	1071.2
Well No. 5	1729.5	1737.8	1232.6
Well No. 6	1954.1	1971.9	1183.1
Well No. 7	1883.1	1900.8	1151.1

3.3.16 Boundary Conditions

For each of the SWIFT models provided in this demonstration, all the lateral boundaries are “open”. This serves to maximize waste plume movement and reflects the local geology in that there are no nearby faults which would potentially “bound” the reservoir. This is accomplished by imposing transmissive Carter-Tracy boundaries on the sides using the same transmissivities and porosity-thickness values that are used throughout the model.

Permeability-Thickness and Porosity-Thickness

The aquifer transmissivity, Kh, and porosity thickness, ϕh, were calculated for the lateral migration models and reservoir pressure models as given below. The reservoir thickness value (h) is the average thickness of the grid block cells along the edges (boundary) of the subject SWIFT models.

For the Washita-Fredericksburg Injection Interval, the Carter-Tracy boundary inputs for the <u>light density plume model</u> were calculated using the following values:

$$Kh = (3.716 \text{ ft/day})(112.69 \text{ ft}) = 418.7 \text{ feet}^2\text{/day}$$
$$\phi h = (0.24)(112.69 \text{ feet}) = 27 \text{ feet}$$

For the Tuscaloosa Massive Sand, the Carter-Tracy boundary inputs for the <u>light density plume model</u> were calculated using the following values:

$$Kh = (5.405 \text{ ft/day})(192.34 \text{ ft}) = 1039.6 \text{ feet}^2\text{/day}$$
$$\phi h = (0.25)(163.73 \text{ feet}) = 48 \text{ feet}$$

The aquifer transmissivity, Kh, and porosity thickness, ϕh, were similarly calculated for each lateral migration model and reservoir pressure model based on the average thickness of the grid block cells along the edges (boundary) of the subject SWIFT.

Equivalent Aquifer Radius

For purposes of this discussion, it is important to distinguish between the term "reservoir" and the term "aquifer." The reservoir is that portion of the system for which the simulation is desired. The aquifer is the area outside the reservoir that provides boundary conditions for the reservoir. The radius of the reservoir (r_e) for a Cartesian geometry is typically chosen as the radius of a circle of equal surface area. The radius of the aquifer (r_q) may be chosen to be either finite or infinite (HIS GeoTrans, 2000). For this model demonstration, a finite equivalent aquifer radius was assigned. The RAQ value was derived by determining the radius of a circle of surface area equal to the width of the SWIFT model multiplied by three (3) and length of the SWIFT model multiplied by three (3). Within this approximate area, "aquifer" properties are expected to mimic the modeled "reservoir" properties. For the light-density Washita-Fredericksburg SWIFT model, the model dimensions are 74,000 feet wide and 142,000 feet in length. Thus,

$$RAQ = r$$
$$\pi r^2 = (74{,}000 \text{ feet x } 3)(142{,}000 \text{ feet x } 3)$$
$$RAQ = r = 173{,}503 \text{ feet}$$

The RAQ value was similarly calculated for each light density waste plume, high density waste plume and reservoir pressurization model.

Angle of Influence

The angle of influence was assigned to be 360 degrees in each SWIFT model, based on the location of the injection wells with respect to the model boundaries (aquifer-influence boundaries).

3.3.17 Coefficient of Thermal Expansion

For the Washita-Fredericksburg Injection Interval, the initial reservoir temperature at the reference depth of 9,888.6 feet subsea was estimated to be 243.6 °F. For the Tuscaloosa Massive Sand, the initial reservoir temperature at the reference depth of 9,511.6 feet subsea was estimated to be 236.4 °F. Based on these temperature values, the coefficient of thermal expansion of the fluid based on Reeves and others (1986, p. 14, Figure 3-1) lies within the range given for experimental data as bracketed by the constant values of 0.0002 $°F^{-1}$ and 0.0005 $°F^{-1}$. Although a coefficient of thermal expansion value is between 0.0002 $°F^{-1}$ and 0.0005 $°F^{-}$, a value of **0.00 $°F^{-1}$** is utilized to be conservative.

3.3.18 Fluid and Rock Heat Capacities

The fluid heat capacity input is only used if the equations for heat flow are being solved. In the simulations, only the brine and pressure equations are solved. The value of **1.0 Btu/lb-°F** was input for completeness and has no impact on the SWIFT calculated pressure or brine concentration.

The rock heat capacity input is only used if the equations for heat flow are being solved. In the simulations, only the brine and pressure equations are solved. The value of **1.0**

Btu/ft^3-°F was input for completeness and has no impact on the SWIFT calculated pressure or brine concentration.

3.3.19 Thermal Conductivity of the Fluid Saturated Porous Medium

The thermal conductivity of the fluid saturated porous medium in the x, y and z directions was assigned to be **116 Btu/ft-d-°F**. This input is only used if the equations for heat flow are being solved. In the Chemours facility simulations, only the brine and pressure equations are solved. The value of 116 Btu/ft-d-°F was input for completeness and has no impact on the SWIFT calculated pressure or brine concentration.

3.3.20 Solid Particle Density of the Formation

The solid particle density of the formation is chosen to be **165 lb/ft^3**. This input is only used if the equations for heat flow or radionuclide movement are being solved. In the Chemours facility simulations, only the brine and pressure equations are solved. The value of 165 lb/ft^3 was input for completeness and has no impact on the SWIFT calculated pressure or brine concentration.

3.3.21 Gridding Scheme and Gridded Area

Grid size is an important parameter in the SWIFT model. To ensure that proper grid sizes are implemented in the Chemours SWIFT models, additional evaluations were performed. This evaluation is provided in Appendix 3-7.

The SWIFT model grid employed for light density lateral migration modeling for the Washita-Fredericksburg Injection Interval has 767 grid blocks in the X direction and 1180 grid blocks in the Y direction. The model distance is 74,000 feet along the X axis and 142,000 feet along the Y axis. Figure 3-10 illustrates the SWIFT model grid employed for Washita-Fredericksburg Injection Interval light density waste plume lateral migration model. The gridding scheme for the Washita-Fredericksburg Injection Interval model is as follows:

X SPACING
50 20*300 80*150 586*75.0 80*150

Y SPACING
250 127*300 44*150 854*75 88*150 66*300

The SWIFT model grid employed for light density lateral migration modeling for the Tuscaloosa Massive Sand has 767 grid blocks in the X direction and 1246 grid blocks in the Y direction. The model distance is 74,000 feet along the X axis and 142,000 feet along the Y axis. Figure 3-11 illustrates the SWIFT model grid employed for Tuscaloosa Massive Sand light density waste plume lateral migration model. The gridding scheme for the Tuscaloosa Massive Sand model is as follows:

X SPACING
100*150 548*75 118*150 200

Y SPACING
250 127*300 132*150 854*75 132*150

The SWIFT model grid employed for high density lateral migration modeling for both the Washita-Fredericksburg Injection Interval and the Tuscaloosa Massive Sand has 560 grid blocks in the X direction and 1467 grid blocks in the Y direction. The model distance is 50,000 feet along the X axis and 120,000 feet along the Y axis. Figure 3-12 illustrates the SWIFT model grid employed for high density waste plume lateral migration model. The gridding scheme is as follows:

X SPACING
24*150 454*75 81*150 200

Y SPACING
83*150 1334*75 50*150

The SWIFT model grid employed for reservoir pressure modeling for both the Washita-Fredericksburg Injection Interval and the Tuscaloosa Massive Sand has 700 grid blocks in the X direction and 700 grid blocks in the Y direction. The model distance is 67,500 feet along the X axis and 67,500 feet along the Y axis. Figure 3-13 illustrates the SWIFT model grid employed for reservoir pressurization model. The gridding scheme is as follows:

X SPACING
100*150 500*75 100*150

Y SPACING
100*150 500*75 100*150

Well locations (bottom-hole locations) within the Washita-Fredericksburg Injection Interval and Tuscaloosa Massive Sand light density plume migration models are as follows:

Washita-Fredericksburg Light Density Waste Plume Migration Model				
Well No.	Grid Block		Distance (feet)	
	x-direction	y-direction	x-direction	y-direction
Monitor Well No. 1	378	431	38,788	70,938
Well No. 2	365	480	37,813	74,613
Well No. 3	350	485	36,688	74,988
Well No. 4	355	478	37,063	74,463
Well No. 5	354	505	36,988	76,488
Well No. 6	382	518	39,088	77,463
Well No. 7	383	491	39,163	75,438

Tuscaloosa Massive Sand Light Density Waste Plume Migration Model				
Well No.	Grid Block		Distance (feet)	
	x-direction	y-direction	x-direction	y-direction
Monitor Well No. 1	417	431	38,738	70,938
Well No. 2	398	480	37,313	74,613
Well No. 3	390	485	36,713	74,988
Well No. 4	394	478	37,013	74,463
Well No. 5	393	505	36,938	76,488
Well No. 6	421	518	39,038	77,463
Well No. 7	422	491	39,113	75,438

Well locations (bottom-hole locations) for the Washita-Fredericksburg Injection Interval and Tuscaloosa Massive Sand high density plume migration models are identical and are as follows:

Heavy Density Waste Plume Migration Models				
Well No.	Grid Block		Distance (feet)	
	x-direction	y-direction	x-direction	y-direction
Monitor Well No. 1	333	1205	26,738	96,563
Well No. 2	320	1253	25,763	100,163
Well No. 3	305	1259	24,463	100,613
Well No. 4	310	1251	25,013	100,013
Well No. 5	309	1278	24,938	102,038
Well No. 6	337	1291	27,038	103,013
Well No. 7	338	1264	27,113	100,988

Well locations (bottom-hole locations) for the reservoir pressure models for the Washita-Fredericksburg and Tuscaloosa Massive Sand models are identical and are as follows:

Reservoir Pressurization Models				
Well No.	**Grid Block**		**Distance (feet)**	
	x-direction	y-direction	x-direction	y-direction
Monitor Well No. 1	374	305	35,513	30,338
Well No. 2	361	353	34,538	33,938
Well No. 3	346	359	33,413	34,388
Well No. 4	351	351	33,788	33,788
Well No. 5	350	378	33,713	35,813
Well No. 6	378	391	35,813	36,788
Well No. 7	379	364	35,888	34,763

3.3.22 SWIFT Model Reference Point and Grid Block Centers

Washita-Fredericksburg Injection Interval: For the Washita-Fredericksburg Injection Interval reservoir modeling, a model reference point was selected in the approximate middle of the Washita-Fredericksburg Injection Interval within the Injection Interval at the Chemours Well No. 4 location. The top of the Washita-Fredericksburg Injection Interval is present at a depth of approximately 9,810 feet below sea level (subsea). A depth of **9,888.6 feet subsea** was chosen as the **reference depth** for the depth specific SWIFT model parameters for the Washita-Fredericksburg Injection Interval.

For the Washita-Fredericksburg Injection Interval SWIFT model runs, the depth to the **center of the grid block** at which Well No. 4 is located was set at 9,876 feet subsea. For a model reservoir thickness of 160 feet, the top of the grid block at the well location is at about 9,796 feet subsea.

Tuscaloosa Massive Sand: For the Tuscaloosa Massive Sand reservoir modeling, a model reference point was selected near the middle of the Tuscaloosa Massive Sand at the Chemours facility Well No. 4 location. The top of the Tuscaloosa Massive Sand is present at a depth of about 9,413 feet subsea. A depth of **9,511.6 feet subsea** was chosen as the **reference depth** for the depth specific SWIFT model parameters for the Tuscaloosa Massive Sand.

For the Tuscaloosa Massive Sand SWIFT model runs, the depth to the **center of the grid bloc**k at which Well No. 4 is located was set at about 9,508 feet subsea. For a model reservoir thickness of 200 feet, the top of the grid block at the well location is at about 9,408 feet subsea.

3.3.23 Time Step Allocation and Model Solution Method

The two-line successive-overrelaxation (L2SOR) solution was used for the SWIFT models. The minimum number of outer (nonlinear-property due to density variation) iterations in the subroutine was set at two. The maximum number of outer (nonlinear-property due to density variation) iterations in the subroutine was set at five. The number of time steps (transient) after which the optimum parameters for the inner iterations are recalculated for the L2SOR was set at five (default value is five).

Time step allocation is an important parameter in the SWIFT model. To ensure that time steps are implemented in the Chemours SWIFT models, additional evaluations were performed. These evaluations are provided in Appendix 3-7. During the stabilization period, the smallest automatic time step allowed was 0.01 days, with a maximum of 30 days. During injection for the pressure buildup and low density lateral migration plume models, the smallest time steps allowed was 1.0 day, which was allowed to automatically increase to maximums of 30 days. After injection ceased, the automatic time step was as small as 1.0 day initially, and then allowed to increase over time to a maximum of 5,000 days. For the pressure model, after injection ceases, the smallest time step was maintained at 1.0 day, and the maximum time step was maintained at 30 days. During injection for the high density lateral migration plume models, the smallest time steps allowed was 1.0 day, which was allowed to automatically increase to maximums of 30 days. After injection ceased, the automatic time step was as small as 1.0 day initially, and then allowed to increase over time to a maximum of 730 days.

3.3.24 Stabilization Period

The length of the stabilization period for each the Chemours facility model was chosen to be 10,000 days. Automatic time stepping was allowed to take incrementally larger time steps from 0.01 days to 30 days until the 10,000-day stabilization period ended.

3.3.25 Darcy Velocity

During the SWIFT model stabilization period, small residual background velocity gradients occur. These remnant velocity values are inherently present due to the variable structure nature (variable dip in X and/or Y direction) of the models, and decrease in magnitude through time. The resultant X and Y Darcy velocity values and directional vectors from the pre-injection stabilization periods for the light injectate model after 10,000 days are included as Figures 3-14 (Washita-Fredericksburg Injection Interval) and 3-15 (Tuscaloosa Massive Sand). The contour/vector maps illustrate the small residual background velocity gradient present in the SWIFT models prior to initiating injection.

The 10,000-year plume movement distances for the Injection Interval models were not adjusted to account for the resultant background velocities at the end of the 10,000-day stabilization period. The Darcy velocity from the Injection Interval velocity maps (Figure 3-14 and Figure 3-15) is small, and on the order of approximately 4.0 x 10^{-6} ft/day (average), within the area of light density plume movement. The Darcy velocity (in ft/day) was converted to an average linear velocity by dividing by the Injection Interval's porosity value (24 percent). The linear movement over the 10,000-year period was calculated to be approximately 61 feet. This distant is negligible (less than 1.0 percent of up-dip plume movement distance) given the extent of the 10,000-year plume dimensions.

3.3.26 Flowing and Static Bottom-Hole Pressure Data

Flowing and static BHP data for the Washita-Fredericksburg Injection Interval were gathered from historical fall-off test analyses of the Chemours injection wells. The historical static BHP data (Tables 3-3, 3-5, 3-6 and 3-11) suggests that there has been very little pressure buildup in the Washita-Fredericksburg Injection Interval due to the operation of the subject Class I injection wells. The initial static BHP values for the Chemours injection wells are discussed in Section 7.3.3.

3.3.27 Nearby Oil and Gas Production

Hydrocarbons are actively produced approximately five (5) miles to the west of the Chemours facility. However, all of the active production is from much deeper horizons (approximate depth of 13,000 to 14,000 feet). There is no nearby oil and gas production from the Washita-Fredericksburg Injection Interval or Tuscaloosa Massive Sand. Therefore, nearby oil and gas production will have no effect on the SWIFT model predicted lateral plume movement or predicted reservoir pressure buildup.

3.4 Cone of Influence

The Cone of Influence (COI) is defined to be "the potentiometric surface area around the injection well within which increased Injection Zone pressures caused by injection of wastes would be sufficient to drive fluids into a USDW or a fresh water aquifer." The SWIFT model was used to determine the Chemours pressure buildup and COI for this application. SWIFT models the pressure increase that will be created in the injection reservoir sands during, and at the end of the operational life of the Chemours injection wells.

The methodology used in this petition for calculating the COI was developed by E. I. du Pont de Nemours and Company (DuPont) for its injection well sites, and it is also generally consistent with previous methods (Price, 1971; Johnston and Greene, 1979; Barker, 1981; Collins, 1986; Davis, 1986; Johnston and Knape, 1986; Warner and Syed, 1986; Clark and others, 1987; Warner, 1988). The basic underlying assumption in the approach is that in the absence of naturally-occurring, vertically transmissive conduits (faults and fractures), the only potential pathway between the Injection Zone and USDW is through an artificial penetration (active or inactive oil and gas well(s). To pose a potential threat to a USDW (i.e., pressure build-up from injection operations must be sufficient to drive fluids into a USDW), the pressure increase in the Injection Zone would have to be greater than the pressure necessary to displace the material residing within the borehole (drilling mud). This pressure is defined as the allowable pressure build-up. Therefore, the COI is defined as the area within which Injection Zone pressures are greater than the allowable pressure build-up.

3.4.1 Mud Weight

Barker (1981) was the first to document the development of the basic theoretical equation for calculating maximum allowable formation pressure at an abandoned borehole in terms of mud properties. The equation includes the effects of both weight and gel strength of the mud. Resistance to upward migration based on mud weight alone can be determined by examining the records of inactive artificial penetrations for their respective abandonment mud weights. In cases where abandonment mud weights are unknown, a reasonable worst-case value of 9.0 lb/gal is widely accepted for the Gulf Coast region (Barker, 1981; Johnston and Knape, 1986).

At the DeLisle Plant, however, site-specific drilling records from wells drilled throughout the area support the application of a 9.3 lb/gal mud weight. This mud weight (9.3 lb/gal) is recorded as the minimum mud weight used within the 2.0-mile AOR and in the wells in offset oil and gas fields west of the AOR. Barker (1981) advocates a similar method of determining the minimum mud weight in the AOR based upon well data in a particular area. Consequently, 9.3 lb/gal is used as one of the factors in determining allowable pressure buildup at DeLisle Plant.

3.4.2 Gel Strength

Gel strength is the property of borehole fluid (mud) which suspends particles (solids) in the static mud column when circulation ceases, e.g., drilling mud left in an abandoned borehole. Gel strength is a function of: 1) the amount and type of clays in suspension, 2) time, 3) temperature, and 4) mud additives (chemistry). The significance of mud gel strength is that it increases the pressure that is required for the onset of fluid migration in the borehole (Figure 3-24).

The pressure required to displace borehole mud can be large, and gel strength can be the main factor in preventing fluid migration within an abandoned wellbore (Collins, 1986 and 1989; Johnston and Knape, 1986; and Pearce, 1989b). Collins further states that in order to properly model abandoned boreholes, it is important to use ". . . realistic values for mud and hole properties," and that ". . . in most cases the contribution of the gel property (gel strength) to the critical pressure increase required for fluid entry into the well may be more significant than previously thought."

For the purpose of calculating the pressure due to gel at DeLisle Plant, a conservative gel strength value of 20 lb/100 ft^2 is used. Grey and Darley (in Collins, 1986) determined that approximately 20 lb/100 ft^2 is the lowest possible gel strength that could occur. Studies indicate that with time the gel strength of drilling mud may be more than an order of magnitude higher (Pierce, 1989). A plot of the increase in mud gel strength with time is shown in Figure 3-12.

Pressure due to gel strength for an open borehole is more conservative than for a cased borehole, and is calculated by the following formula:

$$Pg = \frac{0.00333 \text{ x G x h}}{\text{d}}$$

Where:

Pg = pressure due to gel strength (psia)
G = gel strength (lb/100 ft^2)
d = borehole diameter (inches)
h = the shallowest depth within the AOR of the top of the Washita-Fredericksburg Injection Interval (this is 9,520 feet for the DeLisle Plant site AOR)
h = the shallowest depth within the AOR of the top of the Tuscaloosa Massive Sand (this is 9,160 feet for the DeLisle Plant site AOR)

And 0.00333 is the conversion factor such that Pg is in psi

$$Pg = \frac{0.00333 \text{ x } 20 \text{ x } 9{,}520}{14.325} = 44 \text{ psi (Washita} - \text{Fredericksburg)}$$

$$Pg = \frac{0.00333 \text{ x } 20 \text{ x } 9{,}160}{14.325} = 43 \text{ psi (Tuscaloosa Massive Sand)}$$

3.4.3 Calculating the Allowable Pressure Buildup

The initial step in calculating the allowable pressure buildup (COI) for the injection sands at the plant site is to determine the original formation pressure gradient. The original formation pressure gradient of an injection sand is calculated by dividing the original formation pressure by the depth at which the pressure was recorded. At the DeLisle Plant, the original formation pressure gradient for the Washita-Fredericksburg injection interval was recorded as 0.462 psi/ft.

The maximum pressure buildup is then calculated by subtracting the original formation pressure from the conservative 9.3 lb/gal mud column pressure and adding the gel strength to this value, as demonstrated by the following:

0.052 x 9.3 lb/gal = 0.484 psi/ft	(mud column gradient, modified from Barker, 1981; 0.052 is a conversion factor)
0.484 psi/ft x 9,520 ft = 4608 psi	(9,520 feet to the shallowest Injection Interval within the AOR x 0.484 psi/ft exerted by the mud column)
0.462 psi/ft x 9,520 feet = 4,398 psi	(original formation pressure gradient x depth to the shallowest injection interval within the AOR)
4,608 psi – 4,398 psi + 44 psi = 254 psi	(mud column pressure minus original formation pressure, + pressure due to gel strength = allowable pressure buildup)

Therefore, **254 psi** is the maximum pressure buildup allowed in the Washita-Fredericksburg Injection Interval sand prior to the onset of possible fluid movement in an artificial penetration. The COI for Washita-Fredericksburg Injection Interval is therefore defined as the area within which the Injection Zone pressure increase is greater than **254 psi**. Following the same methodology, **244 psi** is the maximum pressure buildup allowed in the Tuscaloosa Massive Sand prior to the onset of possible fluid movement in an artificial penetration. The COI for Tuscaloosa Massive Sand is therefore defined as the area within which the Injection Zone pressure increase is greater than **244 psi**.

3.5 SWIFT Model Results – Reservoir Pressurization Modeling

The Washita-Fredericksburg Injection Interval and Tuscaloosa Massive Sand pressurization models were run to estimate reservoir pressure at the end-of-operations. The SWIFT pressurization models use the minimum flow capacity (hydraulic conductivity) and average injectate density and viscosities. The reservoir pressure buildup is determined by subtracting the initial reservoir pressures (10,000 days) from the reservoir pressures at the time of interest during the operational period. The simulated pressure buildup is indicative of the formation buildup outside the wellbore. A Table of Contents is included at the beginning of Appendix 3-7 which lists the pressure buildup cases by injection sand as well as showing the input and output file names for each of the model runs.

Reservoir pressurization modeling was performed to determine the area within which reservoir pressure increases due to injection activities exceed the Cone of Endangering Influence (COI). Injection Interval pressurization modeling was performed for the Washita-Fredericksburg Injection Interval and the Tuscaloosa Massive Sand.

3.5.1 SWIFT Washita-Fredericksburg Injection Interval Pressure Model

Reservoir pressure buildup in the Washita-Fredericksburg Injection Interval was considered for three (3) different scenarios. Currently, the calendar-month-average permitted injection rates are: 550 gpm for Well Nos. 2, 3 and 4; 1000 gpm for Well No. 5; and 1,200 gpm for Well No. 6 Total instantaneous injection rate is limited to no more than 2,200 gpm (cumulative for all five wells). This application is not seeking to increase the instantaneous injection rate limit even as it seeks to approval for future injection into Well No. 1 and construction of a second new well (Well No. 7).

The first scenario (Chemours WF Prs) assumes all future injection (January 1, 2016 to December 31, 2050) into the Washita-Fredericksburg Injection Interval will occur into each well (Well Nos. 2, 3, 4 and 5) at 550 gpm (2,200 gpm cumulative).

The second scenario (Chemours WF Prs(2)) assumes all future injection (January 1, 2016 to December 31, 2050) into the Washita-Fredericksburg Injection Interval will occur into Well Nos. 2, 3 and 4 at 400 gpm and at 1,000 gpm into Well No. 5 (2,200 gpm cumulative).

The final scenario (Chemours WF Prs(3)) assumes all future injection (January 1, 2016 to December 31, 2050) into the Washita-Fredericksburg Injection Interval will occur at 1,200 gpm into Well No. 6 and at 250 gpm into Well Nos. 2, 3, 4 and 5 (2,200 gpm cumulative).

The SWIFT reservoir pressure model input parameters are summarized on Table 3-1. For each scenario historical injection was incorporated into the demonstration to account for historically injected volumes (see Section 7.3.1). Historical annual average flow rates into the wells are depicted on Table 3-10. The Washita-Fredericksburg Injection Interval pressure model(s) (Chemours WF Prs and, Chemours WF Prs(2), and Chemours WF Prs(3)) input and output data are included in Appendix 3-8.

Figure 3-16 provides a well bore pressure buildup comparison of the three modeled scenarios. Well bore pressure buildup is included for Well No. 5 for the first and second scenario and for Well No. 6 for the final scenario. The model predicted flowing BHPs (well bore) for each scenario are included on Table 3-13. Pressure buildup was determined by subtracting the initial Injection Interval well bore pressures from the well bore pressure build up at the end of the operational year. The initial pressures were determined from a pre-operation period (no injection) in which the model was run for 10,000 days. The initial Injection Interval pressures (10,000 days) are included in the output files in Appendix 3-8.

For the first scenario (Chemours WF Prs), the maximum predicted flowing bottom-hole grid block pressure at the location of Well No. 5 on December 31, 2050 is 5,394 psi. The maximum predicted flowing bottom-hole well bore pressure on December 31, 2050 is 5,530 psi. The pre-injection native static reservoir pressure at the location of Well No. 5 is 4,563 psi. Therefore, the pressure buildup in the grid block cell is no more than 831 psi and the pressure buildup predicted at the well is no more than 967 psi.

For the second scenario (Chemours WF Prs(2)), the maximum predicted flowing bottom-hole grid block pressure at the location of Well No. 5 on December 31, 2050 is 5,551 psi. The maximum predicted flowing bottom-hole well bore pressure on December 31, 2050 is 5,800 psi. The pre-injection native static reservoir pressure at the location of Well No. 5 is 4,563 psi. Therefore, the pressure buildup in the grid block cell is no more than 988 psi and the pressure buildup predicted at the well is no more than 1,237 psi.

For the third scenario (Chemours WF Prs(3)) considers injection at the location of Well No. 6 at 1,200 gpm. The maximum predicted flowing bottom-hole grid block pressure in at the location of Well No. 6 on December 31, 2050 is 5,556 psi. The maximum predicted flowing bottom-hole well bore pressure on December 31, 2050 is 5,880 psi. The pre-injection native static reservoir pressure at the location of Well No. 6 is 4,554 psi. Therefore, the pressure buildup in the grid block cell is no more than 1,002 psi and the pressure buildup predicted at the well is no more than 1,326 psi.

The simulated Injection Interval pressure buildup for the first scenario (Chemours WF Prs) at the end-of-operation (December 31, 2050) is shown in Figure 3-17. The simulated Injection Interval pressure buildup for the second scenario (Chemours WF Prs(2)) at the end-of-operation (December 31, 2050) is shown in Figure 3-18. The simulated Injection Interval pressure buildup for the third scenario (Chemours WF Prs(3)) at the end-of-operation (December 31, 2050) is shown in Figure 3-19. Figures 3-17A, 3-18A and 3-19A are expanded depictions of the Injection Interval pressure buildup around the Chemours DeLisle property boundaries and injection wells. Each figure shows pressure isobars, representing the pressure buildup (the difference between the injection pressure at the end-of-operation and initial reservoir pressure) within the Injection Interval, radiating outward from the injection wells.

Of the three (3) scenarios, the first scenario (Chemours WF Prs) results in the largest area enclosed within the Cone of Endangering Influence (COI). The COI includes the area within the pressure isopleth representing a 254 psi increase in reservoir pressure. The predicted increase at a radius of 2.0-mile radius Area of Review is approximately 360 psi (northeast and southeast of the wells). Note that the areal distribution in pressure does not change significantly for each model case away from the well field. The COI extends approximately 23,100 feet from the Chemours injection wells. At the end of the model period (year-end 2050), the Cone of Influence extends approximately 12,500 feet beyond the 2.0-mile radius Area of Review.

Comparison to Historical Well Tests and Pressure Measurements: Monitoring Well No. 1 is completed into the Washita-Fredericksburg Injection Interval, and was converted to a monitoring well in 1978 (Egler, 1978). The wellhead pressure of Monitoring Well No. 1 is read approximately weekly by plant personnel. The readings were averaged to obtain a monthly wellhead pressure value for the monitoring well (see Table 3-11 for a tabulation of the monthly average pressures).

The historical measured pressure values from Monitoring Well No. 1 are plotted with the pressure increase predicted by the Chemours WF Prs SWIFT model in Figure 3-19B with time. Note that the figure has been updated through year end 2015, and the model run and output files are contained in Appendix 3-8. From 1979 to 2006, the SWIFT model consistently over-predicts of the reservoir pressure increase compared to those of the measured pressures recorded at Monitoring Well No. 1. From 2006 to 2015, the SWIFT predicted BHP increase more closely matches the measured pressure increases recorded at Monitoring Well No. 1. This comparison suggests that the SWIFT model construct and permeability value can provide a reasonable approximately of reservoir pressure buildup in the Washita-Fredericksburg Injection Interval.

3.5.2 SWIFT Tuscaloosa Massive Sand Pressure Model

For this demonstration, injection into the Tuscaloosa Massive Sand would commence on January 1, 2020 and would include the operation of Well Nos. 2, 3, 4, 5 and 6.

The first scenario (Chemours TMS Prs) assumes all future injection (January 1, 2020 to December 31, 2050) into the Tuscaloosa Massive Sand will occur into each well (Well Nos. 2, 3, 4 and 5) at 550 gpm (2,200 gpm cumulative).

The second scenario (Chemours TMS Prs(2)) assumes all future injection (January 1, 2020 to December 31, 2050) into the Tuscaloosa Massive Sand will occur into Well Nos. 2, 3 and 4 at 400 gpm and at 1,000 gpm into Well No. 5 (2,200 gpm cumulative).

The final scenario (Chemours TMS Prs(3)) assumes all future injection (January 1, 2020 to December 31, 2050) into the Tuscaloosa Massive Sand will occur at 1,200 gpm into Well No. 6 and at 250 gpm into Well Nos. 2, 3, 4 and 5 (2,200 gpm cumulative).

The SWIFT reservoir pressure model input parameters are summarized on Table 3-1. The Tuscaloosa Massive Sand pressure model(s) (Chemours TMS Prs and, Chemours TMS Prs(2), and Chemours TMS Prs(3)) input and output data are included in Appendix 3-8.

Figure 3-20 provides a well bore pressure buildup comparison of the three modeled scenarios. Well bore pressure buildup is included for Well No. 5 for the first and second scenario and for Well No. 6 for the final scenario. The model predicted flowing BHPs (well bore) for each scenario are included on Table 3-14. Pressure buildup was determined by subtracting the initial Injection Interval well bore pressures from the well bore pressure build up at the end of the operational year. The initial pressures were determined from a pre-operation period (no injection) in which the model was run for 10,000 days. The initial Injection Interval pressures (10,000 days) are included in the output files in Appendix 3-8.

For the first scenario (Chemours TMS Prs), the maximum predicted flowing bottom-hole grid block pressure at the location of Well No. 5 on December 31, 2050 is 4,689 psi. The maximum predicted flowing bottom-hole well bore pressure on December 31, 2050 is 4,740 psi. The pre-injection native static reservoir pressure at the location of Well No. 5 is 4,396 psi. Therefore, the pressure buildup in the grid block cell is no more than 293 psi and the pressure buildup predicted at the well is no more than 344 psi.

For the second scenario (Chemours TMS Prs(2)), the maximum predicted flowing bottom-hole grid block pressure at the location of Well No. 5 on December 31, 2050 is 4,746 psi. The maximum predicted flowing bottom-hole well bore pressure on December 31, 2050 is 4,840 psi. The pre-injection native static reservoir pressure at the location of Well No. 5 is 4,396 psi. Therefore, the pressure buildup in the grid block cell is no more than 350 psi and the pressure buildup predicted at the well is no more than 444 psi.

For the third scenario (Chemours TMS Prs(3)) considers injection at the location of Well No. 6 at 1,200 gpm. The maximum predicted flowing bottom-hole grid block pressure in at the location of Well No. 6 on December 31, 2050 is 4,750 psi. The maximum predicted flowing bottom-hole well bore pressure on December 31, 2050 is 4,870 psi. The pre-injection native static reservoir pressure at the location of Well No. 6 is 4,403 psi. Therefore, the pressure buildup in the grid block cell is no more than 347 psi and the pressure buildup predicted at the well is no more than 467 psi.

The simulated Injection Interval pressure buildup for the first scenario (Chemours TMS Prs) at the end-of-operation (December 31, 2050) is shown in Figure 3-21. The simulated Injection Interval pressure buildup for the second scenario (Chemours TMS Prs(2)) at the end-of-operation (December 31, 2050) is shown in Figure 3-22. The simulated Injection Interval pressure buildup for the third scenario (Chemours TMS Prs(3)) at the end-of-operation (December 31, 2050) is shown in Figure 3-23. Each figure shows pressure isobars, representing the pressure buildup (the difference between the injection pressure at the end-of-operation and initial reservoir pressure) within the Injection Interval, radiating outward from the injection wells.

Of the three (3) scenarios, the first scenario (Chemours TMS Prs) results in the largest areal extent of reservoir pressure buildup (relative to the second and third scenario) and the second scenario has the largest reservoir pressure buildup at the injection well location (Well No. 5). The COI includes the area within the pressure isopleth representing a 244 psi increase in reservoir pressure. The predicted increase at a radius of 2.0-mile radius Area of Review is no more than 135 psi (see Figure 3-21). However, at the end of the model period (year-end 2050) the COI for any of the three scenarios extends no farther than 500 feet from the wellbore.

3.5.3 Determination of Cone of Influence

The COI for Washita-Fredericksburg Injection Interval is defined as the area within which Injection Zone pressure increase is greater than **254 psi**. The COI for Tuscaloosa Massive Sand is defined as the area within which Injection Zone pressure increase is greater than **244 psi**.

The COI calculation for this petition application uses a conservative modeling approach where all four existing injection wells and Well No. 6 (and Well No. 7) are completed in either the Washita-Fredericksburg Injection Interval or the Tuscaloosa Massive Sand and modeled using the worst-case scenario of 2,200 gpm through year-end 2050. Actual injection volumes and average injection rates were used through year-end 2015 for the Washita-Fredericksburg reservoir pressure model, and maximum injection rates were used for the years 2016 through year-end 2050 to provide a conservative (large) estimate of reservoir pressure buildup. Maximum injection rates were used in the Tuscaloosa Massive Sand for the years 2020 through year-end 2050 to provide a conservative (large) estimate of reservoir pressure buildup.

A totals of six reservoir pressure models were considered (three for the Washita-Fredericksburg Injection Interval and three for the Tuscaloosa Massive Sand. Of all six scenarios, the first scenario (Chemours WF Prs) results in the largest areal extent of the area enclosed within the Cone of Endangering Influence (COI). The COI includes the area within the pressure isopleth representing a **254 psi** increase in reservoir pressure. The COI extends approximately 23,100 feet from the Chemours injection wells. At the end of the model period (year-end 2050), the Cone of Influence extends approximately 12,500 feet beyond the 2.0-mile radius Area of Review.

3.6 SWIFT Model Results – Lateral Migration Modeling

The lateral SWIFT model was used to simulate lateral waste plume migration during the 10,000-year post operational period. Lateral migration modeling was performed for the Washita-Fredericksburg Injection Interval. A Table of Contents is included at the beginning of Appendix 3-8 which lists the various SWIFT model runs as well as showing the input and output file names for each model run.

The lateral transport model consists of three components: 1) fluid displacement due to injection; 2) buoyant fluid movement and 3) dispersive and diffusive contaminant transport for a conservative species (no adsorption, hydrolysis or other fate mechanism). In this fashion, the outline of the isopleth for the 9-order of magnitude reduction in initial concentration for a 10,000-year post-operational period is obtained. This is the appropriate concentration reduction factor in that it will render the initial waste constituent concentrations non-hazardous.

3.6.1 Low Density Injectate SWIFT Model (Chemours WF-LD Lat Plume)

The up-dip lateral waste transport model (Chemours WF-LD Lat) models waste plume movement in the Washita-Fredericksburg Injection Interval and incorporates variable structure, variable thickness and assumes a waste specific gravity of a light density fluid. The injected waste density was modeled as 62.43 lb/ft^3 at 243.6 °F, and waste viscosity was 0.231 cP at 243.6 °F. The rate of ground water movement in the Injection Interval was assumed to be 0.0 ft/year. Historical injection from October 1979 until December 31, 2015 was modeled as injected into Well Nos. 2, 3, 4 and 5. Future injection from January 1, 2016 until December 31, 2050 was modeled at an injection rate of 550 gpm each (2,200 gpm cumulative) into Well Nos 2, 3, 4 and 5. The lateral model boundaries are left open (Carter-Tracy boundary conditions). The model results for Chemours WF-LD Lat are presented in the output file in Appendix 3-8. The Chemours WF-LD Lat SWIFT model grid, end-of-operations and 10,000-year waste plumes are depicted on Figure 3-10. The low-density waste plume orientations and dimensions at the end of the operational period and after 10,000 years are depicted on Plates 3-1 and 3-2. The base map for Plate 3-1 is the structure map on top of the Washita-Fredericksburg Injection Interval. Plate 3-2 shows the buoyant plume outlines on the Washita-Fredericksburg isopach map.

The shape of both the end-of-operations waste plume and the 10,000-year waste plume are affected by the structural top and the stratigraphic thinning to the southeast. The end-of-operation waste plume is roughly circular in shape. The end-of-operations waste plume (9-order magnitude reduction in concentration) is approximately 21,500 feet in diameter. The 10,000-year low-density waste plume extends 32,000 feet up-gradient and 18,000 feet down-gradient (measured from the Well No. 4 well location). The 10,000-year waste low-density plume (9-order magnitude reduction in concentration) extends about 14,000 feet to the southwest and 16,000 feet northeast from Well No. 4.

A discussion of the wells (non-freshwater artificial penetrations) that are intersected by the plumes during the modeled operational (end time of 12/31/2050) and post-operational (10,000-year) time periods is included in the Area of Review discussion. These wells meet non-endangerment standards (due to pressure increases) and/or no-migration standards (due to waste movement), as discussed in the Area of Review Section.

3.6.2 Low Density Injectate SWIFT Model (Chemours TMS-LD Lat)

The up-dip lateral waste transport model (Chemours TMS-LD Lat) models waste plume migration in the Tuscaloosa Massive Sand and incorporates variable structure, variable thickness and assumes a waste specific gravity of a light density fluid. The injected waste density was modeled as 62.43 lb/ft^3 at 236.4 °F, and waste viscosity was 0.240 cP at 236.4 °F. The rate of ground water movement in the Injection Interval was assumed to be 0.0 ft/year. Future injection from January 1, 2016 until December 31, 2050 was modeled at an injection rate of 550 gpm each (2,200 gpm cumulative) into Well Nos 2, 3, 4 and 5. The lateral model boundaries are left open (Carter-Tracy boundary conditions). The model results for Chemours TMS-LD Lat are presented in the output file in Appendix 3-8. The Chemours TMS-LD Lat SWIFT model grid, end-of-operations and 10,000-year waste plumes are depicted on Figure 3-11. The low-density waste plume orientations and dimensions at the end of the operational period and after 10,000 years are depicted on Plates 3-3 and 3-4. The base map for Plate 3-3 is the structure map on top of the Tuscaloosa Massive Sand. Plate 3-4 shows the buoyant plume outlines on the Tuscaloosa Massive Sand isopach map.

The shape of both the end-of-operations waste plume and the 10,000-year waste plume are affected by the structural top and the stratigraphic thinning to the southeast. The end-of-operation low-density waste plume is roughly circular in shape. The low-density end-of-operations waste plume (9-order magnitude reduction in concentration) is approximately 18,250 feet in diameter. The 10,000-year waste plume extends 34,500 feet up-gradient and 13,500 feet down-gradient (measured from the Well No. 4 well location). The 10,000-year waste plume (9-order magnitude reduction in concentration) extends about 13,500 feet to the southwest and 6,000 feet northeast from Well No. 4.

A discussion of the wells (non-freshwater artificial penetrations) that are intersected by the plumes during the modeled operational (end time of 12/31/2050) and post-operational (10,000-year) time periods is included in the Area of Review discussion. These wells meet non-endangerment standards (due to pressure increases) and/or no-migration standards (due to waste movement), as discussed in the Area of Review Section.

3.6.3 High Density Injectate SWIFT Model (Chemours WF-HD Lat)

The down-dip lateral waste transport model (Chemours WF-HD Lat) models waste plume movement in the Washita-Fredericksburg Injection Interval and incorporates variable structure, variable thickness and assumes a waste specific gravity of a light density fluid. The injected waste density was modeled as 81.16 lb/ft^3 at 243.6 °F, and waste viscosity was 0.608 cP at 243.6 °F. The rate of ground water movement in the Injection Interval was assumed to be 0.0 ft/year. Historical injection from October 1979 until December 31, 2015 was modeled as injected into Well Nos. 2, 3, 4 and 5. Future injection from January 1, 2016 until December 31, 2050 was modeled at an injection rate of 550 gpm each (2,200 gpm cumulative) into Well Nos 2, 3, 4 and 5. The lateral model boundaries are left open (Carter-Tracy boundary conditions). The model results for Chemours WF-HD Lat are presented in the output file in Appendix 3-8. In order to simulate plume movement in response to a background flow gradient of 0.5 ft/year, the 10,000-year waste plume center of mass was shifted down-dip by 5,000 feet (10,000 years x 0.5 ft/year).

The Chemours WF-HD Lat SWIFT model grid, end-of-operations and 10,000-year waste plumes are depicted on Figure 3-12. The waste plume orientations and dimensions at the end of the operational period and after 10,000 years are depicted on Plates 3-5 and 3-6. The base map for Plate 3-5 is the structure map on top of the Washita-Fredericksburg Injection Interval. Plate 3-6 shows the buoyant plume outlines on the Washita-Fredericksburg isopach map.

The shape of both the end-of-operations waste plume and the 10,000-year waste plume are affected by the structural top and the stratigraphic thinning to the southeast. The end-of-operation waste plume is roughly circular in shape. The end-of-operations waste plume (9-order magnitude reduction in concentration) is approximately 21,500 feet in diameter. The 10,000-year waste plume extends 96,000 feet down-gradient (measured from the Well No. 4 well location). The 10,000-year waste plume (9-order magnitude reduction in concentration) extends about 11,000 feet to the southwest and 10,500 feet northeast from Well No. 4.

A discussion of the wells (non-freshwater artificial penetrations) that are intersected by the plumes during the modeled operational (end time of 12/31/2050) and post-operational (10,000-year) time periods is included in the Area of Review discussion. These wells meet non-endangerment standards (due to pressure increases) and/or no-migration standards (due to waste movement), as discussed in the Area of Review Section.

3.6.4 High Density Injectate SWIFT Model (Chemours TMS-HD)

The down-dip lateral waste transport model (Chemours TMS-LD Lat) models waste plume migration in the Tuscaloosa Massive Sand and incorporates variable structure, variable thickness and assumes a waste specific gravity of a high density fluid. The injected waste density was modeled as 81.16 lb/ft^3 at 236.4 °F, and waste viscosity was 0.627 cP at 236.4 °F. The rate of ground water movement in the Injection Interval was assumed to be 0.0 ft/year. Future injection from January 1, 2016 until December 31, 2050 was modeled at an injection rate of 550 gpm each (2,200 gpm cumulative) into Well Nos 2, 3, 4 and 5. The lateral model boundaries are left open (Carter-Tracy boundary conditions). The model results for Chemours TMS-HD Lat are presented in the output file in Appendix 3-8. In order to simulate plume movement in response to a background flow gradient of 0.5 ft/year, the 10,000-year waste plume center of mass was shifted down-dip by 5,000 feet (10,000 years x 0.5 ft/year).

The Chemours TMS-HD Lat SWIFT model grid, end-of-operations and 10,000-year waste plumes are depicted on Figure 3-12A. The waste plume orientations and dimensions at the end of the operational period and after 10,000 years are depicted on Plates 3-7 and 3-8. The base map for Plate 3-7 is the structure map on top of the Tuscaloosa Massive Sand. Plate 3-8 shows the buoyant plume outlines on the Tuscaloosa Massive Sand isopach map.

The shape of both the end-of-operations waste plume and the 10,000-year waste plume are affected by the structural top and the stratigraphic thinning to the southeast. The end-of-operation waste plume is roughly circular in shape. The end-of-operations waste plume (9-order magnitude reduction in concentration) is approximately 18,500 feet in diameter. The 10,000-year waste plume extends 82,500 feet down-gradient (measured from the Well No. 4 well location). The 10,000-year waste plume (9-order magnitude reduction in concentration) is about 28,000 feet wide after 10,000 years of waste plume migration.

A discussion of the wells (non-freshwater artificial penetrations) that are intersected by the plumes during the modeled operational (end time of 12/31/2050) and post-operational (10,000-year) time periods is included in the Area of Review discussion. These wells meet non-endangerment standards (due to pressure increases) and/or no-migration standards (due to waste movement), as discussed in the Area of Review Section.

3.7 Vertical Advective and Diffusive Waste Transport Model

The determination of vertical transport of injected waste constituents included two components. The first component is advection, which arises from pressurization of the Injection Interval during the operational period. The second component is diffusion, which arises from the concentration gradient of injectate from the Injection Interval vertically upward into the overlying Injection Zone strata. The two components of transport are added together to obtain the total predicted vertical plume migration.

The vertical transport model, which includes both advection and diffusion, was designed to focus on the worst-case vertical movement of injection constituents over the total time frame (operational period and 10,000-year post-operational period). This was done by employing a one-dimensional model, whereby no dilution through lateral dispersion is allowed and invoking conservative constraints and input parameters. Also, the injectate constituent which was modeled, chromium, was modeled as a fully conservative species with no transport retardation through sorption, and no decay through hydrolysis or reaction.

In the advective component of vertical transport, the primary transport mechanism (pressure buildup within the Injection Interval during the operational period) is set at the maximum value from the beginning of operations (October 1979), through the end of the future operational period (December 31, 2050), and for an additional five years after the operational period (75.25 years total). The additional five years of advective movement was included in the calculation to account for the time required for the reservoir pressure to return to a static level. Although it is anticipated that reservoir pressure will decline rapidly at the end-of-operations, and that near static reservoir pressures will be reached in a matter of a few months, five years is included in the calculation to be conservative. The Injection Interval pressure buildup is determined from the SWIFT pressure buildup model (Chemours WF Prs(3)) and is calculated to occur at the end of the future operational period (December 31, 2050), just before Well No. 6 is shut in (Note that the pressure buildup in the grid block at Well No. 6 in the Chemours WF Prs(3) model run is the greatest pressure buildup for any of the Washita-Fredericksburg Injection Interval or Tuscaloosa Massive Sand reservoir pressure models). In reality, the pressure during the majority of the operational period is significantly less, since the historical injection rates are less than the future injection rates. The result is a conservatively higher value for the vertical pressure gradient. An additional advective component arises from the buoyancy of the injectate (light density case) due to the density contrast between the injectate and native formation brine. The advective component due to the density contrast is calculated for both the operational and 10,000-year post-operational periods. In this model, it is conservatively assumed that the density contrast remains at its maximum, without allowing any decrease in the density contrast through dispersion or diffusion.

In calculating the diffusive component of vertical transport, it is assumed that the source strength within the Injection Interval remains constant at its maximum value during the entire 10,000-year post operational period. In reality, the source strength within the Injection Interval decreases after injection ceases, since no additional injectate mass is added to the Injection Interval. The result is a conservatively greater transport distance, since the concentration gradient remains at the initial maximum value during the entire 10,000-year period.

3.7.1 Advective Transport Model and Results

The vertical advective transport of the injectate is made up of two components: 1) transport due to pressure buildup within the Injection Interval during operational period; and, 2) transport due to buoyancy of injectate arising from density contrast between injectate and native formation fluid (for light density case) over entire operational and 10,000-year post-operational periods.

To ensure the most conservative case, it is assumed that the Injection Interval pressure buildup reaches the maximum value at the beginning of the operational period on October 1979, and remains at this maximum value for a period of 5 years after injection has ceased (injection ceased on December 31, 2050), for a total pressure buildup period of 75.25 years at the maximum pressure. Additionally, it is assumed that the density contrast between the injectate and formation fluid remains at its maximum during the entire operational and 10,000-year post-operational period. In this way, the advective component of transport is over-estimated.

3.7.1.1 Vertical Advection During Operational Period

The advective component of transport in general can be found through Darcy's Law written in terms of the total head gradient and hydraulic conductivity:

$$q = -K \frac{\Delta h}{\Delta l}$$

where, q = Darcy velocity

$\frac{\Delta h}{\Delta l}$ = total head gradient

K = hydraulic conductivity

Vertical Head Gradient During Operational Period

The total head gradient was defined in terms of pressure buildup within the Injection Interval, elevation and buoyancy (due to a density contrast between injectate and native formation fluid):

$$\frac{\Delta h}{\Delta l} = \frac{\frac{\Delta p}{\rho g} + \Delta z + H_{buoy}}{L}$$

where,

L	=	distance (thickness in this case)
Δp	=	pressure change across distance L
ρg	=	fluid specific weight (density)
Δz	=	elevation change across L
H_{buoy}	=	buoyant head

The quantities in the equation were specified using the conditions at the Chemours facility to define the total vertical head gradient across the first containing shale sequence overlying the Injection Interval.

The distance, L, was defined as the thickness of 150 feet of shale between the top of the Injection Interval and the top of the Injection Zone. The total net shale thickness between the top of the Injection Interval and the top of the Injection Zone is well over 1,200 feet. The total net shale thickness above the top of the Tuscaloosa Massive Sand is well over 1,000 feet. Therefore, the gradient determined here is greater than would be determined for the net containing interval. This results in a conservative overestimate of the advective transport.

Because vertical gradient is being calculated, and the native reservoir fluid gradient within the Injection Interval is equivalent to the native reservoir fluid gradient the overlying shale layer (hydrostatically equilibrated fluid column), a natural fluid gradient does not exist, therefore Δz is zero (0) and is ignored in the calculation.

The pressure change was defined as the difference between the maximum pressure in the Injection Interval (which occurs at the end-of-operation), and the initial pressure within the

Injection Interval. The Washita-Fredericksburg SWIFT pressurization model (Chemours WF Prs(3)) output was used to determine the maximum Injection Interval pressure at the end-of-operation. The initial pressure within the Injection Interval was determined based on the initial (before operation) pressure measured in the Injection Interval at Well No. 6. The maximum Injection Interval pressure buildup, 970 psi (grid block pressure), occurs at the end of the operation period at Well No. 6, as shown in the SWIFT output file (Chemours WF Prs(3)).

The buoyant head (H_{buoy}) is defined as a function of the maximum possible density contrast between the injectate and formation fluid (assuming light density injectate), and the thickness of the total waste-swept pore volume. The Washita-Fredericksburg Injection Interval is considered in this demonstration, since it is the shallowest interval which currently utilized for injection. The waste swept pore thickness, D, of the Washita-Fredericksburg Injection Interval is 160 feet (approximate net sand thickness of the Washita-Fredericksburg at the location of Well No. 4 [see Section 3.3.1]). Density contrast was considered as part of the calculation of the injection pressure differential (native reservoir brine density and injection fluid density are components of the Washita-Fredericksburg SWIFT pressurization model (Chemours WF Prs(3)). Although the density differential portion of the buoyant head determination is incorporated in the Δp_{inj} term, it is considered separately to add additional conservatism to the calculation.

With these definitions of terms, the equation now becomes:

$$\frac{\Delta h}{\Delta l} = \frac{\dfrac{\Delta p_{inj}}{\rho g} + \dfrac{\Delta \rho g D}{(\rho g)_{inj}}}{L}$$

Where:

Δp_{inj}	=	injection pressure differential = 970 psi
ρg	=	formation fluid density at reservoir temperature = 68.49 lb/ft^3 (at reservoir temperature, 243.6 ºF)
$(\rho g)_{inj}$	=	injectate density at reservoir temperature = 62.43 lb/ft^3 (least dense waste density at 243.6 ºF)
$\Delta \rho g$	=	maximum possible density contrast between injectate and formation fluid = 6.06 lb/ft^3
D	=	thickness of total waste-swept pore volume of Injection Interval = 160 feet
L	=	shale thickness = 150 feet (first 150 feet of shale above the injection reservoir)

The vertical head gradient across the thickness of the first shale sequence overlying the Washita-Fredericksburg Injection Interval for the operational period was then determined using the parameters defined above:

$$\frac{\Delta h}{\Delta l} = \frac{\frac{(970\ lb/in^2)(144\ in^2/ft^2)}{68.49\ lb/ft^3} + \frac{(6.06\ lb/ft^3)(160\ ft)}{62.43\ lb/ft^3}}{150\text{ ft}} = 13.7\ ft/ft$$

Vertical Hydraulic Conductivity

The total head gradient calculated above, along with the vertical hydraulic conductivity for the containing shale sequence overlying the Injection Interval were used to determine the vertical Darcy velocity through the first shale sequence overlying the Washita-Fredericksburg Injection Interval (or Tuscaloosa Massive Sand)(using a shale permeability of 6.2 x 10^{-5} mD). A discussion of shale permeability is included in Section 7.3.2. The hydraulic conductivity was determined to be 7.36 x 10^{-7} ft/day using an injectate viscosity of 0.231 cP, and an injectate specific weight of 62.43 lb/ft^3 (at reservoir conditions):

With the vertical head gradient defined from the top of the Injection Interval through the first overlying shale, and the vertical hydraulic conductivity of the shale overlying the Injection Interval, the Darcy flow velocity can be calculated from the Darcy equation as written above:

$$q = 7.36 \times 10^{-7}\text{ ft/day } (13.7\text{ ft/ft}) = 1.01 \times 10^{-5}\text{ft/day}$$

Using the vertical Darcy velocity determined above, and the shale porosity of 0.20, the vertical average linear velocity was determined by dividing the Darcy velocity by the porosity:

$$v = (1.35 \times 10^{-5}\text{ ft/day})/0.20 = 5.04 \times 10^{-5}\text{ ft/day}$$

The vertical advective transport was then calculated by applying the average linear velocity for the entire 70.25-year operational and 5 post-operational period (75.25 years total) in which Injection Interval pressure was elevated due to injection operations. This is an over-estimation because the maximum pressure buildup (and therefore velocity) is used for the entire combined period. The pressure gradient builds up to the maximum value over time, and then falls off sharply when injection is ceased.

Using the approach outlined above, the advective transport distance of waste into the first containing shale sequence overlying the Washita-Fredericksburg Injection Interval (or Tuscaloosa Massive Sand) is found by:

$$z_{advection1} = v \cdot t$$

where, v = vertical average linear velocity = 5.04×10^{-5} ft/day
t = advective transport period = 75.25 yr x 365.25 day/yr
$z_{advection1}$ = 5.04×10^{-5} ft/day x 75.25 yr x 365.25 day/yr =
1.4 feet of advective transport during modeled period

3.7.1.2 Vertical Advection During 10,000-Year Post-Operational Period

As discussed above, an additional component of advective transport may also arise due to the continued density contrast between the injectate and native brine, which remains even after the operational period has ended.

Vertical Head Gradient During 10,000 Post-Operational Period

If it is assumed that the injectate is not diluted due to dispersion or other mixing, the advective transport due to this density contrast arising from the buoyant component of the head gradient as defined above can be calculated over the 10,000-year post-operational period.

$$\frac{\Delta h}{\Delta l} = \frac{\frac{(6.06\ lb/ft^3)(160\ ft)}{62.43\ lb/ft^3}}{150\text{ ft}} = 0.1\, ft/ft$$

The resulting Darcy flow velocity from the buoyant head component can be calculated using the vertical hydraulic conductivity as calculated above in the Darcy equation:

$$q = 7.36 \times 10^{-7} \text{ ft/day } (0.1 \text{ ft/ft}) = 7.36 \times 10^{-8} \text{ ft/day}$$

Using the vertical Darcy velocity determined above, and the shale porosity of 0.20, the vertical average linear velocity was determined by dividing the Darcy velocity by the porosity:

$$v = (7.36 \times 10^{-8} \text{ ft/day})/0.20 = 3.68 \times 10^{-7} \text{ ft/day}$$

The vertical advective transport due to the buoyant head gradient during the 10,000-year post-operational period is then calculated by applying the average linear velocity for the entire 10,000-year period.

$$z_{advection2} = v \cdot t$$

where, v = vertical average linear velocity = 3.68×10^{-7} ft/day
t = advective transport period = 10,000 yr x 365.25 day/yr

$z_{advection2}$ = 3.68×10^{-7} ft/day x 10,000 yr x 365.25 day/yr = **1.3 feet** advective transport during 10,000-year post-operational period due to buoyancy of injectate

The total advective transport of injectate during the operational and 10,000-year post-operational periods is the sum of the two advective transport distances:

$$Z_{(advection)Total} = z_{advection1} + z_{advection2} = 1.4 \text{ feet} + 1.3 \text{ feet} = 2.7 \text{ feet}$$

The total advective distance, 2.7 feet, is much less than the net shale interval thickness between to the top of the Injection Interval and the top of the Injection Zone.

The advective transport calculated here is over-estimated due to several reasons. First, the Injection Interval pressure buildup was assumed to reach its maximum value at the beginning of injection operations on October 1979, and continue at this maximum value through the post-operational fall-off period, for a total Injection Interval pressure buildup period of 75.25 years at the maximum value (the pressure builds up to its maximum value, and then falls of rapidly during the post-operational fall-off period). Secondly, the shale sequence overlying the Washita-Fredericksburg Injection Interval (and Tuscaloosa Massive Sand) was used to define the hydraulic gradient over which vertical advection occurred. The thickness of this shale sequence, 150 feet, is only 15 percent of cumulative net shale thickness in the Injection Zone overlying the Washita-Fredericksburg Injection Interval (or Tuscaloosa Massive Sand). Finally, it is assumed that the density contrast between the injectate and native formation fluid remains at its maximum during the entire operational and 10,000-year post-operational periods. By invoking these model considerations, the model results were conservatively overestimated.

3.7.2 Diffusive Transport Model and Results

The second component of vertical transport is diffusion which arises from the concentration gradient of injectate from the Injection Interval vertically upward into the overlying Injection Zone strata. The governing equation for diffusive transport through a porous medium in one-dimension is given by Fick's second law (Freeze and Cherry, 1979; Daniel and Shackelford, 1988; Carslaw and Jaeger, 1959):

$$\frac{\partial c}{\partial t} = D * \frac{\partial^2 c}{\partial z^2}$$

The vertical extent of molecular diffusion through a porous media in one dimension at any time, t, is calculated from the following solution (Freeze and Cherry, 1979) to Fick's second law:

$$\frac{C(z,t)}{C_0} = \text{erfc}\left[\frac{z}{\sqrt{4D^* t}}\right]$$

where:

$C(z,t)$	=	concentration at location z and time t ;
C_o	=	initial concentration at t = 0, z = 0;
$C(z,t)/C_o$	=	inverse of concentration reduction factor = 1×10^{-9} for the Chemours facility's waste;
z	=	diffusive plume extent = quantity to be calculated;
t	=	time = 10,000 years;
D^*	=	effective molecular diffusivity = $D_o \times G$ = 0.219 ft^2/yr using:
D_o	=	molecular diffusivity of chromium in water = 1.61×10^{-8} m^2/sec = 5.47 ft^2/yr;
G	=	geometric correction factor = ϕ^n where n is approximately 2 for shales
ϕ	=	porosity = 0.20
erfc	=	complimentary error function = 1- erf (error function)

It should be noted that an inherent boundary condition required for the above solution is that the source strength remains constant ($C(z,t)=C_o$) at the top of the Injection Interval for all times, namely, during the entire 10,000-year post-operational period. This is conservative since the source strength of injectate will begin to decay after the end of the operational period, and no additional mass will be introduced to the Injection Interval to keep the source strength constant at its maximum value.

$$1x10^{-9} = 1 - erf\left[\frac{z}{\sqrt{(4)(0.219)(10{,}000)}}\right]$$

$$0.999999999 = erf\left[\frac{z}{93.6}\right]$$

from error function tables;

$$4.32 = \frac{z}{93.6}$$

$$z_{\text{diffusion}} = 404 \text{ feet}$$

The total vertical transport for the injected waste at the Chemours facility, as determined using the one-dimensional analytical models for both advection, due to injection pressure buildup and density contrast, and diffusion, due to concentration gradient between the Injection Interval and overlying Injection Zone is the sum of the two:

$$Z_{total} = z_{(advection)Total} + z_{\ diffusion}$$

$$Z_{total} = 2.7 \text{ feet} + 404 \text{ feet}$$

$$Z_{total} = 406.7 \text{ feet}$$

Thus, the calculated total vertical transport distance is **406.7 feet**. The top of the Washita-Fredericksburg Injection Interval is separated from the top of the Injection Zone by about 1,750 feet of alternating sand and shale sequences, with more than 1,000 feet of total net shale present within the sequence. The top of the Tuscaloosa Massive Sand is separated from the top of the Injection Zone by about 1,250 feet of alternating sand and shale sequences, with more than 1,000 feet of total net shale present within the sequence.

Subtracting 406.7 feet from 9,752 feet (approximate top of Washita-Fredericksburg Injection Interval), places the top of vertical migration in 10,000 years at approximately 9,345, which is well below the top of the permitted Injection Zone which is present at about 8,000 feet.

Subtracting 406.7 feet from 9,282 feet (approximate top of the Tuscaloosa Massive Sand), places the top of vertical migration in 10,000 years at approximately 8,875 feet, which is also well below the top of the permitted Injection Zone which is present at about 8,000 feet. Therefore, the standard for no-migration is met for the vertical model simulation.

3.8 Molecular Diffusion Through Mud Filled Boreholes

The modeling results discussed in Section 3.7 above address the issue of vertical waste movement by advection-diffusion through a porous medium. This section assesses the extent of vertical diffusion over 10,000 years through a mud filled borehole that could penetrate the Injection Zone and intersect the location of the 10,000-year plume.

The calculation is conservative because it assumes that full strength waste would be at the location of a mud filled borehole for 10,000 years. Also, the calculation employs a tortuosity of 0.5 and porosity of 0.9 for the drilling mud. This provides the maximum calculated vertical diffusion distance for the given molecular diffusivity.

The vertical extent of molecular diffusion through a mud filled borehole which penetrates the waste plume present in the Washita-Fredericksburg Injection Interval was calculated from the following solution (Freeze and Cherry, 1979) to Fick's second law:

$$\frac{C(z,t)}{C_0} = erfc\left[\frac{z}{\sqrt{4D^{*}t}}\right]$$

where:

$C(z,t)$	=	concentration at location z and time t ;
C_o	=	initial concentration at t = 0, z = 0;
$C(z,t)/C_o$	=	1×10^{-9} for the Chemours facility's waste
$C(z,t)/C_o$	=	1×10^{-8} for the Chemours facility's waste (Tuscaloosa Massive Sand)
z	=	diffusive extent = quantity to be calculated;
t	=	time = 10,000 years;
D_o	=	molecular diffusivity of chromium in water = 1.61×10^{-8} m^2/sec = 5.47 ft^2/yr;
G	=	geometric correction factor = 0.5 for tortuosity x 0.9 porosity (drilling mud)
D*	=	D_o x G = 2.462 ft^2/yr

As demonstrated in the above equation, the vertical diffusive distance is a function of the concentration reduction factor and the molecular diffusivity of the compound in water. As reported previously, chromium had the highest molecular diffusivity in water for the chemical species of interest to this demonstration. The concentration reduction factor necessary to reach the health based limit given the petitioned concentration for lead is 1.00 x 10^{-8}. Both the molecular diffusivity for chromium and the concentration reduction factor for lead are the most conservative values for the waste constituents considered in this demonstration (Table 3-8 includes actual Vertical Diffusion Distance Through a Mud-Filled Borehole for each waste constituent for the maximum request waste concentration). The diffusive contaminant transport through a mud-filled borehole which penetrates the waste plume in the Washita-Fredericksburg Injection Interval was calculated as follows:

$$1.00x10^{-9} = 1 - erf\left[\frac{z}{\sqrt{(4)(2.462)(10{,}000)}}\right]$$

$$0.999999999 = erf\left[\frac{z}{313.8}\right]$$

from error function tables;

$$4.32 = \frac{z}{313.8}$$

$$z_{\text{diffusion}} = 1{,}356 \text{ feet}$$

Subtracting 1,356 feet from 9,752 feet (approximate top of Washita-Fredericksburg Injection Interval), places the top of vertical migration in 10,000 years at approximately 8,396, which is well the top of the permitted Injection Zone which is present at about 8,000 feet. Therefore, the standard for no-migration from the Washita-Fredericksburg Injection Interval is met for the vertical model simulation with respect to a mud-filled borehole.

Although the concentration reduction factors employed in all other plume delineation and vertical migration calculations is 1.00 x 10^{-9}, the actual concentration reduction factor of 1.00 x 10^{-8} is used for the Tuscaloosa Massive Sand. The diffusive contaminant transport through a mud-filled borehole which penetrates a waste plume present in the Tuscaloosa Massive Sand was calculated as follows:

$$1.00x10^{-8} = 1 - erf\left[\frac{z}{\sqrt{(4)(2.462)(10{,}000)}}\right]$$

$$0.99999999 = erf\left[\frac{z}{313.8}\right]$$

from error function tables;

$$4.052 = \frac{z}{313.8}$$

$$z_{\text{diffusion}} = 1{,}272 \text{ feet}$$

Subtracting 1,272 feet from 9,282 feet (approximate top of the Tuscaloosa Massive Sand), places the top of vertical migration in 10,000 years at approximately 8,010 feet, which is 10 feet below the top of the permitted Injection Zone which is present at about 8,000 feet. Therefore, the standard for no-migration from the Tuscaloosa Massive Sand would be met for the vertical model simulation with respect to a mud-filled borehole.

3.9 Reservoir Modeling Conclusions

This modeling effort provides a demonstration of "no-migration" in accordance with applicable regulations. This has been accomplished by demonstrating that the Chemours facility's injected waste will not migrate out of the Injection Zone and will be contained both vertically and laterally within the Injection Zone for a period of at least 10,000 years.

The modeling accounts for: (1) Injection Interval pressurization during the operational period; (2) end-of-operations light density injectate lateral waste transport; (3) post-operation light density injectate 10,000-year lateral waste transport; (4) end-of-operations heavy density injectate lateral waste transport; (5) post-operation heavy density injectate 10,000-year lateral waste transport; and (6) vertical waste transport. Conservative numerical and analytical models have been constructed and used to determine the maximum pressure buildup, and lateral and vertical waste transport distances. The modeling results demonstrate that no harm or impairment to the environment will occur from continued injection operations at the Chemours facility, through either endangerment (Injection Interval pressurization), lateral waste transport (up-dip or down-dip) or vertical waste transport.

For the Washita-Fredericksburg Injection Interval, lateral (low density) plume migration is depicted on Plates 3-1 and 3-2. The low density injectate model results (Chemours WF-LD Lat) indicate that, for a 9-order magnitude reduction in the initial concentration, the end-of-operations (12/31/2050) is approximately 21,500 feet in diameter. In 10,000 years, the light density waste plume extends 32,000 feet up-gradient and 18,000 feet down-gradient (measured from the Well No. 4 well location). The 10,000-year waste plume (9-order magnitude reduction in concentration) extends about 14,000 feet to the southwest and 16,000 feet northeast from Well No. 4

For the Tuscaloosa Massive Sand, lateral (low density) plume migration is depicted on Plates 3-3 and 3-4. The low density injectate model results (Chemours TMS-LD Lat) indicate that, for a 9-order magnitude reduction in the initial concentration, the end-of-operations (12/31/2050) is approximately 18,250 feet in diameter. In 10,000 years, the light density waste plume extends 34,500 feet up-gradient and 13,500 feet down-gradient (measured from the Well No. 4 well location). The 10,000-year waste plume (9-order magnitude reduction in concentration) extends about 13,500 feet to the southwest and 6,000 feet northeast from Well No. 4.

For the Washita-Fredericksburg Injection Interval, lateral (high density) plume migration is depicted on Plates 3-5 and 3-6. The high density injectate model results (Chemours WF-HD Lat) indicate that, for a 9-order magnitude reduction in the initial concentration, the end-of-operations (12/31/2050) is approximately 21,500 feet in diameter. In 10,000 years, the high density waste plume extends 96,000 feet down-gradient (measured from the Well No. 4 well location). The 10,000-year waste plume (9-order magnitude reduction in concentration) extends about 11,000 feet to the southwest and 10,500 feet northeast from Well No. 4.

For the Tuscaloosa Massive Sand, lateral (high density) plume migration is depicted on Plates 3-7 and 3-8. The high density injectate model results (Chemours TMS-HD Lat) indicate that, for a 9-order magnitude reduction in the initial concentration, the end-of-operations (12/31/2050) is approximately 18,500 feet in diameter. In 10,000 years, the waste plume extends 82,500 feet down-gradient (measured from the Well No. 4 well location). The 10,000-year waste plume (9-order magnitude reduction in concentration) is about 28,000 feet wide after 10,000 years of waste plume migration.

Washita-Fredericksburg Injection Interval pressure buildup isopleths are depicted on Figures 3-17, 3-18 and 3-19. The calculated COI is defined as that area around the Chemours injection well(s) within which the modeled reservoir pressure increase due to injection operations exceeds **254 psi**. For the SWIFT pressure model run Chemours WF Prs, the largest COI is observed (largest areal extent of the COI for all of the Washita-Fredericksburg reservoir pressure models or for the Tuscaloosa Massive Sand reservoir pressure models). For Chemours WF Prs, the maximum predicted flowing bottom-hole grid block pressure at the location of Well No. 5 on December 31, 2050 is 5,394 psi. The maximum predicted flowing bottom-hole well bore pressure on December 31, 2050 is 5,530 psi. The pre-injection native static reservoir pressure at the location of Well No. 5 is 4,563 psi. Therefore, the pressure buildup in the grid block cell is no more than 831 psi and the pressure buildup predicted at the well is no more than 967 psi.

The predicted increase at a radius of 2.0-mile radius Area of Review is approximately 360 psi (northeast and southeast of the wells). The COI extends approximately 23,100 feet from the Chemours injection wells. At the end of the model period (year-end 2050), the Cone of Influence extends approximately 12,500 feet beyond the 2.0-mile radius Area of Review.

As indicated in the previous paragraph, the largest COI is observed in the Washita-Fredericksburg reservoir pressure models. Of the three (3) reservoir pressure buildup scenarios for the Tuscaloosa Massive Sand, Chemours TMS Prs results in the largest areal extent of reservoir pressure buildup. The COI includes the area within the pressure isopleth representing a **244 psi** increase in reservoir pressure. The predicted increase at a radius of 2.0-mile radius Area of Review is no more than 135 psi (see Figure 3-21). However, at the end of the model period (year-end 2050) the COI extends no farther than 500 feet from the wellbore.

A conservative analytical model was used to determine the vertical advective transport resulting from the pressure buildup during the historical and projected operational periods. The results indicate that the vertical advective transport during the operational period would be 2.7 feet above the Washita-Fredericksburg Injection Interval. In addition, 404 feet of vertical migration was calculated by the 10,000-year molecular diffusion analytical model for chromium, for a total modeled predicted vertical migration in 10,000 years of 406.7 feet above the top of Washita-Fredericksburg Injection Interval. Subtracting 406.7 feet from 9,752 feet (approximate top of Washita-Fredericksburg Injection Interval), places the top of vertical migration in 10,000 years at approximately 9,345 feet, which is well below the top of the permitted Injection Zone which is present at about 8,000 feet. In addition, subtracting 406.7 feet from 9,282 feet (approximate top of the Tuscaloosa Massive Sand), places the top of vertical migration in 10,000 years at approximately 8,875 feet, which is also well below the top of the permitted Injection Zone which is present at about 8,000 feet. Therefore, the standard for no-migration is met for the vertical model simulation.

A conservative analytical model was used to determine the vertical transport resulting from the vertical migration through a mud-filled borehole which penetrates the waste plume present in the Washita-Fredericksburg Injection Interval. The results indicate that the vertical transport during the 10,000-year modeled timeframe would be 1,249 feet above the top of the Washita-Fredericksburg Injection Interval. The vertical migration was calculated by the 10,000-year molecular diffusion analytical model for chromium (worst case constituent). Subtracting 1,249 feet from 9,752 feet (approximate top of Washita-Fredericksburg Injection Interval), places the top of vertical migration in 10,000 years at approximately 8,503 feet, which is below the top of the permitted Injection Zone which is present at about 8,000 feet. Therefore, the standard for no-migration from the Washita-

Fredericksburg Injection Interval is met for the vertical model simulation with respect to a mud-filled borehole.

A conservative analytical model was also used to determine the vertical transport resulting from the vertical migration through a mud-filled borehole which penetrates a waste plume present in the Tuscaloosa Massive Sand. The results indicate that the vertical transport during the 10,000-year modeled timeframe would be 1,272 feet above the top of the Tuscaloosa Massive Sand. Subtracting 1,272 feet from 9,282 feet (approximate top of the Tuscaloosa Massive Sand), places the top of vertical migration in 10,000 years at approximately 8,010 feet, which is 10 feet below the top of the permitted Injection Zone which is present at about 8,000 feet. Therefore, the standard for no-migration from the Tuscaloosa Massive Sand is met for the vertical model simulation with respect to a mud-filled borehole.

In conclusion, the modeling results demonstrate no harm to the environment will occur from continued operations at the facility resulting from endangerment or migration of waste. All the artificial penetrations located within the boundaries of the waste plumes are plugged or constructed to prevent the migration of waste from the Injection Zone to satisfy the no-migration standard.

REFERENCES

Adams, E.E., and L.W. Gelhar, 1992, "Field Study of Dispersion in a Heterogeneous Aquifer: 2. Spatial Moments Analysis", Water Resources Research, v. 28, n. 12, p. 3293-3307.

Anderson, M.P., 1984, Movement of Contaminants in Groundwater: Groundwater Transport-Advection and Dispersion: Groundwater Contamination, National Academy Press, Washington, D.C., p. 33-45.

Barker, S. E., 1981, Determining the Area of Review for Hazardous Waste Disposal Wells: M.S. Thesis, University of Texas at Austin.

Baroid, 1931, Composition and method for dual function soil grouting excavating or boring fluid, Baroid Corporation, 1931.

Bethke, C. M., 1986, Inverse hydrologic analysis of the distribution and origin or Gulf Coast-type geopressured zones: Journal of Geophysical Research, 91, 6535-6545 (also 93, 9211).

Borst, R. L., 1983, Methods of Calculating Shale Permeability: Society of Petroleum Engineers, Paper No. 11768.

Bryant, W. D., W. R. Hoffman, and P. Trabant, 1975, Permeability of Unconsolidated and Consolidated Marine Sediments, Gulf of Mexico: Marine Geotechnology, v. 1, p. 1-14.

Carslaw, H. S., and J. C. Jaeger, 1959, Conduction of heat in Solids, Oxford University Press, Oxford England, 2nd Edition, 510 p.

Clark, J. E., M. R. Howard, and D. K. Sparks, 1987, Factors that can Cause Abandoned Wells to Leak as Verified by Case Histories from Class II injection, Texas Railroad Commission files: International Symposium on Subsurface Injection of Oilfield Brines, Underground Injection Practices Council, New Orleans, La., p. 166-223.

Clark, J. E., 1989, Groundwater Flow in Deep Saline Aquifers: Proceedings of the International Symposium on Class I and II Injection Well Technology, p. 151-176.

Clark, J. E., P. W. Papadeas, D. K. Sparks, and R. R. McGowen, 1991, Gulf Coast Borehole Closure Test Well, Orangefield, Texas, *in* Proceedings of the UIPC Underground Injection Practices Council, 1991 Winter and Summer Meetings: Underground Injection Practices Council, Oklahoma City, OK, p. 219-238.

Collins, R. E. 1986, Technical basis for area of review, an engineering study prepared for Chemical Manufacturers Association: CMA Reference Number 80 160 000 4. (0110859).

Constant, W. D. and D. A. Clark, 1989, Evaluation of Shale Permeability Associated With Deep-Well Hazardous Waste Injection Zone Confining Layers: Proceedings of the International Symposium on Class I and II Injection Well Technology, pp. 253-280.

CRC Handbook of Chemistry and Physics, 1979, Lide, D. R., editor, CRC Press, Boston, 58th Edition.

CRC Handbook of Chemistry and Physics, 1991, Lide, D. R., editor, CRC Press, Boston, 83th Edition.

Daniel, D. E., and C. D. Shackelford, 1988, Disposal Barriers that Release Contaminants Only by Molecular Diffusion, Nuclear and Chemical Waste Management, v. 8, p. 299-305.

Davis, S.N., D.J. Campbell, H.W. Bentley, and T.J. Flynn, 1985, Ground-Water Tracers, National Water Well Assn. and U.S. EPA Robert S. Kerr Environmental Research Laboratory, U.S. EPA and University of Arizona cooperative agreement CR-81003601-0, 200 p.

Davis, K. E., 1986, Factors Effecting the Area of Review for Hazardous Waste Disposal Wells: Proceedings of the International Symposium on Subsurface Injection of Liquid Wastes, New Orleans, National Water Well Association, Dublin, OH, p. 148-194.

Domenico, P. A., and F. W. Schwartz, 1990, Physical and Chemical Hydrogeology, J. Wiley and Sons, New York, 824 p.

Earlougher, R.C., 1977, Advances in Well Test Analysis: H.L. Doherty Series, Monograph Vol. 5, Society of Petroleum Engineers of AIME, 264 p.

Finley, N.C., and M. Reeves, 1982, SWIFT Self-Teaching Curriculum: NUREG/CR-1968, SAND81-0410, Sandia National Laboratories, Albuquerque, NM, 169 p.

Freeze, A.R., and J.A. Cherry, 1979, Groundwater: Prentice-Hall, Inc., Englewood Cliffs, N.J., 604 p.

Gelhar, L.W., 1986, Stochastic Subsurface Hydrology From Theory to Applications: Water Resources Research, v. 22, n. 9, p. 135s-145s.

Gelhar, L.W., A.L. Gutjahr, and R.L. Naff, 1979, Stochastic Analysis of Macrodispersion in a Stratified Aquifer: Water Resources Research, v. 15, p. 1383-1397.

Gelhar, L. W., C. Welty, and K. R. Rehfeldt, 1992, A Critical Review of Data on Field-Scale Dispersion in Aquifers, Water Resources Research, v. 28, p. 1955-1974.

Hewlett Packard, 1982, HP41C Petroleum Fluids Pac Manual, Hewlett Packard Corporation, Fort Collins, Colorado, 199 p.

HSI Geotrans, 2000, Swift for Windows Sandia Waste Isolation Flow and Transport Model, 45060 Manekin Pl, Suite 100 C, Sterling, VA 20166.

Intercomp Resources Development and Engineering, Inc., 1976, Development of Model for Calculating Disposal in Deep Saline Aquifers, Parts I and II: USGS/WRI 76-61, National Technical Information Service, Washington, D.C., 236 p.

Johnson, R. L., J. A. Cherry, and J. F. Pankow, 1989, Diffusive Contaminant Transport in Natural Clay: A field Example and Implications for Clay-Lined Waste Disposal Sites: Environmental Science and Technology, v. 23, p. 340-349.

Johnston, 0. C., and Green, C. J., 1979, Investigation of Artificial Penetrations in the Vicinity of Subsurface Disposal Wells: Texas Department of Water Resources.

Johnston, O. C. and B. K. Knape, 1986, Pressure Effects of the Static Mud Column in Abandoned Wells: Texas Water Commission, Limited Publication 86-06, Austin, Texas.

Lerman, A., 1979, Geochemical Processes Water and Sediment Environments: John Wiley and Sons, New York, N.Y., 481 p.

MacKay, D.M., P.V. Roberts, and J.A. Cherry, 1985, Transport of Organic Contaminants in Groundwater: Environmental Science and Technology, v. 19, n. 5, p. 384-392.

Magara, K., 1969, “Porosity-Permeability Relationship of Shale,” Society of Petroleum Engineers Paper No. 2430.

Neuman, S. P., 1993, Comment on A Critical Review of Data on Field-Scale Dispersion in Aquifers *by* L. W. Gelhar, C. Welty, and K. R. Rehfeldt, Water Resources Research, v. 29, p. 1863-1865.

Neuman, S. P., 1990, Universal Scaling of Hydraulic Conductivities and Dispersivities in Geologic Media, Water Resources Research, v. 26, p. 1749-1758.

Numbere, D., W. E. Brigham, and M. B. Standing, 1977, Correlations for Physical Properties of Petroleum Reservoir Brines, Petroleum Research Institute, Stanford University, November, 1977, p. 16.

Perry, R.H., 1984, Perry’s Chemical Engineers’ Handbook: Sixth Edition, McGraw-Hill Book Company, New York, N.Y.

Perry, R.H., 1979, Perry’s Chemical Engineers’ Handbook: McGraw-Hill Book Company, New York, N.Y.

Perry, R.H., 1997, Perry’s Chemical Engineers’ Handbook: Seventh Edition, McGraw-Hill Book Company, New York, N.Y.

Potter, R.W., and Brown, D. L., 1977, The Volumetric Properties of Aqueous Sodium Chloride Solutions from 0° to 500°C at Pressures up to 2000 Bars Based on a Regression of Available Data in the Literature: USGS Bull 1421-C.

Reeves, M.D., and D.S. Ward, 1986, SWIFT II Self-Teaching Curriculum: NUREG/CR-3925, Sandia National Laboratories, Albuquerque, NM, 105 p.

Reeves, M.D., D.S. Ward, N.D. Johns, and R.M. Cranwell, 1986, Theory and Implementation for SWIFT II, the Sandia Waste-Isolation Flow and Transport Model for Fractured Media, Release 4.84: NUREG/CR-3328 or SAND83-1159, Sandia National Laboratories, Albuquerque, NM, 189 p.

Reeves, M.D., D.S. Ward, P.A. Davis, and E.J. Bonano, 1987, SWIFT II Self-Teaching Curriculum: Illustrative Problems for the Sandia Waste-Isolation Flow and Transport Model for Fractured Media: NUREG/CR-3925 or SAND84-1586, Sandia National Laboratories, Albuquerque, NM, 94 p.

Sandia Technologies, LLC., 2000, Merisol 2000 HWDIR Exemption Petition Reissuance Request.

URM 1986, Technical Report.

Ward, D.S., M. Reeves, and L.E. Duda, 1984, "Verification and Field Comparison of the Sandia Waste-Isolation Flow and Transport Model (SWIFT)", NUREG/CR-3316 or SAND83-1154, Sandia National Laboratories, Albuquerque, NM.

Ward, D.S., M. Reeves, and L.E. Duda, 1984, Verification and Field Comparison of the Sandia Waste-Isolation Flow and Transport Model (SWIFT): NUREG/CR-3316 or SAND83-1154, Sandia National Laboratories, Albuquerque, NM.

Ward, D.S., D.R. Buss, J.W. Mercer, and S.S. Hughes, 1987, Evaluation of a Groundwater Corrective Action at the Chem-Dyne Hazardous Waste Site Using a Telescopic Mesh Refinement Modeling Approach: Water Resources Research, v. 23, n. 4, p. 603-617.

Warner, D. L., and T. Syed, 1986, Confining layer study-supplemental report: prepared for U.S. EPA Region V, Chicago, Illinois

Warner, D. L., 1988, Abandoned oil and gas industry wells and their environmental implications: prepared for the American Petroleum Institute.

Schlumberger, 1989, Cased Hole Log Interpretation Principles/Applications: Schlumberger Educational Services.

Xu, M. and Y Eckstein, 1995, Use of Weighted Least-Squares Method in Evaluation of the Relationship Between Dispersivity and Field Scale, Ground Water, v. 33, pp 905-90.

TABLES

TABLE 3-1

SWIFT MODEL PARAMETER VALUES

PARAMETER	SYMBOL, UNITS	SWIFT MNEMONIC	Washita-Fredericksburg	Tuscaloosa Massive Sand
NATIVE FORMATION FLUID				
Specific Gravity	γ (at reference temperature)		1.097	1.098
Density	ρ (T, P), lb/ft^3 (at reference temperature)	BWRN	68.49	68.55
Viscosity	μ (T, P), cP (at reference temperature)	VISRR	0.405	0.418
Compressibility	C (T, P), psi-1	CW	2.33E-06	2.31E-06
WASTE, Least Dense				
Specific Gravity	γ (at reference temperature)		1.00	1.00
Density	ρ (T, P), lb/ft^3 (at reference temperature)	BWRI	62.43	62.43
Viscosity	μ (T, P), cP (at reference temperature)	VISIR	0.231	0.240
WASTE, Average Density				
Specific Gravity	γ (at surface conditions)		1.20	1.20
Density	ρ (T, P), lb/ft^3 (at reference temperature)	BWRI	71.80	71.92
Viscosity	μ (T, P), cP (at reference temperature)	VISIR	0.482	0.497
WASTE, Most Dense				
Specific Gravity	γ (T/60, P) [γ 60/60, 1 atm; surface):		1.30	1.30
Density	ρ (T, P), lb/ft^3 (at reference temperature)	BWRI	81.16	81.16
Viscosity	μ (T, P), cP (at reference temperature)	VISIR	0.482	0.497
INJECTION INTERVAL				
Reference Depth	D, ft (subsea)	HINIT	9,889	9,512
Initial Pressure (at reference depth)	P, psia	PBWR, PINIT	4,581	4,406
Temperature (at reference depth)	T, ° F	TBWR, TRR, TIR, TD, TO	243.6	236.4
Hydraulic Conductivity				
Plume movement:	K (kρ/μ), feet/day	KX, KY	3.716	5.405
Pressurization:	K (kρ/μ), feet/day	KX, KY	1.561	3.243
Rock Density	ρ, lb/ft^3	BROCK	165	165
Porosity	ϕ	PHI	0.24	0.25
Rock Compressibility	C, psi^{-1}	CR	3.20E-06	3.20E-06
Dispersivity				
Longitudinal	α_L, feet	ALPHL	50	50
Transverse	α_T, feet	ALPHT	5	5
Molecular Diffusivity (effective)	D^{*}, ft^2/d ($D^{*} = D° \tau \phi$)	DMEFF	2.32E-03	2.46E-04
Molecular Diffusivity (free water)	D°, ft^2/d (free water)		1.49E-02	1.49E-02
Tortuosity				
Sand	τ		0.24	0.25
Shale	τ		0.07	0.07
Thickness	ft	DELZ(K), UTH	200	160
Well Index	ft^2/day	WI		
High Conductivity (Well No. 4)	ft^2/day	WI	958.7	1,743.1
Low Conductivity (Well No. 4)	ft^2/day	WI	402.7	1,045.8
Carter-Tracy Boundary				
Permeability-Thickness (high conductivity)	Kh	KH	383.6	895.8
Permeability-Thickness (low conductivity)	Kh	KH	161.2	537.5
Porosity-Thickness	ϕh	PHIH	25	41
Coefficient of thermal expansion	°F^{-1}	CTW	0.00	0.00
Fluid heat capacity	BTU/lb-°F	CPW	1	1
Rock heat capacity	BTU/lb-°F	CPR	1	1
Thermal conductivity	BTU/ft-d-°F	UKTX, UKTY, UKTZ	116	116

TABLE 3-2

WASHITA-FREDERICKSBURG RESERVOIR TEST RESULTS

Test Date	Well No.	Values Measured From Well Test k (mD)	h (ft)	µ (cP)	kh/µ (mD-ft/cP)
2015	3	422.7	160	0.42	161,029
2014	2	135.8	160	0.42	51,733
2013	5	64.0	160	0.42	24,381
2012	4	89.9	160	0.60	23,973
2011	3	330.0	160	0.42	125,714
2010	2	147.5	160	0.42	54,324
2009	5	86.0	160	0.42	56,190
2008	4	142.6	160	0.42	54,324
2007	3	236.3	160	0.42	90,019
2006	2	144.1	160	0.42	54,895
2005	5	223.3	160	0.42	85,074
2004	4	186.0	160	0.42	70,857
2003	3	158.2	160	0.42	60,247
2002	2	319.9	160	0.42	121,867
2001	5	189.8	160	0.42	72,305
2000	4	142.3	160	0.42	54,201
1999	3	170.0	160	0.60	45,333

TABLE 3-3

DELISLE PLANT BOTTOM-HOLE PRESSURE MEASUREMENTS IN MONITORING WELL NO. 1

Test Well No.	Date	Stabilized Pressure Reading @ Depth	Pressure Gradient (psi/ft)	Calculated Pressure at 9,850'* (psia)
Well No. 1	1974**	4,626 psia @ 9,893 ft.	0.4670	4,606
	Sep-92	4,580 psia @ 9,775 ft.	0.4685	4,615
	Dec-92	4,553 psia @ 9,760 ft.	0.4665	4,595
	Dec-92	4,516 psia @ 9,760 ft.	0.4627	4,558

* Assumes midpoint of Washita-Fredericksburg Sand at 9,850 ft
** Original measured formation pressure from DST values

TABLE 3-4

WASHITA-FREDERICKSBURG HISTORICAL BOTTOMHOLE PRESSURE SURVEY DATA

Date	Well No.	Stabilized Pressure Reading @ Depth	Static Pressure (psia)*
April 2015	3	4,719 psia @ 9,740 ft.	4,750
April 2014	2	4,699 psia @ 9,748 ft.	4,751
May 2013	5	4,619 psia @ 9,685 ft.	4,707
April 2012	4	5,070 psia @ 9,748 ft.	5,122
April 2011	3	4,679 psia @ 9,794 ft.	4,707
April 2010	2	4,620 psia @ 9,643 ft	4,675
April 2009	5	4,579 psia @ 9,685 ft.	4,679
April 2008	4	4,627 psia @ 9,746 ft.	4,680
March 2007	3	4,636 psia @ 9,730 ft.	4,696
April 2006	2	4,639 psia @ 9,748 ft.	4,690
March 2005	5	4,665 psia @ 9,730 ft.	4,726
March 2004	4	4,704 psia @ 9,750 ft.	4,755
February 2003	3	4,618 psia @ 9,800 ft	4,644
March 2002	2	4,661 psia @ 9,775 ft.	4,699
May 2001	5	4,613 psia @ 9,743 ft.	4,668
April 2000	4	4,623 psia @ 9,737 ft.	4,681
April 1999	3	4,618 psia @ 9,800 ft.	4,643
March 1998	2	4,610 psia @ 9,775 ft.	4,648
September 1997	5	4,564 psia @ 9,743 ft.	4,618
April 1996	5	4,547 psia @ 9,743 ft.	4,602
December 1996	4	4,572 psia @ 9,750 ft.	4,628
March 1995	5	4,430 psia @ 9,500 ft.	4,593
November 1995	2	4,599 psia @ 9,842 ft.	4,603
December 1995	4	4,569 psia @ 9,750 ft.	4,620
May 1994	5	4,473 psia @ 9,750 ft.	4,519
July 1994	4	4,617 psia @ 9,670 ft.	4,703
September 1993	4	4,581 psia @ 9,736 ft.	4,635
December 1992	4	4,249 psia @ 9,207 ft.	4,546
December 1992	2	4,277 psia @ 9,272 ft.	4,563
November 1989	4	4,523 psia @ 9,750 ft.	4,568
1974 **	1**	4,626 psia @ 9,893 ft.	** 4,606 **

* Corrected to the reference depth of 9,850 feet

** Data from Drill Stem Formation Pressure Test measurement taken during drilling of Well No. 1

TABLE 3-5

DELISLE PLANT BOTTOM-HOLE PRESSURE MEASUREMENTS IN PLANT WELL NOS. 2 AND 3

Test Well No.	Date	Stabilized Pressure Reading @ Depth	True Vertical Depth (TVD)	Pressure Gradient (psi/ft)	Calculated Pressure at 9,850 ft* (psia)
Well No. 2	Dec-92	4,277 psia @ 9,272 ft	9232 ft	0.4633	4,563
	Aug-93	4,586 psia @ 9,787 ft	9743 ft	0.4707	4,637
	Mar-95	4,315 psia @ 9,272 ft	9232 ft	0.4674	4,604
	Nov-95	4,599 psia @ 9,842 ft	9808 ft		4,603
	Mar-98	4,610 psia @ 9,775 ft	9741 ft		4,648
	Mar-02	4,661 psia @ 9,775 ft	9741 ft	0.5093	4,699
	Apr-06	4,639 psia @ 9,748 ft	9759 ft	0.5012	4,690
	Apr-10	4,620 psia @ 9,643 ft	9609 ft	0.5064	4,675
	Apr-14	4,699 psia @ 9,748 ft	9759 ft	0.5033	4,751
Well No. 3	Nov-89	4,501 psia @ 9,750 ft	9696 ft	0.4642	4,573
	Dec-92	4,251 psia @ 9,238 ft	9189 ft	0.4626	4,557
	Dec-92	4,238 psia @ 9,238 ft	9189 ft	0.4612	4,543
	Dec-92	4,252 psia @ 9,238 ft	9189 ft	0.4627	4,558
	Dec-92	4,215 psia @ 9,238 ft	9189 ft	0.4587	4,518
	Sep-93	4,544 psia @ 9,767 ft	9713 ft	0.4678	4,608
	Apr-99	4,618 psia @ 9,800 ft	9745 ft		4,643
	Feb-03	4,618 psia @ 9,800 ft	9745 ft	0.5088	4,644
	Mar-07	4,636 psia @ 9,730 ft	9675 ft	0.5044	4,696
	Apr-11	4,679 psia @ 9,794 ft	9739 ft	0.5013	4,707
	Apr-15	4,719 psia @ 9,740 ft	9686 ft	0.5250	4,750

* Assumes midpoint of Washita-Fredericksburg Sand at 9,850 ft

TABLE 3-6

DELISLE PLANT BOTTOM-HOLE PRESSURE MEASUREMENTS IN PLANT WELL NOS. 4 AND 5

Test Well No.	Date	Stabilized Pressure Reading @ Depth	Pressure Gradient (psi/ft)	Calculated Pressure at 9,850 ft* (psia)
Well No. 4	Nov-89	4,523 psia @ 9,750 ft	0.4639	4,568
	Dec-92	4,249 psia @ 9,207 ft	0.4615	4,546
	Sep-93	4,581 psia @ 9,736 ft	0.4705	4,635
	Jul-94	4,617 psia @ 9,670 ft	0.4775	4,703
	Mar-95	4,315 psia @ 9,207 ft	0.4687	4,616
	Dec-95	4,569 psia @ 9,750 ft	0.5100	4,620
	Dec-96	4,572 psia @ 9,750 ft	0.5600	4,628
	Apr-00	4,623 psia @ 9,737 ft	0.5133	4,681
	Mar-04	4,704 psia @ 9,750 ft	0.5106	4,755
	Apr-08	4,627 psia @ 9,746 ft	0.5098	4,680
	May-12	5,093 psia @ 9,750 ft	0.5090	5,122
Well No.5	May-94	4,473 psia @ 9,750 ft	0.4588	4,519
	Mar-95	4,430 psia @ 9,500 ft	0.4663	4,594
	Apr-96	4,547 psia @ 9,743 ft	0.5140	4,602
	Sep-97	4,564 psia @ 9,743 ft	0.5047	4,618
	May-01	4,613 psia @ 9,743 ft	0.5140	4,668
	Mar-05	4,665 psia @ 9,730 ft	0.5106	4,726
	Apr-09	4,579 psia @ 9,685 ft	0.5041	4,679
	May-13	4,619 psia @ 9,685 ft	0.5192	4,707

* Assumes midpoint of Washita-Fredericksburg Sand at 9,850 ft

* Assumes midpoint of Washita-Fredericksburg Sand at 9,850 ft
** Original measured formation pressure from DST values

TABLE 3-7

FORMATION TEMPERATURE VALUES AT DELISLE PLANT
(Graph of Temperature Data in Figure 7-5)

Depth (ft)	Temperature (°F)	Data Source
0	70	Estimate
3,808	130	Well No. 1 DST #1
4,505	140	Well No. 1 DST #4
9,410	190	Well No. 1 DST #5
9,865	215	Well No. 1 DST #6
9,535	184	Electrical Log, Well No. 1
10,025	181	Electrical Log, Well No. 2
10,057	179	Electrical Log, Well No. 3
10,045	180	Electrical Log, Well No. 4
9,352	183	Electrical Log, Well No. 5
10,050	183	Electrical Log Well No. 5

TABLE 3-8

VERTICAL DIFFUSION DISTANCES FOR PETITIONED CONSTITUENTS THROUGH FORMATION AND MUD-FILLED BOREHOLES

VERTICAL MIGRATION MOLECULAR DIFFUSION DISTANCES

Chemical Name	Waste Codes	Land Ban Health Based Limit (mg/L)	Detection Limit (1) (mg/L)	Injected Fluid Maximum Concentration (2) (mg/L)	Concentration Reduction Factor (C/Co)	Molecular Diffusivity In Water (3) (cm2/sec)	Molecular Diffusivity In Water (ft2/day)	Effective Diffusion Coefficient in Injection Interval (ft2/day)	Effective Diffusion Coefficient in Containment Interval (ft2/day)	Effective Diffusion Coefficient in Mud Filled Borehole (ft2/day)	Vertical Diffusion Distance Through Containment Interval (ft)	Vertical Diffusion Distance Through Mud-Filled Borehole (ft)
Arsenic	D004	5.0E-02		100,000	5.0E-07	1.54E-04	1.43E-02	2.23E-03	5.71E-04	6.43E-03	324	1088
Barium	D005	2.0E+00		100,000	2.0E-05	4.39E-05	4.08E-03	6.37E-04	1.63E-04	1.84E-03	147	493
Cadmium	D006	5.0E-03		100,000	5.0E-08	5.17E-05	4.81E-03	7.50E-04	1.92E-04	2.16E-03	209	702
Chromium	D007	1.0E-01		100,000	1.0E-06	1.61E-04	1.49E-02	2.33E-03	5.97E-04	6.72E-03	322	1081
Lead	D008		1.0E-03	100,000	1.0E-08	7.52E-05	6.99E-03	1.09E-03	2.80E-04	3.15E-03	254	851
Mercury	D009	2.0E-03		100,000	2.0E-08	6.20E-05	5.76E-03	8.99E-04	2.31E-04	2.59E-03	230	771
Selenium	D010	5.0E-02		100,000	5.0E-07	1.68E-04	1.56E-02	2.44E-03	6.26E-04	7.04E-03	339	1139
Silver	D011	5.0E-03		100,000	5.0E-08	7.52E-05	6.99E-03	1.09E-03	2.80E-04	3.15E-03	252	847

RfD - Reference Dose
RSD- Risk Specific Dose

MCL taken from Drinking Water Regulations and Health Advisories, 10/96.

RFD and RSD taken from IRIS, 3/97.
RfD (mg/L) = RfD (mg/kg/day) x 70 kg / 2L/day

(1) The Practical Quantitation Limit (PQL) was employed when available, using a ground water matrix.

(2) Maximum yearly averages. See Appendix K for measured concentrations in waste stream.

(3) Calculated using methodology given by Johnson and others (1989), p. 347.
Molecular diffusivity of inorganic constituents with multiple valences calculated using highest valence ion (Daniel & Shackleford, 1988)

TABLE 3-9

COMPILATION OF MONTHLY PLANT WELL INJECTION RATES (IN GALLONS PER MINUTE)

Month	Inj. Well 2 MSI-1001 (GPM)	Inj. Well 3 MSI-1001 (GPM)	Inj. Well 4 MSI-1001 (GPM)	Inj. Well 5 MSI-1001 (GPM)
Oct-79	25.3	25.3	0.0	0.0
Nov-79	88.4	88.4	0.0	0.0
Dec-79	62.5	73.9	0.0	0.0
Jan-80	174.0	0.0	0.0	0.0
Feb-80	101.8	0.0	0.0	0.0
Mar-80	166.8	0.0	0.0	0.0
Apr-80	10.1	181.3	0.0	0.0
May-80	44.4	185.3	0.0	0.0
Jun-80	104.6	64.6	0.0	0.0
Jul-80	95.7	50.8	0.0	0.0
Aug-80	86.3	102.9	0.0	0.0
Sep-80	117.2	47.0	0.0	0.0
Oct-80	100.1	36.5	0.0	0.0
Nov-80	156.3	0.0	0.0	0.0
Dec-80	182.7	0.0	0.0	0.0
Jan-81	187.1	0.0	0.0	0.0
Feb-81	171.0	21.8	0.0	0.0
Mar-81	149.5	0.0	0.0	0.0
Apr-81	123.5	86.3	0.0	0.0
May-81	100.8	129.1	0.0	0.0
Jun-81	28.8	172.6	0.0	0.0
Jul-81	4.4	171.9	0.0	0.0
Aug-81	76.3	111.1	0.0	0.0
Sep-81	152.3	38.6	0.0	0.0
Oct-81	115.3	58.0	0.0	0.0
Nov-81	13.3	167.7	0.0	0.0
Dec-81	68.5	10.5	0.0	0.0
Jan-82	126.5	22.9	0.0	0.0
Feb-82	23.2	152.3	0.0	0.0
Mar-82	75.1	130.5	0.0	0.0
Apr-82	25.3	126.3	0.0	0.0
May-82	40.7	160.9	0.0	0.0
Jun-82	16.1	102.5	0.0	0.0
Jul-82	130.1	58.5	0.0	0.0
Aug-82	172.9	45.6	0.0	0.0
Sep-82	141.8	32.0	0.0	0.0
Oct-82	62.7	158.1	0.0	0.0
Nov-82	212.2	40.2	0.0	0.0
Dec-82	95.4	7.0	0.0	0.0
Jan-83	119.1	32.3	142.7	0.0
Feb-83	147.1	44.9	37.2	0.0
Mar-83	154.4	0.0	88.7	0.0
Apr-83	102.0	0.0	122.8	0.0
May-83	138.9	69.5	0.0	0.0
Jun-83	140.1	8.4	77.9	0.0
Jul-83	116.5	20.6	50.1	0.0
Aug-83	74.6	39.1	109.9	0.0
Sep-83	128.0	77.9	13.1	0.0
Oct-83	37.7	105.7	97.1	0.0
Nov-83	110.4	0.0	77.4	0.0
Dec-83	131.5	73.0	0.0	0.0
Jan-84	109.0	0.0	117.7	0.0
Feb-84	8.0	0.0	226.7	0.0
Mar-84	245.4	0.0	0.0	0.0
Apr-84	32.3	0.0	194.9	0.0
May-84	197.7	0.0	39.3	0.0
Jun-84	166.1	0.0	82.8	0.0
Jul-84	51.2	0.0	189.2	0.0
Aug-84	98.9	0.0	128.7	0.0
Sep-84	10.5	0.0	214.7	0.0
Oct-84	128.2	0.0	119.1	0.0
Nov-84	143.6	0.0	118.6	0.0
Dec-84	114.9	0.0	142.5	0.0

Month	Inj. Well 2 MSI-1001 (GPM)	Inj. Well 3 MSI-1001 (GPM)	Inj. Well 4 MSI-1001 (GPM)	Inj. Well 5 MSI-1001 (GPM)
Jan-85	53.3	0.0	156.7	0.0
Feb-85	52.6	0.0	168.9	0.0
Mar-85	151.6	0.0	134.5	0.0
Apr-85	180.8	0.0	55.2	0.0
May-85	4.2	0.0	274.9	0.0
Jun-85	142.5	0.0	143.4	0.0
Jul-85	242.8	0.0	39.3	0.0
Aug-85	133.8	0.0	124.4	0.0
Sep-85	228.1	0.0	0.0	0.0
Oct-85	259.9	0.0	0.0	0.0
Nov-85	219.9	0.0	0.0	0.0
Dec-85	222.7	0.0	0.0	0.0
Jan-86	161.9	0.0	87.8	0.0
Feb-86	201.3	0.0	19.0	0.0
Mar-86	212.9	0.0	22.0	0.0
Apr-86	226.0	0.0	2.3	0.0
May-86	171.7	0.0	79.5	0.0
Jun-86	13.3	0.0	251.5	0.0
Jul-86	0.0	0.0	300.1	0.0
Aug-86	142.0	0.0	120.5	0.0
Sep-86	206.5	0.0	0.2	0.0
Oct-86	129.8	0.0	92.4	0.0
Nov-86	115.3	121.9	45.8	0.0
Dec-86	133.4	36.5	71.8	0.0
Jan-87	76.4	127.5	14.9	0.0
Feb-87	81.1	26.0	58.6	0.0
Mar-87	85.5	139.0	0.0	0.0
Apr-87	33.2	187.8	9.9	0.0
May-87	0.5	250.7	0.0	0.0
Jun-87	88.1	125.8	15.0	0.0
Jul-87	155.3	58.3	7.4	0.0
Aug-87	104.1	0.0	165.9	0.0
Sep-87	175.0	0.0	0.0	0.0
Oct-87	253.6	0.0	0.0	0.0
Nov-87	219.2	0.0	9.2	0.0
Dec-87	239.5	0.0	14.7	0.0
Jan-88	219.1	3.8	18.0	0.0
Feb-88	162.3	0.0	72.7	0.0
Mar-88	252.9	0.0	0.0	0.0
Apr-88	244.9	0.0	0.0	0.0
May-88	285.2	0.0	0.0	0.0
Jun-88	257.8	0.0	0.3	0.0
Jul-88	240.3	0.0	0.0	0.0
Aug-88	255.4	0.0	0.0	0.0
Sep-88	255.2	9.6	0.0	0.0
Oct-88	261.8	0.0	0.0	0.0
Nov-88	236.9	0.0	0.0	0.0
Dec-88	207.3	0.0	0.0	0.0
Jan-89	196.4	0.0	0.0	0.0
Feb-89	197.4	0.0	0.0	0.0
Mar-89	209.2	0.0	0.0	0.0
Apr-89	226.9	0.0	0.0	0.0
May-89	249.2	0.0	0.0	0.0
Jun-89	252.1	0.0	0.0	0.0
Jul-89	257.5	0.0	18.5	0.0
Aug-89	246.8	0.0	0.0	0.0
Sep-89	255.7	0.0	0.0	0.0
Oct-89	279.6	0.0	0.0	0.0
Nov-89	217.3	0.0	0.0	0.0
Dec-89	210.8	0.0	0.0	0.0

Month	Inj. Well 2 MSI-1001 (GPM)	Inj. Well 3 MSI-1001 (GPM)	Inj. Well 4 MSI-1001 (GPM)	Inj. Well 5 MSI-1001 (GPM)
Jan-90	205.4	205.4	0.0	0.0
Feb-90	215.6	215.6	0.0	0.0
Mar-90	200.4	200.4	0.0	0.0
Apr-90	193.9	0.0	3.9	0.0
May-90	221.9	0.0	0.0	0.0
Jun-90	163.2	0.0	54.5	0.0
Jul-90	250.1	0.0	0.4	0.0
Aug-90	183.2	8.4	0.0	0.0
Sep-90	146.3	43.6	0.8	0.0
Oct-90	215.9	23.0	5.7	0.0
Nov-90	234.9	0.0	0.0	0.0
Dec-90	87.6	149.7	0.0	0.0
Jan-91	147.3	151.9	0.0	0.0
Feb-91	109.3	81.3	0.0	0.0
Mar-91	67.3	103.8	43.0	0.0
Apr-91	136.2	2.9	86.4	0.0
May-91	30.2	0.0	213.4	0.0
Jun-91	67.9	98.9	90.6	0.0
Jul-91	90.1	114.7	47.8	0.0
Aug-91	77.8	6.5	122.8	0.0
Sep-91	226.4	29.3	69.2	0.0
Oct-91	164.9	172.2	1.9	0.0
Nov-91	12.5	170.2	118.0	0.0
Dec-91	0.0	111.9	221.6	0.0
Jan-92	117.4	220.4	337.8	0.0
Feb-92	134.5	184.2	318.8	0.0
Mar-92	190.9	110.5	301.5	0.0
Apr-92	17.5	205.5	150.7	0.0
May-92	270.5	33.7	84.2	0.0
Jun-92	202.7	46.8	43.2	0.0
Jul-92	245.1	41.3	110.2	0.0
Aug-92	269.1	64.0	4.7	0.0
Sep-92	252.6	15.2	109.8	0.0
Oct-92	254.1	17.7	76.7	0.0
Nov-92	246.3	51.2	91.4	0.0
Dec-92	159.2	3.2	89.4	0.0
Jan-93	267.0	21.1	176.6	0.0
Feb-93	257.9	78.1	44.8	0.0
Mar-93	229.9	26.7	211.8	0.0
Apr-93	244.3	74.8	98.2	0.0
May-93	284.0	55.2	23.3	0.0
Jun-93	284.8	16.2	87.6	0.0
Jul-93	171.6	139.1	45.4	0.0
Aug-93	212.6	0.0	163.0	0.0
Sep-93	201.8	0.6	128.5	0.0
Oct-93	115.5	2.2	187.6	0.0
Nov-93	271.8	26.6	24.6	0.0
Dec-93	225.7	77.1	3.0	0.0
Jan-94	211.1	54.8	70.1	0.0
Feb-94	293.3	76.1	0.0	0.0
Mar-94	321.2	108.0	0.0	0.0
Apr-94	288.6	109.5	0.0	0.0
May-94	279.5	115.8	0.0	0.0
Jun-94	299.9	129.5	0.0	0.0
Jul-94	256.8	123.4	0.0	0.0
Aug-94	240.7	72.2	0.0	1.1
Sep-94	153.5	120.4	0.0	115.1
Oct-94	0.5	49.8	0.0	325.0
Nov-94	124.0	46.4	0.0	144.2
Dec-94	209.8	0.0	0.0	138.3

Month	Inj. Well 2 MSI-1001 (GPM)	Inj. Well 3 MSI-1001 (GPM)	Inj. Well 4 MSI-1001 (GPM)	Inj. Well 5 MSI-1001 (GPM)
Jan-95	92.0	94.2	0.0	124.3
Feb-95	187.6	81.7	0.0	87.1
Mar-95	164.2	208.0	0.0	0.0
Apr-95	183.3	163.3	0.0	19.1
May-95	218.2	91.3	0.0	54.9
Jun-95	227.1	126.3	0.0	0.0
Jul-95	188.3	65.4	0.0	146.5
Aug-95	187.2	76.7	0.0	75.4
Sep-95	67.2	92.7	189.8	13.5
Oct-95	0.0	63.6	58.9	175.6
Nov-95	0.0	51.8	103.6	214.9
Dec-95	0.0	0.0	162.6	158.0
Jan-96	0.0	0.0	80.5	264.6
Feb-96	1.6	0.0	163.3	124.0
Mar-96	212.4	0.0	82.3	39.5
Apr-96	90.3	0.0	141.5	84.7
May-96	288.2	0.0	47.5	51.2
Jun-96	163.7	0.0	130.8	46.5
Jul-96	259.4	0.0	68.1	22.7
Aug-96	257.5	0.0	105.0	72.0
Sep-96	263.4	0.0	43.0	73.9
Oct-96	240.0	0.0	206.1	0.0
Nov-96	265.7	0.0	88.9	0.5
Dec-96	353.0	0.0	62.0	19.9
Jan-97	256.3	0.0	201.8	0.3
Feb-97	215.8	0.0	112.0	85.1
Mar-97	302.3	0.0	194.0	0.7
Apr-97	178.2	0.0	167.8	139.0
May-97	326.9	0.0	103.7	3.2
Jun-97	271.5	0.0	132.2	11.0
Jul-97	276.4	0.0	71.7	77.9
Aug-97	305.5	0.0	64.9	35.3
Sep-97	152.5	0.0	51.5	243.7
Oct-97	173.4	0.0	97.5	162.9
Nov-97	135.0	0.0	111.8	167.0
Dec-97	261.7	0.0	80.8	0.0
Jan-98	49.7	0.0	73.1	324.8
Feb-98	179.4	0.0	93.6	159.1
Mar-98	190.8	0.0	48.5	198.9
Apr-98	35.6	0.0	0.0	447.6
May-98	112.5	0.0	40.4	226.7
Jun-98	109.1	0.0	65.8	295.8
Jul-98	123.0	0.0	2.6	283.5
Aug-98	81.7	0.0	20.7	367.3
Sep-98	78.0	0.0	0.0	330.7
Oct-98	269.8	0.0	177.0	0.0
Nov-98	247.0	0.0	99.4	174.3
Dec-98	105.6	0.0	97.5	178.4
Jan-99	95.0	0.0	115.7	274.2
Feb-99	212.0	0.0	194.1	180.8
Mar-99	288.6	0.0	135.4	52.3
Apr-99	165.6	0.0	155.1	193.0
May-99	214.5	0.0	130.9	147.5
Jun-99	136.2	0.0	66.9	301.6
Jul-99	13.6	15.6	77.3	334.7
Aug-99	101.2	0.0	82.7	309.8
Sep-99	45.9	0.0	73.1	332.7
Oct-99	160.4	0.0	98.2	256.7
Nov-99	178.1	0.0	96.0	235.1
Dec-99	187.4	0.0	97.7	240.4

TABLE 3-9

COMPILATION OF MONTHLY PLANT WELL INJECTION RATES (IN GALLONS PER MINUTE)

Month	Inj. Well 2 MSI-1001 (GPM)	Inj. Well 3 MSI-1001 (GPM)	Inj. Well 4 MSI-1001 (GPM)	Inj. Well 5 MSI-1001 (GPM)	Month	Inj. Well 2 MSI-1001 (GPM)	Inj. Well 3 MSI-1001 (GPM)	Inj. Well 4 MSI-1001 (GPM)	Inj. Well 5 MSI-1001 (GPM)	Month	Inj. Well 2 MSI-1001 (GPM)	Inj. Well 3 MSI-1001 (GPM)	Inj. Well 4 MSI-1001 (GPM)	Inj. Well 5 MSI-1001 (GPM)	Month	Inj. Well 2 MSI-1001 (GPM)	Inj. Well 3 MSI-1001 (GPM)	Inj. Well 4 MSI-1001 (GPM)	Inj. Well 5 MSI-1001 (GPM)
Jan-00	52.3	0.0	59.1	309.6	Jan-05	232.8	315.0	186.0	0.0	Jan-10	228.4	104.5	0.0	366.6	Jan-15	148.1	67.8	313.2	180.9
Feb-00	173.8	0.0	97.7	172.8	Feb-05	76.2	233.2	200.4	197.1	Feb-10	295.7	167.1	19.0	182.4	Feb-15	36.5	233.2	25.0	372.3
Mar-00	206.9	7.3	177.7	217.1	Mar-05	51.1	130.8	230.6	319.3	Mar-10	273.2	149.6	144.0	232.3	Mar-15	129.9	102.7	13.8	379.5
Apr-00	156.1	300.4	0.4	111.2	Apr-05	1.7	88.0	317.7	312.0	Apr-10	113.7	202.6	105.7	303.7	Apr-15	119.0	168.1	155.9	303.4
May-00	73.6	384.7	101.6	6.0	May-05	31.9	306.2	43.6	372.3	May-10	0.0	283.0	0.0	439.2	May-15	299.1	182.3	242.9	0.0
Jun-00	66.0	0.0	101.3	311.8	Jun-05	165.7	128.3	215.5	240.8	Jun-10	216.1	191.7	194.6	105.5	Jun-15	285.0	157.8	253.3	0.0
Jul-00	0.0	330.5	212.4	68.2	Jul-05	11.0	203.8	317.7	312.0	Jul-10	188.1	22.6	146.5	325.9	Jul-15	278.9	189.9	289.5	0.0
Aug-00	60.1	349.6	7.4	107.2	Aug-05	26.9	144.4	202.8	315.8	Aug-10	44.1	160.6	197.3	418.8	Aug-15	254.5	157.2	236.6	0.0
Sep-00	63.9	124.6	7.4	317.8	Sep-05	0.0	0.0	0.0	0.0	Sep-10	170.4	199.4	197.1	161.2	Sep-15	281.2	56.2	279.0	33.1
Oct-00	0.0	249.3	136.0	159.1	Oct-05	0.0	0.0	0.0	0.0	Oct-10	216.1	89.2	195.4	304.0	Oct-15	176.0	101.0	183.2	209.8
Nov-00	223.7	31.8	67.5	116.7	Nov-05	0.0	0.0	0.0	0.0	Nov-10	262.1	0.0	73.0	363.9	Nov-15	284.3	132.0	149.9	0.0
Dec-00	149.0	150.2	67.5	33.6	Dec-05	2.1	0.0	0.0	0.0	Dec-10	260.2	168.2	363.9	86.1	Dec-15	360.7	105.8	278.2	40.4
Jan-01	55.7	293.4	50.7	141.0	Jan-06	0.0	1.1	0.0	0.2	Jan-11	217.1	255.0	90.4	198.7					
Feb-01	130.7	332.9	17.0	0.0	Feb-06	0.0	207.6	35.9	316.0	Feb-11	59.6	247.2	0.1	356.2					
Mar-01	209.0	122.1	17.0	0.3	Mar-06	0.0	157.5	104.5	396.4	Mar-11	290.9	290.6	30.7	112.1					
Apr-01	259.6	0.0	7.8	1.0	Apr-06	100.1	31.7	193.4	334.2	Apr-11	99.1	240.0	155.1	204.6					
May-01	111.4	88.8	113.5	185.1	May-06	75.1	180.1	89.1	277.8	May-11	157.0	239.0	180.7	158.6					
Jun-01	39.5	128.9	160.8	157.6	Jun-06	294.7	80.2	311.4	23.6	Jun-11	219.5	171.3	0.0	293.9					
Jul-01	66.4	159.4	82.3	243.6	Jul-06	62.4	256.8	292.4	85.8	Jul-11	75.0	244.9	49.1	333.6					
Aug-01	70.2	319.0	40.4	165.5	Aug-06	269.9	200.0	56.6	188.6	Aug-11	104.5	90.1	122.5	334.3					
Sep-01	142.0	143.9	40.4	224.8	Sep-06	83.5	85.6	239.8	290.1	Sep-11	158.3	92.6	139.5	303.0					
Oct-01	18.8	175.7	96.0	277.7	Oct-06	60.1	165.0	282.2	178.9	Oct-11	13.8	157.8	209.1	368.3					
Nov-01	194.5	269.3	0.0	124.1	Nov-06	292.2	87.7	82.5	234.6	Nov-11	133.0	20.9	70.9	286.5					
Dec-01	106.5	82.2	0.0	35.9	Dec-06	193.0	0.0	198.0	291.4	Dec-11	161.9	82.7	85.7	330.5					
Jan-02	55.7	293.4	50.5	141.3	Jan-07	26.2	265.5	323.3	60.0	Jan-12	139.6	206.5	174.7	199.5					
Feb-02	131.0	332.9	17.1	0.0	Feb-07	11.7	226.0	112.8	286.8	Feb-12	54.8	169.6	136.9	402.9					
Mar-02	209.0	122.1	17.1	0.3	Mar-07	160.8	212.0	159.9	164.3	Mar-12	131.7	106.3	117.6	243.9					
Apr-02	150.8	205.1	139.9	101.5	Apr-07	0.0	116.6	195.9	388.2	Apr-12	198.2	157.8	171.2	312.9					
May-02	152.0	224.4	235.9	24.8	May-07	87.5	258.6	56.9	302.5	May-12	168.2	117.0	53.9	220.5					
Jun-02	0.0	117.9	242.6	233.4	Jun-07	248.2	163.5	54.4	241.0	Jun-12	208.1	104.5	140.8	298.6					
Jul-02	126.9	57.5	143.2	293.2	Jul-07	55.5	176.3	188.3	287.2	Jul-12	183.2	161.2	127.6	343.7					
Aug-02	73.6	361.5	39.6	121.3	Aug-07	126.9	242.5	189.1	33.4	Aug-12	97.9	50.6	48.8	233.3					
Sep-02	180.8	211.0	44.7	100.6	Sep-07	281.7	123.2	11.5	239.5	Sep-12	198.9	61.5	53.0	241.4					
Oct-02	54.3	101.5	161.8	263.0	Oct-07	175.6	209.6	245.0	47.3	Oct-12	130.1	27.4	81.3	103.4					
Nov-02	199.4	126.5	97.5	116.4	Nov-07	113.5	81.0	163.3	328.9	Nov-12	224.6	36.6	34.1	270.2					
Dec-02	306.3	50.7	101.8	84.3	Dec-07	0.0	243.9	290.6	136.7	Dec-12	275.0	0.0	106.1	57.4					
Jan-03	154.2	161.5	189.2	135.3	Jan-08	0.0	40.7	286.0	340.3	Jan-13	119.1	47.9	40.0	301.1					
Feb-03	124.6	86.8	69.7	263.3	Feb-08	55.6	70.8	101.6	384.9	Feb-13	0.0	48.2	4.8	519.8					
Mar-03	89.4	0.2	103.1	416.2	Mar-08	160.4	142.8	7.0	412.8	Mar-13	0.1	48.1	0.0	474.3					
Apr-03	152.3	0.0	137.5	318.2	Apr-08	123.2	136.7	134.2	312.6	Apr-13	5.1	155.9	0.0	425.6					
May-03	221.0	0.0	64.2	257.1	May-08	291.0	292.4	45.7	87.5	May-13	0.0	229.5	0.0	329.5					
Jun-03	323.5	0.0	219.9	47.6	Jun-08	268.0	123.5	162.9	127.8	Jun-13	0.0	234.6	0.0	370.2					
Jul-03	319.9	0.0	269.5	38.6	Jul-08	59.0	79.4	70.9	417.4	Jul-13	0.0	161.5	0.0	441.0					
Aug-03	187.5	0.0	91.6	262.8	Aug-08	265.9	82.0	14.2	324.7	Aug-13	0.0	5.4	0.0	432.4					
Sep-03	75.8	0.0	110.1	355.8	Sep-08	218.6	115.6	99.8	164.1	Sep-13	0.0	172.7	0.0	423.0					
Oct-03	0.0	0.0	210.1	434.0	Oct-08	216.2	298.5	66.2	135.5	Oct-13	0.0	131.2	5.4	467.9					
Nov-03	52.7	94.5	122.1	323.2	Nov-08	126.6	142.4	0.0	0.0	Nov-13	0.0	55.1	137.3	365.7					
Dec-03	188.0	45.9	165.7	227.1	Dec-08	16.4	75.1	13.7	41.7	Dec-13	0.0	135.1	219.3	179.1					
Jan-04	58.3	341.1	184.0	0.6	Jan-09	0.0	247.8	2.6	376.9	Jan-14	0.0	211.3	237.7	144.0					
Feb-04	205.8	362.5	63.3	0.1	Feb-09	178.8	292.1	36.5	0.0	Feb-14	0.0	131.2	99.0	286.4					
Mar-04	299.4	121.6	276.2	40.0	Mar-09	198.5	89.6	0.0	193.8	Mar-14	224.5	129.3	101.6	231.8					
Apr-04	59.0	339.1	310.1	0.0	Apr-09	135.4	238.8	172.9	68.7	Apr-14	124.7	160.7	40.3	418.8					
May-04	303.9	383.4	29.0	0.0	May-09	162.3	311.9	26.1	178.6	May-14	196.9	132.1	27.4	403.8					
Jun-04	306.5	146.8	196.1	0.0	Jun-09	84.1	233.2	257.1	38.6	Jun-14	271.1	92.0	0.0	388.6					
Jul-04	232.1	220.0	279.4	0.0	Jul-09	173.8	175.5	72.4	261.9	Jul-14	54.9	114.3	11.1	404.8					
Aug-04	345.0	329.1	76.2	0.0	Aug-09	116.6	177.6	26.9	378.6	Aug-14	0.0	84.4	0.0	491.7					
Sep-04	290.7	138.6	205.2	0.0	Sep-09	259.6	139.6	179.9	92.8	Sep-14	0.0	87.4	0.0	482.3					
Oct-04	239.3	280.6	247.7	0.0	Oct-09	231.1	239.0	225.9	17.9	Oct-14	0.0	162.8	0.0	409.3					
Nov-04	311.2	216.0	219.4	0.0	Nov-09	211.6	249.8	171.3	73.1	Nov-14	345.4	106.2	100.1	114.0					
Dec-04	400.9	37.4	278.3	0.0	Dec-09	168.2	157.1	73.1	269.2	Dec-14	174.7	28.4	349.9	17.4					

TABLE 3-10

COMPILATION OF ANNUAL PLANT WELL INJECTION RATES (IN GALLONS PER MINUTE)

Year	Inj. Well 2 MSI-1001 (GPM)	Inj. Well 2 MSI-1001 (GPM)	Inj. Well 4 MSI-1001 (GPM)	Inj. Well 5 MSI-1001 (GPM)
1979	14.3	15.2		
1980	108.9	54.3		
1981	96.8	78.7		
1982	91.2	84.3		
1983	113.8	38.3	66.4	
1984	106.1	0.0	127.9	
1985	153.8	0.0	89.2	
1986	139.3	12.9	88.8	
1987	122.9	74.4	24.0	
1988	234.0	1.1	7.4	
1989	227.5	0.0	1.5	
1990	188.4	68.8	5.3	
1991	91.8	84.8	82.5	
1992	191.8	80.8	139.7	
1993	224.9	42.1	97.1	
1994	217.7	81.8	5.7	58.8
1995	123.1	90.6	41.9	86.9
1996	194.7	0.0	99.1	65.0
1997	232.1	0.0	113.0	75.3
1998	128.6	0.0	58.4	242.8
1999	146.2	1.3	107.5	232.4
2000	99.6	156.7	84.2	157.0
2001	114.1	172.0	50.9	126.5
2002	133.3	179.2	105.0	120.3
2003	153.5	31.6	142.5	250.3
2004	248.1	237.0	192.2	3.3
2005	48.7	126.0	139.3	168.2
2006	116.3	118.1	153.3	212.8
2007	104.7	188.5	161.8	204.5
2008	146.4	130.0	81.5	223.5
2009	156.1	207.4	101.2	158.5
2010	184.4	141.3	133.0	267.4
2011	137.3	173.3	92.2	266.6
2012	168.2	99.9	104.0	243.4
2013	10.5	119.0	34.1	393.1
2014	116.2	120.0	80.9	315.9
2015	222.4	137.2	203.1	125.1

TABLE 3-11

DUPONT DELISLE PLANT MONITORING WELL NO. 1 PRESSURES

Month-Year	Wellhead Pressure (psig)	Month-Year	Wellhead Pressure (psig)	Month-Year	Wellhead Pressure (psig)	Month-Year	Wellhead Pressure (psig)	Month-Year	Wellhead Pressure (psig)	Month-Year	Wellhead Pressure (psig)
Jan-81	--	Jan-87	34	Jan-93	58	Jan-99	65	Jan-05	31	Jan-11	148
Feb-81	--	Feb-87	32	Feb-93	57	Feb-99	68	Feb-05	32	Feb-11	142
Mar-81	27	Mar-87	33	Mar-93	58	Mar-99	68	Mar-05	65	Mar-11	149
Apr-81	28	Apr-87	31	Apr-93	58	Apr-99	69	Apr-05	134	Apr-11	145
May-81	29	May-87	32	May-93	57	May-99	71	May-05	133	May-11	149
Jun-81	30	Jun-87	32	Jun-93	57	Jun-99	71	Jun-05	135	Jun-11	145
Jul-81	--	Jul-87	32	Jul-93	51	Jul-99	67	Jul-05	138	Jul-11	141
Aug-81	--	Aug-87	33	Aug-93	51	Aug-99	67	Aug-05	136	Aug-11	144
Sep-81	--	Sep-87	33	Sep-93	51	Sep-99	68	Sep-05	126	Sep-11	146
Oct-81	--	Oct-87	32	Oct-93	50	Oct-99	71	Oct-05	116	Oct-11	143
Nov-81	--	Nov-87	32	Nov-93	52	Nov-99	71	Nov-05	106	Nov-11	137
Dec-81	--	Dec-87	33	Dec-93	50	Dec-99	75	Dec-05	96	Dec-11	134
Jan-82	26	Jan-88	32	Jan-94	49	Jan-00	69	Jan-06	96	Jan-12	140
Feb-82	29	Feb-88	32	Feb-94	55	Feb-00	68	Feb-06	83	Feb-12	141
Mar-82	27	Mar-88	33	Mar-94	58	Mar-00	74	Mar-06	100	Mar-12	140
Apr-82	27	Apr-88	34	Apr-94	53	Apr-00	78	Apr-06	109	Apr-12	146
May-82	27	May-88	34	May-94	58	May-00	77	May-06	113	May-12	151
Jun-82	24	Jun-88	34	Jun-94	60	Jun-00	75	Jun-06	123	Jun-12	124
Jul-82	32	Jul-88	34	Jul-94	61	Jul-00	77	Jul-06	125	Jul-12	142
Aug-82	32	Aug-88	34	Aug-94	50	Aug-00	78	Aug-06	126	Aug-12	142
Sep-82	30	Sep-88	34	Sep-94	53	Sep-00	79	Sep-06	127	Sep-12	130
Oct-82	31	Oct-88	34	Oct-94	48	Oct-00	79	Oct-06	127	Oct-12	124
Nov-82	34	Nov-88	35	Nov-94	53	Nov-00	74	Nov-06	129	Nov-12	118
Dec-82	28	Dec-88	32	Dec-94	53	Dec-00	76	Dec-06	125	Dec-12	119
Jan-83	30	Jan-89	32	Jan-95	48	Jan-01	79	Jan-07	129	Jan-13	120
Feb-83	35	Feb-89	29	Feb-95	50	Feb-01	76	Feb-07	129	Feb-13	115
Mar-83	35	Mar-89	30	Mar-95	51	Mar-01	77	Mar-07	132	Mar-13	115
Apr-83	36	Apr-89	31	Apr-95	52	Apr-01	77	Apr-07	133	Apr-13	118
May-83	37	May-89	31	May-95	54	May-01	76	May-07	136	May-13	120
Jun-83	36	Jun-89	32	Jun-95	53	Jun-01	77	Jun-07	138	Jun-13	122
Jul-83	37	Jul-89	32	Jul-95	55	Jul-01	77	Jul-07	138	Jul-13	123
Aug-83	34	Aug-89	32	Aug-95	54	Aug-01	80	Aug-07	141	Aug-13	114
Sep-83	35	Sep-89	32	Sep-95	52	Sep-01	57	Sep-07	137	Sep-13	119
Oct-83	35	Oct-89	33	Oct-95	49	Oct-01	80	Oct-07	141	Oct-13	120
Nov-83	32	Nov-89	33	Nov-95	45	Nov-01	83	Nov-07	139	Nov-13	121
Dec-83	32	Dec-89	30	Dec-95	46	Dec-01	81	Dec-07	139	Dec-13	123
Jan-84	33	Jan-90	29	Jan-96	46	Jan-02	78	Jan-08	136	Jan-14	126
Feb-84	35	Feb-90	29	Feb-96	45	Feb-02	82	Feb-08	134	Feb-14	126
Mar-84	33	Mar-90	28	Mar-96	48	Mar-02	88	Mar-08	136	Mar-14	121
Apr-84	33	Apr-90	28	Apr-96	48	Apr-02	88	Apr-08	143	Apr-14	133
May-84	35	May-90	28	May-96	49	May-02	89	May-08	145	May-14	138
Jun-84	36	Jun-90	28	Jun-96	50	Jun-02	89	Jun-08	148	Jun-14	139
Jul-84	36	Jul-90	28	Jul-96	50	Jul-02	91	Jul-08	128	Jul-14	134
Aug-84	37	Aug-90	28	Aug-96	55	Aug-02	88	Aug-08	127	Aug-14	125
Sep-84	36	Sep-90	28	Sep-96	53	Sep-02	88	Sep-08	134	Sep-14	123
Oct-84	34	Oct-90	26	Oct-96	57	Oct-02	84	Oct-08	138	Oct-14	121
Nov-84	36	Nov-90	28	Nov-96	55	Nov-02	87	Nov-08	125	Nov-14	126
Dec-84	35	Dec-90	39	Dec-96	57	Dec-02	86	Dec-08	98	Dec-14	132
Jan-85	35	Jan-91	49	Jan-97	58	Jan-03	90	Jan-09	108	Jan-15	129
Feb-85	37	Feb-91	42	Feb-97	59	Feb-03	89	Feb-09	121	Feb-15	124
Mar-85	35	Mar-91	38	Mar-97	60	Mar-03	90	Mar-09	117	Mar-15	132
Apr-85	35	Apr-91	33	Apr-97	61	Apr-03	93	Apr-09	117	Apr-15	135
May-85	35	May-91	34	May-97	65	May-03	89	May-09	125	May-15	145
Jun-85	37	Jun-91	40	Jun-97	61	Jun-03	95	Jun-09	129	Jun-15	143
Jul-85	39	Jul-91	40	Jul-97	61	Jul-03	97	Jul-09	128	Jul-15	146
Aug-85	40	Aug-91	35	Aug-97	59	Aug-03	92	Aug-09	127	Aug-15	137
Sep-85	37	Sep-91	35	Sep-97	61	Sep-03	87	Sep-09	134	Sep-15	142
Oct-85	38	Oct-91	41	Oct-97	62	Oct-03	91	Oct-09	139	Oct-15	139
Nov-85	36	Nov-91	25	Nov-97	63	Nov-03	93	Nov-09	142	Nov-15	135
Dec-85	35	Dec-91	40	Dec-97	55	Dec-03	94	Dec-09	136	Dec-15	143
Jan-86	35	Jan-92	48	Jan-98	60	Jan-04	104	Jan-10	134		
Feb-86	37	Feb-92	53	Feb-98	63	Feb-04	118	Feb-10	138		
Mar-86	35	Mar-92	51	Mar-98	63	Mar-04	123	Mar-10	143		
Apr-86	35	Apr-92	57	Apr-98	63	Apr-04	125	Apr-10	142		
May-86	37	May-92	49	May-98	61	May-04	119	May-10	137		
Jun-86	37	Jun-92	43	Jun-98	63	Jun-04	123	Jun-10	144		
Jul-86	35	Jul-92	51	Jul-98	62	Jul-04	86	Jul-10	141		
Aug-86	35	Aug-92	43	Aug-98	62	Aug-04	28	Aug-10	141		
Sep-86	36	Sep-92	60	Sep-98	65	Sep-04	25	Sep-10	145		
Oct-86	34	Oct-92	60	Oct-98	64	Oct-04	30	Oct-10	146		
Nov-86	34	Nov-92	64	Nov-98	66	Nov-04	30	Nov-10	144		
Dec-86	35	Dec-92	50	Dec-98	61	Dec-04	31	Dec-10	149		

TABLE 3-12

FORMATION FLUID TOTAL DISSOLVED SOLIDS (TDS) VALUES AT DELISLE PLANT

2007 MDEQ Permit Application Data

Depth (ft)	TDS (ppm)	Data Source
2,700	10,000	USDW
3,900	57,000	Measured DST
5,900	85,000	Literature*
9,370	114,000	Measured DST
9,855	155,000	Calculated**

* Literature Value from Wilcox value in USGS Open File Report 80-595

** Calculated Value from NaCl Concentration

Salinity (NaCl) Calculated from Resistivity Log

Depth (ft)	Rwa (calculated)	Temperature (calculated)	Salinity (NaCl ppm)
2940	0.600	120	6,000
3,090	0.358	123	10,000
3,370	0.224	128	16,500
4,000	0.067	140	58,000
9,600	0.037	243	65,000
9,870	0.037	248	65,000

Monitoring Well No. 1 DST in 1974

Depth (ft)	Cl (ppm)	TDS* (ppm)
3,911	53,500	- - -
9,898	102,500	180,000

* calculated based on Cl concentration

Well No. 2 Sidetrack Recompletion in 1995

Depth (ft)	TDS (mg/L)	Notes
9,560	165,986	Tuscaloosa Massive Sand
9,966	187,898	Washita-Fredericksburg

Well No. 3 Sidetrack Recompletion in 1999

Depth (ft)	TDS (mg/L)	Data Source
9,496	130,000	Tuscaloosa Massive Sand
9,996	140,000	Washita-Frederickburg

TABLE 3-13

WASHITA-FREDERICKSBURG INJECTION INTERVAL
RESERVOIR PRESSURE BUILDUP DATA

Chemours WF Prs

Date	Model Days	Well 5 Bottom Hole Pressure (psi)	Well 5 Pressure Buildup (psi)	Date	Model Days	Well 5 Bottom Hole Pressure (psi)	Well 5 Pressure Buildup (psi)
10/1/79	10,000	4,563	0	12/31/17	23,971	5,400	837
12/31/79	10,091	4,570	7	12/31/18	24,336	5,430	867
12/31/80	10,457	4,590	27	12/31/19	24,701	5,450	887
12/31/81	10,822	4,600	37	12/31/20	25,067	5,460	897
12/31/82	11,187	4,600	37	12/31/21	25,432	5,460	897
12/31/83	11,552	4,610	47	12/31/22	25,797	5,470	907
12/31/84	11,918	4,610	47	12/31/23	26,162	5,470	907
12/31/85	12,283	4,620	57	12/31/24	26,528	5,470	907
12/31/86	12,648	4,620	57	12/31/25	26,893	5,480	917
12/31/87	13,013	4,620	57	12/31/26	27,258	5,490	927
12/31/88	13,379	4,620	57	12/31/27	27,623	5,490	927
12/31/89	13,744	4,620	57	12/31/28	27,989	5,500	937
12/31/90	14,109	4,620	57	12/31/29	28,354	5,500	937
12/31/91	14,474	4,630	67	12/31/30	28,719	5,500	937
12/31/92	14,840	4,650	87	12/31/31	29,084	5,500	937
12/31/93	15,205	4,650	87	12/31/32	29,450	5,500	937
12/31/94	15,570	4,680	117	12/31/33	29,815	5,500	937
12/31/95	15,935	4,700	137	12/31/34	30,180	5,500	937
12/31/96	16,301	4,640	77	12/31/35	30,545	5,500	937
12/31/97	16,666	4,700	137	12/31/36	30,911	5,510	947
12/31/98	17,031	4,810	247	12/31/37	31,276	5,510	947
12/31/99	17,396	4,810	247	12/31/38	31,641	5,510	947
12/31/00	17,762	4,780	217	12/31/39	32,006	5,510	947
12/31/01	18,127	4,760	197	12/31/40	32,372	5,510	947
12/31/02	18,492	4,770	207	12/31/41	32,737	5,520	957
12/31/03	18,857	4,850	287	12/31/42	33,102	5,520	957
12/31/04	19,223	4,730	167	12/31/43	33,467	5,520	957
12/31/05	19,588	4,800	237	12/31/44	33,833	5,520	957
12/31/06	19,953	4,840	277	12/31/45	34,198	5,520	957
12/31/07	20,318	4,850	287	12/31/46	34,563	5,520	957
12/31/08	20,684	4,850	287	12/31/47	34,928	5,520	957
12/31/09	21,049	4,820	257	12/31/48	35,294	5,520	957
12/31/10	21,414	4,900	337	12/31/49	35,659	5,520	957
12/31/11	21,779	4,900	337	12/31/50	36,024	5,530	967
12/31/12	22,145	4,870	307	12/31/51	36,389	4,800	237
12/31/13	22,510	4,950	387	12/31/52	36,755	4,750	187
12/31/14	22,875	4,920	357	12/31/53	37,120	4,720	157
12/31/15	23,240	4,810	247	12/31/54	37,485	4,690	127
12/31/16	23,606	5,350	787	12/31/55	37,850	4,670	107

Chemours WF Prs(1)

Date	Model Days	Well 5 Bottom Hole Pressure (psi)	Well 5 Pressure Buildup (psi)	Date	Model Days	Well 5 Bottom Hole Pressure (psi)	Well 5 Pressure Buildup (psi)
10/1/79	10,000	4,563	0	12/31/17	23,971	5,670	1,107
12/31/79	10,091	4,570	7	12/31/18	24,336	5,690	1,127
12/31/80	10,457	4,590	27	12/31/19	24,701	5,710	1,147
12/31/81	10,822	4,600	37	12/31/20	25,067	5,720	1,157
12/31/82	11,187	4,600	37	12/31/21	25,432	5,730	1,167
12/31/83	11,552	4,610	47	12/31/22	25,797	5,730	1,167
12/31/84	11,918	4,610	47	12/31/23	26,162	5,730	1,167
12/31/85	12,283	4,620	57	12/31/24	26,528	5,740	1,177
12/31/86	12,648	4,620	57	12/31/25	26,893	5,750	1,187
12/31/87	13,013	4,620	57	12/31/26	27,258	5,750	1,187
12/31/88	13,379	4,620	57	12/31/27	27,623	5,760	1,197
12/31/89	13,744	4,620	57	12/31/28	27,989	5,760	1,197
12/31/90	14,109	4,620	57	12/31/29	28,354	5,760	1,197
12/31/91	14,474	4,630	67	12/31/30	28,719	5,760	1,197
12/31/92	14,840	4,650	87	12/31/31	29,084	5,770	1,207
12/31/93	15,205	4,650	87	12/31/32	29,450	5,770	1,207
12/31/94	15,570	4,680	117	12/31/33	29,815	5,770	1,207
12/31/95	15,935	4,700	137	12/31/34	30,180	5,770	1,207
12/31/96	16,301	4,640	77	12/31/35	30,545	5,770	1,207
12/31/97	16,666	4,700	137	12/31/36	30,911	5,770	1,207
12/31/98	17,031	4,810	247	12/31/37	31,276	5,770	1,207
12/31/99	17,396	4,810	247	12/31/38	31,641	5,780	1,217
12/31/00	17,762	4,780	217	12/31/39	32,006	5,780	1,217
12/31/01	18,127	4,760	197	12/31/40	32,372	5,780	1,217
12/31/02	18,492	4,770	207	12/31/41	32,737	5,780	1,217
12/31/03	18,857	4,850	287	12/31/42	33,102	5,780	1,217
12/31/04	19,223	4,730	167	12/31/43	33,467	5,780	1,217
12/31/05	19,588	4,790	227	12/31/44	33,833	5,780	1,217
12/31/06	19,953	4,840	277	12/31/45	34,198	5,780	1,217
12/31/07	20,318	4,850	287	12/31/46	34,563	5,790	1,227
12/31/08	20,684	4,850	287	12/31/47	34,928	5,790	1,227
12/31/09	21,049	4,820	257	12/31/48	35,294	5,790	1,227
12/31/10	21,414	4,900	337	12/31/49	35,659	5,790	1,227
12/31/11	21,779	4,890	327	12/31/50	36,024	5,790	1,227
12/31/12	22,145	4,870	307	12/31/51	36,389	4,800	237
12/31/13	22,510	4,950	387	12/31/52	36,755	4,760	197
12/31/14	22,875	4,910	347	12/31/53	37,120	4,720	157
12/31/15	23,240	4,810	247	12/31/54	37,485	4,690	127
12/31/16	23,606	5,610	1,047	12/31/55	37,850	4,670	107

Chemours WF Prs(2)

Date	Model Days	Well 6 Bottom Hole Pressure (psi)	Well 6 Pressure Buildup (psi)	Date	Model Days	Well 6 Bottom Hole Pressure (psi)	Well 6 Pressure Buildup (psi)
10/1/79	10,000	4,554	0	12/31/17	23,971	5,740	1,186
12/31/79	10,091	4,560	6	12/31/18	24,336	5,770	1,216
12/31/80	10,457	4,580	26	12/31/19	24,701	5,790	1,236
12/31/81	10,822	4,580	26	12/31/20	25,067	5,790	1,236
12/31/82	11,187	4,590	36	12/31/21	25,432	5,800	1,246
12/31/83	11,552	4,590	36	12/31/22	25,797	5,800	1,246
12/31/84	11,918	4,600	46	12/31/23	26,162	5,800	1,246
12/31/85	12,283	4,600	46	12/31/24	26,528	5,800	1,246
12/31/86	12,648	4,600	46	12/31/25	26,893	5,820	1,266
12/31/87	13,013	4,600	46	12/31/26	27,258	5,830	1,276
12/31/88	13,379	4,600	46	12/31/27	27,623	5,830	1,276
12/31/89	13,744	4,600	46	12/31/28	27,989	5,830	1,276
12/31/90	14,109	4,610	56	12/31/29	28,354	5,840	1,286
12/31/91	14,474	4,610	56	12/31/30	28,719	5,840	1,286
12/31/92	14,840	4,630	76	12/31/31	29,084	5,840	1,286
12/31/93	15,205	4,630	76	12/31/32	29,450	5,840	1,286
12/31/94	15,570	4,630	76	12/31/33	29,815	5,840	1,286
12/31/95	15,935	4,630	76	12/31/34	30,180	5,850	1,296
12/31/96	16,301	4,620	66	12/31/35	30,545	5,850	1,296
12/31/97	16,666	4,640	86	12/31/36	30,911	5,850	1,296
12/31/98	17,031	4,650	96	12/31/37	31,276	5,850	1,296
12/31/99	17,396	4,660	106	12/31/38	31,641	5,850	1,296
12/31/00	17,762	4,660	106	12/31/39	32,006	5,850	1,296
12/31/01	18,127	4,660	106	12/31/40	32,372	5,850	1,296
12/31/02	18,492	4,670	116	12/31/41	32,737	5,860	1,306
12/31/03	18,857	4,680	126	12/31/42	33,102	5,860	1,306
12/31/04	19,223	4,690	136	12/31/43	33,467	5,860	1,306
12/31/05	19,588	4,670	116	12/31/44	33,833	5,860	1,306
12/31/06	19,953	4,680	126	12/31/45	34,198	5,860	1,306
12/31/07	20,318	4,690	136	12/31/46	34,563	5,860	1,306
12/31/08	20,684	4,690	136	12/31/47	34,928	5,860	1,306
12/31/09	21,049	4,690	136	12/31/48	35,294	5,860	1,306
12/31/10	21,414	4,710	156	12/31/49	35,659	5,860	1,306
12/31/11	21,779	4,710	156	12/31/50	36,024	5,870	1,316
12/31/12	22,145	4,700	146	12/31/51	36,389	4,790	236
12/31/13	22,510	4,690	136	12/31/52	36,755	4,750	196
12/31/14	22,875	4,700	146	12/31/53	37,120	4,710	156
12/31/15	23,240	4,700	146	12/31/54	37,485	4,680	126
12/31/16	23,606	5,680	1,126	12/31/55	37,850	4,660	106

TABLE 3-14

TUSCALOOSA MASSIVE SAND
RESERVOIR PRESSURE BUILDUP DATA

Chemours TMS Prs

Date	Model Days	Well 5 Bottom Hole Pressure (psi)	Well 5 Pressure Buildup (psi)	Date	Model Days	Well 5 Bottom Hole Pressure (psi)	Well 5 Pressure Buildup (psi)
12/31/19	10,000	4,397	0	12/31/38	16,940	4,730	333
12/31/20	10,366	4,650	253	12/31/39	17,305	4,730	333
12/31/21	10,731	4,670	273	12/31/40	17,671	4,730	333
12/31/22	11,096	4,690	293	12/31/41	18,036	4,730	333
12/31/23	11,461	4,700	303	12/31/42	18,401	4,730	333
12/31/24	11,827	4,700	303	12/31/43	18,766	4,730	333
12/31/25	12,192	4,710	313	12/31/44	19,132	4,730	333
12/31/26	12,557	4,710	313	12/31/45	19,497	4,740	343
12/31/27	12,922	4,710	313	12/31/46	19,862	4,740	343
12/31/28	13,288	4,710	313	12/31/47	20,227	4,740	343
12/31/29	13,653	4,720	323	12/31/48	20,593	4,740	343
12/31/30	14,018	4,720	323	12/31/49	20,958	4,740	343
12/31/31	14,383	4,720	323	12/31/50	21,323	4,740	343
12/31/32	14,749	4,720	323	1/1/51	21,324	4,590	193
12/31/33	15,114	4,720	323	12/31/51	21,688	4,490	93
12/31/34	15,479	4,730	333	12/31/52	22,054	4,480	83
12/31/35	15,844	4,730	333	12/31/53	22,419	4,470	73
12/31/36	16,210	4,730	333	12/31/54	22,784	4,470	73
12/31/37	16,575	4,730	333				

Chemours TMS Prs(1)

Date	Model Days	Well 5 Bottom Hole Pressure (psi)	Well 5 Pressure Buildup (psi)	Date	Model Days	Well 5 Bottom Hole Pressure (psi)	Well 5 Pressure Buildup (psi)
12/31/19	10,000	4,397	0	12/31/38	16,940	4,830	433
12/31/20	10,366	4,750	353	12/31/39	17,305	4,830	433
12/31/21	10,731	4,770	373	12/31/40	17,671	4,830	433
12/31/22	11,096	4,790	393	12/31/41	18,036	4,830	433
12/31/23	11,461	4,800	403	12/31/42	18,401	4,830	433
12/31/24	11,827	4,800	403	12/31/43	18,766	4,830	433
12/31/25	12,192	4,810	413	12/31/44	19,132	4,840	443
12/31/26	12,557	4,810	413	12/31/45	19,497	4,840	443
12/31/27	12,922	4,810	413	12/31/46	19,862	4,840	443
12/31/28	13,288	4,810	413	12/31/47	20,227	4,840	443
12/31/29	13,653	4,820	423	12/31/48	20,593	4,840	443
12/31/30	14,018	4,820	423	12/31/49	20,958	4,840	443
12/31/31	14,383	4,820	423	12/31/50	21,323	4,840	443
12/31/32	14,749	4,820	423	1/1/51	21,324	4,600	203
12/31/33	15,114	4,820	423	12/31/51	21,688	4,490	93
12/31/34	15,479	4,830	433	12/31/52	22,054	4,480	83
12/31/35	15,844	4,830	433	12/31/53	22,419	4,470	73
12/31/36	16,210	4,830	433	12/31/54	22,784	4,470	73
12/31/37	16,575	4,830	433				

Chemours TMS Prs(2)

Date	Model Days	Well 6 Bottom Hole Pressure (psi)	Well 6 Pressure Buildup (psi)	Date	Model Days	Well 6 Bottom Hole Pressure (psi)	Well 6 Pressure Buildup (psi)
12/31/19	10,000	4,403	0	12/31/38	16,940	4,860	457
12/31/20	10,366	4,780	377	12/31/39	17,305	4,860	457
12/31/21	10,731	4,800	397	12/31/40	17,671	4,860	457
12/31/22	11,096	4,820	417	12/31/41	18,036	4,860	457
12/31/23	11,461	4,830	427	12/31/42	18,401	4,860	457
12/31/24	11,827	4,830	427	12/31/43	18,766	4,860	457
12/31/25	12,192	4,840	437	12/31/44	19,132	4,860	457
12/31/26	12,557	4,840	437	12/31/45	19,497	4,870	467
12/31/27	12,922	4,840	437	12/31/46	19,862	4,870	467
12/31/28	13,288	4,840	437	12/31/47	20,227	4,870	467
12/31/29	13,653	4,840	437	12/31/48	20,593	4,870	467
12/31/30	14,018	4,850	447	12/31/49	20,958	4,870	467
12/31/31	14,383	4,850	447	12/31/50	21,323	4,870	467
12/31/32	14,749	4,850	447	1/1/51	21,324	4,590	187
12/31/33	15,114	4,850	447	12/31/51	21,688	4,500	97
12/31/34	15,479	4,850	447	12/31/52	22,054	4,490	87
12/31/35	15,844	4,860	457	12/31/53	22,419	4,480	77
12/31/36	16,210	4,860	457	12/31/54	22,784	4,470	67
12/31/37	16,575	4,860	457				

FIGURES

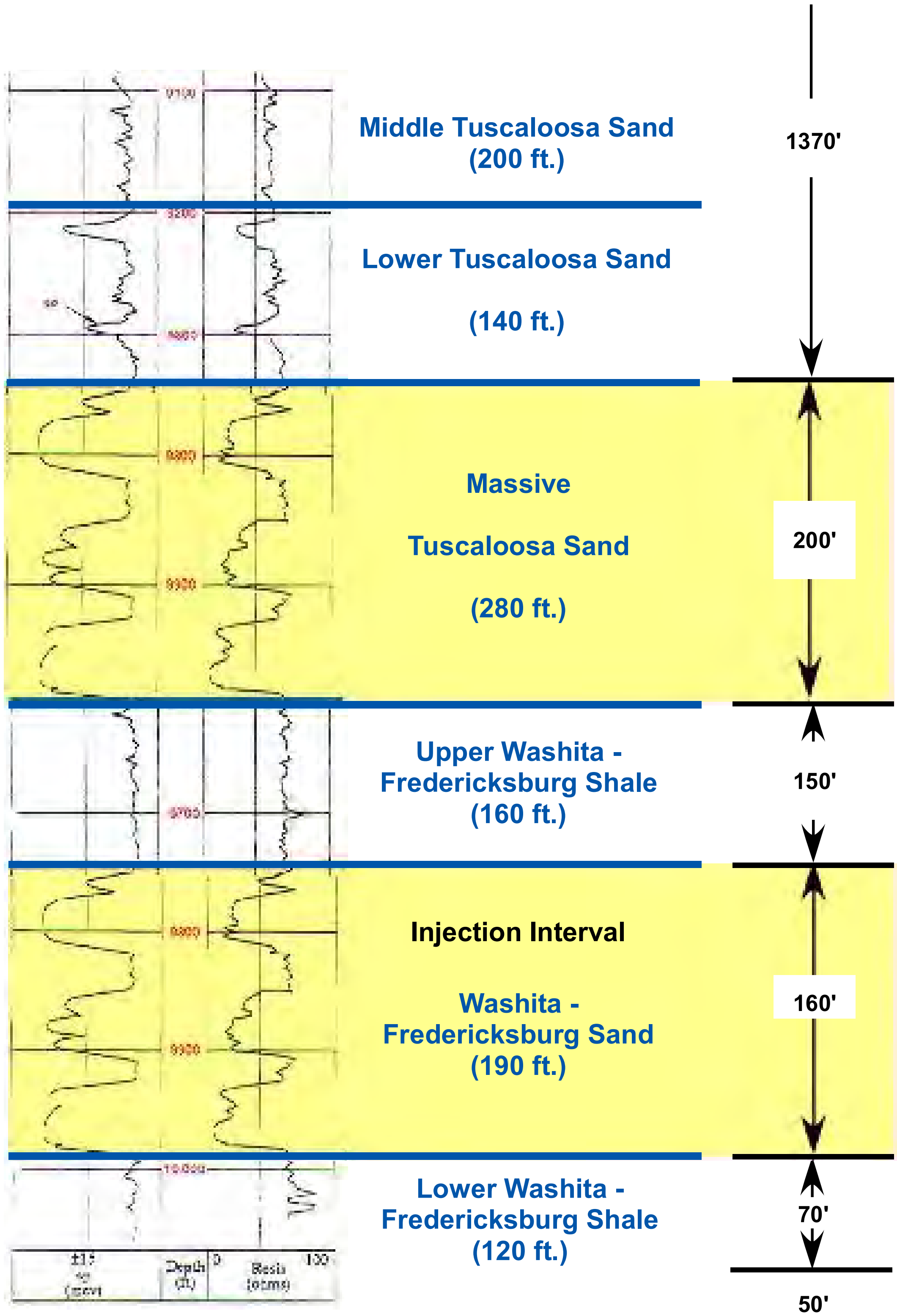

Sandia Technologies, LLC
recreated by: (ESSJ) Sandia; 12/19/06

FIGURE 3-1

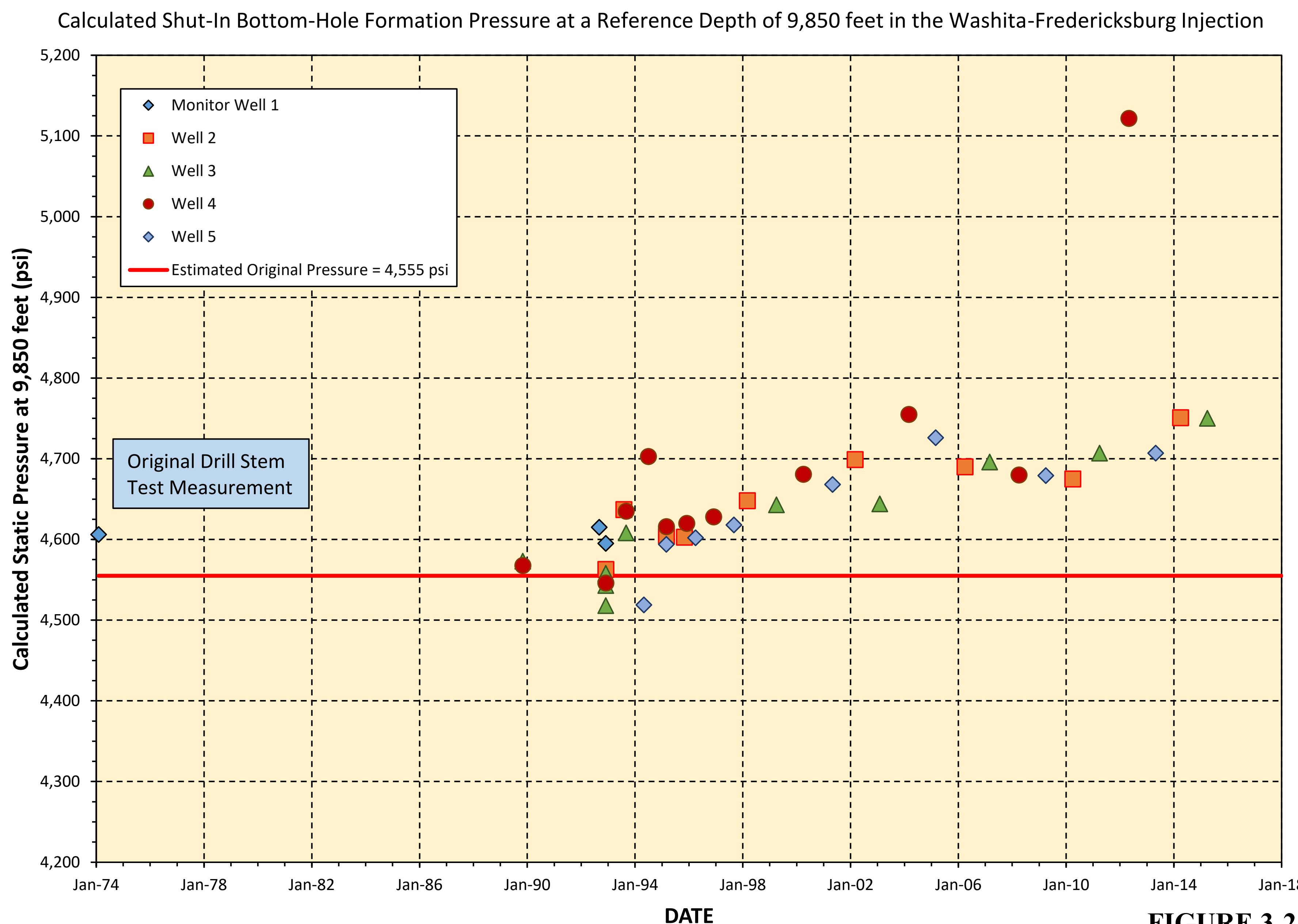

Terra Dynamics Incorporated

FIGURE 3-2

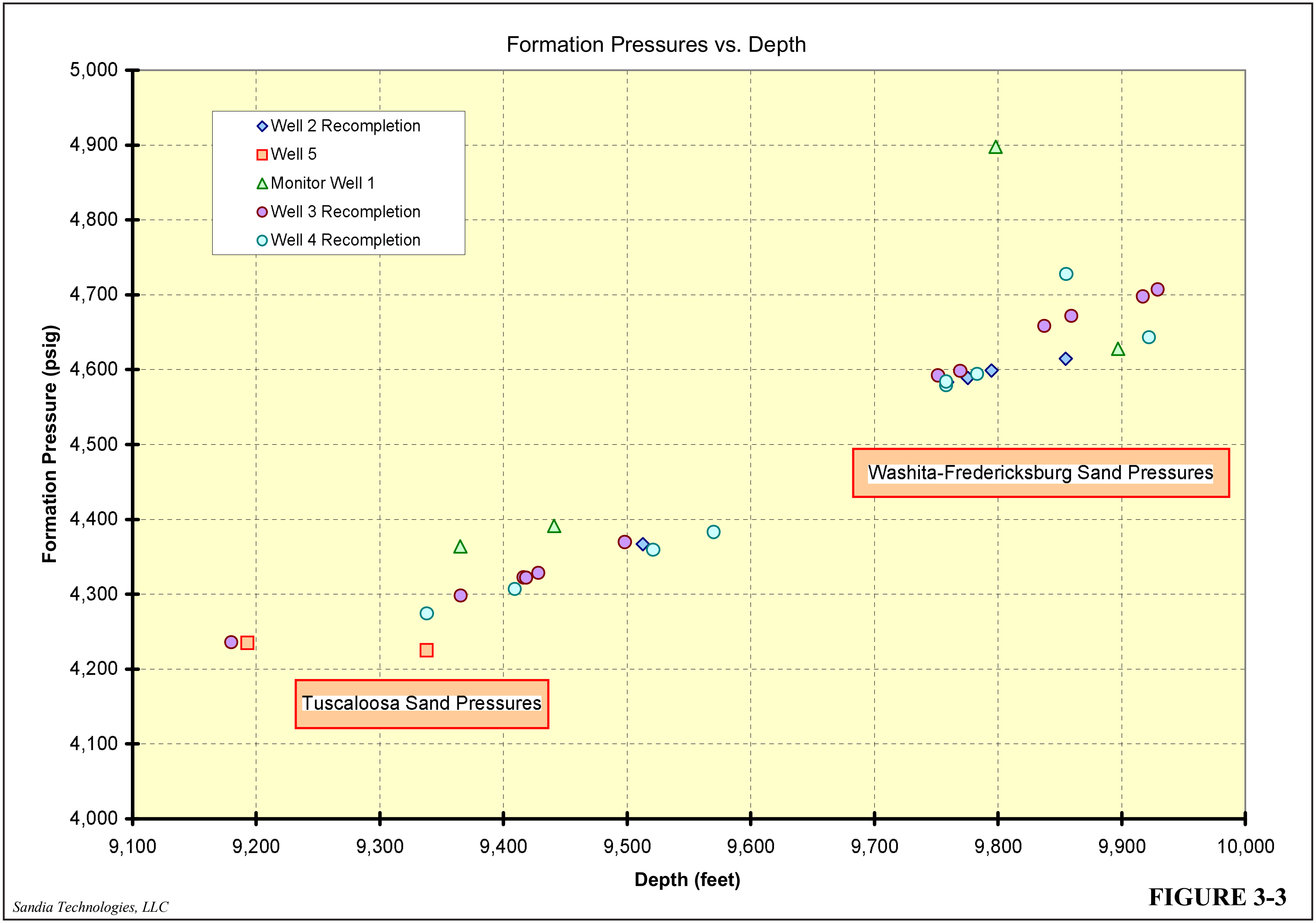

Formation Pressures vs. Depth
Well 2 Recompletion
Well 5
Monitor Well 1
Well 3 Recompletion
Well 4 Recompletion
Washita-Fredericksburg Sand Pressures
Tuscaloosa Sand Pressures
Formation Pressure (psig)
5,000
4,900
4,800
4,700
4,600
4,500
4,400
4,300
4,200
4,100
4,000
9,100
9,200
9,300
9,400
9,500
9,600
9,700
9,800
9,900
10,000
Depth (feet)
Sandia Technologies, LLC

FIGURE 3-3

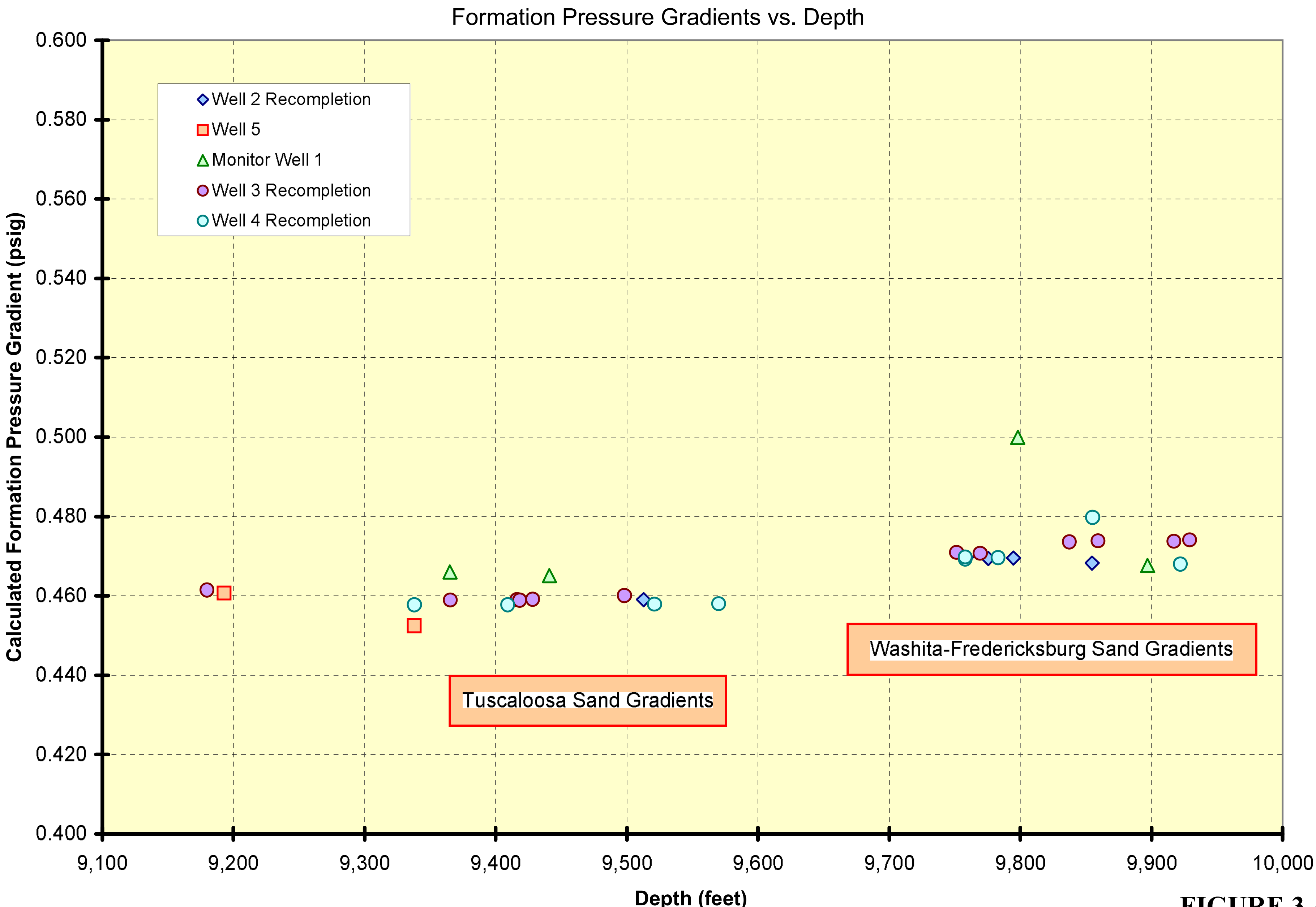

Sandia Technologies, LLC

FIGURE 3-4

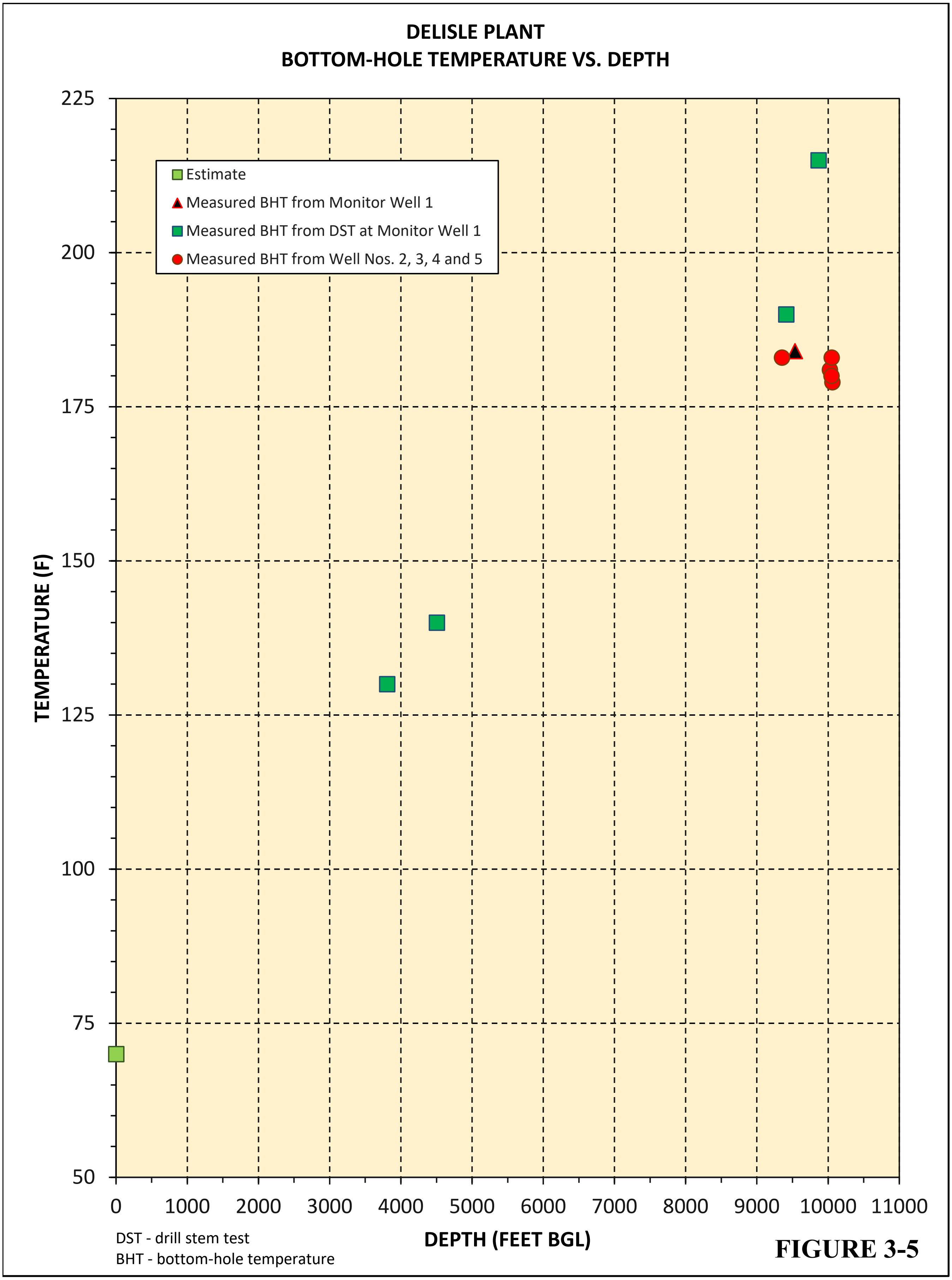
DELISLE PLANT
BOTTOM-HOLE TEMPERATURE VS. DEPTH
Estimate
Measured BHT from Monitor Well 1
Measured BHT from DST at Monitor Well 1
Measured BHT from Well Nos. 2, 3, 4 and 5
TEMPERATURE (F)
225
200
175
150
125
100
75
50
0
1000
2000
3000
4000
5000
6000
7000
8000
9000
10000
11000
DEPTH (FEET BGL)
DST - drill stem test
BHT - bottom-hole temperature

FIGURE 3-5

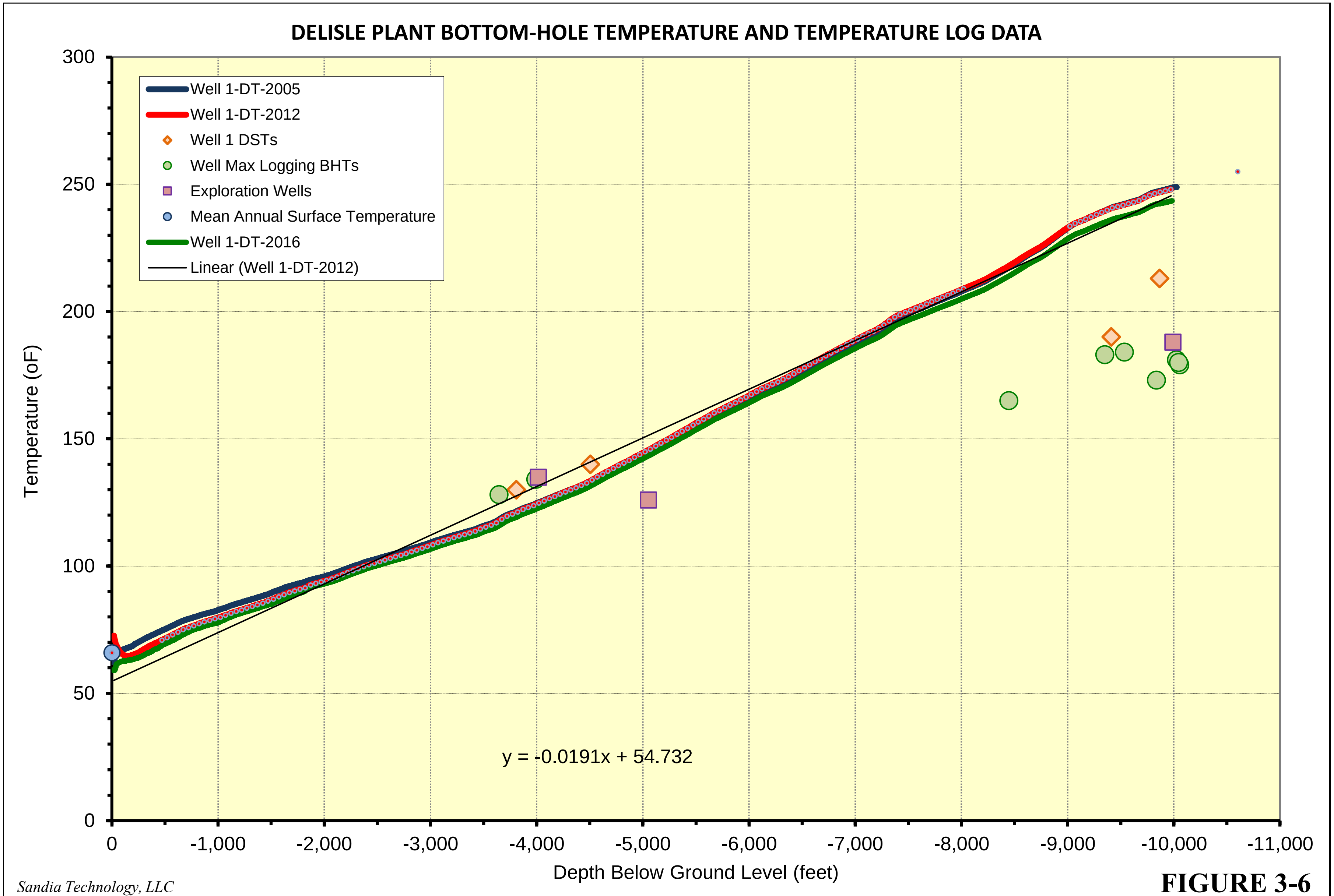
DELISLE PLANT BOTTOM-HOLE TEMPERATURE AND TEMPERATURE LOG DATA
Well 1-DT-2005
Well 1-DT-2012
Well 1 DSTs
Well Max Logging BHTs
Exploration Wells
Mean Annual Surface Temperature
Well 1-DT-2016
Linear (Well 1-DT-2012)
300
250
200
150
100
50
0
Temperature (oF)
y = -0.0191x + 54.732
0
-1,000
-2,000
-3,000
-4,000
-5,000
-6,000
-7,000
-8,000
-9,000
-10,000
-11,000
Depth Below Ground Level (feet)
Sandia Technology, LLC

FIGURE 3-6

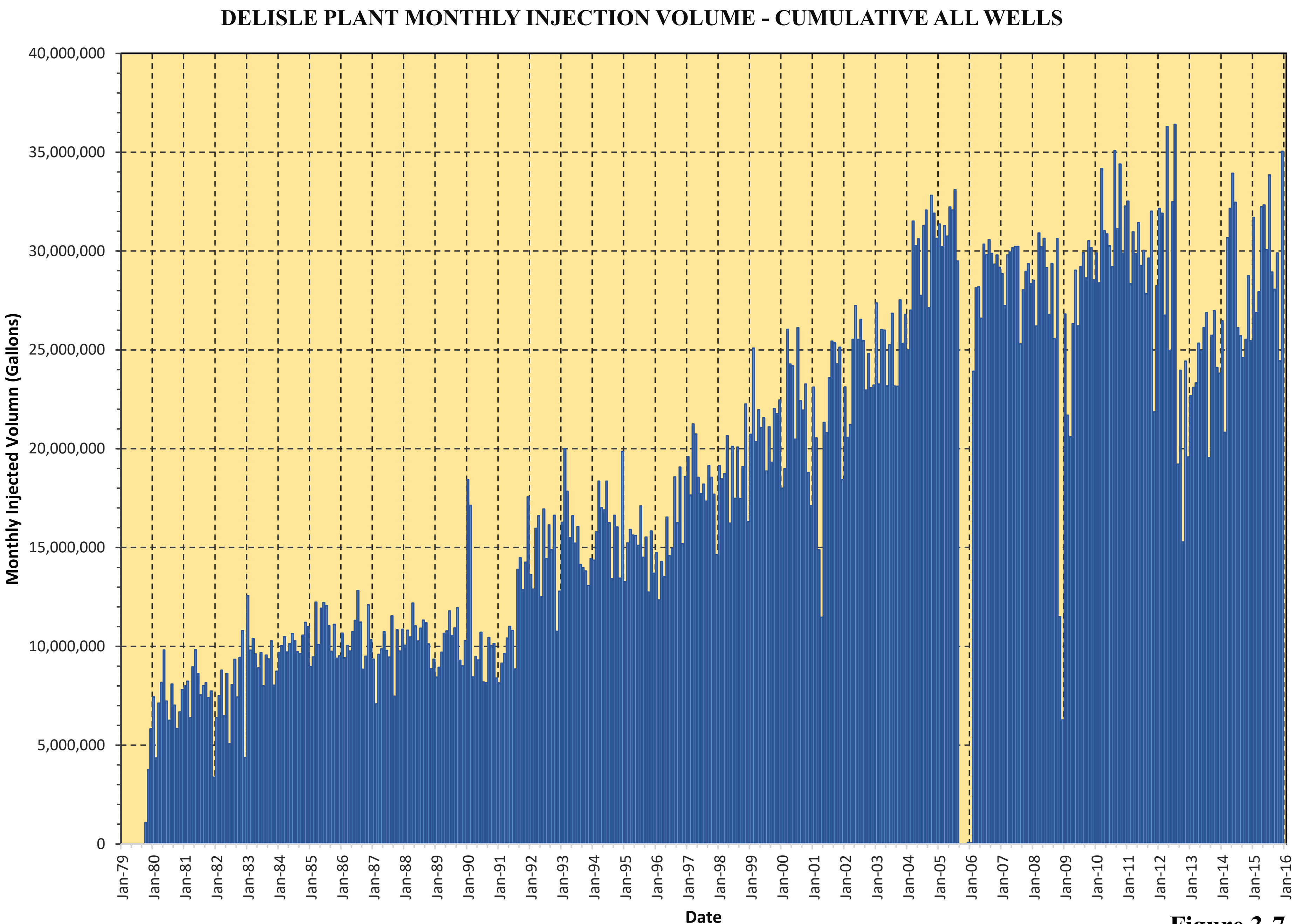

DELISLE PLANT MONTHLY INJECTION VOLUME - CUMULATIVE ALL WELLS
40,000,000
35,000,000
30,000,000
25,000,000
20,000,000
15,000,000
10,000,000
5,000,000
0
Monthly Injected Volumn (Gallons)
Jan-79
Jan-80
Jan-81
Jan-82
Jan-83
Jan-84
Jan-85
Jan-86
Jan-87
Jan-88
Jan-89
Jan-90
Jan-91
Jan-92
Jan-93
Jan-94
Jan-95
Jan-96
Jan-97
Jan-98
Jan-99
Jan-00
Jan-01
Jan-02
Jan-03
Jan-04
Jan-05
Jan-06
Jan-07
Jan-08
Jan-09
Jan-10
Jan-11
Jan-12
Jan-13
Jan-14
Jan-15
Jan-16
Date

Figure 3-7

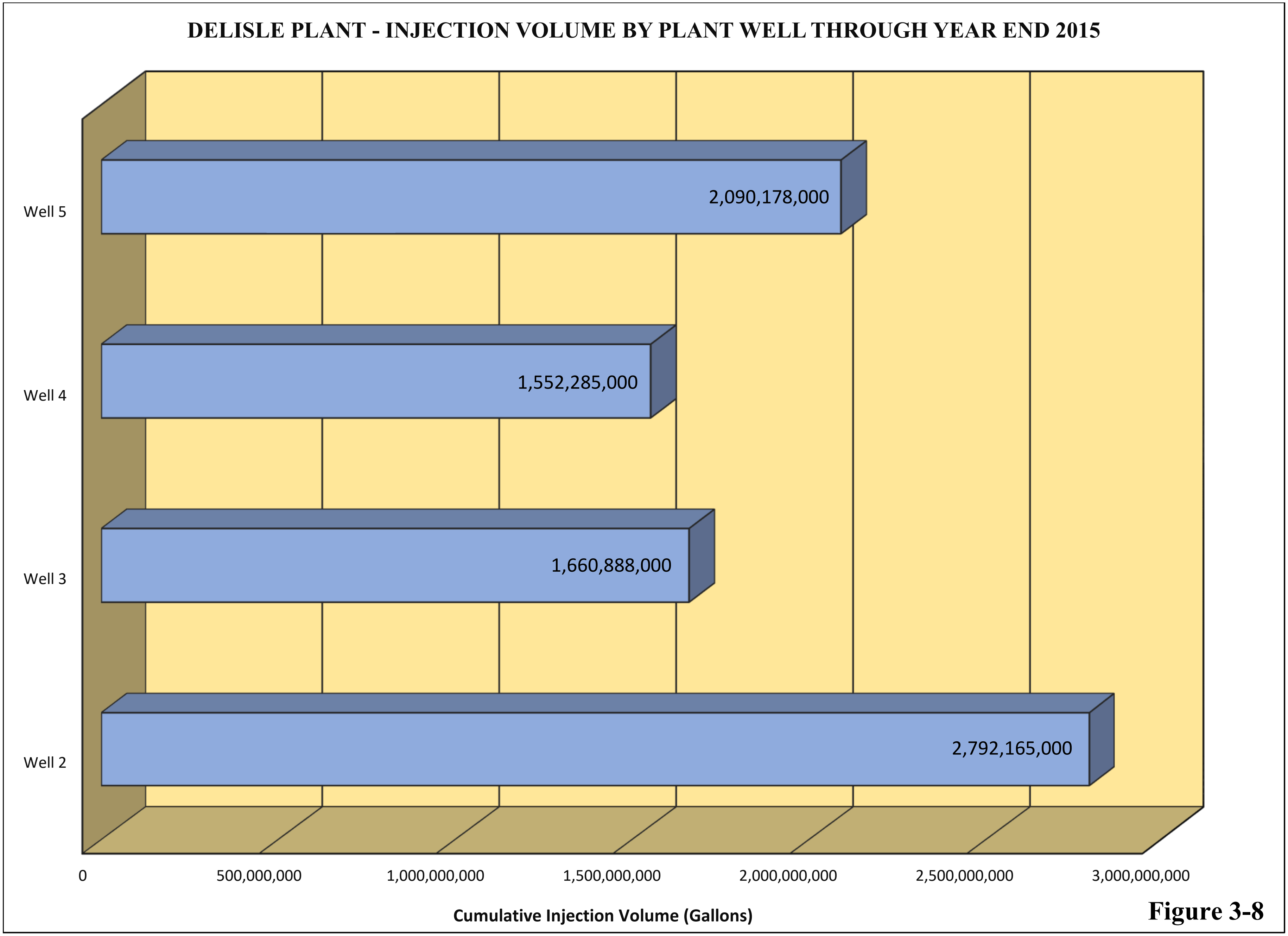
DELISLE PLANT - INJECTION VOLUME BY PLANT WELL THROUGH YEAR END 2015
Well 5
2,090,178,000
Well 4
1,552,285,000
Well 3
1,660,888,000
Well 2
2,792,165,000
0
500,000,000
1,000,000,000
1,500,000,000
2,000,000,000
2,500,000,000
3,000,000,000
Cumulative Injection Volume (Gallons)

Figure 3-8

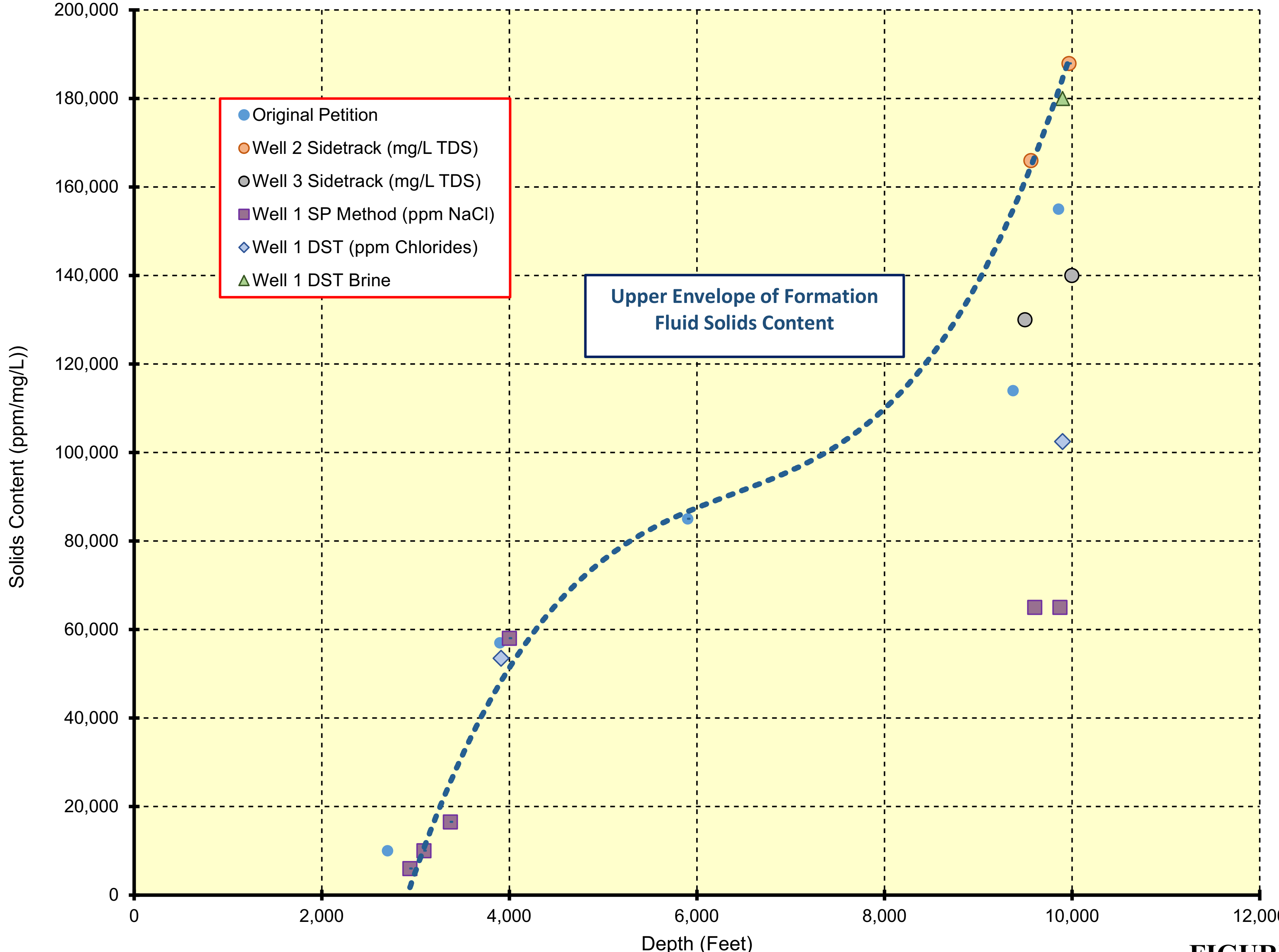

Sandia Technologies, LLC

FIGURE 3-9

Washita-Fredericksburg Injection Interval
Light Density Waste Plume Migration Model
Model and Grid Block Dimensions

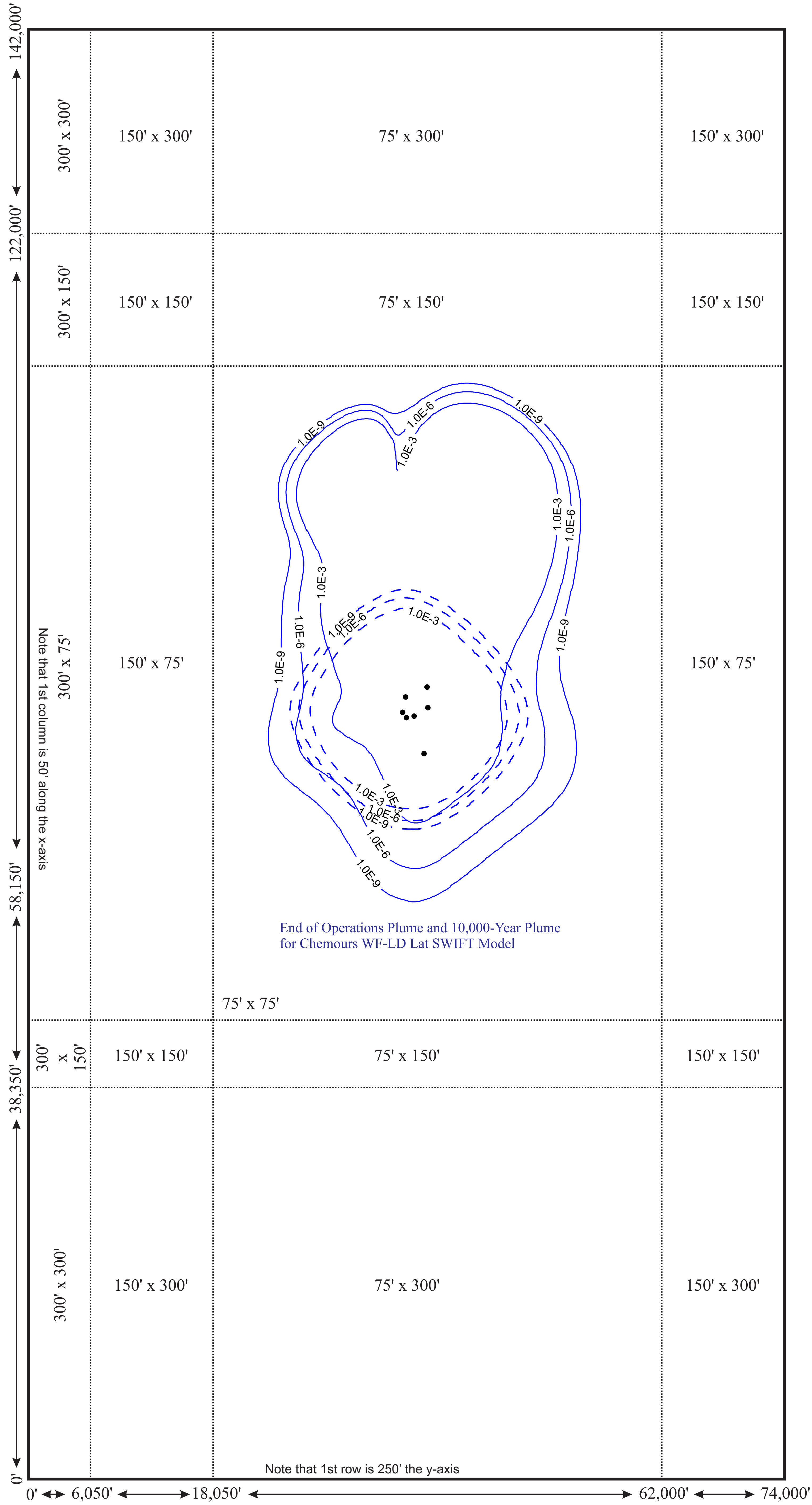

Explanation: for each dimension (ie., 150' x 300'), the first number is the grid block length along the x-axis and the second number is the grid block length along the y-axis.
X SPACING: 50' 20*300' 80*150' 586*75' 80*150'
Y SPACING: 250' 127*300' 132*150' 854*75' 132*150'

FIGURE 3-10

Tuscaloosa Massive Sand
Light Density Waste Plume Migration Model
Model and Grid Block Dimensions

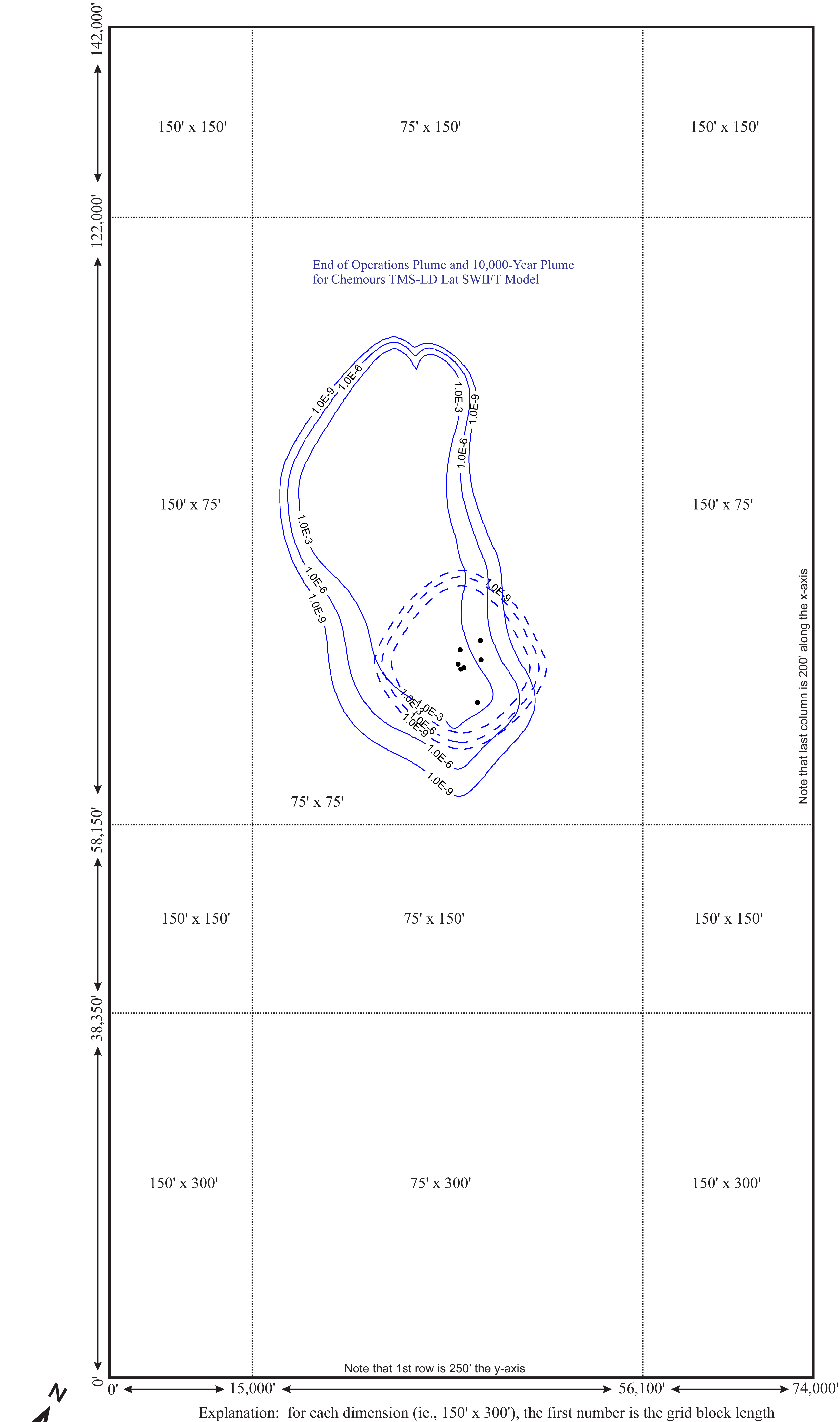

Explanation: for each dimension (ie., 150' x 300'), the first number is the grid block length along the x-axis and the second number is the grid block length along the y-axis.
X SPACING: 100*150' 548*75' 118*150' 200'
Y SPACING: 250' 127*300' 132*150' 854*75' 132*150'

FIGURE 3-11

Washita-Fredericksburg Injection Interval
High Density Waste Plume Migration Model
Model and Grid Block Dimensions

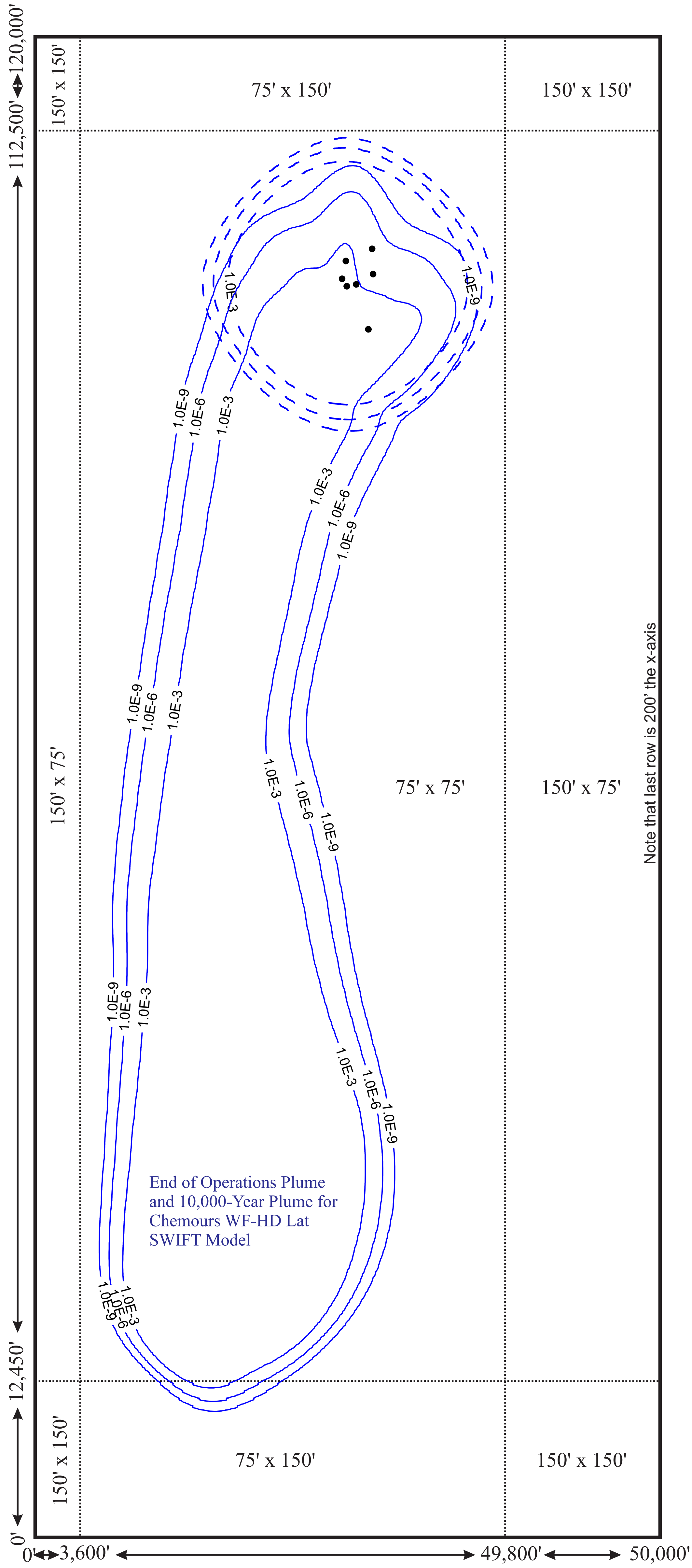

Explanation: for each dimension (ie., 150' x 150'), the first number is the grid block length along the x-axis and the second number is the grid block length along the y-axis.
X SPACING: 24*150' 454*75' 81*150' 200'
Y SPACING: 83*150' 1334*75' 50*150'

FIGURE 3-12

Tuscaloosa Massive Sand
High Density Waste Plume Migration Model
Model and Grid Block Dimensions

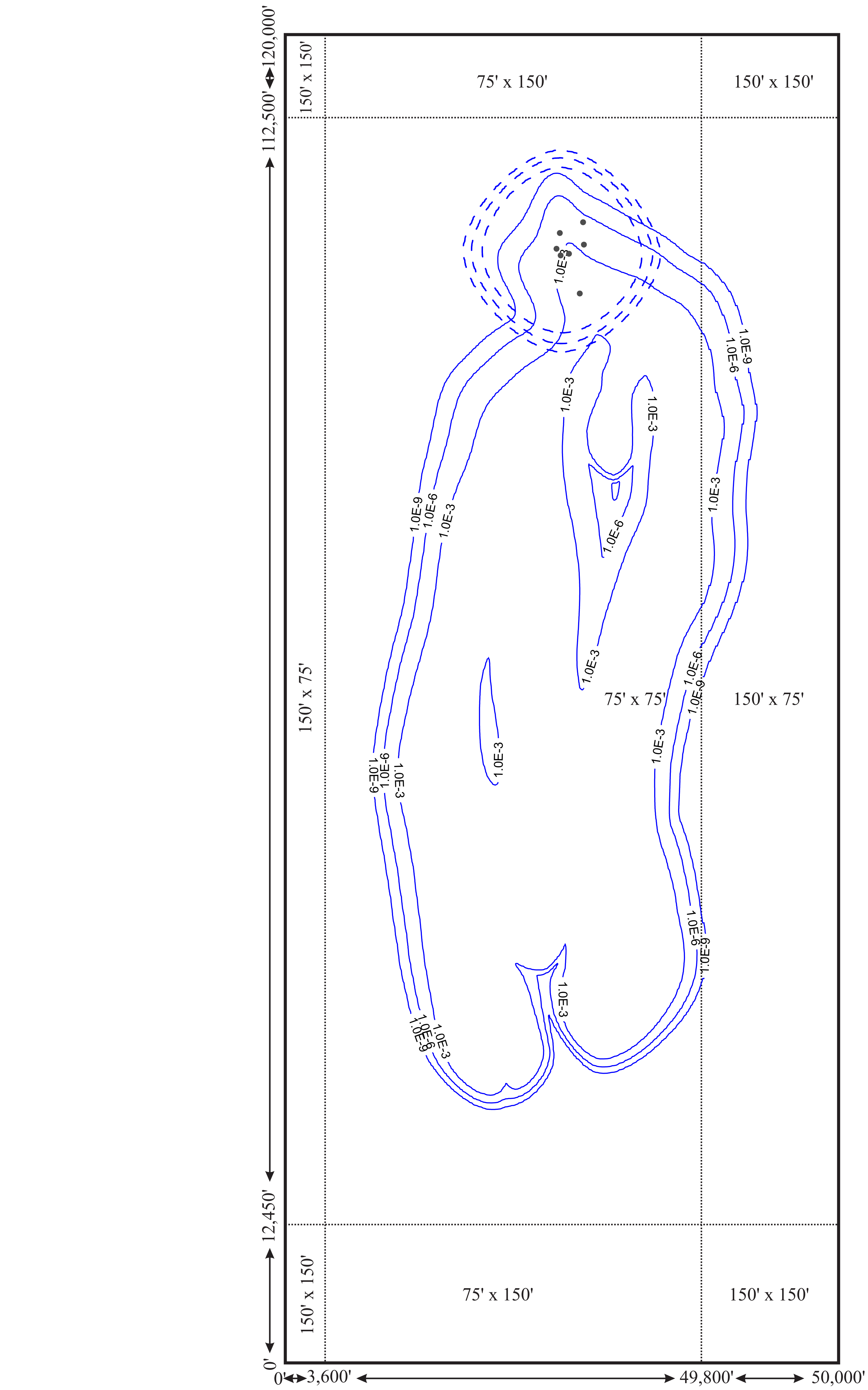

Explanation: for each dimension (ie., 150' x 300'), the first number is the grid block length along the x-axis and the second number is the grid block length along the y-axis.
X SPACING: 24*150' 454*75' 81*150' 200'
Y SPACING: 83*150' 1334*75' 50*150'

FIGURE 3-12A

Reservoir Pressurization Model
Model and Grid Block Dimensions

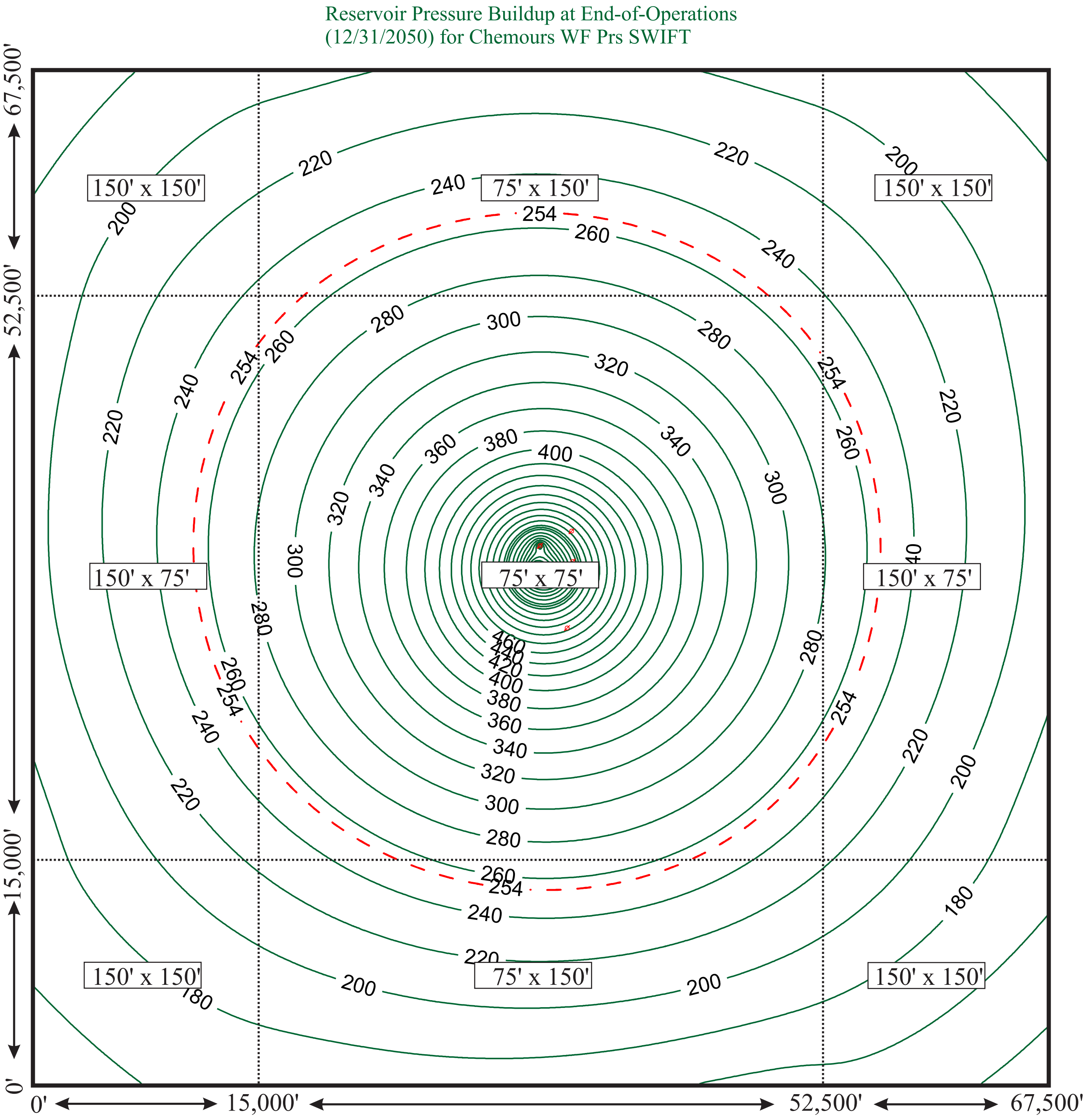

Explanation: for each dimension (ie., 150' x 300'), the first number is the grid block length along the x-axis and the second number is the grid block length along the y-axis.
X SPACING: 100*150' 500*75' 100*150'
Y SPACING: 100*150' 500*75' 100*150'

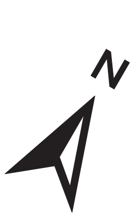

FIGURE 3-13

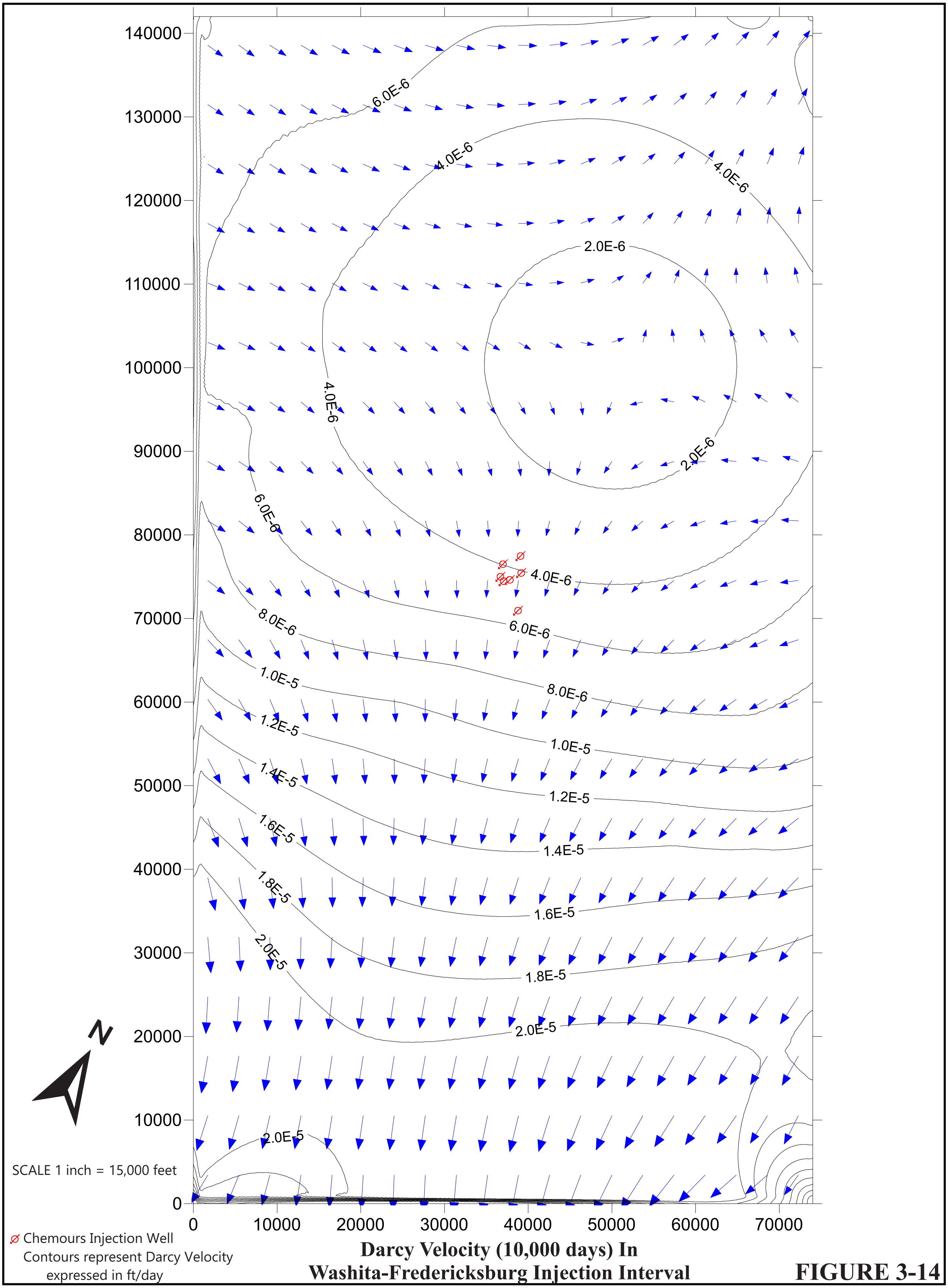

Darcy Velocity (10,000 days) In
Washita-Fredericksburg Injection Interval

FIGURE 3-14

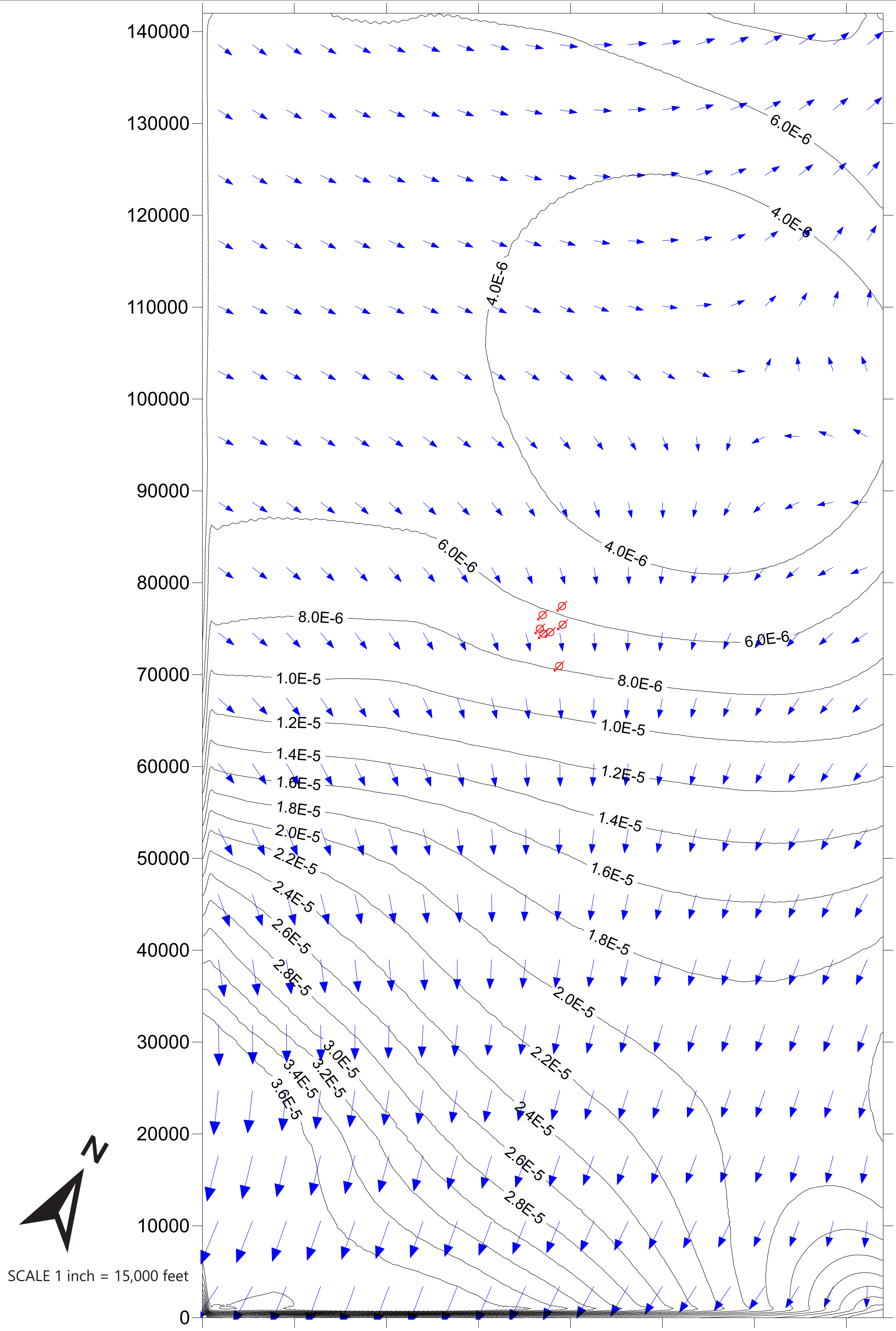

Chemours Injection Well
Contours represent Darcy Velocity expressed in ft/day

Darcy Velocity (10,000 days) In Tuscaloosa Massive Sand

FIGURE 3-15

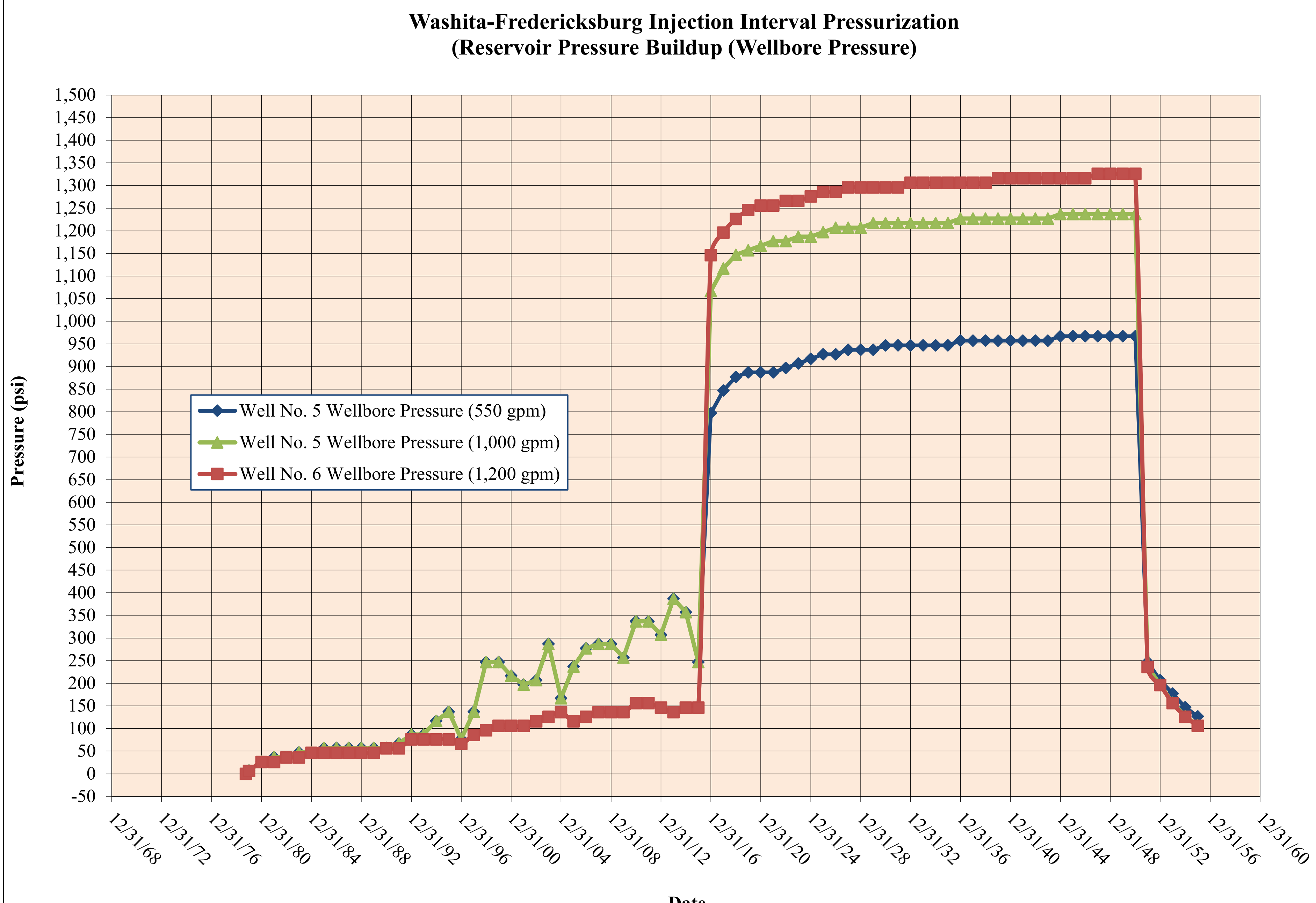
Washita-Fredericksburg Injection Interval Pressurization
(Reservoir Pressure Buildup (Wellbore Pressure)
Pressure (psi)
1,500
1,450
1,400
1,350
1,300
1,250
1,200
1,150
1,100
1,050
1,000
950
900
850
800
750
700
650
600
550
500
450
400
350
300
250
200
150
100
50
0
-50
Well No. 5 Wellbore Pressure (550 gpm)
Well No. 5 Wellbore Pressure (1,000 gpm)
Well No. 6 Wellbore Pressure (1,200 gpm)
12/31/68
12/31/72
12/31/76
12/31/80
12/31/84
12/31/88
12/31/92
12/31/96
12/31/00
12/31/04
12/31/08
12/31/12
12/31/16
12/31/20
12/31/24
12/31/28
12/31/32
12/31/36
12/31/40
12/31/44
12/31/48
12/31/52
12/31/56
12/31/60
Date

FIGURE 3-16

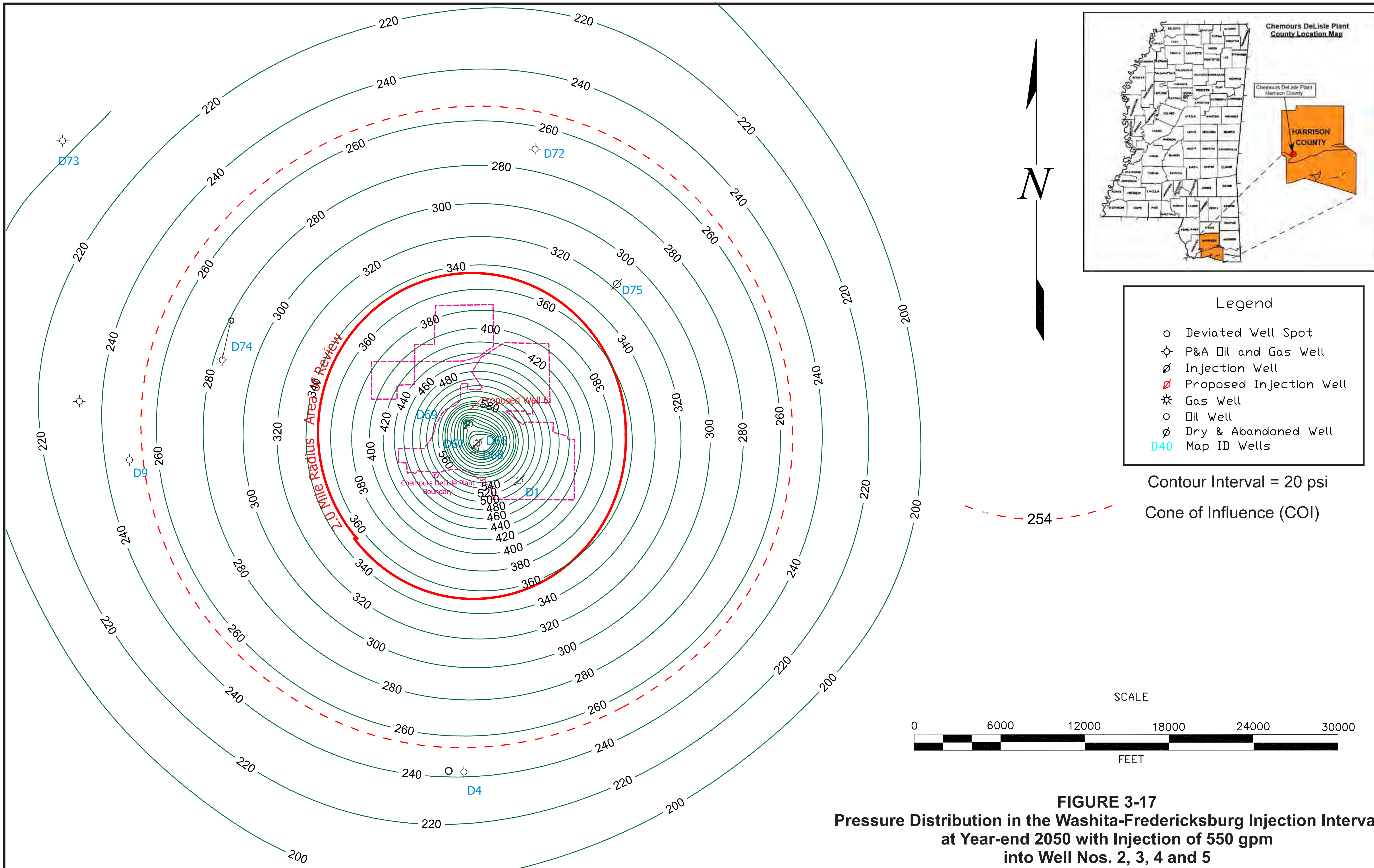

FIGURE 3-17
Pressure Distribution in the Washita-Fredericksburg Injection Interval at Year-end 2050 with Injection of 550 gpm into Well Nos. 2, 3, 4 and 5

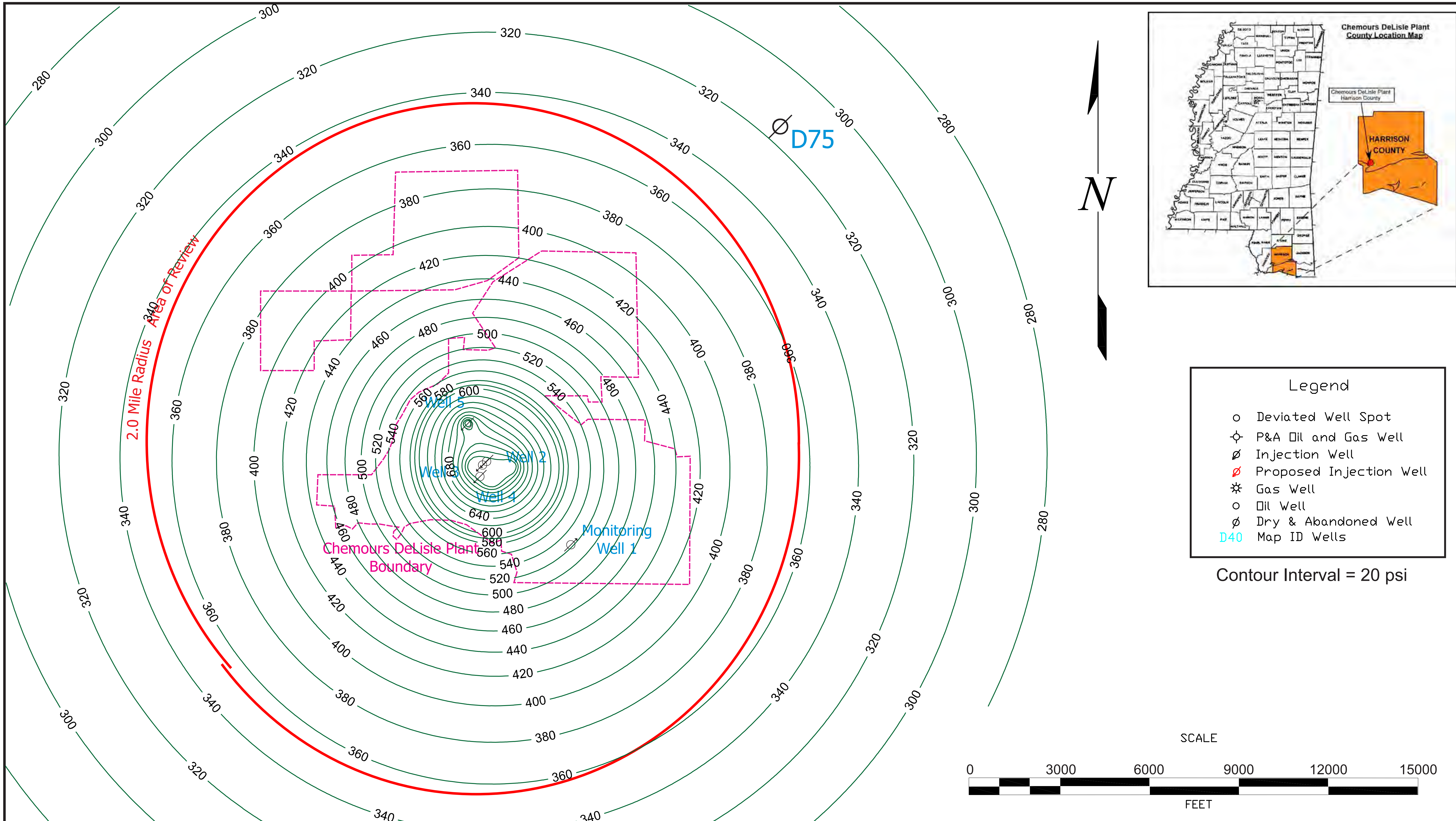

FIGURE 3-17A
Pressure Distribution in the Washita-Fredericksburg Injection Interval at Year-end 2050 with Injection of 550 gpm into Well Nos. 2, 3, 4 and 5 (Expanded)

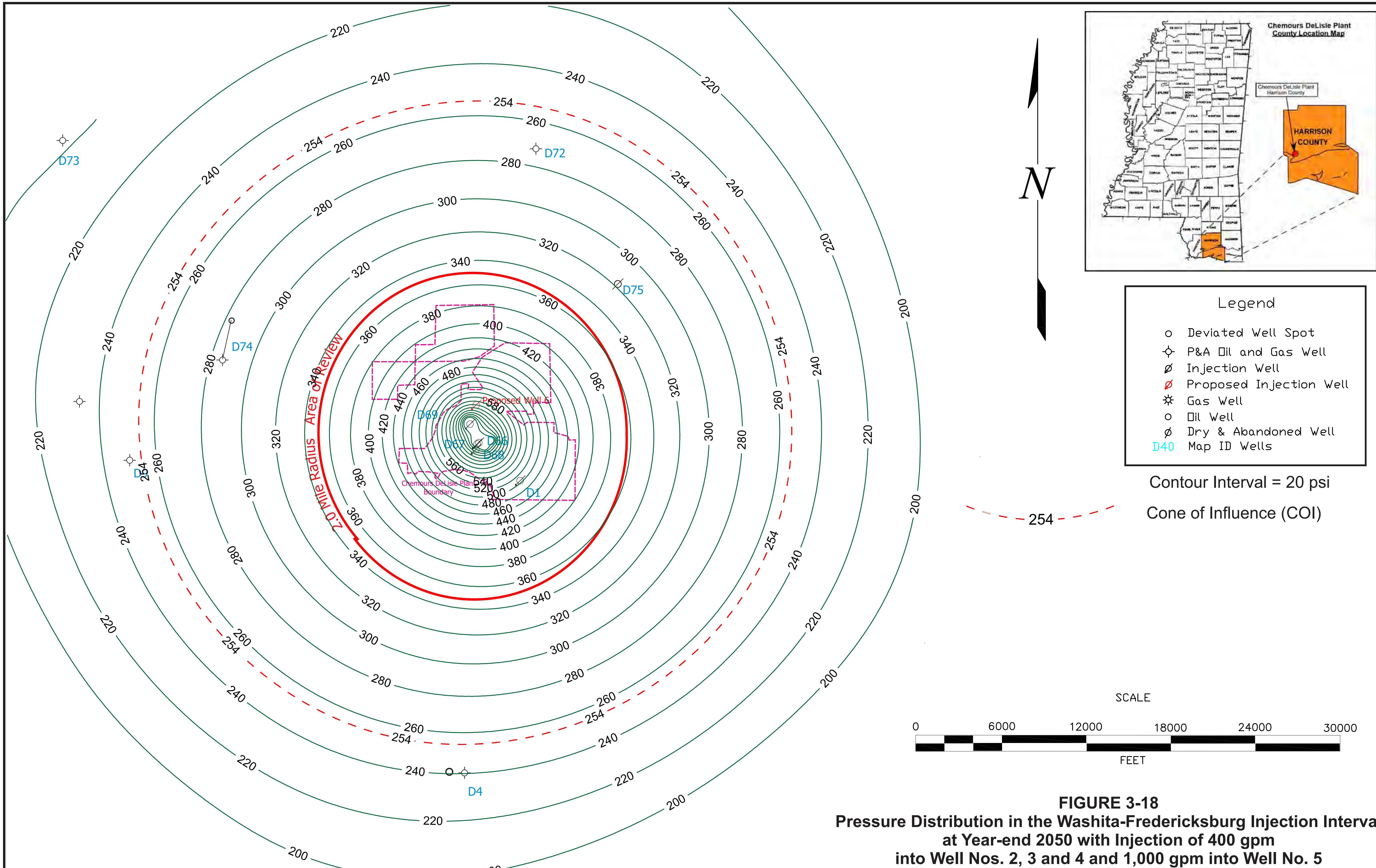

FIGURE 3-18

Pressure Distribution in the Washita-Fredericksburg Injection Interval at Year-end 2050 with Injection of 400 gpm into Well Nos. 2, 3 and 4 and 1,000 gpm into Well No. 5

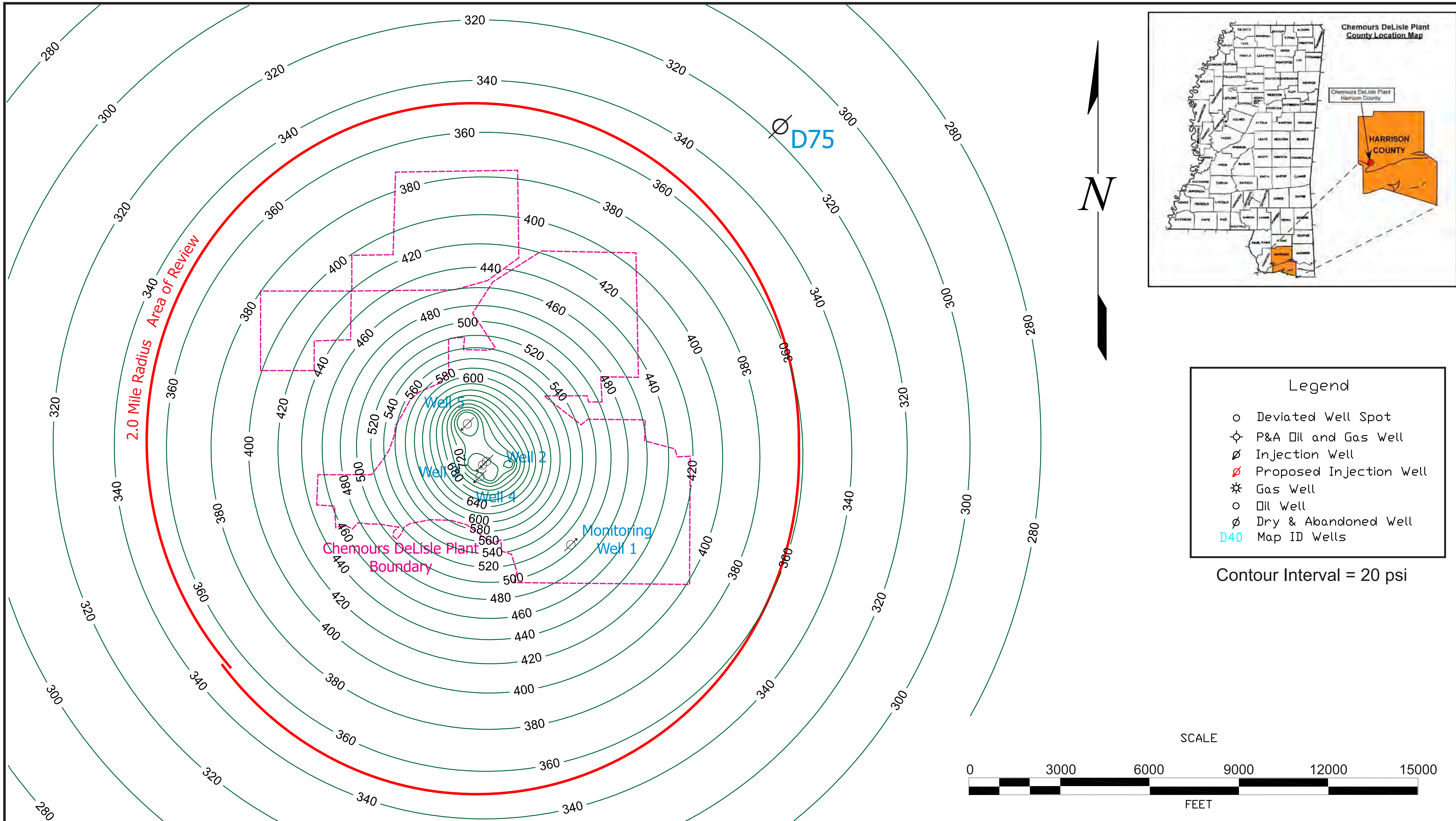

FIGURE 3-18A
Pressure Distribution in the Washita-Fredericksburg Injection Interval at Year-end 2050 with Injection of 400 gpm into Well Nos. 2, 3 and 4 and 1,000 gpm into Well No. 5 (Expanded)

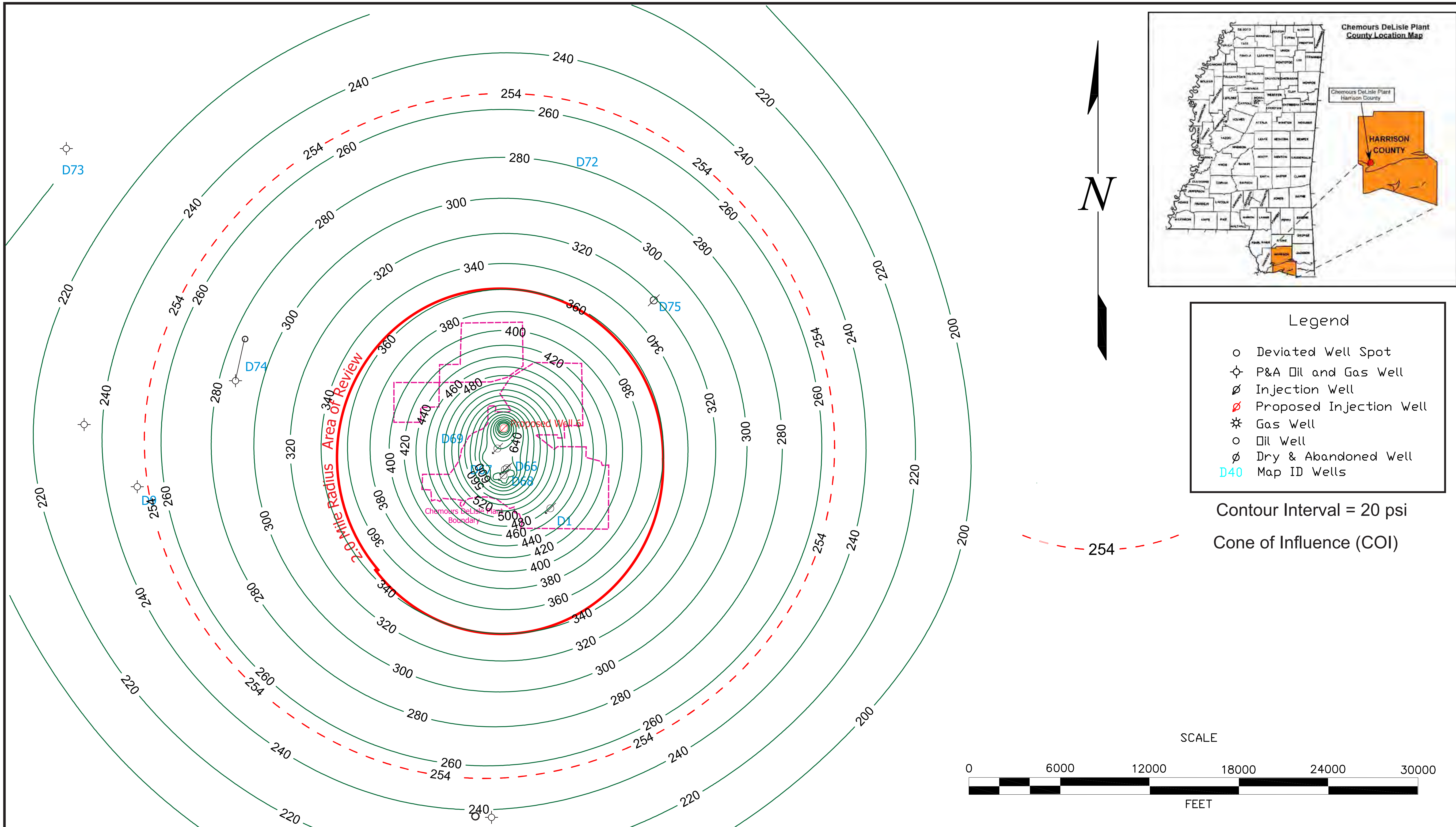

FIGURE 3-19
Pressure Distribution in the Washita-Fredericksburg Injection Interval at Year-end 2050 with Injection of 250 gpm into Well Nos. 2, 3, 4 and 5 and 1,200 gpm into Well No. 6

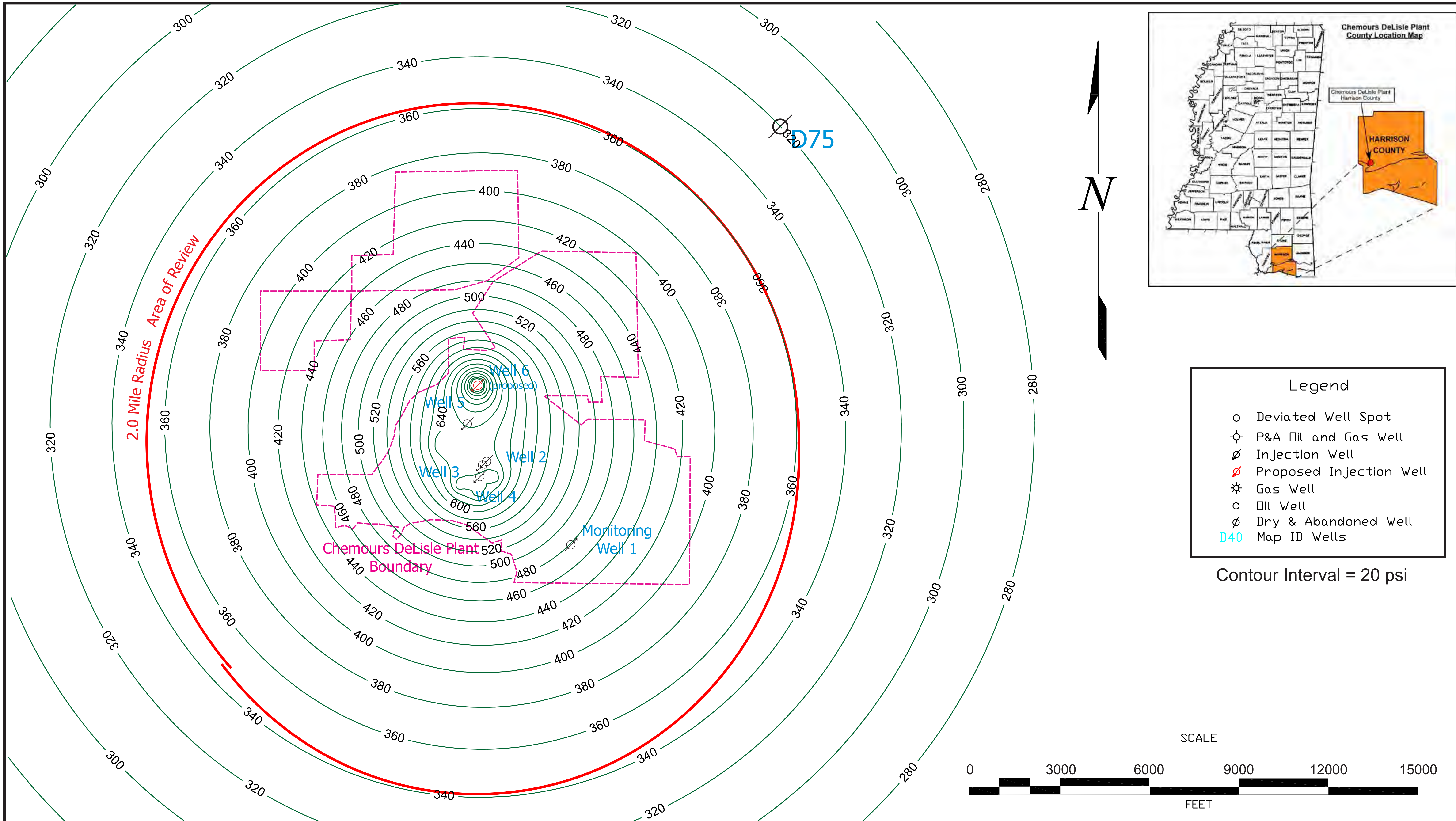

FIGURE 3-19A
Pressure Distribution in the Washita-Fredericksburg Injection Interval at Year-end 2050 with Injection of 250 gpm into Well Nos. 2, 3, 4 and 5 and 1,200 gpm into Well No. 6 (Expanded)

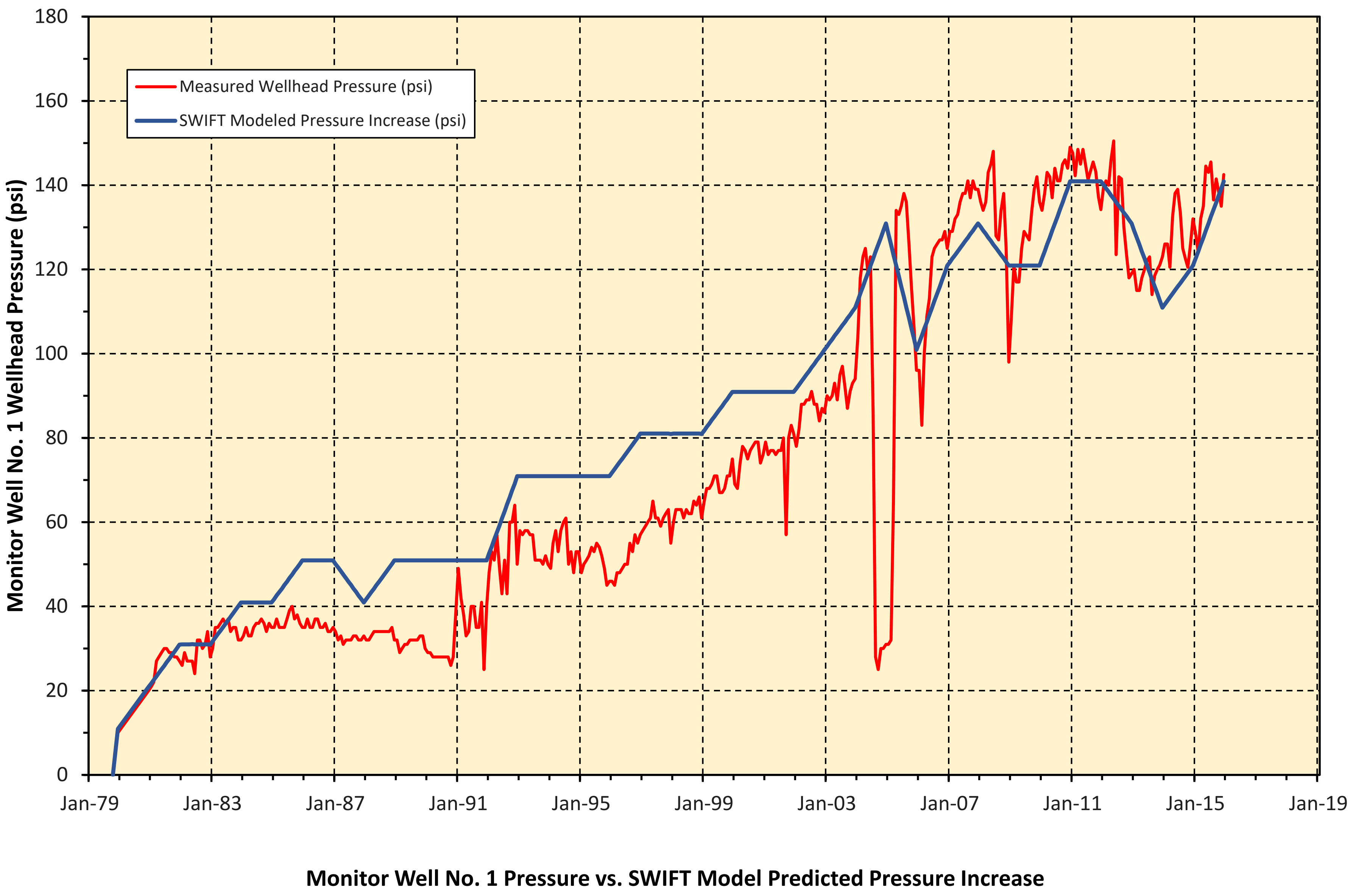
Measured Wellhead Pressure (psi)
SWIFT Modeled Pressure Increase (psi)
Monitor Well No. 1 Wellhead Pressure (psi)
180
160
140
120
100
80
60
40
20
0
Jan-79
Jan-83
Jan-87
Jan-91
Jan-95
Jan-99
Jan-03
Jan-07
Jan-11
Jan-15
Jan-19
Monitor Well No. 1 Pressure vs. SWIFT Model Predicted Pressure Increase

FIGURE 3-19B

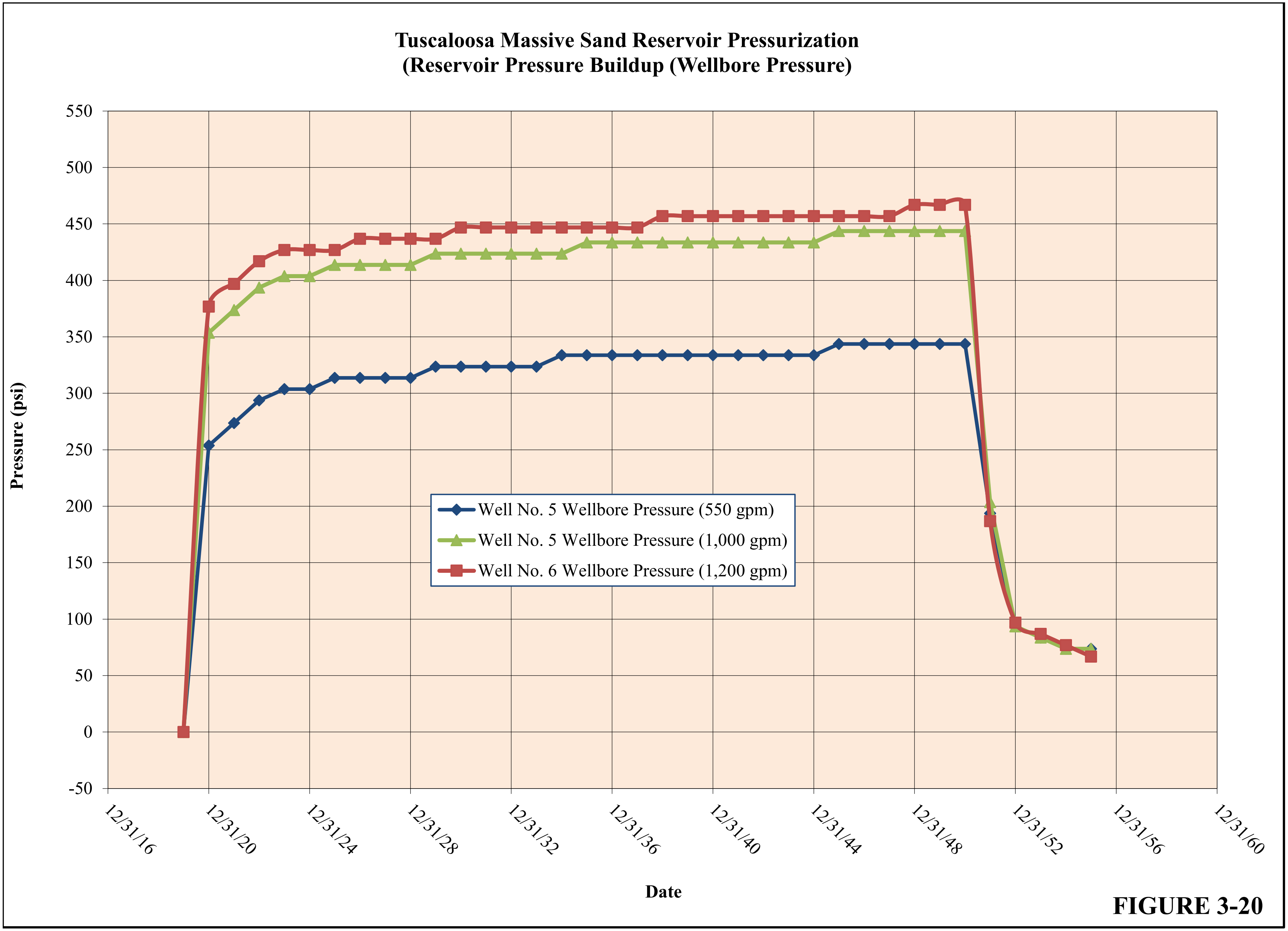

Tuscaloosa Massive Sand Reservoir Pressurization
(Reservoir Pressure Buildup (Wellbore Pressure)
Pressure (psi)
550
500
450
400
350
300
250
200
150
100
50
0
-50
Well No. 5 Wellbore Pressure (550 gpm)
Well No. 5 Wellbore Pressure (1,000 gpm)
Well No. 6 Wellbore Pressure (1,200 gpm)
12/31/16
12/31/20
12/31/24
12/31/28
12/31/32
12/31/36
12/31/40
12/31/44
12/31/48
12/31/52
12/31/56
12/31/60
Date

FIGURE 3-20

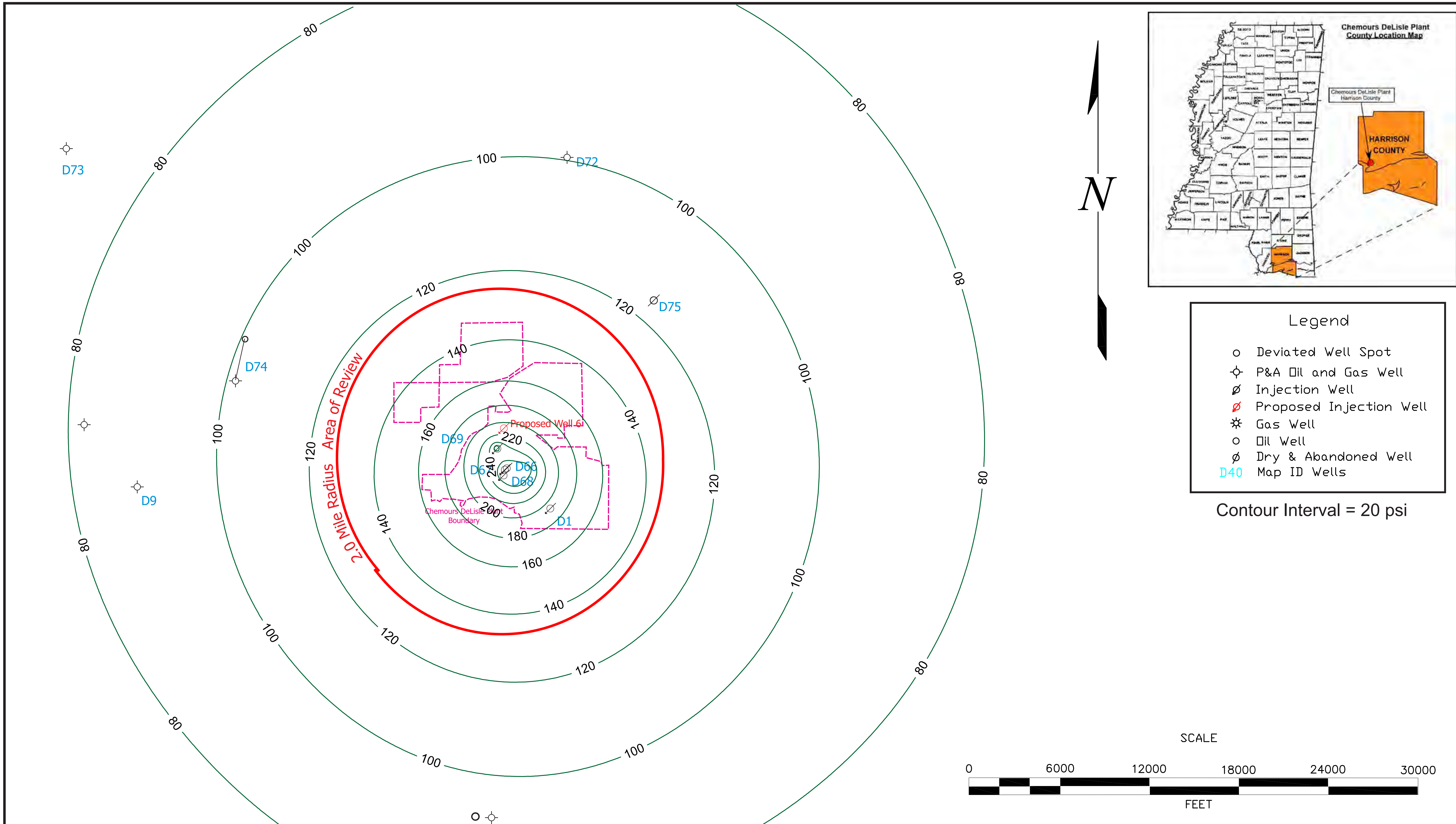

FIGURE 3-21
Pressure Distribution in the Tuscaloosa Massive Sand at Year-end 2050 with Injection of 550 gpm into Well Nos. 2, 3, 4 and 5

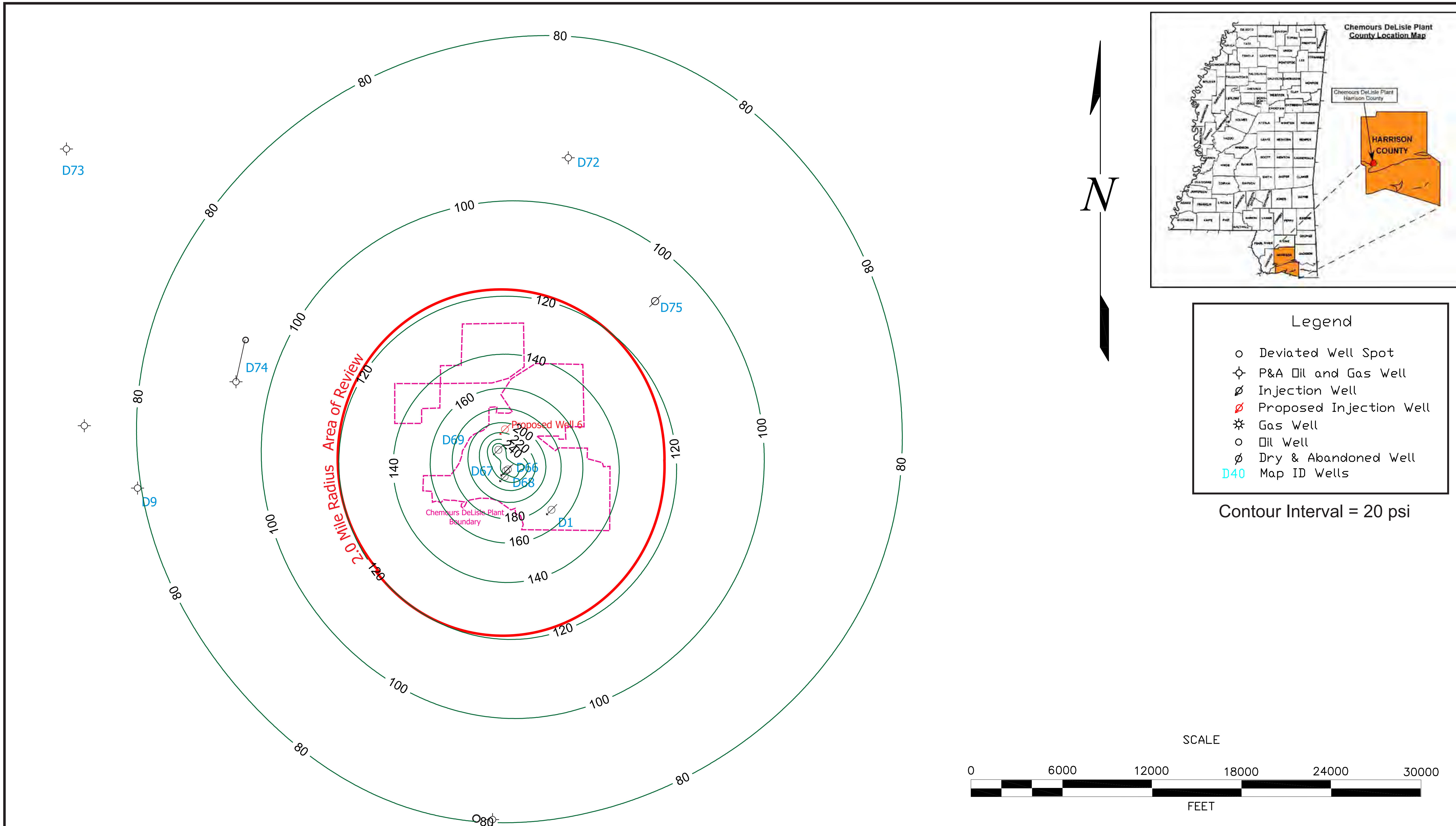

FIGURE 3-22
Pressure Distribution in the Tuscaloosa Massive Sand at Year-end 2050 with Injection of 400 gpm into Well Nos. 2, 3 and 4 and 1,000 gpm into Well No. 5

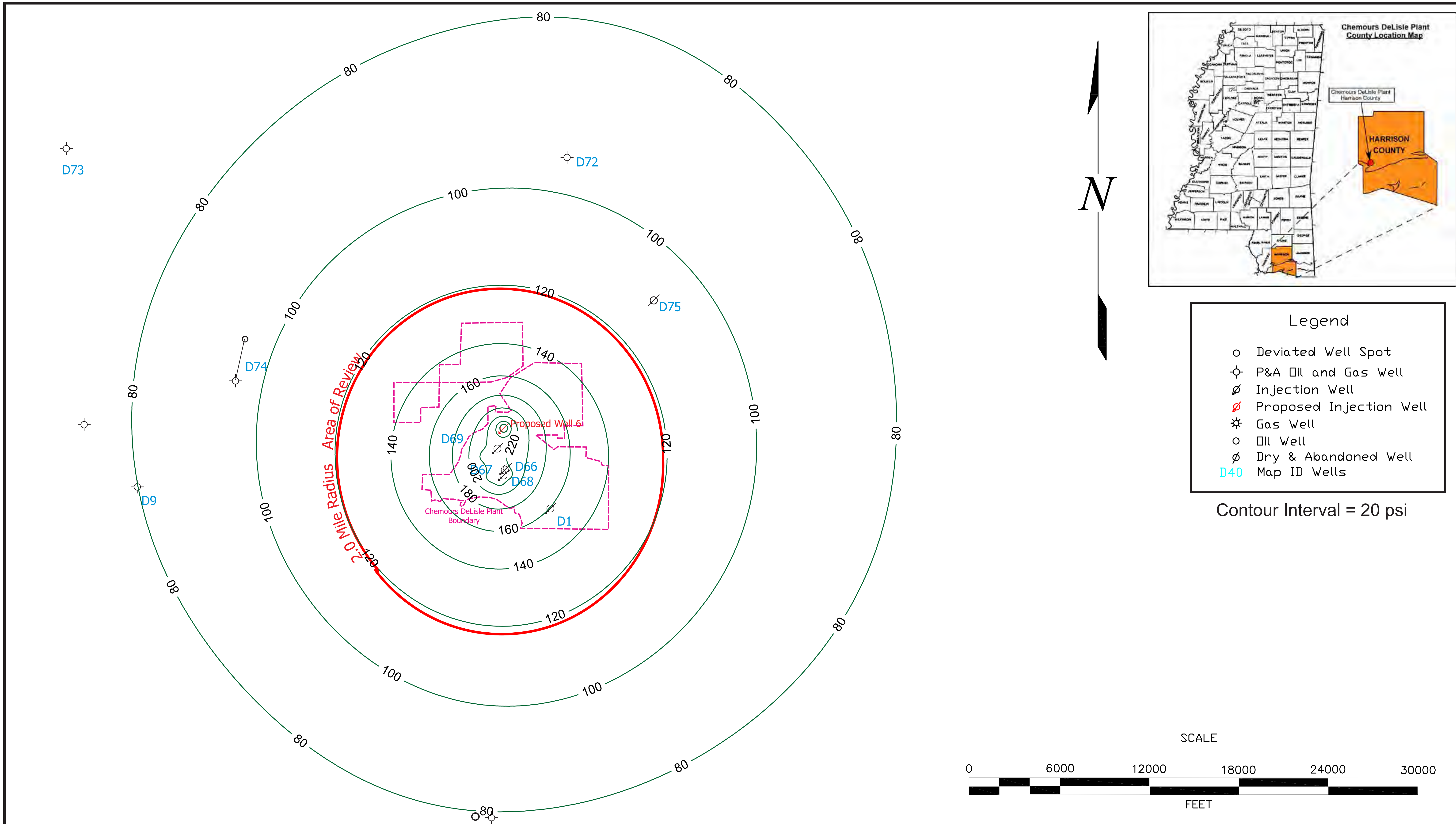

FIGURE 3-23
Pressure Distribution in the Tuscaloosa Massive Sand at Year-end 2050 with Injection of 250 gpm into Well Nos. 2, 3, 4 and 5 and 1,200 gpm into Well No. 6

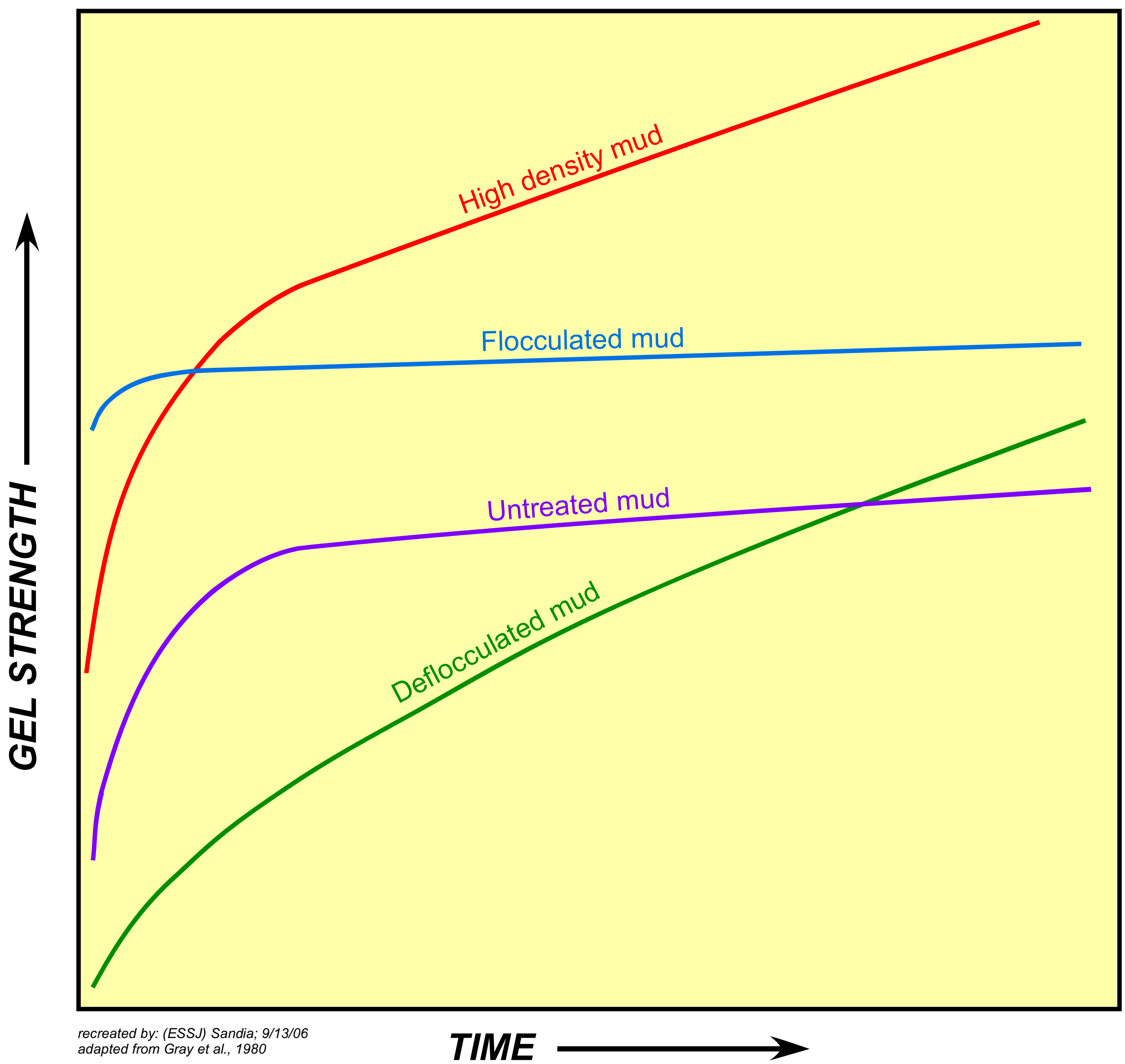

Gel Strength Increase Through Time (Adapted from: Gray et al., 1980)

PLATES

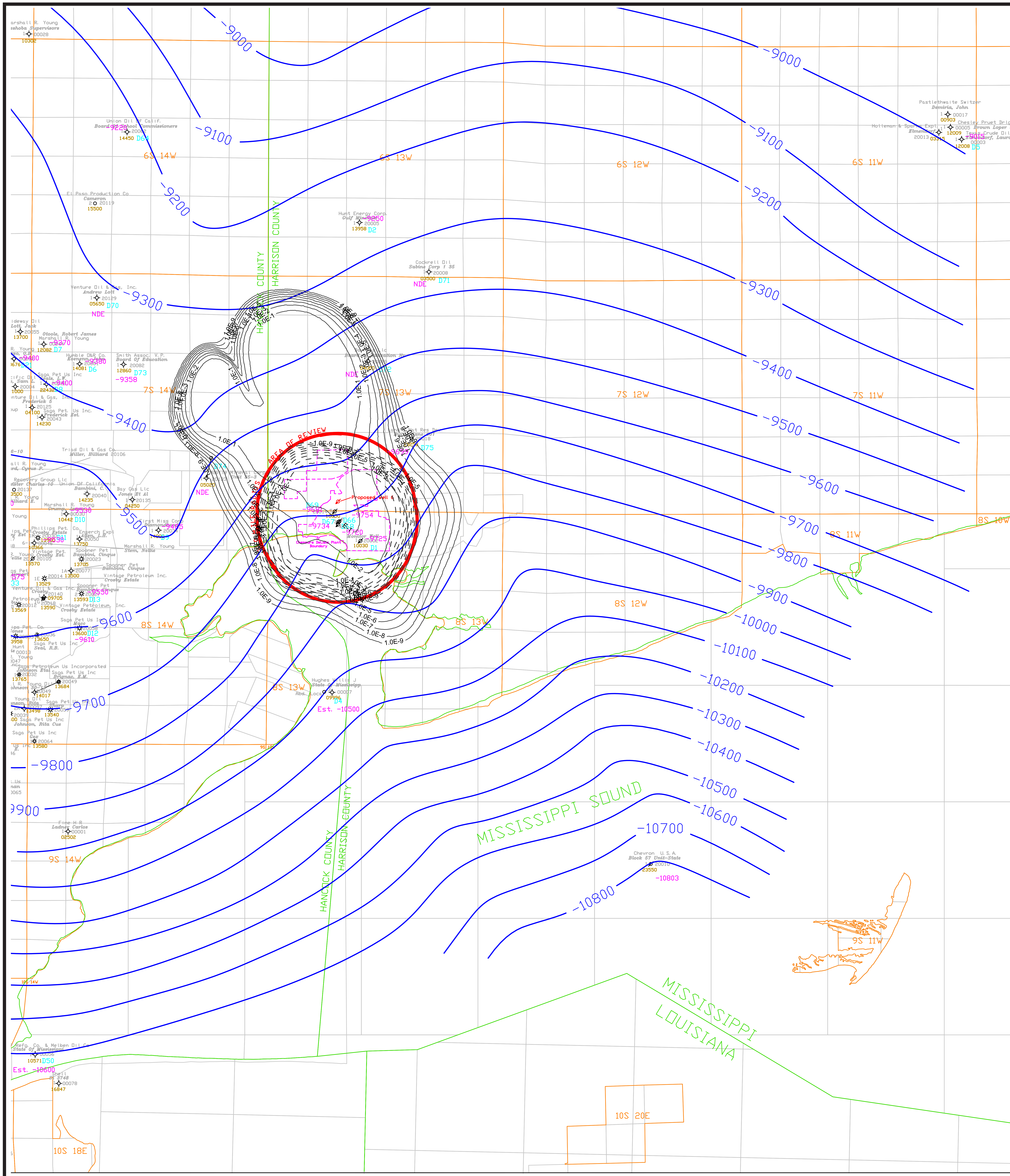

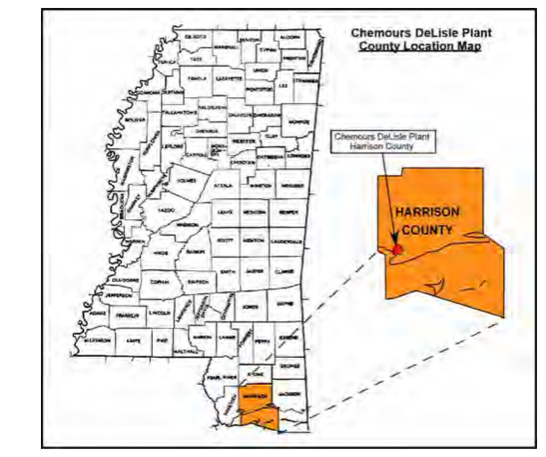

Legend

○	Deviated Well Spot
⌖	P&A Oil and Gas Well
ø	Injection Well
ø	Proposed Injection Well
☼	Gas Well
○	Oil Well
ø	Dry & Abandoned Well
-4650	Post Numbers
D40	Map ID Wells
11600	Total Depth
31290	API Number
NDE	Log Not Deep Enough
NL	No Log

- - - - - - End of Operations (12/31/2050) Waste Plume

———— 10,000-Year Waste Plume

Waste Plume Contours Represent Magnitude of Reduction In Initial Waste Constituent Concentration

SCALE

0 6000 12000 18000 24000 30000

FEET

PLATE 3-1

Washita-Fredericksburg Injection Interval Structure Map Showing Location of Light-Density Plume at End of Operations (2050) and After 10,000 Years (Chemours WF-LD Lat SWIFT MODEL)

BASE MAP FROM:

Chemours™

The Chemours Company FC, LLC
DeLisle Plant
Pass Christian, MS

Appendix 2-11: Top of Washita-Fredericksburg Sand (Injection Interval) Structure Map

Contour Interval = 100'

Base Map Prepared & compiled from Tobin International, Ltd. digital Map Data

Compiled & Drafted by: (ESSJ, WGK) Sandia	Scale: 1" = 6000'	Date: 3/2016

GEOSTOCK SANDIA ENTREPOSE

6731 Theall Road Houston, Tx 77066 USA • Tel: (832) 286 0471 • Fax: (832) 286 0477
Web : www.geostocksandia.com

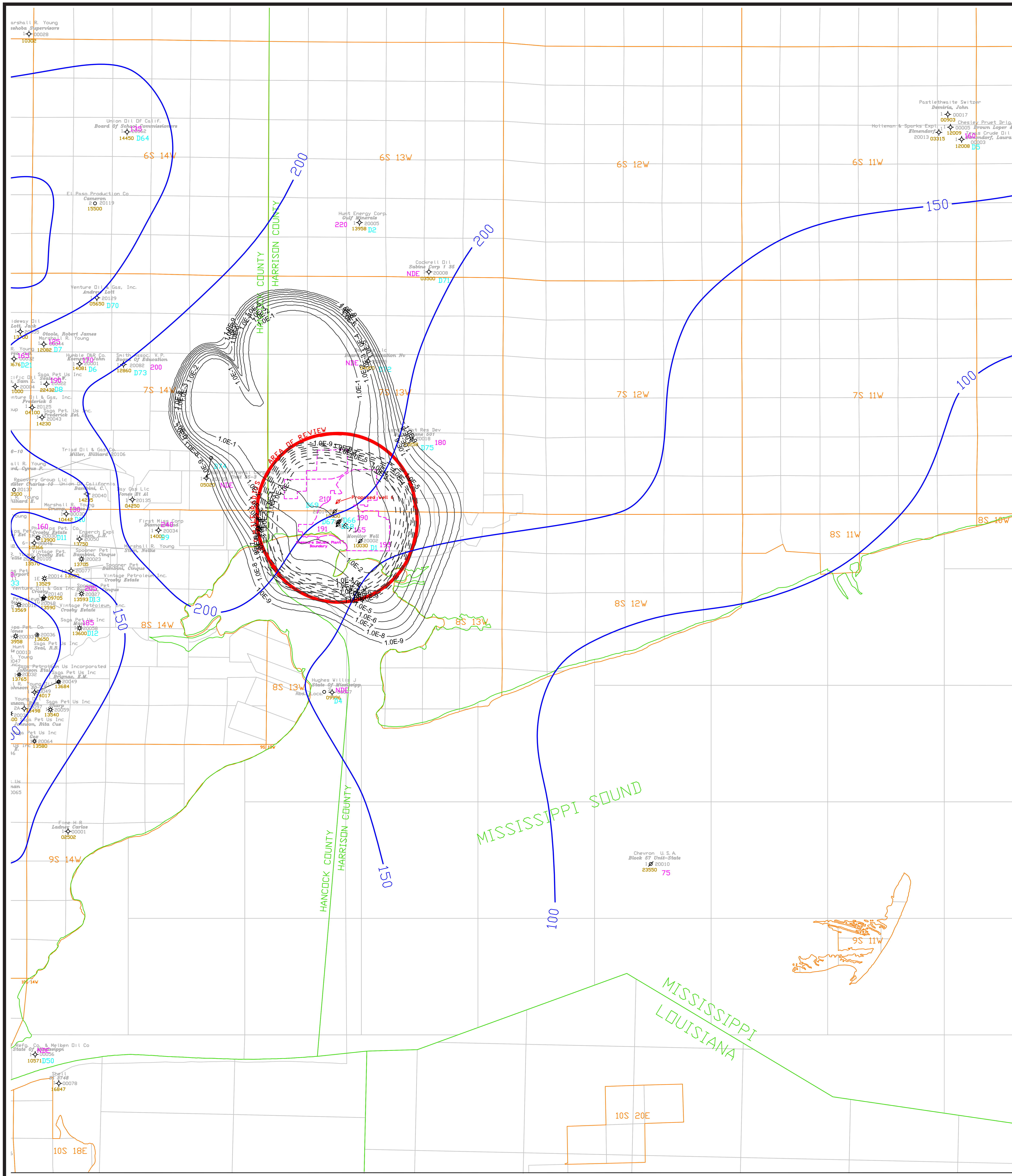

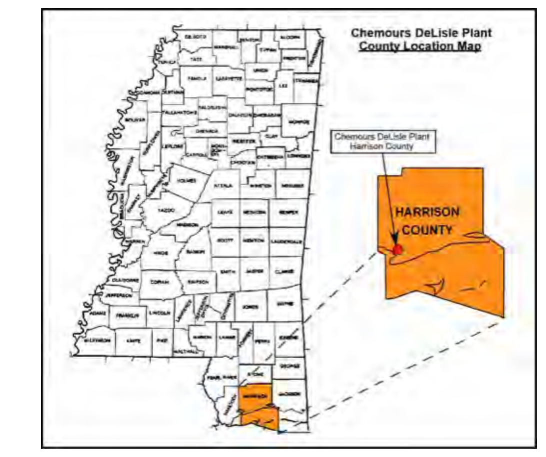

N

Legend

- Deviated Well Spot
- P&A Oil and Gas Well
- Injection Well
- Proposed Injection Well
- Gas Well
- Oil Well
- Dry & Abandoned Well
- -4650 Post Numbers
- D40 Map ID Wells
- 11600 Total Depth
- 31290 API Number
- NDE Log Not Deep Enough
- NL No Log

End of Operations (12/31/2050) Waste Plume

10,000-Year Waste Plume

Waste Plume Contours Represent Magnitude of Reduction In Initial Waste Constituent Concentration

SCALE

0 6000 12000 18000 24000 30000

FEET

PLATE 3-2

Washita-Fredericksburg Injection Interval Isopach Map Showing Location of Light-Density Plume at End of Operations (2050) and After 10,000 Years (Chemours WF-LD Lat SWIFT MODEL)

BASE MAP FROM:

The Chemours Company FC, LLC
DeLisle Plant
Pass Christian, MS

Appendix 2-18: Washita-Fredericksburg Sand (Injection Interval) Isopach Map

Contour Interval = 50'

Base Map Prepared & compiled from Tobin International, Ltd. digital Map Data

Compiled & Drafted by: (ESSJ, WGK) Sandia	Scale: 1" = 6000'	Date: 3/2016

GEOSTOCK SANDIA ENTREPOSE

6731 Theall Road Houston, Tx 77066 USA • Tel: (832) 286 0471 • Fax: (832) 286 0477
Web : www.geostocksandia.com

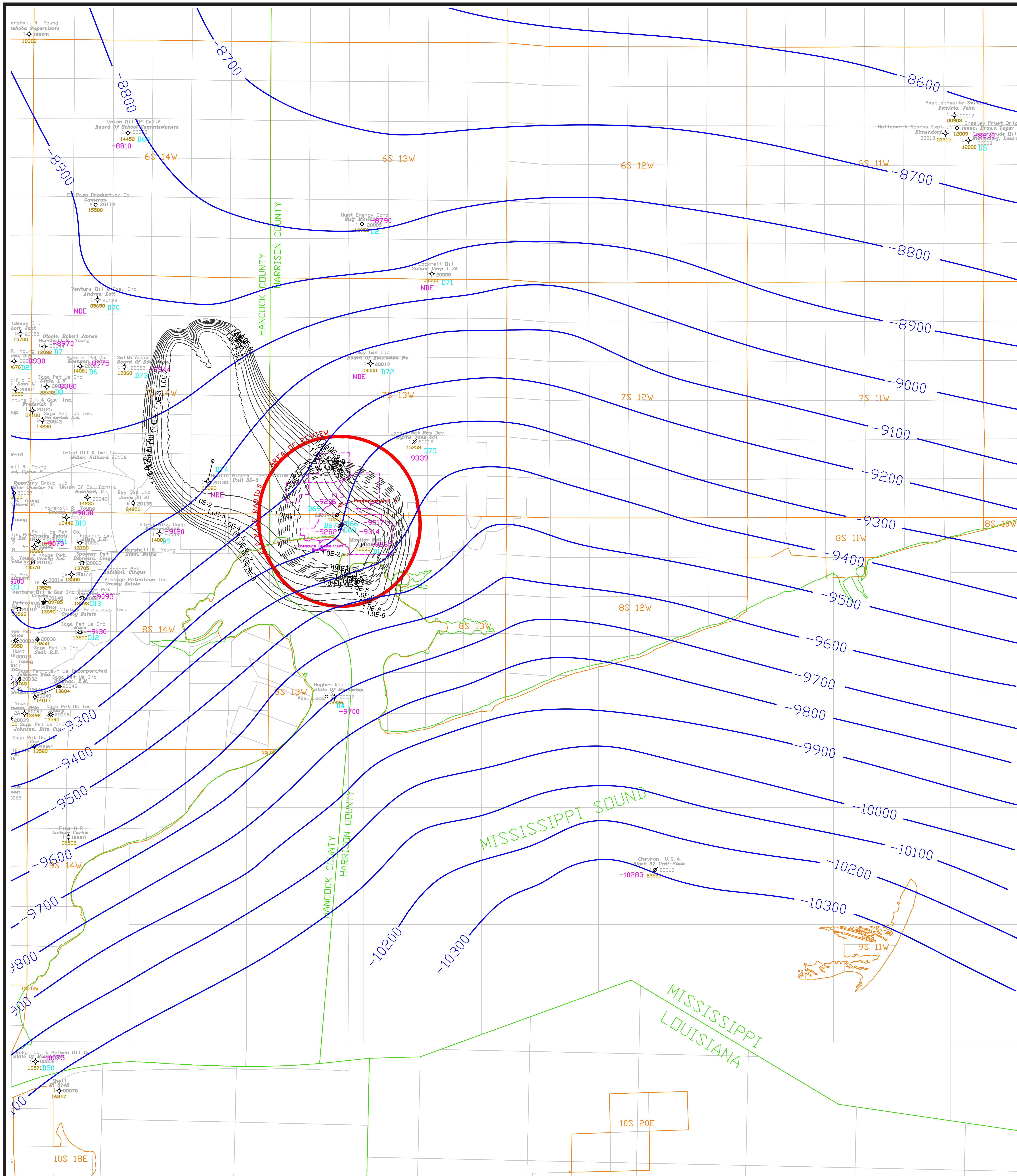

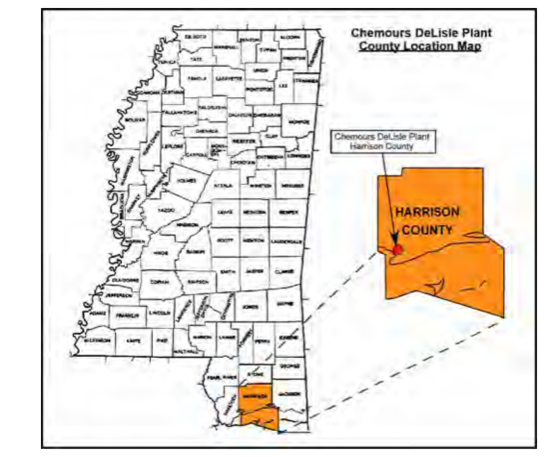

N

Legend

- Deviated Well Spot
- P&A Oil and Gas Well
- Injection Well
- Proposed Injection Well
- Gas Well
- Oil Well
- Dry & Abandoned Well
- -4650 Post Numbers
- D40 Map ID Wells
- 11600 Total Depth
- 31290 API Number
- NDE Log Not Deep Enough
- NL No Log

End of Operations (12/31/2050) Waste Plume
10,000-Year Waste Plume

Waste Plume Contours Represent Magnitude of Reduction In Initial Waste Constituent Concentration

SCALE
0 6000 12000 18000 24000 30000
FEET

PLATE 3-3

Tuscaloosa Massive Sand Structure Map Showing Location of Light-Density Plume at End of Operations (2050) and After 10,000 Years (Chemours TMS-LD Lat SWIFT MODEL)

BASE MAP FROM:

Chemours

The Chemours Company FC, LLC
DeLisle Plant
Pass Christian, MS

Appendix 2-10: Top of Tuscaloosa Massive Sand Structure Map
Contour Interval = 100'

Base Map Prepared & compiled from Tobin International, Ltd. digital Map Data

Compiled & Drafted by: (ESSJ, WGK) Sandia	Scale: 1" = 6000'	Date: 3/2016

GEOSTOCK SANDIA ENTREPOSE

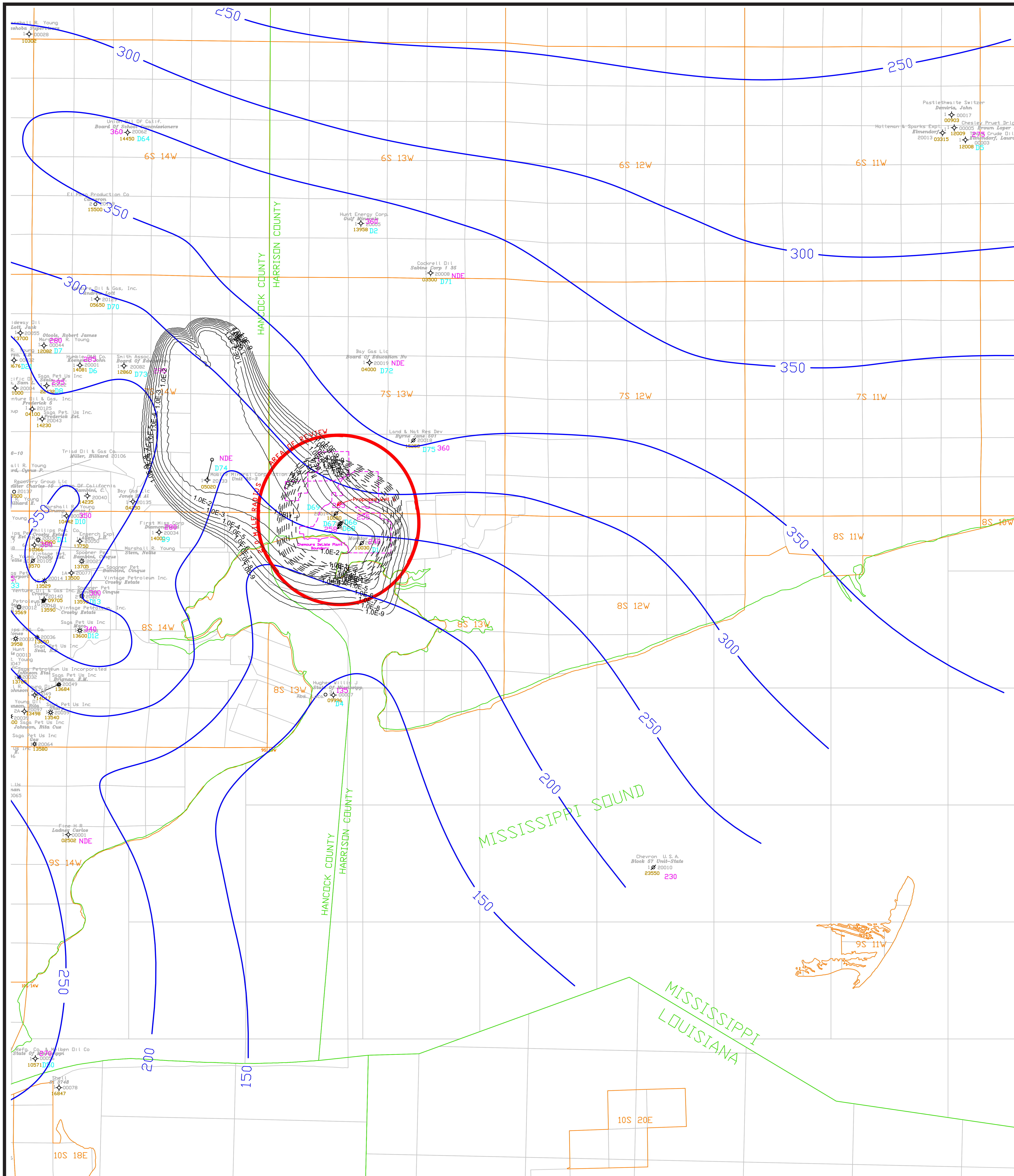

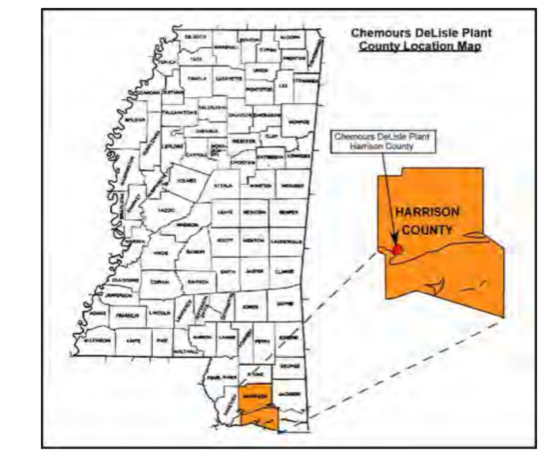

Legend

- Deviated Well Spot
- P&A Oil and Gas Well
- Injection Well
- Proposed Injection Well
- Gas Well
- Oil Well
- Dry & Abandoned Well
- -4650 Post Numbers
- D40 Map ID Wells
- 11600 Total Depth
- 31290 API Number
- NDE Log Not Deep Enough
- NL No Log

End of Operations (12/31/2050) Waste Plume

10,000-Year Waste Plume

Waste Plume Contours Represent Magnitude of Reduction In Initial Waste Constituent Concentration

SCALE

0 6000 12000 18000 24000 30000

FEET

PLATE 3-4

Tuscaloosa Massive Sand Isopach Map
Showing Location of Light-Density Plume
at End of Operations (2050) and After 10,000 Years
(Chemours TMS-LD Lat SWIFT MODEL)

BASE MAP FROM:

The Chemours Company FC, LLC
DeLisle Plant
Pass Christian, MS

Appendix 2-17: Tuscaloosa Massive Sand
(Net Sand) Isopach Map
Contour Interval = 50'

Base Map Prepared & compiled from Tobin International, Ltd. digital Map Data

Compiled & Drafted by: (ESSJ, WGK) Sandia	Scale: 1" = 6000'	Date: 3/2016

GEOSTOCK SANDIA ENTREPOSE
6731 Theall Road Houston, Tx 77066 USA • Tel: (832) 286 0471 • Fax: (832) 286 0477

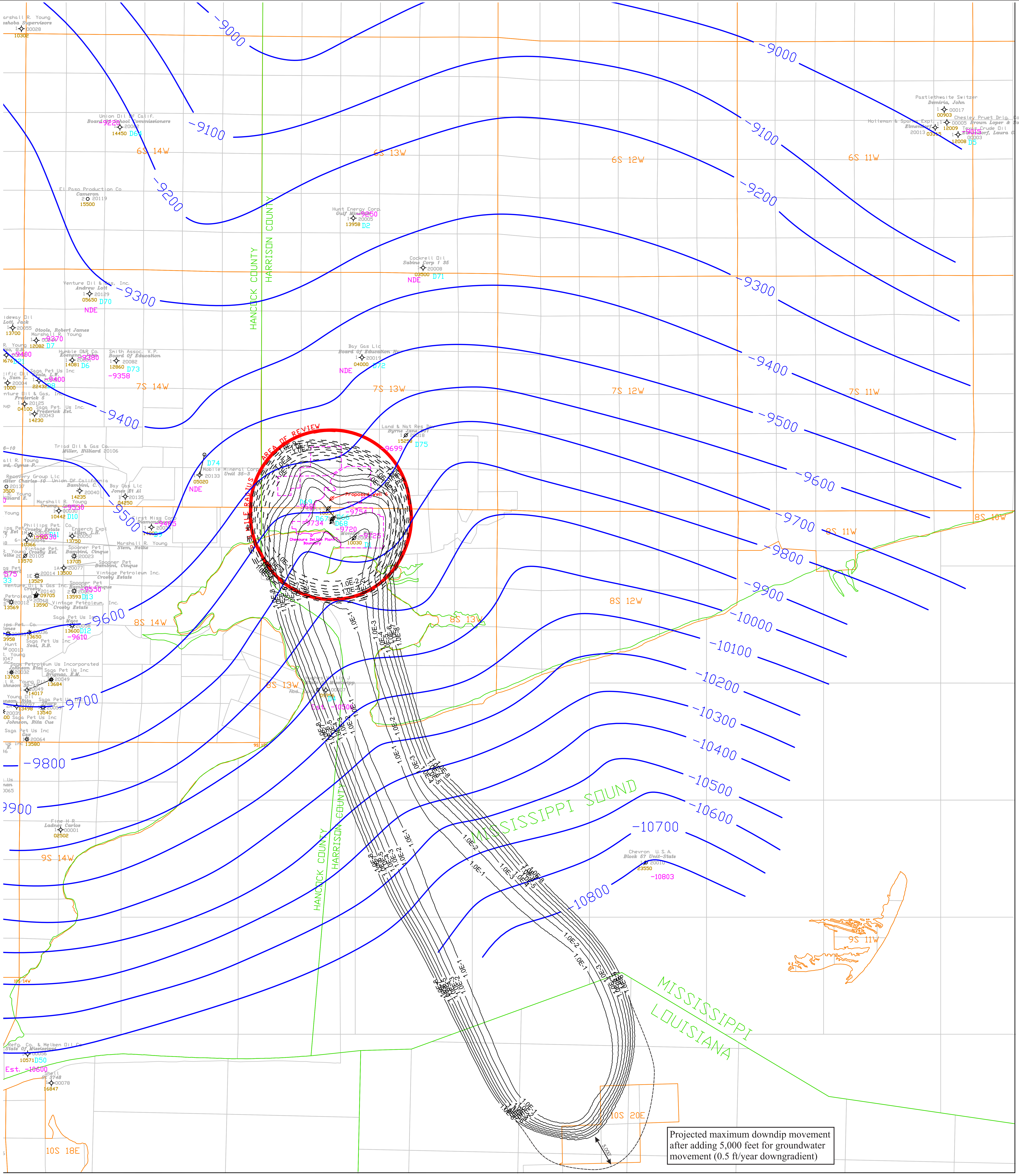

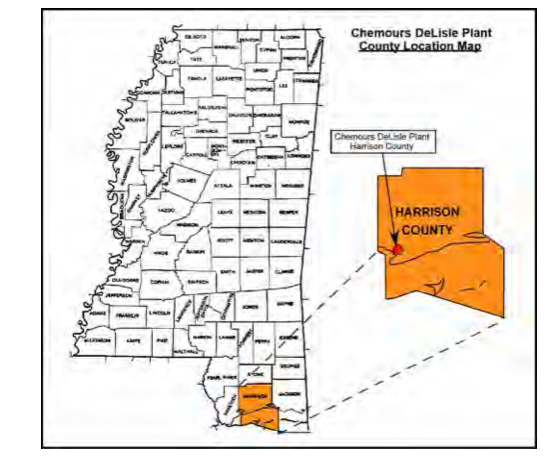

N

Legend

- Deviated Well Spot
- P&A Oil and Gas Well
- Injection Well
- Proposed Injection Well
- Gas Well
- Oil Well
- Dry & Abandoned Well
- -4650 Post Numbers
- D40 Map ID Wells
- 11600 Total Depth
- 31290 API Number
- NDE Log Not Deep Enough
- NL No Log

End of Operations (12/31/2050) Waste Plume

10,000-Year Waste Plume

Waste Plume Contours Represent Magnitude of Reduction In Initial Waste Constituent Concentration

SCALE

0 6000 12000 18000 24000 30000

FEET

PLATE 3-5

Washita-Fredericksburg Injection Structure Map Showing Location of Heavy-Density Plume at End of Operations (2050) and After 10,000 Years (Chemours WF-HD Lat SWIFT MODEL)

BASE MAP FROM:

Chemours

The Chemours Company FC, LLC
DeLisle Plant
Pass Christian, MS

Appendix 2-11: Top of Washita-Fredericksburg Sand (Injection Interval) Structure Map
Contour Interval = 100'

Base Map Prepared & compiled from Tobin International, Ltd. digital Map Data

Compiled & Drafted by: (ESSJ, WGK) Sandia	Scale: 1" = 6000'	Date: 3/2016

GEOSTOCK SANDIA
ENTREPOSE

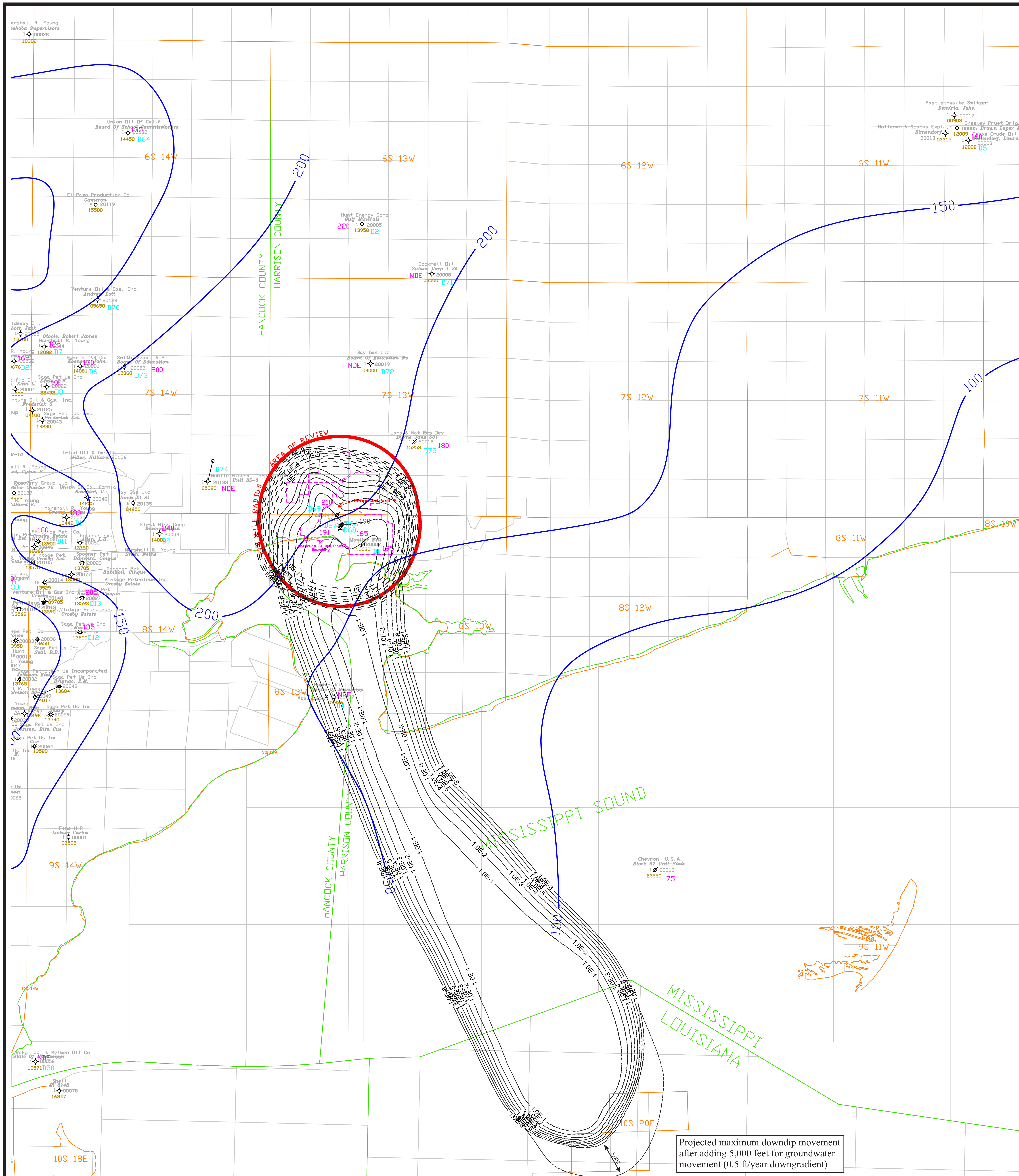

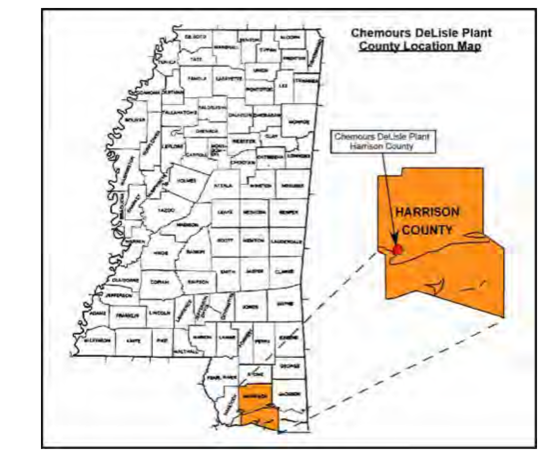

Legend

	Deviated Well Spot
	P&A Oil and Gas Well
	Injection Well
	Proposed Injection Well
	Gas Well
	Oil Well
	Dry & Abandoned Well
-4650	Post Numbers
D40	Map ID Wells
11600	Total Depth
31290	API Number
NDE	Log Not Deep Enough
NL	No Log

- - - - - - End of Operations (12/31/2050) Waste Plume

——— 10,000-Year Waste Plume

Waste Plume Contours Represent Magnitude of Reduction In Initial Waste Constituent Concentration

SCALE

0 6000 12000 18000 24000 30000

FEET

PLATE 3-6

Washita-Fredericksburg Injection Isopach Map Showing Location of Heavy-Density Plume at End of Operations (2050) and After 10,000 Years (Chemours WF-HD Lat SWIFT MODEL)

BASE MAP FROM:

The Chemours Company FC, LLC
DeLisle Plant
Pass Christian, MS

Appendix 2-18: Washita-Fredericksburg Sand (Injection Interval) Isopach Map

Contour Interval = 50'

Base Map Prepared & compiled from Tobin International, Ltd. digital Map Data

Compiled & Drafted by: (ESSJ, WGK) Sandia	Scale: 1" = 6000'	Date: 3/2016

GEOSTOCK SANDIA ENTREPOSE

6731 Theall Road Houston, Tx 77066 USA • Tel: (832) 286 0471 • Fax: (832) 286 0477
Web : www.geostocksandia.com

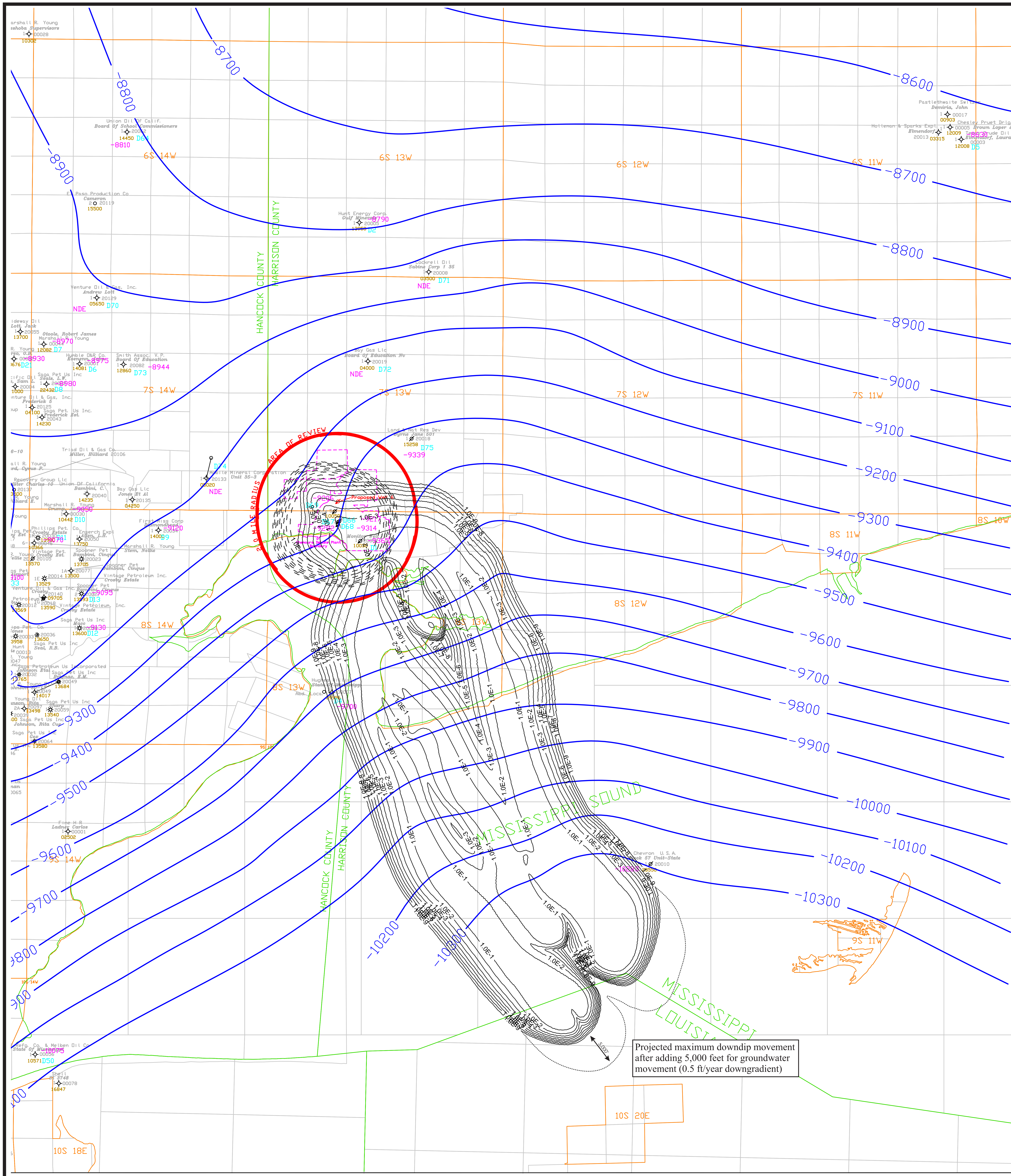

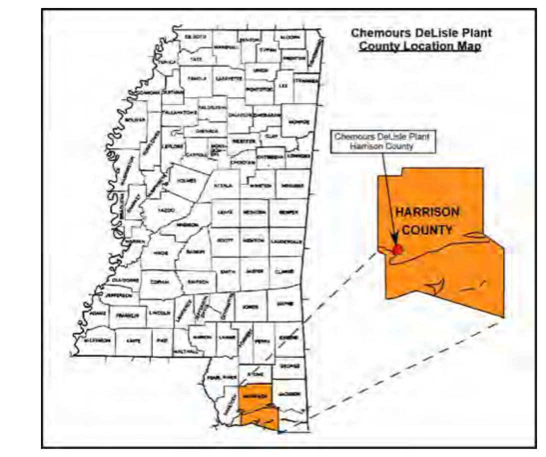

N

Legend

- Deviated Well Spot
- P&A Oil and Gas Well
- Injection Well
- Proposed Injection Well
- Gas Well
- Oil Well
- Dry & Abandoned Well
- -4650 Post Numbers
- D40 Map ID Wells
- 11600 Total Depth
- 31290 API Number
- NDE Log Not Deep Enough
- NL No Log

End of Operations (12/31/2050) Waste Plume
10,000-Year Waste Plume

Waste Plume Contours Represent Magnitude of Reduction In Initial Waste Constituent Concentration

SCALE

0 6000 12000 18000 24000 30000

FEET

PLATE 3-7

Tuscaloosa Massive Sand Structure Map Showing Location of Heavy-Density Plume at End of Operations (2050) and After 10,000 Years (Chemours TMS-HD Lat SWIFT MODEL)

BASE MAP FROM:

Chemours

The Chemours Company FC, LLC
DeLisle Plant
Pass Christian, MS

Appendix 2-10: Top of Tuscaloosa Massive Sand Structure Map

Contour Interval = 100'

Base Map Prepared & compiled from Tobin International, Ltd. digital Map Data

Compiled & Drafted by: (ESSJ, WGK) Sandia	Scale: 1" = 6000'	Date: 3/2016

GEOSTOCK SANDIA ENTREPOSE

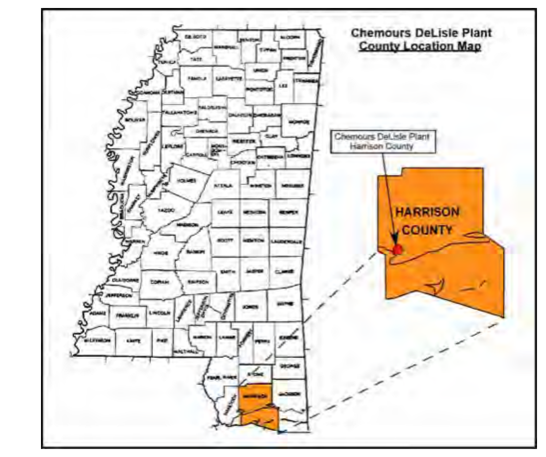

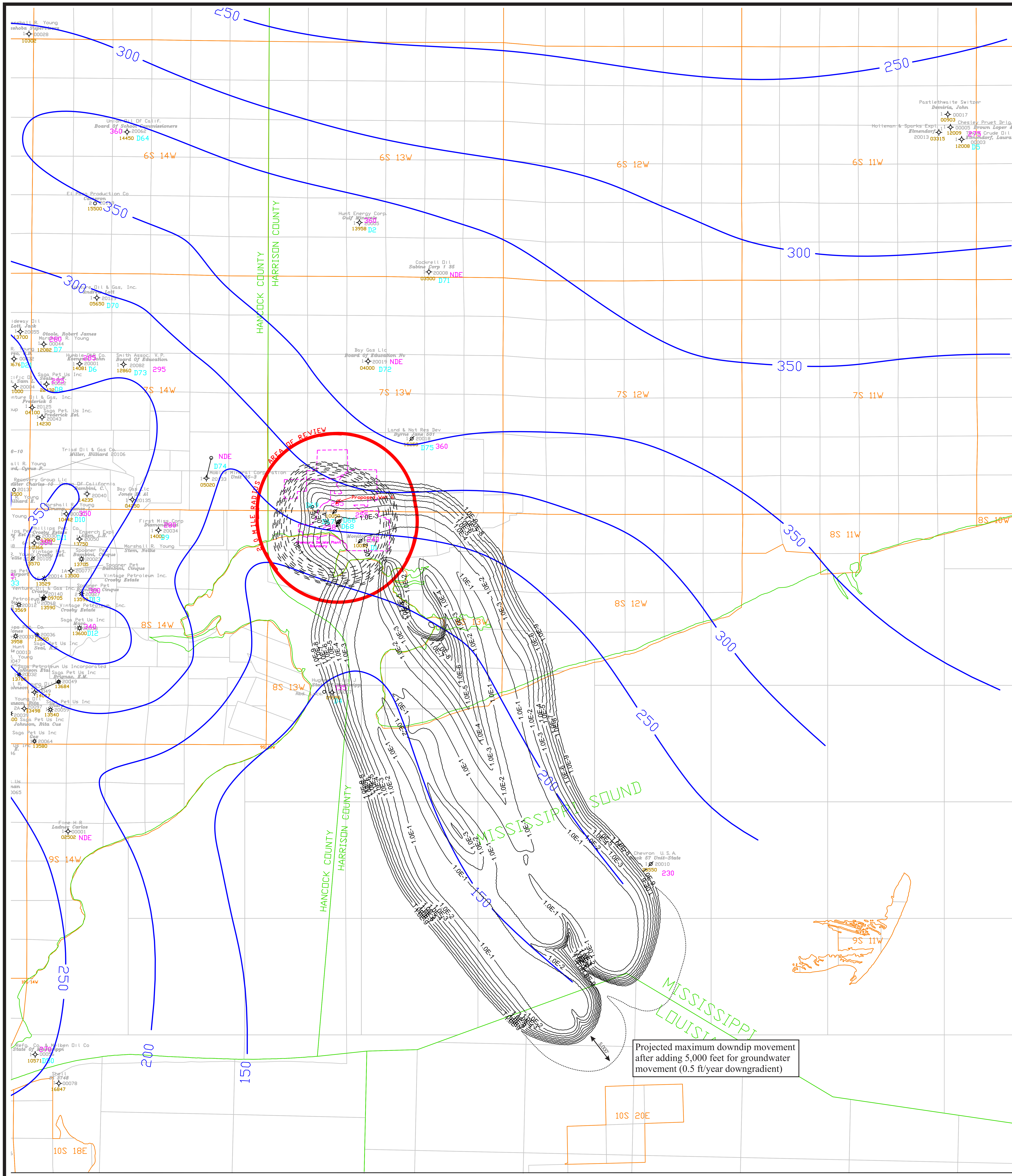

N

Legend

- Deviated Well Spot
- P&A Oil and Gas Well
- Injection Well
- Proposed Injection Well
- Gas Well
- Oil Well
- Dry & Abandoned Well
- -4650 Post Numbers
- D40 Map ID Wells
- 11600 Total Depth
- 31290 API Number
- NDE Log Not Deep Enough
- NL No Log

End of Operations (12/31/2050) Waste Plume

10,000-Year Waste Plume

Waste Plume Contours Represent Magnitude of Reduction In Initial Waste Constituent Concentration

SCALE

0 6000 12000 18000 24000 30000

FEET

PLATE 3-8

Tuscaloosa Massive Sand Isopach Map Showing Location of Heavy-Density Plume at End of Operations (2050) and After 10,000 Years (Chemours TMS-HD Lat SWIFT MODEL)

BASE MAP FROM:

Chemours

The Chemours Company FC, LLC
DeLisle Plant
Pass Christian, MS

Appendix 2-17: Tuscaloosa Massive Sand (Net Sand) Isopach Map

Contour Interval = 50'

Base Map Prepared & compiled from Tobin International, Ltd. digital Map Data

Compiled & Drafted by: (ESSJ, WGK) Sandia	Scale: 1" = 6000'	Date: 3/2016

GEOSTOCK SANDIA ENTREPOSE

APPENDICES

APPENDIX 3-1
COMPREHENSIVE RESERVOIR TESTING AND ANALYSIS –
RESERVOIR DESCRIPTION SERVICES (1992)

Pressure History Simulation Study
for
Du Pont DeLisle Plant
Pass Christian, Mississippi

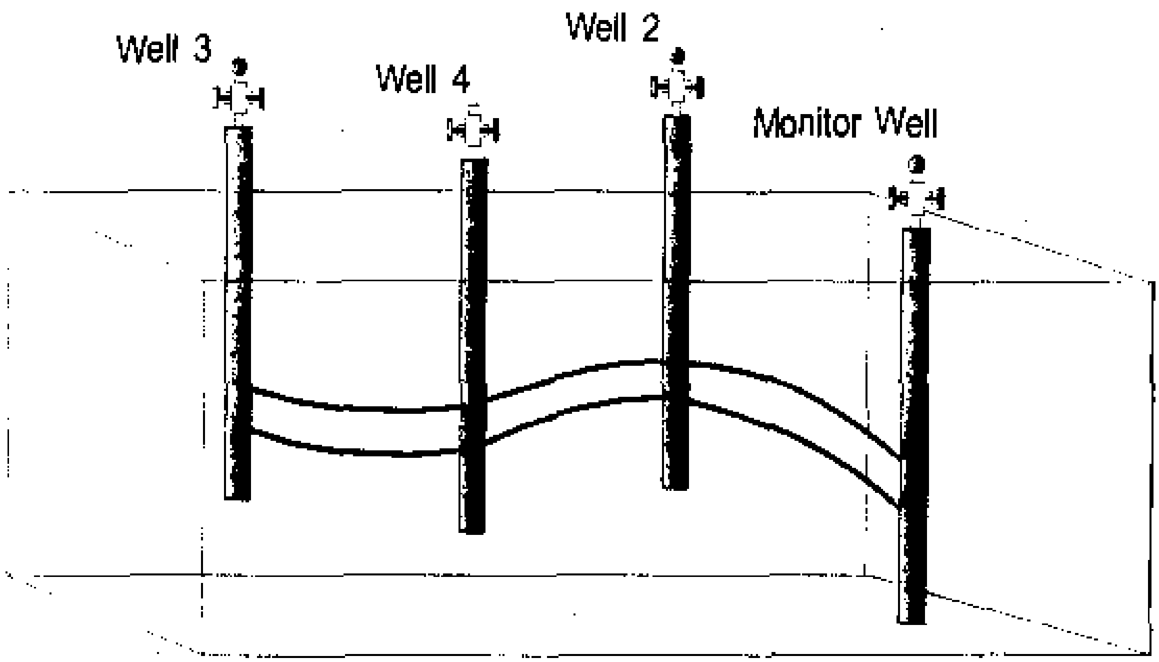

This Study Conducted by
Reservoir Description Services
915 Bayou Parkway
Houston, Texas 77077
(713) 531-5850

Table of Contents

Pressure History Simulation Study

for

Du Pont DeLisle Plant

Pass Christian, Mississippi

Section 1 - Summary of Results

Executive Summary

The Du Pont DeLisle plant, in Pass Christian, Mississippi, uses three injection wells to dispose of effluent generated during the production of titanium dioxide. One additional well located on the plant site is dedicated to monitoring pressure in the permitted injection interval.

This report evaluates the pressure transient interference testing project which started on December 5, 1992. An interference test involves placing gauges in a monitor well while injection is established in offset wells. The magnitude of the pressure increase in the monitor well, and the time delay from when the pressure pulse is observed in the monitor well, yields valuable information about the average permeability (k) , and storativity ($\phi c_t h$) of the reservoir rock between the wells. This information is critical for the accurate prediction of the waste stream movement and pressure increase in the reservoir over time.

The three injection wells – Well 2, Well 3, Well 4 -- and Monitor Well 1 were used in the study to characterize well and reservoir properties in the permitted injection interval. These wells are completed in the Washita-Fredericksburg formation which is a massive sand inter-bedded with shale stringers. A spinner survey was also run prior to the start of the interference testing program to help establish which sand bodies within the permitted injection interval were taking fluid in each well. Section 4 of this report establishes the effective injection intervals based on the spinner information, while Section 5 makes additional recommendations on future follow-up testing.

Bottomhole pressures were continuously monitored for roughly 12 days in Monitor Well 1, and periodically monitored in each of the injection wells. Pressure gauges were not left in the injection wells during the injection of ferric chloride waste because of its acidity. Instead, the injection wells were flushed with brine and gauges were placed in each well to monitor interference between the injection wells at specified intervals. Section 2 of this report provides a detailed review of the sequence of events during the test.

The analysis of the monitor well data is felt to be the most reliable while the analysis of the injection well data is less reliable due to wellbore effects that occur during the test. Overall, the objective of the testing program was met, with establishment of a good description of the hydraulic conductivity of the reservoir system.

Discussion

Communication Between Wells

The intent of the interference test was to identify reservoir properties between all of the wells completed in the injection interval. An additional well, Well 5, was being drilled at the time of this test and is not included in the this study but can be reviewed at a later date when completed.

Diagram S1-G1 to the right shows the paths of pressure communication determined from this study. All of the wells are in prassure communication and an estimate of the reservoir properties between wells has been established. The overall pressure change observed in each well was clearly a result of injection from offset wells and cannot be mistaken for gauge drift or fluctuations.

S1-G1, Paths of Pressure Communication

Between Wells

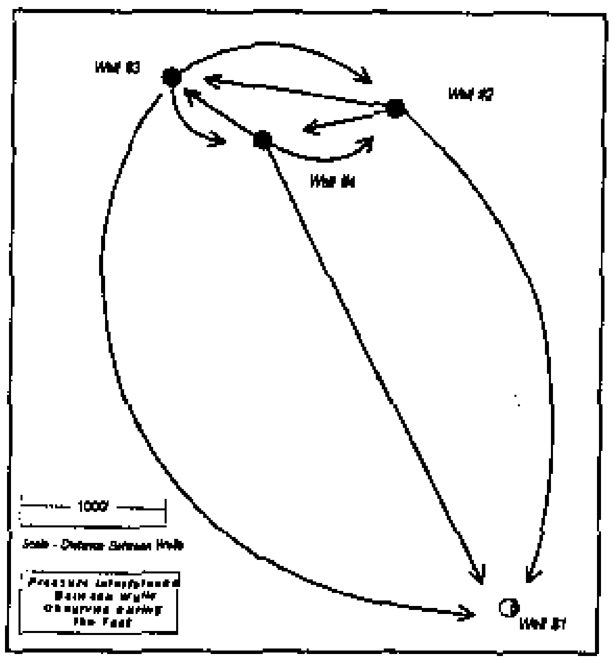

The largest overall pressure change, 80 psi, was observed in Well 4 while Well 2 was injecting. The smallest pressure changes were observed in Well 3.

Overall Quality of the Results

The summary of results presented in this section of the report are a compilation of the analysis of the best transient test data collected from four wells over a twelve day period. In general, ths data collected in Monitor Well 1 yields the most reliable estimate of inter-well ressrvoir properties because ths well and gauge were "stable" throughout the entire test period. The gauges were not run in and out of Monitor Well 1, and no injection occurred in Monitor Well 1 itself. The Pressure History Simulation matches ths Monitor Well 1 measured data very well and the most confidence can be placed in the values between Monitor Well 1 and the three other injectors.

This is not true of ths injection wells. Each of the injection wells was flushed with brine prior to running gauges, and in some cases the gauges were pulled to flush the wells again due to the acidity of the injectate. Unfortunately, the pressure data following the brine flush periods is inconsistent with the a priori reservoir response. Density "drift" in the wellbore, and the gauge's inability to adjust to temperature changes are the suspected cause of the erratic pressure behavior observed during portions of the test.

Although some sections of the injection well data were affected by wellbore problems, there are still several transient periods between the injection wells that yield good results.

- Between *Well 2 and Well 3* : The period starting on December 13, 1992 while Well #2 was injecting yields a good match between Well 2 and Well 3. (Elapsed time 340 to 430 hours).

- Between *Well 4 and Well 3* : The period when Well 4 stopped injection on December 9, 1992 provides a good evaluation of reservoir properties between Well 4 and Well 3. (Elapsed time 140 to 290 hours).

- Between *Well 4 and Well 2* : The period when Well 2 stopped injection on December 15, 1992 provides a good evaluation of reservoir properties between Well 4 and Well 2. (Elapsed time 350 to 400 hours).

Analysis Technique

The analysis of the interference test data is complicated by the fact that there isn't a single transient period created as a result of injection from only one well. Instead, the entire range of test data is influenced by multiple underlying pressure trends created by injection into two or more disposal wells at or about the same time. In some cases, the pressure influence caused by the flush period is present in the well, further complicating the interpretation.

Traditional interference techniques are limited, at best, when dealing with multiple well interference tests. Instead a Pressure History Simulation technique is required to analyze the interference test data. The Pressure History Simulation technique is an iterative method that involves generating the sum of the theoretical pressure responses at the observation well created by each active well given inter-well reservoir properties (transmissibility, storativity, pi, model type, distance between wells, etc.) and the wells' rate history. The simulated pressure data is statistically compared to the measured observation well pressure, the reservoir parameters are automatically adjusted for each well in the system, and the process is repeated until the best statistical match is obtained. The analyst's role in this type of problem involves choosing the appropriate reservoir model to use in the process, and applying "weighting factors" to help the optimizer find the best solution. A great deal of time is spent before the start of the modeling process preparing the data. The rate history from each well has to be synchronized to the same elapsed gauge time, and the gauge data has to be checked and in some cases filtered to alleviate data that is not part of the transient test.

In some cases, the best statistical match does not come close to explaining the measured pressure response. This can be caused by faulty gauge data, poor test conditions, or the choice of a reservoir model that does not fit the system requirements (i.e. a homogeneous model when a 2 porosity model is required). The objective is to generate a pressure history simulation that matches the entire range of pressure data. The Pressure History Simulation of Monitor Well 1 is an example of an excellent match, while Section 3 Graph S3-G7 is an example of the best match that can be obtained with a homogeneous system model when a 2 porosity model is required.

The results presented below are felt to be the best estimate of inter-well reservoir properties derived from the analysis of multiple transient periods in the four wells using the Pressure History Simulation technique.

Transmissibility Between Wells

Transmissibility [(k h) / (μ B)] is a measure of the hydraulic conductivity of the rock, or in other words, the ability of the fluid to move through the total cross sectional area of the reservoir rock. Transmissibility is derived as a unit term in the analysis of the pressure date. Although permeability is included in the definition of transmissibility, a high transmissibility value does not necessarily indicate high permeability and vice versa. A low permeability, but thick, zone can have the same apparent transmissibility as a thin, high permeability zone.

- The highest apparent transmissibility [(k h) / (μ B)] exists between Well 4 and Monitor Well 1 and between Well 3 and Monitor Well 1.

- The lowest apparent transmissibility [(k h) / (μ B)] exists between Injection Well 4 and Injection Well 2. This is qualitatiuely indicated by the 80 psi increase in pressure in Well 4 while Well 2 is injecting. In this case it is felt that the low transmissibility is a result of a smaller effective zone height between the wells as opposed to a low permeability.

- Table S1-T1, below, is a listing of the best estimate of transmissibility [(k h) / (μ B)] between wells. The column to the right is the 95% confidence interval based on the Pressure History Simulation analysis.

- The small pressure signal seen in Well 1 while Well 3 was injecting is the cause of the large variance in transmissibility between Well 3 and Well 1. A larger injection rate in Well 3 , and the absence of the underlying pressure trends created by injection from Wells 2 and 4, would have created a more unique signal, and provided more confidence in the answer.

• The analysis of the pressure observed in Well 1 while Well 2 was injecting has a small error range and provides a good estimate of inter-well properties.

Graph S1-G2, and S1-G3 compare the estimated transmissibility between wells from several perspectives. Graph S1-G2 is a bar chart comparison of the values while Graph S1-G3 shows the proximity of injection and monitor wells to each other, and also graphically compares the estimated transmissibility between the wells. The size of the box in Graph S1-G3 is relative to the calculated transmissibility between wells.

Table S1-T1, Transmissibility [(k h) / (uB)] Between Wells

	Transmissibility [(k h) / (μ B)]	95 % Confidence Interval
Well 1 <--> Well 2	129,477	125,970 to 133,080
Well 1 <--> Well 3	167,573	98,249 to 285,810
Well 1 <--> Well 4	196,460	162,780 to 237,110
Well 2 <--> Well 3	87,787	81,203 to 94,905
Well 2 <--> Well 4	12,038	11,000 to 13,170
Well 3 <--> Well 4	42,547	38,357 to 47,194

Graph S1-G2, Bar Chart Effective Transmissibility Between Wells

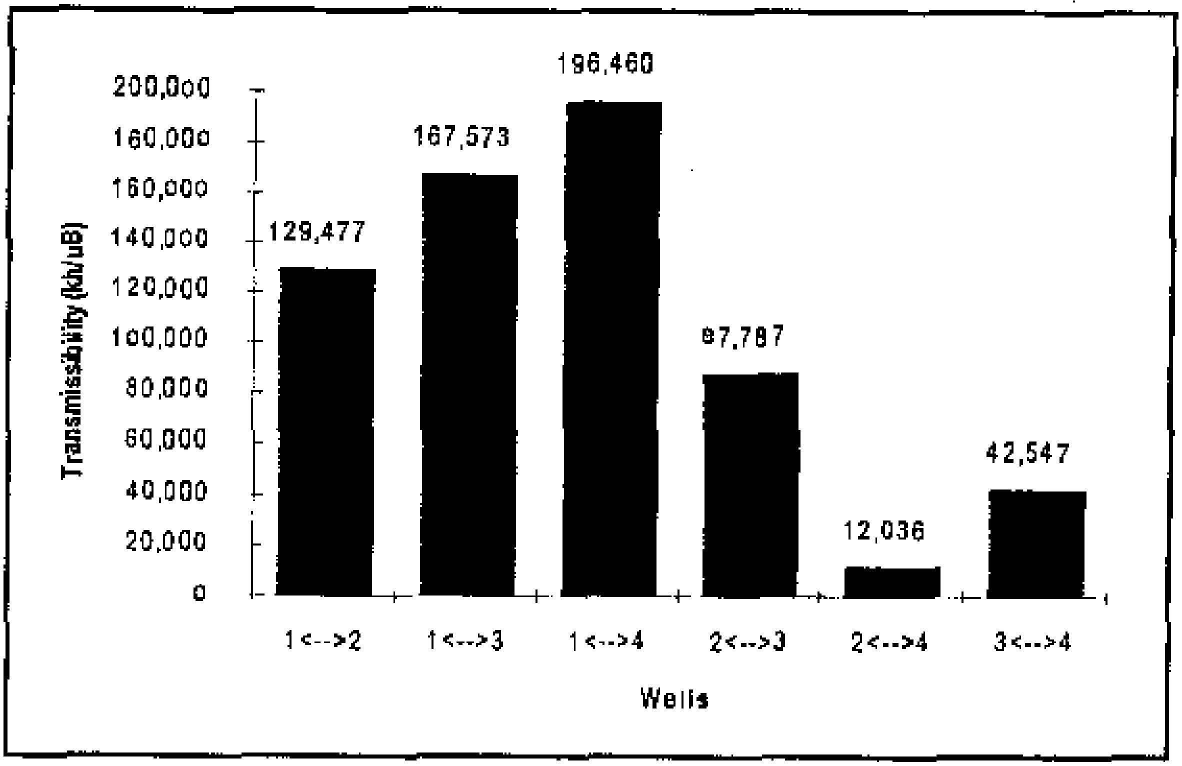

Graph S1-G3, Effective Transmissibility Between Well

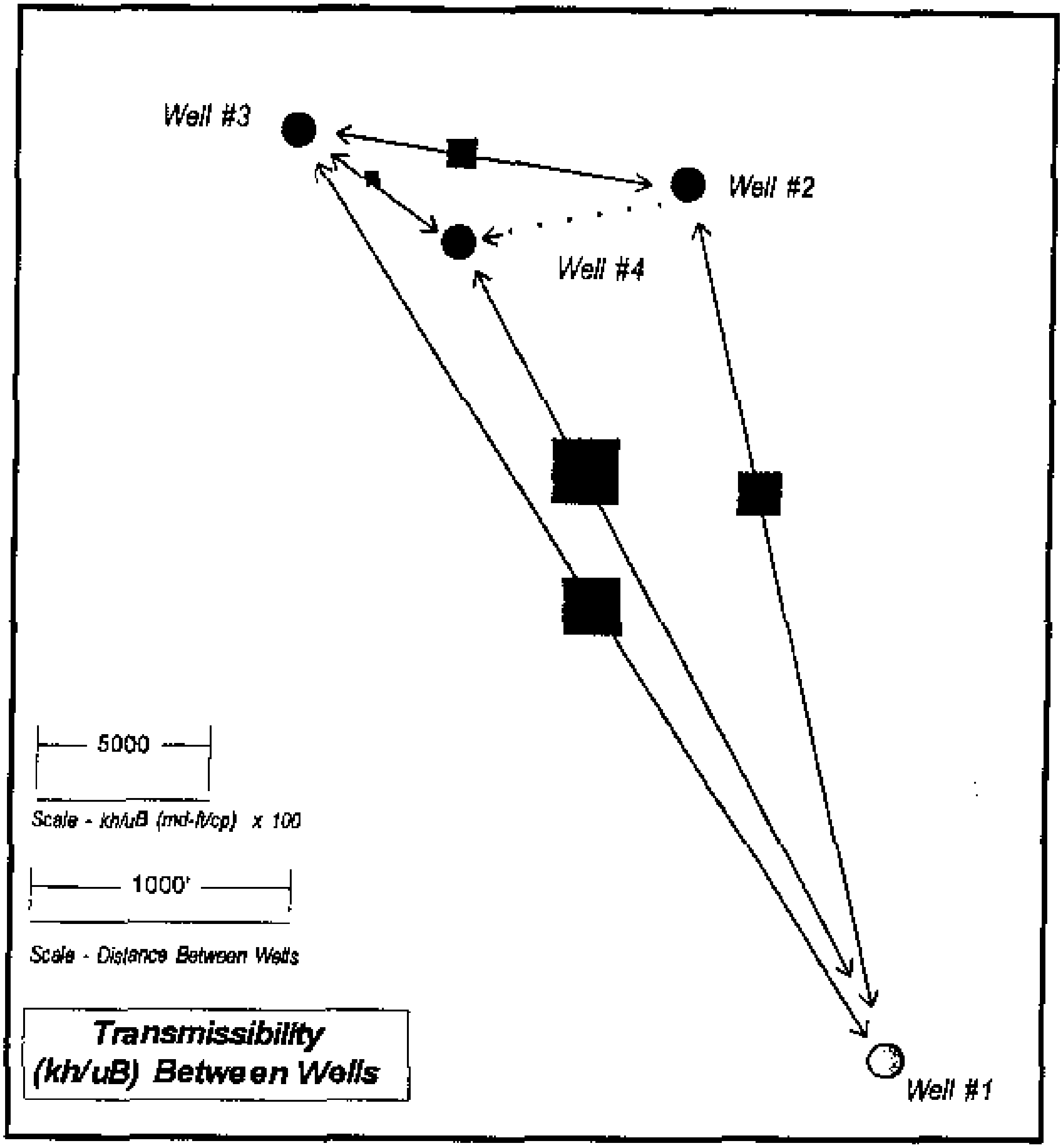

Storativity

Storativity ($\phi\ c_t\ h$) is a measure of the formation's ability to amass fluid. The formation's ability to store fluid is a direct function of the zone thickness, compressibility of the rock, compressibility of the fluid, and the formation's porosity. A larger storativity value indicates either a larger zone thickness exists between wells, the zone is more porous, or the fluid is more compressible. Changes in fluid compressibility will not explain the noted differences in storativity given the nature of the injectate and the relatively small difference in average pressure between wells. Either a difference in porosity, a difference in zone thickness, or statistical variation in the analysis, are the suspected causes of the difference in the storativity values between wells.

Table S1-T2 shows the average storativity values between wells and the 95% confidence interval. Graph S1-G4 is a bar chart of the values, and Graph S1-G5 on the following page is a diagram showing storativity in relationship to well position.

Table S1-T2, Storativity ($phi^*c_t{}^*h$) Between Wells

	Storativity ($\phi\ c_t\ h$)	95 % Confidence Interval
Well 1 <--> Well 2	1.074E-4	1.84E-04 to 1.11E-04
Well 1 <--> Well 3	2.916E-4	2.02E-84 to 4.20E-04
Well 1 <--> Well 4	1.608E-4	1.44E-04 to 1.79E-84
Well 2 <--> Well 3	1.625E-4	1.428E-84 to 1.843E-04
Well 2 <--> Well 4	1.655E-5	1.233E-05 to 2.221E-05
Well 3 <--> Well 4	8.268E-5	7.392E-05 to 9.240E-05

Graph S1-G4, Bar Chart of Effective Storativity Between Wells

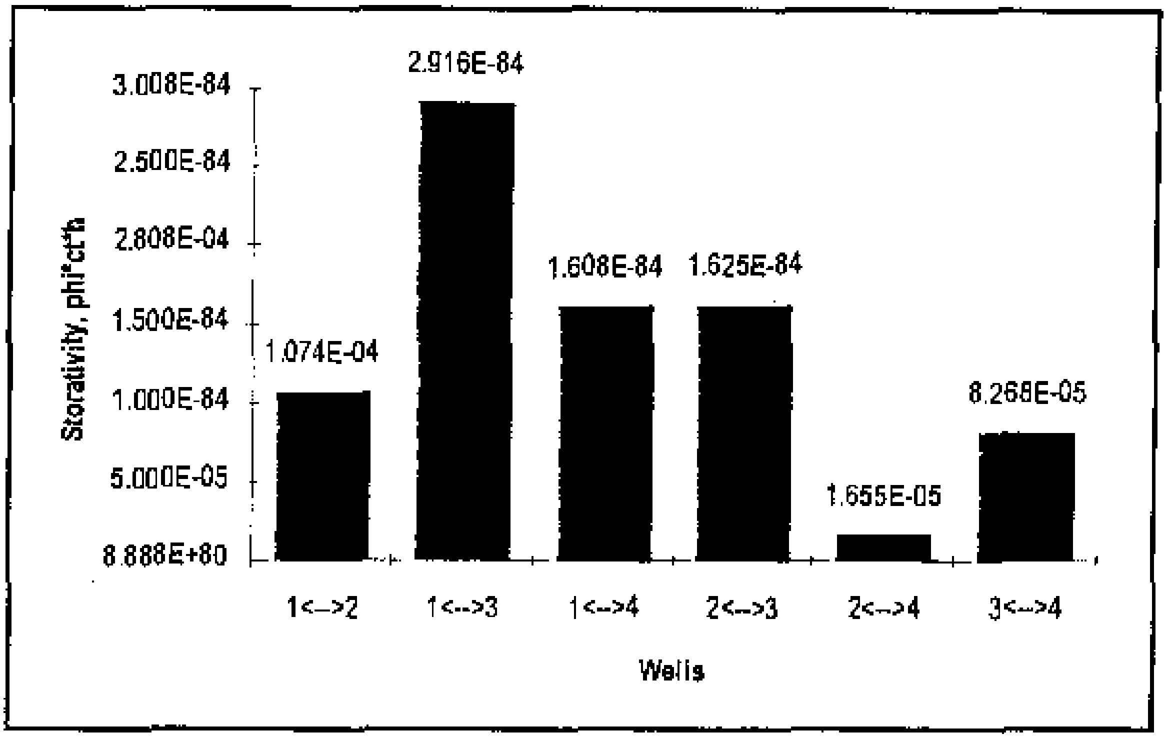

Graph S1-G5, Effective Storativity Between Wells

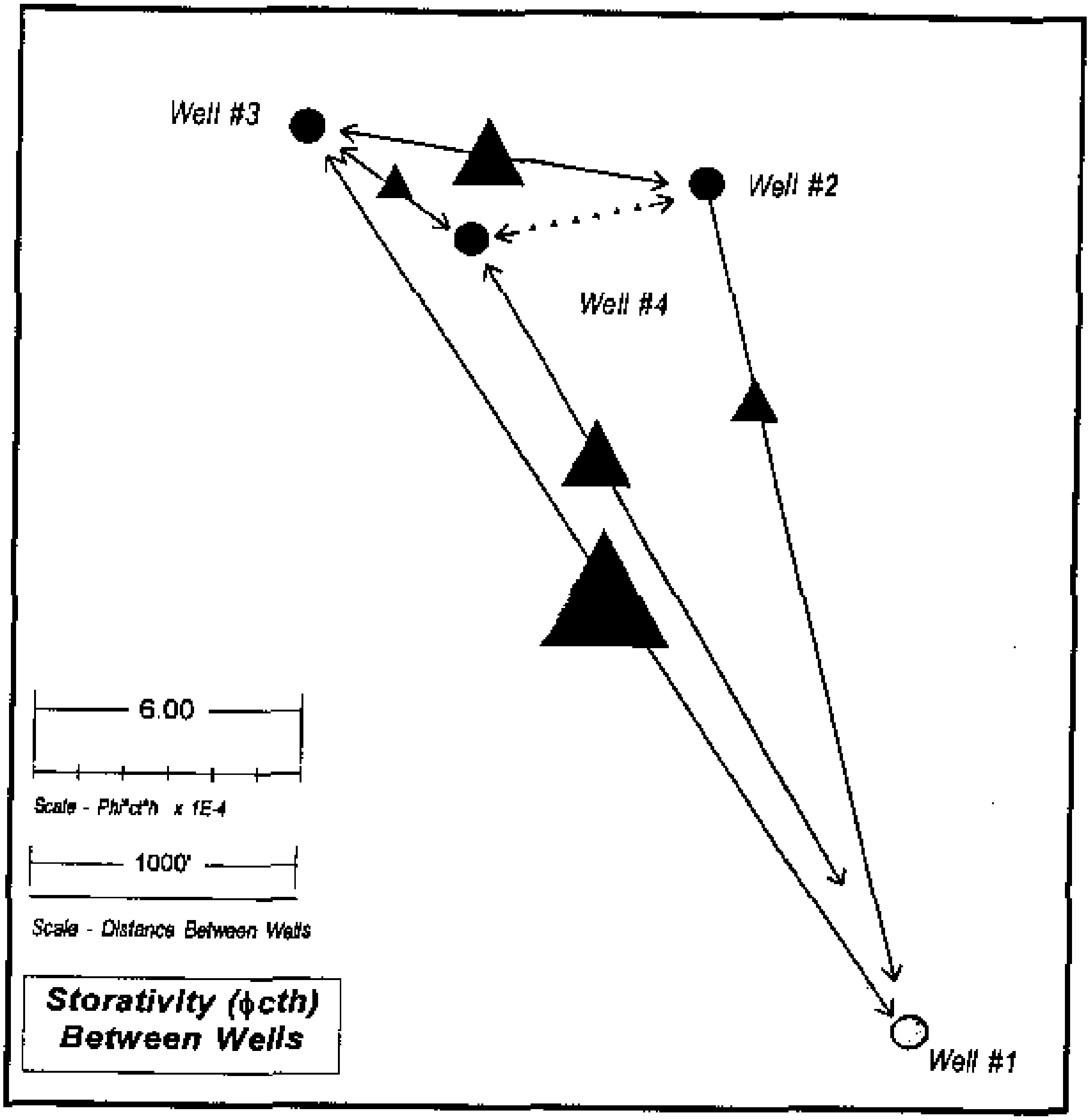

Effective Zone Thickness

As mentioned previously, Storativity is the product of porosity, total compressibility, and zone thickness. Thus, the effective zone thickness between wells can be estimated using the storativity value from the analysis if one assumes an average compressibility and porosity.

$$\text{Storativity} = \Phi c_t h$$

where:

h = zone thickness (ft)

c_t = total compressibility (1/psi)

Φ = porosity (fraction)

Then;

$$\text{zone thickness } (h) = \text{Storativity} / \Phi c_t$$

Graph S1-G7, Diagram of Effective Zone Thickness Between Wells

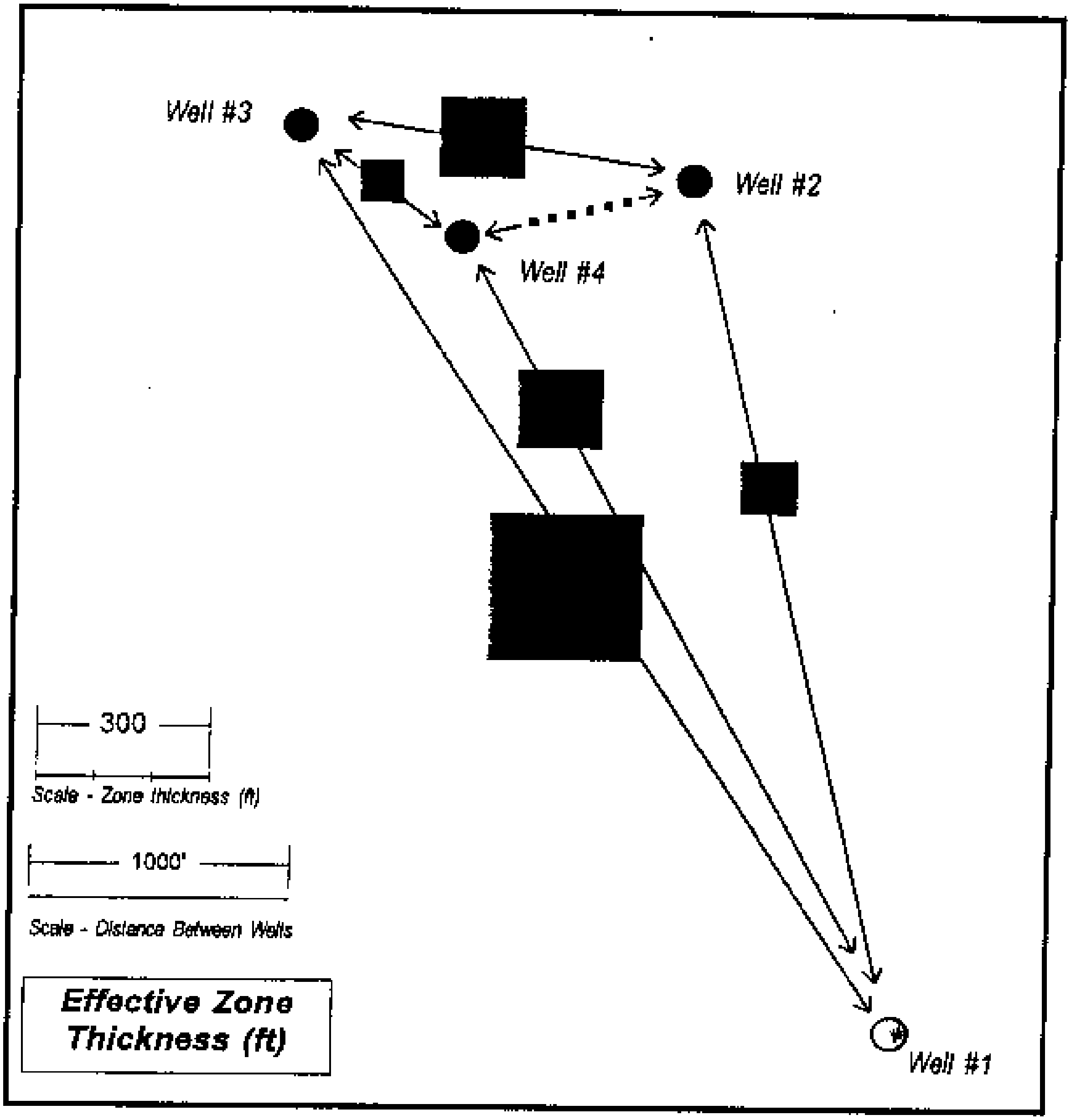

Note the thickest effective zone interval appears to be between Well 3 and Well 1 and decreasing to the northeast. This may be indicative of a geologic feature of the effective injection interval. This raises geologic questions of about the depositional environment of the system.

Effective Permeability

Transmissibility comes directly from the interference analysis as a unit term. Permeability can only be estimated if one knows zone thicknesa, viscosity, and formation volume factor. An estimate of zone

Section 2 presents a discussion of the pressure-volume-temperature relationship of the injectate fluid. Based on this information the estimated total compressibility at 226° F and 4550 psia is 4.659E-06 1/psi. The estimated average porosity of the permitted injection sand is 23.5% as stated in the original petition. Table S1-T3 shows the estimated inter-well zone thickness calculated using the storativity values derived from the interference analysis and using the estimated porosity and total compressibility values mentioned above.

Table S1-T3 , Effective Zone Thickness Between Wells

	Effective Zone Thickness (ft)	95 % Confidence Interval (ft)
Well 1 <--> Well 2	98	95 to 101
Well 1 <--> Well 3	266	184 to 384
Well 1 <--> Well 4	147	132 to 163
Well 2 <--> Well 3	148	130 to 166
Well 2 <--> Well 4	15	11 to 20
Well 3 <--> Well 4	76	68 to 84

Below, Graph S1-G6 is a bar chart of the estimated zone thickness between wells and Graph S1-G7 on the following page is a diagram showing effective zone thickness in relationship to well position.

Graph S1-G6, Bar Chart Effective Zone Thickness Between Wells

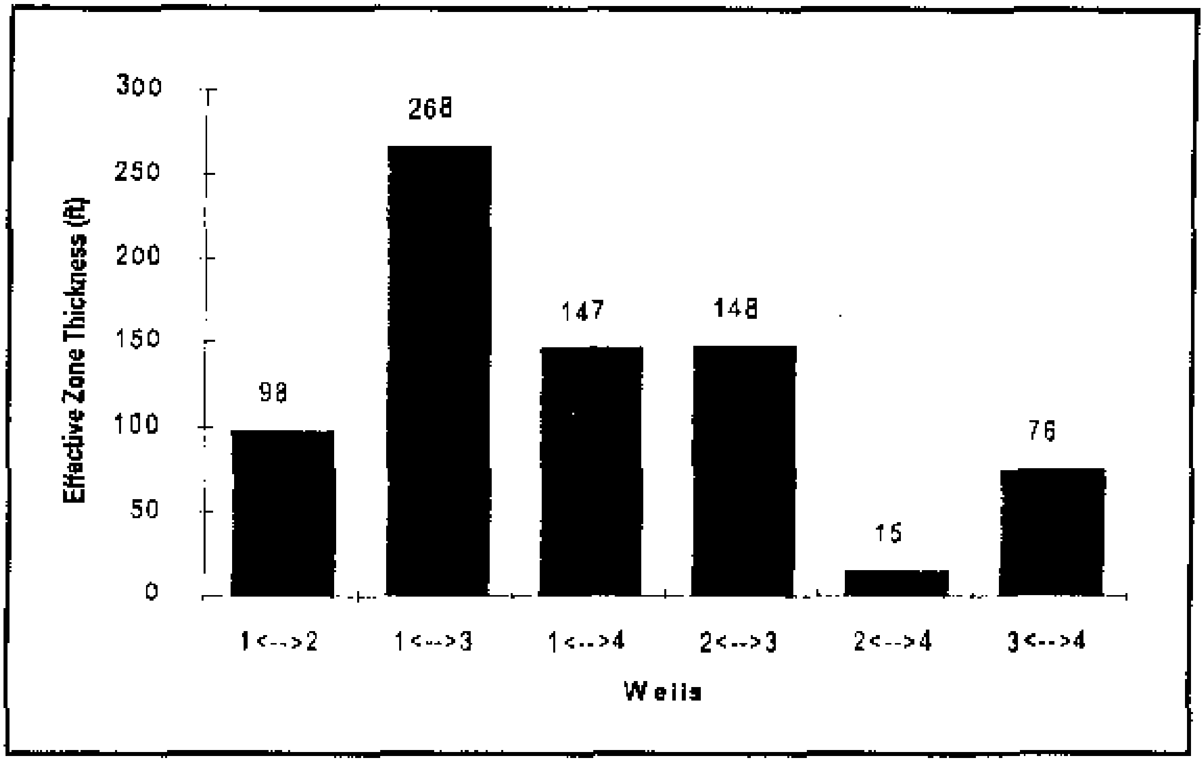

thickness has been made using the effective storativity between wells, and assuming an average value for porosity and total compressibility.

The effective permeability between wells has been estimated using the effective zone thickness between wells and an average viscosity of 0.303 cp. Table S1-T4 presents the calculated permeability between wells, and Graph S1-G8 shows the data in bar chart form. Graph S1-G9 illustrates average permeability between wells in relationship to well position.

Table S1-T4, Effective Permeability Between Wells

	Effective Permeability md)	95 % Confidence Interval (md)
Well 1 <--> Well 2	400	377 to 425
Well 1 <--> Well 3	191	78 to 469
Well 1 <--> Well 4	406	302 to 546
Well 2 <--> Well 3	180	146 to 220
Well 2 <--> Well 4	242	165 to 355
Well 3 <--> Well 4	171	135 to 208

Graph S1-G8, Bar Chart of Effective Permeability Between Wells

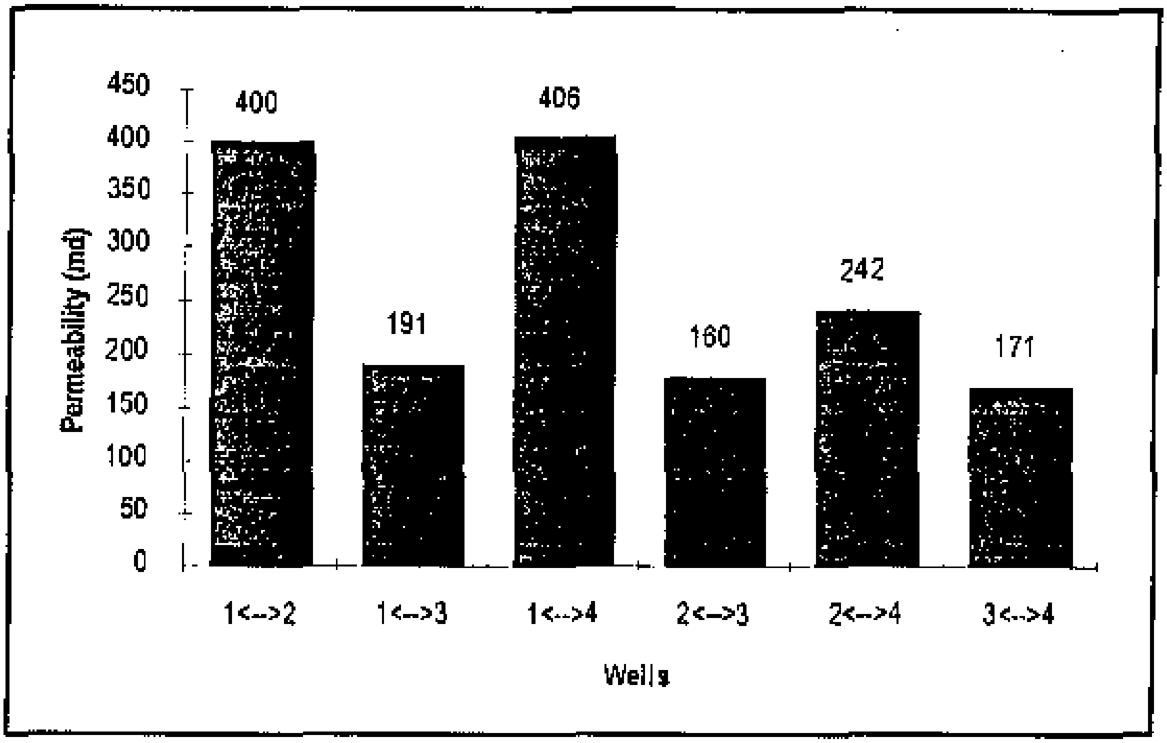

Graph S1-G9, Diagram Effective Permeability Between Wells

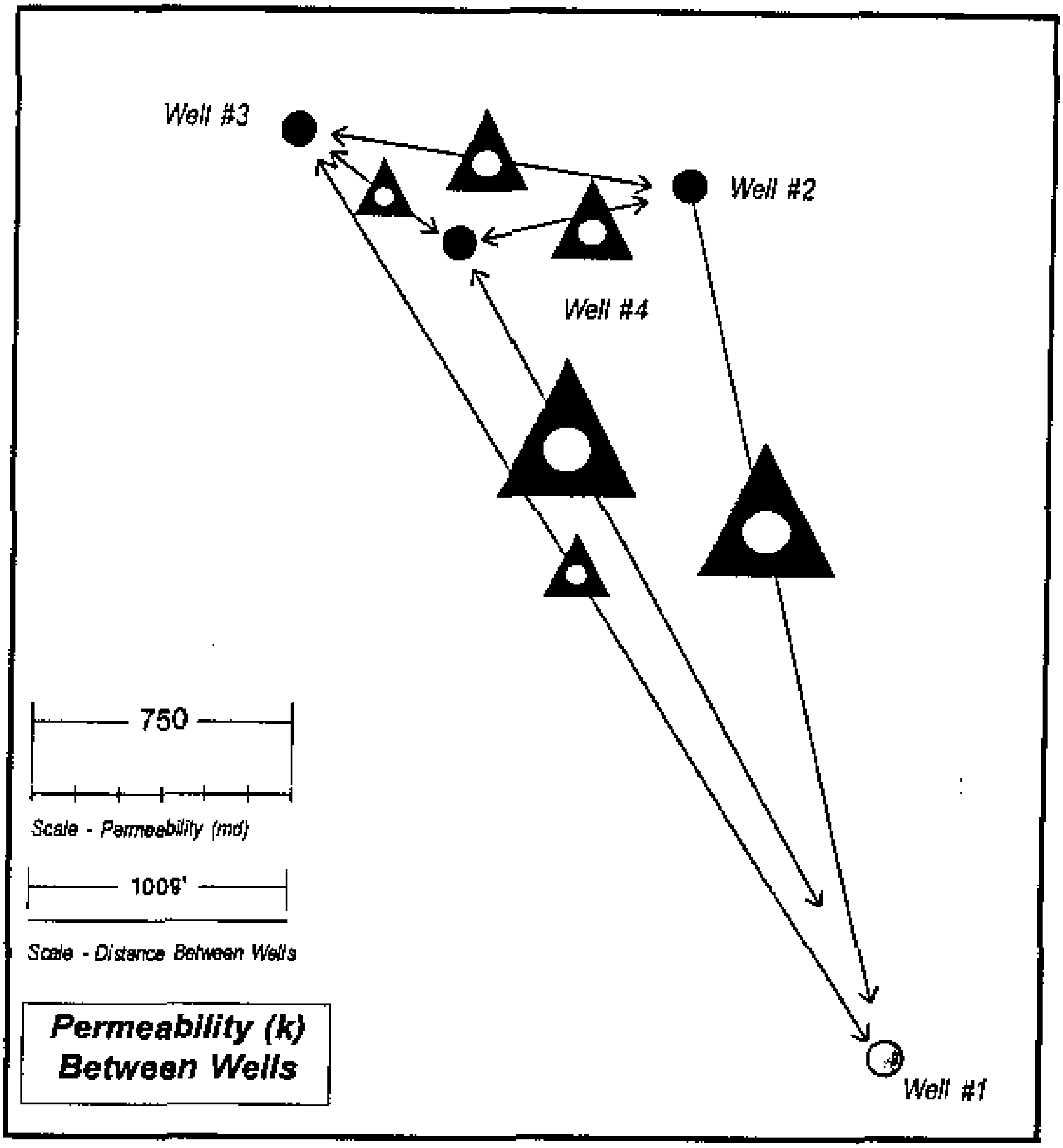

Conclusions

In general, the inter-well properties are similar with the exception of the results obtained between Well 2 and Well 4. The effective transmissibility, and storativity between Well 2 and 4 is an order of magnitude smaller than evidenced in the other wells. It is suspected that Well 2 and Well 4 may communicate through an isolated sand stringer. Examination of the spinner survey results presented in Section 4 indicate that the majority of injection in Well 2 is emplaced in the Upper sand. Additional spinner surveys should be run to confirm this behavior (see Section 4).

The effective zone thickness between Monitor Well 1 and Well 3 appears to be the thickest, which may indicate the center of the fluvial stream bed, with some thinning toward the eastern flank. The largest transmissibility is also evidenced in the North-westerly direction, perhaps confirming the direction of the fluvial deposition.

The effectiue permeability among the wells is most pronounced between Monitor Well 1 and Well 4, and Monitor Well 1 and Well 2. This is most probably a result of geologic conditions in the Injection sand, regional geologic dip and sand thickness.

Additional interference testing between new Well 5 and the all of the Wells presented in this study, as well as, additional falloff testing in each injection Well will help confirm these conclusions.

Section 2 -- Sequence of Events and Data Review

Overview of The DeLisle Interference Testing Program

Spinner Surveys

On December 3, 1992, prior to the start of the interference test, a spinner survey and radioactive tracer survey (R.A.T.) were run in Injection Well 2. The following day, December 4, 1992, a spinner survey was run in Well 3 and on December 16, 1992 a spinner survey wss run in Well 4. Section 4 of this report provides a summary of the spinner data acquired by Gulf Coast Well Analysis of Pearland, Texas.

Pressure Data

Pressure data acquisition was also performed by Gulf Coast Well Analysis. A surface pressure readout (SPRO) Panex quartz capacitsnce gauge, and Panex memory quartz capacitance gauge were used in each well to measure pressure data during the test. The SPRO gauge yields the best data and was used in the analysis. Each gauge recorded thousands of pressure readings which were filtered for use in the analysis. Sections 6, 7, 8 and 9 of this report provide a listing of the filtered pressure response.

Sequence of Events

Graph S2-G1 located on Page 4 in this Section showa the pressure and rate history for each well during the test. This plot helps put the complexity of the test and analysis procedure in perspective. Points A through Q on the plot are the major events that occurred during the test and are discussed below.

A) On December 2, 1992 at 15:20:00, gauges were run into Monitor Well 1 and the SPRO gauge was placed at a depth of 9760 feet. The gauge was 15 feet below the top of the Washita-Fredericksburg Sand located at approximately 9745 feet measured depth in Monitor Well 1. The lowermost set of perforations in Monitor Well 1 are at 9974 feet.

B) On December 3, 1992 at 20:37:00 gauges were run into Well 2 and the SPRO gauge was placed at s depth of 9272 feet. The top of the Washita-Fredericksburg is at approximately 9803 feet measured depth in Well 2. Top of fill in Well 2 was recorded at approximately 9974 feet as determined during the spinner survey of December 3rd. Gauges were pulled from Well 2 on December 6, 1992 at 9:46:00 prior to the start of injection into Well 2.

C) On December 3, 1992 at 16:56:00 gauges were run into Well 3. The SPRO gauge was placed at a depth of 9236 feet. The top of the Washita-Fredericksburg is at approximately 9797 feet measured depth in Well 3. Top of fill in Well 3 was recorded at approximately 10,000 feet as determined during the spinner survey. Gauges were pulled from Well 3 on December 10, 1992 12:06:00 prior to the start of injection into Well 3.

Section 2 -- Sequence of Events and Data Review

Overview of The DeLisle Interference Testing Program

Spinner Surveys

On December 3, 1992, prior to the start of the interference test, a spinner survey and radioactive tracer survey (R.A.T.) were run in Injection Well 2. The following day, December 4, 1992, a spinner survey was run in Well 3 and on December 16, 1992 a spinner survey was run in Well 4. Section 4 of this report provides a summary of the spinner data acquired by Gulf Coast Well Analysis of Pearland, Texas.

Pressure Data

Pressure data acquisition was also performed by Gulf Coast Well Analysis. A surface pressure readout (SPRO) Panex quartz capacitance gauge, and Panex memory quartz capacitance gauge were used in each well to measure pressure data during the test. The SPRO gauge yields the best data and was used in the analysis. Each gauge recorded thousands of pressure readings which were filtered for use in the analysis. Sections 6, 7, 8 and 9 of this report provids a listing of the filtered pressure response.

Sequence of Events

Graph S2-G1 located on Page 4 in this Section shows the pressure and rate history for each well during the test. This plot helps put the complexity of the test and analysis procedure in perspective. Points A through Q on the plot are the major events that occurred during the test and are discussed below.

A) On December 2, 1992 at 15:20:00, gauges were run into Monitor Well 1 and the SPRO gauge was placed at a depth of 9760 feet. The gauge was 15 feet below the top of the Washita-Fredericksburg Sand located at approximately 9745 feet measured depth in Monitor Well 1. The lowermost set of perforations in Monitor Well 1 are at 9974 feet.

B) On December 3, 1992 at 20:37:00 gauges were run into Well 2 and the SPRO gauge was placed at a depth of 9272 feet. The top of the Washita-Fredericksburg is at approximately 9803 feet measured depth in Well 2. Top of fill in Well 2 was recorded at approximately 9974 feet as determined during the spinner survey of December 3rd. Gauges were pulled from Well 2 on December 6, 1992 at 9:48:00 prior to the start of injection into Well 2.

C) On December 3, 1992 at 16:58:00 gauges were run into Well 3. The SPRO gauge was placed at a depth of 9238 feet. The top of the Washita-Fredericksburg is at approximately 9797 feet measured depth in Well 3. Top of fill in Well 3 was recorded at approximately 10,000 feet as determined during the spinner survey. Gauges were pulled from Well 3 on December 10, 1992 12:08:00 prior to the start of injection into Well 3.

D - H) Injection was initiated in Well 4 on December 5, 1992 at 21:00:00 and continued until December 9, 1992 at 12:00:00. The average rate was approximately 120 gpm and interference created from the injection was observed in Well 3, Monitor Well 1, and for a short period in Well 2.

E - F) Injection was initiated in Well 2 on December 6, 1992 at 13:35 and continued until December 8, 1992 12:40:00. This injection period was not scheduled but was required to handle waste storage volume. The average rate was approximately 238 gpm. During this time interference created from the injection was observed in Well 3 and Monitor Well 1.

G) On December 9, 1992 at 9:02:00 gauges were run back into Well 2 and the SPRO gauge was placed at a depth of 9272 feet. The gauge was pulled from Well 2 on December 13, 1992 at 4:12:00.

I) Well 2 was flushed with Brine at approximately 12:30 on December 1g, 1992.

J) Gauges were placed in Well 4 on December 10, 1992 at 16:49:80 at a depth of 9207 feet. The approximate top of the Washita-Fredericksburg in Well 4 is 9753 measured depth.

K - L) Injection was initiated in Well 3 on December 11, 1992 at 3:36:00 end ended on December 12, 1992 at 4:46:00. The average rate was 110 gpm and interference was observed in Monitor Well 1, Well 2, end Well 4.

M) Well 4 was flushed with brine on December 13, 1992 at 6:55:80.

N) On December 13, 1992 at 8:18:00 gauges were run back into Well 3. However, due to mechanical problems with the wireline equipment the gauges could only be run to 5880 feet instead of the original depth of 9238 feet. The pressure data presented in graph S2-G2 for Well 3 after point M has been adjusted by adding 2120 psi to the data. This is the estimated difference in hydrostatic pressure between the gauge depth of 5000 feet and the original depth of 923B feet.

O-P) Injection was initiated in Well 2 at an average rate of 330 gpm sterting on December 13, 1992 at 17:36:00 and continuing until December 15, 1992 at 9:30:00. Interference was observed in Monitor Well 1, Well 3, and Well 4.

Q) Pressure gauges were pulled from Monitor Well 1 on December 16, 1992 at 7:58:80, from Well 3 December 16, 1992 at 8:55:08 and from Well 4 on December 16, 1992 at 8:57:00. This concluded the interference portion of the test.

Rate History

The previous discussion outlines the rato history during the test, but an additional one month of injection history for each active well wae used in the anelysis to account for the underlying effects previous rates may have had on the pressure response. The influence of injection prior to the start of this test is evidenced in Monitor Well 1 pressure data.

There was no injection into the field from November 29, 1992 until the start of injection into Well 4 on December 5, 1992 at 21:00:00. An attempt was made to establish a "stable" pressure profile in the field, however, inspection of Monitor Well 1 pressure data from December 3rd to December 5th shows the pressure continually declining. This observed decline is felt to be a result of prior injection into the field linked with the relatively low transmissibility of the reservoir.

The entire rate history used in the analysis is presented in Sections 10, 11 and 12 of this report. The rate data was provided by the DeLisle Plant and was downloaded from the plant's computer system.

Graph S2-G1, 1992 Interference Test - Rate and Pressure History

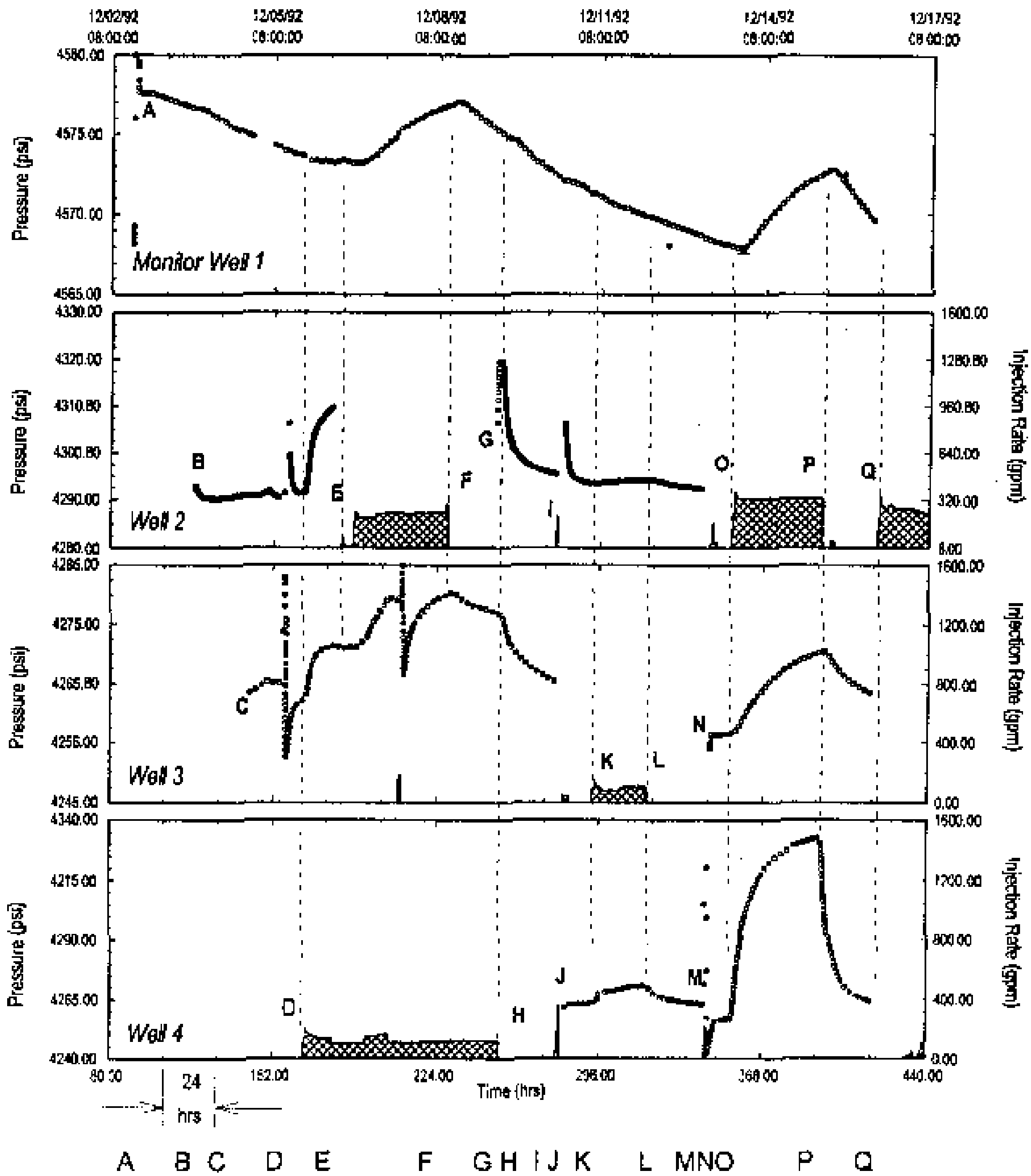

Data Quality

Gauge Drift

Graph S2-G2, below, is an expended view of the Monitor Well 1 pressure response while Well 3 was injecting. The change in the Monitor Well 1 pressure trend over a 36 hour period during the test ie only 0.65 psi, or 0.018 psi / hour. Because of the small pressure response observed in Monitor Well 1 caused by Well 3, a drift calibration was run on the Monitor Well Gauge to make sure the observed pressure change was actually interference and not just gauge drift.

Graph S2-G2; Monitor Well 1 Pressure While Well 3 Was Injecting

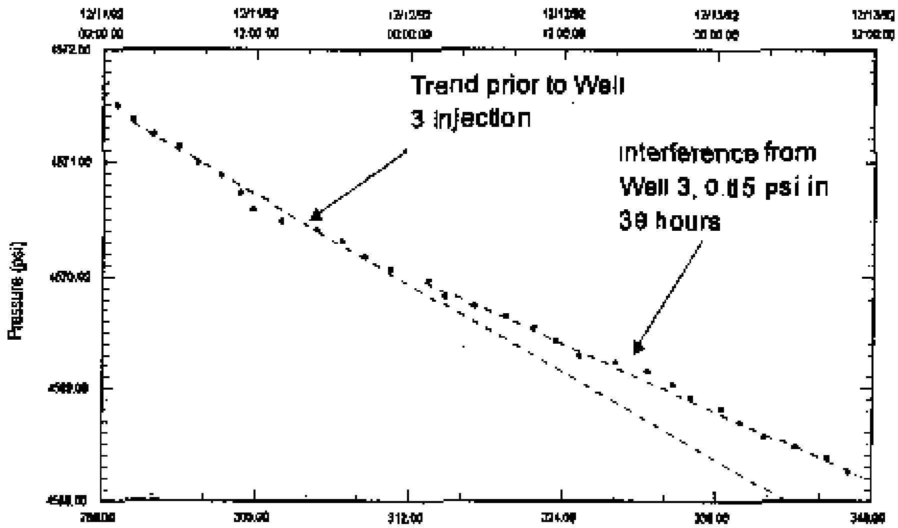

Graph S2-G3; Monitor Well Gauge Calibration

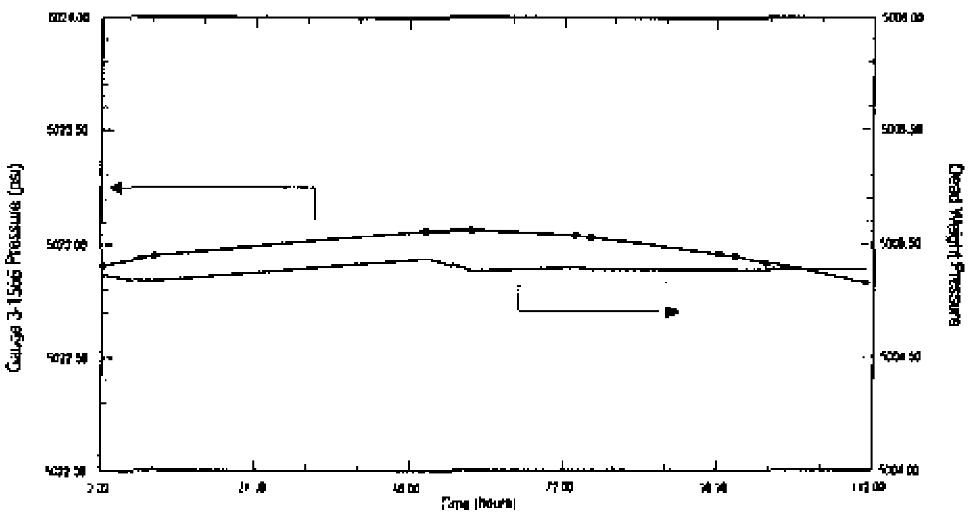

Graph S2-G4, above, is a graph of the Monitor Well 1 gauge placed in a calibration bath for 5 days at a constant temperature of 140 degrees and pressure of 5000 psig. The maximum gauge drift in the bath over 60 hours is approximately 0.2 psi, or 0.0033 psi / hr. This is a far smaller pressure response than seen in Monitor Well 1 thus indicating the pressure change in Monitor Well 1 is a result of interference from Well 3.

Gauge Depths

Graph S2-G5, below, shows the gauge depths during the interference test compared to the formation depths for each well. Note the top of the Washita-Fredericksberg Sand is indicated by the dashed line in the drawing. With the exception of Monitor Well 1 the gauges were over five hundred feet above the completed interval in each well. Also note the top of fill recorded in Well 2 and Well 3 at 9974 feet and 10,000 feet respectively. There was no fill noted in Well 4.

Graph S2-G5; Gauge Depths During the Test

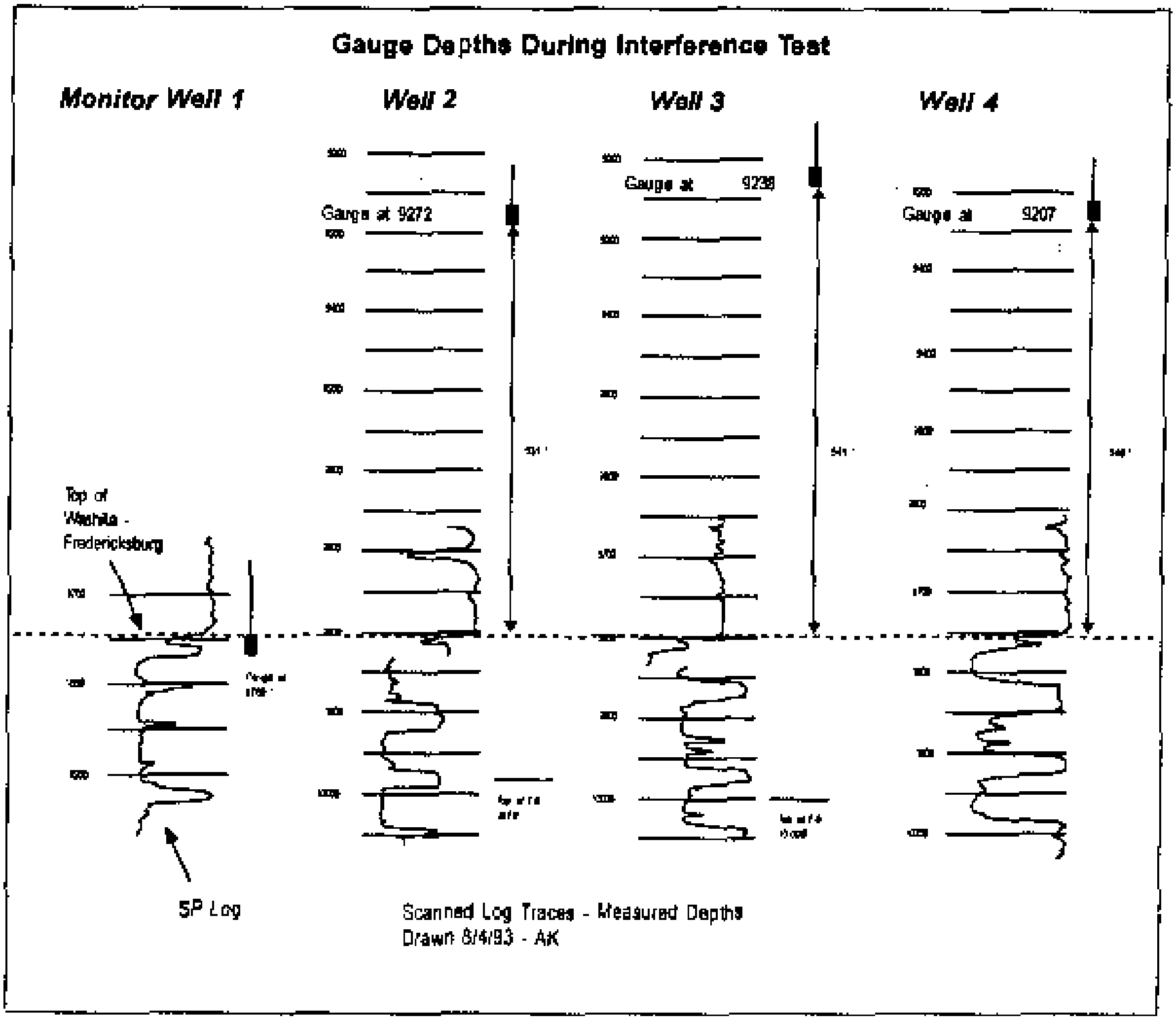

Well locations

At the time of this test there were three wells permitted for waste disposal with one Monitor well located on the DeLisle Plant (the completion on Well 5 was still ongoing). Graph S2-G6 below shows the wells' proximity to each other and the distance between wells used in the analysis. Distance between wells is used in the analysis to determine storativity ($\phi\ c_t\ h$) between wells. The calculated storativity values presented in this report are proportional to the square root of distance between wells.

Monitor Well 1, and Well 4 are vertical. Well 3 and Well 2 are deviated approximately 8 degrees.

S2-G6, Well Positions

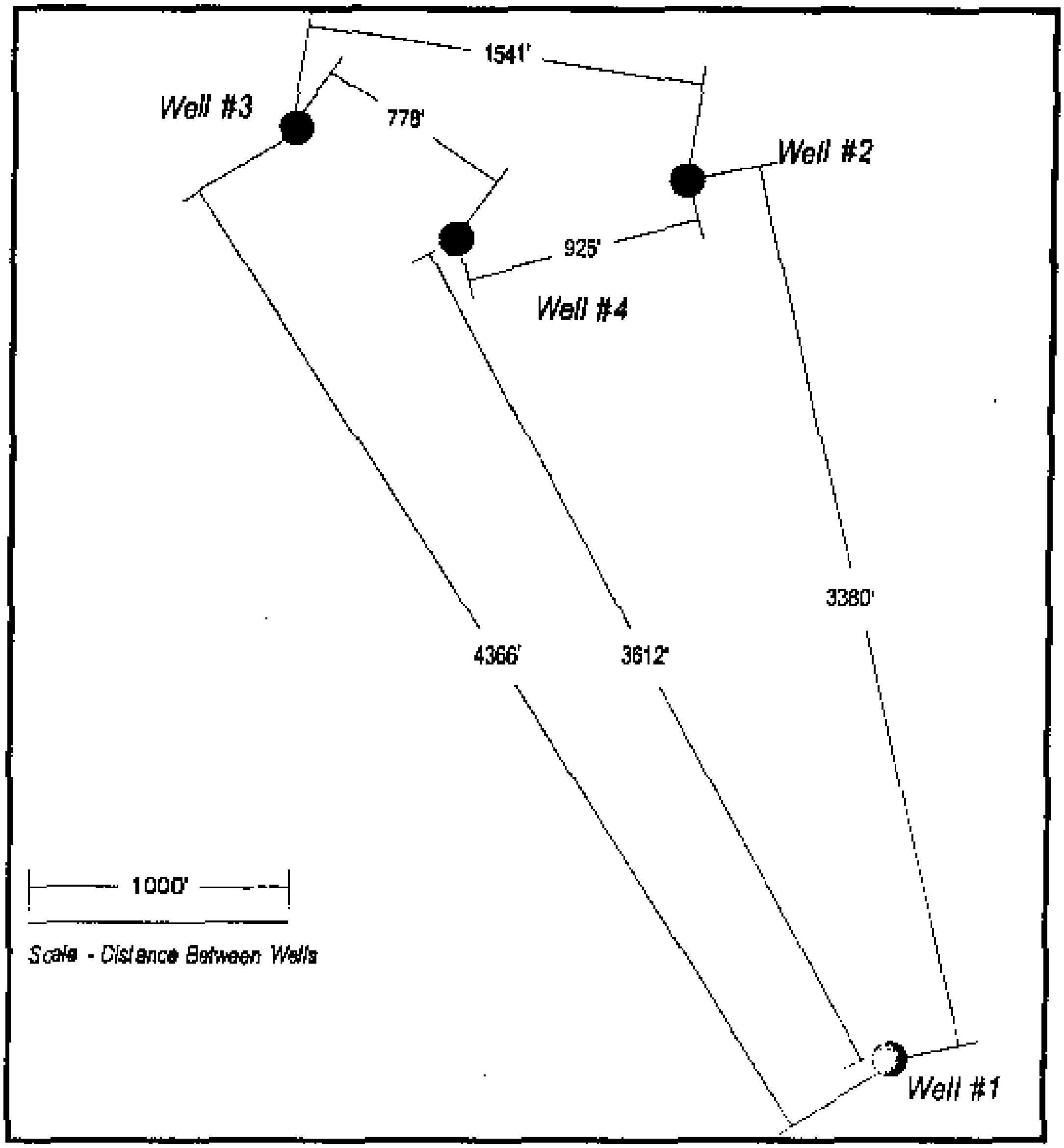

Fluid Properties Used in the Analysis

Graph S2-G7 shows the calculated total compressibility and fluid viscosity over the range of pressure encountered during the interference test. Graph S2-G8 presents the calculated total compressibility and fluid viscosity versus temperature. Viscosity is represented by the dashed line in both graphs.

Graph S2-G7; Total compressibility and viscosity versus pressure.

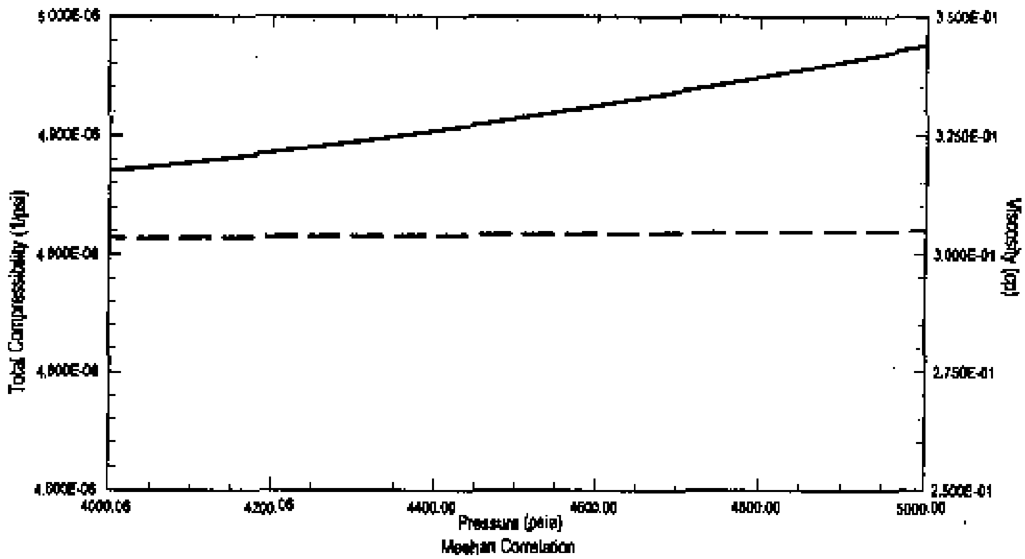

Graph S2-G7; Total compressibility and viscosity versus temperature.

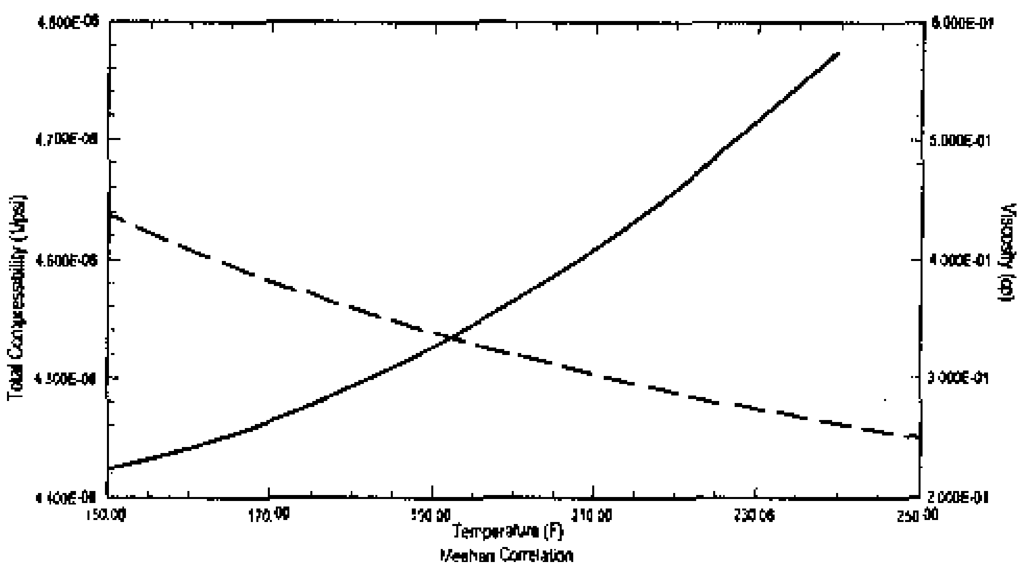

Table S2-T1 and Table S2-T2, below, show the calculated viscosity and total compressibility data presented in the previous graphs. Table S2-T1 is evaluated at 226° F and Table S2-T2 is evaluated at 4500 psia.

Table S2-T1; Pressure vs Fluid Properties

Pressure vs Total Compressibility*		Pressure vs Viscosity*	
4000.00	4.87E-06	4000.00	0.303
4052.63	4.67E-06	4052.63	0.304
4105.26	4.88E-06	4105.26	0.364
4157.90	4.68E-06	4157.90	0.304
4210.53	4.89E-06	4210.53	4.304
4263.16	4.89E-06	4263.16	0.304
4315.79	4.90E-06	4315.79	0.304
4368.42	4.90E-06	4368.42	0.304
4421.05	4.91E-06	4421.05	0.304
4473.68	4.91E-06	4473.68	0.304
4526.32	4.92E-06	4526.32	0.304
4578.95	4.92E-06	4578.96	0.304
4631.58	4.93E-06	4631.58	0.304
4684.21	4.94E-08	4684.21	0.305
4736.84	4.94E-06	4736.84	0.305
4789.47	4.95E-06	4789.47	0.305
4842.11	4.95E-06	4842.11	0.305
4894.74	4.96E-06	4894.74	0.305
4947.37	4.97E-06	4947.37	0.305
5000.00	4.98E-08	5000.00	0.305

**Evaluated at 226° F*

Table S2-T2; Temperature vs Fluid Properties

Temperature vs Total Compressibility[+]		Temperature vs Viscosity[+]	
150.00	4.42E-06	150.00	0.438
155.26	4.43E-06	155.26	0.422
160.53	4.44E-06	160.53	0.407
165.79	4.45E-06	165.79	0.393
171.05	4.47E-06	171.05	0.380
176.32	4.48E-06	176.32	0.368
181.58	4.50E-06	181.58	0.356
186.84	4.52E-06	186.84	0.345
192.11	4.53E-06	192.11	0.335
197.37	4.55E-06	197.37	0.325
202.63	4.58E-06	202.63	0.316
207.90	4.60E-06	207.90	0.307
213.16	4.63E-06	213.16	0.298
218.42	4.65E-06	218.42	0.290
223.68	4.68E-06	223.68	0.283
228.95	4.71E-06	228.95	0.276
234.21	4.74E-06	234.21	0.269
239.47	4.77E-06	239.47	0.262
244.74	4.81E-06	244.74	0.256
250.00	4.85E-06	250.00	0.250

[+]*Evaluated at 4550 psia*

An accurate evaluation of fluid properties is important because the estimation of effective zone height is proportional to total compressibility using the Storativity (ϕ c_t h) value from the interference analysis. Also, estimated permeability is proportional to viscosity using the transmissibility [(k h) / (μ B)] from the interference analysis.

Inspection of the pressure-volume-temperature relationships shows that viscosity and total compressibility is insensitive to pressure change yet a bigger variance is evidenced when temperature changes. The fluid properties used in this study were evaluated at 226° F and 4550 psia. The estimated viscosity at these conditions is 0.303 cp and the total compressibility is 4.659E-06 1/psi. The temperature of 226° F was the average bottomhole temperature as measured by the Monitor Well gauge during the interference test.

Section 3 -- Interference Analysis

Description of an Interference Test

A simple interference test is conducted by placing pressure gauges in one well while a rate change is made at an offset well. The change in pressure at the observation well is a function of the average reservoir properties between the wells. Graph S3-G1, below, shows a simple two well interference test. The well on the right is the *observation* well while the well on the left is the *active*, or *interfering* well.

Graph S3-G1; Two Well Interference Test

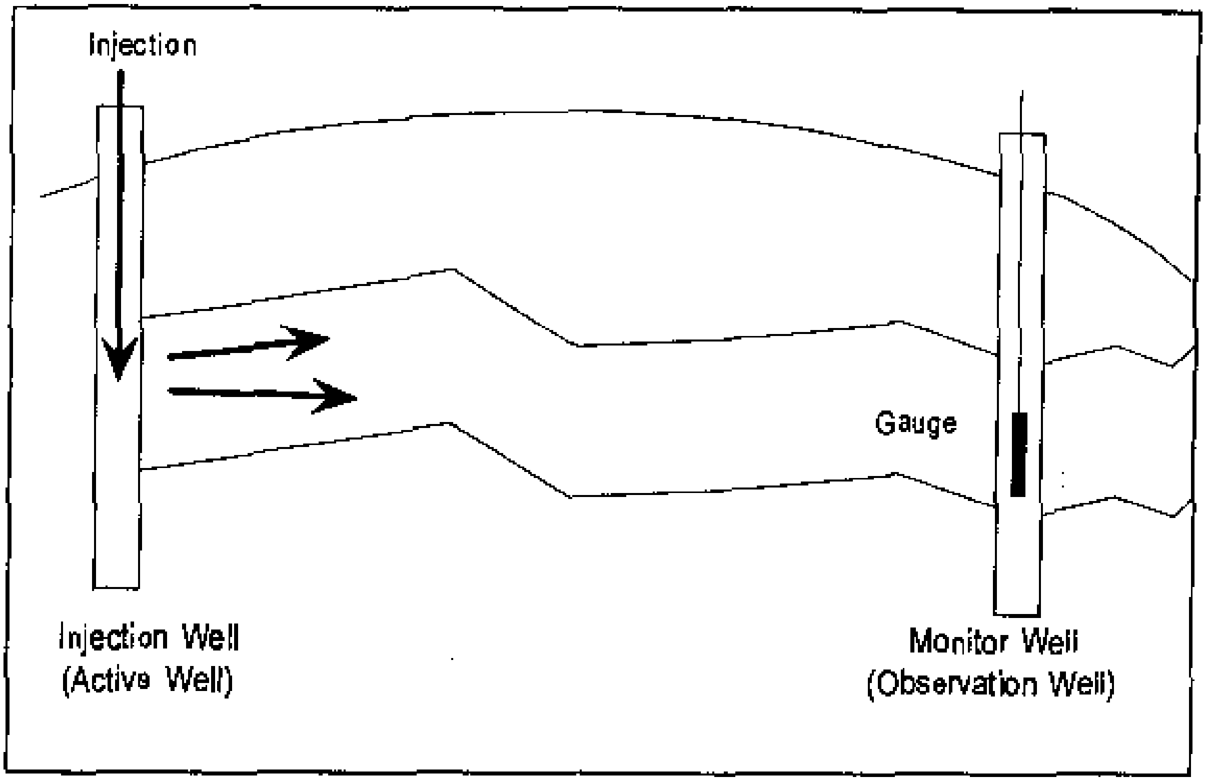

Graph S3-G2 on the next page shows the theoretical pressure response created in the observation well during injection into the active well. Pressure will increase exponentially, and proportionally to the distance and reservoir properties between the wells. The magnitude of the pressure increase is governed by the rate, the distance between wells, and the average transmissibility between wells.

√ The lower the transmissibility, the bigger the pressure increase at the observation well.

√ The higher the injection rate, the bigger the pressure increase at the observation well.

√ The closer the wells, the bigger the pressure increase at the observation well.

Graph S3-G2; Conceptual Pressure Response - Two Well Interference Test

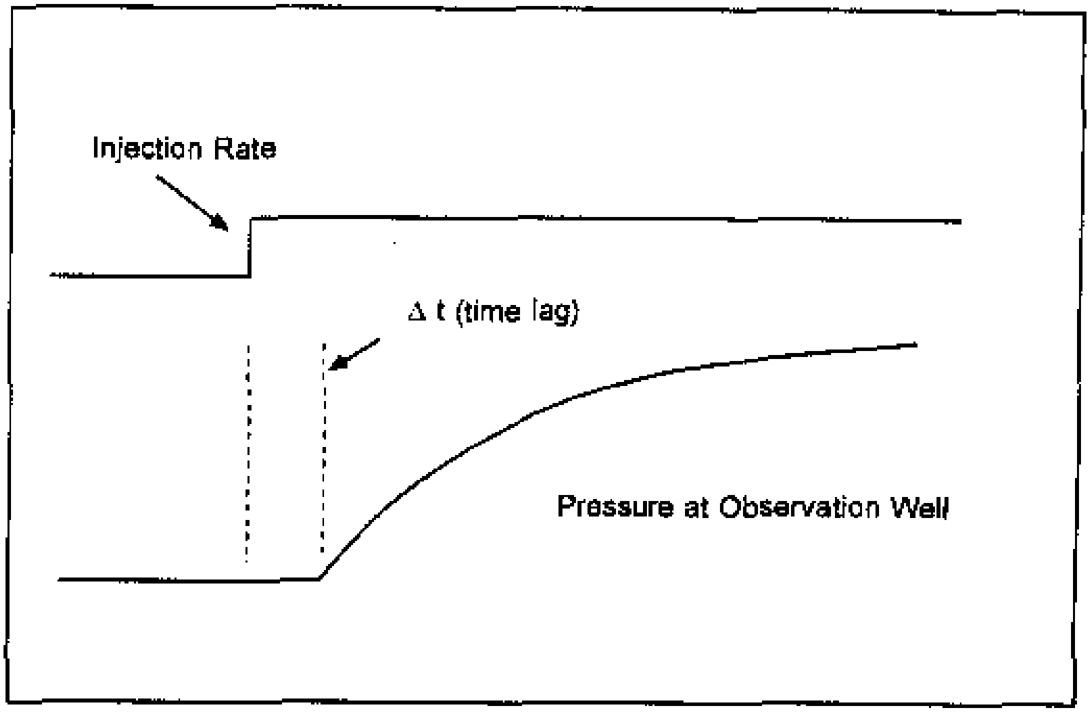

The dashed line in Graph S3-G2 shows a time lag from when injection starts in the active well and the observed pressure increase in the observation well. This time lag is a function of the rock and fluid properties between the wells. The term that defines the time lag is known as the diffusivity constant[1] and is defined as

$$\eta = \frac{k}{\phi c_t \mu}$$

Where,

k =	Permeability (md)
ϕ =	Porosity (fraction)
c_t =	total compressaibility (1/psi)
μ =	Viscosity (cp)

A decrease in porosity, viscosity and total compressibility , or an increase in permeability, will decrease the time required to see the pressure response in the observation well.

The common technique used to analyze the simple two well interference test is the type curve matching method. The type-curve matching technique requires aligning a plot of log delta pressure vs log delta time from the start of injection at the active well to the theoretical pressure solution. The theoretical solution is the basic analytical model known as the Exponential Integral and the ratio of the measured data

[1] Craft and Hawkins, *Applied Petroleum Reservoir Engineering*, (Prentice Hall, 1959), 275

to the theoretical solution yields transmissibility [(k h) / (μ B)], and the diffusivity constant. The diffusivity term is further reduced to the Storativity ($\phi\ c_t\ h$) term, by dividing by transmissibility.

The type curve matching technique is outlined in detail in *SPE Monograph Volume 5, Advances in Well Test Analysis*, available through the Society of Petroleum Engineers (SPE) . The SPE headquarters are located in Richardson, Texas.

The simple type-curve matching procedure works fine when the pressure in the observation well is stable prior to the start of injection in the active well, and when there are no other active wells in the field. However, the simple two-well situation does not exist with the DeLisle interference test. In the DeLisle study there are multiple interfering wells, and in some cases the observation well itself is active prior to becoming an observation well. Therefore a more sophisticated approach is required to analyze the data.

Description of the Pressure History Matching Technique

The Pressure History Simulation technique is used to analyze complex interference tests, such as the DeLisle test where there are multiple interfering wells. Pressure History Simulation involves generating the theoretical pressure response at the observation well given the observation well's rate history and the rate history of all of the surrounding wells.

The pressure change (relative to the initial pressure) in the observation well at any point in time is the sum of the pressure changes due to the surrounding wells rate history, inter-well properties, boundary conditions, and reservoir characteristics. The pressure in the observation well is calculated using superposition techniques described in various publications. SPE Volume 5, *Advances in Well Test Analysis* is one source that provides some Insight into the superposition techniques used in this study.

The pressure at any given time (t), in the observation well, is calculated from the following equation.

$$p_{(t)} = p_o - \frac{141.2B\mu}{kh}\sum_{i=1}^{n}(q_i - q_{i-1})P_{D[(t-t_{i-1})_D]} - \sum_{j=1}^{z}\frac{141.2B\mu}{kh}\sum_{i=1}^{n}(q_{ji} - q_{j,i-1})P_{D[(t-t_{j,i-1})_D, R_D]}$$

PD =	Dimensionless Pressure (model dependent)
TD =	Dimensionless Time (model dependent)
k =	Permeability (md)
B =	Formation Volume Factor (dim)
h =	Net zone thickness (ft)
μ =	viscosity (cp)
n =	Number of rates influencing each well
z =	Number of interfering wells
RD =	Dim. Distance from the observation well
p_o =	Initial pressure

A regression routine is needed to help find the set of reservoir parameters that gives the best agreement between the model response and the measured data given the infinite number of combinations of parameter values that can be used to predict the pressure response at the observation well.

The Pressure History Simulstion technique used in the analysis of this data "systematically varies" the model parameters ($kh/\mu B$, $\phi c_t h$, p_e, etc..) using a modified[2] Marquardt-Levenberg regression algorithm. The modified Marquardt-Levenberg algorithm uses the derivative of pressure error (p model - p measured) with respect to each model parameter of interest to steer the match toward the best statistical fit.

The engineer's role in the Pressure History Simulation process is in data preparation, the choice of model to use in the simulation (i.e. homogeneous, two-porosity, bounded), finding the starting point for each parameter, setting limits on parameters to keep the solution away from unrealistic answers, and to "weight" the data. Data weighting is a means to have the optimizer concentrate on portions of the data the analyst feels csn be best represented by the model.

The adequacy of the Pressure History Simulation can be judged statistically, as well as by visual inspection. When the simulated pressure goes through every point the match is deemed perfect.

Models

The three analytical models used in this simulation study were the homogeneous, two-porosity, and homogeneous with outer no-flow boundaries. Each model is briefly discussed below.

The homogeneous model assumes "horizontal flow, negligible gravity effects, a homogeneous and isotropic porous medium, a single fluid of constant compressibility, applicability of Darcy's law, and that μ, c_t, k, and ϕ are independent of pressure."[3] The homogeneous model is solved in Laplace space and inverted through the use of Stefhest inversion algorithm to generate the constant rate dimensionless pressure solution (PD). This solution is then used in the superposition technique presented on page 3.

The two-porosity model contains the assumptions of the homogeneous solution with the exception of constant permeability and porosity. The two-porosity model assumes a higher permeability, higher porosity system (such as fractures or s layer) takes the majority of injection fluid snd that the fluid "leaks" off into s secondary system with lower permeability and porosity. See SPE Paper 7977 for a detailed description of the two-porosity model.

The homogeneous model with no-flow boundaries has all the implicit assumptions of the basic homogeneous model but with the addition of four barriers to flow at various distances from the well. A modified Green's function solution[4] is used to generate the dimensionless pressure response for a well inside a closed rectangle.

---

[2]Maghsood Abbaszadeh and Medhat Kamal, "Automatic Type-curve Matching for Well Test Data", September 1988, SPE Formation Evaluation magazine

[3]*Advances in Well Test Analysis*, pg. 4

[4]Gringarten, Alain, "The Use of Source and Green's Functions in Solving Unsteady-Flow Problems in Reservoirs"

Interpretation Periods

Section 1 of this report presents a summary of the inter-well properties derived from the Pressure History Simulation of the interference data. These values are felt to be the most representative inter-well properties available given the data collected during the testing process.

There were fourteen individual Pressure History Simulations conducted using various models and focusing on distinct transient periods to arrive at the values presented in Section 1 of this report. Table S3-T1, below, gives a summary of all the results from each Pressure History Simulation run.

Table S3-T1; Summary of the Results From Each Pressure History Simulation

	1 <--> 2 kh/uB / ϕ cth	1 <--> 3 kh/uB / ϕ cth	1 <--> 4 kh/uB / ϕ cth	Pi (psia)	Σ err^2	Model Type	Graph
Monitor Well 1	125,477 1.07E-4	167,573 2.92E-4	196,460 1.61E-4	4538	1.68	Closed Rectangle	S3-G3
Monitor Well 1	142,227 1.13E-4	521,603 4.13E-4	288,471 1.94E-4	4566	3.16	Homogen. Infinite	S3-G4

	2 <--> 3 kh/uB / ϕ cth	2 <--> 4 kh/uB / ϕ cth	At Well 2 kh/uB	Pi (psia)	Σ err^2	Model Type	Graph
Well 2	147,671 5.48E-6	21,175 4.50E-6	76,941	4281	1.49	2 Porosity	S3-G5
Well 2		12,879 1.36E-5		4255	1.74	2 Porosity	S3-G6
Well 2		42,932 4.29E4		4276	165.78	Homogen.	S3-G7
Well 2		28,816 2.42E-5		4284	2.53	2 Porosity	S3-G8
Well 2		41,327 3.45E-5		4283	3.03	Homogen.	S3-G9

	3 <-->2 kh/uB / ϕ cth	3 <--> 4 kh/uB / ϕ cth	At Well 3 kh/uB	Pi (psia)	Σ err^2	Model Type	Graph
Well 3	51,806 1.56E-4	42,547 8.42E-5		4244	1.59	2 Porosity	S3-G10
Well 3	179,646 2.12E-4	82,437 9.51E-5		4252	6.74	Homogen.	S3-G11
Well 3	112,413 1.64E-4			2128*	2.86	Homogen.	S3-G12
Well 3	67,787 1.63E-4			2129*	1.46	2 Porosity	S3-G13

*Gauge at 5000 ft.

Table S3-T1 Continued

	4 <-->2 kh/uB / ϕ cth	4 <--> 3 kh/uB / ϕ cth	At Well 4 kh/uB	Pi (psia)	Σ err^2	Model Type	Graph
Well 4	12,838 1.65E-5	66,885 7.53E-5	123,344 N/A	4182	30.92	2 Porosity	S3-G14
Well 4	23,328 2.97E-5	87,508 1.11E-4	148,128	4244	3.03	2 Porosity	S3-G15
Well 4	194,021 8.27E-5	77,821 9.67E-5	148,883	4250	8.99	Homogen.	S3-G16

Discussion of Interference Testing Results

Table S3-T1 is broken into four parts, one for each well. Part 1 shows the results from the analysis of Monitor Well 1 pressure data, part 2 shows the results of Well 2's pressure data, and so on. Columns two through four show the inter-well properties determined from the analysis of the pressure data. For instance, the column labeled "1 <--> 2" indicates that Monitor Well 1 was the observation well and Well 2 was the active Well. The data in the row below this column shows the transmissibility and storativity values determined from the analysis.

The fourth column, in the case of the injectors, shows the transmissibility value derived from the pressure response created when the well itself was injecting. In general these results are not very reliable because the gauges were taken out of the well during the injection of waste so no data exists with distinct character to derive near well properties. The gauges were in the well during brine flushes but the brine flush has the effect of distorting the pressure response due to density changes. This "distorted" behavior can be observed in Graphs S3-G10 and S3-G11, (located at the back of this section), when Well 3 was flushed at an elapsed time of approximately 207 hours. Notice the gauge response in relationship to what the theoretical response predicts for this period. It is felt that because the brine is heavier than the in-situ waste the pressure at the gauge is lower following the flush, then as waste creeps into the wellbore the gauge pressure will slowly increase. The data seems to be back on track near 230 hours.

The fifth column in Table S3-T1 shows the reservoir pressure at the start of the injection history. As noted in Section 2, one month of prior injection history was used in the analysis so the initial pressure is the estimated pressure, at gauge depth, on November 1, 1992. Initial pressure is the p_0 term in the equation presented on page 3 of this section.

The sixth column shows the sum of error squared determined form the comparison of the measured response to the simulated response; the smaller the value the better the fit. Zero indicates there is no difference between the measured and simulated data. Graph S3-G7 is a match of Well 2 data while Well 4 was injecting and has a Σerr^2 value of 185.7. This is an example of the best match possible with a model that doesn't explain the pressure response. Graph S3-G6 is a match of the same data, but using a two-porosity model, and is a much better fit as indicated by the Σerr^2 value of 1.74.

The seventh column references the graph located at the back of this section for each match presented in the table.

As mentioned previously the Monitor Well pressure response gives the best model results. Graph S3-G3 and Graph S3-G4 show the simulations given a homogeneous model with boundaries, and a homogeneous model without boundaries.

The initial match of Monitor Well 1 data was made without boundaries with very good results (see Graph S3-G4) but there seems to be an underlying pressure trend in the data. Boundaries were added to the model to see if they would improve this match by explaining the underlying trend. The diagram in Graph S3-G3 shows the well's location in relationship to four no-flow boundaries as determined from the Pressure History Simulation. The addition of boundaries to the model helped the match but the distances to the boundaries should be used qualitatively based on their statistical significance in explaining the pressure response. Table S3-T2 shows the 95% confidence interval for the estimated boundary locations. The distances are relative to Monitor Well 1, so that L-> means the boundary to the right of Monitor Well 1, <-L to the left and so on.

Tables S3-T2; 95 % Confidence Interval - Distance to Boundaries from Monitor Well 1

7028 '	L->	121,580 '
6253 '	<-L	15,652 '
2663 '	L^^	16,440 '
2643 '	Lvv	26,223 '

Also mentioned previously is the fact the apparent transmissibility between Well 2 and 4 is lower than between other Wells. This is evident in all of the transient periods between Well 2 and Well 4 with the exception of the analysis presented in Graph S3-G16. In this case transmissibility between Well 2 and Well 4 is reported as 194,021 md-ft/cp. Inspection of this analysis shows that this value came from a period when Well 2 was injecting at a very low rate at the same time Well 3 was injecting. The 95% confidence interval for this transmissibility ranges from 9.1643E02 md-ft/cp to 4.1077E07 md-ft/cp This is a good example of how the values presented in this table shouldn't be taken at face value.

Perhaps the most difficult section of data to match from the entire test can be seen in Graphs S3-G14, S3-G15, and S3-G16. This is the pressure response observed in Well 4 while Well 3 was injecting and while Well 2 was injecting. The previous Graph S3-G13 shows an excellent match of the response between Well 3 and Well 4 using a two-porosity model focusing on the section when only well 3 was injecting. However, when the simulation is extended to the entire range of data a match cannot be found using the same two porosity model.

The root of the problem in matching the entire range of Well 4 pressure data is felt to be the gauge distance above the injection interval and the changing fluid density below the gauge. The effects of multi-layer response in Well 4 is also a potential explanation of the pressure behavior, however, there is not information available to quantify this aspect. Rate data from each of the layers would have to be collected during the interference portion of the test which is not feasible due to the acidity of the waste stream.

Only sections of the data collected in Well 4 can be successfully matched. Graph S3-G14 matches the last part of the data when Well 2 stops injection. This is felt to be the most reliable estimate of properties between Well 4 and Well 2 because we know exactly what the rate is from Well 2 (zero) and the gauge and wellbore have had the longest amount of time to stabilize. Graph S3-G15 shows the simulation when Well 2 starts injection but this match is unable to reproduce the falloff response when Well 2 stops injection.

State .... Mississippi	**Du Pont DeLisle Plant**	**Test Date** 5-Dec-92
County .... Harrison	**Monitor Well 1**	**Analysis Date** 1-Jun-93
Field .... DeLisle Plant	**Graph S3-G3**	**Report Number** 930201

Pressure History Simulation - Closed Rectangle Model

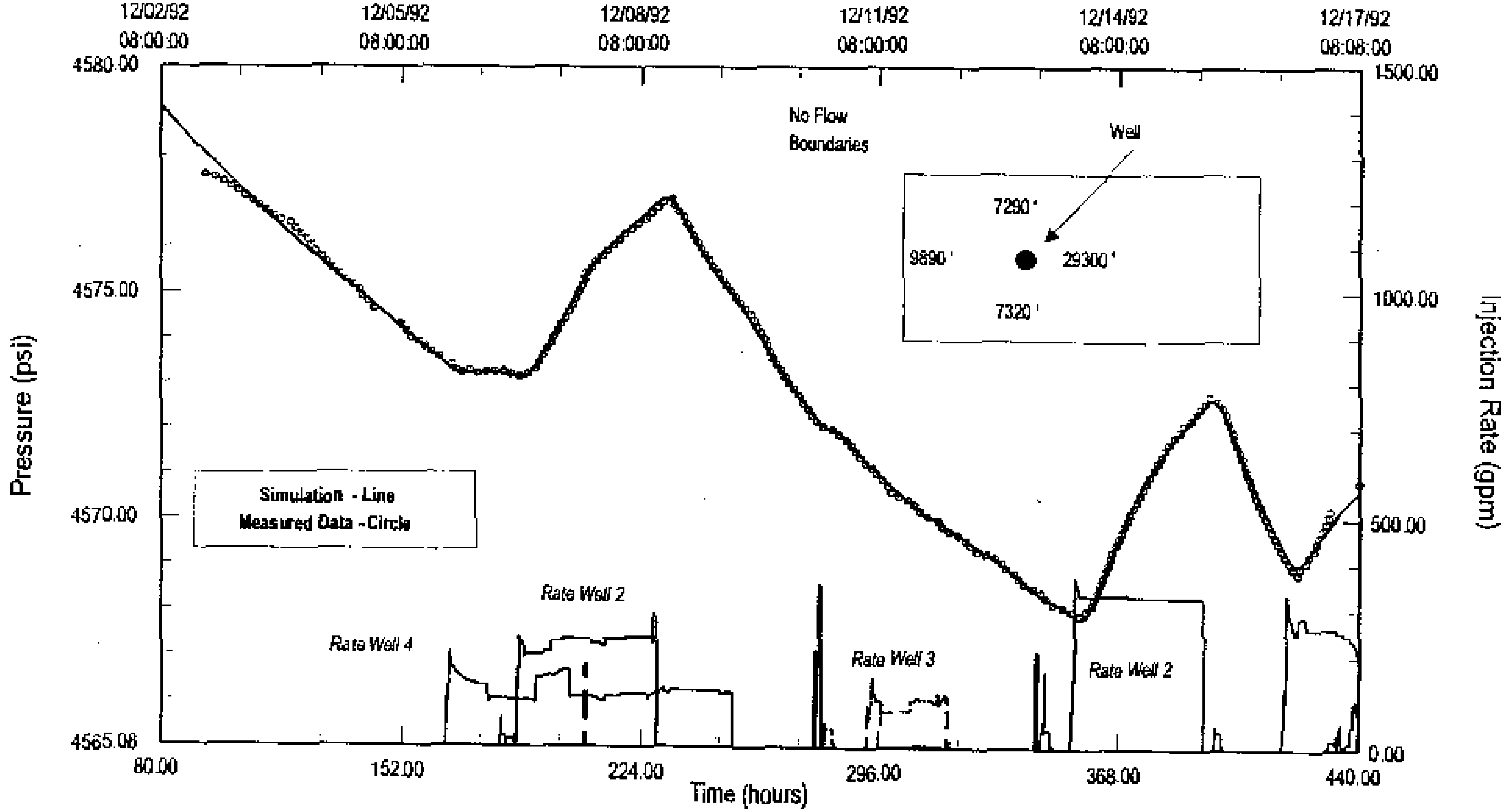

	1 <-> 2	1 <-> 3	1 <-> 4		
kh/uo (md-ft/cp)	129,477	167,573	196,460	pi (psi at gauge depth)	4,530
phi*ct*h (ft/psi)	1.07E-04	2.92E-04	1.61E-04	Sum Square Error	1.68

State .... Mississippi **County** .... Harrison **Field** .... DeLisle Plant	**Du Pont DeLisle Plant** ***Monitor Well 1*** ***Graph S3-G4***	**Test Date** .... 5-Dec-92 **Analysis Date** .... 1-Jun-93 **Report Number** 930201

Pressure History Simulation - Infinite System Model

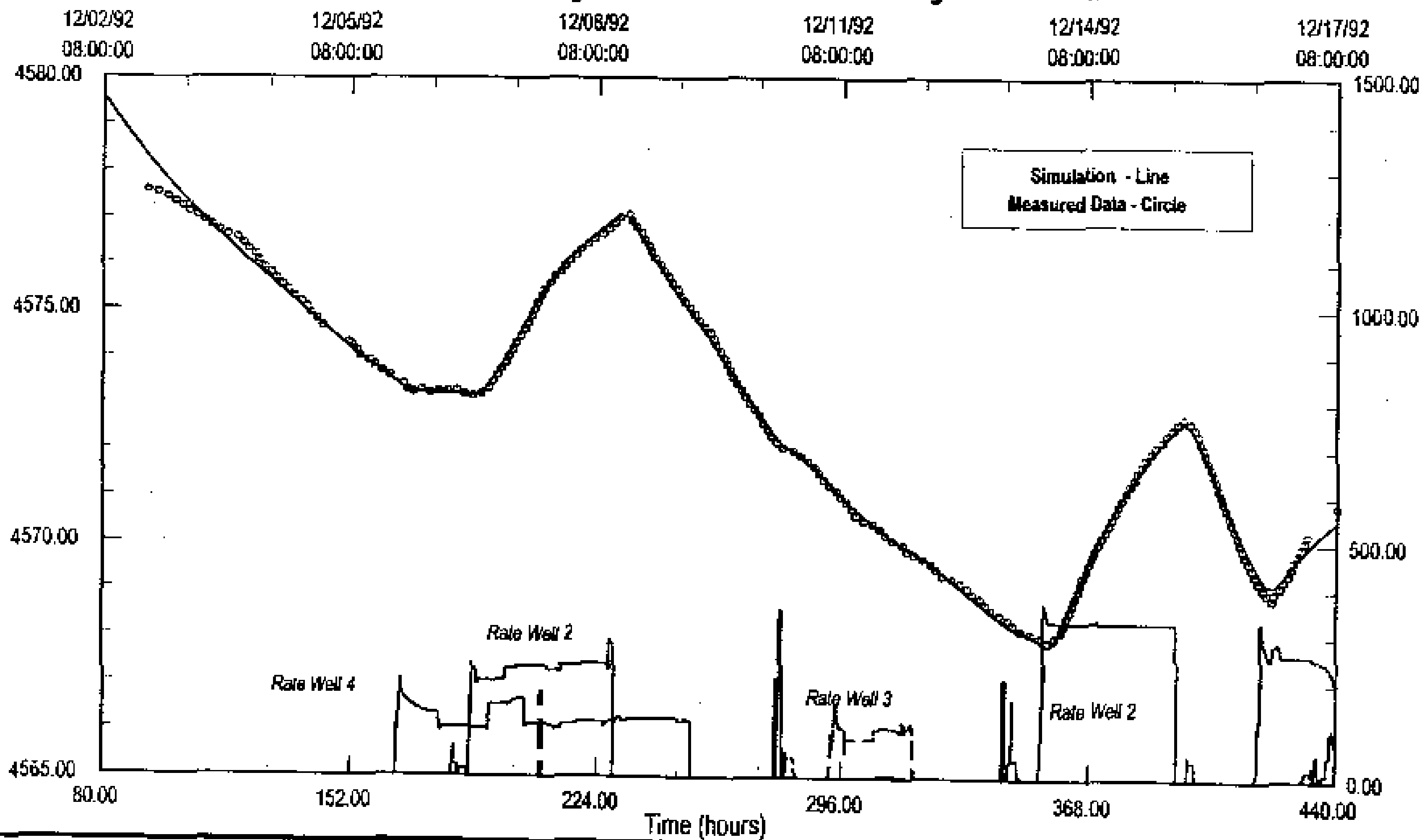

	1 <-> 2	1 <-> 3	1 <-> 4		
kh/ub (md-ft/cp)	142,227	521,603	206,471	pi (psi at gauge depth)	4,566
phi*ct*h (ft/psi)	1.13E-04	4.13E-04	1.94E-04	Sum Square Error	3.18

State .... Mississippi **County** .... Harrison **Field** .... DeLisle Plant	**Du Pont DeLisle Plant** ***Well 2*** ***Graph S3-G5***	**Test Date** .... 5-Dec-92 **Analysis Date** .... 1-Jun-93 **Report Number** 930201

Pressure History Simulation - 2 Porosity Model

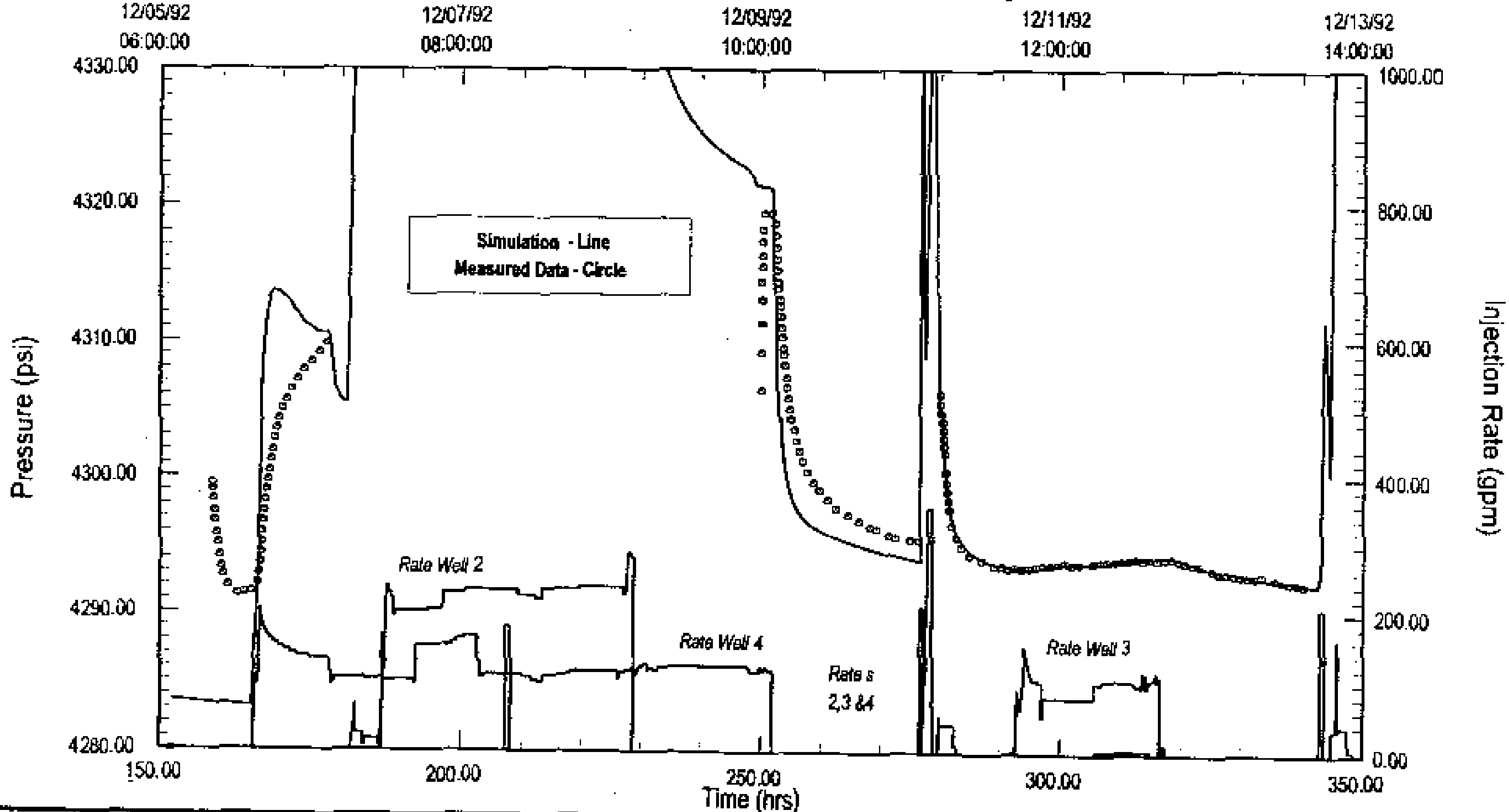

	At 2	2 <-> 3	2 <-> 4		
kh/ub (md-ft/cp)	70,941	147,671	21,175	pi (psi at gauge depth)	4,251
phi*ct*h (ft/psi)		5.40E-06	4.50E-06	Sum Square Error	1.49

Z13

State .... Mississippi	**Du Pont DeLisle Plant**	***Test Date*** 5-Dec-92
County .... Harrison	***Well 2***	***Analysis Date*** 1-Jun-93
Field .... DeLisle Plant	***Graph S3-G6***	***Report Number*** 930201

Pressure History Simulation - 2 Porosity Model

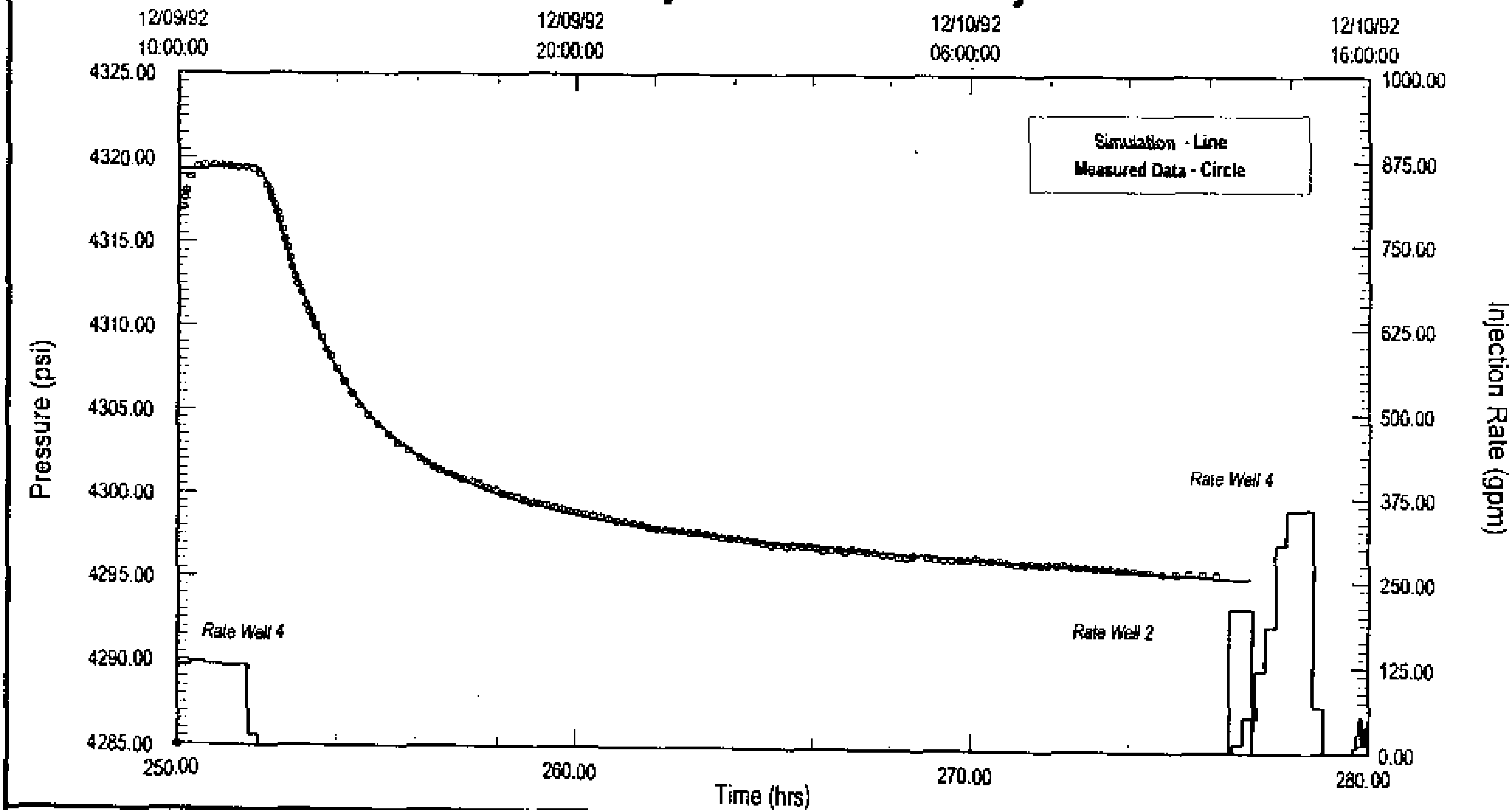

	2 <-> 4		
kh/ub (md-ft/cp)	12,879	pi (psi at gauge depth)	4,255
phi*ct*h (ft/psi)	1.36E-05	Sum Square Error	1.74

z12

State	Mississippi
County	Harrison
Field	DeLisle Plant

Du Pont DeLisle Plant

Well 2

Graph S3-G7

Test Date	5-Dec-92
Analysis Date	1-Jun-93
Report Number	930201

Pressure History Simulation - Homogeneous Model

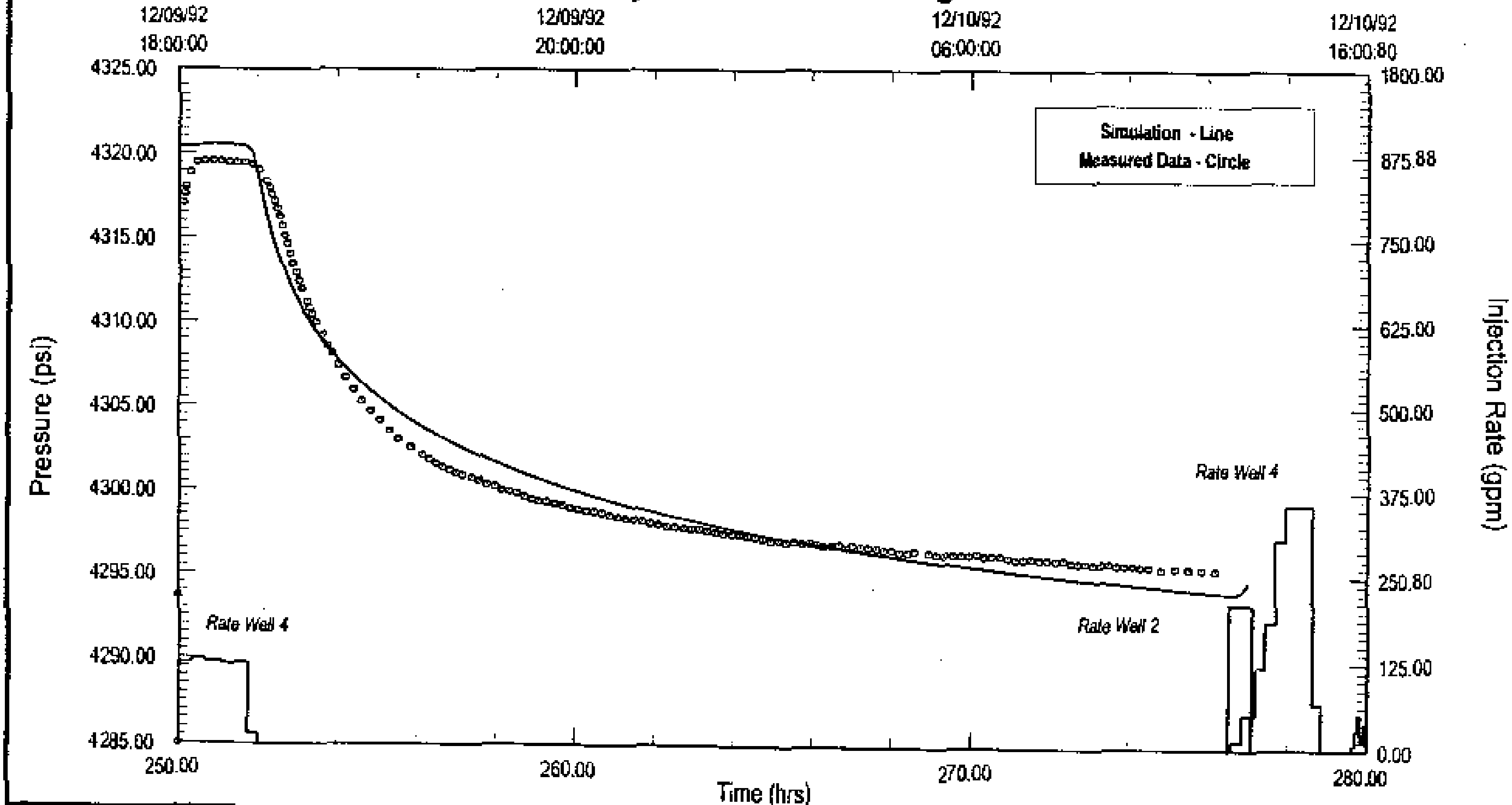

	2 <-> 4
kh/ub (md-ft/cp)	42,932
phi*ct*h (ft/psi)	4.29E+04

pi (psi at gauge depth)	4,276
Sum Square Error	185.78

211

State .... Mississippi	**Du Pont DeLisle Plant**	**Test Date** 5-Dec-92
County .... Harrison	***Well 2***	**Analysis Date** 1-Jun-93
Field .... DeLisle Plant	***Graph S3-G8***	**Report Number** 930201

Pressure History Simulation - 2 Porosity Model

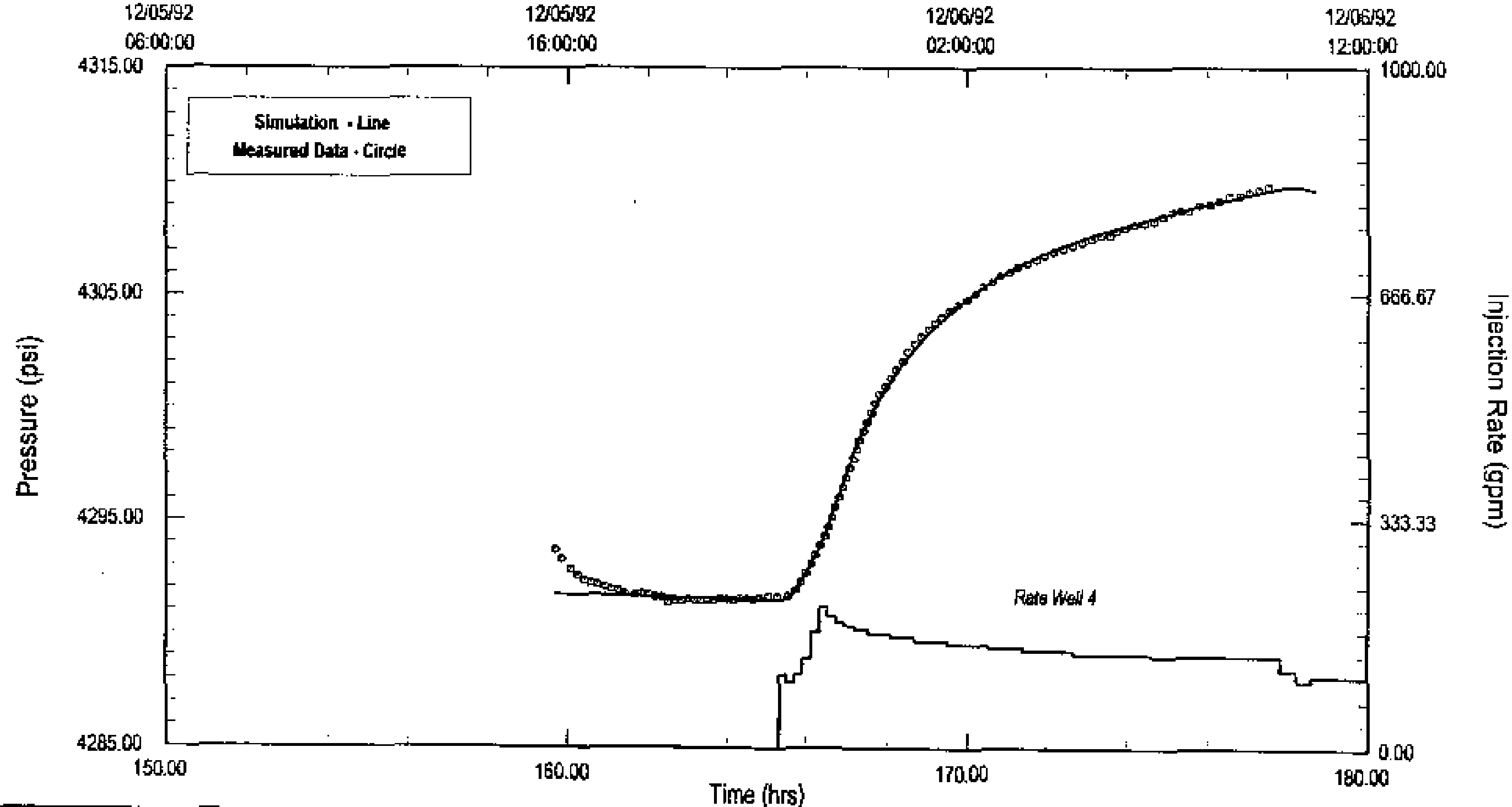

	2<-> 4		
kh/ub (md-ft/cp)	26,016	pi (psi at gauge depth)	4,284
phi*ct*h (ft/psi)	2.42E-05	Sum Square Error	2.53

z10

State .... Mississippi *County* .... Harrison *Field* .... DeLisle Plant	**Du Pont DeLisle Plant** ***Well 2*** ***Graph S3-G9***	*Test Date* .... 5-Dec-92 *Analysis Date* .... 1-Jun-93 *Report Number* 930201

Pressure History Simulation - Homogeneous Model

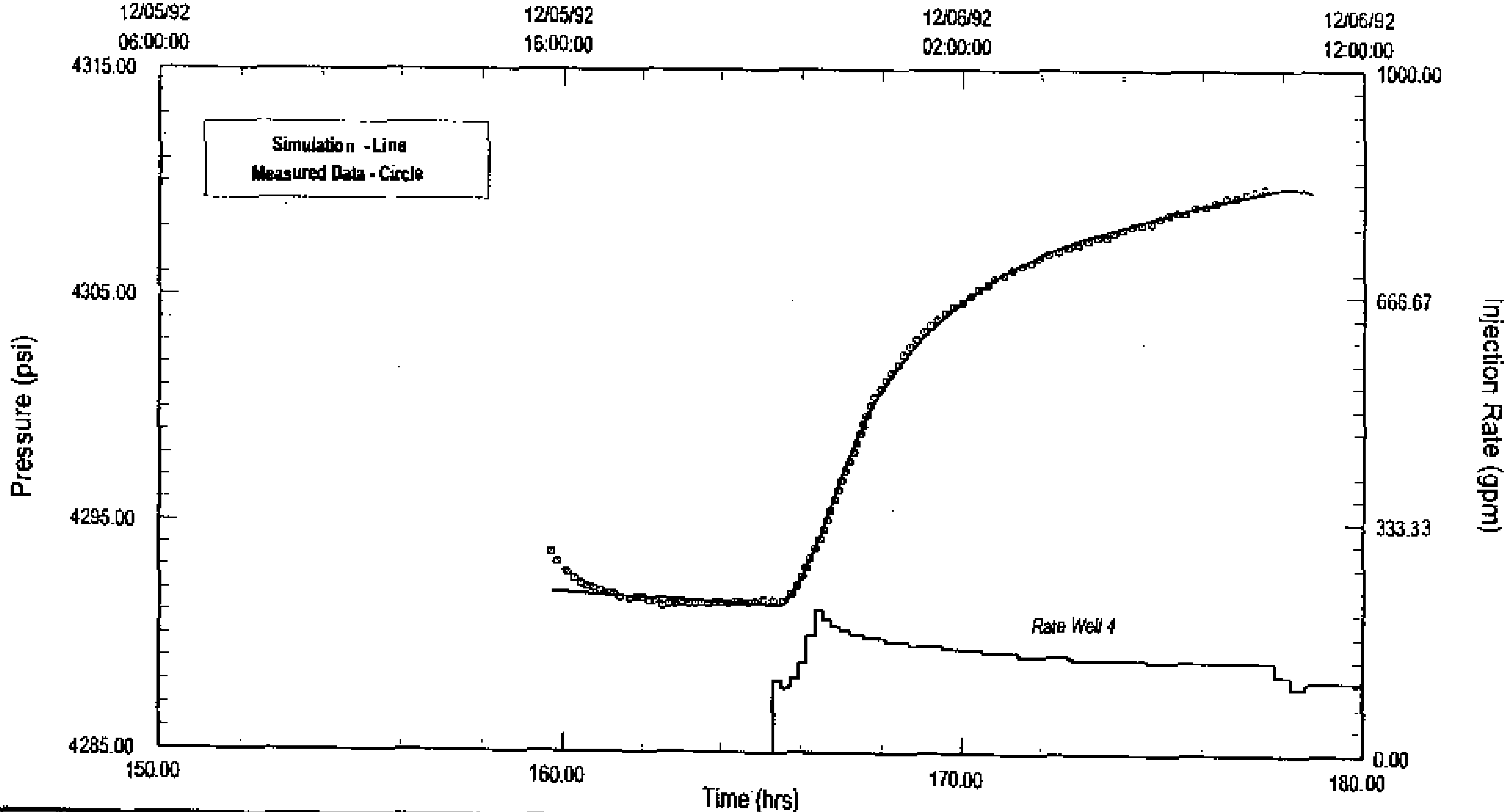

	2 <-> 4		
kh/ub (md-ft/cp)	41,327	pi (psi at gauge depth)	4,283
phi*ct*h (ft/psi)	3.45E-05	Sum Square Error	3.03

State .... Mississippi
County .... Harrison
Field .... DeLisle Plant

Du Pont DeLisle Plant

Well 3

Graph S3-G10

Test Date 5-Dec-92
Analysis Date 1-Jun-93
Report Number 930201

Pressure History Simulation - 2 Porosity Model

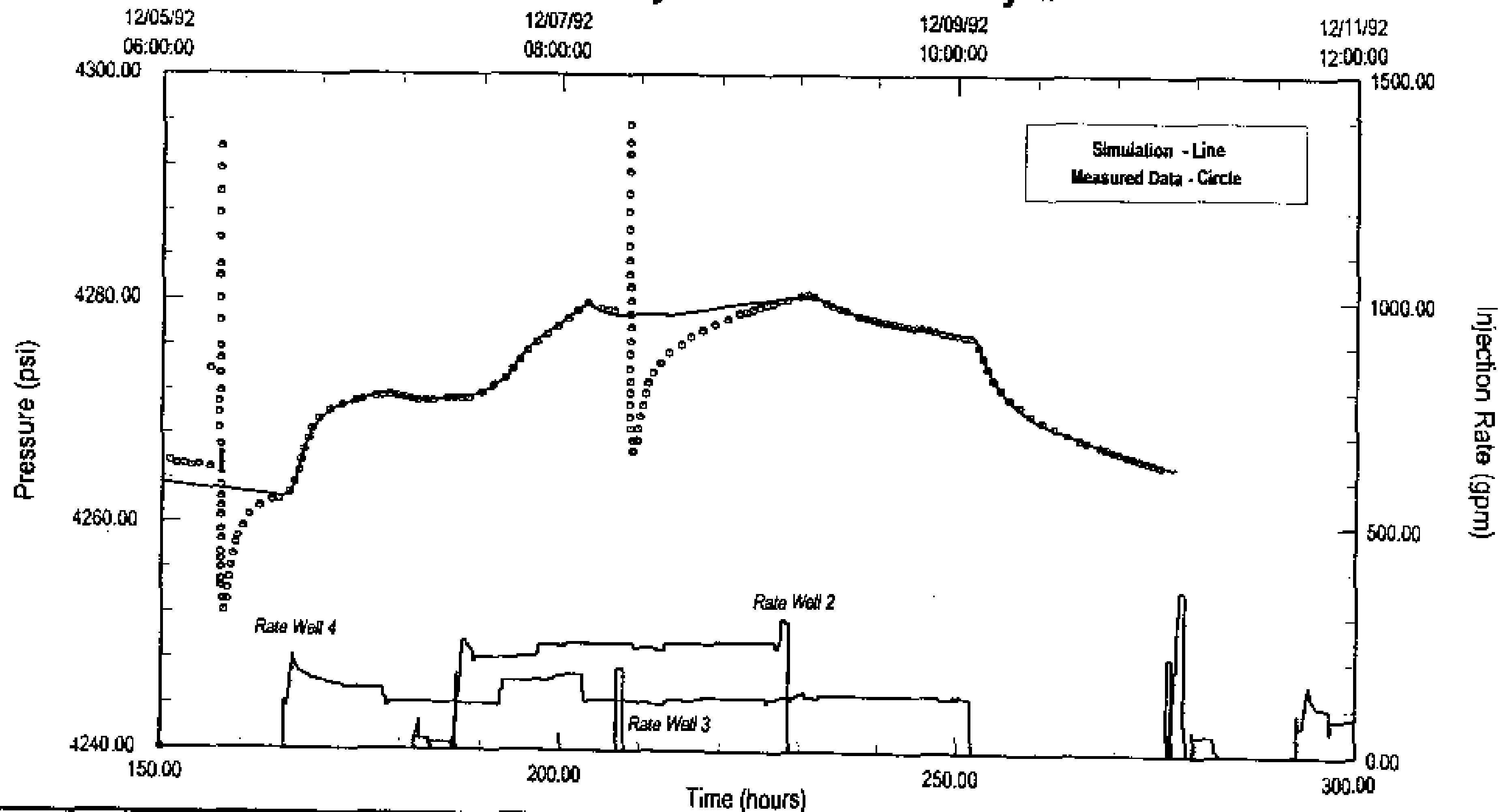

	3 <-> 2	3 <-> 4
kh/ub (md-ft/cp)	51,806	42,547
phi*ct*h (ft/psi)	1.56E-04	8.42E-06

pi (psi at gauge depth)	4,244
Sum Square Error	1.89

215

State .... Mississippi	**Du Pont DeLisle Plant**	**Test Date** 5-Dec-92
County .... Harrison	***Well 3***	**Analysis Date** 1-Jun-93
Field .... DeLisle Plant	***Graph S3-G11***	**Report Number** 930201

Pressure History Simulation - Homogeneous Model

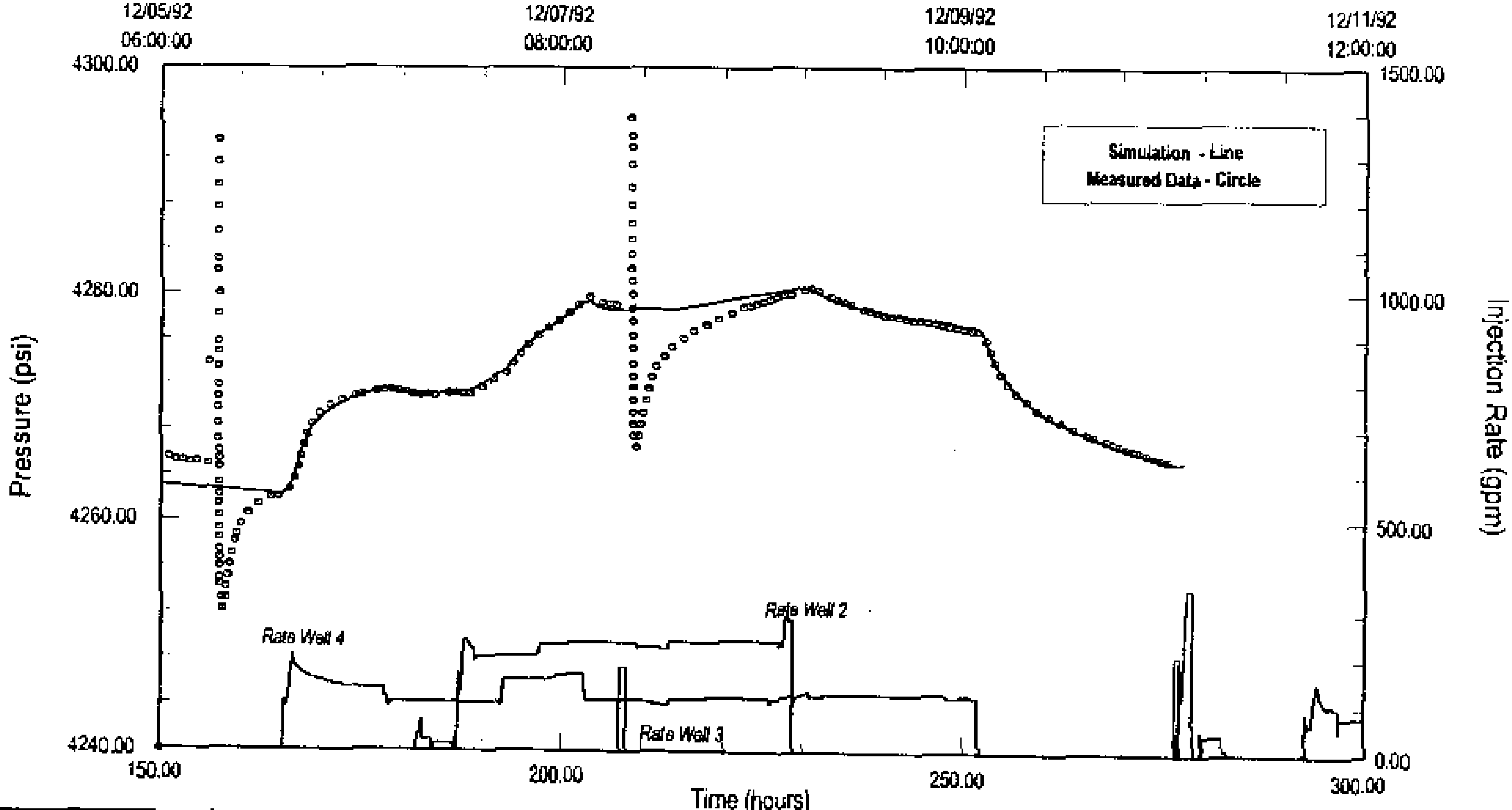

	3 <-> 2	3 <-> 4
kh/ub (md-ft/cp)	179,646	82,437
phi*ct*h (ft/psi)	2.12E-04	9.51E-05

pi (psi at gauge depth)	4,252
Sum Square Error	6.74

214

State .... Mississippi	**Du Pont DeLisle Plant**	**Test Date** 5-Dec-92
County .... Harrison	***Well 3***	**Analysis Date** 1-Jun-93
Field .... DeLisle Plant	***Graph S3-G12***	**Report Number** 930201

Pressure History Simulation - Homogeneous Model

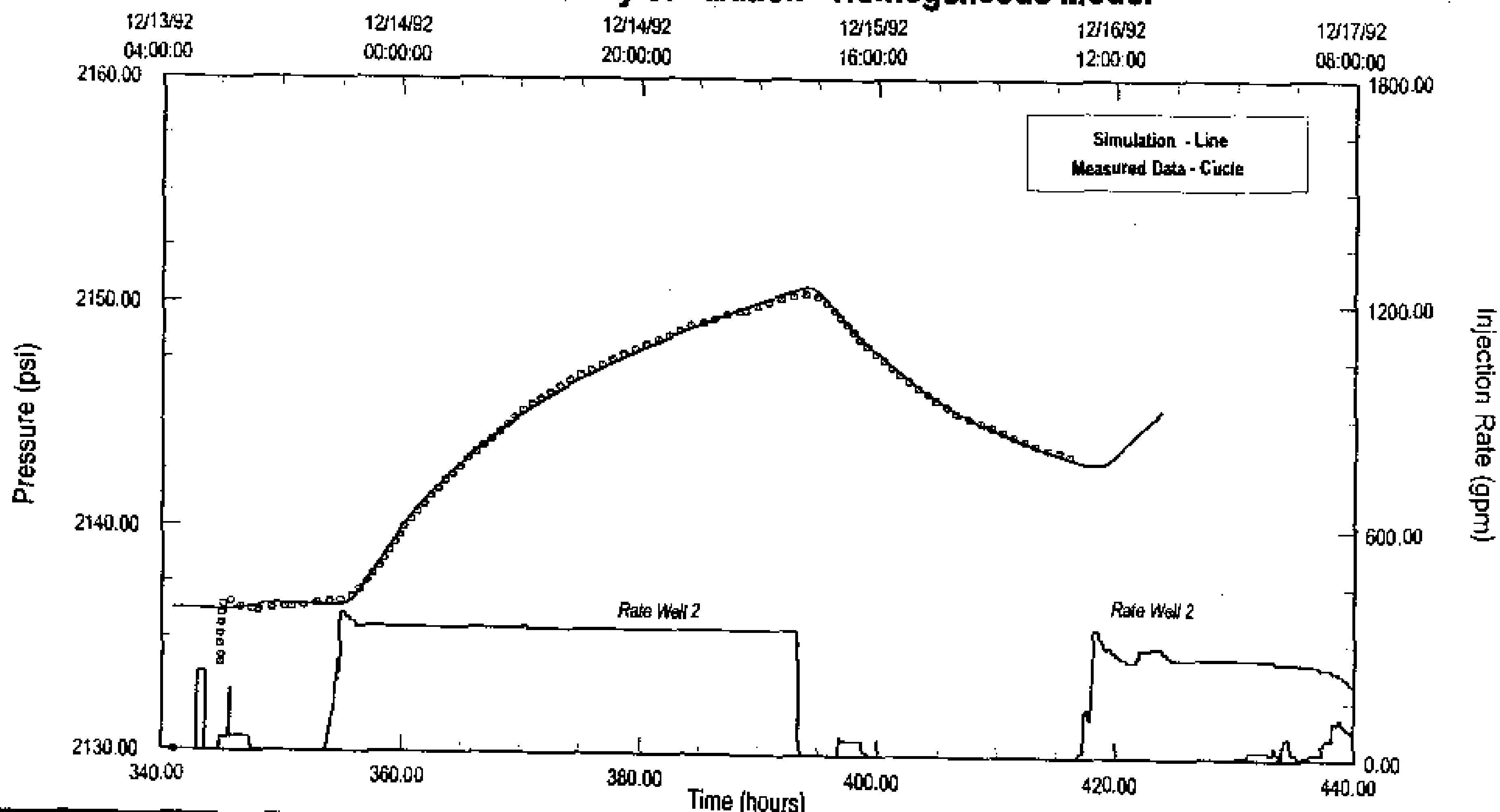

	3 <-> 2
kh/ub (md-ft/cp)	112,413
phi*ct*h (ft/psi)	1.64E-04

pi (psi at gauge depth)	2,128	* Gauge at 5000 ft
Sum Square Error	2.88	

State .... Mississippi	**Du Pont DeLisle Plant**	**Test Date** 5-Dec-92
County .... Harrison	***Well 3***	**Analysis Date** 1-Jun-93
Field .... DeLisle Plant	***Graph S3-G13***	**Report Number** 930201

Pressure History Simulation - 2 Porosity Model

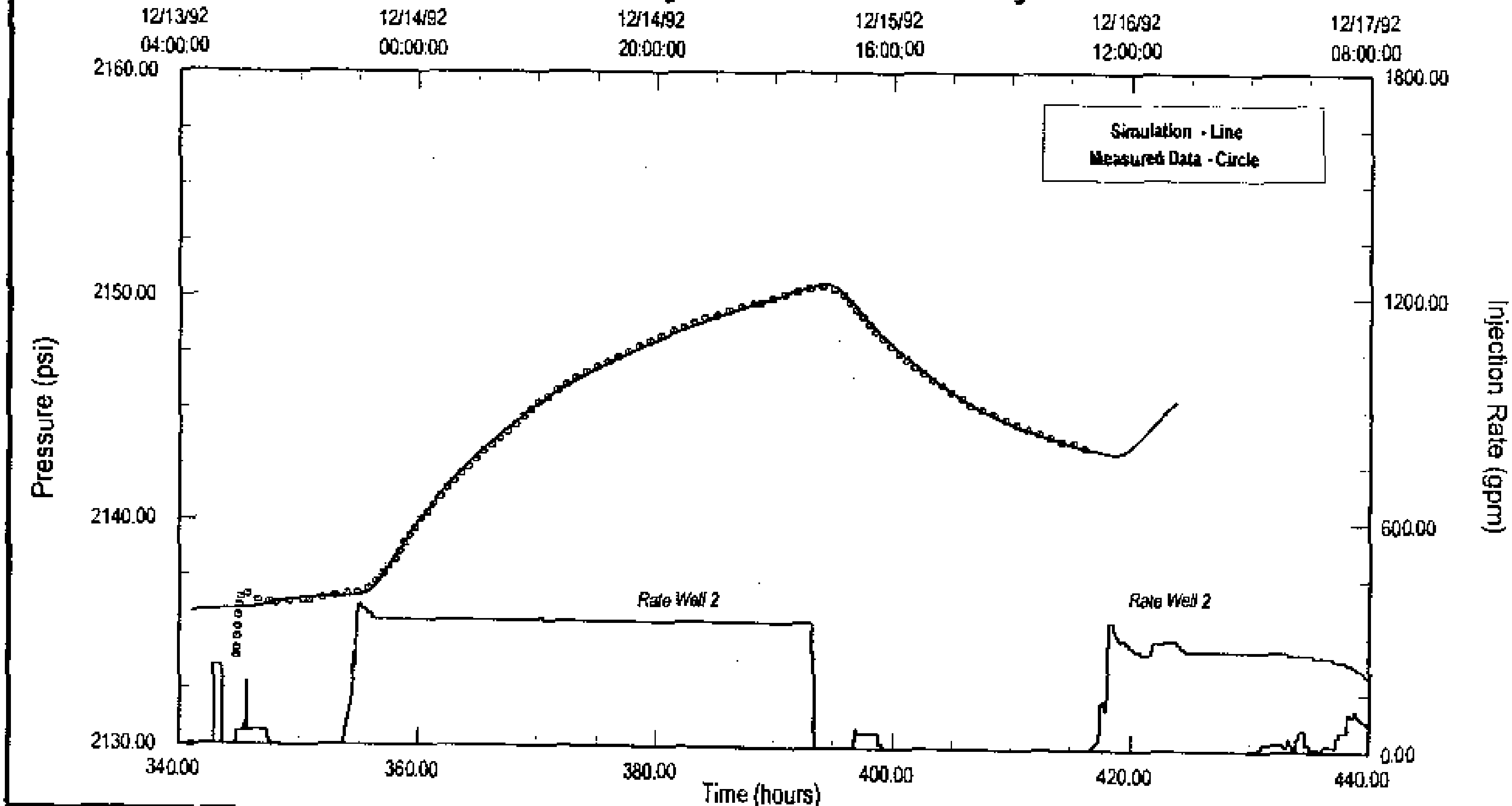

	3 <--> 2			
kh/ub (md-ft/cp)	87,787	pi (psi at gauge depth)	2,129	* Gauge at 5000 ft
phi*ct*h (ft/psi)	1.63E-04	Sum Square Error	1.46	

State .... Mississippi *County* .... Harrison *Field* .... DeLisle Plant	**Du Pont DeLisle Plant** ***Well 4*** ***Graph S3-G14***	*Test Date* .... 5-Dec-92 *Analysis Date* .... 1-Jun-93 *Report Number* 930201

Pressure History Simulation - 2 Porosity Model

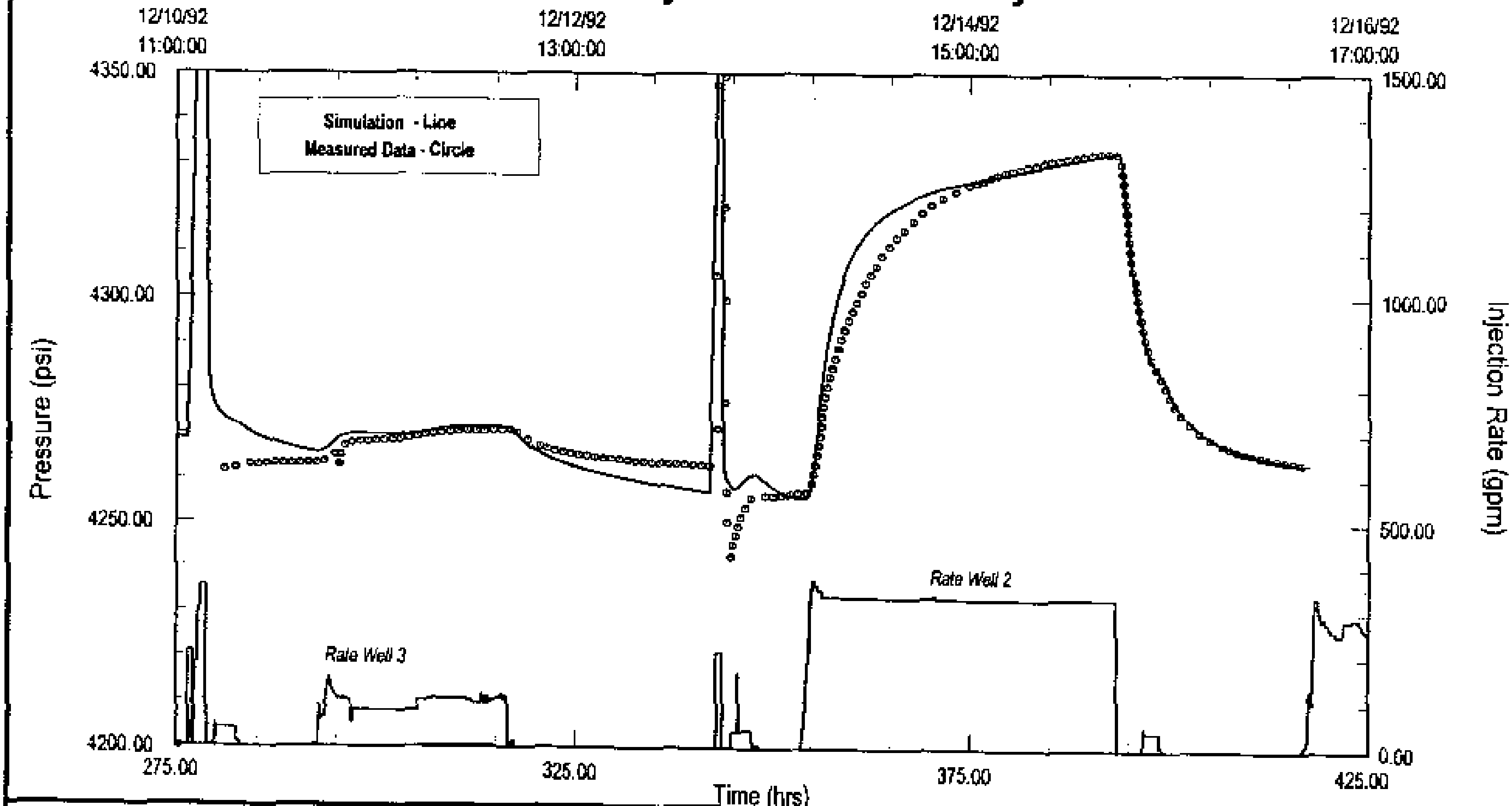

	AI 4	4 <-> 2	4 <-> 3		
kh/ub (md-ft/cp)	123,344	12,036	66,885	pi (psi at gauge depth)	4,182
phi*ct*h (ft/psi)	N/A	1.65E-05	7.53E-05	Sum Square Error	30.92

z7

State .... Mississippi	**Du Pont DeLisle Plant**	**Test Date** 5-Dec-92
County .... Harrison	***Well 4***	**Analysis Date** 1-Jun-93
Field .... DeLisle Plant	***Graph S3-G15***	**Report Number** 930201

Pressure History Simulation - 2 Porosity Model

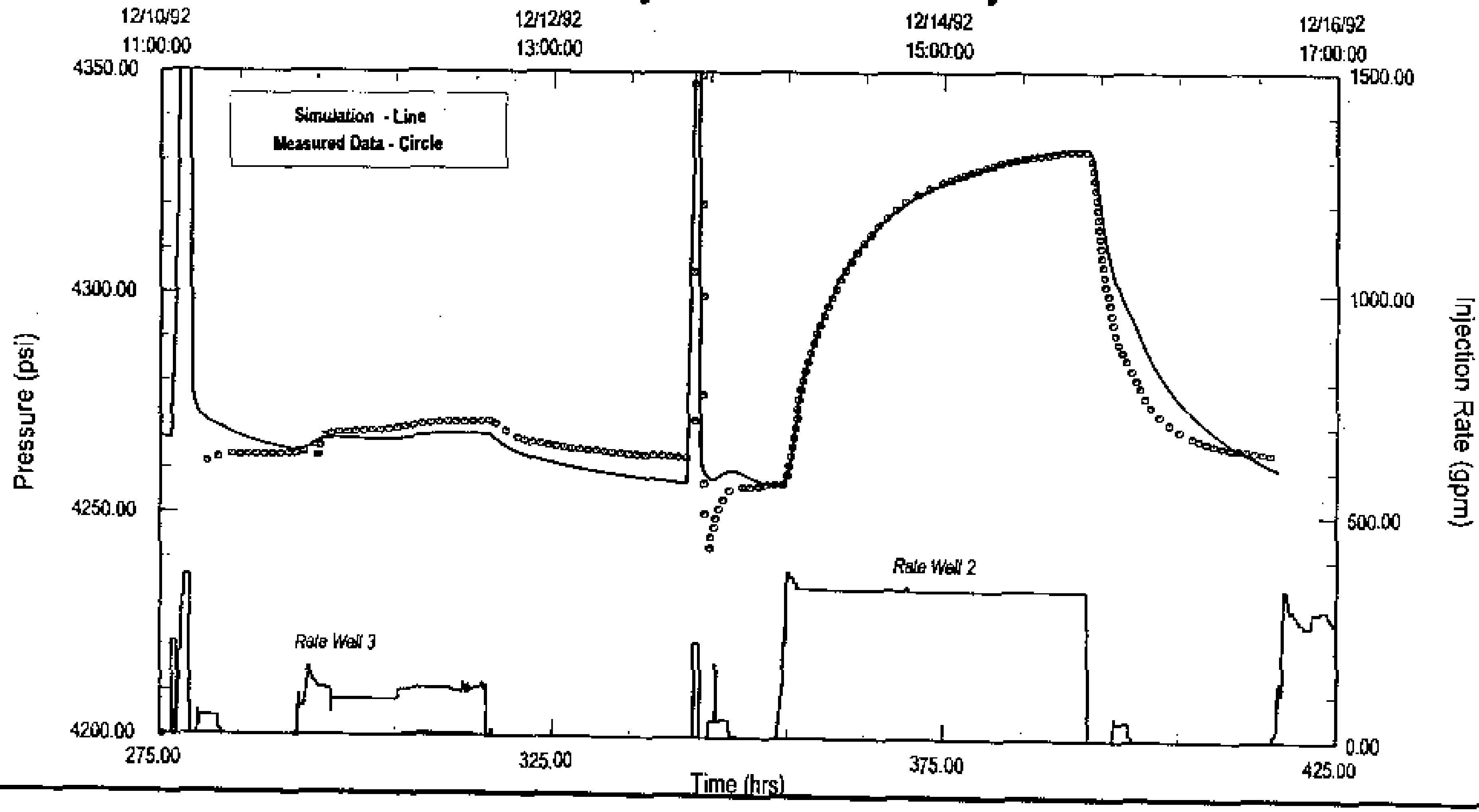

	At 4	4 <--> 2	4 <--> 3		
kh/ub (md-ft/cp)	148,120	23,320	87,508	pi (psi at gauge depth)	4,244
phi*ct*h (ft/psi)	N/A	2.97E-05	1.11E-04	Sum Square Error	3.03

State .... Mississippi **County** .... Harrison **Field** .... DeLisle Plant	**Du Pont DeLisle Plant** ***Well 4*** ***Graph S3-G16***	**Test Date** .... 5-Dec-92 **Analysis Date** .... 1-Jun-93 **Report Number** 930201

Pressure History Simulation - Homogeneous Model

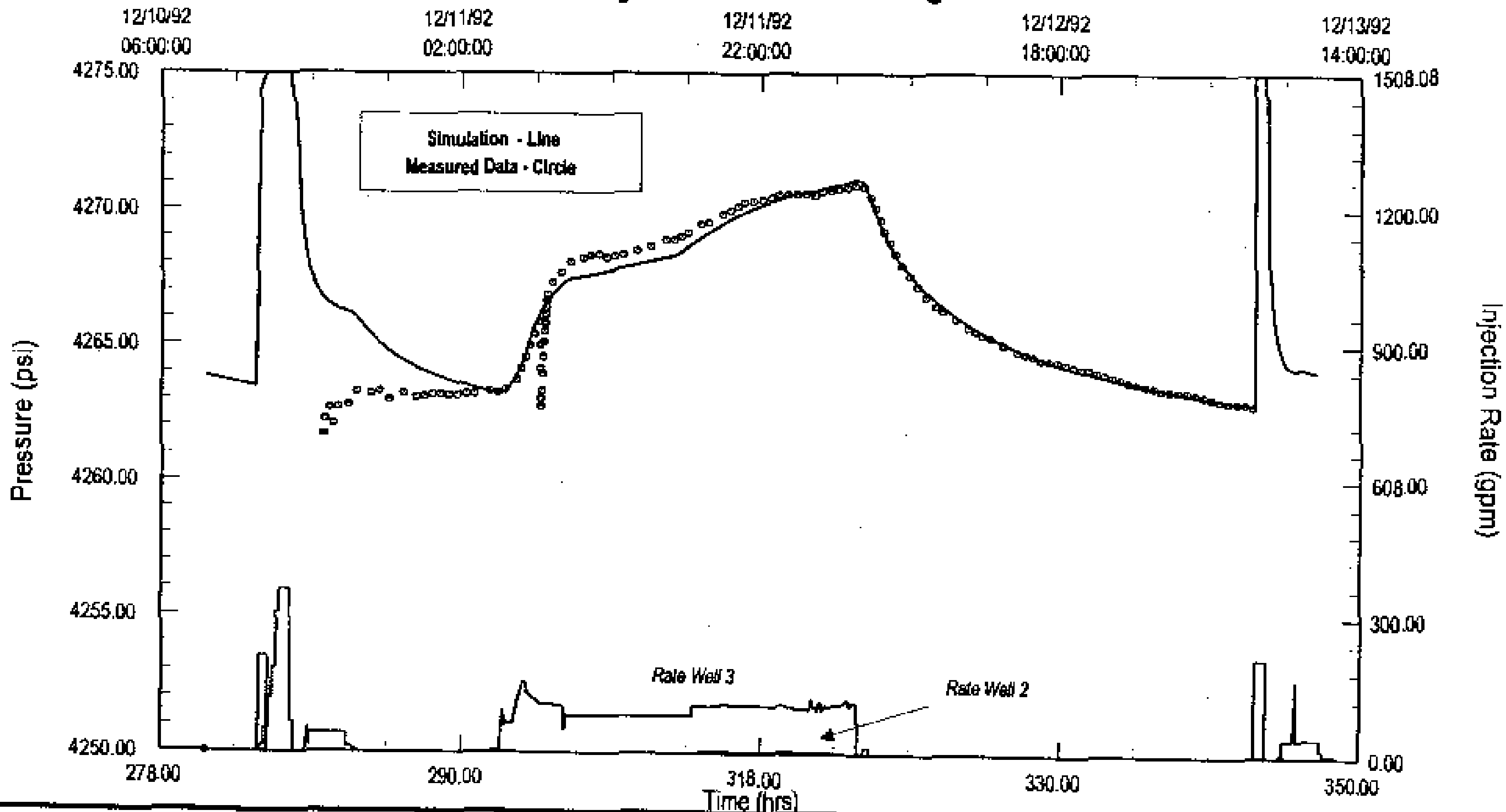

	At 4	4 <--> 2	4 <--> 3		
kh/ub (md-ft/cp)	140,863	194,021	77,021	pi (psi at gauge depth)	4,250
phi*ct*h (ft/psi)	N/A	8.27E-05	9.67E-05	Sum Square Error	0.99

z6

Section 4 -- Production Log Data

Gulf Coast Well Analysis ran Spinner and RAT surveys on Well 2, and Spinner Surveys on Well 3 and Well 4 in conjunction with the testing program. The stationary spinner involves placing the tool in the well as fluid is injected. A base measurement is established with the tool above all of the intervals to determine the total number of spinner counts for a given injection rate. The tool is then lowered into the well and as fluid moves into the various layers the velocity at the tool decreases. The tool should measure zero rotations below all of the perforations. Implicit in the interpretation of the data is the assumption that fluid is single phase, and also that the wellbore diameter is constant throughout the completion interval.

Graph S4-G1 on the following page shows the interpretation of the stationary spinner survey measured in each well. The Well 2 survey was measured at 200 gpm, and the Well 3 and Well 4 surveys were taken at 160 gpm in each well. The spinner profiles are overlaid against the SP curve from each well.

Qualitative Interpretation

Note that 50% of the fluid seems to be going into the upper sand body Well 2, and there appears to be no flow below 9920 feet. Top of fill in Well 2 was estimated at 9974 feet. All of the brine in Well 3 is injected below 9920 feet with the majority going into the zone above the shale stringer at 9965 feet. It is speculated that the previous cement squeeze job in Well 3 may have blocked portions of the upper intervals in Well 3. The brine in Well 4 is evenly distributed over zones with the exception of the middle zone at 9800 ft. which appears to be taking very little or no fluid.

This spinner survey should be used qualitatively because there are several factors that can influence the apparent injection profile.

1) If the layers have different pressures then the spinner profile will vary with rate. The spinner should be run using a range of rates to check for the possibility of varying layer pressures.

2) The spinner only shows where the fluid leaves the wellbore. It does not show where fluid is going in the formation.

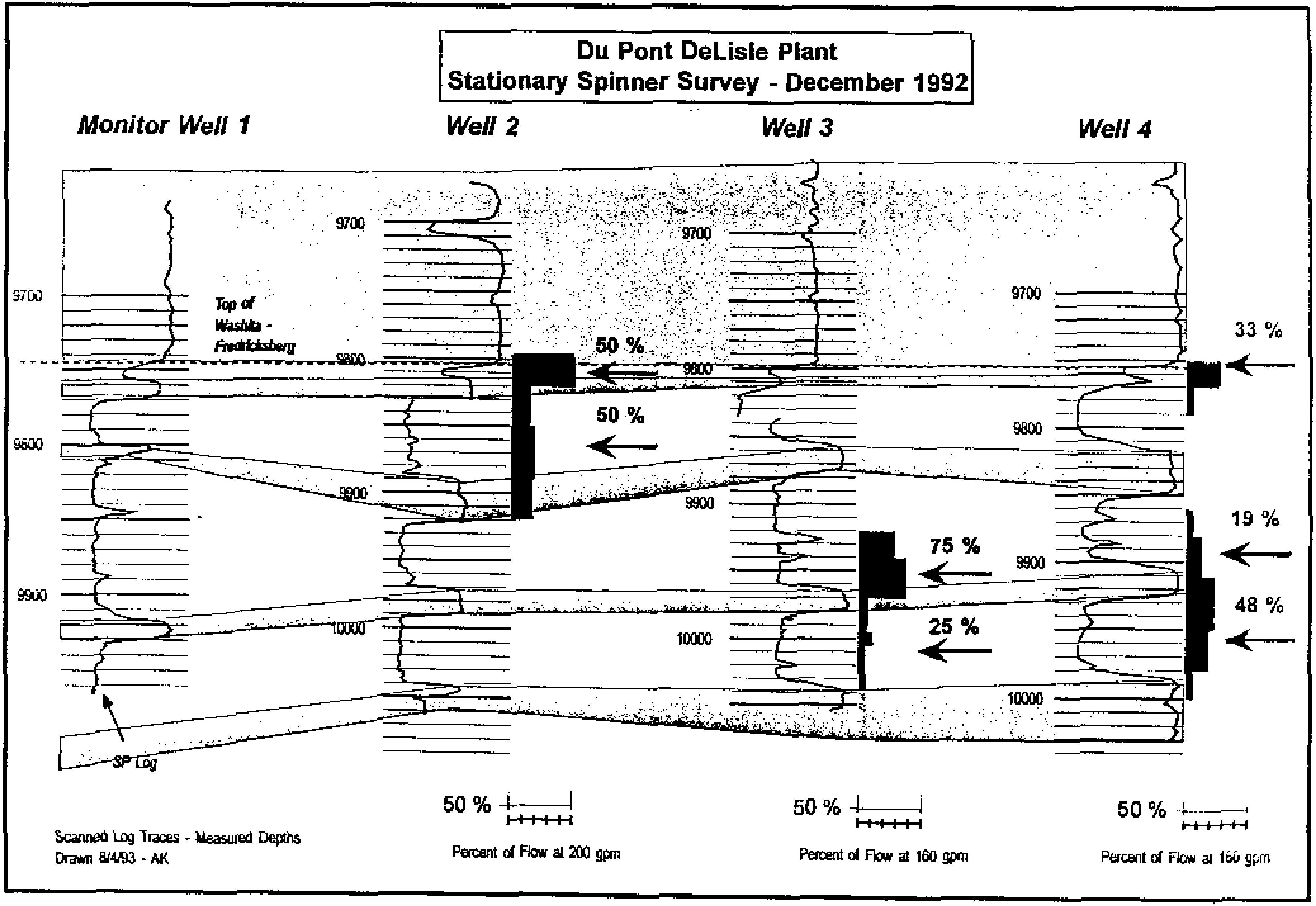

Du Pont DeLisle Plant
Stationary Spinner Survey - December 1992
Monitor Well 1
Well 2
Well 3
Well 4
9700
9800
9900
10000
Top of Washita - Fredricksberg
SP Log
50 %
50 %
75 %
25 %
33 %
19 %
48 %
Percent of Flow at 200 gpm
Percent of Flow at 160 gpm
Percent of Flow at 160 gpm
Scanned Log Traces - Measured Depths
Drawn 8/4/93 - AK

Section 5 -- Future Testing Recommendations

In general the testing program was very useful in helping define inter-well reservoir properties. There are still a few areas of uncertainty that can be clarified through additional reservoir testing and analysis. Some of the areas of uncertainty and action that can be taken to clarify these issues are listed below.

Comprehensive Spinner Survey

This reservoir test was not able to define individual zone pressures or properties. Therefore, a comprehensive spinner survey should be run to help deterime these parameters. A relatively simple *SIP* procedure can be employed to determine layer pressures and a gross estimate of the layer transmissibility-skin product.

The SIP enteils running a pressure gauge and spinner tool, in combination, at each layer, over a range of rates. The pressure and rate data is used to construct an inflow performance relationship for each zone which in turn is used to estimate reservoir pressure and the transmissibility-skin product for esch layer.

The SIP will help determine if fluid injection is confined to only the the upper zones in Well 2 and only the lower zones in Well 3. This information is important to help predict the long term waste migration. Knowing individual layer pressures will also help the modeling of

Falloff Testing

There were no transient periods in which near well properties could be determined. Falloff tests in the Injection Wells will help verify near well preperties which can then be compared to inter-well properitles. Thia information will help determine if the appsrently lower transmissibility between Well 2 and 4 is isolated to a single stringer or is regional in nature.

Inteference Testing Between Injection Wells and the New Well 5

A comprehensive interference test between Well 5 and the existing wells will help verify directional transmissibility and storativity in the reservoir. This information will be very useful in helping delineate the reservoir in the North-esst direction.

State .... Mississippi	**Du Pont DeLisle Plant**	**Test Date** 5-Dec-92
County .... Harrison	***Monitor Well 1***	**Analysis Date** 1-Jun-93
Field .... DeLisle Plant		**Report Number** 930201

Pressure Data

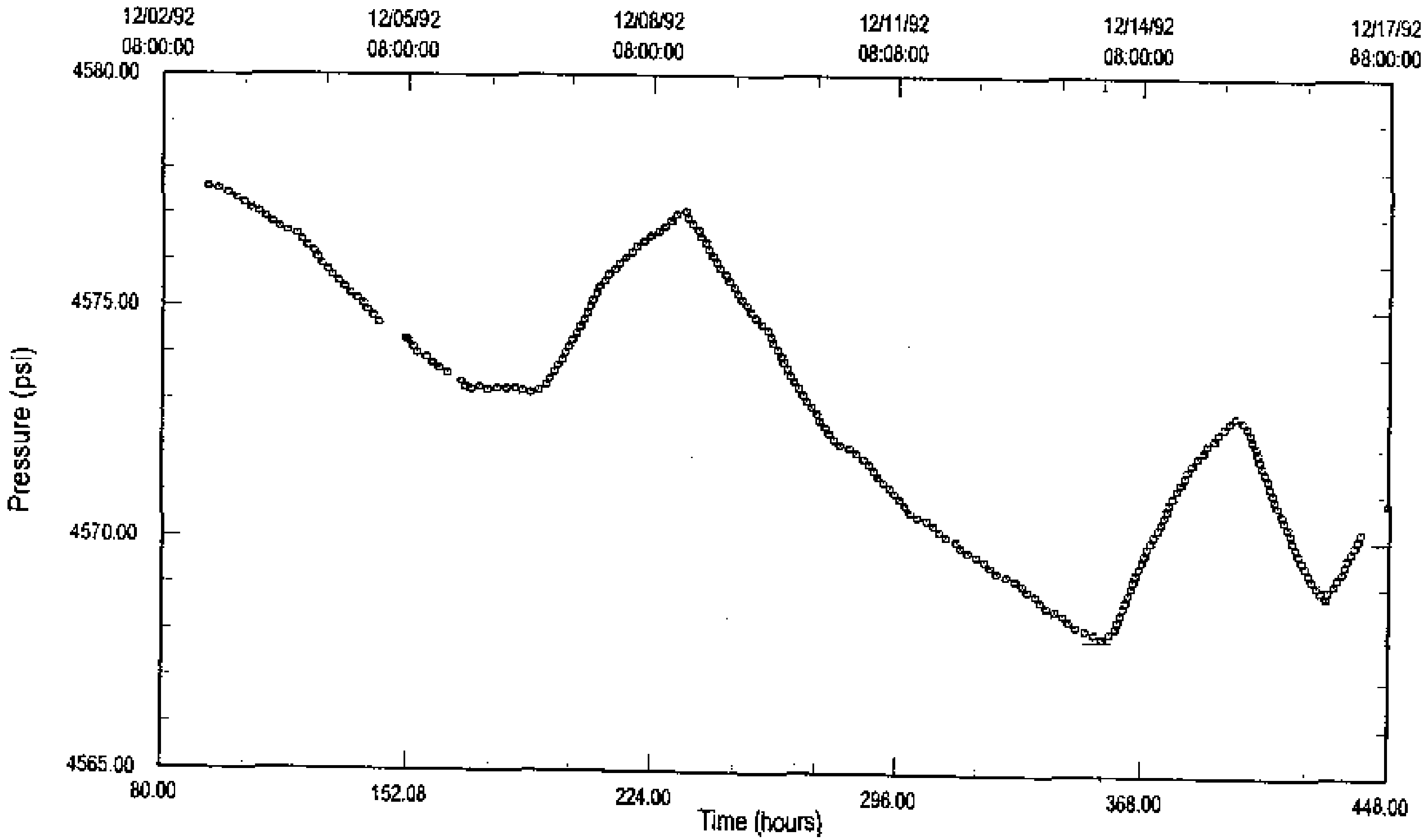

Pressure Data - Monitor Well 1			
Point Number	Real Time of Day (mm/dd/yy hh:mm:ss)	Elapsed Time (hours)	Measured Pressure
1)	12/2/92 19:00:00	91.000	577.637
2)	12/2/92 19:10:00	91.167	577.487
3)	12/2/92 21:10:00	93.167	4577.597
4)	12/3/92 0:05:00	96.083	4577.550
5)	12/3/92 2:50:00	98.833	4577.460
6)	12/3/92 5:05:00	101.083	4577.350
7)	12/3/92 7:15:00	103.250	4577.250
8)	12/3/92 9:20:00	105.333	4577.137
9)	12/3/92 11:40:00	107.667	4577.037
10)	12/3/92 13:40:00	109.667	4576.930
11)	12/3/92 15:45:00	111.750	4576.827
12)	12/3/92 17:50:00	113.833	4576.717
13)	12/3/92 20:15:00	116.250	4576.627
14)	12/3/92 23:00:00	119.000	4576.560
15)	12/4/92 0:35:00	120.583	4576.433
16)	12/4/92 2:10:00	122.167	4576.318
17)	12/4/92 4:05:00	124.083	4576.197
18)	12/4/92 5:10:00	125.167	4576.057
19)	12/4/92 6:30:00	126.500	4575.913
20)	12/4/92 8:20:00	128.333	4575.797
21)	12/4/92 9:40:00	129.667	4575.670
22)	12/4/92 11:30:00	131.500	4575.543
23)	12/4/92 13:15:00	133.250	4575.427
24)	12/4/92 15:00:00	135.000	4575.283
25)	12/4/92 17:05:00	137.083	4575.177
26)	12/4/92 18:55:00	138.917	4575.060
27)	12/4/92 19:55:00	139.917	4574.927
28)	12/4/92 21:45:00	141.750	4574.813
29)	12/4/92 23:30:00	143.500	4574.660
30)	12/5/92 7:20:00	151.333	4574.320
31)	12/5/92 8:00:00	152.000	4574.260
32)	12/5/92 9:30:00	153.500	4574.143
33)	12/5/92 10:45:00	154.750	4574.016
34)	12/5/92 13:15:00	157.250	4573.923
35)	12/5/92 15:00:00	159.000	4573.803
36)	12/5/92 17:00:00	161.000	4573.680
37)	12/5/92 19:20:00	163.333	4573.560
38)	12/5/92 23:19:00	167.317	4573.403
39)	12/6/92 0:40:00	168.667	4573.277
40)	12/6/92 2:16:00	170.267	4573.229
41)	12/6/92 4:43:00	172.717	4573.268
42)	12/6/92 7:01:00	175.017	4573.216
43)	12/6/92 9:41:00	177.683	4573.249
44)	12/6/92 12:21:00	180.350	4573.253
45)	12/6/92 15:00:00	183.000	4573.269
46)	12/6/92 17:10:00	185.167	4573.196
47)	12/6/92 19:40:00	187.667	4573.153

Pressure Data - Meniter Well 1			
Point Number	Real Time of Day (mm/dd/yy hh:mm:ss)	Elapsed Time (hours)	Measured Pressure
48)	12/6/92 22:06:00	190.100	4573.218
49)	12/7/92 0:21:00	192.350	4573.323
50)	12/7/92 1:25:00	193.417	4573.483
51)	12/7/92 2:42:00	194.706	4573.607
52)	12/7/92 3:45:00	195.750	4573.747
53)	12/7/92 5:07:00	197.117	4573.877
54)	12/7/92 5:55:00	197.917	4574.028
55)	12/7/92 7:02:00	199.033	4574.153
56)	12/7/92 7:59:06	199.983	4574.300
57)	12/7/92 9:19:00	201.317	4574.443
58)	12/7/92 10:24:00	202.400	4574.590
59)	12/7/92 11:33:00	203.558	4574.740
60)	12/7/92 12:26:00	204.433	4574.880
61)	12/7/92 13:13:00	205.217	4575.023
62)	12/7/92 14:09:06	206.150	4575.160
63)	12/7/92 15:08:00	207.133	4575.303
64)	12/7/92 15:58:06	287.987	4575.447
65)	12/7/92 17:35:06	209.583	4575.573
66)	12/7/92 18:43:00	219.717	4575.710
67)	12/7/92 20:32:06	212.533	4575.823
68)	12/7/92 21:52:00	213.867	4575.950
69)	12/7/92 23:42:00	215.700	4576.077
70)	12/8/92 1:29:00	217.483	4576.193
71)	12/8/92 2:55:06	218.917	4576.320
72)	12/8/92 5:04:00	221.067	4576.433
73)	12/8/92 6:58:00	222.967	4578.550
74)	12/8/92 9:19:06	225.317	4576.643
75)	12/8/92 11:12:06	227.206	4576.760
76)	12/8/92 12:57:00	228.950	4576.890
77)	12/8/92 14:28:06	230.467	4577.817
78)	12/8/92 17:10:06	233.187	4577.087
79)	12/8/92 17:50:06	233.833	4576.947
80)	12/8/92 19:19:06	235.317	4576.818
81)	12/8/92 20:56:06	236.933	4576.687
82)	12/8/92 21:44:06	237.733	4576.537
83)	12/8/92 23:04:06	239.067	4576.410
84)	12/8/92 23:57:06	239.950	4576.278
85)	12/9/92 1:05:06	241.083	4578.133
86)	12/9/92 2:14:00	242.233	4576.000
87)	12/9/92 3:18:00	243.167	4575.860
88)	12/9/92 4:45:06	244.750	4575.737
89)	12/9/92 5:45:00	245.767	4575.587
90)	12/9/92 7:26:06	247.433	4575.457
91)	12/9/92 8:20:00	248.333	4575.317
92)	12/9/92 9:36:06	249.606	4575.187
93)	12/9/92 11:07:00	251.117	4575.063
94)	12/9/92 12:21:00	252.350	4574.923

Pressure Data - Monitor Well 1			
Point Number	Real Time of Day (mm/dd/yy hh:mm:ss)	Elapsed Time (hours)	Measured Pressure
95)	12/9/92 13:44:86	253.733	4574.797
96)	12/9/92 15:33:00	255.550	4574.663
97)	12/9/92 17:22:86	257.367	4574.547
98)	12/9/92 18:15:00	258.250	4574.418
99)	12/9/92 18:56:86	258.933	4574.273
100)	12/9/92 20:14:86	260.233	4574.137
101)	12/9/92 21:23:00	261.383	4573.987
102)	12/9/92 22:06:00	282.186	4573.843
103)	12/9/92 23:07:86	263.117	4573.697
104)	12/10/92 8:04:00	264.067	4573.550
105)	12/10/92 1:18:00	285.267	4573.420
106)	12/10/92 2:35:00	260.583	4573.287
107)	12/10/92 3:50:86	287.833	4573.137
108)	12/10/92 4:54:00	288.900	4573.086
109)	12/10/92 8:25:00	270.417	4572.873
110)	12/10/92 8:01:00	272.817	4572.733
111)	12/10/92 8:53:00	272.883	4572.570
112)	12/10/92 18:28:00	274.467	4572.437
113)	12/10/92 11:35:00	275.583	4572.297
114)	12/10/92 13:07:00	277.117	4572.167
115)	12/10/92 14:59:00	278.983	4572.047
118)	12/10/92 17:48:00	281.800	4571.990
117)	12/10/92 19:59:00	283.983	4571.873
118)	12/10/92 22:08:86	286.133	4571.750
119)	12/10/92 23:44:86	287.733	4571.630
120)	12/11/92 1:06:00	289.083	4571.586
121)	12/11/92 2:21:00	290.350	4571.367
122)	12/11/92 4:86:86	292.000	4571.243
123)	12/11/92 6:81:86	294.817	4571.133
124)	12/11/92 7:20:00	295.333	4571.000
125)	12/11/92 9:04:86	297.867	4570.880
126)	12/11/92 10:37:00	298.617	4570.737
127)	12/11/92 11:39:00	299.850	4578.593
128)	12/11/92 13:52:00	301.867	4570.493
129)	12/11/92 16:35:00	304.583	4570.423
130)	12/11/92 18:37:00	300.617	4570.317
131)	12/11/92 20:21:00	308.350	4570.183
132)	12/11/92 22:23:00	310.383	4570.073
133)	12/12/92 1:21:00	313.350	4569.973
134)	12/12/92 2:40:00	314.667	4569.047
135)	12/12/92 4:45:00	316.750	4569.740
138)	12/12/92 7:24:00	319.400	4569.657
137)	12/12/92 9:37:00	321.617	4569.550
138)	12/12/92 11:19:00	323.317	4569.430
139)	12/12/92 13:14:00	325.233	4569.297
140)	12/12/92 16:81:00	328.017	4560.233
141)	12/12/92 18:36:00	330.600	4569.150

Pressure Data - Monitor Well 1			
Point Number	Real Time of Day (mm/dd/yy hh:mm:ss)	Elapsed Time (hours)	Measured Pressure
142)	12/12/92 28:39:00	332.650	4569.643
143)	12/12/92 21:59:00	333.983	4568.917
144)	12/13/92 0:22:06	336.367	4568.820
145)	12/13/92 1:52:00	337.867	4568.693
146)	12/13/92 3:38:00	339.633	4568.573
147)	12/13/92 6:06:00	342.100	4568.477
148)	12/13/92 8:33:00	344.550	4568.387
149)	12/13/92 10:10:00	346.167	4568.260
150)	12/13/92 12:15:00	348.250	4568.143
151)	12/13/92 15:07:00	351.117	4568.070
152)	12/13/92 17:44:00	353.733	4567.993
153)	12/13/92 20:06:00	356.100	4567.903
154)	12/13/92 22:11:00	358.183	4568.010
155)	12/14/92 0:06:00	360.000	4568.130
156)	12/14/92 0:44:00	360.733	4568.270
157)	12/14/92 1:32:06	361.533	4568.423
158)	12/14/92 2:18:00	362.300	4568.570
159)	12/14/92 3:06:00	363.133	4568.707
160)	12/14/92 3:52:00	363.867	4568.850
161)	12/14/92 4:41:00	364.683	4569.000
162)	12/14/92 5:19:00	365.317	4568.147
163)	12/14/92 5:55:06	365.917	4569.290
164)	12/14/92 6:57:00	366.950	4569.433
165)	12/14/92 7:45:00	367.750	4569.580
166)	12/14/92 8:33:06	368.550	4569.720
167)	12/14/92 9:19:00	369.317	4568.851
168)	12/14/92 10:21:00	370.350	4569.990
169)	12/14/92 11:16:00	371.267	4570.133
170)	12/14/92 12:32:00	372.533	4570.273
171)	12/14/92 13:29:00	373.483	4570.407
172)	12/14/92 14:21:80	374.350	4570.543
173)	12/14/92 15:21:00	375.350	4570.677
174)	12/14/92 16:10:69	376.167	4570.817
175)	12/14/92 17:10:00	377.167	4570.957
176)	12/14/92 18:24:00	378.400	4571.120
177)	12/14/92 19:33:00	379.550	4571.263
178)	12/14/92 20:45:00	380.750	4571.409
179)	12/14/92 21:30:00	381.500	4571.550
180)	12/14/92 22:47:00	382.783	4571.683
181)	12/15/92 0:19:00	384.317	4571.833
182)	12/15/92 2:04:06	386.067	4571.960
183)	12/15/92 3:11:00	387.183	4572.118
184)	12/15/92 5:17:06	389.283	4572.223
185)	12/15/92 6:30:69	390.500	4572.360
186)	12/15/92 8:06:00	392.100	4572.480
187)	12/15/92 9:37:06	393.617	4572.603
188)	12/15/92 11:16:06	395.267	4572.723

Pressure Data - Monitor Well 1			
Point Number	Real Time of Day (mm/dd/yy hh:mm:ss)	Elapsed Time (hours)	Measured Pressure
189)	12/15/92 13:26:00	397.433	4572.623
190)	12/15/92 14:45:00	398.750	4572.497
191)	12/15/92 15:42:00	399.700	4572.363
192)	12/15/92 16:16:00	400.267	4572.217
193)	12/15/92 17:22:00	401.367	4572.063
194)	12/15/92 17:56:00	401.933	4571.943
195)	12/15/92 18:23:00	402.383	4571.797
196)	12/15/92 19:14:00	403.233	4571.653
197)	12/15/92 20:16:00	404.167	4571.507
198)	12/15/92 20:55:00	404.917	4571.376
199)	12/15/92 21:35:00	405.583	4571.203
200)	12/15/92 22:22:00	406.367	4571.060
201)	12/15/92 22:57:00	406.950	4570.920
202)	12/15/92 23:44:00	407.733	4570.783
203)	12/16/92 0:39:00	408.650	4570.617
204)	12/16/92 1:25:00	409.417	4570.488
205)	12/16/92 2:21:00	410.350	4570.337
206)	12/16/92 3:11:00	411.183	4570.193
207)	12/16/92 3:47:00	411.783	4570.050
208)	12/16/92 4:35:00	412.583	4569.913
209)	12/16/92 5:23:00	413.383	4569.776
210)	12/16/92 6:28:00	414.467	4569.630
211)	12/16/92 7:25:00	415.417	4569.497
212)	12/16/92 8:22:00	416.367	4569.357
213)	12/16/92 9:21:00	417.350	4569.213
214)	12/16/92 10:41:00	418.683	4569.080
215)	12/16/92 11:51:00	419.850	4568.958
216)	12/16/92 13:30:00	421.500	4568.820
217)	12/16/92 14:02:00	422.033	4568.963
218)	12/16/92 15:48:00	423.800	4569.087
219)	12/16/92 16:44:00	424.733	4569.227
220)	12/16/92 18:12:00	426.200	4569.353
221)	12/16/92 19:02:00	427.083	4568.516
222)	12/16/92 19:37:00	427.617	4568.657
223)	12/16/92 20:44:00	428.733	4569.793
224)	12/16/92 21:46:00	429.767	4569.933
225)	12/16/92 22:42:00	430.700	4570.076
226)	12/16/92 23:31:00	431.517	4570.217
227)	12/17/92 7:54:00	439.900	4570.830
228)	12/10/92 20:43:00	284.717	4294.377
229)	12/10/92 21:41:00	285.683	4294.163
230)	12/10/92 22:48:00	286.800	4294.027
231)	12/10/92 23:47:00	287.783	4293.820
232)	12/11/92 0:51:00	288.850	4293.647
233)	12/11/92 2:02:00	290.033	4293.570
234)	12/11/92 3:09:00	291.150	4293.400
235)	12/11/92 4:19:00	292.317	4293.487

Pressure Data - Monitor Well 1			
Point Number	Real Time of Day (mm/dd/yy hh:mm:ss)	Elapsed Time (hours)	Measured Pressure
236)	12/11/92 5:30:00	293.500	4293.383
237)	12/11/92 6:42:00	294.700	4293.440
238)	12/11/92 7:52:00	295.867	4293.540
239)	12/11/92 9:02:00	297.033	4293.638
240)	12/11/92 10:14:00	298.233	4293.657
241)	12/11/92 11:26:00	299.433	4293.743
242)	12/11/92 12:36:00	300.633	4293.667
243)	12/11/92 13:45:00	301.750	4293.733
244)	12/11/92 14:57:00	302.950	4293.760
245)	12/11/92 15:59:00	303.983	4293.973
246)	12/11/92 17:08:00	305.133	4293.843
247)	12/11/92 18:20:00	306.333	4293.937
248)	12/11/92 19:32:00	307.533	4293.983
249)	12/11/92 20:44:00	308.733	4293.933
250)	12/11/92 21:56:00	309.933	4293.997
251)	12/11/92 23:08:00	311.133	4294.037
252)	12/12/92 0:18:00	312.300	4294.123
253)	12/12/92 1:30:00	313.500	4294.047
254)	12/12/92 2:40:00	314.667	4294.133
255)	12/12/92 3:52:00	315.867	4294.067
256)	12/12/92 5:04:00	317.067	4294.130
257)	12/12/92 6:16:00	318.267	4294.163
258)	12/12/92 7:24:00	319.400	4294.033
259)	12/12/92 8:30:00	320.500	4293.883
260)	12/12/92 9:42:00	321.700	4293.768
261)	12/12/92 10:54:00	322.900	4293.713
262)	12/12/92 11:56:00	323.933	4293.500
263)	12/12/92 13:06:00	325.100	4293.370
264)	12/12/92 14:14:00	326.233	4293.167
265)	12/12/92 15:24:00	327.400	4293.083
266)	12/12/92 16:36:00	328.600	4292.983
267)	12/12/92 17:48:00	329.787	4292.893
268)	12/12/92 18:58:00	330.967	4292.827
269)	12/12/92 20:10:00	332.167	4292.807
270)	12/12/92 21:20:00	333.333	4292.917
271)	12/12/92 22:18:00	334.300	4292.783
272)	12/12/92 23:30:00	335.500	4292.650
273)	12/13/92 0:40:00	336.667	4292.533
274)	12/13/92 1:50:00	337.833	4292.418
275)	12/13/92 3:02:00	339.033	4292.397
276)	12/13/92 4:18:00	340.167	4292.287

State	Mississippi
County	Harrison
Field	DeLisle Plant

Du Pont DeLisle Plant
Well 2 Pressure Data

Test Date	5-Dec-92
Analysis Date	1-Jun-93
Report Number	930201

Pressure Data

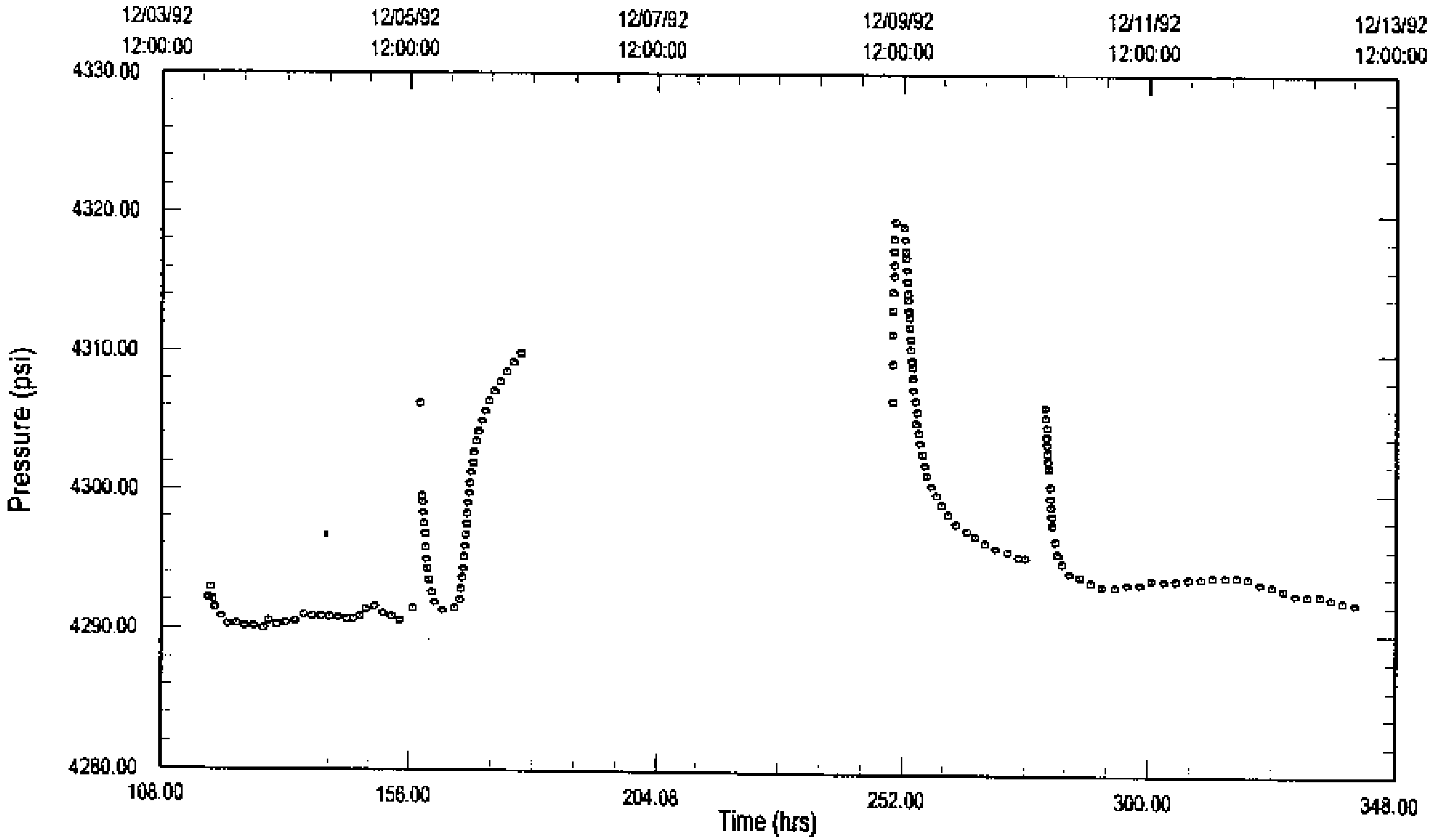

Pressure Data - Well 2

Point Number	Real Time of Day (mm/dd/yy hh:mm:ss)	Elapsed Time (hours)	Measured Pressure
1)	12/3/92 20:37:00	116.617	4205.130
2)	12/3/92 20:38:00	116.633	4251.820
3)	12/3/92 21:05:00	117.083	4292.210
4)	12/3/92 21:30:00	117.500	4292.960
5)	12/3/92 21:55:00	117.917	4292.110
6)	12/3/92 22:20:00	118.333	4291.550
7)	12/3/92 22:45:00	118.750	4291.280
8)	12/3/92 23:10:00	119.167	4291.160
9)	12/3/92 23:35:00	119.583	4290.918
10)	12/4/92 0:00:00	120.000	4290.740
11)	12/4/92 0:25:00	120.417	4290.590
12)	12/4/92 0:50:00	120.833	4290.360
13)	12/4/92 1:15:00	121.250	4290.570
14)	12/4/92 1:40:00	121.667	4290.440
15)	12/4/92 2:05:00	122.083	4290.390
16)	12/4/92 2:30:00	122.500	4290.410
17)	12/4/92 2:55:00	122.917	4290.240
19)	12/4/92 3:26:00	123.333	4290.410
19)	12/4/92 3:45:00	123.750	4290.350
20)	12/4/92 4:10:00	124.107	4290.240
21)	12/4/92 4:35:00	124.583	4290.460
22)	12/4/92 5:00:00	125.000	4290.270
23)	12/4/92 5:25:00	125.417	4290.250
24)	12/4/92 5:50:00	125.833	4290.220
25)	12/4/92 6:15:00	126.250	4290.270
26)	12/4/92 6:40:00	126.667	4290.280
27)	12/4/92 7:05:00	127.083	4290.310
28)	12/4/92 7:46:00	127.667	4290.080
29)	12/4/92 8:05:00	120.083	4290.420
30)	12/4/92 0:30:00	128.500	4290.600
31)	12/4/92 8:55:00	128.917	4290.480
32)	12/4/92 9:20:00	129.333	4290.480
33)	12/4/92 9:45:00	129.750	4290.460
34)	12/4/92 10:10:00	130.167	4290.330
35)	12/4/92 10:35:00	136.583	4290.590
36)	12/4/92 11:00:00	131.000	4290.620
37)	12/4/92 11:25:00	131.417	4290.570
39)	12/4/92 11:50:00	131.833	4290.460
39)	12/4/92 12:15:00	132.250	4290.560
40)	12/4/92 12:40:00	132.667	4290.570
41)	12/4/92 13:05:00	133.083	4290.660
42)	12/4/92 13:30:00	133.500	4290.600
43)	12/4/92 13:55:00	133.917	4290.790
44)	12/4/92 14:20:00	134.333	4290.930
45)	12/4/92 14:45:00	134.750	4290.950
46)	12/4/92 15:10:00	135.167	4291.830
47)	12/4/92 15:35:00	135.583	4290.980

Pressure Data - Well 2			
Point Number	Real Time of Day (mm/dd/yy hh:mm:ss)	Elapsed Time (hours)	Measured Pressure
48)	12/4/92 16:00:00	136.000	4290.910
49)	12/4/92 16:25:00	136.417	4290.960
50)	12/4/92 16:50:00	136.833	4290.930
51)	12/4/92 17:15:00	137.250	4291.060
52)	12/4/92 17:40:00	137.667	4290.840
53)	12/4/92 18:05:00	138.083	4290.860
54)	12/4/92 18:30:00	138.500	4290.930
55)	12/4/92 18:55:00	138.917	4290.960
56)	12/4/92 19:20:00	139.333	4290.960
57)	12/4/92 19:45:00	139.750	4290.900
58)	12/4/92 20:10:00	140.167	4290.880
59)	12/4/92 20:35:00	140.583	4290.830
60)	12/4/92 21:00:00	141.000	4290.920
61)	12/4/92 21:25:00	141.417	4290.930
62)	12/4/92 21:50:00	141.833	4290.878
63)	12/4/92 22:15:00	142.250	4290.760
64)	12/4/92 22:40:00	142.667	4290.780
65)	12/4/92 23:05:00	143.083	4290.960
66)	12/4/92 23:30:00	143.500	4290.740
67)	12/4/92 23:55:00	143.917	4290.848
68)	12/5/92 0:25:00	144.417	4290.740
69)	12/5/92 0:50:00	144.833	4290.720
70)	12/5/92 1:20:00	145.333	4290.940
71)	12/5/92 1:45:00	145.750	4291.050
72)	12/5/92 2:10:00	146.167	4290.930
73)	12/5/92 2:35:00	146.583	4291.150
74)	12/5/92 3:00:00	147.000	4291.310
75)	12/5/92 3:25:00	147.417	4291.420
76)	12/5/92 3:50:00	147.833	4291.540
77)	12/5/92 4:15:00	148.250	4291.580
78)	12/5/92 4:40:00	148.667	4291.650
79)	12/5/92 5:05:00	149.083	4291.640
80)	12/5/92 5:30:00	149.500	4291.690
81)	12/5/92 5:55:00	149.917	4291.850
82)	12/5/92 6:20:00	150.333	4291.680
83)	12/5/92 6:45:00	150.750	4291.150
84)	12/5/92 7:10:00	151.147	4291.160
85)	12/5/92 7:35:00	151.563	4291.118
86)	12/5/92 8:00:00	152.000	4290.748
87)	12/5/92 8:25:00	152.417	4290.930
88)	12/5/92 8:50:00	152.833	4290.800
89)	12/5/92 9:15:00	153.250	4290.560
90)	12/5/92 9:39:00	153.650	4290.690
91)	12/5/92 10:03:00	154.050	4290.660
92)	12/5/92 12:00:00	156.000	4212.240
93)	12/5/92 12:12:30	156.208	4269.010
94)	12/5/92 12:36:38	156.608	4291.520

Pressure Data - Well 2			
Point Number	Real Time of Day (mm/dd/yy hh:mm:ss)	Elapsed Time (hours)	Measured Pressure
95)	12/5/92 12:49:38	156.825	4355.970
96)	12/5/92 12:53:00	156.883	4414.388
97)	12/5/92 13:18:00	157.287	4470.870
98)	12/5/92 13:24:30	157.408	4414.650
99)	12/5/92 13:32:00	157.533	4356.238
100)	12/5/92 13:56:00	157.933	4306.278
101)	12/5/92 14:32:00	158.533	4299.577
102)	12/5/92 14:36:36	158.608	4299.100
103)	12/5/92 14:39:38	158.658	4298.707
104)	12/5/92 14:43:00	158.717	4299.340
105)	12/5/92 14:49:30	158.775	4297.936
106)	12/5/92 14:51:00	159.650	4297.548
107)	12/5/92 14:54:30	158.908	4297.130
108)	12/5/92 14:59:30	158.975	4296.767
109)	12/5/92 15:02:30	159.042	4296.313
110)	12/5/92 15:09:00	159.150	4295.843
111)	12/5/92 15:13:30	159.225	4295.447
112)	12/5/92 15:19:00	159.300	4295.073
113)	12/5/92 15:24:00	159.400	4294.667
114)	12/5/92 15:31:00	159.517	4294.267
115)	12/5/92 15:37:30	159.625	4293.843
116)	12/5/92 15:47:00	159.783	4293.477
117)	12/5/92 15:54:38	159.909	4293.113
118)	12/5/92 16:10:00	160.167	4292.863
119)	12/5/92 16:25:00	160.417	4292.290
120)	12/5/92 17:00:00	161.000	4291.930
121)	12/5/92 17:45:00	161.750	4291.920
122)	12/5/92 18:30:00	162.500	4291.327
123)	12/5/92 19:40:00	163.667	4291.427
124)	12/5/92 20:50:00	164.933	4291.523
125)	12/5/92 21:41:50	165.697	4291.773
126)	12/5/92 21:50:00	165.833	4292.133
127)	12/5/92 21:56:38	165.942	4292.530
128)	12/5/92 22:05:00	166.083	4292.890
129)	12/5/92 22:10:50	166.181	4293.300
130)	12/5/92 22:17:50	166.297	4293.670
131)	12/5/92 22:22:50	166.391	4294.030
132)	12/5/92 22:29:16	166.488	4294.418
133)	12/5/92 22:33:18	166.553	4294.800
134)	12/5/92 22:38:00	166.633	4295.160
135)	12/5/92 22:41:50	166.697	4295.563
136)	12/5/92 22:45:40	166.761	4295.933
137)	12/5/92 22:51:16	166.853	4296.293
138)	12/5/92 22:57:16	166.953	4296.723
139)	12/5/92 23:01:30	167.025	4297.113
140)	12/5/92 23:06:00	167.100	4297.490
141)	12/5/92 23:11:00	167.163	4297.897

Pressure Data - Well 2			
Point Number	Real Time of Day (mm/dd/yy hh:mm:ss)	Elapsed Time (hours)	Measured Pressure
142)	12/5/92 23:18:00	167.267	4298.283
143)	12/5/92 23:20:10	167.336	4298.653
144)	12/5/92 23:26:30	167.442	4299.023
145)	12/5/92 23:31:30	167.525	4299.413
146)	12/5/92 23:36:40	167.611	4296.777
147)	12/5/92 23:41:40	167.694	4300.143
148)	12/5/92 23:47:30	167.792	4300.507
149)	12/5/92 23:54:20	167.906	4300.887
150)	12/6/92 0:03:00	168.050	4301.247
151)	12/6/92 0:09:20	168.156	4301.640
152)	12/6/92 0:19:40	168.328	4301.997
153)	12/6/92 0:29:38	168.492	4302.397
154)	12/6/92 0:38:20	168.639	4302.767
155)	12/6/92 0:50:30	168.842	4303.130
156)	12/6/92 1:02:20	169.839	4303.533
157)	12/6/92 1:13:20	169.222	4303.910
158)	12/6/92 1:30:30	169.508	4304.270
159)	12/6/92 1:50:30	169.842	4304.637
160)	12/6/92 2:11:00	170.183	4304.987
161)	12/6/92 2:22:00	170.367	4305.350
162)	12/6/92 2:43:00	170.717	4305.697
163)	12/6/92 3:04:30	171.075	4306.110
164)	12/6/92 3:35:30	171.592	4306.437
165)	12/6/92 4:00:00	172.000	4306.783
166)	12/6/92 4:32:30	172.542	4307.157
167)	12/6/92 5:07:30	173.125	4307.490
168)	12/6/92 5:38:30	173.642	4307.863
169)	12/6/92 6:06:00	174.100	4308.227
170)	12/6/92 6:54:00	174.900	4308.523
171)	12/6/92 7:38:00	175.633	4308.850
172)	12/6/92 0:10:00	176.167	4309.177
173)	12/6/92 8:58:00	176.967	4309.450
174)	12/6/92 9:30:00	177.500	4309.630
175)	12/9/92 9:53:00	249.883	4306.527
176)	12/9/92 9:55:00	249.917	4309.270
177)	12/9/92 9:57:00	249.950	4311.417
178)	12/9/92 9:59:00	249.983	4313.157
179)	12/9/92 10:01:00	250.017	4314.473
180)	12/9/92 10:03:00	250.050	4315.587
181)	12/9/92 10:05:00	250.083	4318.423
182)	12/9/92 10:08:00	250.133	4317.418
183)	12/9/92 10:12:00	250.200	4310.290
184)	12/9/92 18:26:00	250.433	4319.477
185)	12/9/92 10:52:00	250.867	4319.596
186)	12/9/92 11:39:00	251.650	4319.460
187)	12/9/92 12:02:00	252.033	4319.103
188)	12/9/92 12:10:00	252.167	4318.663

Pressure Data - Well 2			
Point Number	Real Time of Day (mm/dd/yy hh:mm:ss)	Elapsed Time (hours)	Measured Pressure
189)	12/9/92 12:15:00	252.250	4318.210
190)	12/9/92 12:20:00	252.333	4317.783
191)	12/9/92 12:23:00	252.383	4317.397
192)	12/9/92 12:28:00	252.467	4316.916
193)	12/9/92 12:31:00	252.517	4316.523
194)	12/9/92 12:35:00	252.583	4316.023
195)	12/9/92 12:38:00	252.633	4315.597
196)	12/9/92 12:41:00	252.683	4315.220
197)	12/9/92 12:44:00	252.733	4314.823
198)	12/9/92 12:47:00	252.783	4314.400
199)	12/9/92 12:50:00	252.833	4313.927
200)	12/9/92 12:53:00	252.883	4313.527
201)	12/9/92 12:56:00	252.933	4313.097
202)	12/9/92 13:00:00	253.000	4312.633
203)	12/9/92 13:03:00	253.050	4312.260
204)	12/9/92 13:06:00	253.100	4311.887
205)	12/9/92 13:11:00	253.183	4311.453
206)	12/9/92 13:15:00	253.250	4311.067
207)	12/9/92 13:19:00	253.317	4310.673
208)	12/9/92 13:24:00	253.400	4310.313
209)	12/9/92 13:28:00	253.467	4309.937
210)	12/9/92 13:34:00	253.567	4309.517
211)	12/9/92 13:40:00	253.667	4309.030
212)	12/9/92 13:44:00	253.733	4308.663
213)	12/9/92 13:50:00	253.833	4308.260
214)	12/9/92 13:55:00	253.917	4307.837
215)	12/9/92 14:02:00	254.003	4307.397
216)	12/9/92 14:07:00	254.117	4307.023
217)	12/9/92 14:13:00	254.217	4306.623
218)	12/9/92 14:20:00	254.333	4306.217
219)	12/9/92 14:27:00	254.450	4305.790
220)	12/9/92 14:33:00	254.550	4305.426
221)	12/9/92 14:41:00	254.683	4305.023
222)	12/9/92 14:50:00	254.833	4304.653
223)	12/9/92 14:59:00	254.983	4304.287
224)	12/9/92 15:06:00	255.100	4303.890
225)	12/9/92 15:18:00	255.300	4303.517
226)	12/9/92 15:30:00	255.500	4303.137
227)	12/9/92 15:41:00	255.683	4302.753
228)	12/9/92 15:55:00	255.917	4302.363
229)	12/9/92 16:12:00	256.200	4301.980
230)	12/9/92 16:26:00	256.433	4301.603
231)	12/9/92 16:42:00	256.700	4301.243
232)	12/9/92 17:03:00	257.050	4300.890
233)	12/9/92 17:34:00	257.567	4300.470
234)	12/9/92 18:03:00	258.050	4300.127
235)	12/9/92 18:32:00	258.533	4299.783

Pressure Data - Well 2			
Point Number	Real Time of Day (mm/dd/yy hh:mm:ss)	Elapsed Time (hours)	Measured Pressure
236)	12/9/92 18:59:00	258.983	4299.423
237)	12/9/92 19:36:00	259.600	4299.113
238)	12/9/92 20:13:00	289.217	4299.803
239)	12/9/92 20:54:00	260.900	4298.463
240)	12/9/92 21:35:00	261.583	4298.157
241)	12/9/92 22:19:00	262.317	4297.797
242)	12/9/92 23:21:00	263.350	4297.593
243)	12/10/92 0:16:00	264.267	4297.347
244)	12/10/92 0:58:00	264.967	4297.047
245)	12/10/92 2:08:00	288.100	4296.907
246)	12/10/92 3:11:00	267.183	4296.727
247)	12/10/92 4:06:00	268.100	4296.450
248)	12/10/92 5:12:00	269.200	4296.300
249)	12/10/92 6:14:06	270.233	4296.097
250)	12/10/92 7:19:00	271.317	4295.923
251)	12/10/92 8:31:00	272.517	4295.853
252)	12/10/92 8:35:00	273.583	4295.880
253)	12/10/92 10:45:00	274.750	4295.500
254)	12/10/92 12:10:00	276.167	4295.432
255)	12/10/92 16:00:00	280.000	4306.193
256)	12/10/92 16:05:00	280.083	4305.463
257)	12/10/92 16:10:00	280.187	4304.797
258)	12/10/92 16:15:80	280.250	4304.143
259)	12/10/92 18:20:00	280.333	4303.547
280)	12/10/92 16:25:00	280.417	4302.957
261)	12/10/92 16:30:80	280.500	4302.400
262)	12/10/92 16:40:00	280.667	4301.883
263)	12/10/92 16:45:00	280.750	4301.413
264)	12/10/92 16:56:00	280.833	4300.493
265)	12/10/92 18:55:00	280.917	4300.067
266)	12/10/92 17:80:00	281.000	4299.680
267)	12/10/92 17:10:00	291.167	4299.047
268)	12/10/92 17:20:00	281.333	4298.403
269)	12/10/92 17:30:00	281.500	4297.757
270)	12/10/92 17:48:00	281.667	4297.330
271)	12/10/92 17:55:80	281.917	4296.567
272)	12/10/92 18:15:00	282.250	4296.193
273)	12/10/92 18:30:00	282.600	4295.713
274)	12/10/92 19:58:00	282.967	4295.353
275)	12/10/92 18:17:00	283.283	4294.987
276)	12/10/92 20:00:00	284.000	4294.673
277)	12/10/92 20:43:00	284.717	4294.377
278)	12/10/92 21:41:00	285.693	4294.163
279)	12/10/92 22:48:00	288.600	4294.027
280)	12/10/92 23:47:00	287.783	4293.820
281)	12/11/92 0:51:00	288.850	4293.647
282)	12/11/92 2:02:00	290.033	4293.570

Pressure Data - Wsll 2			
Point Number	Real Time of Bay (mm/dd/yy hh:mm:ss)	Elapsed Time (hours)	Measured Pressure
283)	12/11/92 3:09:00	291.150	4293.400
284)	12/11/92 4:19:00	292.317	4293.487
285)	12/11/92 5:30:00	293.500	4293.383
286)	12/11/92 6:42:00	294.700	4293.440
287)	12/11/92 7:52:00	295.867	4293.540
288)	12/11/92 9:02:00	297.033	4293.830
289)	12/11/92 18:14:00	298.233	4293.657
290)	12/11/92 11:26:00	299.433	4293.743
291)	12/11/92 12:38:00	300.633	4293.887
292)	12/11/92 13:45:00	301.750	4293.733
293)	12/11/92 14:57:00	302.950	4293.768
294)	12/11/92 15:59:00	303.983	4293.973
295)	12/11/92 17:08:00	305.133	4293.843
296)	12/11/92 18:20:00	306.333	4293.937
297)	12/11/92 19:32:00	307.533	4293.983
298)	12/11/92 20:44:00	308.733	4293.933
299)	12/11/92 21:56:00	309.933	4293.997
300)	12/11/92 23:08:00	311.133	4294.007
301)	12/12/92 o:18:00	312.300	4294.123
382)	12/12/92 1:38:00	313.500	4294.047
303)	12/12/92 2:40:00	314.667	4294.133
304)	12/12/92 3:52:00	315.867	4294.067
305)	12/12/92 5:04:00	317.067	4294.138
306)	12/12/92 6:16:00	318.267	4294.183
307)	12/12/92 7:24:00	319.400	4294.003
308)	12/12/92 8:30:00	320.500	4293.893
309)	12/12/92 9:42:00	321.700	4293.760
318)	12/12/92 19:54:00	322.900	4293.713
311)	12/12/92 11:58:00	323.933	4293.500
312)	12/12/92 13:06:00	325.100	4293.378
313)	12/12/92 14:14:00	326.233	4293.187
314)	12/12/92 15:24:00	327.400	4293.083
315)	12/12/92 18:36:00	328.600	4292.983
318)	12/12/92 17:46:00	329.767	4292.893
317)	12/12/92 18:58:00	330.967	4292.827
318)	12/12/92 20:10:00	332.167	4292.807
319)	12/12/92 21:28:00	333.333	4292.917
328)	12/12/92 22:18:00	334.300	4292.763
321)	12/12/92 23:30:00	335.500	4292.650
322)	12/13/92 8:48:00	336.667	4292.533
323)	12/13/92 1:50:00	337.833	4292.418
324)	12/13/92 3:02:00	339.033	4292.397
325)	12/13/92 4:18:00	340.187	4292.267

State .... Mississippi	**Du Pont DeLisle Plant**	**Test Date** 5-Dec-92
County .... Harrison	***Well 3***	**Analysis Date** 1-Jun-93
Field .... DeLisle Plant		**Report Number** 930201

Pressure Data

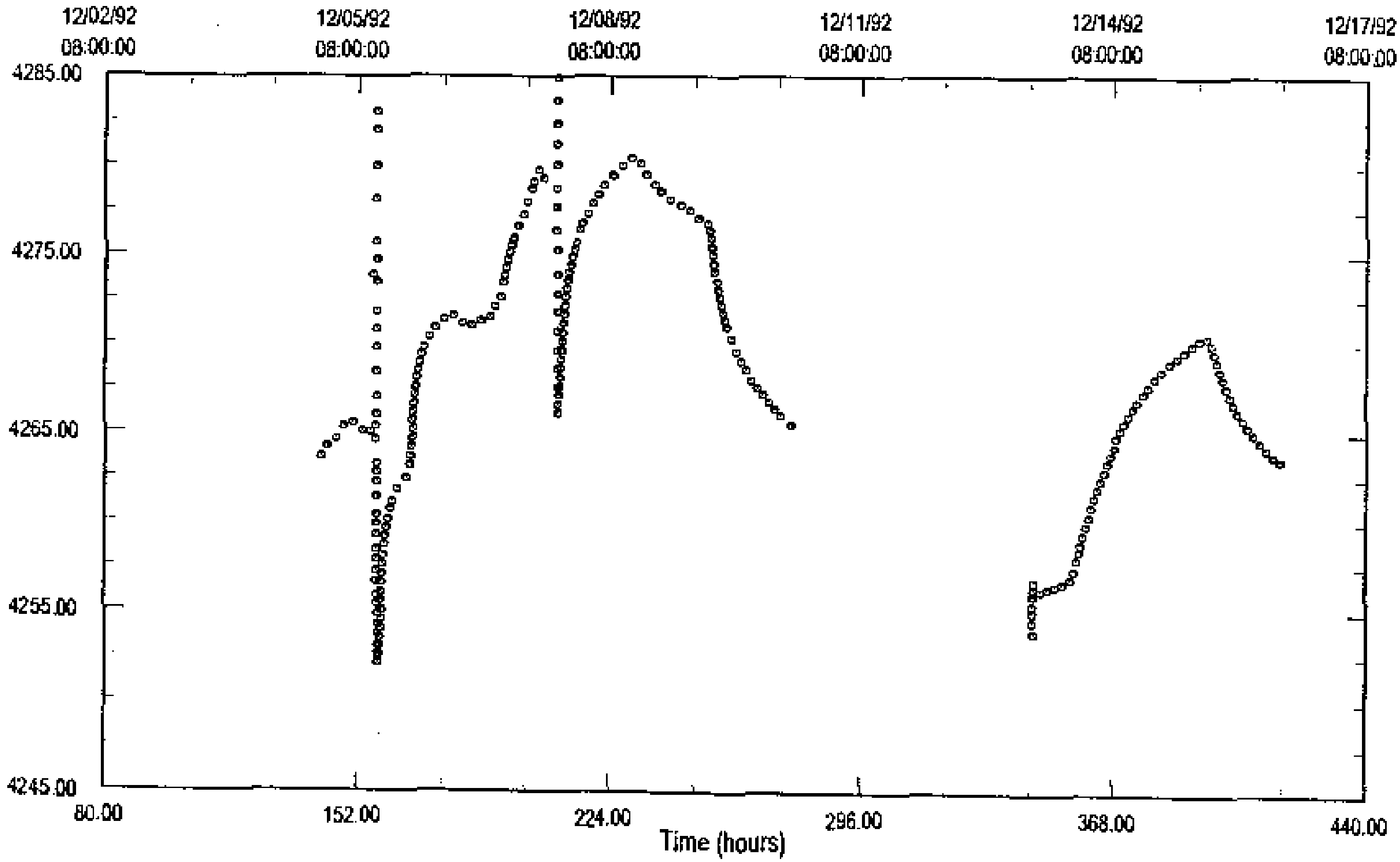

Pressure Data - Well 3			
Point Number	Real Time of Day (mm/dd/yy hh:mm:ss)	Elapsed Time (hours)	Measured Pressure
1)	12/4/92 20:40:00	140.667	263.250
2)	12/4/92 21:20:00	141.333	4263.630
3)	12/4/92 22:10:00	142.167	4263.880
4)	12/4/92 23:00:00	143.000	4264.240
5)	12/4/92 23:55:00	143.917	4264.180
6)	12/5/92 0:50:00	144.833	4264.370
7)	12/5/92 1:40:00	145.667	4264.630
0)	12/5/92 2:35:00	146.583	4264.650
9)	12/5/92 3:30:00	147.500	4264.880
10)	12/5/92 4:10:00	148.167	4265.340
11)	12/5/92 5:05:00	149.083	4265.500
12)	12/5/92 6:00:00	150.000	4265.540
13)	12/5/92 6:55:00	150.917	4265.550
14)	12/5/92 7:45:00	151.750	4265.270
15)	12/5/92 8:40:00	152.667	4265.260
16)	12/5/92 9:31:30	153.525	4265.090
17)	12/5/92 10:25:30	154.425	4265.180
10)	12/5/92 11:14:00	155.233	4265.420
19)	12/5/92 11:45:30	155.758	4265.030
20)	12/5/92 11:54:00	155.900	4273.850
21)	12/5/92 12:00:00	156.000	4547.480
22)	12/5/92 12:12:00	156.200	4725.900
23)	12/5/92 12:26:00	156.433	4748.540
24)	12/5/92 12:38:00	156.633	4780.770
25)	12/5/92 12:50:00	156.833	4411.460
26)	12/5/92 13:01:00	157.017	4293.620
27)	12/5/92 13:01:30	157.025	4291.640
28)	12/5/92 13:02:00	157.033	4289.580
29)	12/5/92 13:02:30	157.042	4287.690
30)	12/5/92 13:03:00	157.050	4285.470
31)	12/5/92 13:03:30	157.058	4203.010
32)	12/5/92 13:04:00	157.067	4201.990
33)	12/5/92 13:04:30	157.075	4279.980
34)	12/5/92 13:05:00	157.083	4278.100
35)	12/5/92 13:06:00	157.100	4275.700
36)	12/5/92 13:06:30	157.108	4274.730
37)	12/5/92 13:07:00	157.117	4273.480
38)	12/5/92 13:07:30	157.125	4271.820
39)	12/5/92 13:08:00	157.133	4270.820
40)	12/5/92 13:00:30	157.142	4269.800
41)	12/5/92 13:09:00	157.150	4268.410
42)	12/5/92 13:10:00	157.167	4267.050
43)	12/5/92 13:10:30	157.175	4266.066
44)	12/5/92 13:11:00	157.103	4265.370
45)	12/5/92 13:11:30	157.192	4264.610
46)	12/5/92 13:12:30	157.208	4263.240
47)	12/5/92 13:13:00	157.217	4262.766

Pressure Data - Well 3			
Point Number	Real Time of Day (mm/dd/yy hh:mm:ss)	Elapsed Time (hours)	Measured Pressure
48)	12/5/92 13:13:30	157.226	4262.220
49)	12/5/92 13:14:00	157.233	4261.370
50)	12/5/92 13:15:00	157.250	4260.360
51)	12/5/92 13:15:30	157.258	4259.860
52)	12/5/92 13:16:00	157.267	4259.240
53)	12/5/92 13:17:00	157.283	4258.390
54)	12/5/92 13:17:30	157.292	4257.850
55)	12/5/92 13:18:30	157.308	4257.200
56)	12/5/92 13:19:00	157.317	4256.600
57)	12/5/92 13:20:38	157.342	4255.850
58)	12/5/92 13:21:30	157.358	4255.340
59)	12/5/92 13:22:00	157.367	4254.820
60)	12/5/92 13:24:00	157.400	4254.220
61)	12/5/92 13:25:38	157.425	4253.690
62)	12/5/92 13:27:38	157.458	4253.080
63)	12/5/92 13:30:00	157.500	4252.570
64)	12/5/92 13:35:38	157.592	4252.890
65)	12/5/92 13:54:00	157.900	4252.550
66)	12/5/92 14:00:30	158.008	4253.030
67)	12/5/92 14:05:00	150.083	4253.510
68)	12/5/92 14:11:00	158.183	4254.020
69)	12/5/92 14:21:30	158.358	4254.500
70)	12/5/92 14:25:30	158.425	4255.820
71)	12/5/92 14:29:30	158.492	4255.540
72)	12/5/92 14:36:30	158.608	4256.030
73)	12/5/92 14:44:08	158.733	4256.540
74)	12/5/92 14:51:30	158.858	4257.040
75)	12/5/92 15:81:00	158.817	4257.590
76)	12/5/92 15:11:30	159.192	4258.080
77)	12/5/92 15:24:30	158.408	4258.690
78)	12/5/92 15:41:30	159.692	4258.160
79)	12/5/92 16:08:00	160.000	4259.620
80)	12/5/92 16:25:00	160.417	4280.100
01)	12/5/92 16:50:00	180.833	4260.630
82)	12/5/92 17:25:00	161.417	4261.080
83)	12/5/92 18:05:00	162.083	4261.430
84)	12/5/92 19:50:00	162.833	4261.820
85)	12/5/92 19:40:08	183.667	4262.810
86)	12/5/92 20:35:08	164.583	4262.090
87)	12/5/92 21:11:20	165.189	4282.458
88)	12/5/92 21:55:10	165.919	4262.740
89)	12/5/92 22:18:50	166.314	4263.180
90)	12/5/92 22:31:30	166.525	4263.680
91)	12/5/92 22:44:50	166.747	4264.200
92)	12/5/92 23:03:00	167.050	4264.690
93)	12/5/92 23:88:20	167.139	4265.130
94)	12/5/92 23:17:40	167.294	4265.680

Pressure Data - Well 3			
Point Number	Real Time of Day (mm/dd/yy hh:mm:ss)	Elapsed Time (hours)	Measured Pressure
95)	12/5/92 23:31:00	167.517	4266.150
96)	12/5/92 23:41:50	167.697	4266.630
97)	12/5/92 23:59:00	197.967	4297.090
99)	12/6/92 9:14:30	169.242	4297.560
99)	12/6/92 9:28:10	168.469	4268.040
100)	12/6/92 8:49:06	169.800	4269.490
181)	12/6/92 1:11:50	169.197	4268.930
102)	12/6/92 1:43:39	169.725	4269.390
103)	12/6/92 2:22:00	179.367	4269.778
104)	12/6/92 3:01:06	171.817	4279.110
105)	12/6/92 3:46:30	171.775	4270.390
106)	12/6/92 4:33:39	172.558	4270.640
197)	12/6/92 5:19:30	173.308	4270.920
108)	12/6/92 6:12:30	174.209	4270.900
109)	12/6/92 7:02:39	175.042	4271.090
118)	12/6/92 7:50:06	175.833	4271.350
111)	12/6/92 9:44:00	176.733	4271.369
112)	12/6/92 9:38:00	177.933	4271.450
113)	12/6/92 19:32:00	178.533	4271.540
114)	12/6/92 11:26:06	179.433	4271.410
115)	12/6/92 12:20:00	180.333	4271.290
116)	12/6/92 13:12:00	181.200	4271.130
117)	12/6/92 14:06:00	182.100	4271.949
119)	12/6/92 15:00:06	193.000	4271.080
119)	12/6/92 15:54:00	183.900	4271.020
120)	12/6/92 16:42:00	184.700	4271 240
121)	12/6/92 17:36:06	195.600	4271.240
122)	12/6/92 19:38:06	186.500	4271.270
123)	12/6/92 19:24:00	187.400	4271.249
124)	12/6/92 20:18:00	188.300	4271.220
125)	12/6/92 21:06:40	189.061	4271.490
126)	12/6/92 21:59:30	189.842	4271.749
127)	12/6/92 22:31:28	190.522	4272.080
129)	12/6/92 23:17:20	191.299	4272.350
129)	12/7/92 0:06:48	192.911	4272.660
138)	12/7/92 9:48:40	192.811	4273.000
131)	12/7/92 1:17:18	193.296	4273.430
132)	12/7/92 1:43:30	193.725	4273.859
133)	12/7/92 2:11:00	194.183	4274.278
134)	12/7/92 2:37:06	194.617	4274.700
135)	12/7/92 3:95:06	195.993	4275.150
136)	12/7/92 3:37:50	195.631	4275.540
137)	12/7/92 4:10:40	196.179	4275.930
139)	12/7/92 4:49:20	196.806	4276.280
139)	12/7/92 5:27:00	197.450	4279.640
140)	12/7/92 6:05:39	199.092	4276.980
141)	12/7/92 6:47:00	198.793	4277.290

Pressure Data - Well 3			
Point Number	Real Time of Day (mm/dd/yy hh:mm:ss)	Elapsed Time (hours)	Measured Pressure
142)	12/7/92 7:24:58	199.414	4277.650
143)	12/7/92 8:01:00	200.017	4276.818
144)	12/7/92 8:43:00	200.717	4278.348
145)	12/7/92 9:16:00	201.300	4278.730
146)	12/7/92 9:54:00	201.900	4279.118
147)	12/7/92 10:32:00	202.533	4279.470
148)	12/7/92 11:15:00	203.250	4279.780
149)	12/7/92 12:03:00	204.850	4279.560
150)	12/7/92 12:50:00	284.833	4279.318
151)	12/7/92 13:43:00	205.717	4279.200
152)	12/7/92 14:37:00	206.617	4279.120
153)	12/7/92 15:16:00	207.300	4556.380
154)	12/7/92 15:27:00	207.450	4715.840
155)	12/7/92 15:36:00	207.600	4756.220
156)	12/7/92 15:45:00	207.750	4759.660
157)	12/7/92 15:54:00	207.900	4756.760
158)	12/7/92 16:03:68	268.060	4716.650
159)	12/7/92 16:12:00	208.200	4453.030
160)	12/7/92 16:16:00	208.300	4358.370
161)	12/7/92 16:24:18	206.403	4300.700
162)	12/7/92 16:27:30	208.450	4295.718
163)	12/7/92 16:28:00	208.467	4294.118
164)	12/7/92 16:26:20	208.472	4293.116
165)	12/7/92 16:28:50	268.481	4291.530
160)	12/7/92 16:29:30	208.492	4289.560
167)	12/7/92 16:30:18	208.503	4288.000
168)	12/7/92 16:30:50	206.514	4286.400
169)	12/7/92 16:31:30	208.525	4264.940
178)	12/7/92 16:32:18	208.536	4283.670
171)	12/7/92 16:32:50	206.547	4282.360
172)	12/7/92 16:33:50	208.564	4261.230
173)	12/7/92 16:34:40	208.578	4280.668
174)	12/7/92 16:35:50	206.597	4278.800
175)	12/7/92 16:36:50	268.614	4277.710
176)	12/7/92 16:38:68	208.633	4276.400
177)	12/7/92 16:39:00	206.650	4275.270
176)	12/7/92 16:48:30	288.675	4273.900
179)	12/7/92 16:42:68	208.700	4272.790
188)	12/7/92 16:43:20	208.722	4271.790
181)	12/7/92 16:45:00	208.750	4270.700
182)	12/7/92 16:47:00	206.783	4269.610
183)	12/7/92 16:49:30	268.625	4268.568
194)	12/7/92 16:53:10	209.886	4267.560
165)	12/7/92 16:59:40	286.994	4266.590
186)	12/7/92 17:06:20	209.139	4268.110
167)	12/7/92 17 20:30	209.342	4267 120
186)	12/7/92 17:31:20	289.522	4267.600

Pressure Data - Well 3

Point Number	Real Time of Day (mm/dd/yy hh:mm:ss)	Elapsed Time (hours)	Measured Pressure
189)	12/7/92 17:37:30	209.625	4268.110
190)	12/7/92 17:45:10	209.753	4268.630
191)	12/7/92 17:51:50	209.864	4269.120
192)	12/7/92 18:00:00	210.000	4269.620
193)	12/7/92 18:07:00	210.117	4270.120
194)	12/7/92 18:17:10	210.286	4270.620
195)	12/7/92 18:28:30	210.442	4271.180
196)	12/7/92 18:40:30	210.675	4271.670
197)	12/7/92 18:49:30	210.825	4272.150
198)	12/7/92 19:00:00	211.000	4272.640
199)	12/7/92 19:17:30	211.292	4273.120
200)	12/7/92 19:36:30	211.608	4273.590
201)	12/7/92 19:58:00	211.967	4274.050
202)	12/7/92 20:29:00	212.483	4274.460
203)	12/7/92 20:53:30	212.892	4274.920
204)	12/7/92 21:29:30	213.492	4275.320
205)	12/7/92 22:08:30	214.142	4275.690
206)	12/7/92 22:51:00	214.850	4276.050
207)	12/7/92 23:28:00	215.467	4276.410
208)	12/8/92 0:11:00	216.183	4276.780
209)	12/8/92 0:57:30	216.958	4277.030
210)	12/8/92 1:41:00	217.683	4277.330
211)	12/8/92 2:20:00	218.333	4277.670
212)	12/8/92 3:07:00	219.117	4277.910
213)	12/8/92 3:53:30	219.892	4278.170
214)	12/8/92 4:42:00	220.700	4278.410
215)	12/8/92 5:28:30	221.475	4278.670
216)	12/8/92 6:15:30	222.258	4278.930
217)	12/8/92 7:08:00	223.133	4279.050
218)	12/8/92 7:58:00	223.967	4279.280
219)	12/8/92 8:48:00	224.800	4279.470
220)	12/8/92 9:40:00	225.667	4279.650
221)	12/8/92 10:32:00	226.533	4279.800
222)	12/8/92 11:22:00	227.367	4280.000
223)	12/8/92 12:16:00	228.267	4280.070
224)	12/8/92 13:04:00	229.067	4280.340
225)	12/8/92 13:58:00	229.967	4280.440
226)	12/8/92 14:52:00	230.867	4280.580
227)	12/8/92 15:44:00	231.733	4280.420
228)	12/8/92 16:32:00	232.533	4280.150
229)	12/8/92 17:18:00	233.300	4279.880
230)	12/8/92 18:08:00	234.133	4279.570
231)	12/8/92 18:58:00	234.967	4279.380
232)	12/8/92 19:50:00	235.833	4279.210
233)	12/8/92 20:38:00	236.633	4278.980
234)	12/8/92 21:30:00	237.500	4278.740
235)	12/8/92 22:22:00	238.367	4278.590

Pressure Data - Well 3			
Point Number	Real Time of Day (mm/dd/yy hh:mm:ss)	Elapsed Time (hours)	Measured Pressure
236)	12/8/92 23:1d:00	239.233	4276.460
237)	12/9/92 8:04:00	240.067	4278.250
238)	12/9/92 8:58:90	248.967	4278.180
239)	12/9/92 1:52:00	241.867	4278.880
248)	12/9/92 2:46:00	242.767	4277.968
241)	12/9/92 3:40:90	243.667	4277.858
242)	12/9/92 4:32:00	244.533	4277.720
243)	12/9/92 5:26:00	245.433	4277.660
244)	12/9/92 6:26:00	246.333	4277.540
245)	12/9/92 7:12:90	247.200	4277.400
248)	12/9/92 8:04:00	248.067	4277.258
247)	12/9/92 9:00:00	248.000	4277.120
246)	12/9/92 8:55:90	248.917	4277.000
249)	12/9/92 10:50:90	250.833	4278.860
250)	12/9/92 11:44:00	251.733	4276.810
251)	12/9/92 12:22:00	252.367	4278.440
252)	12/9/92 12:41:90	252.683	4275.990
253)	12/9/92 12:57:00	252.950	4275.480
254)	12/9/92 13:13:00	253.217	4275.020
255)	12/9/92 13:30:00	253.500	4274.530
256)	12/9/92 13:47:00	253.783	4274.070
257)	12/9/92 14:08:90	254.133	4273.530
258)	12/9/92 14:31:00	254.517	4273.078
259)	12/9/92 14:55:00	254.817	4272.618
260)	12/9/92 15:26:00	255.433	4272.100
261)	12/9/92 15:56:00	255.933	4271.790
262)	12/9/92 16:38:00	256.500	4271.360
263)	12/9/92 17:06:90	257.100	4270.980
264)	12/9/92 17:50:90	257.833	4278.690
265)	12/9/92 18:28:00	258.467	4270.290
266)	12/9/92 19:08:90	259.133	4269.960
267)	12/9/92 19:52:90	259.867	4269.640
268)	12/9/92 28:36:00	260.600	4269.358
268)	12/9/92 21:22:00	261.367	4269.090
270)	12/9/92 22:08:90	262.133	4268.820
271)	12/9/92 22:52:90	262.867	4268.540
272)	12/9/92 23:48:00	263.667	4268.238
273)	12/10/92 8:24:00	264.400	4267.940
274)	12/10/92 1:16:00	265.267	4267.750
275)	12/10/92 2:06:90	266.100	4267.590
276)	12/10/92 2:54:00	266.900	4267.310
277)	12/10/92 3:46:00	267.767	4267.100
278)	12/10/92 4:36:00	268.600	4266.970
278)	12/10/92 5:26:90	269.433	4266.778
280)	12/10/92 6:18:00	270.300	4266.558
281)	12/10/92 7:10:00	271.167	4266.370
282)	12/10/92 8:82:00	272.833	4266.228

Pressure Data - Well 3				
Point Number	Real Time of Day (mm/dd/yy hh:mm:ss)	Elapsed Time (hours)	Measured Pressure	
283)	12/10/92 8:52:00	272.867	4268.000	
284)	12/10/92 9:44:00	273.733	4265.830	
285)	12/10/92 10:36:00	274.600	4265.670	
286)	12/10/92 11:28:00	275.467	4265.480	
287)	12/13/92 8:52:00	344.867	2133.920	2120 psi
288)	12/13/92 8:53:00	344.883	2134.250	added to these
288)	12/13/92 8:54:00	344.900	2134.490	values
290)	12/13/92 8:55:00	344.917	2134.750	
291)	12/13/92 8:56:00	344.933	2135.019	
292)	12/13/92 8:57:00	344.950	2135.190	
293)	12/13/92 8:58:00	344.967	2135.419	
294)	12/13/92 9:00:00	345.000	2136.680	
295)	12/13/92 9:82:00	345.033	2136.950	
296)	12/13/92 9:04:00	345.067	2138.130	
297)	12/13/92 8:07:00	345.117	2136.350	
298)	12/13/92 9:11:00	345.183	2136.530	
299)	12/13/92 9:17:00	345.283	2138.720	
300)	12/13/92 9:48:00	345.800	2136.660	
301)	12/13/92 10:12:00	346.200	2136.520	
382)	12/13/92 18:37:00	346.617	2136.400	
303)	12/13/92 11:08:00	347.133	2138.216	
304)	12/13/92 11:34:00	347.567	2136.320	
305)	12/13/92 12:07:00	348.117	2136.280	
306)	12/13/92 12:39:00	348.650	2138.348	
307)	12/13/92 13:12:00	349.200	2136.360	
308)	12/13/92 13:44:00	349.733	2136.390	
309)	12/13/92 14:17:00	350.283	2139.410	
310)	12/13/92 14:50:00	350.833	2136.400	
311)	12/13/92 15:19:00	351.317	2136.500	
312)	12/13/92 15:52:00	351.867	2136.480	
313)	12/13/92 16:24:00	352.400	2138.550	
314)	12/13/92 1g:56:00	352.933	2136.580	
315)	12/13/92 17:27:00	353.450	2136.640	
316)	12/13/92 17:58:00	353.967	2139.708	
317)	12/13/92 18:25:19	354.419	2136.840	
31D)	12/13/92 18:51:00	354.850	2136.720	
319)	12/13/92 19:17:59	355.297	2136.930	
329)	12/13/92 19:46:36	355.775	2130.929	
321)	12/13/92 28:05:19	356.088	2137.090	
322)	12/13/92 20:25:48	356.428	2137.250	
323)	12/13/92 28:44:50	356.747	2137.400	
324)	12/13/92 20:59:00	356.983	2137.579	
325)	12/13/92 21:13:20	357.222	2137.748	
326)	12/13/92 21:28:00	357.467	2137.919	
327)	12/13/92 21:41:00	357.683	2138.090	
328)	12/13/92 22:02:49	358.044	2138.230	
329)	12/13/92 22:13:28	358.222	2138.400	

Pressure Data - Well 3			
Point Number	Real Time of Day (mm/dd/yy hh:mm:ss)	Elapsed Time (hours)	Measured Pressure
330)	12/13/92 22:23:50	358.397	2138.580
331)	12/13/92 22:35:50	358.597	2138.800
332)	12/13/92 22:51:48	358.861	2138.960
333)	12/13/92 23:03:30	359.050	2139.148
334)	12/13/92 23:18:30	359.308	2139.300
335)	12/13/92 23:32:20	359.539	2139.470
336)	12/13/92 23:48:10	350.803	2139.640
337)	12/14/92 8:02:00	368.033	2139.830
338)	12/14/92 0:13:10	360.219	2140.028
339)	12/14/92 0:33:20	360.556	2140.180
340)	12/14/92 8:48:40	360.811	2140.348
341)	12/14/92 1:03:00	361.050	2140.510
342)	12/14/92 1:20:00	361.333	2140.700
343)	12/14/92 1:37:60	301.617	2140.870
344)	12/14/92 1:54:00	381.900	2141.030
345)	12/14/92 2:13:00	362.217	2141.218
346)	12/14/92 2:26:60	362.433	2141.428
347)	12/14/92 2:44:00	362.733	2141.570
348)	12/14/92 3:02:60	363.033	2141.740
349)	12/14/92 3:17:60	363.283	2141.900
350)	12/14/92 3:37:00	363.617	2142.090
351)	12/14/92 3:56:00	363.933	2142.240
352)	12/14/92 4:14:00	364.233	2142.390
353)	12/14/92 4:32:00	364.533	2142.550
354)	12/14/92 4:52:00	364.867	2142.720
355)	12/14/92 5:12:00	365.280	2142.880
356)	12/14/92 5:30:00	365.900	2143.080
357)	12/14/92 5:49:00	365.817	2143.230
35a)	12/14/92 6:11:00	366.183	2143.370
359)	12/14/92 6:29:00	368.433	2143.530
360)	12/14/92 6:47:60	366.783	2143.670
361)	12/14/92 7:08:00	367.133	2143.820
362)	12/14/92 7:27:00	367.450	2143.970
363)	12/14/92 7:50:60	367.833	2144.120
364)	12/14/92 8:08:00	368.133	2144.280
365)	12/14/92 8:26:00	368.433	2144.460
366)	12/14/92 8:50:00	368.833	2144.810
367)	12/14/92 9:04:00	369.037	2144.810
368)	12/14/92 9:31:00	369.517	2144.920
369)	12/14/92 9:51:00	399.650	2145.008
378)	12/14/92 18:13:00	378.217	2145.240
371)	12/14/92 10:38:00	378.633	2145.360
372)	12/14/92 10:57:00	370.950	2145.510
373)	12/14/92 11:20:00	371.333	2145.640
374)	12/14/92 11:42:00	371.760	2145.788
375)	12/14/92 12:09:00	372.150	2145.900
376)	12/14/92 12:28:00	372.467	2146.050

Pressure Data - Well 3			
Point Number	Real Time of Day (mm/dd/yy hh:mm:ss)	Elapsed Time (hours)	Measured Pressure
377)	12/14/92 12:49:00	372.817	2146.190
378)	12/14/92 13:15:00	373.250	2146.340
379)	12/14/92 13:42:00	373.708	2146.460
380)	12/14/92 14:06:00	374.100	2148.590
381)	12/14/92 1d:31:00	374.517	2146.720
382)	12/14/92 14:58:00	374.967	2146.830
383)	12/14/92 15:24:06	375.400	2146.940
384)	12/14/92 15:50:00	375.833	2147.050
385)	12/14/92 16:17:00	378.283	2147.170
388)	12/14/92 16:44:00	376.733	2147.300
387)	12/14/92 17:08:00	377.133	2147.430
388)	12/14/92 17:36:00	377.600	2147.530
389)	12/14/92 18:00:00	378.000	2147.680
390)	12/14/92 18:30:00	378.500	2147.780
391)	12/14/92 18:58:00	378.967	21d7.890
392)	12/14/92 19:28:00	379.467	2147.990
393)	12/14/92 19:52:06	379.867	2148.180
394)	12/14/92 20:24:00	380.400	2148.220
395)	12/14/92 20:56:00	380.933	2148.340
396)	12/14/92 21:24:00	381.400	2148.440
397)	12/14/92 21:48:00	381.767	2148.580
398)	12/14/92 22:18:00	382.300	2148.619
399)	12/14/92 22:48:00	382.667	2148.750
400)	12/14/92 23:18:00	383.167	2148.838
401)	12/14/92 23:38:00	383.633	2148.940
402)	12/15/92 0:06:00	384.100	2149.050
403)	12/15/92 0:36:00	384.600	2149.120
404)	12/15/92 1:10:00	385.187	2148.160
405)	12/15/92 1:38:00	385.633	2149.320
406)	12/15/92 2:10:00	386.167	2149.360
487)	12/15/92 2:42:00	386.700	2149.450
408)	12/15/92 3:12:00	387.200	2149.550
409)	12/15/92 3:44:00	387.733	2149.610
d10)	12/15/92 d:14:00	388.233	2149.690
411)	12/15/92 4:48:00	388.800	2149.730
412)	12/15/92 5:18:00	389.267	2149.890
413)	12/15/92 5:50:00	389.833	2149.940
414)	12/15/92 8:20:00	390.333	2150.030
415)	12/15/92 8:52:00	390.867	2150.120
416)	12/15/92 7:21:00	391.350	2150.220
417)	12/15/92 7:54:00	391.900	2150.250
418)	12/15/92 8:23:00	392.383	2150.340
419)	12/15/92 8:57.00	392.950	2150.390
420)	12/15/92 9:25:10	393.419	2150.490
421)	12/15/92 9:57:40	393.961	2150.490
422)	12/15/92 10:30:30	394.508	2150.480
423)	12/15/92 18:58:38	394.975	2158.378

Pressure Data - Well 3			
Point Number	Real Time of Day (mm/dd/yy hh:mm:ss)	Elapsed Time (hours)	Measured Pressure
424)	12/15/92 11:22:30	395.375	2150.230
425)	12/15/92 11:46:00	395.767	2150.090
426)	12/15/92 12:01:00	396.017	2149.910
427)	12/15/92 12:17:30	396.292	2149.750
428)	12/15/92 12:38:00	396.633	2149.610
429)	12/15/92 12:50:00	396.833	2149.440
430)	12/15/92 13:09:00	397.150	2149.290
431)	12/15/92 13:24:00	397.400	2149.130
432)	12/15/92 13:40:00	397.667	2148.976
433)	12/15/92 13:55:00	397.917	2148.810
434)	12/15/92 14:09:00	398.150	2148.630
435)	12/15/92 14:27:30	398.458	2148.480
436)	12/15/92 14:48:30	398.808	2148.340
437)	12/15/92 15:04:00	399.067	2148.180
438)	12/15/92 15:26:00	399.433	2148.030
439)	12/15/92 15:48:00	399.800	2147.840
440)	12/15/92 16:08:00	400.133	2147.660
441)	12/15/92 16:29:00	400.483	2147.520
442)	12/15/92 16:46:00	400.767	2147.360
443)	12/15/92 17:08:00	401.133	2147.210
444)	12/15/92 17:33:00	401.550	2147.060
445)	12/15/92 17:48:00	401.800	2146.900
446)	12/15/92 18:13:00	402.217	2146.780
447)	12/15/92 18:34:00	402.567	2146.620
448)	12/15/92 18:59:00	402.983	2146.460
449)	12/15/92 19:21:00	403.350	2146.320
450)	12/15/92 19:45:00	403.750	2146.190
451)	12/15/92 20:10:00	404.167	2146.060
452)	12/15/92 20:36:00	404.600	2145.930
453)	12/15/92 20:53:00	404.883	2145.770
454)	12/15/92 21:21:00	405.350	2145.630
455)	12/15/92 21:49:00	405.817	2145.500
456)	12/15/92 22:12:00	406.200	2145.350
457)	12/15/92 22:34:00	406.567	2145.210
458)	12/15/92 23:05:00	407.083	2145.150
459)	12/15/92 23:34:00	407.567	2145.010
460)	12/16/92 0:02:00	408.033	2144.900
461)	12/16/92 0:33:00	408.550	2144.820
462)	12/16/92 1:02:00	409.033	2144.720
463)	12/16/92 1:28:00	409.467	2144.580
464)	12/16/92 1:57:00	409.950	2144.490
465)	12/16/92 2:24:00	410.400	2144.370
466)	12/16/92 2:54:00	410.900	2144.280
467)	12/16/92 3:19:00	411.317	2144.160
468)	12/16/92 3:49:00	411.817	2144.080
469)	12/16/92 4:17:00	412.283	2143.980
470)	12/16/92 4:43:00	412.717	2143.960

Pressure Data - Well 3			
Point Number	Real Time of Day (mm/dd/yy hh:mm:ss)	Elapsed Time (hours)	Measured Pressure
471)	12/16/92 5:13:00	413.217	2143.790
472)	12/16/92 5:43:00	413.717	2143.716
473)	12/16/92 6:11:00	414.183	2143.610
474)	12/16/92 6:41:00	414.683	2143.500
475)	12/16/92 7:13:00	415.217	2143.540
476)	12/16/92 7:35:00	415.583	2143.400
477)	12/16/92 8:07:00	416.117	2143.350
478)	12/16/92 8:39:00	416.650	2143.270

State .... Mississippi

County .... Harrison

Field .... DeLisle Plant

Du Pont DeLisle Plant

Well 4

Test Date 5-Dec-92

Analysis Date 1-Jun-93

Report Number 930201

Pressure Data

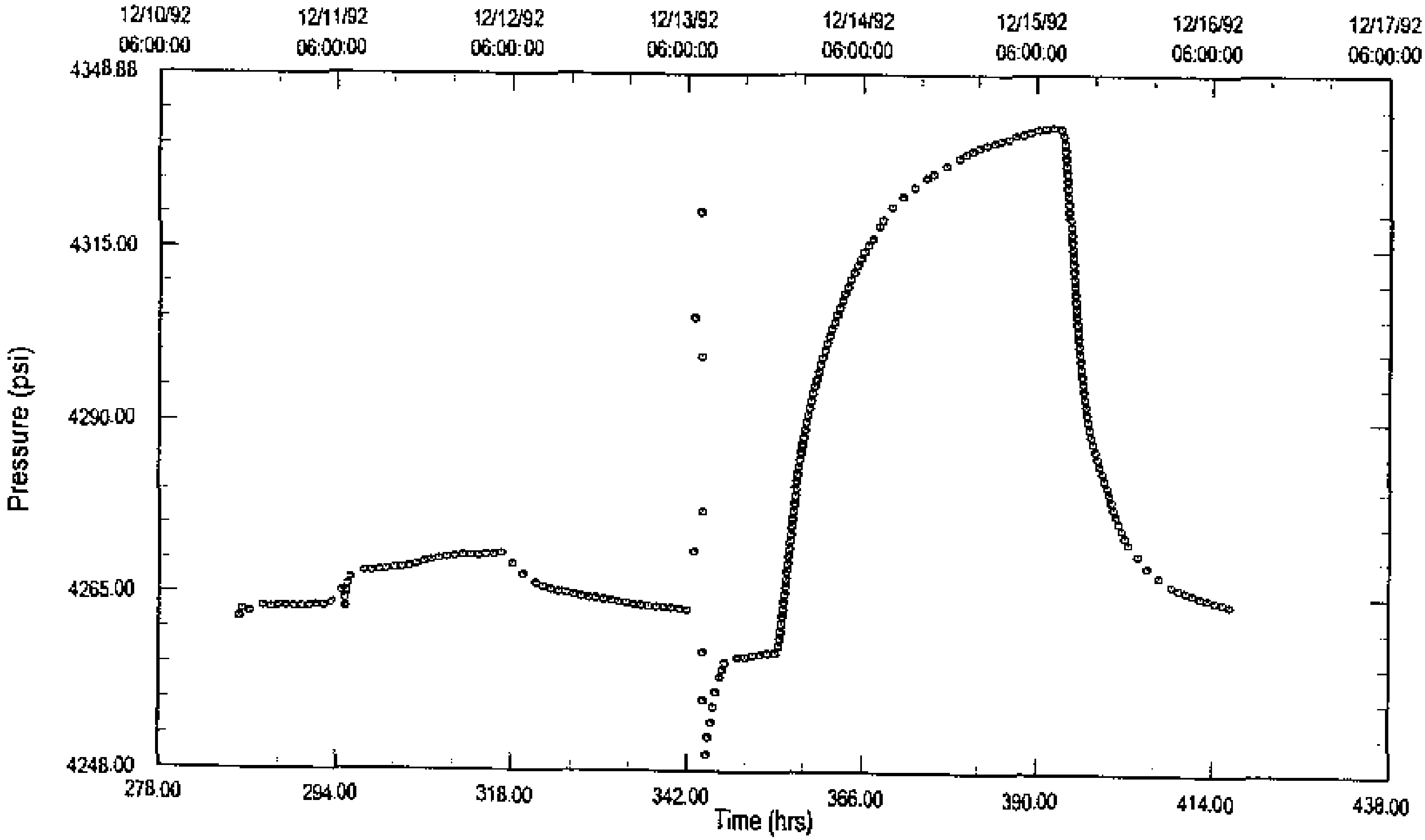

Pressure Data - Well 4			
Point Number	Real Time of Day (mm/dd/yy hh:mm:ss)	Elapsed Time (hours)	Measured Pressure
1)	12/10/92 16:49:00	280.817	4261.620
2)	12/10/92 17:11:60	281.183	4262.680
3)	12/10/92 18:12:00	282.200	4262.380
4)	12/10/92 18:56:00	282.933	4263.218
5)	12/10/92 19:59:00	283.983	4263.158
6)	12/10/92 21:01:30	285.025	4262.990
7)	12/10/92 22:03:30	286.058	4263.200
8)	12/10/92 23:06:30	287.108	4263.200
9)	12/11/92 0:09:30	288.158	4263.130
10)	12/11/92 1:12:30	289.208	4263.140
11)	12/11/92 2:15:30	290.258	4263.190
12)	12/11/92 3:18:30	291.300	4263.318
13)	12/11/92 4:21:30	292.358	4263.278
14)	12/11/92 5:19:00	293.317	4263.718
15)	12/11/92 6:07:40	294.128	4264.390
16)	12/11/92 6:41:50	294.697	4265.280
17)	12/11/92 7:11:30	295.192	4264.228
18)	12/11/92 7:13:30	295.225	4263.020
19)	12/11/92 7:24:30	295.408	4265.100
20)	12/11/92 7:31:30	295.525	4266.250
21)	12/11/92 7:55:30	295.925	4267.278
22)	12/11/92 8:40:30	296.668	4267.870
23)	12/11/92 9:49:00	297.817	4268.230
24)	12/11/92 10:52:00	298.867	4268.190
25)	12/11/92 11:54:00	299.900	4268.390
26)	12/11/92 12:57:00	300.950	4268.490
27)	12/11/92 14:00:03	302.000	4268.668
28)	12/11/92 15:03:00	303.050	4268.720
29)	12/11/92 16:06:00	304.100	4268.930
30)	12/11/92 17:08:00	305.133	4269.240
31)	12/11/92 18:08:00	306.133	4269.590
32)	12/11/92 19:10:00	307.167	4269.810
33)	12/11/92 20:12:00	308.200	4270.070
34)	12/11/92 21:16:00	309.267	4270.268
35)	12/11/92 22:20:00	310.333	4270.470
36)	12/11/92 23:24:00	311.400	4270.620
37)	12/12/92 0:28:00	312.467	4270.600
38)	12/12/92 1:32:00	313.533	4270.550
39)	12/12/92 2:34:00	314.567	4270.760
40)	12/12/92 3:38:00	315.633	4270.780
41)	12/12/92 4:40:40	316.678	4270.928
42)	12/12/92 5:32:20	317.539	4270.290
43)	12/12/92 6:08:20	318.139	4269.418
44)	12/12/92 6:49:50	318.831	4268.600
45)	12/12/92 7:34:03	319.567	4267.850
46)	12/12/92 8:23:30	320.392	4267.160
47)	12/12/92 9:18:00	321.300	4266.618

Pressure Data - Well 4			
Point Number	Real Time of Day (mm/dd/yy hh:mm:ss)	Elapsed Time (hours)	Measured Pressure
48)	12/12/92 18:15:00	322.250	4266.120
49)	12/12/92 11:16:00	323.267	4265.770
58)	12/12/92 12:16:00	324.300	4265.530
51)	12/12/92 13:19:00	325.317	4265.260
52)	12/12/92 14:21:00	326.350	4265.818
53)	12/12/92 15:22:00	327.367	4264.738
54)	12/12/92 16:25:00	328.417	4264.560
55)	12/12/92 17:26:00	329.467	4264.510
56)	12/12/92 16:30:00	330.500	4264.320
57)	12/12/92 19:33:00	331.550	4264.160
56)	12/12/92 20:35:00	332.583	4263.950
59)	12/12/92 21:36:00	333.633	4263.660
60)	12/12/92 22:40:00	334.667	4263.660
61)	12/12/92 23:43:00	335.717	4263.538
62)	12/13/92 9:46:00	336.787	4263.360
63)	12/13/92 1:49:00	337.817	4263.318
64)	12/13/92 2:52:00	338.667	4263.270
65)	12/13/92 3:55:00	339.917	4263.150
66)	12/13/92 4:58:00	340.967	4263.040
67)	12/13/92 6:01:00	342.817	4262.890
68)	12/13/92 8:59:00	342.983	4271.270
69)	12/13/92 7:00:00	343.000	4305.020
78)	12/13/92 7:01:00	343.817	4347.440
71)	12/13/92 7:02:00	343.033	4388.540
72)	12/13/92 7:00:00	343.050	4425.780
73)	12/13/92 7:04:00	343.067	4461.540
74)	12/13/92 7:05:00	343.083	4494.130
75)	12/13/92 7:06:00	343.100	4521.090
76)	12/13/92 7:87:00	343.117	4544.620
77)	12/13/92 7:06:00	343.133	4561.500
76)	12/13/92 7:18:00	343.167	4588.800
79)	12/13/92 7:12:00	343.200	4608.550
80)	12/13/92 7:21:00	343.350	4620.918
61)	12/13/92 7:31:00	343.517	4688.870
62)	12/13/92 7:36:00	343.600	4627.760
63)	12/13/92 7:42:00	343.700	4613.718
64)	12/13/92 7:43:00	343.717	4593.490
85)	12/13/92 7:44:00	343.733	4562.988
66)	12/13/92 7:46:00	343.767	4503.190
87)	12/13/92 7:46:50	343.781	4481.750
88)	12/13/92 7:49:00	343.817	4433.920
69)	12/13/92 7:50:00	343.633	4415.520
90)	12/13/92 7:52:30	343.875	4376.830
91)	12/13/92 7:54:48	343.911	4349.360
92)	12/13/92 7:57:48	343.961	4328.280
93)	12/13/92 9:00:40	344.011	4299.510
94)	12/13/92 8:05:50	344.097	4277.100

Pressure Data - Well 4			
Point Number	Real Time of Day (mm/dd/yy hh:mm:ss)	Elapsed Time (hours)	Measured Pressure
95)	12/13/92 8:12:10	344.203	4257.000
96)	12/13/92 8:19:48	344.328	4250.190
97)	12/13/92 8:49:00	344.817	4242.490
98)	12/13/92 9:02:00	345.033	4244.940
99)	12/13/92 9:29:30	345.475	4247.090
100)	12/13/92 9:42:20	345.706	4249.230
181)	12/13/92 19:02:40	346.044	4251.340
192)	12/13/92 19:35:50	349.597	4253.450
103)	12/13/92 10:57:30	346.958	4254.479
104)	12/13/92 11:19:19	347.319	4255.490
105)	12/13/92 12:00:40	348.811	4256.290
108)	12/13/92 13:04:00	349.067	4256.249
187)	12/13/92 14:97:00	350.117	4256.218
109)	12/13/92 15:08:00	351.133	4256.518
199)	12/13/92 16:11:00	352.183	4256.920
110)	12/13/92 17:13:00	353.217	4256.830
111)	12/13/92 19:15:49	354.261	4256.949
112)	12/13/92 18:41:00	354.683	4257.920
113)	12/13/92 18:51:30	354.958	4258.960
114)	12/13/92 19:58:49	354.978	4260.020
115)	12/13/92 19:05:40	355.094	4291.090
118)	12/13/92 19:12:20	355.208	4262.140
117)	12/13/92 19:18:40	355.311	4263.190
119)	12/13/92 19:25:20	355.422	4264.260
118)	12/13/92 18:31:00	355.517	4265.338
120)	12/13/92 19:36:30	355.608	4266.380
121)	12/13/92 19:42:18	355.703	4267.460
122)	12/13/92 19:47:50	355.797	4268.580
123)	12/13/92 19:53:20	355.889	4290.640
124)	12/13/92 19:58:56	355.991	4270.748
125)	12/13/92 20:03:49	356.061	4271.930
126)	12/13/92 20:09:00	356.150	4272.890
127)	12/13/92 29:14:40	356.244	4273.940
128)	12/13/92 20:20:50	356.347	4275.060
120)	12/13/92 20:27:00	356.450	4279.120
130)	12/13/92 20:33:30	356.558	4277.179
131)	12/13/92 20:40:10	356.669	4276.260
132)	12/13/92 20:47:39	356.792	4279.330
133)	12/13/92 20:55:50	356.931	4280.430
134)	12/13/92 21:04:10	357.069	4281.500
135)	12/13/92 21:12:40	357.211	4292.560
138)	12/13/92 21:22:50	357.381	4283.620
137)	12/13/92 21:32:19	357.536	4284.660
138)	12/13/92 21:42:19	357.703	4285.749
139)	12/13/92 21:52:18	357.869	4286.800
149)	12/13/92 22:93:10	358.053	4287.879
141)	12/13/92 22:14:50	358.247	4289.930

Pressure Data - Well 4			
Point Number	Real Time of Day (mm/dd/yy hh:mm:ss)	Elapsed Time (hours)	Measured Pressure
142)	12/13/92 22:26:00	358.433	4289.970
143)	12/13/92 22:37:10	358.619	4291.040
144)	12/13/92 22:50:00	358.833	4292.070
145)	12/13/92 23:02:50	359.047	4283.120
146)	12/13/92 23:16:29	359.272	4294.168
147)	12/13/92 23:38:20	358.506	4295.200
148)	12/13/92 23:45:30	359.756	4296.220
149)	12/14/92 0:00:40	368.011	4297.260
150)	12/14/92 0:15:50	368.264	4298.298
151)	12/14/92 8:32:20	360.539	4299.320
152)	12/14/92 0:49:50	360.831	4300.348
153)	12/14/92 1:07:20	361.122	4301.360
154)	12/14/92 1:27:00	361.450	4302.470
155)	12/14/92 1:47:00	361.783	4303.510
156)	12/14/92 2:07:00	362.117	4304.520
157)	12/14/92 2:27:00	362.450	4305.578
158)	12/14/92 2:47:00	362.783	4306.670
159)	12/14/92 3:08:00	363.133	4307.610
160)	12/14/92 3:30:00	363.500	4308.628
161)	12/14/92 3:54:00	363.900	4309.610
162)	12/14/92 4:16:00	364.300	4310.640
163)	12/14/92 4:45:00	364.750	4311.698
164)	12/14/92 5:18:00	365.1e7	4312.700
165)	12/14/92 5:38:00	365.833	4313.650
166)	12/14/92 6:06:00	366.100	4314.660
167)	12/14/92 6:36:00	366.600	4315.600
168)	12/14/92 7:10:00	367.167	4316.540
169)	12/14/92 7:43:00	367.717	4317.440
170)	12/14/92 8:17:00	368.283	4316.330
171)	12/14/92 8:48:00	368.800	4319.260
172)	12/14/92 9:24:00	369.400	4328.160
173)	12/14/92 10:00:00	370.000	4321.060
174)	12/14/92 10:48:00	370.667	4321.890
175)	12/14/92 11:29:00	371.483	4322.570
176)	12/14/92 12:18:00	372.300	4323.278
177)	12/14/92 13:67:00	373.117	4323.930
178)	12/14/92 13:56:00	373.933	4324.620
179)	12/14/92 14:45:00	374.750	4325.340
180)	12/14/92 15:42:00	375.700	4325.860
181)	12/14/92 16:35:00	376.563	4326.490
182)	12/14/92 17:26:00	377.467	4327.080
183)	12/14/92 16:21:00	376.350	4327.650
184)	12/14/92 19:16:00	379.267	4328.210
185)	12/14/92 20:12:00	380.200	4328.770
186)	12/14/92 21:09:00	3b1.150	4329.220
187)	12/14/92 22.05:00	382.083	4329.730
188)	12/14/92 23:65:00	383.083	4330.090

Pressure Data - Well 4			
Point Number	Real Time of Day (mm/dd/yy hh:mm:ss)	Elapsed Time (hours)	Measured Pressure
189)	12/15/92 0:06:00	384.100	4330.400
190)	12/15/92 1:07:00	385.117	4330.750
191)	12/15/92 2:09:00	386.150	4331.018
192)	12/15/92 3:09:00	387.150	4331.370
193)	12/15/92 4:11:00	388.183	4331.570
194)	12/15/92 5:10:00	389.167	4331.940
195)	12/15/92 6:11:00	390.183	4332.290
196)	12/15/92 7:14:00	391.233	4332.460
197)	12/15/92 8:17:00	392.283	4332.560
198)	12/15/92 9:19:50	393.331	4332.440
199)	12/15/92 9:42:20	393.706	4331.450
200)	12/15/92 9:49:50	393.831	4330.350
201)	12/15/92 9:54:50	393.914	4329.300
202)	12/15/92 9:59:40	393.994	4328.220
203)	12/15/92 10:04:18	394.089	4327.100
204)	12/15/92 10:08:30	394.142	4326.048
205)	12/15/92 10:12:40	394.211	4324.978
206)	12/15/92 18:16:20	394.272	4323.870
207)	12/15/92 10:20:40	394.344	4322.740
208)	12/15/92 10:24:40	394.411	4321.618
209)	12/15/92 10:28:20	394.472	4320.530
210)	12/15/92 10:32:28	394.539	4319.450
211)	12/15/92 10:36:00	394.600	4318.330
212)	12/15/92 10:40:00	394.667	4317.250
213)	12/15/92 18:43:58	394.731	4316.198
214)	12/15/92 10:47:40	394.794	4315.100
215)	12/15/92 10:51:40	394.861	4314.820
216)	12/15/92 18:55:40	394.928	4312.978
217)	12/15/92 10:59:50	394.997	4311.920
218)	12/15/92 11:03:50	395.064	4310.828
219)	12/15/92 11:08:20	395.139	4309.750
220)	12/15/92 11:12:50	395.214	4308.690
221)	12/15/92 11:17:30	395.292	4307.598
222)	12/15/92 11:22:40	395.378	4306.498
223)	12/15/92 11:27:30	395.458	4305.440
224)	12/15/92 11:32:40	395.544	4304.310
225)	12/15/92 11:37:30	395.625	4303.260
226)	12/15/92 11:43:00	395.717	4302.218
227)	12/15/92 11:49:00	395.817	4301.080
228)	12/15/92 11:55:00	395.917	4300.820
229)	12/16/92 12:01:00	396.017	4298.960
230)	12/15/92 12:07:30	396.125	4297.870
231)	12/15/92 12:14:00	396.233	4296.818
232)	12/16/92 12:21:30	396.358	4295.678
233)	12/15/92 12:29:00	396.483	4294.580
234)	12/15/92 12:37:00	396.617	4293.500
235)	12/15/92 12:45:30	396.758	4292.390

Pressure Data - Well 4			
Point Number	Real Time of Day (mm/dd/yy hh:mm:ss)	Elapsed Time (hours)	Measured Pressure
236)	12/15/92 12:54:30	396.908	4291.320
237)	12/15/92 13:04:30	397.075	4290.240
238)	12/15/92 13:16:38	397.275	4289.150
239)	12/15/92 13:30:30	397.508	4288.090
240)	12/15/92 13:46:30	397.775	4287.060
241)	12/15/92 14:04:00	398.067	4285.970
242)	12/15/92 14:23:30	398.392	4284.920
243)	12/15/92 14:42:00	398.700	4283.918
244)	12/15/92 15:81:90	399.817	4282.880
245)	12/15/92 15:18:00	399.300	4281.830
246)	12/15/92 15:34:00	399.567	4288.800
247)	12/15/92 15:50:00	399.833	4279.770
248)	12/15/92 16:06:00	400.100	4278.740
249)	12/15/92 16:23:00	400.383	4277.690
256)	12/15/92 16:44:00	400.733	4276.670
251)	12/15/92 17:06:00	401.100	4275.860
252)	12/15/92 17:30:00	401.500	4274.680
253)	12/15/92 17:57:00	401.950	4273.590
254)	12/15/92 18:28:00	402.407	4272.620
255)	12/15/92 19:01:00	403.817	4271.720
253)	12/15/92 19:38:00	403.833	4270.850
257)	12/15/92 29:16:00	404.287	4270.000
258)	12/15/92 21:00:00	405.000	4269.240
259)	12/15/92 21:47:00	405.783	4268.530
260)	12/15/92 22:38:00	406.600	4287.670
261)	12/15/92 23:28:00	407.467	4287.260
262)	12/16/92 0:23:00	408.383	4266.700
263)	12/16/92 1:28:00	409.333	4266.220
264)	12/16/92 2:20:00	418.333	4285.360
265)	12/16/92 3:19:00	411.317	4265.470
266)	12/16/92 4:28:00	412.333	4265.110
267)	12/16/92 5:22:00	413.387	4264.830
268)	12/16/92 6:23:00	414.383	4264.490
269)	12/16/92 7:26:06	415.433	4264.320
270)	12/16/92 8:26:06	416.433	4263.990

State .... Mississippi	**Du Pont DeLisle Plant**	**Test Date** 5-Dec-92
County .... Harrison	***Well 2***	**Analysis Date** 1-Jun-93
Field .... DeLisle Plant		**Report Number** 930201

Rate History

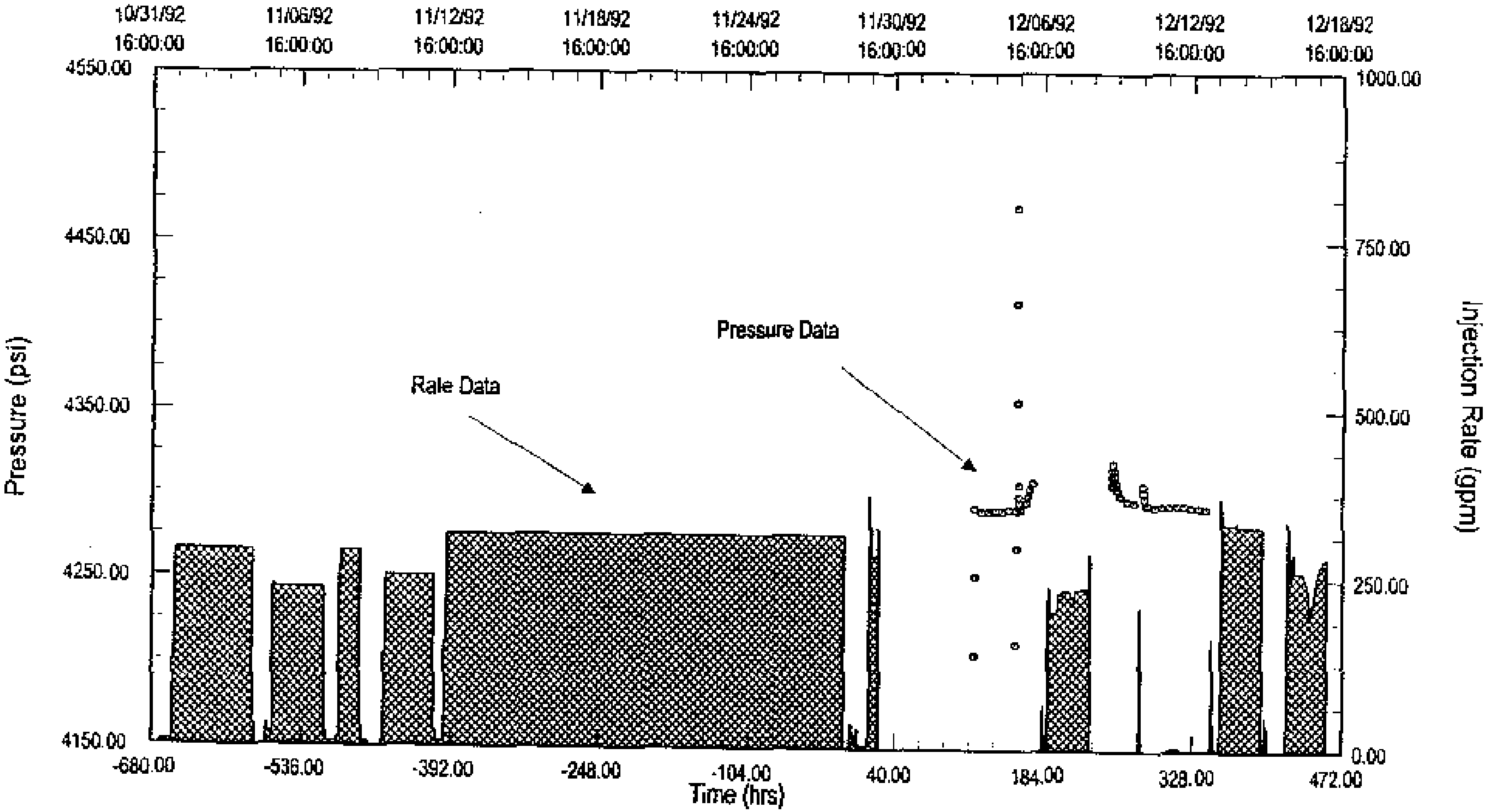

Rato History - Well 2				
Point Number	Real Time of Day (mm/dd/yy hh:mm:ss)	Elapsed Time (hours)	Injection Rate (GPM)	Injection Rate (BBLD)
1)	11/1/92 0:00:00	-672.000	6.632	227.383
2)	11/1/92 11:00:00	-661.000	6.632	227.383
3)	11/1/92 11:00:00	-661.000	123.221	4224.720
4)	11/1/92 13:00:00	-659.000	289.642	9930.583
5)	11/4/92 15:45:00	-584.250	31.723	1087.646
6)	11/4/92 17:46:00	-592.233	0.000	9.900
7)	11/5/92 4:46:00	-571.233	30.794	1055.794
8)	11/5/92 6:46:00	-569.233	16.336	626.963
9)	11/5/92 9:00:00	-567.000	13.599	466.251
10)	11/5/92 11:00:00	-565.000	236.086	8094.377
11)	11/5/92 13:00:00	-563.000	232.110	7958.057
12)	11/7/92 14:15:00	-513.750	19.954	653.280
13)	11/7/92 16:15:00	-511.750	5.713	195.874
14)	11/8/92 2:31:00	-501.483	11.785	404.057
15)	11/8/92 4:46:00	-499.233	264.086	9054.377
16)	11/8/92 6:48:00	-497.233	267.919	9671.200
17)	11/9/92 1:00:00	-479.000	28.745	985.543
18)	11/9/92 3:00:00	-477.000	6.953	228.103
19)	11/9/92 9:00:00	-471.000	9.173	5.931
20)	11/9/92 11:00:00	-469.000	9.000	0.000
21)	11/9/92 21:45:00	-458.250	8.219	281,794
22)	11/9/92 23:45:00	-458.250	136.771	4689.291
23)	11/10/92 1:45:00	-454.250	250.191	6577.634
24)	11/11/92 23:14:00	-408.767	22.191	760.491
25)	11/12/92 1:15:00	-406.750	7.621	249.720
26)	11/12/92 7:14:00	-400.767	8.678	235.817
27)	11/12/92 9:14:00	-398.767	153.559	5264.889
28)	11/12/92 11:15:00	-396.750	312.538	19715.588
29)	11/28/92 13:15:00	-19.758	0.000	0.000
30)	11/28/92 19:45:00	-4.250	35.140	1204.600
31)	11/28/92 21:45:00	-2.250	21.696	750.720
32)	11/28/92 23:45:00	-0.250	12.587	439.869
33)	11/29/92 1:45:00	1.750	29.835	1022.914
34)	11/29/92 3:45:00	3.758	4.750	162.057
35)	11/29/92 14:00:00	14.000	20.887	719.126
36)	11/29/92 14:31:00	14.517	88.151	3922.320
37)	11/28/92 14:45:00	14.750	253.385	9687.488
38)	11/29/92 15:00:00	15.000	362.370	12424.114
39)	11/29/92 15:15:00	15.250	373.307	12799.097
40)	11/29/92 15:31:00	15.517	343.535	11778.343
41)	11/29/92 16:00:00	16.000	327.391	11224.934
42)	11/29/92 16:31:00	16.517	282.843	9697.474
43)	11/29/92 22:45:00	22.750	324.381	11121.635
44)	11/29/92 23:45.00	23.750	9.000	9.000
45)	12/6/92 13:35:00	181.583	2.992	102.563
46)	12/6/92 13:40.00	181.667	9.976	397.749
47)	12/6/92 13:45:00	161.750	29.198	692.503

Rate History - Well 2				
Point Number	Real Time of Day (mm/dd/yy hh:mm:ss)	Elapsed Time (hours)	Injection Rate (GPM)	Injection Rate (BBLD)
48)	12/6/92 13:55:00	181.917	37.483	1282.369
49)	12/6/92 14:10:00	182.167	50.864	1743.909
50)	12/6/92 14:15:00	182.250	58.344	2000.366
51)	12/6/92 14:20:00	182.333	65.825	2256.857
52)	12/6/92 14:25:00	182.417	24.123	827.074
53)	12/6/92 15:41:00	183.683	5.339	183.051
54)	12/6/92 15:55:00	183.917	15.678	537.531
55)	12/6/92 16:20:00	186.333	5.469	187.589
56)	12/6/92 16:25:00	186.417	18.640	639.886
57)	12/6/92 16:36:00	186.600	27.533	943.989
58)	12/6/92 18:46:00	186.767	4.297	147.328
59)	12/6/92 18:51:00	186.850	71.875	2464.286
60)	12/6/92 18:55:00	186.917	168.285	5769.772
61)	12/6/92 19:00:00	187.000	114.341	3920.263
62)	12/6/92 19:04:00	187.067	131.771	4517.863
63)	12/6/92 19:09:00	187.150	153.908	5276.777
64)	12/6/92 18:14:00	187.233	126.432	4334.811
65)	12/6/92 19:19:00	187.317	158.203	5424.103
66)	12/6/92 19:24:00	187.400	211.189	7240.080
67)	12/6/92 19:30:00	187.500	223.032	7646.811
68)	12/6/92 19:35:00	187.583	239.171	8200.149
69)	12/6/92 20:04:00	188.007	229.453	7866.960
70)	12/6/92 20:24:00	188.400	222.547	7630.163
71)	12/6/92 20:45:00	188.750	217.132	7444.526
72)	12/6/92 20:54:00	188.900	195.321	6696.720
73)	12/6/92 21:08:00	189.150	201.856	6920.777
74)	12/7/92 2:36:00	194.600	205.158	7033.969
75)	12/7/92 4:55:00	196.617	212.305	7279.826
76)	12/7/92 5:18:00	197.167	229.266	7860.549
77)	12/7/92 6:45:00	200.750	233.810	8016.343
78)	12/7/92 17:15:00	209.250	225.352	7720.354
79)	12/7/92 20:09:00	212.150	219.778	7535.177
80)	12/7/92 21:09:00	213.150	234.582	8042.811
81)	12/8/92 3:25:00	219.417	238.634	8181.737
82)	12/8/92 11:00:00	227.000	227.661	7785.634
83)	12/8/92 11:19:00	227.317	233.044	7990.080
84)	12/8/92 11:30:00	227.500	241.537	8281.269
85)	12/8/92 11:35:00	227.583	282.161	9674.092
86)	12/8/92 11:40:00	227.667	289.134	9913.188
87)	12/8/92 12:10:00	228.167	282.298	9678.789
88)	12/8/92 12:40:00	228.667	0.000	0.000
89)	12/10/92 12:30:00	276.500	218.000	7200.000
90)	12/10/92 13:05:00	277.083	0.000	0.000
91)	12/11/92 17:20:00	305.333	0.344	11.794
92)	12/11/92 17:25:00	305.417	0.688	23.589
93)	12/11/92 17:31:00	305.517	1.333	45.703
94)	12/11/92 17:41:00	305.683	2.323	79.646

Rate History - Well 2				
Point Number	Real Time of Day (mm/dd/yy hh:mm:ss)	Elapsed Time (hours)	Injection Rate (GPM)	Injection Rate (BBLs)
95)	12/11/92 17:55:00	365.917	4.457	152.811
96)	12/12/92 2:45:00	314.750	6.679	23.280
97)	12/12/92 2:50:00	314.833	6.000	0.000
98)	12/13/92 6:35:00	344.583	6.469	16.080
99)	12/13/92 6:40:00	344.667	2.613	96.446
100)	12/13/92 6:45:00	344.756	6.901	238.606
101)	12/13/92 6:50:00	344.833	36.133	1238.846
102)	12/13/92 9:30:00	345.500	57.422	1968.754
103)	12/13/92 9:35:00	345.583	47.563	1630.731
184)	12/13/92 9:46:00	345.667	165.755	5683.629
105)	12/13/92 9:45:00	345.750	37.283	1275.531
106)	12/13/92 10:16:00	346.167	39.666	1359.977
107)	12/13/92 11:24:00	347.400	16.217	556.011
108)	12/13/92 11:35:00	347.583	5.807	199.097
109)	12/13/92 12:24:00	348.400	1.458	49.989
118)	12/13/92 12:38:00	348.500	8.000	8.000
111)	12/13/92 17:36:00	353.600	6.664	228.486
112)	12/13/92 17:41:00	353.683	19.991	685.406
113)	12/13/92 17:46:00	353.767	45.912	1574.126
114)	12/13/92 17:55:00	353.917	66.636	2284.663
115)	12/13/92 18:01:00	354.017	83.295	2855.829
116)	12/13/92 18:05:00	354.083	99.954	3426.994
117)	12/13/92 18:10:00	354.167	103.776	3558.034
118)	12/13/92 18:15:00	354.250	124.088	4254.446
119)	12/13/92 18:20:00	354.333	154.297	5290.183
120)	12/13/92 18:25:00	354.417	185.905	6373.886
121)	12/13/92 18:31:00	354.517	217.576	7459.417
122)	12/13/92 18:36:00	354.600	245.247	8408.468
123)	12/13/92 18:41:00	354.683	216.677	7223.211
124)	12/13/92 18:46:00	354.767	348.280	11941.029
125)	12/13/92 18:55:00	354.917	371.216	12727.47d
128)	12/13/92 19:14:00	355.233	359.558	12327.428
127)	12/13/92 19:40:00	355.667	347.715	11921.657
128)	12/13/92 20:09:00	356.150	333.707	11441.383
129)	12/13/92 22:35:00	358.583	331.752	11374.355
130)	12/14/92 10:14:00	370.233	337.344	11566.080
131)	12/14/92 10:35:00	378.583	329.092	11283.155
132)	12/15/92 9:14:00	393.233	252.018	8640.617
133)	12/15/92 9:24:00	393.400	39.453	1352.674
134)	12/15/92 9:30:00	393.500	0.000	6.000
135)	12/15/92 12:35:00	396.583	2.296	78.729
138)	12/15/92 12:40:00	396.667	13.778	472.389
137)	12/15/92 12:45:00	396.750	25.260	866.057
138)	12/15/92 12:50:00	396.833	51.042	1750.811
139)	12/15/92 12:55:00	396.917	38.687	1328.411
140)	12/15/92 14:45:00	398.750	16.538	361.629
141)	12/15/92 15:05:00	399.083	3.535	121.200

Rate History - Well 2				
Point Number	Real Time of Day (mm/dd/yy hh:mm:ss)	Elapsed Time (hours)	Injection Rate (GPM)	Injection Rate (BeLO)
142)	12/15/92 15:15:00	399.250	0.471	16.149
143)	12/15/92 15:20:00	399.333	0.000	0.000
144)	12/16/92 8:35:00	416.583	0.603	20.674
145)	12/16/92 8:40:00	416.667	3.618	124.046
146)	12/16/92 8:45:00	416.750	7.707	264.248
147)	12/16/92 8:54:00	416.900	14.514	497.623
148)	12/16/92 9:09:00	417.150	23.387	789.097
149)	12/16/92 9:19:00	417.317	44.792	1535.726
150)	12/16/92 9:24:00	417.400	125.651	4308.034
151)	12/16/92 9:30:00	417.500	120.052	4116.069
152)	12/16/92 9:35:00	417.583	131.445	4506.686
153)	12/16/92 9:40:00	417.667	121.328	4159.817
154)	12/16/92 9:45:00	417.750	105.587	3620.126
155)	12/16/92 9:55:00	417.917	135.990	4662.514
156)	12/16/92 10:00:00	418.000	202.734	6950.888
157)	12/16/92 10:05:00	418.083	275.391	9441.977
158)	12/16/92 10:10:00	418.167	335.338	11497.303
159)	12/16/92 10:35:00	418.583	315.187	10803.668
160)	12/16/92 10:45:00	418.750	303.071	10391.006
161)	12/16/92 10:55:00	418.917	291.927	10008.926
162)	12/16/92 11:05:00	419.083	285.417	9785.725
163)	12/16/92 11:10:00	419.167	290.571	9962.435
164)	12/16/92 11:35:00	419.583	280.013	9600.446
165)	12/16/92 11:55:00	419.917	269.984	9256.595
166)	12/16/92 12:15:00	420.250	261.306	8959.063
167)	12/16/92 12:50:00	420.833	252.558	8659.131
168)	12/16/92 13:40:00	421.667	265.929	9117.565
169)	12/16/92 13:50:00	421.833	283.893	9733.474
170)	12/16/92 14:50:00	422.833	289.396	9922.148
171)	12/16/92 15:50:00	423.833	278.635	9553.200
172)	12/16/92 16:10:00	424.167	268.898	9219.360
173)	12/16/92 16:31:00	424.517	260.974	8947.680
174)	12/17/92 1:20:00	433.333	253.288	8684.160
175)	12/17/92 3:25:00	435.417	246.403	8448.103
176)	12/17/92 5:05:00	437.083	237.275	8135.143
177)	12/17/92 6:05:00	438.083	229.993	7885.474
178)	12/17/92 6:41:00	438.683	222.457	7627.097
179)	12/17/92 7:04:00	439.067	214.747	7362.754
180)	12/17/92 7:24:00	439.400	206.458	7078.560
181)	12/17/92 7:35:00	439.583	199.005	6823.029
182)	12/17/92 7:45:00	439.750	197.083	6757.131
183)	12/17/92 8:40:00	440.667	203.969	6993.223
184)	12/17/92 9:30:00	441.500	209.711	7190.091
185)	12/17/92 10:14:00	442.233	216.318	7416.617
186)	12/17/92 11:05:00	443.083	224.466	7695.977
187)	12/17/92 11:55:00	443.917	232.296	7964.434
188)	12/17/92 12:35:00	444.583	239.587	8214.412

Rate History - Well 2				
Point Number	Real Time of Day (mm/dd/yy hh:mm:ss)	Elapsed Time (hours)	Injection Rate (GPM)	Injection Rate (BBLD)
189)	12/17/92 13:31:00	445.517	247.024	8469.394
190)	12/17/92 14:05:00	446.083	254.869	8738.366
191)	12/17/92 15:00:00	447.000	263.419	9031.509
192)	12/17/92 16:31:00	448.517	271.491	9308.263
193)	12/17/92 19:45:00	451.750	279.725	9590.572
194)	12/17/92 23:30:00	455.500	283.264	9711.909
195)	12/17/92 23:55:00	455.917	282.943	9700.903

State .... Mississippi	**Du Pont DeLisle Plant**	**Test Date** 5-Dec-92
County .... Harrison	***Well 3***	**Analysis Date** 1-Jun-93
Field .... DeLisle Plant		**Report Number** 930201

Rate History

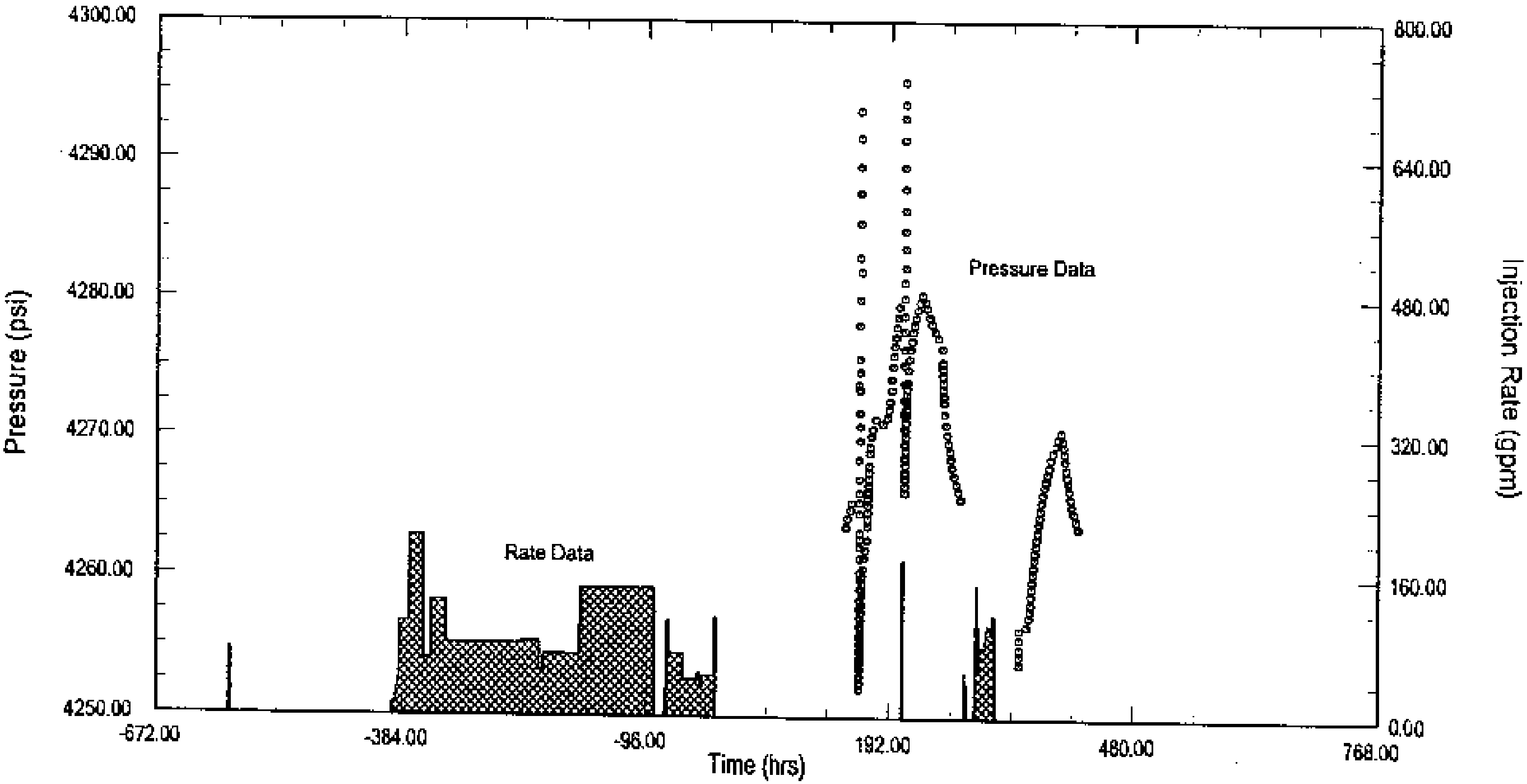

Rato History - Well 3				
Point Number	Real Time of Day (mm/dd/yy hh:mm:ss)	Elapsed Time (hours)	Injection Rate (GPM)	Injection Rate (BBLD)
1)	11/1/92 0:00:00	-672.000	0.808	9.806
2)	11/4/92 14:15:00	-585.750	0.000	9.808
3)	11/4/92 14:15:00	-585.750	75.754	2597.280
4)	11/4/92 18:15:00	-583.750	0.000	0.808
5)	11/12/92 11:30:00	-396.500	15.157	519.889
6)	11/12/92 13:31:00	-394.483	14.280	489.600
7)	11/12/92 15:31:00	-392.483	31.056	1064.777
8)	11/12/92 17:31:00	-390.483	42.309	1450.594
9)	11/12/92 19:45:00	-388.250	107.912	3668.983
10)	11/13/92 7:45:00	-376.250	205.866	7058.263
11)	11/14/92 0:15:00	-359.750	64.467	2210.297
12)	11/14/92 9:45:00	-350.250	132.061	4527.808
13)	11/15/92 3:15:00	-332.750	85.503	2931.531
14)	11/15/92 5:15:00	-330.750	82.162	2816.993
15)	11/18/92 21:14:00	-242.767	84.794	2907.223
16)	11/19/92 19:14:00	-220.767	51.907	1779.669
17)	11/19/92 23:45:00	-216.250	70.425	2414.572
19)	11/21/92 19:00:00	-173.000	146.074	5008.252
19)	11/25/92 9:45:00	-86.250	9.269	9.189
20)	11/25/92 15:45:00	-80.250	9.027	9.926
21)	11/25/92 17:46:00	-78.233	0.000	0.000
22)	11/25/92 20:30:00	-75.500	4.919	168.343
23)	11/25/92 22:30:00	-73.500	32.687	1120.697
24)	11/26/92 0:31:00	-71.483	100.889	3767.623
25)	11/26/92 2:31:00	-69.483	72.281	2479.206
26)	11/26/92 20:14:00	-51.767	42.965	1473.088
27)	11/27/92 13:00:00	-35.000	50.021	1715.006
28)	11/27/92 16:00:00	-32.000	33.975	1184.857
29)	11/27/92 18:01:00	-29.983	47.303	1621.817
30)	11/28/92 8:45:00	-15.250	113.588	3894.446
31)	11/28/92 10:45:00	-13.250	0.000	0.808
32)	12/7/92 15:00:00	207.150	180.000	6171.429
33)	12/7/92 16:00:00	209.000	9.000	9.806
34)	12/10/92 15:36:00	279.600	8.073	276.789
35)	12/10/92 15:41:00	279.693	28.906	991.063
36)	12/10/92 15:45:00	279.750	53.516	1834.834
37)	12/10/92 15:50:00	279.833	15.820	542.400
38)	12/10/92 15:55:00	279.917	40.881	1491.634
39)	12/10/92 18:20:00	282.333	10.933	374.846
40)	12/10/92 18:46:00	282.767	4.557	156.246
41)	12/10/92 19:00:00	283.000	1.491	51.129
42)	12/10/92 19:09:00	283.150	0.569	19.509
43)	12/10/92 19:19:00	283.317	0.228	7.817
44)	12/10/92 19:24:00	283.400	0.033	1.131
45)	12/10/92 19:30:00	283.500	0.000	0.000
46)	12/11/92 3:36:00	291.600	0.245	8.400
47)	12/11/92 3:41:00	291.683	1.130	38.743

Point Number	Real Time of Day (mm/dd/yy hh:mm:ss)	Elapsed Time (hours)	Injection Rate (GPM)	Injection Rate (BBLS)
Rate History - Well 3				
48)	12/11/92 3:58:00	291.833	2.267	77.728
49)	12/11/92 4:00:00	292.000	4.013	137.589
50)	12/11/92 4:20:00	292.333	5.239	179.623
51)	12/11/92 4:36:00	292.600	65.104	2232.137
52)	12/11/92 4:41:00	292.683	91.927	3151.783
53)	12/11/92 4:46:00	292.767	57.552	1973.211
54)	12/11/92 4:50:00	292.833	75.912	2602.697
55)	12/11/92 4:55:00	292.917	64.180	2200.457
56)	12/11/92 5:25:00	293.417	81.771	2803.577
57)	12/11/92 5:31:00	293.517	90.817	3086.297
58)	12/11/92 5:36:00	293.600	98.542	3378.583
59)	12/11/92 5:41:00	293.683	115.104	3946.423
60)	12/11/92 5:46:00	293.767	123.413	4231.393
61)	12/11/92 5:51:00	293.850	134.440	4609.372
62)	12/11/92 5:56:00	293.917	143.262	4911.840
63)	12/11/92 6:01:00	294.017	153.177	5251.783
64)	12/11/92 6:15:00	294.250	142.424	4883.108
65)	12/11/92 6:20:00	294.333	129.584	4442.880
66)	12/11/92 6:31:00	294.517	122.396	4196.434
67)	12/11/92 6:41:00	294.683	118.438	4060.732
68)	12/11/92 6:51:00	294.850	114.595	3928.971
69)	12/11/92 7:00:00	295.000	110.614	3792.480
70)	12/11/92 7:09:00	295.150	106.771	3660.720
71)	12/11/92 7:19:00	295.317	103.854	3560.708
72)	12/11/92 7:24:00	295.400	105.898	3630.789
73)	12/11/92 7:45:00	295.750	104.167	3571.440
74)	12/11/92 7:50:00	295.833	107.262	3677.554
75)	12/11/92 8:09:00	296.150	102.913	3528.446
76)	12/11/92 8:45:00	296.750	100.929	3458.994
77)	12/11/92 8:50:00	296.833	52.865	1812.514
78)	12/11/92 8:54:00	296.900	83.463	2861.589
79)	12/11/92 9:00:00	297.000	80.587	2762.983
80)	12/11/92 17:20:00	305.333	101.595	3483.257
81)	12/11/92 18:41:00	306.683	105.685	3623.489
82)	12/11/92 19:19:00	307.317	107.490	3685.371
83)	12/11/92 19:49:00	307.817	104.966	3598.834
84)	12/11/92 20:14:00	308.233	105.658	3622.560
85)	12/11/92 21:14:00	309.233	104.533	3583.988
86)	12/11/92 23:18:00	311.167	105.926	3631.749
87)	12/11/92 23:40:00	311.667	102.644	3519.223
88)	12/12/92 0:15:00	312.250	98.262	3368.983
89)	12/12/92 1:10:00	313.167	95.508	3274.560
90)	12/12/92 1:15:00	313.250	102.606	3517.851
91)	12/12/92 1:20:00	313.333	118.525	4063.714
92)	12/12/92 1:31:00	313.517	102.204	3504.137
93)	12/12/92 1:45:00	313.750	96.994	3296.651
94)	12/12/92 1:50:00	313.833	112.370	3852.668

Rate History - Well 3				
Point Number	Real Time of Day (mm/dd/yy hh:mm:ss)	Elapsed Time (hours)	Injection Rate (GPM)	Injection Rate (BBLD)
95)	12/12/92 1:55:06	313.917	106.380	3647.314
96)	12/12/92 2:06:06	314.000	115.972	3945.326
97)	12/12/92 2:95:06	314.083	94.922	3254.468
98)	12/12/92 2:10:06	314.167	192.422	3511.611
99)	12/12/92 2:20:06	314.333	106.120	3639.400
100)	12/12/92 2:25:06	314.417	101.498	3479.931
101)	12/12/92 2:40:00	314.667	105.383	3612.446
102)	12/12/92 3:06:00	315.000	187.681	3691.920
103)	12/12/92 3:31:06	315.517	112.628	3861.531
104)	12/12/92 3:41:06	315.683	116.893	4067.760
105)	12/12/92 3:55:06	315.917	103.972	3564.754
106)	12/12/92 4:05:06	316.093	111.382	3818.812
107)	12/12/92 4:25:00	316.417	69.792	2392.969
108)	12/12/92 4:31:00	316.517	8.980	2.743
109)	12/12/92 4:41:06	316.683	0.029	8.994
110)	12/12/92 4:46:00	318.767	0.000	8.000
111)	12/12/92 4:55:06	316.917	14.218	467.400
112)	12/12/92 5:29:06	317.333	8.000	0.000
113)	12/17/92 23:55:06	455.917	0.000	0.000

State .... Mississippi
County .... Harrison
Field .... DeLisle Plant

Du Pont DeLisle Plant

Well 4

Test Date 5-Dec-92
Analysis Date 1-Jun-93
Report Number 930201

Rate History

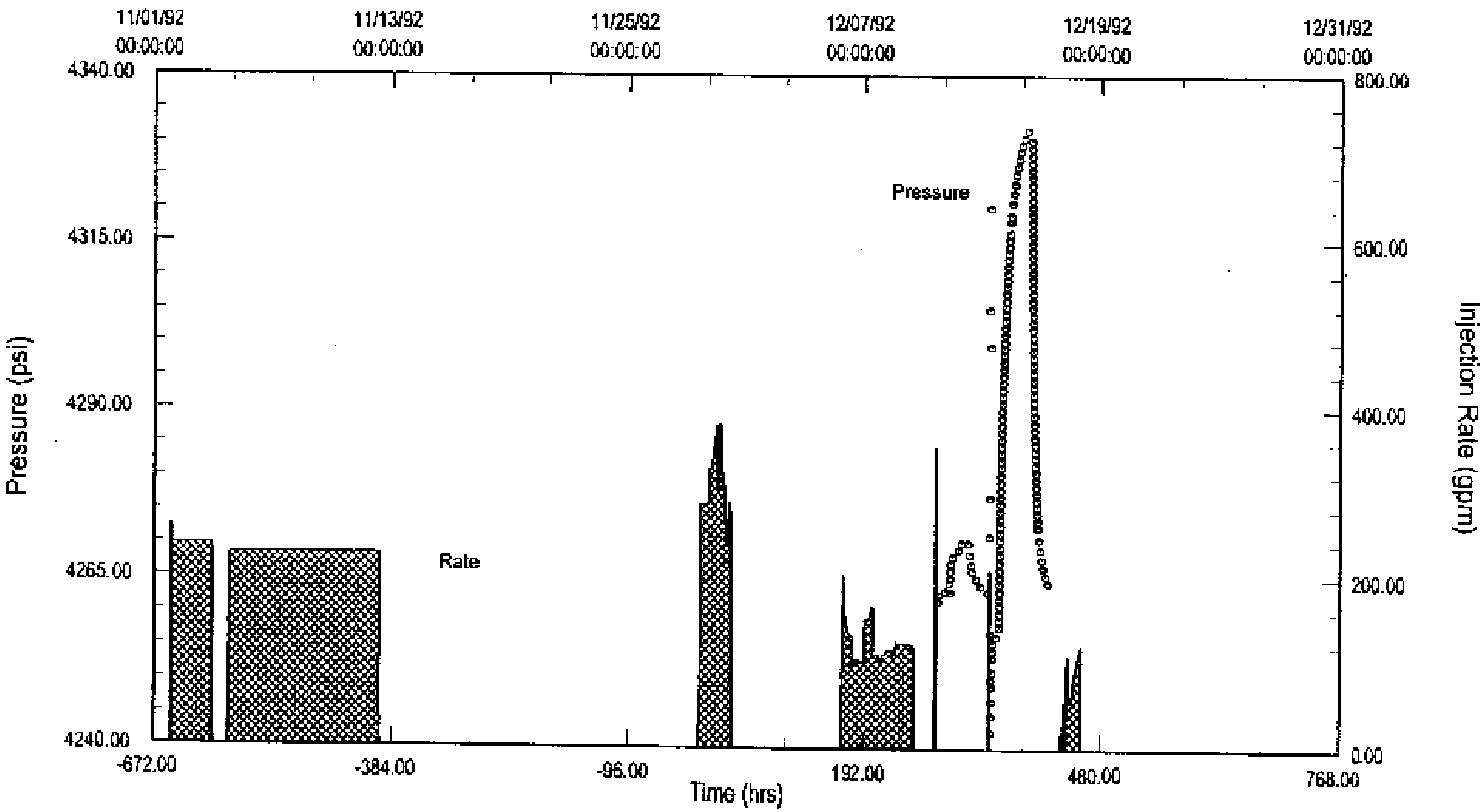

Rate History - Well 4				
Point Number	Real Time of Day (mm/dd/yy hh:mm:ss)	Elapsed Time (hours)	Injection Rate (GPM)	Injection Rate (BBLD)
1)	11/1/92 0:00:00	-672.000	0.000	0.000
2)	11/1/92 18:48:01	-653.233	8.246	8.434
3)	11/1/92 19:45:06	-652.250	0.115	3.943
4)	11/1/92 20:45:06	-651.250	268.042	8915.725
5)	11/1/92 21:45:00	-650.250	236.833	8119.988
6)	11/3/92 22:30:00	-601.500	43.341	1485.977
7)	11/3/92 23:30:00	-606.506	8.581	294.206
8)	11/4/92 0:31:81	-599.463	2.075	71.143
9)	11/4/92 1:31:01	-598.483	0.459	15.737
10)	11/4/92 5:46:01	-594.233	0.000	0.000
11)	11/4/92 17:15:06	-582.750	13.410	460.046
12)	11/4/92 18:15:06	-581.750	33.475	1147.714
13)	11/4/92 19:13:59	-580.767	186.661	6399.806
14)	11/4/92 20:13:58	-579.767	227.459	7798.594
15)	11/12/92 0:30:00	-399.500	38.658	1325.417
10)	11/12/92 9:30:06	-398.500	6.337	217.268
17)	11/12/92 10:30:06	-397.500	0.435	14.914
18)	11/12/92 11:30:06	-396.500	0.000	8.000
19)	11/28/92 12:45:00	-11.250	26.250	900.000
20)	11/28/92 13:45:00	-10.250	68.222	2339.040
21)	11/28/92 14:45:00	-9.250	287.097	9843.325
22)	11/29/92 1:00:06	1.000	329.058	11281.980
23)	11/29/92 5:06:00	5.000	341.372	11704.183
24)	11/29/92 7:06:00	7.000	355.606	12192.205
25)	11/29/92 8:00:06	8.000	367.698	12606.789
26)	11/29/92 9:30:06	9.500	380.879	13031.280
27)	11/29/92 11:15:06	11.250	304.658	10441.989
28)	11/29/92 12:15:06	12.250	363.804	12473.280
29)	11/29/92 13:15:00	13.250	381.468	13070.902
30)	11/29/92 16:31:01	16.517	330.759	11340.309
31)	11/29/92 17:31:81	17.517	321.425	11020.285
32)	11/29/92 19:30:00	19.500	309.161	10599.806
33)	11/29/92 20:30:00	20.506	291.106	9900.777
34)	11/29/92 21:30:00	21.500	269.725	9247.714
35)	11/29/92 22:30:06	22.500	254.048	8709.943
36)	11/29/92 23:38:06	23.580	240.948	8261.074
37)	11/30/92 0:45:06	24.758	253.279	8683.852
38)	11/30/92 1:45:06	25.750	290.833	9943.980
39)	11/30/92 2:45:06	26.750	277.787	9524.125
40)	11/30/92 3:45:06	27.750	211.102	7237.783
41)	11/30/92 4:48:01	28.767	77.341	2651.692
42)	11/30/92 5:46:01	29.767	0.000	0.000
43)	12/5/92 21:00:06	165.000	8.130	4.457
44)	12/5/92 21:19:01	165.317	104.786	3592.663
45)	12/5/92 21:31:08	165.519	94.341	3234.549
46)	12/5/92 21:43:19	165.722	106.645	3656.406
47)	12/5/92 21:55:19	165.922	129.649	4445.109

Rate History - Well 4				
Point Number	Real Time of Day (mm/dd/yy hh:mm:ss)	Elapsed Time (hours)	Injection Rate (GPM)	Injection Rate (BBLD)
48)	12/5/92 22:07:28	166.124	168.412	5774.126
49)	12/5/92 22:19:59	166.333	204.996	7028.434
50)	12/5/92 22:31:59	166.533	191.082	6551.383
51)	12/5/92 22:44:10	166.736	181.748	6231.360
52)	12/5/92 22:56:17	166.938	175.924	6031.680
53)	12/5/92 23:12:00	167.200	170.298	5838.789
54)	12/5/92 23:32:17	167.538	164.794	5650.080
55)	12/6/92 0:04:59	168.083	158.943	5483.760
56)	12/6/92 0:40:01	168.667	154.640	5301.943
57)	12/6/92 1:31:01	169.517	149.576	5128.328
58)	12/6/92 2:31:01	170.517	145.161	4976.948
59)	12/6/92 3:25:01	171.417	140.575	4819.714
60)	12/6/92 4:40:59	172.683	135.933	4660.560
61)	12/6/92 6:36:00	174.600	132.691	4549.406
62)	12/6/92 9:49:59	177.833	112.910	3871.200
63)	12/6/92 10:13:59	178.233	96.131	3295.920
64)	12/6/92 10:34:59	178.583	103.577	3551.212
65)	12/6/92 11:30:00	179.500	103.541	3549.977
66)	12/6/92 15:25:01	183.417	106.281	3643.920
67)	12/6/92 15:40:59	183.683	103.095	3534.686
68)	12/6/92 18:15:00	186.250	104.703	3589.617
69)	12/6/92 18:55:01	186.917	101.292	3472.869
70)	12/6/92 20:54:00	186.900	102.033	3498.274
71)	12/7/92 0:10:01	192.167	96.948	3323.931
72)	12/7/92 0:24:00	192.400	131.151	4496.606
73)	12/7/92 0:40:01	192.667	151.250	5185.714
74)	12/7/92 4:25:01	196.417	153.693	5269.474
75)	12/7/92 5:40:59	197.683	150.738	5168.160
76)	12/7/92 5:55:01	197.917	151.728	5202.103
77)	12/7/92 6:31:01	198.517	155.260	5357.486
78)	12/7/92 7:19:01	199.317	161.362	5532.411
79)	12/7/92 8:30:00	200.500	165.713	5681.560
80)	12/7/92 10:45:00	202.750	127.461	4370.091
81)	12/7/92 11:00:00	203.000	106.362	3646.697
82)	12/7/92 11:19:01	203.317	106.267	3643.440
83)	12/7/92 11:34:59	203.583	109.852	3766.354
84)	12/7/92 17:49:59	209.833	106.649	3656.537
85)	12/7/92 19:19:01	211.317	101.999	3497.109
86)	12/7/92 20:13:59	212.233	99.495	3411.257
87)	12/7/92 21:09:00	213.150	106.511	3651.806
88)	12/7/92 21:24:00	213.400	109.649	3766.251
89)	12/8/92 1:00:00	217.000	111.177	3811.783
90)	12/8/92 1:49:59	217.833	115.407	3956.611
91)	12/8/92 9:49:59	225.833	105.553	3618.966
92)	12/8/92 10:04:59	226.083	113.840	3903.086
93)	12/8/92 11:04 59	227.083	116.746	4002.789
94)	12/8/92 12:10:01	228.167	119.818	4108.046

Rate History - Well 4				
Point Number	Real Time of Day (mm/dd/yy hh:mm:ss)	Elapsed Time (hours)	Injection Rate (GPM)	Injection Rate (BBLD)
95)	12/8/92 12:45:00	228.750	110.323	3782.503
96)	12/6/92 13:00:00	229.000	116.444	3992.386
97)	12/8/92 13:19:59	229.333	120.552	4133.211
98)	12/8/92 13:49:59	229.833	124.339	4263.051
99)	12/8/92 14:19:59	230.333	127.139	4359.851
100)	12/8/92 14:49:59	230.833	117.842	4040.297
101)	12/8/92 15:04:59	231.083	119.504	4097.288
182)	12/8/92 15:49:59	231.833	117.095	4014.686
100)	12/8/92 16:38:00	232.800	123.828	4216.103
104)	12/9/92 7:54:00	247.900	115.728	3967.817
105)	12/9/92 9:34:59	249.583	122.365	4195.371
106)	12/9/92 9:49:59	249.833	117.521	4029.292
107)	12/9/92 18:19:01	250.317	122.924	4214.537
108)	12/9/92 18:40:01	250.867	118.862	4075.269
109)	12/9/92 11:04:59	251.083	116.782	4003.269
118)	12/9/92 11:24:00	251.400	118.169	4052.194
111)	12/9/92 11:45:00	251.750	15.166	519.977
112)	12/9/92 12:00:00	252.000	0.000	8.000
113)	12/10/92 12:34:59	276.583	12.662	434.128
114)	12/10/92 12:49:59	276.833	51.299	1758.823
115)	12/10/92 13:18:01	277.167	119.195	4086.686
116)	12/16/92 13:24:00	277.400	184.701	6332.686
117)	12/10/92 13:40:81	277.667	305.167	10462.968
118)	12/10/92 13:55:01	277.917	356.579	12226.566
119)	12/10/92 14:36:09	278.600	66.747	2288.469
120)	12/16/92 14:49:59	278.833	8.000	9.000
121)	12/13/92 6:55:01	342.917	219.000	7200.000
122)	12/13/92 7:40:81	343.667	0.000	8.000
123)	12/16/92 21:49:59	429.833	8.939	32.194
124)	12/16/92 22:04:59	430.083	2.379	61.568
125)	12/16/92 22:19:81	438.317	3.754	128.709
126)	12/16/92 22:34:59	430.583	7.818	240.617
127)	12/16/92 23:00:00	431.000	19.231	659.349
128)	12/17/92 0:49:59	432.833	12.281	421.063
129)	12/17/92 1:18:01	433.167	33.106	1135.063
130)	12/17/92 1:25:01	433.417	18.478	633.463
131)	12/17/92 1:40.01	433.667	1.593	54.617
132)	12/17/92 1:55:01	433.917	34.669	1188.309
133)	12/17/92 2:10:01	434.167	53.294	1827.223
134)	12/17/92 2:25:81	434.417	56.246	1928.434
135)	12/17/92 2:40:91	434.667	16.748	574.217
136)	12/17/92 3:18:01	435.167	6.579	225.568
137)	12/17/92 3:55:01	435.917	2.343	80.331
138)	12/17/92 4:10:81	436.167	13.643	467.766
139)	12/17/92 5.00:86	437.000	11.718	401.691
140)	12/17/92 5:15:00	437.250	37.042	1270.811
141)	12/17/92 5:31:81	437.517	50.496	1731 291

Rate History - Well 4				
Point Number	Real Time of Day (mm/dd/yy hh:mm:ss)	Elapsed Time (hours)	Injection Rate (GPM)	Injection Rate (BBLD)
142)	12/17/92 6:10:01	438.167	99.502	3411.497
143)	12/17/92 6:25:01	438.417	93.717	3213.154
144)	12/17/92 6:40:59	438.683	109.339	3748.766
145)	12/17/92 6:55:59	438.933	94.952	3255.497
146)	12/17/92 7:09:00	439.150	86.841	2977.406
147)	12/17/92 7:24:00	439.400	81.040	2778.514
148)	12/17/92 7:40:01	439.667	75.881	2601.634
149)	12/17/92 7:54:00	439.900	70.575	2419.714
150)	12/17/92 8:09:00	440.150	65.858	2258.023
151)	12/17/92 8:24:00	440.400	63.247	2168.469
152)	12/17/92 8:40:01	440.667	60.607	2077.954
153)	12/17/92 9:00:00	441.000	58.309	1999.166
154)	12/17/92 9:19:01	441.317	56.813	1947.074
155)	12/17/92 11:04:59	443.083	59.483	2039.417
156)	12/17/92 11:49:59	443.833	61.335	2102.914
157)	12/17/92 12:15:00	444.250	63.247	2168.469
158)	12/17/92 12:40:01	444.667	65.361	2240.949
159)	12/17/92 13:10:01	445.167	67.501	2314.320
160)	12/17/92 13:34:59	445.583	70.102	2403.497
161)	12/17/92 14:00:00	446.000	81.361	2789.520
162)	12/17/92 14:15:00	446.250	81.718	2801.760
163)	12/17/92 15:00:00	447.000	85.378	2927.246
164)	12/17/92 15:25:01	447.417	88.072	3019.611
165)	12/17/92 15:55:01	447.917	91.140	3125.006
166)	12/17/92 16:25:01	448.417	94.179	3228.994
167)	12/17/92 17:00:00	449.000	97.335	3337.200
168)	12/17/92 17:36:00	449.600	100.452	3444.069
169)	12/17/92 18:15:00	450.250	103.254	3540.137
170)	12/17/92 19:04:01	451.067	106.808	3661.989
171)	12/17/92 20:04:01	452.067	110.402	3785.211
172)	12/17/92 20:54:00	452.900	113.766	3900.549
173)	12/17/92 21:55:01	453.917	117.239	4019.623
174)	12/17/92 23:04:59	455.083	120.630	4135.886
175)	12/17/92 23:55:01	455.917	122.191	4189.406

APPENDIX 3-2
SHALE POROSITY AND PERMEABILITY (PORTER AND NEWSOM, 1987)

SHALE POROSITY AND PERMEABILITY

W. M. Porter, S. W. Newsom 4/06/87

OVERVIEW

Hydrologic characteristics of shales are required for pressure modeling and determination of maximum upward permeation. Site-specific data on porosity and vertical permeability of shales are usually not available, and generalized data must be used. This paper presents guidelines for determining shale parameters so that modeling assumptions may have a uniform basis.

DATA LIMITATIONS

Porosity and permeability data for shales, at depths of concern in waste injection, are scarce and frequently unreliable. Sampling opportunities arise in the course of petroleum exploration, but attention has primarily been focused on sand reservoirs. When samples are obtained, they are usually sidewall core plugs whose porosity and permeability can be affected by rupturing or shearing associated with the sampling process. Hydrologic properties of whole cores may also be affected by drilling (Magara, 1978).

Several techniques are commonly used to determine porosity. The results are not always comparable. Oilfield service companies frequently use a vacuum porosimeter, which yields values that are less than true porosity, especially in lower porosity materials (Legate, 1974). Another technique involves measurement of bulk wet density and dry weight, accompanied by assumptions on the density of fluid and solid constituents. This method is sensitive to drying time and temperature, since some of the water removed is more closely bound to clay particles. Singer and Mueller (1974) maintain that a significant part of the total "immobilized" water content may be removed during sample drying at elevated temperatures. Also, the extent to which "bound" layers of water are involved in flow processes (the question of effective porosity) is apparently unresolved.

Shale permeability can be measured by steady-state techniques involving equilibrium flow conditions, or by transient pulse hydraulic and mechanical tests. Steady-state permeabilities have generally been determined without confining pressures typical of the sample depth. Application of confining pressure can decrease permeability by an order of magnitude or more (Young et al., 1964). Sample orientation can be very significant, due to the presence of fine laminae of coarser material, but is often not stated in reports; sidewall core data generally represent horizontal permeability.

Steady or quasi-steady state fluid permeability measurements of shales require long time periods, usually on the order of weeks. Large hydraulic gradients and thin samples can reduce the measurement times to some extent, but also increase the possibility of inaccuracies associated with sample rupture, bypassing flow, and small scale inhomogeneities.

Gas permeants are often used because of their low viscosity, but corrections for gas slippage are required (Scheidegger, 1974). Because of physicochemical interactions, the relationship between gas and liquid permeabilities in shale is uncertain (Neuzil, 1986).

Transient techniques can measure permeability at lower gradients, but have been infrequently used. They also suffer from some inacuracies associated with spatial and temporal variations in hydraulic properties (Neuzil, 1986). Transient tests and mechanical consolidation tests (an indirect measure of permeability) appear to agree fairly well with carefully conducted steady-state flow tests.

The above caveats suggest caution in the use of porosity and permeability values, whether obtained from literature or from site-specific data. Values that do not represent the actual behavior of the shale may produce anomalous modeling results. Modification of porosity and permeability inputs for shale (within reasonable limits) is justified by uncertainties associated with shale properties.

The range of shale porosity and permeability values, as cited in various references, is indicated by the data in Table 1. This table should not be used for estimating permeabitity, since methods are undocumented. Neuzil (1987, personal communication) has stated that most techniques yietd values which are upper limits of permeability.

POROSITY

Shale porosity depends primarily on compaction due to burial, but is also dependent on chemical and mineralogical phenomena (Magara, 1978). Compaction is generally regarded as irreversible (Mueller, 1967). In most Gulf Coast situations, erosion and uplift have been minimal and porosity should represent present burial depth.

Where fluid pressures are near hydrostatic and shales are at compaction equilibrium, porosity wilt vary with depth in a regular fashion. A number of authors (cited in Rieke and Chillingarian, 1974) have produced curves representing variations in shale porosity with burial depth. These curves are shown in Fig. 1. Differences between curves are probably related to several factors inherent to the data used:

- o Different porosity measurement techniques were employed (porosity logs, bulk density measurements, etc.).

- o Sediments differed in the amount of cementation, which limited the effectiveness of compaction.

- o Composition and texture of shales varied.

- o Shales had been subjected to different stress histories.

- o Increased fluid pressure due to thermal expansion or mineral transformations, generally at depths of 7000 ft. or more, may have affected compaction in some cases.

- o Compaction disequilibrium, caused by burial rates that exceed the shale's ability to release water, may have been a factor in some sediments.

Since many factors can affect porosity-depth relationships, it is clearly best to apply generalized data trends from the area of interest.

Curve 6 in Fig. 1 is from Dickinson's (1953) data for Tertiary shales from the Louisiana Gulf Coast, and agrees fairly well with curves 9 (Gulf Coast data) and 10 (Louisiana offshore). Magara (1978) commented that this curve showed an exponential relationship (normal compaction) above 7000 ft., with higher than normal porosities at greater depths reflecting overpressure. This curve is replotted in Fig. 2., along with other curves for sets of Gulf Coast data.

Dickinson's curve is probably the best representation of average porosity, considering the geographical area of our plants. Curve (b) in Fig 2 may be taken to represent the minimum average shale porosity in the area.

Clay porosity figures represent actual pore water plus a considerable amount of water bound to clay minerals (relatively immobile). For modeling, the effective porosity (involved in flow) is needed, but no estimates have been found in the literature.

One approach to estimating effective porosity is to determine the quantity of bound water from theoretical considerations.

Powers (1967) cited work showing that four monomolecular water layers remain on smectite at a burial depth of about 3000 ft. The net thickness of these layers is the same as that of the smectite unit layer, that is 10 Angstroms. One of the water layers is gradually lost by progressive burial to 20,000 ft., so the proportion of smectite to interlayer water should be approximately correct for depths of interest to us. The interlayer water is thought to represent most of the bound water, and has a density of 1.4 gm/cc. (Powers, 1967). This is sufficient information to calculate the volume of water immobilized by smectite. The volume of water held on other clay species may be estimated by considering their relative surface areas (about 80sq. m/gm for illite vs. 700 sq. m/gm for smectite).

To apply this method, core data from the Kaiser disposal well near Du Pont's Pontchartrain Plant was used. A core from 3067 ft. appears to be fairly typical of confining layers at our sites. Total water content (all water driven off at 1200 F) is approximately 28% of <u>bulk volume</u> (Davis Assoc., 1986) The petrographic analysis of this core was used to determine the percentage of bulk volume occupied by individual clay species. If smectite and smectite/illite interlayers are assumed to immobilize water to the same extent, and allowing for the greater density of interlayer water, 16% of the <u>bulk volume</u> is bound water. Effective porosity is thus reduced to 28%-16%, or 12%.

The result will vary with sample mineralogy, but this is probably a typical case. If the ratio of bound to unbound water is assumed to be constant (pore and interlayer water lost at a proportional rate), the effective porosity curve will follow the normal compaction slope. Curve (c) in Fig. 2 has been drawn on this basis. Since the porosity of this sample (19.8%) measured by conventional techniques is near curve (b) which represents minimum porosity shales, curve (c) gives the approximate minimum effective porosity of Gulf Coast shales. For convenience, porosity values at various depths from this curve are tabulated in Table 2.

The minimum effective porosity is suggested for use in calculating maximum upward permeation into confining layers, unless site-specific shale data support use of different values.

PERMEABILITY

Vertical shale permeability is required for model inputs. The horizontal permeability of a shale sample can be significantly larger. Modelers should be aware that values of permeability obtained by testing sidewall and whole cores typically represent horizontal flow, unless otherwise stated.

Permeability varies with porosity, and several empirical equations have been devised to express this relationship for sands. The Kozeny-Carman equation is the best known relationship, and involves factors for grain size, packing and shape. But other factors (pore geometry, pore throat sizes, interconnection of the pores) are so important that actual sand permeability can easily vary several orders of magnitude from computed values. Considering the above difficulties and the potential for complex water-clay interactions in shales, these relationships are of little value for estimating shale permeability.

Magara (1978), Bethke (1985) and others have concluded that an exponential relationship exists between shale permeability and porosity. Neuzil (1987, personal communication) has stated that this relationship is not particularly useful for computing permeability where porosity is known, due to the amount of scatter in the data. Additionally, some of the better documented studies of shale permeability have not included data on porosity.

Shale permeability and sample depth are plotted in Fig. 3, representing several sets of data with uniform measurement techniques. Data form Neglia (1979) exhibits a fair amount of scatter, and comes form several different locations in Italy. Magara's data comes from two areas in Japan, and each location shows a similiar trend of decreasing permeability with depth. The measurements of Young et al. (1964) for shales from Alberta, and Neuzil (1986) for the Pierre Shale in South Dakota, are the best documented and also indicate the lowest permeabilities. The range of permeabilities in this figure spans six orders of magnitude.

To establish a useful relationship between depth and permeability, a straight line was drawn through the log-log plot of Pierre Shale permeability vs. pressure in Fig. 4. This plot includes many data points from mechanical consolidation tests, and covers a wide range of pressures (and equivalent depths). A straight line relationship would be expected on the basis of the previously assumed exponential relationships among burial depth, porosity, and permeability. In Fig. 5, this line has been transferred to the semi-log plot of permeability vs. depth, and thesame curve with different intercepts has been superimposed on data points for each of Magara's locations. The observed fit to locations in Japan indicates that this curve may be generally valid for normally compacted sediments above geopressure.

Bethke (1986) computed a series of curves defining the maximum shale permeability which would permit geopressuring on the Gulf Coast, for different sedimentation rates. He also states that current sedimentation rates on the Gulf Coast have been estimated at 1 to 5 mm/yr. Curves for these rates are shown in Fig. 6. A curve derived from the Pierre Shale data is drawn so that the intercept with Bethke's limit falls at 7000 ft., the typical depth of geopressures. This curve should indicate the maximum average shale permeability for Gulf Coast locations, and can be used for worst-case computations of upward permeation into shales.

Permeability values from this upper-limit curve are tabulated in Table 3.

Actual shale permeabilities at specific locations may be two to three orders of magnitude lower than this upper-limit curve, but probably follow similiar depth relationships. If site-specific shale data is available and can be considered reliable, similar curves may be constructed to estimate permeability at different depths.

SUMMARY

- o Site-specific data for porosity and permeability of shales are unlikely to exist in most cases. When available, it should be used with considerable caution and judgement.
- o In the absence of other reliable data, minimum effective shale porosity may be estimated using curve (c) in Fig. 2, or from Table 2.
- o Maximum shale permeability may be estimated from Fig. 6 or Table 3. If reliable measurements of shale permeability have been made at a site, the curve shown in Fig. 6 can be used to extrapolate the data to different depths.

REFERENCES

Bethke, C. M., 1985, A numerical model of compaction-driven groundwater flow and heat transfer and its application to the paleohydrology of intercratonic sedimentary basins: J. Geophys Res., v. 90 (B8), p. 6817-6828.

Bethke, C. M., 1986, Inverse hydrologic analysis of the distribution and origin of Gulf Coast-type geopressured zones: J. Geophys Res., v. 91 (B6), p. 6535-6545.

Dickinson, G., 1953, Geological aspects of abnormal reservoir pressures in Gulf Coast Louisiana: Am. Assoc. Pet. Geol. Bull., v. 37, p. 410-432.

Isherwood, D., 1981, Geoscience data base handbook for modeling a nuclear waste repository, v. 2: Lawrence Livermore Laboratory, Livermore, California (NUREG/CR-0912, v. 2, UCRL-52719, v. 2) p. 1-84.

Legate, R. A., 1974, Letter accompanying data report from Location Sampling Service to Du Pont De Lisle Plant, [0107399].

Magara, K., 1978, Compaction and fluid migration - practical petroleum geology: New York, Elsevier, p. 319.

Mueller, G., 1967, Diagenesis in argillaceous sediments, in Larsen, G. and Chilingar, G. V., eds., Diagenesis in sediments: Amsterdam, Elsevier, p. 127-177.

Neglia, S., 1979, Migration of fluids in sedimentary basins: Am. Assoc. Pet. Geol. Bull., v. 63, p. 573-597.

Neuzil, C. E., 1986, Groundwater flow in low-permeability environments: Water Resources Research, v. 22, p. 1163-1195.

Powers, M. C., 1967, Fluid release mechanisms in compacting marine mudrocks and their importance in oil exploration: Am. Assoc. Pet. Geol. Bull., v. 51, p. 1240-1254.

Rieke, H. H. and Chilingarian, G. V., 1974, Compaction of argillaceous sediments: Amsterdam, Elsevier.

Scheidegger, A. E., 1974, The physics of flow through porous media, 3rd ed.: Univ. of Toronto Press, Toronto, p. 353.

Schmidt, G. W., 1973, Interstitial water composition and geochemistry of deep Gulf Coast shales and sandstones: Am. Assoc. Pet. Geol. Bull., v. 57, p. 321-337.

Singer, A., and Mueller, G., 1979., Diagenesis in argillaceous sediments, in Larsen, G. and Chilingar, G. V., eds., Diagenesis in sediments and sedimentary rocks, 2: Amsterdam, Elsevier, p. t15-205.

Young, A., Low., P. F., and McLatchie, A. S., 1964, Permeability studies in argillaceous rocks: J. Geophys. Res., v. 69, p. 4237-4245.

TABLE 1

REPRESENTATIVE POROSITY AND PERMEABILITY DATA
FOR YOUNG SHALES AND RELATED SEDIMENTS, CITED IN LITERATURE

Note: Detailed descriptions of methods used to obtain these data are not found in cited references. Most permeability measurement techniques will tend to yield erroneously high values. These data are presented as typical of values found in the literature, and may not be accurate.

Description	Depth (ft)	Porosity (%)	Permeability (mD) Vertical	Horizontal	Unknown	Ref.
Clay, marine		48.5	1.6 E-2			1
Clay, lacustrine? (CA)	838	44.1	1.1 E-2	1.1 E-2		1
Clay, lacustrine? (CA)	946	40.5	1.1 E-2	2.8 E-1		1
Clay, silty (CA)	1558	41.1	1.1 E-1			1
Silt, Clayey	1527	34.1	5.5			1
Clay, Olig. subsurface (MS)		33.3			1.1 E-2	1
Silt, Mio. subsurface (MS)		33.7			3.8 E-2	1
Shale, Crtaceous					4 E-3	1
Shale, Oligocene & Miocene		21.1 (a)				1
Shale, u. Cret., G. C. (TX)		10.1				2
Shale, u. Cret.? (east TX)		14.5				2
Shale, u. Cret.? (east TX)	10945	27.5				2
Shale, u. Cret.? (TX)		10-15			8.6	2
Shale, sandy (south TX)	8245	23 (b)			5.1 E+1	2
Shale, Gulf Coast	3990	20 (d)			1.8 E-2 (d)	2
Shale, Gulf Coast	13970	14 (d)			1.7 E-4 (d)	2
Shale, "normally compacted"	2000	22 (c)				3
Shale, "normally compacted"	10000	12 (c)				3
Shale, "geopressured" (LA)	11000	17 (c)				3
Shale, "geopressured" (LA)	14000	12 (c)				3
Na-Montmorilonite		70.2			1.4 E-2 (e)	4
Na-Bentonite (WY)		84.5			1.0 E-1 (e)	4
Na-Bentonite (WY)		66.7			3.5 E-2 (e)	4
Bentonite, compacted (WY)		34			4.0 E-6 (f)	4
Na-Kaolinite		61.8			1.7 (e)	4
Kaolinite, compacted		57.5			2.0 E-2 (g)	4
Kaolinite, compacted		22.5			2.9 E-2 (h)	4

TABLE 1 (cont'd)

(a) Average for nine samples.
(b) Average for three samples.
(c) Range from plot of data for LA wells. Extrapolated values above 7000 ft.
(d) Range of values - max. and min. assumed to correlate with depth as shown.
(e) Permeant de-ionized or distilled water.
(f) Compaction load = 2.76 E+10 Pa. Permeant 2.5 N NaCl.
(g) Compaction load = E+6 Pa. Permeant distilled water.
(h) Compaction load = 3.5 E+8 Pa. Permeant 0.002 N NaCl.

References

1. Davis, S. N., 1969, Porosity and permeability of natural materials, in De Wiest, R. J. M., ed., Flow through porous media: Academic Press, New York, p. 530.

2. Isherwood, D., 1981, Geoscience data base handbook for modeling a nuclear waste repository, v. 2: Lawrence Livermore Laboratory, Livermore CA (NUREG/CR-0912, v. 2, UCRL-52719, v. 2) p. 1-84.

3. Schmidt, G. W., 1973, Interstitial water composition and geochemistry of deep Gulf Coast shales and sandstones: AAPG Bull. 58, p. 321-337.

4. Bredehoeft, J. D., and Hanshaw, B. B., 1968, On the maintenance of anomalous fluid pressures: I. thick sedimentary sequences: GSA Bull. 79, p. 1097-1106.

TABLE 2
MINIMUM EFFECTIVE SHALE POROSITY
IN GULF COAST ENVIRONMENTS

Depth (ft.)	Porosity (%)
1000	18
1500	15.5
2000	13.5
2500	12.5
3000	12
3500	11.5
4000	11
5000	10.5
6000	9.5
7000	9

Porosities for depths over 7000 ft. are not tabulated, since this data appears to reflect low-density, overpressured shales (Magara, 1978). Where overpressuring exists, shale densities and porosities can vary widely and generalized data are not valid.

TABLE 3
GENERALIZED UPPER-LIMIT VALUES OF SHALE PERMEABILITY
IN GULF COAST ENVIRONMENTS

Depth (ft.)	Permeability (mD)
1000	3.5 E-2
1500	1.5 E-2
2000	8.5 E-3
2500	5.5 E-3
3000	3.7 E-3
3500	2.9 E-3
4000	2.3 E-3
4500	1.9 E-3
5000	1.6 E-3
5500	1.3 E-3
6000	1.1 E-3
6500	9.5 E-4
7000	8.2 E-4

limit values for average shale permeability

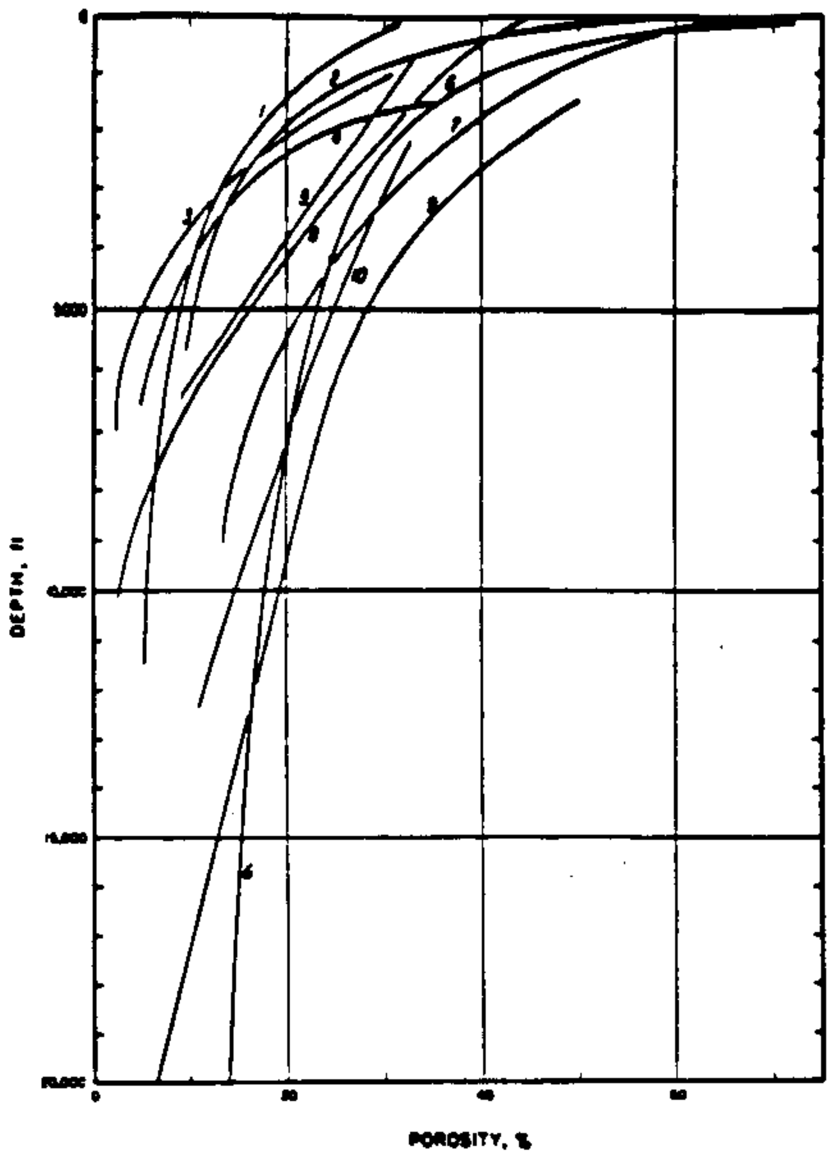

Relationship between porosity and depth of burial for shales and argillaceous sediments.
1=Proshlyakhov (1960); 2=Meade (1966); 3=Athy (1930); 4=Hosoi (1963); 5=Hedberg (1936); 6=Dickinson (1953); 7=Magara (1968); 8=Weller (1959); 9=Ham (1966); 10=Foster and Whalen (1966).

Figure 1 (from Rieke and Chillingarian, 1974, p. 42)

Locations of data used to construct curve:

1 = USSR, 2 = California? 3 = Oklahoma, 4 = Japan,
5 = Venezuela (Tertiary), 6 = Louisiana Gulf Coast,
7 = Japan, 8 = combined data from from various areas, 9 = Gulf Coast (core data), 10 = Louisiana offshore.

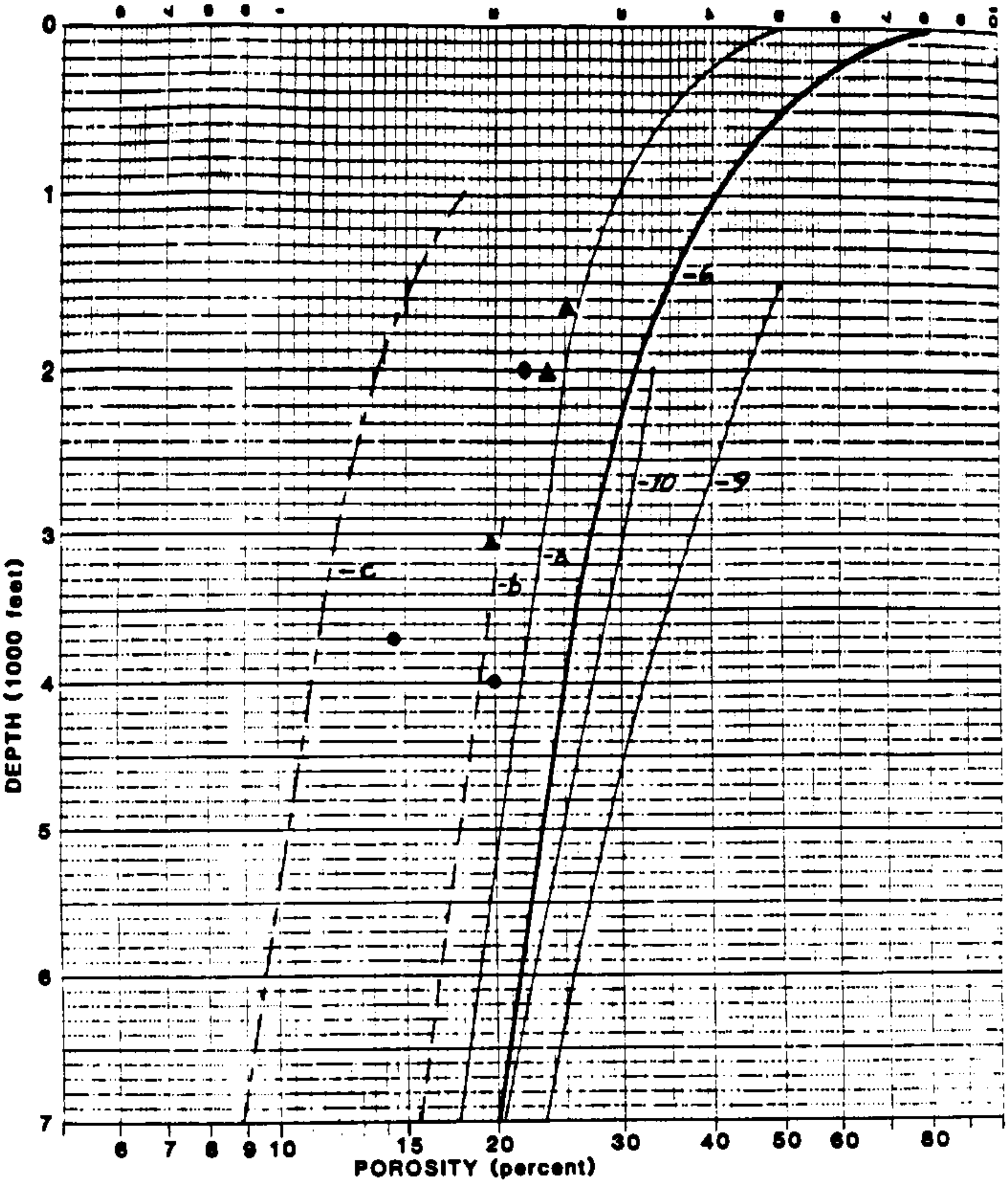

Figure 2
Porosity curves for Gulf Coast Shales: (6) Tertiary shales, Louisiana (Dickinson, 1953), (9) Gulf Coast shales, core data (Ham, 1966), (10) Louisiana offshore (Foster and Whalen, 1966), (a) curve for "typical" porosities, Tertiary shales, Texas and Louisiana (Bradley, 1975), (b) data from shale cuttings of Anahuac and Frio formations in a Louisiana well (Schmidt, 1973), extrapolated by Isherwood (1981) to depths above 7000 ft., (c) estimated minimum effective porosity. Plotted points: (s) gulf Coast data from Table 1, (s) whole core data from Louisiana disposal well (Davis and Assoc., 1986).

KEY FOR FIGURES 3, 5, AND 6

Δ Mudstones, Kambara and Obuchi wells, Japan. Porosity 20-43%, av. porosity = 30%. Steady state measurement, 8000-10,000 mg/l NaCl. (Magara, 1978)

▲ Mudstones, Yuza well, Japan. Porosity 15-38% average porosity = 21.5%. Steady state measurement, 10,000 mg/l NaCl. (Magara, 1978).

◩ Pliocene and Miocene shales, Italy. Steady state permeability measurement, permeant not stated. (Neglia, 1979).

Lower Cretaceous clayey siltstones and sandstones, Western Canada. Porosity not given. Steady state measurement, water permeant. (Young et al., 1964).

◇ - vertical permeability, no confining pressure.

◆ - vertical permeability, confining pressures 76 to 400 bars, equivalent to burial depths of 3500 to 11,100 ft.

⊚ Pierre Shale, Cretaceous, South Dakota. Initial porosity 25-45%, compacted at stress equivalent to depths shown. Transient pulse hydraulic test (numerous mechanical compaction test results not shown). (Neuzil, 1986).

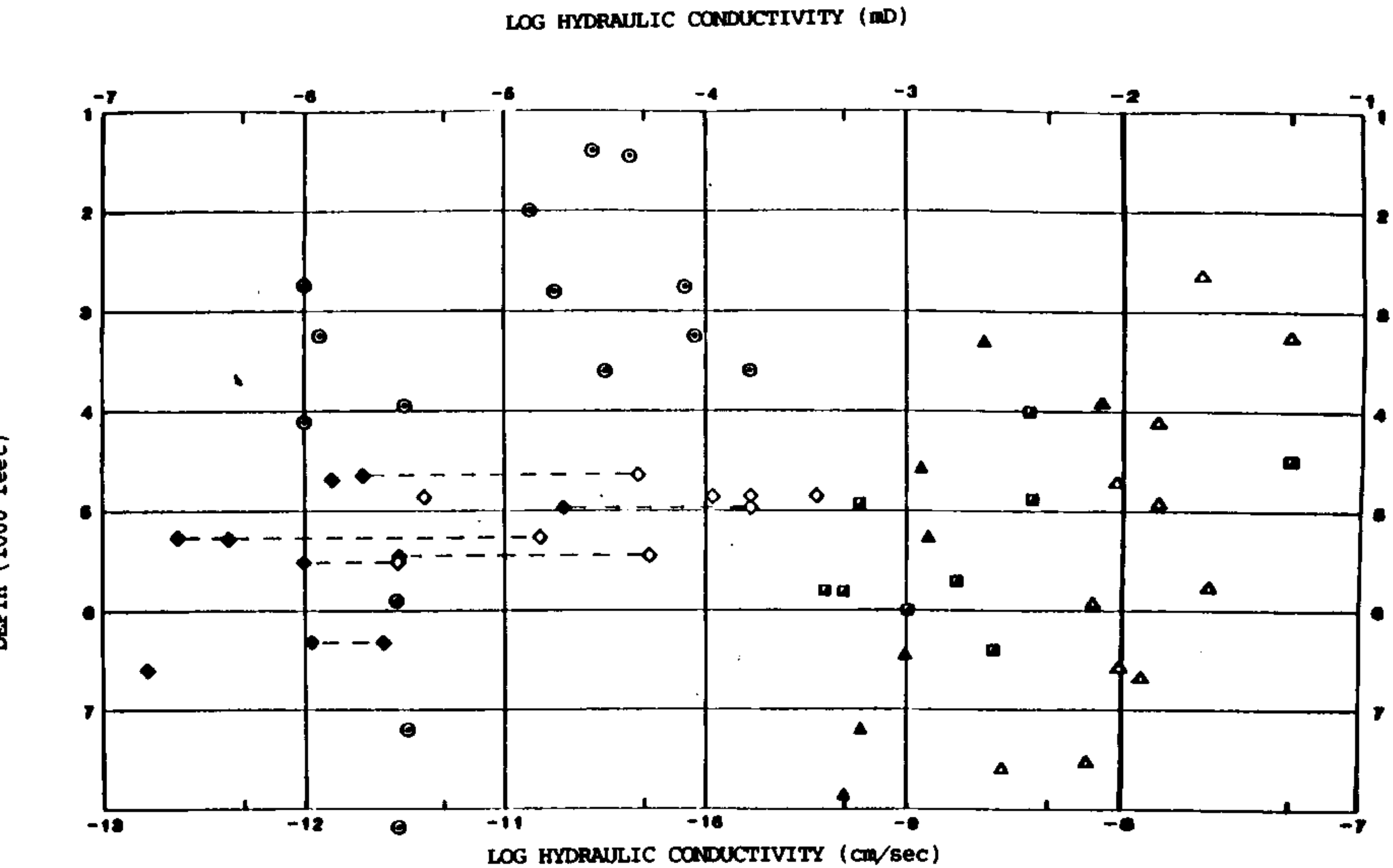

FIGURE 3

SHALE PERMEABILITIES vs. DEPTH,
DATA FROM VARIOUS STUDIES
(SEE KEY, PRECEDING PAGE)

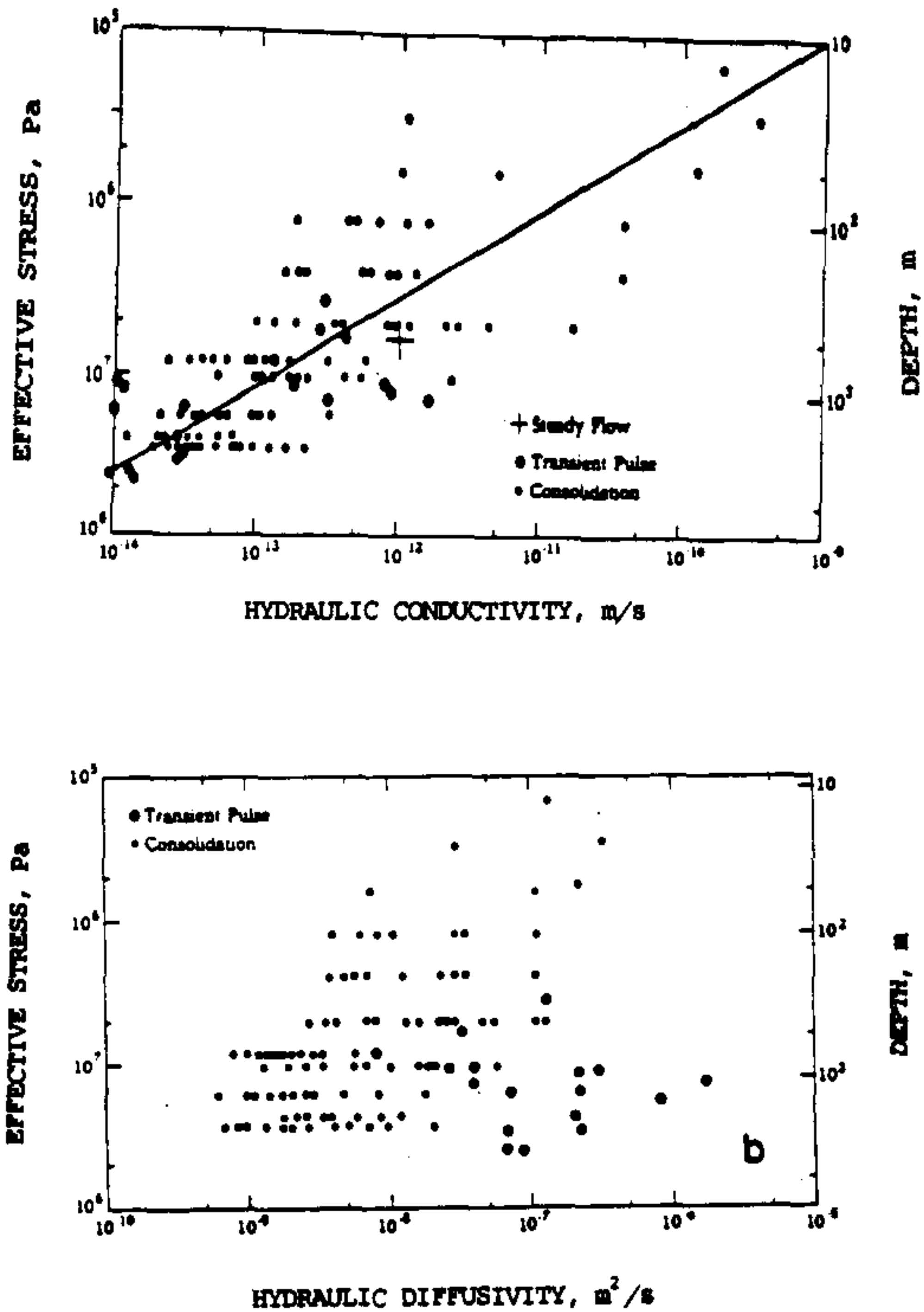

Hydraulic properties of the Pierre Shale derived from a steady flow test and transient hydraulic and mechanical tests. The transient hydraulic test methodology used was that described by Hsieh et al. (1981) and Neuzil et al. (1981); the transient mechanical tests were step load consolidation (e.g., Scott, 1963). The data are plotted against effective stress and as equivalent depth in meters using the convention that effective stress increases at approximately 1.3×10^4 Pa/m.

FIGURE 4

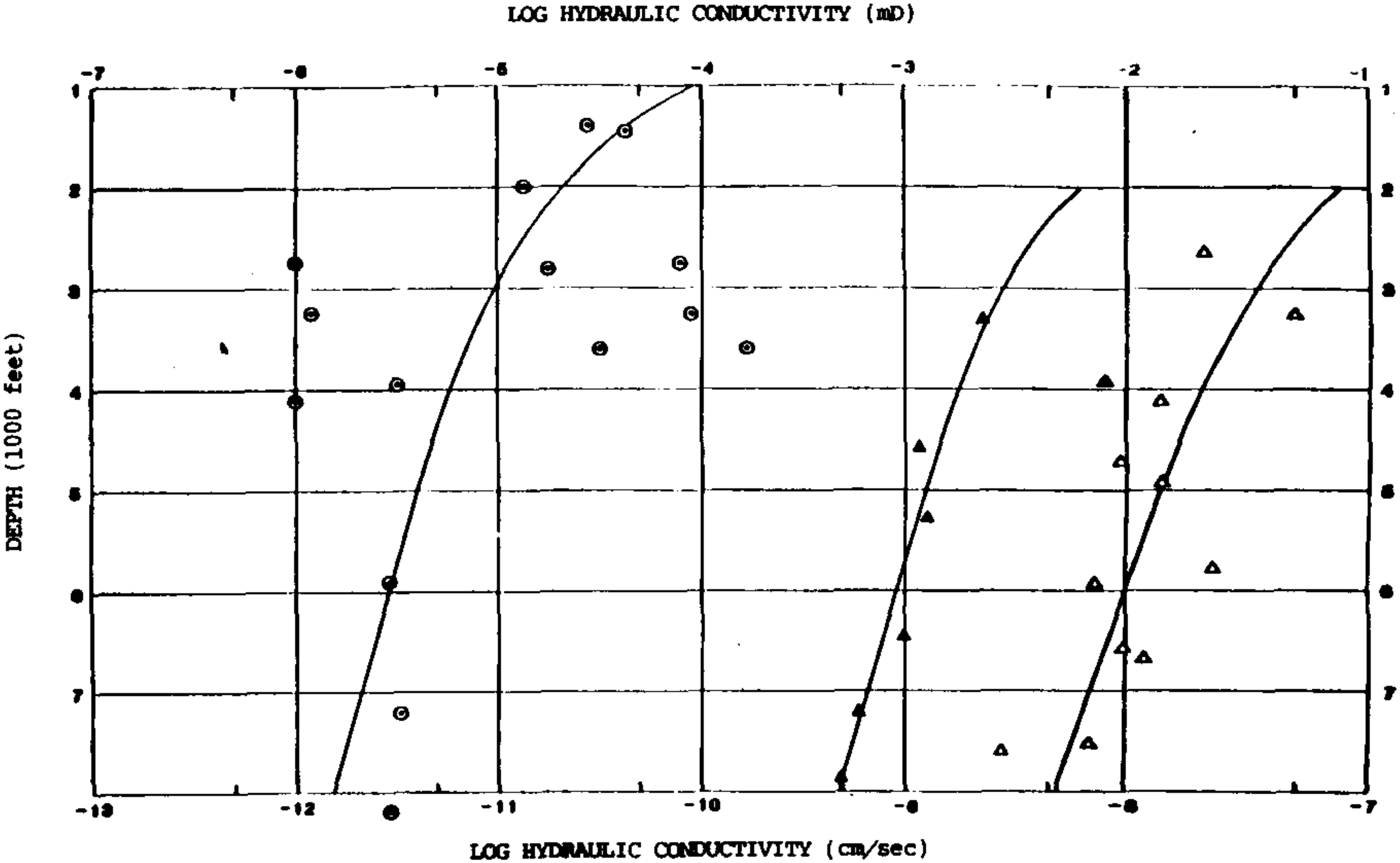

FIGURE 5

CURVE FROM FIGURE 4 APPLIED TO DATA FROM MAGARA (1978)

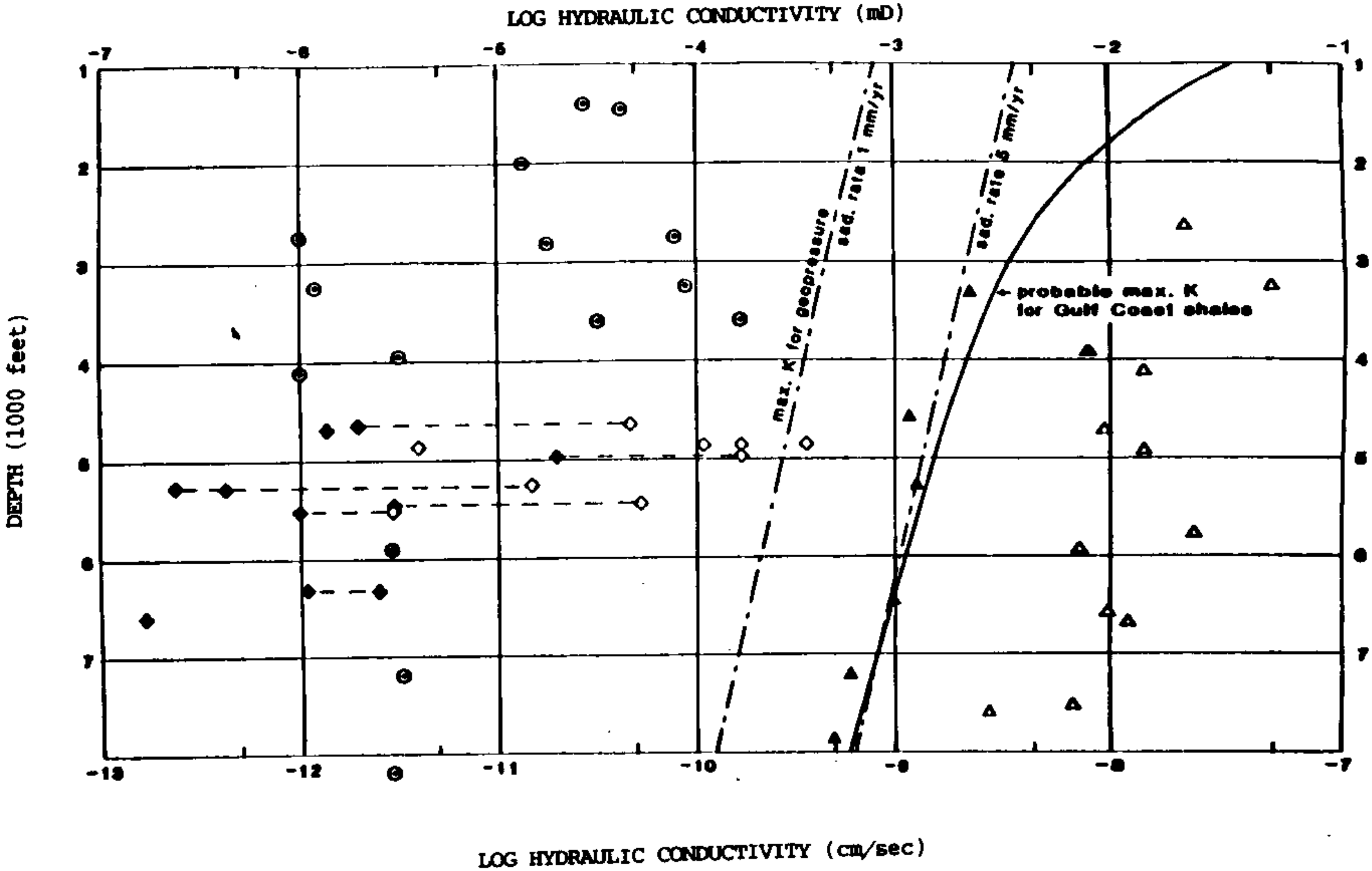

FIGURE 6

CURVES FROM BETHKE (1986) SHOWING MAXIMUM PERMEABILITY FOR GULF COAST GEOPRESSURING, AND CURVE OF PROBABLE MAXIMUM SHALE PERMEABILITY.

APPENDIX 3-3
MOLECULAR DIFFUSION MODEL

BLANK

TABLE OF CONTENTS

CONTENTS
(CONTINUED)

LIST OF FIGURES

LIST OF TABLES

1.0 INTRODUCTION

Molecular diffusion is a transport process occurring exclusively in solution. It results in the movement of solute molecules or ions from regions of high concentration to regions of low concentration, driven by the random thermal agitation (Brownian motion) and collisions of solute and solvent molecules.

At underground injection sites, molecular diffusion of a dissolved contaminant species can take place vertically within the injection zone, in the water-saturated aquitard layer overlying the layer containing the bulk waste plume. This type of transport can be visualized (see Figure 1) as a cloud or halo of contaminant molecules rising above the bulk plume. The highest concentration of dissolved contaminant will be found at the base of the aquitard, and will decrease with vertical distance into this layer. This is illustrated schematically by the gradation of shading shown in Figure 1.

Molecular diffusion can also occur in the horizontal direction. However, this effect will normally be negligible compared to the lateral movement of contaminants resulting from other transport mechanisms, such as hydrodynamic dispersion. Horizontal diffusion will typically contribute less than 500 ft to the lateral movement (calculated using the methods presented in Section 4.0), even on a 10,000 year time scale.

2.0 KEY CONSIDERATIONS

In evaluating molecular (or ionic) diffusion of contaminant species within an aquitard layer, it is necessary to consider two key factors: (1) the magnitude of the concentration reduction (i.e., the concentration reduction factor or CRF) required to render the most toxic and/or most mobile species non-hazardous and (2) the vertical distance into the aquitard layer needed to obtain this CRF after 10,000 years of diffusion (recall that species concentration decreases with increasing vertical distance into the aquitard).

The required CRF is determined on the basis of published health-based standards or detectability limits on the species under consideration, as outlined in the underground injection regulations, together with the concentration of the species in the waste stream. This aspect of the molecular diffusion calculation is not addressed in the present discussion, which focuses primarily on the prediction of the species transport. It is assumed, for the present purposes, that the required CRF has been established beforehand for a given site and waste stream.

Confident prediction of the vertical distance required to obtain the necessary CRF for the most toxic species after 10,000 years dictates the use of a conservative model for molecular diffusion. Such a model must calculate the concentration profile as a function of vertical distance, based on a conservative value for the effective diffusion coefficient of the species through the water-saturated porous matrix of the aquitard layer. The following sections will describe the molecular diffusion model adopted in the present no-migration demonstration, and the approach developed for establishing a conservative value for the effective diffusion coefficient.

3.0 MODEL DESCRIPTION

The present molecular diffusion model is based on the application of Fick's well-known Second Law of Diffusion, which is expressed as:

$$\frac{\partial C}{\partial t} = D* \quad \frac{\partial^2 C}{\partial z^2} \tag{1}$$

where C is the relative species concentration (with respect to the contaminant concentration in the waste stream) at time t and vertical position z within the overlying aquitard layer. The distance z is measured upward relative to the top boundary of the bulk waste, as it slowly advances by advective seepage into the aquitard layer. The location of this top boundary (versus time) can be determined using the Multilayer Vertical Permeation Model (Appendix D).

The parameter D* in Equation 1 is the "effective diffusion coefficient" for the contaminant species within the water-saturated porous aquitard layer, defined on the basis of the mass transfer rate per unit cross sectional area of material. In this definition, only the portion of the total cross section occupied by the pores is included in specifying the area. (It is significant to note that diffusion through the solid matrix will virtually always be negligible compared to diffusion within the pore space, because diffusivities in solids are several orders of magnitude lower than in liquids (Lerman, 1988).)

This form of Fick's Second Law, together with the associated definition of the diffusion coefficient, is consistent with the description employed in number of key literature references, including Freeze and Cherry (1979), Bear (1972), Walton (1985), Javandel et al. (1984), Fried (1975), and Greenkorn (1981). On the other hand, an <u>equivalent</u> alternate representation, which also frequently appears in the literature (Lerman, 1988; Huyakorn and Pinder, 1983; Currie, 1960; and Intercomp, 1976) deserves some comment. This form of Fick's Second Law for porous media is given by:

$$\frac{\partial C}{\partial t} = \frac{D}{\phi} * \quad \frac{\partial^2 C}{\partial z^2} \tag{1}$$

where ϕ is the porosity of the medium, and D is the "nominal diffusion coefficient" of the contaminant species within the porous matrix, defined on the basis of the mass transfer rate per unit total cross sectional area, including both matrix and pores (rather than solely the pore cross sectional area).

The two equivalent formulations of Fick's Second Law given in Equations 1 and 2 are related by an expression linking the two diffusion coefficients D and D*:

$$D = D^*\phi \tag{3}$$

These two diffusion coefficients differ by a factor of the porosity ϕ, and, since ϕ is always less than 1, D is always less than D*.

In discussing diffusion phenomena in porous media, it is extremely important to make the distinction between which of these two diffusion coefficients is being referred to. There appears to be considerable ambiguity and misinterpretation of information in the literature as a result of overlooking this distinction.

Gillham and Cherry (1982) alluded to both D and D* in their discussions of porous matrix diffusion. However, Walton (1985) later incorrectly assumed that they were referring to D* in their evaluation of the effect of porosity on the diffusion coefficient, when, in reality, they were referring to D. This led Walton to an unfounded conclusion.

Manheim (1970) discussed ionic diffusion in porous media on the basis of the Fick's Second Law formulation given by Equation 1, which involves D*. However, he then expressed D* in terms of the so called "formation resistivity factor" F, using an equation valid strictly for D. It is not clear whether the relationship between the diffusion coefficient and porosity plotted by Manheim for NaCl in porous media refers to D or to D*.

In the present development, Equation 1 is solved for the concentration reduction factor C as a function of time t and vertical position z, assuming that, at the lower boundary z = 0, the contaminant concentration is identical to the value in the waste stream at all times (i.e., C = 1 at z = 0). This assumption is conservative, since the diffusion process itself will act to cause the concentration at z = 0 to drop below the waste concentration. Diffusion occurring upward into the region above z = 0 will tend to deplete the neighborhood near z =0 of contaminants. Of course, these contaminants can be replenished, to a certain extent, by upward diffusion out of the region beneath the lower boundary of the model (z <0), comprising the lower portion of the aquitard layer and the upper portion of the bulk waste plume. However, in order for such diffusion to take place, it is necessary for a concentration driving force to be established, and thus, for the relative concentration at z = 0 to drop below C = 1. The actual relative concentration at z=0 must always lie somewhere between C = 0 and C = 1. Therefore, the assumption that C=1 at z=0 for all times automatically guarantees that the predicted relative concentrations above z=0 will be overestimates of the true values.

Based on the assumption that C=1 at z=0, the solution to Fick's Second Law of Diffusion (Equation 1) for the relative concentration profile C(t,z) of a contaminant species in the aquitard layer overlying the bulk waste plume is given by

$$C(t,z) \quad = \quad erfc\left[\frac{z}{2\sqrt{D*t}}\right] \tag{4}$$

where erfc is the "complementary error function," widely available in published tabulations and virtually all computer function libraries.

Equation 4 constitutes a complete statement of the present model of molecular diffusion in a water-saturated porous aquitard layer. Figure 2 shows a plot of Equation 4, expressed in terms of the relative concentration C, while Figure 3 shows the same results, plotted using a logarithmic scale for the relative concentration. These figures indicate that the concentration of a contaminant species decreases monotonically with vertical distance above the bulk waste plume.

To apply the results embodied in Equation 4 and Figures 2 and 3 on a practical basis, it is necessary to convert the dimensionless distance parameter

$$\frac{z}{2\sqrt{D*t}}$$

into true vertical distance z in space. This can be accomplished once a defensible value for the effective diffusion coefficient D* of the contaminant species in the porous matrix is known. Determination of the effective diffusion coefficient is addressed next.

4.0 DETERMINATION OF EFFECTIVE DIFFUSION COEFFICIENT

In general, very few direct experimental measurements of the effective diffusion coefficient of a contaminant species in the water saturated aquitard layer will be available. Therefore, it is necessary to predict a value for the coefficient on the basis of physical property data and other reliable information extracted from the literature. Fortunately, a considerable body of such information is available to achieve this with sufficient accuracy and confidence to provide a conservative estimate of molecular diffusion in the aquitard layer, consistent with the requirements of the no-migration demonstration.

The effective diffusion coefficient of a solute species within a water-saturated porous medium is always lower than in free water solution (i.e., without the solid framework). This behavior can be attributed primarily to the complexities inherent in the porous medium microgeometry (see Figure 4). Constrictions in the pore channels inhibit the rate of diffusion along the pores, and tortuosity of the channels lengthens the total path over which molecules must travel. These geometric effects have been studied extensively in the literature, both theoretically and experimentally. In general, it is found that the influence of the microgeometry can be characterized in terms of a "geometric correction factor" G for the porous matrix, equal to the ratio of the effective diffusion coefficient in the matrix D^* to the diffusion coefficient in free solution D_o:

$$G = D^* / D_0 \leq 1 \tag{5}$$

In the absence of various complicated chemical phenomena discussed below, G is expected to be a property of the matrix only, independent of the solvent and diffusing solute. It will typically be a function of both the matrix porosity and of the lithology. For a specified lithology, G will generally decrease with decreasing porosity.

In addition to the reduction in effective diffusion coefficient associated with the geometrical complexities of the porous matrix, there are frequently chemical phenomena present which act to reduce the extent of contaminant movement further. These chemical phenomena include adsorption, ion exchange, steric hindrance, and osmotic exclusion, which slow or prevent the movement of contaminants. They also include hydrolysis and decomposition, which destroy the contaminants. Although these chemical effects are sometimes difficult to quantify in practice, their presence will always result in a reduction in the extent of contaminant movement.

Therefore neglecting these effects in the diffusion assessment automatically leads to an added margin of safety in the calculations (see Section V for details).

The first step in determining the effective diffusion coefficient for a contaminant species within the water-saturated aquitard layer is predict the value of the diffusivity in free aqueous solution, D_o. This is accomplished by making use of the extensive correlations available in the open literature (Section 4.1).

The next step is to predict the geometric correction factor G for the porous matrix, for a given matrix porosity and lithology. Using information assembled from a variety of literature sources, including both theoretical and experimental studies (Section 4.2), a correlation for accomplishing this has been developed, and is presented in Section 4.2. This correlation expresses the geometric correction factor G as a simple function of the porosity, for various generic lithologies.

4.1 Predicting Diffusion Coefficient In Free Solution

A number of well-validated correlations for predicting with confidence the diffusivity of solutes in free aqueous solution are documented in the literature, both for electrolytes (ionic solutes) and non-electrolytes (non-ionic solutes). Techniques applicable to non-electrolytes include those of Othmer and Thakar (1953), Wilke (1949), Li and Chang (1955), and Wilke and Chang (1955). For electrolytes, diffusivities can be predicted very accurately (Perry and Chilton, 1973) using the so-called Nernst equation (Nernst, 1888), which expresses the diffusivity in terms of known values for the cationic and anionic electrical conductances at infinite dilution. Detailed instructions on applying these techniques, in some cases together with examples, are presented in a number of references, including the standard Chemical Engineers' Handbook (Perry and Chilton, 1973), as well as other well-regarded texts and handbooks by Treybal (1955), Lerman (1988), and Horvath (1985). Also contained in these references are extensive tabulations of species- and chemical group-specific physical property data required as input parameters to the correlations. De Kee and Laudie (1973) have published a nomograph, based on the method of Othmer and Thakar (1953), for predicting the diffusivities of 65 frequently-encountered non-electrolytes, including many organics, as a function of temperature. The average accuracy of the various predictive methods is roughly ±10% (Perry and Chilton, 1973; Bird et al., 1960). This high degree of accuracy is possible because of the very narrow range typically observed for the diffusivities of most solutes, both ionic and non-ionic. With few exceptions, the total range of variation at a given temperature is less than a factor of 10.

In addition to the highly accurate techniques described above, there are frequently measured values of diffusivities for specific solutes in water available in the literature. Broad tabulations of observed diffusivities have occasionally been published (Johnson and Babb, 1956; Reid and Sherwood, 1958; Perry and Chilton, 1973; Lobo, 1984). Of course, a directly measured value for the diffusivity is often preferable to a value predicted using a correlation.

4.2 Predicting Geometric Correction Factor For Porous Medium

4.2.1 Theoretical

A great many theoretical studies have been conducted to gain a fundamental mechanistic understanding of the diffusion phenomenon in porous media, and to develop quantitative relationships for predicting the effect of porosity and microstructure on the geometric correction factor G. The basic approach typically adopted in these studies is to first define an idealized geometric model for the microstructure of the porous medium, and then to solve the basic differential equations for diffusion through the open pore space in this geometry. Subsequent averaging of the solution for the mass flux over the boundaries of the system leads to a prediction of the effective macroscopic diffusion coefficient D* and the geometric correction factor G.

One form of idealized model frequently used for porous media is that of a series of tortuous tubes running at a spatially varying angle across the matrix. If the tubes are assumed uniform in cross section and equal in total length, then the geometric correction factor G is found (Currie, 1960) to be given by the equation:

$$G = (L/L_T)^2 \tag{6}$$

where L represents the length of the direct path for diffusion across the medium, and L_T denotes the tortuous path length contained within the direct distance L. Because of the wide recognition afforded this tortuous tube model, a parameter known as the "tortuosity factor" t is often defined. In general, the tortuosity factor is equal to $(L_T/L)^2$, but, for the idealized tortuous tube model, it also equals the reciprocal of the geometric correction factor G. Even in the case of more complex geometries, the tortuosity factor t is frequently considered to be the reciprocal of G, although, in a strict sense, this interpretation is not valid because G includes both tortuosity and constriction effects.

Another version of tube model often utilized for porous media features constrictions along the length of the tubular pores [see Figure 4(a)]. These constrictions can be included in either a straight-tube form of the model, or in a tortuous tube model. In general, the presence of constrictions results in a reduction in G (relative to the value obtained for uniform straight or tortuous tubes) by a factor equal to the ratio of the harmonic mean cross sectional area to the arithmetic mean area. Unless the cross sectional area varies very drastically along the pores, as in the case of a consolidated medium which features dead-end pores, this ratio will normally not differ greatly from 1. Thus, for unconsolidated media, the effects of pore tortuosity will usually dominate over those of pore constrictions.

Tubular models of porous media generally consider the matrix network of the system to be comprised of a continuous solid phase. In contrast, another frequently-used geometric idealization for porous systems typically describes the matrix as a discontinuous phase, consisting of a two dimensional array of discrete particles arranged in a regular repeating pattern [see Figure 4(b)].

The advantage of this type of representation is that it permits one to examine the potential effects of particle shape on the geometric correction factor. A variety of particle shapes have received consideration using Discrete Particle Array models, including circles and squares, as well as shapes with larger aspect ratios (ratio of maximum to minimum dimension), such as ellipses and rectangles (De Vries, 1950; Maxwell, 1881; Burger, 1919; Weissberg, 1963; Hashim and Shtrikman, 1962; Ryan, 1984; Kim et al., 1987).

Model arrangements with high-aspect ratio particles are expected to be particularly well-suited to describing laboratory and geological systems featuring plate-like particles, such as clays and shales, with their major dimensions aligned roughly along a sedimentary bedding plane. In such configurations, the Discrete Particle Array models predict anisotropic diffusion behavior (Kim et al., 1987), characterized by an effective diffusion coefficient perpendicular to the bedding that is considerably lower than the coefficient parallel to the bedding. This type of anisotropic behavior is, of course, to be anticipated because of the much more tortuous path the molecules must take in migrating perpendicular to the bedding.

The theoretical predictions from Discrete Particle Array models have been found to be in excellent agreement with experimental observations on <u>unconsolidated</u> <u>granular</u> <u>beds</u>, for cases in which the aspect ratio of the particles is close to 1 (Kim et al., 1987), even in systems with highly non-uniform particle size distributions. These results will be discussed in further detail below.

Fewer experimental and theoretical results are available on plate-like particles. Kim et al. (1987) considered an idealized particle array model consisting of plate-like particles in which the major axes were perfectly aligned along the horizontal bedding planes. However, in the accompanying experiments, the particle orientations deviated significantly from perfect horizontal alignment, as revealed by the published photographs of the particle arrangements. It is therefore not surprising that the results of these experiments did not agree well with the predictions. While the theory and experiments both gave a major reduction in the diffusion coefficient perpendicular of the bedding plane (relative to free solution), the observed variations with porosity, and the ratio of the horizontal- to vertical diffusivity, were not in good accord with the simple theory for a perfectly aligned bed.

In laboratory and geological systems consisting of plate-like particles deposited in a sedimentary fashion, it is reasonable to expect that, immediately after deposition has taken place, the particles will be poorly aligned with the bedding planes, and the porosity of the sediment will be fairly high. However, as the system is compacted, either by natural overburden pressure (in the case of a geological system) or by directly imposed mechanical action (in the case of a laboratory system), the porosity will decrease, and the particles will rotate into better alignment with the bedding. This improved particle alignment will result in an increase in the tortuosity of the pore channels, which, in turn, will reduce the effective diffusion coefficient perpendicular to the bedding plane. Therefore, for beds of plate-like particles, the compaction process will act to bring about simultaneous reductions in both the porosity of the sediment and the geometric correction factor for diffusion. Such systems will thus behave as if the geometric correction factor were a unique function of the porosity, decreasing with decreasing porosity.

4.2.2. Experimental

Four different experimental techniques are typically used to establish the relationship between the geometric correction factor G and porous medium microstructure. These techniques are: (1) in-situ field measurements, (2) laboratory experiments on unconsolidated dry packings, (3) diffusivity measurements on platelet-filled plastic barrier films and (4) electrical resistivity measurements on core samples and sediments. This section will briefly describe each of these measurement techniques, and present experimental results obtained with the various methods. These experimental results will then be used, in conjunction with the theory discussed above, to develop a simple relationship for confidently predicting the geometric correction factor G for an arbitrary aquitard layer, based solely on knowledge of the layer porosity and its generic lithology.

4.2.2.1 In-Situ Field Measurements

It is sometimes possible to determine a value for the diffusion coefficient of a solute species in a layer of porous rock using direct in-situ field measurements of concentration profile as a function of vertical position. The applicability of this method depends entirely on whether, at some time in the geological past, a sudden change took place in a concentration boundary condition for the species, brought about by a relatively precipitous geological event, such as rapid uplift or retreat of a glacier. The present-day concentration profile of the species in the porous rock layer can be predicted using an unsteady state diffusion model, such as Equation 4, derived from Fick's Second law. The effective diffusion coefficient D* is an adjustable parameter in the model which is determined by matching the predicted concentration profile to the observed variation.

This technique is not expected to be very accurate for three reasons. First, the precise time in the past at which the sudden geological event occurred is often difficult to establish. Secondly, the observed variations in concentration, relative to the mean concentration profile, are frequently too jagged and noisy to establish a confident value for the diffusion coefficient. And third, the sediments are often stratified, containing several sublayers of distinctly different lithology; the results are thus not characteristic of any one lithology, but, rather, an average over them all. Therefore, values of the effective diffusion coefficient deduced using the direct in-situ measurement technique should only be viewed as first approximations to the true values.

Leythaeuser et al. (1980, 1982) measured diffusion coefficients for light hydrocarbons (C_2 to C_7) through the water-saturated pore space of shales exposed after retreat of the polar ice cap from west Greenland, using the direct in-situ measurement method, and obtained values 10 to 100 times lower than as in free solution. This implies a geometric correction factor G of 0.01 to 0.1. These measurements also mildly suggested that the heavier hydrocarbons were being adsorbed onto the shale to some extent.

Several in-situ determinations of effective diffusion coefficients for ionic radio-isotope species (self-diffusion) and major ions in near-surface unconsolidated silty/clayey deposits at various sites in south-central Canada and north-central USA have been reported in the literature (Cherry et al., 1979; Desaulniers et al., 1981; Desaulniers et al., 1982; Quigley et al., 1983; Desaulniers et al., 1984; Desaulniers et al., 1986, Desaulniers et al., 1987; Desaulniers and Cherry, 1988). These determinations were based on the existence of a sudden change in concentration boundary conditions when glaciers or seawater retreated some 10,000-16,000 years ago. Values reported for the effective diffusion coefficients ranged from $2X10^{-6}$ to $7X10^{-6}$ cm^2/sec, with most values situated at the low end of the range. These are a factor of 2 to 10 as low as for free solution, implying a geometric correction factor of 0.1 to 0.5.

4.2.2.2 Dry Granular Packing Method (DGP)

A great many laboratory studies have been conducted to characterize diffusion behavior in unconsolidated dry porous media (Buckingham, 1904; Penman, 1940; DeVries, 1952; Hoogschagen, 1955; Currie, 1960; Kim et al., 1987). The most extensive of these investigations is the pioneering work of Currie (1960).

In these types of studies, dry samples of granular (particulate) material are loaded into a small cylindrical tube. The samples are supported at the ends of the tube by wire- or fabric meshes. Particlate forms examined include glass spheres (uniform and non-uniform size distributions), sand, carborundum, sodium chloride, soil crumbs, and pumice, as well as plate-like particles such as plastic disks, talc, kaolin, vermiculite, and mica. The effective diffusion coefficient of a trace gas (such as hydrogen or argon) through the air-filled porous medium is measured. Since the geometric correction factor G is expected to be independent of both the solute and the solvent under consideration, the values obtained for G in these experiments should apply equally well to diffusion of contaminant species through water-saturated porous media of the same pore channel geometry.

Figure 5 presents a summary of the available results for dry unconsolidated granular beds, plotted as G versus porosity ϕ. Separate data ranges are shown for "spherical" particles (Currie, 1960; Hoogshagen, 1955; Kim et al., 1987) and higher-aspect-ratio plate-like particles (Currie, 1960; Kim et al., 1987). In the latter case, the porous medium exhibits anisotropic behavior, and the component of G perpendicular to the bedding plane is given. Also provided for comparison is the theoretical curve for low-aspect-ratio particles calculated by Ryan (1984) using a discrete particle array model, and later confirmed by Kim et al. (1987) using the same model. As noted by Kim et al. (1987), this theoretical curve agrees closely with the range of experimental data on "spherical" particles, even for the case of non-uniform particle size distributions.

The most striking feature of this plot is the very large reduction in the geometric correction factor G obtained in going from "spherical particles" to plate-like particles. Of course, such a reduction was anticipated in the theoretical discussion presented earlier. This reduction is caused by the increased tortuosity produced by the alignment of the particles along the bedding plane. The magnitude of the reduction, relative to the spherical case, is on the order of 4X and larger in some instances. Kim et al. (1987) specifically noted a 4X reduction in their experiments on mica particles. Several of the plate-like particle forms included in the range of data in Figure 5 correspond to clay minerals, with particle shapes similar to those found in typical aquitard layers.

The lines $G=\phi^{0.3}$, $G=\phi$, and $G=\phi^2$ are plotted for reference in Figure 5. $G=\phi^{0.3}$ and $G=\phi$ represent the approximate relationships determined by Archie (1952) for a variety of natural (a) unconsolidated sands and (b) consolidated sandstones, respectively (Bear, 1972; Lerman, 1988), using the Electrical Resistivity (ER) Method (see Section 4.2.2.4 for more details).

4.2.2.3 Plastic Barrier Film Method (PBF)

In the food packaging industry, plastic films are frequently used as barriers to limit the diffusion of water vapor and oxygen into and out of foodstuffs. This approach is very effective primarily because of the low diffusivity of dissolved gases through plastic. However, for some applications, the diffusivity is still not low enough to achieve desired shelf life. To overcome this limitation, rigid particulate "filler" material is sometimes added to the plastic. The filler consists of tiny plate-like flake particles distributed uniformly through the thickness, and aligned with the plane of the film. This in-plane particle alignment is achieved automatically as a consequence of the unique manufacturing process that produces the film. The embedded particles act to reduce the effective diffusion coefficient through the film by creating a very tortuous microgeometric diffusion path.

Plate-like fillers are very widely used in the manufacture of commercial packaging films and containers to reduce diffusivity and achieve certain desirable mechanical and thermal properties. In fact, many commercial plastic resin suppliers offer their products in pellet form, with the filler particles predispersed within the pellets (Plastics, Edition 7, 1985; Modern Plastics Encyclopedia, 1988). These pellets are designed to be fed to a plasticating extruder, which then delivers a polymer melt containing suspended filler particles to a film-forming die. When the quenched film is stretched and oriented to develop mechanical properties, the particles will align with the plane of the film. Commercially available plate-like fillers include talc, mica, clays, and aluminum flake.

The diffusion of dissolved gases in a plastic film containing filler particles is completely analogous to the diffusion of soluble substances in a water-saturated porous medium. The plastic material serves the function of the pore water, while the filler particles are analogous to the rock matrix, providing a tortuous barrier to diffusion. Since the geometric correction factor G is dependent primarily on the microgeometry of the system (and is expected to be nearly independent of the specific substances involved), measurements of G for plastic barrier films should translate directly into comparable results for porous media of similar microgeometry.

Because of the commercial importance of plastic barrier films, a considerable body of experimental data has developed on diffusion in such systems, particularly for materials containing plate-like filler particles (e.g., Arina et al., 1979; Kamal et al., 1984; Murthy et al., 1986; Cussler et al., 1988; Bissot, 1988a,b). The quality of this data is typically excellent, owing to the business liabilities inherent in marketing products based on over-optimistic projections. Results are normally reported as diffusion rate reduction factor (i.e., geometric correction factor G) as a function of filler loading. Filler loading can be converted directly into volume fraction plastic (equivalent to porosity of a porous medium).

All available experimental data on diffusion in particle-filled plastic barrier films, both for the case of spherical as well as plate-like particles, are found to fall entirely within the range of behavior presented in Figure 5 for the Dry Granular Packing (DGP) Method. Thus, these two strikingly different measurement techniques provide mutually consistent results, which enhances confidence in findings from both techniques.

4.2.2.4 Electrical Resistivity Method (ER)

The Electrical Resistivity Method (ER) makes use of the physical analogy between conduction of an electrical current through the open pore channels of a medium saturated with an electrolyte solution, and the diffusion of molecules and ions through these same pore channels. In this technique, a quantity known as the "formation factor" F is determined. The formation factor is equal to the ratio of the electrical resistivity of a porous medium saturated with an electrolyte solution to the resistivity of the same electrolyte solution, without the porous medium present. Typically, a sodium chloride solution with over 10g per liter of NaCl is used. Electrical resistivity is defined as the resistance of a unit cube of material subjected to a one-dimensional current flow through one face and out the opposite face. The geometric correction factor G is related to the formation factor F by the equation (Greenkorn, 1981):

$$G = \frac{1}{F\phi} \qquad (7)$$

According to Equation 7, a large value for the formation factor implies a substantial reduction in the effective diffusion coefficient, relative to the case of diffusion in free solution.

Use of the Electrical Resistivity (ER) Method to determine geometric correction factors for porous media is valid, in the strictest sense, only for media that do not conduct electric current. However, as pointed out by Manheim and Waterman (1974), for materials such as clays and shales, which exhibit surface conductivity, the Electrical Resistivity Method will always underestimate the "true" formation factor associated with the pore microgeometry, and thus will automatically produce a conservative overestimate for the geometric correction factor G. Moreover, techniques have been developed (Waxman and Smits, 1968) to correct for the effects of surface conductivity on formation factor, by saturating the porous medium with electrolyte solutions of several different concentrations and measuring the corresponding resistivities.

In an early investigation, Archie (1952) measured formation factors for a variety of natural unconsolidated sands and consolidated sandstones. He found that, over a significant range of porosities, the experimental variations of formation factor with porosity could be described (within a given sediment) by an empirical relationship of the form:

$$F = 1/\phi^{\pi} \qquad (8)$$

The exponent m was found to be approximately 1.3 for unconsolidated sands, and to range between 1.8 and 2.0 (Bear, 1972) for consolidated sandstones. Equation 8 has subsequently come to be known as the "Archie Equation." Substitution of Equation 8 into Equation 7 provides an expression for the geometric correction factor G as a function of the porosity _.

$$G = \phi^{n} \qquad (9)$$

where n = m-1, with n approximately equal to 0.3 for unconsolidated sands, and ranging between 0.8 to 1.0 for consolidated sandstones.

In the intervening years since the pioneering work of Archie (1952), many experimental investigations have been published describing measurements of the relationship between the formation factor and porosity for various types of reservoir rocks, including unconsolidated sands, consolidated/cemented sandstones, and unfractured carbonates (see e.g., Winsauer et al., 1952; Carothers, 1968; Wyllie and Gregory, 1953; Baker and Worthington, 1973; Jackson et al., 1978, Asquith, 1979; Waxman and Thomas, 1974). Survey articles have been published on this subject (Asquith, 1980; Hilchie, 1984), textbooks have summarized the pertinent results (Asquith and Gibson, 1982; Levorsen, 1967; Hilchie, 1982), and comprehensive reports have been issued by the oil service companies recommending guidelines for predicting formation factors in different reservoir lithologies (Welex, 1978; Schlumberger, 1984; Dresser Atlas, 1979). Moreover, for the case of reservoir sediments containing electrically-conductive clay and shale mineral fractions, reliable experimental methods have been established (Waxman and Smits, 1968; Clavier et al., 1984) for determining the "true" formation factor, characteristic solely of the pore microgeometry, from resistivity measurements. This development is particularly relevant in the present context, since it is this "true" formation factor that relates directly to the geometric correction factor G for diffusion.

The results of these extensive electrical resistivity investigations of reservoir sediments have enabled researchers to identify certain well-defined trends in behavior. Typically, for a given sediment, the measured variation in formation factor with porosity can be described over a fairly broad range of ϕ by means of the empirical Archie relationship, Equation 8 (in some cases modified by a constant multiplying-factor close to 1.0). The exponent "m" in Archie's expression (or, equivalently, the exponent "n" in Equation 9 for the geometric correction factor G) normally varies as a function of lithology, increasing with increasing constrictions and tortuosity of the pore channels. Thus, in the case of sands, for example, m rises from a value of 1.3 (n=0.3) for completely unconsolidated sediments, to 1.8 (n=0.8) for moderately cemented sands (Martin, 1953). For this reason, m and n are frequently referred to as "cementation exponents." Such terminology, however, is somewhat of a misnomer, since both m and n are also expected to increase with increasing plate-like character of the sediment particles (since increasing particle aspect-ratio typically gives rise to greater pore tortuosity).

Figure 6 presents a general summary of the extensive measurements on reservoir rocks (including the measurements of Archie, 1952), obtained using the Electrical Resistivity (ER) Method. Note that these findings have been reexpressed in terms of the geometric correction factor G for diffusion, using Equation 7. (Also shown in Figure 6 are results from laboratory measurements on clay sediments, to be described in detail below).

Separate ranges of behavior are indicated in Figure 6 for unconsolidated sands, consolidated/cemented sandstones, and unfractured carbonates. As suggested previously, observed differences between unconsolidated sands and consolidated sandstones are related to the degree of cementation in these deposits. Both types of sediments are comprised of essentially "spherical" sand granules. However, in a consolidated sandstone, the cementation process produces increased constrictions in the pore channels, and dead-end pores. These effects severely retard the overall rate of diffusion, and result in a lower value for the geometric correction factor G. Apparently, G is generally smaller for a consolidated particle matrix than for the equivalent unconsolidated packing.

Very few measurements have been carried out using the Electrical Resistivity (ER) Method to characterize the relationship between formation factor and porosity for clays and shales. This is unfortunate, since many of the aquitard layers used to restrict contaminant movement within the permitted injection zone at underground injection sites are comprised of such sediments, particularly in the Gulf Coast region.

Atkins and Smith (1961) measured formation resistivity factors for <u>slurries</u> of various clay minerals and mica particles in the laboratory, and found that the observed variations of F with porosity were described adequately by the Archie equation (Equation 8). The clay minerals tested included montmorillonite (Na and Ca), illite, kaolinite, and attapulgite. Unfortunately, the results of these measurements could not realistically be expected to provide accurate estimates of the "true" formation factors characteristic of pore microgeometry in actual clay-type geological deposits, for two reasons. First, no attempts were made to correct for the effects of clay surface electrical conductivity on the measured values of the formation factors. Secondly, the clay slurries were agitated immediately before resistivitity measurements were taken, thus disrupting any particle alignments that may have existed and virtually guaranteeing that the majority of the plate-like particles were not oriented perpendicular to the direction of electrical current flow. Both these effects would have resulted in significant underestimates of the true formation factor, and, by Equation 7, overestimates of the geometric correction factor G for diffusion. Therefore, Atkins and Smith's results are not applicable to oriented geological deposits such as clays and shales, and have been omitted from Figure 6. However, even with these rather severe restrictions, Atkins and Smith did find that, for the Na montmorillonite tested, the exponent m in Archie's relationship exceeded the rather large value of 3.0; equivalently, the exponent n in Equation 9 for G was greater than 2.0. According to Equation 9, the larger the value of the exponent n, the greater the reduction in the effective diffusion coefficient relative to free aqueous solution. The large values for m and n observed by Atkins and Smith for the montmorillonite slurries can be attributed to the highly plate-like character of the particles, which resulted in very tortuous conduction paths through the slurries, even though the particles were not aligned.

Jackson et al. (1978) investigated the effect of particle size and shape on the relationship between formation factor and porosity in simulated laboratory sediments comprised of sands and plate-like shell fragments. As in the previous studies, all the observations were adequately described by the Archie equation. The exponent m in Archie's expression was determined to be 1.85 for the shell fragments ($n = 0.85$ in Equation 9 for G). Unfortunately, in these experiments, the resistivity was measured in the direction <u>parallel</u> to the orientation of the fragments, rather than perpendicular. Thus the results are not applicable to conductive or diffusive transport vertically through beds of horizontally oriented plate-like particles (such as clays and shales), and they have therefore been omitted from Figure 6. If the resistivity measurements were made perpendicular to the direction of the particle orientation, the exponent m would almost certainly have been larger than 1.85.

The most definitive measurements to date of formation factors for clays of varying mineralogy were made by Atlan, et al. (1968). These experiments employed simulated laboratory core samples, comprised of kaolinites, illites, and montmorillonites. The results were corrected for the effects of clay surface electrical conductivity, using the well-known method of Waxman and Smits (1968). This enabled Atlan et al. to determine a value for the "true" formation factor for the sediments, characteristic solely of the clay pore-channel microgeometry.

The observed relationship between formation factor and porosity for each of the clay minerals tested was found to agree closely with the Archie equation. Values of the Archie exponent m as high as 5.4 were obtained for the case of the montmorillonite clay. This is equivalent to a value of n=4.4 in Equation 9 for the geometric correction factor G.

Figure 6 presents a plot of the results from this study, reexpressed in terms of G. Separate data ranges are shown for the various clays investigated. A salient feature of this plot is the much lower range of values obtained for G in the clay sediments, compared that found for the sands, sandstones, and carbonates comprising reservoir rocks. These much lower values can be attributed to the greater tortuosity of the pore channels, caused by alignment of the plate-like clay particles in the direction perpendicular to the flow of electrical current or diffusion.

For sediments consisting of illites and montmorillonites (as well as for kaolinites with porosities $\phi < 0.4$), all the data in Figure 6 fall below the reference line $G = \phi^2$. This result is particularly germane to the present situation, since shale and clay aquitard layers in the Gulf Coast region at the depths of underground injection operations are comprised primarily of illites and montmorillonites. Montmorillonites dominate at shallower depths, in relatively uncompacted sediments, whereas illites become a more prevalent component at greater depths. Therefore, the results in Figure 6 strongly suggest that **a conservative upper bound to the geometric correction factor for Gulf Coast clays and shales is provided by the expression:**

$$G \leq \phi^2 \qquad (10)$$

The validity of this bound is supported by a powerful body of additional evidence. This evidence is provided by the remarkable consistency that exists between the results obtained using the Dry Granular Packing (DGP) Method, the Plastic Barrier Film (PBF) Method, and the Electrical Resistivity (ER) Method. Figure 7 combines the data from all three of these markedly different measurement techniques into a single plot. The results for "spherical" particles determined using the Dry Granular Packing Method lie comfortably within the mid-range of results for unconsolidated sands (also consisting of basically "spherical" particles) obtained with the Electrical Resistivity Method. Similarly, the data on high-aspect-ratio plate-like particles (exhibiting shapes comparable to clay minerals) determined using both the Dry Granular Packing Method and the Plastic Barrier Film method are in excellent agreement with the results on illite and montmorillonite plate-like clay particle deposits, determined using the Electrical Resistivity Method. Moreover, virtually all these data sets on plate-like particles fall below the reference line $G \leq \phi^2$. Therefore, it is reasonable to expect that, for high-aspect-ratio plate-like sediments, such as Gulf Coast clays shales, comprised primarily of illites and montmorillonites, the relationship $G \leq \phi^2$ can be used as a conservative upper bound for estimating the geometric correction factor for molecular diffusion in no-migration demonstrations.

4.3 Summary and Conclusions

The rate of diffusion of a dissolved species through a water-saturated porous medium is always lower than in free aqueous solution. Complexities in pore channel microgeometry, resulting from constrictions and tortuosity, are responsible for this reduction in diffusion rate. The effects of pore channel complexities can be quantified in terms of a geometric correction factor G, which expresses the reduction in the effective diffusion coefficient, relative to the diffusivity value in free solution.

The geometric correction factor G is highly dependent upon the lithological characteristics of the porous medium. For unconsolidated beds of low-aspect-ratio "spherical" particles, such as an unconsolidated sand, the value will be relatively high, typically in the range 0.5 to 0.8 for porosities in the working range 0.1 to 0.5. However, for an equivalent consolidated/cemented "spherical" particle bed, such as a sandstone or unfractured carbonate, the geometric correction factor is significantly reduced as a result of the constrictions and dead end pores produced by the cementation process; typical values for G in such a bed could be expected to lie well below 0.5. Sediments consisting of high-aspect-ratio plate-like particles aligned with the bedding planes, such as clays and shales, are characterized by highly tortuous diffusion paths. This increase in tortousity, relative to the "spherical" particle case, will bring about an enormous reduction in the geometric correction factor, with values normally expected to range from 0.01 to 0.1 and below, for typical aquitard layer porosities less than 0.3.

Based on the considerable body of experimental data obtained using several distinctly different, but mutually consistent, measurement techniques, it has been possible to establish reasonable upper bounds to the geometric correction factor G as a function of porosity ϕ for various sediments. These upper bounds can be expressed in terms of an "Archie" type relationship, of the form $G \leq \phi^n$, where the exponent n depends on the sediment. Values of n for various specific sediments are presented in Table 1. The results in Table 1 for both sands and clays/shales are consistent with the relationships recently employed by Ranganathan and Hanor (1988). Values for the geometric correction factor determined using the present procedure will automatically produce overestimates of the extent of molecular diffusion in the porous medium.

According to the current molecular diffusion model, described by Equation 4, the diffusion distance for a contaminant species into the aquitard layer overlying the bulk waste plume is proportional to the square root of the effective diffusion coefficient D*. Since D* is equal to the diffusivity in free solution multiplied by the geometric correction factor, it follows that <u>the diffusion distance of a contaminant species into the overlying aquitard is equal to the diffusion distance for the species in free solution multiplied by the square root of the geometric correction factor G.</u>

Table 1

Upper Bounds To Geometric Correction Factor "G" For Various Sediments

Sediment Type	Exponent n	$G \leq \phi^n$
Unconsolidated sand	0.3	$G \leq \phi^{0.3}$
Consolidated sandstone	0.8	$G \leq \phi^{0.8}$
Tight unfractured limestones and dolomites	1.0	$G \leq \phi^{1.0}$
Gulf coast clays and shales	2.0	$G \leq \phi^{2.0}$

5.0 MARGINS OF SAFETY

A number of margins of safety are inherent in the present molecular diffusion model and in the recommended procedure for determination of the key input parameter, the effective diffusion coefficient D*, guarantee that the predicted diffusion distance is an overestimate of the true extent of vertical contaminant transport.

A. Concentration at z=0 Assumed Equal to the Waste Concentration for All Times

The conservativeness of this assumption was discussed in detail in Section 3.0 of this appendix.

B. Chemical Interactions With Aquitard Neglected

Chemical interactions with the aquitard material, resulting from phenomena such as adsorption, ion exchange, molecular hindrance, and osmosic membrane effects are neglected in the model. Such interactions have often been known to greatly attenuate or totally eliminate solute movement into typical clay and shale aquitard materials (Freeze and Cherry, 1979; Lerman, 1988; Neuzil, 1986; Wayman, 1967; Collins, 1961; Deen, 1987).

Adsorption is a process in which solute molecules or ions adhere to the surfaces of the particles within the aquitard layer. This greatly slows their rate of diffusional transport in the aquitard.

Ion Exchange occurs when contaminant cations (such as heavy metals) interchange places with other cations (non-contaminant) electrostatically bound to the surface of the aquitard particles. This partially immobilizes the contaminant cations, and greatly attenuates their diffusional transport rate.

Molecular hindrance occurs in porous media when the dimensions of the diffusing solute molecule or ion are on the same order as the dimensions of the pores (Deen, 1987; Lerman, 1988). This causes hydrodynamic frictional drag to develop between the diffusing molecule or ion and the walls of the pores, and results in reduced diffusion rate through the matrix. If the solute molecule is sufficiently large, it can be hindered from even entering.

Clays and shales are often known to behave as semipermeable membranes (Collins, 1961; Freeze and Cherry, 1979; Neglia, 1979; Neuzil, 1986), blocking the passage of ionic solutes, including contaminant ions, through the aquitard material. This ionic exclusion phenomenon is referred to as osmosis, and is believed to be an important process in sedimentary basins (Freeze and Cherry, 1979). The basic mechanism for this membrane behavior is typically ascribed to the effects of an unbalance in electrical charges on the surfaces and edges of the sediment particles. As explained in detail by Freeze and Cherry (1979),

> ...the net charge on the clay particles is negative. This results in the adsorption of a large number of hydrated cations onto the clay mineral surfaces. Owing to a much smaller number of positively charged sites on the edges of the clay particles and the local charge imbalance caused by the layer or layers of adsorbed cations, there is also some tendency for anions to be included in this microzone of ions and water molecules around the clay particles. The ability of compacted clays and shales to cause ...[osmosis] develops when clay particles are squeezed so close together that the adsorbed layers of ions and associated water molecules occupy much of the remaining pore space. Since cations are the dominant charged species in the adsorbed microzones around the clay particles, the relatively immobile fluid in the compressed pores develops a net positive charge. Therefore, ... cations in the solution are repelled.

The cationic species (e.g., heavy metal ions) in a waste are often the constituents responsible for its hazardous characteristics. The osmotic membrane phenomenon can prevent these constituents from even entering the overlying aquitard layer.

C. Horizontal Movement of Waste Neglected

The model assumes that the waste plume is not moving horizontally after injection is discontinued, and that, at a given lateral location, the base of the overlying aquitard layer is in contact with the waste for 10,000 years. If a small horizontal velocity exists within the injection zone, driven by the action of natural gradients or buoyancy effects (density differences between the waste and the formation brine) in a dipping formation, the contact time of the waste with the overlying aquitard at a given lateral location can be substantially less than 10,000 years. This will reduce the amount of contaminant that can diffuse into the aquitard at a given lateral location, and will decrease the contaminant concentration in the aquitard.

D. Waste Assumed No More Dense than Formation Brine

If the waste is heavier than the formation brine, it will tend to sink within the injection zone, and eventually lose contact with the overlying aquitard layer. This will reduce the contact time of the waste with the aquitard to less than 10,000 years, which will decrease both the contaminant concentration within the aquitard as well as the vertical extent of diffusional transport.

If the waste is lighter than the formation brine, it will remain in contact with the overlying aquitard for the full 10,000 years, and, thus, the vertical distance for diffusional transport will be the same as with a neutrally buoyant waste.

E. Effective Diffusion Coefficient Determined Conservatively

The procedure for establishing a conservative upper bound for the effective diffusion coefficient of a contaminant species within the water-saturated porous matrix of the overlying aquitard layer is described in detail in Section 4.0.

F. Chemical Destruction of Contaminants is Neglected

The model neglects the chemical destruction of the contaminant constituents diffusing into the overlying aquitard layer. If these constituents decompose with time, exhibiting a half-life even as long as 3,000 years, the buildup of contaminant concentrations in the overlying aquitard will be significantly reduced. This will also translate into a substantial reduction in the extent of vertical movement after 10,000 years.

6.0 SAMPLE CALCULATION

The following sample calculation is provided to illustrate the present methodology:

Problem Statement

A contaminant species is diffusing into a shale aquitard layer overlying a sandstone injection stratum in the Texas Gulf Coast region. From health-based standards, it has been determined that the contaminant concentration would have to be reduced by a factor of a million (i.e., relative concentration $C=10^{-6}$) in order to be considered non-hazardous. The diffusion coefficient for the species in free aqueous solution, at a temperature corresponding to the depth of injection, has been determined, using the method of Wilke and Chang (1955), to be $3X10^{-5}$ cm^2/sec. The porosity of the shale is 0.15. Obtain a conservative, upper bound estimate of the diffusion distance into the aquitard layer after 10,000 years.

Solution

From Figure 3, the dimensionless vertical diffusion distance required to produce a relative concentration of 10^{-6} is found to be 3.45:

$$\frac{z}{2\sqrt{D*t}}=3.45$$

This translates into an actual (dimensional) vertical diffusion distance of:

$$z = 6.9 \sqrt{D*t}$$

For Gulf Coast shales, a conservative estimate of the geometric correction factor G for contaminant diffusion through the water-saturated porous matrix is given by the relationship $G \leq \phi^2$. In the present case of $\phi = 0.15$, this results in an upper bound of 0.0225 for G. Since the diffusivity in free solution is $3X10^{-5}$ cm^2/sec, the effective diffusion coefficient in the porous shale medium is:

$$D^* \leq 3 \times 10^{-5} \times (0.0225) = 6.75 \times 10^{-7}\ cm^2/sec$$

Substituting this value for D* into the equation given above for z, and using a value of 10,000 year (= 3.16×10^{11} sec) for t yields:

$$z \le 6.9\sqrt{\left(6.75\times10^{-7}\right)\times\left(3.16\times10^{11}\right)}$$

$$\le 3190\,\text{cm}$$

$$\le 105\ \text{ft}$$

Thus, the diffusion distance into the overlying aquitard layer after 10,000 years is predicted to be no greater than 105 feet.

REFERENCES

Archie, G.E., The Electrical Resistivity Log as an Aid in Determining Some Reservoir Characteristics, American Institute of Mechanical Engineers Transactions, 146, 54-61, 1952.

Arina, M., Honkanen, A., and Tammela, V., Mineral Fillers in Low Density Polyethylene Films, Polymer Engineering and Science, 19, 30-39, 1979.

Asquith, G.B., Subsurface Carbonate Depositional Models-A Concise Review, PennWell, Tulsa, 1979.

Asquith, G.B., Log Analysis by Microcomputer, PennWell, Tulsa, 1980.

Asquith, G.B., and Gibson, C.R., Basic Well Log Analysis for Geologists, American Association of Petroleum Geologists, Methods in Exploration Series, Tulsa, 1982.

Atkins, E.R., and Smith, G.H., The Significance of Particle Shape in Formation Resistivity Factor-Porosity Relationships, Journal of Petroleum Technology, 13, 285-291, 1961.

Atlan, A., Bardon, C., Minssieux, L., Quint, M., and Delvaux, P., Conductivite en Milieux Poreux Argileux - Interpretation Des Diagraphies, in Comptes Rendus du Troisieme Colloque, Association de Recherche sur les Techniques de Forage et de Production, held September 23-26, 1968, 615-642, 1968.

Baker, R.D., and Worthington, P.F., Some Hydrogeophysical Properties of the Bunter Sandstone of Northwest England, Geoexploration, 11, 151-170. 1973.

Bear, J., Dynamics of Fluids in Porous Media, Elsevier, New York, 1972.

Bird, R.B., Stewart, W.E., and Lightfoot, E.N., Transport Phenomena, Wiley, New York, 1960.

Bissot, T.C., Effect of Platelet Type Fillers on Oxygen Permeability of Ethylene Vinyl Alcohol Resins, E. I. Du Pont De Nemours, Inc., Polymer Products Department, private communication, 1988a.

Bissot, T.C., Effect of Platelet Type Fillers on Water Vapor Permeability of Polyproplyene Resins, E. I. Du Pont De Nemours, Inc., Polymer Products Department, private communication, 1988b.

Buckingham, E., Contributions to our Knowledge of the Aeration of Soils, USDA Bureau of Soils, Bulletin No. 25, 1904.

Burger, H.C., Das Leitvermogen Verdunnter Mischkristallfreier Legierungen, Physikalische Zeitschrift, 20, 73-75, 1919.

Carothers, J.C., A Statistical Study of the Formation Factor Relation to Porosity, The Log Analyst, 9, 38-52, 1968.

Cherry, J.A., Desaulniers, D.E., Frind, E.O., Fritz, P., and Gevaert, D.M., Hydrogeologic Properties and Pore Water Origin and Age: Clayey Till and Clay in South Central Canada, Proceedings of Workshop on Low-Flow, Low-Permeability Measurements in Largely Impermeable Rocks, OECD, Paris, 30-47, 1979.

Clavier, C., Coates, G., and Dumanoir, J., Theoretical and Experimental Bases for the Dual-Water Model for Interpretation of Shaly Sands, Society of Petroleum Engineers Journal, 24, 153-168, 1984.

Collins, R.E., Flow of Fluids Through Porous Materials, PennWell, Tulsa, Oklahoma, 1961.

Currie, J.A., Gaseous Diffusion in Porous Media. Part 2.--Dry Granular Materials, British Journal of Applied Physics, 11, 318-324, 1960.

Cussler, E.L., Hughes, S.E., Ward, W.J. III, and Aris, R., Barrier Membranes, Journal of Membrane Science, 38, 161-174, 1988.

Deen, W.M., Hindered Transport of Large Molecules in Liquid-Filled Pores, AIChE Journal, 33, 9, 1409-1425, 1987.

De Kee, D., and Laudie, H., Diffusivities of Nonelectrolytes in Water at Atmospheric Pressure, Chemical Engineering, 80, 29, 74-75, 1973.

Desaulniers, D.E., Cherry, J.A., and Fritz, P., Origin, Age and Movement of Pore Water in Argillaceous Quaternary Deposits at Four Sites in Southwestern Ontario, Journal of Hydrology, 50, 231-267, 1981.

Desaulniers, D.E., Cherry, J.A., and Fritz, P., Origin, Age and Movement of Pore Water in Clayey Pleistocene Deposits in South Central Canada, in Isotope Studies of Hydrologic Processes, Perry, E.C. Jr., and Montgomery, C.W. (Eds.), Northern Illinois University Press, DeKalb, Illinois, 45-55, 1982.

Desaulniers, D.E., Cherry, J.A., and Gillham, R.W., La Migration Des Solutes a Long Terme dans un Depot Argileux Epais du Quaternaire, in Proceedings of the Canadian Hydrology Symposium No. 15 - 1984, Volume II, University Laval, Quebec, June 10-12, 1984, 528-537, 1984.

Desaulniers, D.E., Kaufmann, R.S., Cherry, J.A., and Bentley, H.W., ^{37}Cl-^{35}Cl Variations in a Diffusion-Controlled Groundwater System, Geochimica et Cosmochimica Acta, 50, 1757-1764, 1986.

Desaulniers, D.E., Bradbury, K.R., and Cherry, J.A., Groundwater origin, age and the Long-Term Solute Migration in the Thick Clayey Tills of Northwestern Wisconsin, Submitted to Ground Water, 1987.

Desaulniers, D.E., and Cherry, J.A., Origin and Movement of Groundwater and Major Ions in a Thick Deposit of Champlain Sea Clay Near Montreal, Submitted to Canadian Geotechnical Journal, 1988.

De Vries, D.A., Some Remarks on Gaseous Diffusion in Soils, Transactions Fourth International Congress Soil Science, II, 41-43, 1950.

De Vries, D.A., Het Warmtegeleidingsvermogen van Grond, Meded. Landbouwhogesch. Wageningen, 52, 1, 1952.

Dresser Atlas, Log Interpretation Charts, Dresser Industries, Houston, 1979.

Freeze, A.R., and Cherry, J.A., Groundwater, Prentice-Hall, Englewood Cliffs, New Jersey, 1979.

Fried, J.J., Developments in Water Science, Elsevier, New York, 1975.

Gillham, R.A., and Cherry, J.A., Contaminant Migration in Saturated Unconsolidated Geologic Deposits, In Recent Trends in Hydrogeology, Narasimhan, T.N. (Ed), Geological Society of America, Special Publication 189, Boulder, Colorado, 31-62, 1982.

Greenkorn, R.A., Steady Flow through Porous Media, AIChE Journal, 27, 4, 529-545, 1981.

Hashim, Z., and Shtrikman, S., A Variational Approach to the Theory of Effective Magnetic Permeability of Multiphase Materials, Journal of Applied Physics, 33, 3125-3131, 1962.

Hilchie, D.W., Advanced Well Log Interpretation, D.W. Hilchie, Golden, Colorado, 1982.

Hilchie, D.W., Reservoir Description Using Well Logs, Journal of Petroleum Technology, 36, 1067-1073, 1984.

Hoogschagen, J., Diffusion in Porous Catalysts and Adsorbents, Industrial and Engineering Chemistry, 47, 906-913, 1955.

Horvath, A.L., Handbook of Aqueous Electrolyte Solutions, Physical Properties, Estimation, and Correlation Methods, Halsted Press, New York, 1985.

Huyakorn, P.S., and Pinder, G.F., Computational Methods in Subsurface Flow, Academic, Harcourt Brace, New York, 1983.

Intercomp Resource Development and Engineering, Inc., A Model for Calculating Effects of Liquid Waste Disposal in Deep Saline Aquifers...Part I--Development, Part II--Documentation, USGS/WRD/WRI-76/056, USGS, Reston, Virginia, 1976.

Jackson, P.D., Taylor Smith, D., and Stanford, P.N., Resistivity-Porosity-Particle Shape Relationships for Marine Sands, Geophysics, 43, 6, 1250-1268, 1978.

Javandel, I., Doughty, C., and Tsang, C.F., Groundwater Transport: Handbook of Mathematical Models, American Geophysical Union, Washington, D.C., 1984.

Johnson, P.A., and Babb, A.L., Liquid Diffusion in Non-Electrolytes, Chemical Reviews, 56, 387-453, 1956.

Kamal, M.R., Jinnah, I.A., and Utracki, L.A., Permeability of Oxygen and Water Vapor Through Polyethylene/Polyamide Films, Polymer Engineering and Science, 24, 1337-1346, 1984.

Kim, J.H., Ochoa, J.A., and Whitaker, S., Diffusion in Anisotropic Porous Media, Transport in Porous Media, 2, 327-356, 1987.

Lerman, A., Geochemical Processes Water and Sediment Environments, Krieger, Malabar, Florida, 1988.

Levorsen, A.I., Geology of Petroleum, Freeman, San Francisco, 1967.

Leythaeuser, D., Schaefer, R.G., and Yukler, A., Diffusion of Light Hydrocarbons Through Near-Surface Rocks, Nature, 284, 10, 522-525, 1980.

Leythaeuser, D., Schaefer, R.G., and Yukler, A., Role of Diffusion in Primary Migration of Hydrocarbons, American Association of Petroleum Geologists Bulletin, 66, 408-429, 1982.

Li, J.C.M., and Chang, P., Journal of Chemical Physics, 23, 518-520, 1955.

Lobo, V.M.M., Electrolyte Solutions: Literature Data on Thermodynamic and Transport Properties, Vols. I - III, Coimbra University Press, Coimbra, Portugal, 1984.

Manheim, F.T., The Diffusion of Ions in Unconsolidated Sediments, Earth and Planetary Science Letters, 9, 307-309, 1970.

Manheim, F.T., and Waterman, L.S., Diffusimetry (Diffusion Constant Estimation) on Sediment Cores by Resistivity Probe, in Initial Reports of the Deep Sea Drilling Project, Vol. 22, U.S. Government Printing Office, Washington, D.C., 663-670, 1974.

Martin, R.I., Resistivity of Water-Saturated Porous Formation, Oil and Gas Journal, 52, 8, 111, 1953.

Maxwell, J.C., Treatise on Electricity and Magnetism, I, 2nd. edn., Clarendon, Oxford, 1881.

Modern Plastics Encyclopedia/88, Juran, R. (Ed.), Mc Graw Hill, New York, 1988.

Murthy, N.S., Kotliar, A.M., Sibilia, J.P., and Sacks, W., Structure and Properties of Talc-Filled Polyethylene and Nylon 6 Films, Journal of Applied Polymer Science, 31, 2569-2582, 1986.

Neglia, S., Migration of Fluids in Sedimentary Basins, American Association of Petroleum Geologists Bulletin, 63, 573-597, 1979.

Nernst, W., Zur Kinetik der in L^sung befindlichen K^rper, Zeitschrift Physic. Chem., 2, 613-637, 1888.

Neuzil, C.E., Groundwater Flow in Low-Permeability Environments, Water Resources Research, 22, 8, 1163-1195, 1986.

Othmer, D.F., and Thakar, M.S., Correlating Diffusion Coefficients in Liquids, Industrial and Engineering Chemistry, 45, 589-593, 1953.

Penman, H.L., Gas and Vapor Movements in the Soil. 1. The Diffusion of Vapor Through Porous Solids, Journal Agricultural Science, 30, 437-462, 1940.

Perry, R.H., and Chilton, C.H., (Eds), Chemical Engineers' Handbook, 5th Edition, McGraw-Hill, New York, 1973.

Plastics, Edition 7, Thermoplastics and Thermosets, Desk-top Data Bank, Cordura Publications, San Diego, 1985.

Quigley, R.M., Gwyn, Q.H.J., White, O.L., Rowe, R.K., Haynes, J.E., and Bohdanowicz, A., Leda Clay from Deep Boreholes at Hawkesbury, Ontario, Part I, Geology and Geotechnique, Canadian Geotechnical Journal, 20, 228-298, 1983.

Ranganathan, V., and Hanor, J.S., Density-Driven Groundwater Flow Near Salt Domes, Chemical Geology, 74, 173-188, 1988.

Reid, R.C., and Sherwood, T.K., The Properties of Gases and Liquids, McGraw-Hill, New York, 1958.

Ryan, D., The Theoretical Determination of Effective Diffusivities for Reactive, Spatially Periodic, Porous Media, MS thesis, Department of Chemical Engineering, University of California at Davis, 1984.

Schlumberger, Log Interpretation Charts, Schlumberger Well Services, Houston, 1984.

Treybal, R.E., Mass-Transfer Operations, McGraw-Hill, New York, 1955.

Walton, W.C., Practical Aspects of Groundwater Modeling, National Water Well Association, Worthington, Ohio, 1985.

Waxman, M.H., and Smits, L.J.M., Electrical Conductivities in Oil-Bearing Shaly Sands, Society of Petroleum Engineers Journal, 8, 107-122, 1968.

Waxman, M.H., and Thomas, E.C., Electrical Conductivities in Shaly Sands - I. The Relation Between Hydrocarbon Saturation and Resistivity Index; II. The Temperature Coefficient of Electrical Resistivity, Journal of Petroleum Technology, 26, 213-225, 1974.

Wayman, C.H., Adsorption on Clay Mineral Surfaces, in Principles and Applications of Water Chemistry, Faust, S.D., and Hunter, J.V. (Eds.), Wiley, New York, 127-167, 1967.

Weissberg, H.L., Effective Diffusion Coefficients in Porous Media, Journal of Applied Physics, 34, 2636-2639, 1963.

Welex, An Introduction to Well Log Analysis, Halliburton, Houston, 1978.

Wilke, C.R., Estimation of Liquid Diffusion Coefficients, Chemical Engineering Progress, 45, 218-224, 1949.

Wilke, C.R., and Chang, P., Correlation of Diffusion Coefficients in Dilute Solutions, AIChE Journal, 1, 264-270, 1955.

Winsauer, W.O., Shearin, H.M. Jr., Masson, P.H., and Williams, M., Resistivity of Brine-Saturated Sands in Relation to Pore Geometry, American Association of Petroleum Geologists Bulletin, 36, 253-277, 1952.

Wyllie, M.R., and Gregory, A.R., Formation Factors of Unconsolidated Porous Media: Influence of Particle Shape and Effect of Cementation, Transactions American Institute of Mining Engineers, 198, 103-110, 1953.

FIGURES

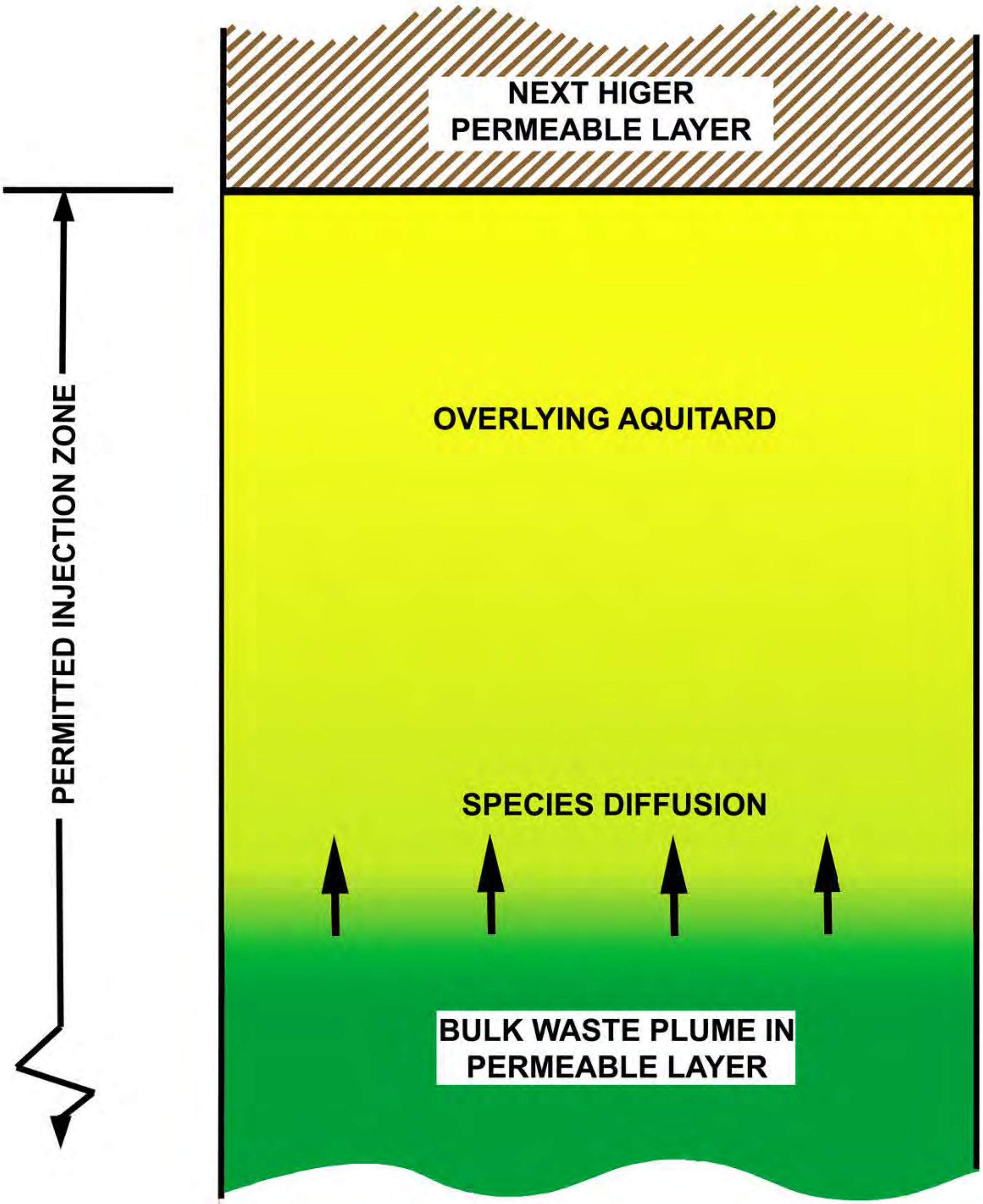

Figure 1: Diffusion Into Overlying Aquitard.

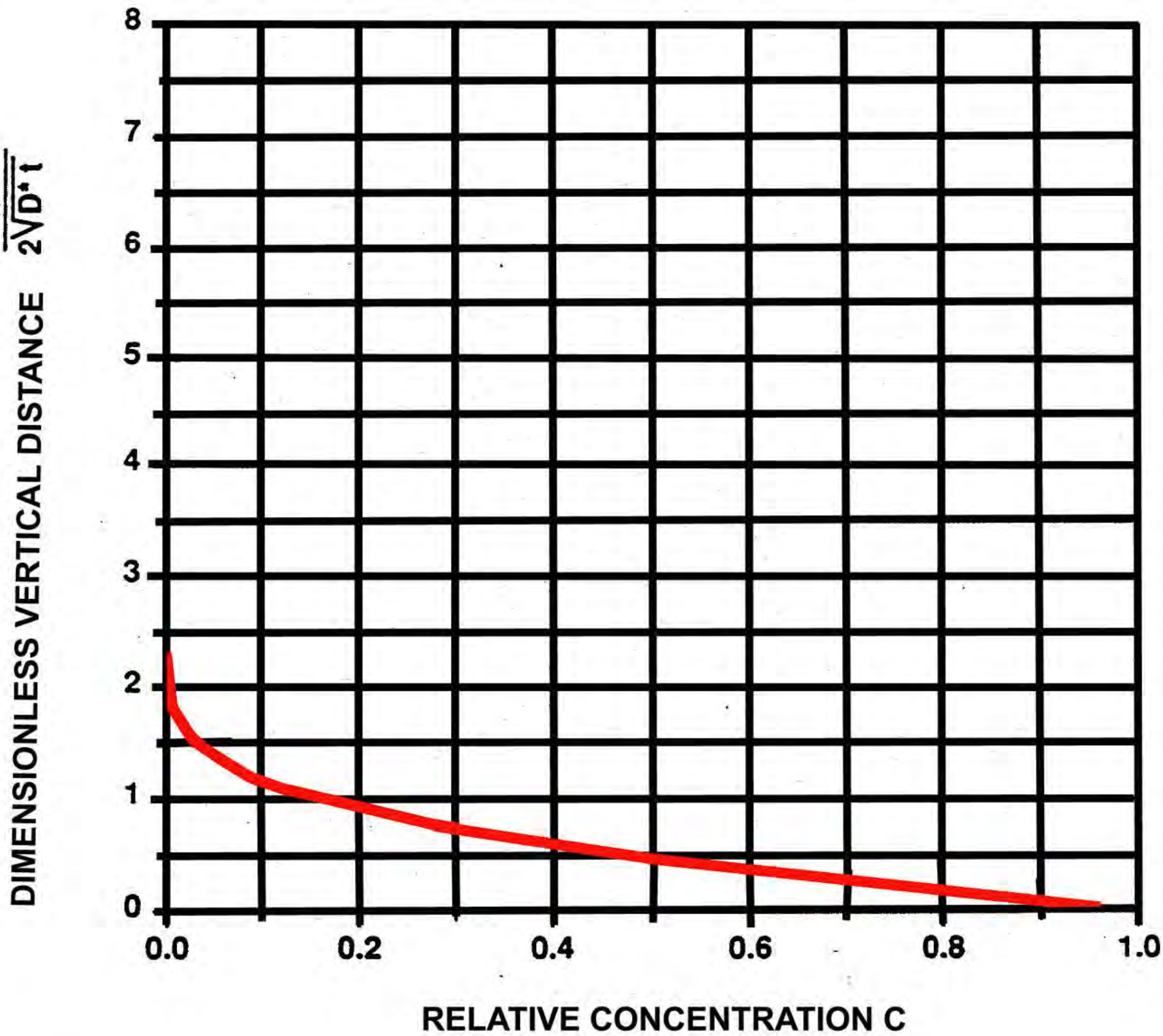

Figure 2: Predicted Concentration Profile.

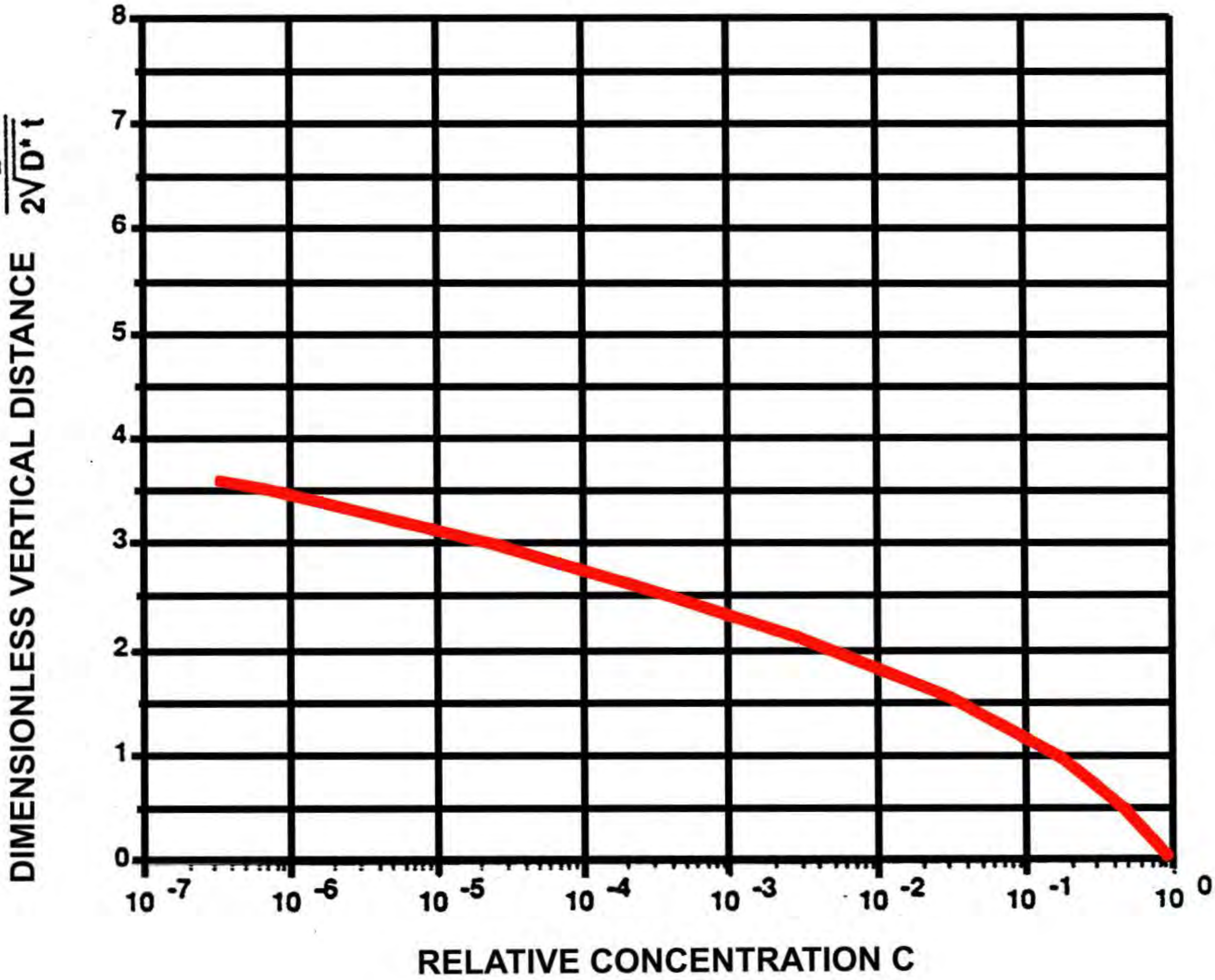

Figure 3: Predicted Concentration Profile (Logarithmic Plot).

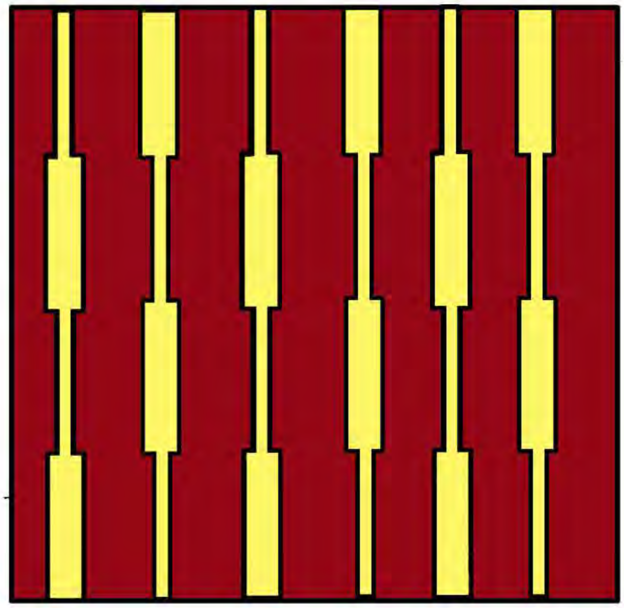

$$\text{FACTOR} = \frac{\text{HARMONIC MEAN AREA}}{\text{ARITHMETIC MEAN AREA}}$$

FIG. 4a CONSTRUCTION EFFECT

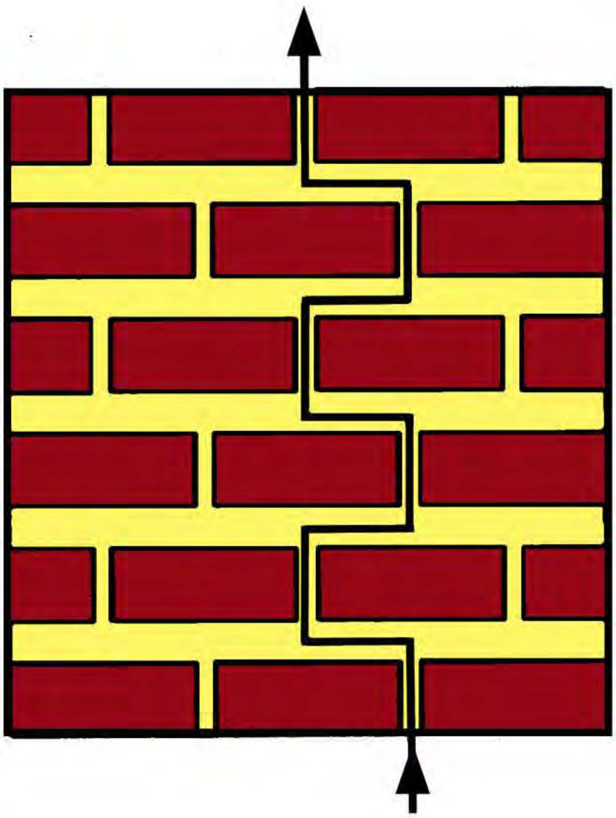

$$\text{FACTOR} = \left[\frac{\text{DIRECT LENGTH}}{\text{TORTUOUS LENGTH}}\right]^2$$

FIG. 4b TORTUOSITY EFFECT

Figure 4: Geometric Correction Factor : Theory.

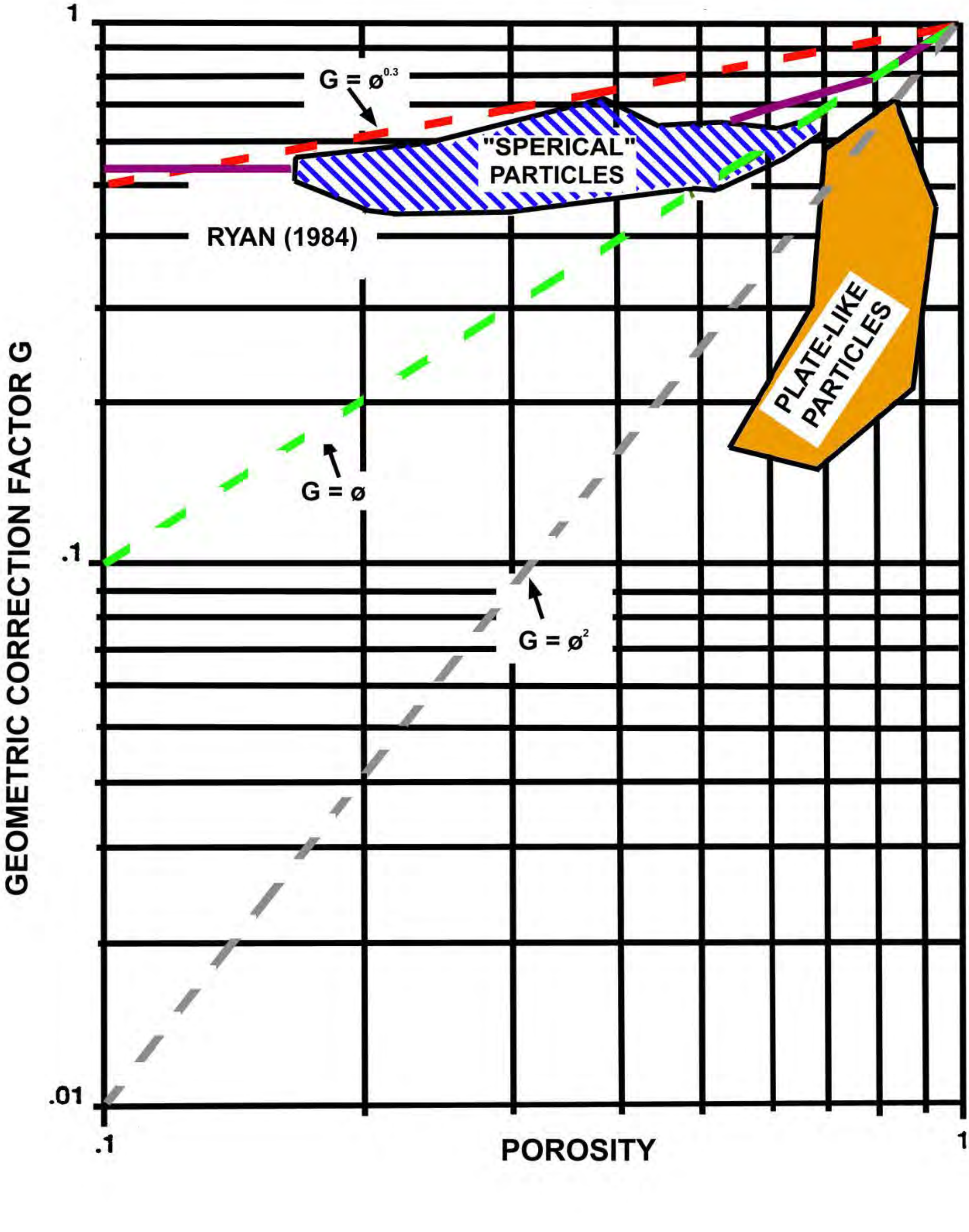

Figure 5: Dry Granular Packing Methods Results.

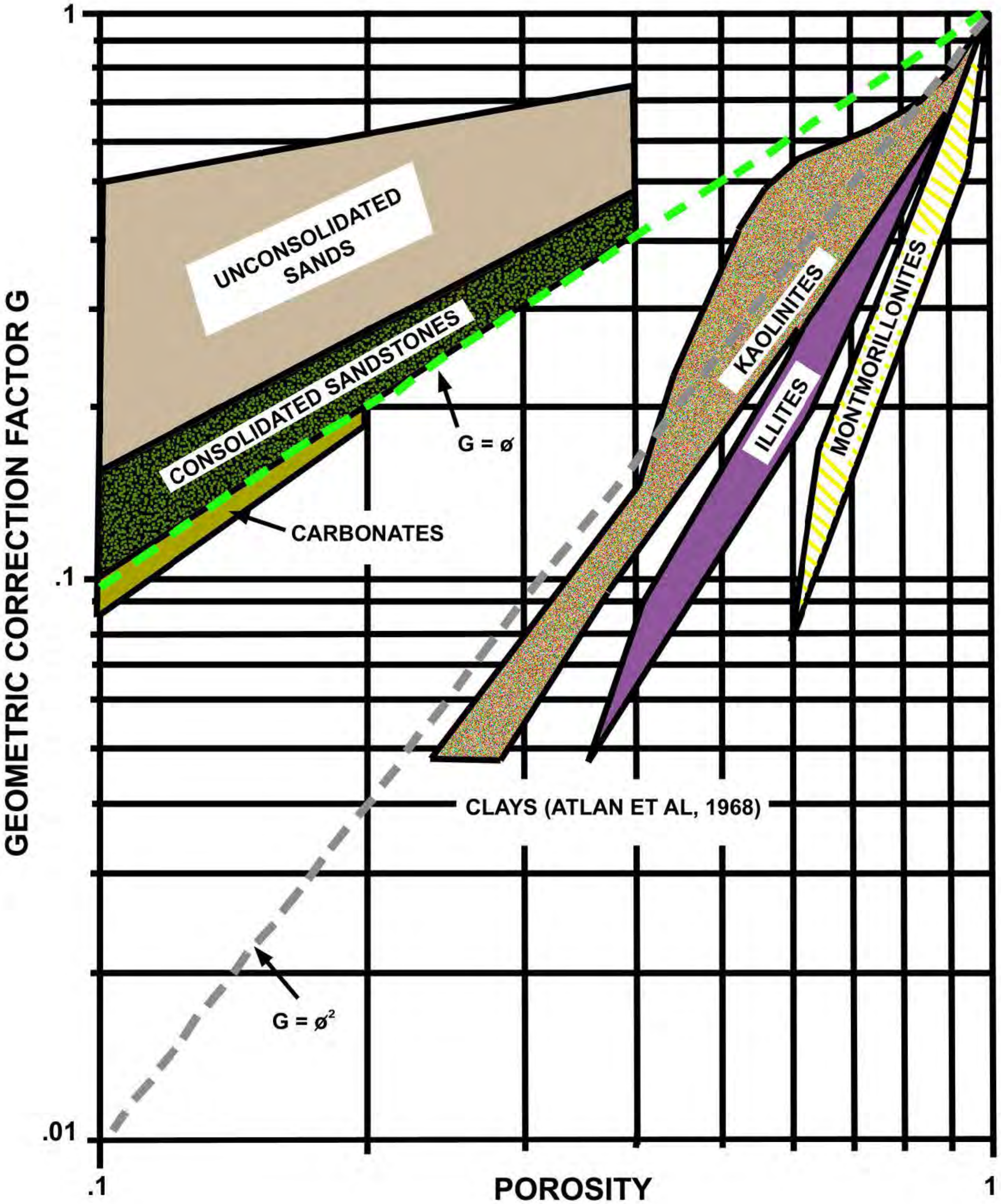

Figure 6: Electrical Resistivity Method Results.

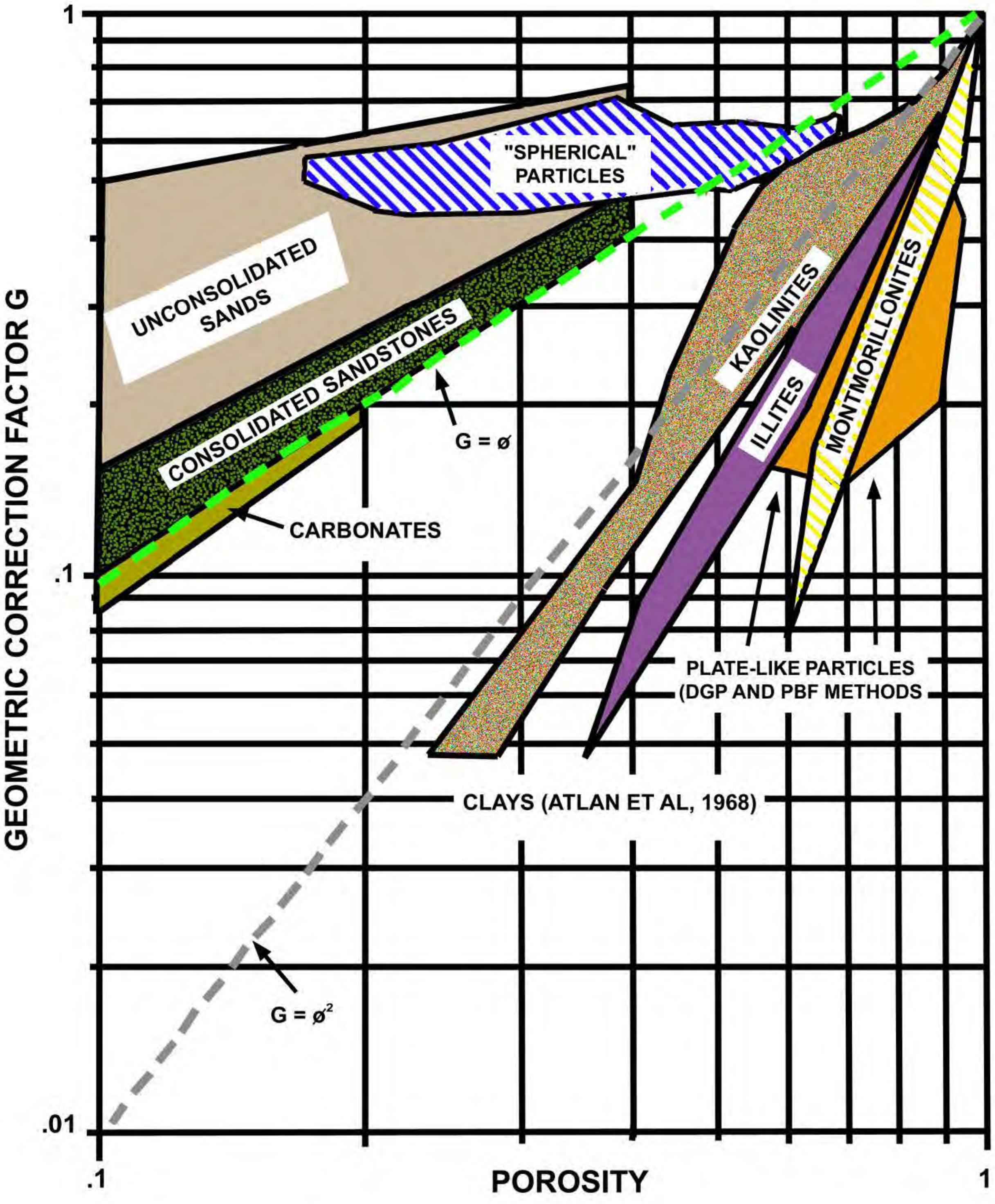

Figure 7: Overall Combined Results.

APPENDIX 3-4
FLUID VISCOSITY GRAPHS

BLANK

Drawing No.: FIG 1-2 Fig1-2.cdr
Date: 8-9-99
Job No.: 99-175.03

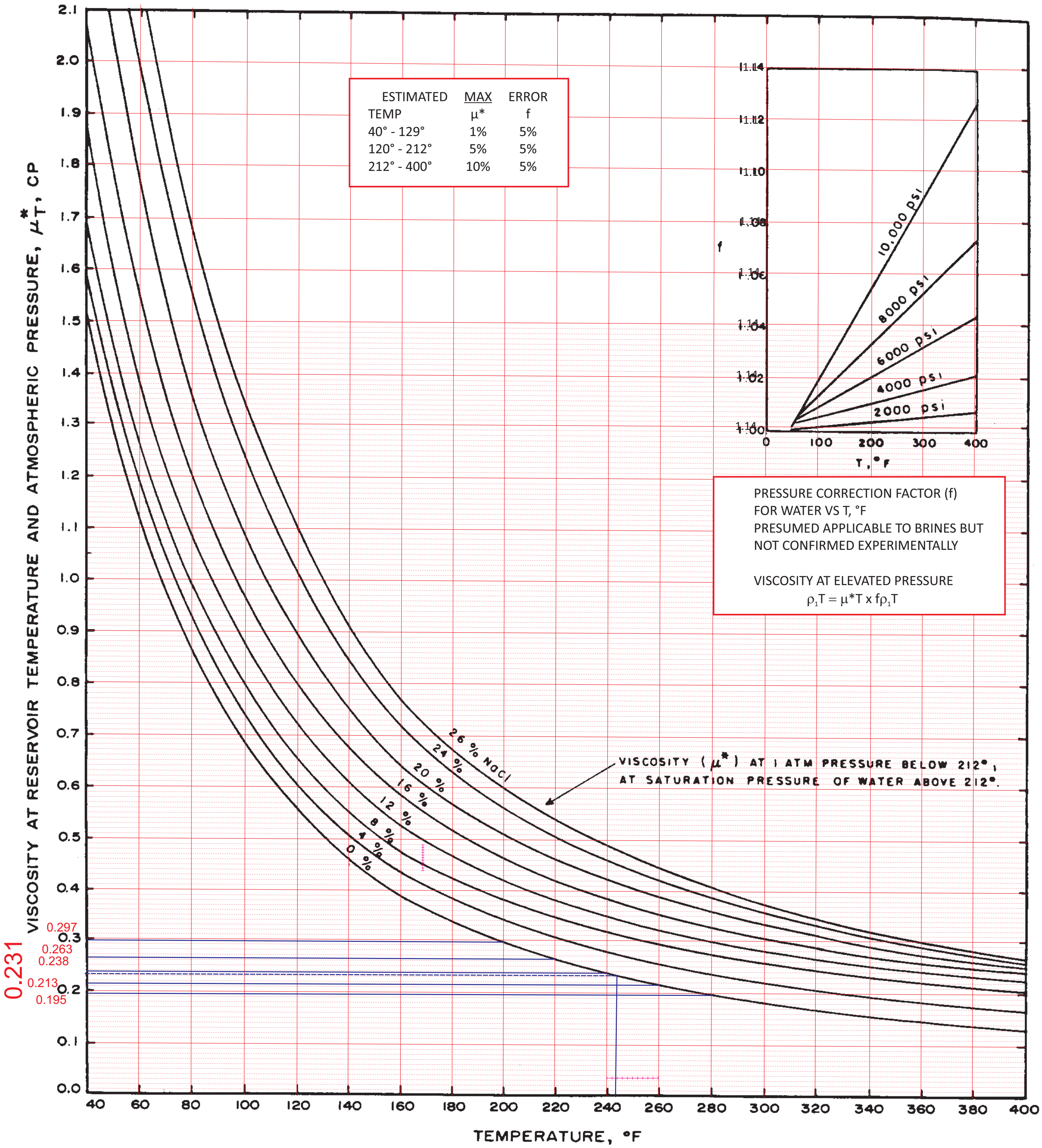

FRESHWATER VISCOSITY
(LIGHT DENSITY INJECTION FLUID)

Drawn By: tdm
Designed By: TDM
Checked By: TDM

Fig. D.35 Water viscosity at various salinities and temperatures After Mathews and Russell, data of Chesnut

Drawing No.: FIG 1-2 Fig1-2.cdr
Date: 8-9-99
Job No.: 99-175.03

Drawn By: tdm
Designed By: TDM
Checked By: TDM

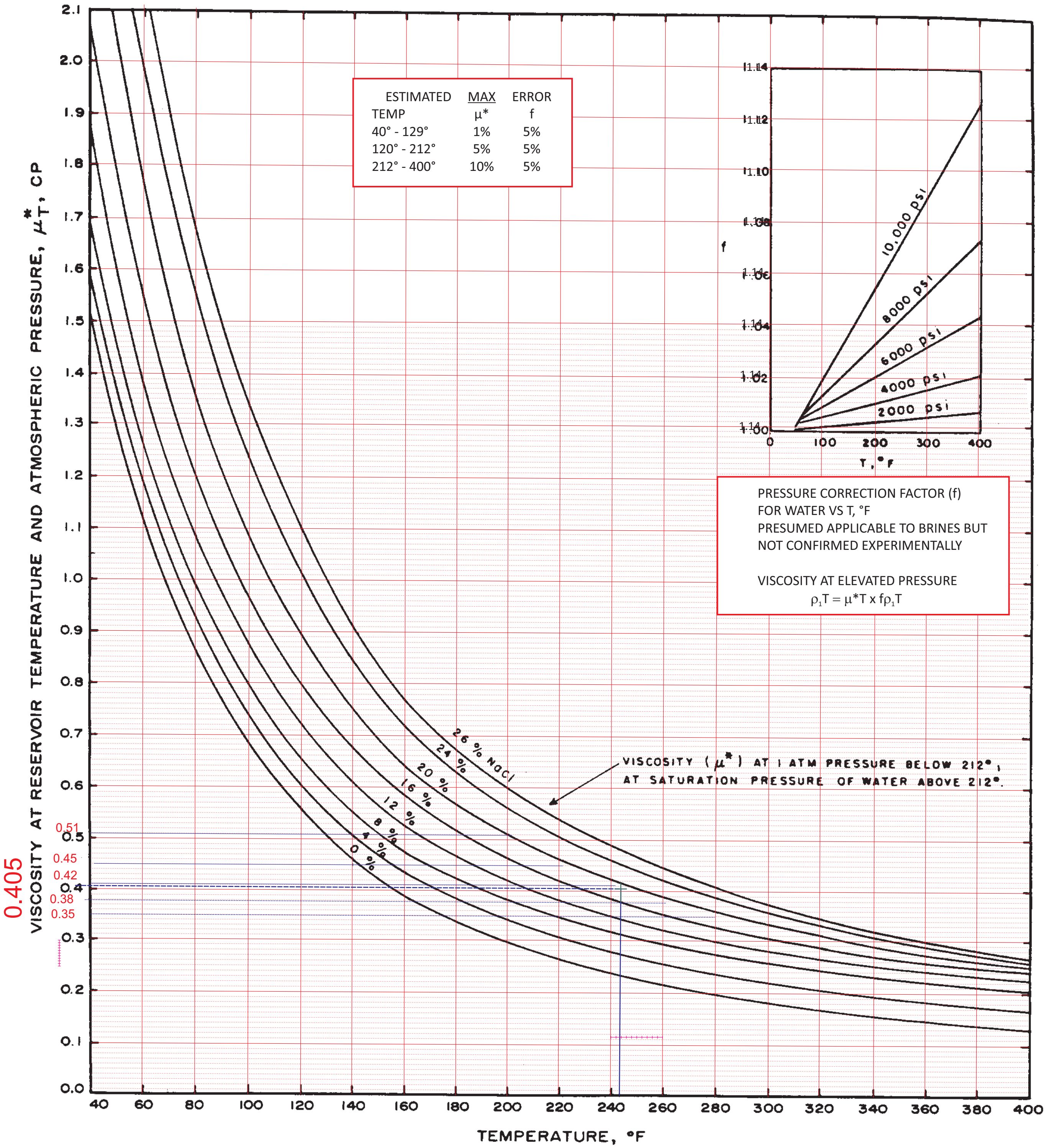

RESERVOIR BRINE VISCOSITY

Fig. D.35 Water viscosity at various salinities and temperatures After Mathews and Russell, data of Chesnut

APPENDIX 3-5
GROUNDWATER FLOW IN DEEP SALINE AQUIFERS (CLARK, 1988)

GROUNDWATER FLOW IN DEEP SALINE AQUIFERS

James E. Clark

E. I. du Pont de Nemours & Co.
P. O. Box 3269
Beaumont, Texas 77704

ABSTRACT

Natural horizontal groundwater flow rates in deep saline aquifers are less than those for shallower freshwater aquifers. Deep saline aquifers have natural groundwater movement measured in inches per year compared to feet per year for shallower freshwater systems. Therefore, the deeper units contain water that is highly mineralized and exhibit a sluggish circulation system compared to the shallow formations. In general, groundwater flow in the deeper saline aquifers is a function of lower permeability of the sand units rather than hydraulic gradients. The preparation of horizontal flow maps for deep saline aquifers can be difficult due to the limited database. This limitation is both in number of data points and quality of the reservoir pressure measurement.

Confining-layer studies in the Gulf Coast indicate that the vertical flow migration rate for these deep saline aquifers to be on the order of 1 foot in 10,000 years. Typical Gulf Coast shale permeabilities were measured under formation pressure, temperature, and salinity. The results indicate shale permeabilities of 10^{-5} to 10^{-6} md. Case histories using geophysical logs, formation tester tools, laboratory simulation of downhole conditions, and actual monitoring illustrate the effectiveness of confining units to restrict vertical flow, both in the Gulf Coast and in a carbonate sequence near Louisville, Kentucky.

Underground Injection Control Program

Subsurface waste disposal operators must demonstrate that there will be no migration of hazardous constituents from the disposal unit or injection zone for as long as the wastes remain hazardous (Hazardous and Solid Waste Amendments of 1984). EPA (1987) has stated that a 10,000 year residence time in the injection zone would be sufficient to render any waste non-hazardous. Currently, an injection well operator must demonstrate that injected fluids will not migrate within the injection zone to a point of discharge over a time span of 10,000 years.

Safe operating well practices such as mechanical integrity, proper well design and compatibility, and suitable injection well siting criteria are necessary to ensure that wastes are injected into the intended disposal formation. Adequate injection well siting criteria include absence of the following: 1) solution collapse features, 2) transmissive faults and joints, 3) improperly plugged abandoned wells that would permit escape of injected wastewaters from the injection interval, and 4) complex geologic structures that cannot be assessed. After injection is terminated, and the pressures needed to achieve injection have dissipated, the injected fluids move at the same rate as the natural brines within a few years (EPA, 1987).

Groundwater Flow

Groundwater flow movement can be predicted using Darcy's law. In 1856 Darcy experimented with the flow of water through sand columns and determined that the flux of water through sand is directly proportional to the hydraulic gradient, which is the difference in head in feet between two points, divided by the distance in feet between them. Darcy's law can be written as:

$$v = -K\, dh/dl \qquad \text{(Equation 1)}$$

where: v = specific discharge

K = hydraulic conductivity

dh = change in hydraulic head

dl = distance between head measurements

By dividing the specific discharge (v) by the porosity (Θ) of the zone of interest we can obtain the average movement (V), seepage velocity, of groundwater through the porous media. The flow of groundwater does depend on many factors including the geologic structure, boundaries, and the recharge/discharge areas. Groundwater is continually in motion from natural and man-made influences;

it flows mainly under the influence of gravity from levels of higher potential energy to levels of lower potential.

Experimental and theoretical evidence (Freeze and Cherry, 1979) show that water can be induced to flow (coupled) through a porous media under the influence of gradients other than the most important one, hydraulic head. The presence of a temperature gradient can cause groundwater to move even if a hydraulic gradient does not exist. Also, chemical gradients can cause the movement of chemical constituents through the water from regions where water has higher salinity to regions where it has lower salinity. Temperature and chemical parameters can be useful indicators in determining if groundwater is flowing from other reservoirs. Temperature has been used by investigators (Smith et al., 1982; Everett, 1986) to indicate potential upwelling of deeper, warmer waters. Smith et al. (1982), using groundwater temperatures within the Oakville aquifer in south Texas, illustrated the effect of relative transmissivity differences within the aquifer and the possibility of leakage of deeper, warmer waters along fault zones. This practical method has usage in the deeper saline aquifers to determine local anomalies in the regional groundwater flow where head data is lacking. Temperature profiles can be a very useful tool in determining fluid movement. In fact, temperature profiles are routinely logged in injection wells to determine if upward fluid movement is occurring.

An increase in total dissolved solids (TDS) was also used by Smith et al. (1982) to show that slower rates of groundwater movement reflect zones of lower permeability and longer residence time. Warner et al. (1986) suggested that geochemical criteria provide an inexpensive method to determine the degree of local and regional confinement of various geologic units. The chloride ion is the most useful indicator of cross-formational movement of fluids. In general, the chloride concentration increases with depth and is not normally affected by ion exchange nor by precipitation of minerals.

LeGrand (1962), in a study relating to the disposal of radioactive wastes in the Atlantic and Gulf Coastal plains, reported on two important features of the Cretaceous and Tertiary age deposits. Individual formations are finer grained and less permeable toward the coast; therefore, most sand beds become finer grained and grade into clay or silt downdip or seaward. The second important factor is the tendency of the permeability and storage capacity of the sediments to decrease with increased depth due to the weight of the overlying sediments which compact and squeeze water out of the system, forcing it upward. Pore space decreases and some sediments may become indurated into relatively dense rock. Generally, clays below 2000 feet become shaly, and sediments below 3000 feet are less permeable than those of the unconsolidated, more shallow formations.

A detailed study of groundwater flow near Cypress Creek and Richton Salt Domes, Mississippi, conducted by the Bentley (1983) confirmed LeGrand's statement that permeability decreases with depth. Table 1 shows that the dominant variable controlling groundwater flow is permeability (K) of the sand units and not hydraulic gradients (dh/dl). In this case study, the permeability and groundwater flow (V) of the freshwater sand units are two orders of magnitude greater than the saline aquifers.

Table 1*

Groundwater Flow Near Cypress Creek
and Richton Salt Domes, Mississippi

Formation	K(ft/day)	dh/dl	θ	V(ft/year)
Freshwater				
Pascagoula and Hattiesburg Formations	140	9/5280	0.30	300
Catahoula Sandstone	180	7/5280	0.30	300
Saline Water				
Cook Mountain Formation	0.86	3.6/5280	0.20	1.0
Sparta Sand	0.11	11/5280	0.20	0.4
Wilcox Group	4.1	3.3/5280	0.20	4.0

*(Bentley, 1983)

Throughout the Atlantic and Gulf Coastal plain, LeGrand (1962) distinguished three general zones in the vertical section in which water moves at different rates. Zone 1 consists of water-table and artesian aquifers and extends from approximately 100 feet to 200 feet below the base of streams where water is discharged. The rate of groundwater movement is on the order of feet per day or feet per year. Zone 2 may be from several hundred feet below surface to the depth where water is salty. The water in this zone has limited discharge paths and flow rates are generally on the order of feet per year. Zone 3 contains salty water and the rate of movement can be described in terms of feet per century. Withdrawal or introduction of fluids in wells could alter the hydraulic gradient in an aquifer and would increase the flow in any of these zones.

Studies of deep saline waters typically rely on a more limited data base than do studies of the more extensively developed freshwater aquifers because fewer wells are drilled to these depths and hydraulic-head data are therefore difficult to obtain.

Hydrodynamics Studies of Deep Saline Aquifers

Many of the studies for deep saline aquifers have been funded by the federal government in search for suitable sites in which to isolate nuclear waste. These studies have shown that groundwater flow rates in deep saline aquifers are less than the rates in more shallow freshwater aquifers. The regional flow picture from these studies indicates that the deeper units have less porosity and permeability, and they contain saline water. This suggests that the water is practically static (Warner et al., 1986). The sluggish circulation further demonstrates that geologic confinement is effective on both a local and regional scale.

Wolfcamp Aquifer System-Palo Duro Basin-West Texas

The deep brine aquifers in the Palo Duro Basin were studied by Bassett and Bentley (1983). Particular importance was placed on the Wolfcamp carbonate saline aquifer of early Permian age, at an approximate depth of 3500 feet. The head data for this study came almost exclusively from drill stem tests (DST) performed in petroleum exploration wells and bottom hole pressures (BHP) measured in the production wells. Since there is no petroleum production in the central Palo Duro Basin, the pressure measurements reflect natural pre-stress conditions. On the basis of the hydraulic-head map (Figure 1) and the average reported permeability of 2 md for this aquifer, the average horizontal flow rate in this saline unit is calculated to be approximately 0.25 inches per year.

Mt. Simon Aquifer-Northern Ohio

The rate of natural groundwater movement of saline water in the Mt. Simon aquifer in Ohio has been calculated by Clifford (1973, 1975—see Figure 2), Warner and Lehr (1981) and Nealon (1982). The Mt. Simon is a well-cemented sandstone of Cambrian age that occurs at a depth of less than 3000 feet below the surface (Bentley et al., 1986). Preinjection well data in the form of DSTs were used to extrapolate and obtain static pressure values. Warner and Lehr (1981) stated that the Mt. Simon Formation has an average permeability of 24 md and a porosity of 10 percent near the Empire-Reeves injection well (see Figure 2). All sets of calculations revealed groundwater flow rates in the Mt. Simon aquifer to be less than 6 inches per year.

Lower Floridan Aquifer-Northwest Florida

The rate of natural groundwater flow for water containing 5000 to 10,000 mg/l chlorides in the lower Floridan aquifer, northwest Florida, has been calculated by Warner and Lehr (1981). The aquifer has a permeability of approximately 1000 md and a porosity of 10 percent. The natural velocity of groundwater flow at a depth of approximately 1300 feet below the surface in the lower Floridan aquifer is less than 27 inches per year (see Figure 3).

Wilcox Aquifer-Gulf Coastal Plain-Mississippi

Groundwater flow rates near Mississippi interior salt domes for a nuclear waste isolation study (Slaughter, 1981) were calculated from observation wells that were constructed individually for each aquifer of interest. Hydraulic-head values were determined from field measurements. Permeability (1000 md) and porosity (25 percent) values were determined from lab and field tests. The results of this study showed that the natural horizontal fluid movement in the Tertiary age Wilcox saline aquifer is approximately 19 inches per year at a depth of nearly 3000 feet (see Figure 4).

Frio Aquifer - Harris County, Texas

The area near Houston, Texas, was studied for horizontal flow velocities because a large number of waste disposal wells which are completed similar to water wells should provide reliable head data measurements. Results (see Figure 5) showed the Frio is recharged in the outcrop area, and the majority of the driving force (head) is lost near the outcrop area, partially due to discharge to rivers. The Frio becomes saline downdip of Grimes County, which is reflected by a lower driving hydraulic gradient. The waste disposal wells located in Harris County would have a hydraulic gradient of 1.6 feet per mile based on basinward or downdip

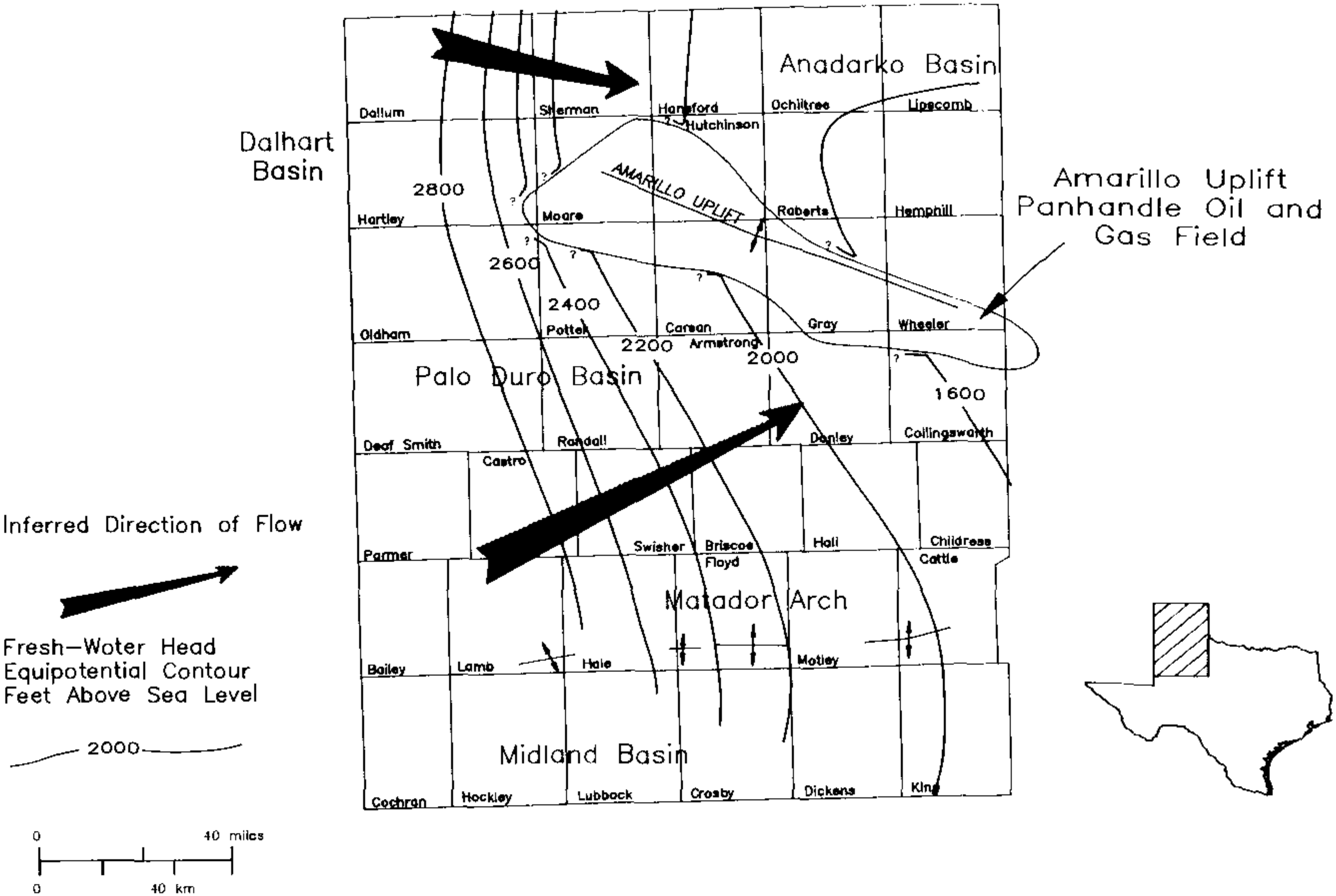

FIGURE 1

POTENTIOMETRIC SURFACE FOR THE WOLFCAMP AQUIFER,
PALO OURO BASIN (BASSETT AND BENTLEY, 1983)

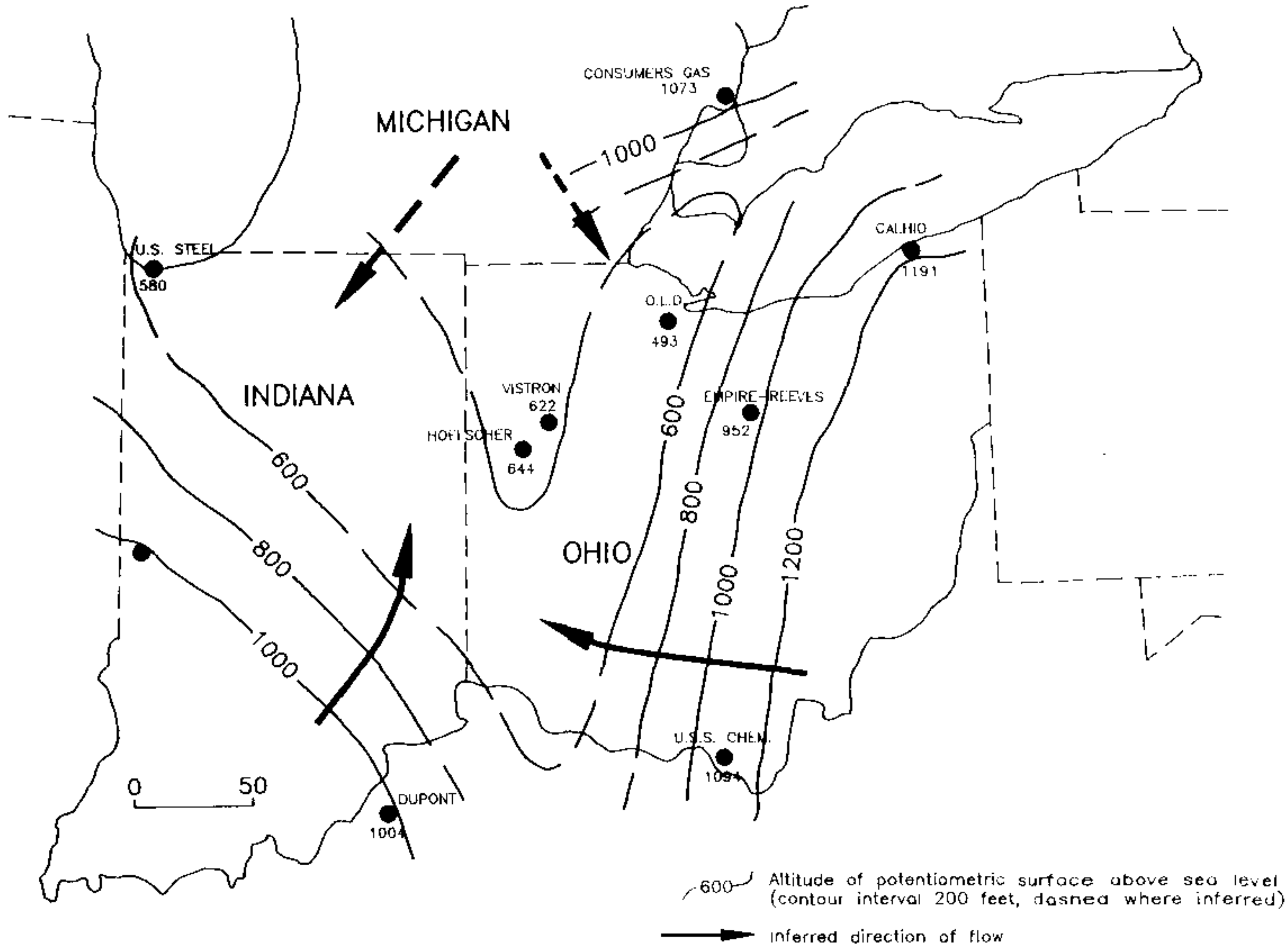

FIGURE 2

POTENTIOMETRIC SURFACE OF THE MT. SIMON FORMATION
IN OHIO AND VICINITY (CLIFFORD, 1973)

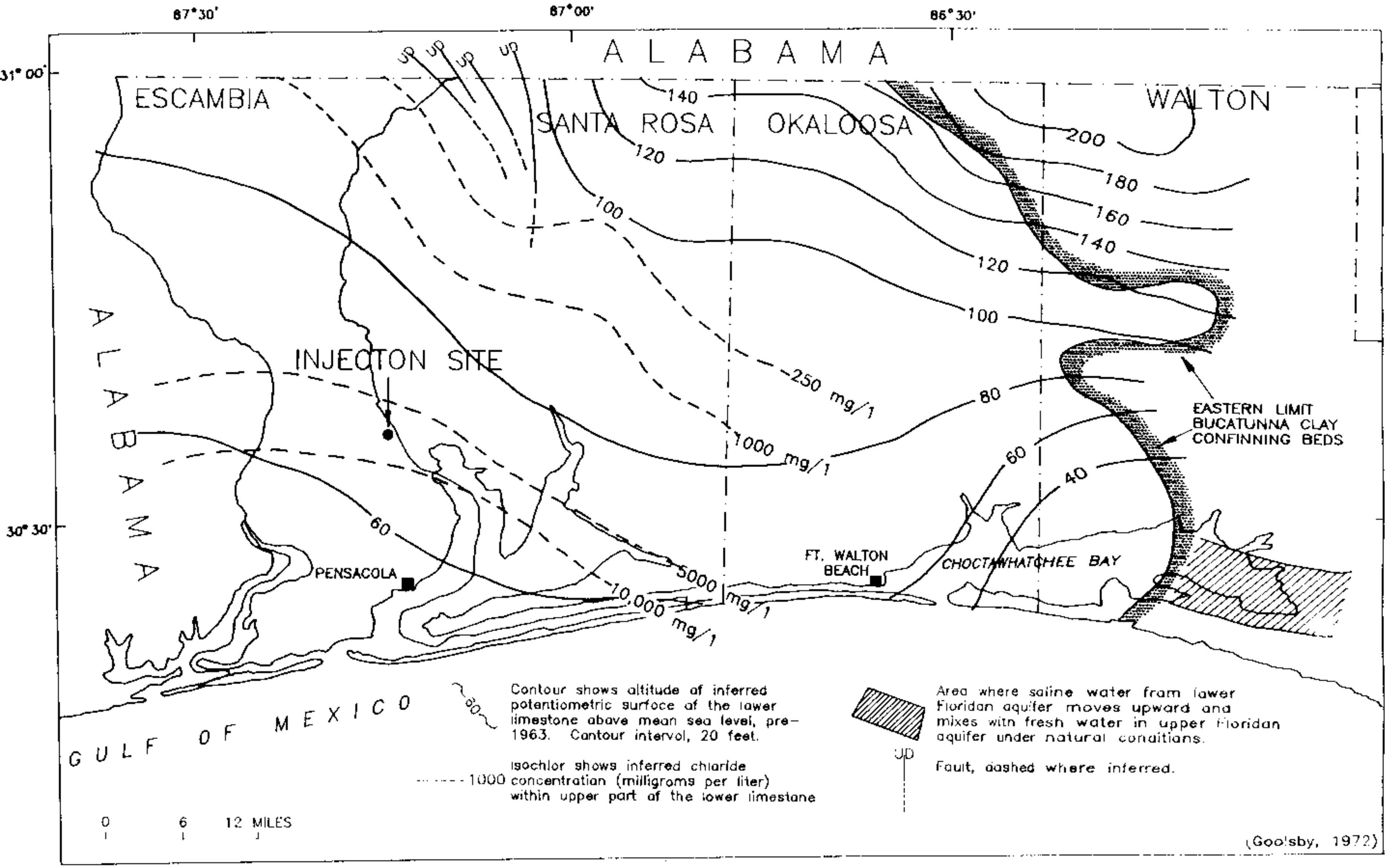

FIGURE 3

POTENTIOMETRIC SURFACE OF THE LOWER FLORIDAN AQUIFER, NORTHWEST FLORIDA

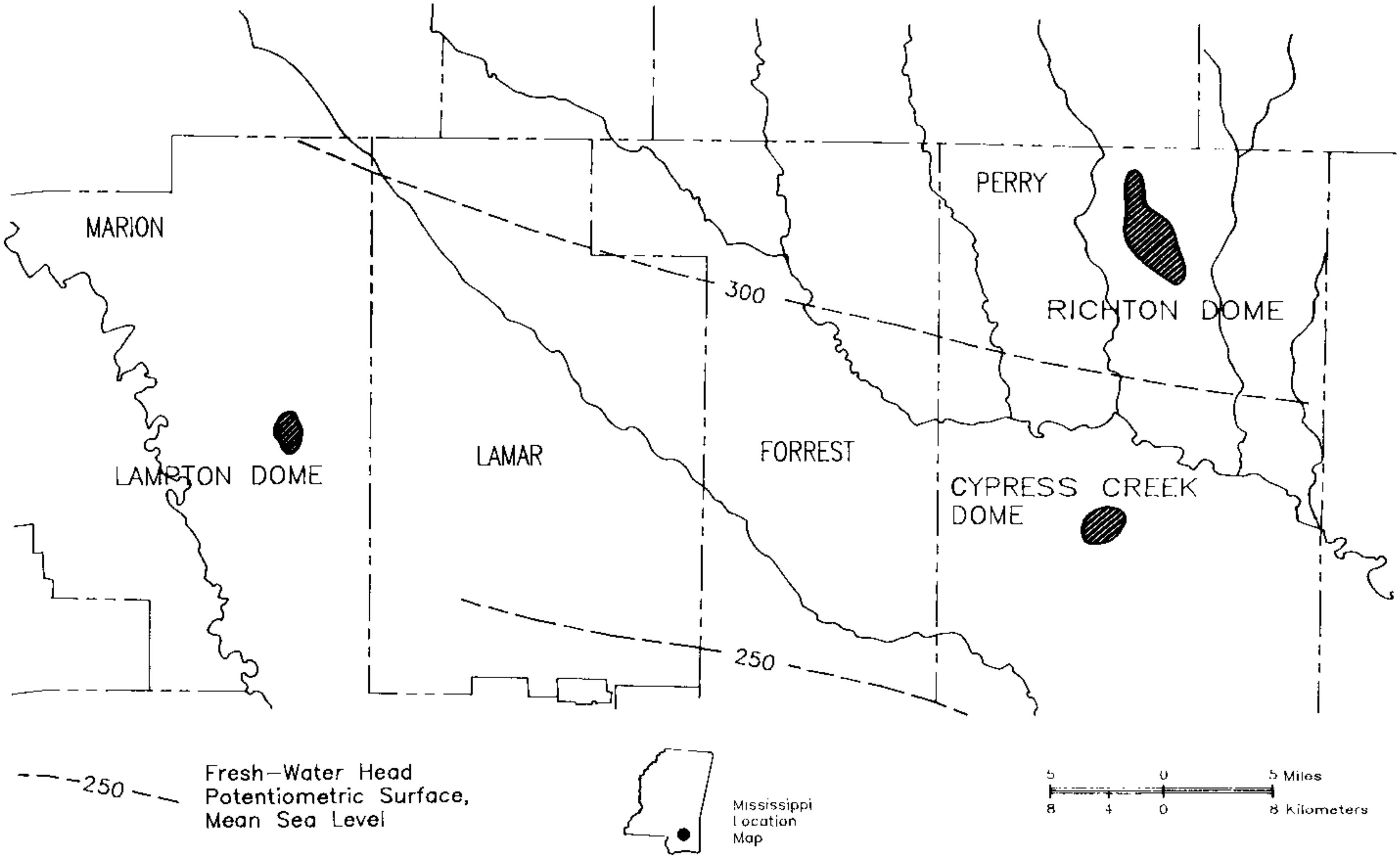

FIGURE 4

POTENTIOMETRIC SURFACE FOR THE WILCOX AQUIFER (–3000 FT. MSL)
SOUTHERN MISSISSIPPI (SLAUGHTER, 1981)

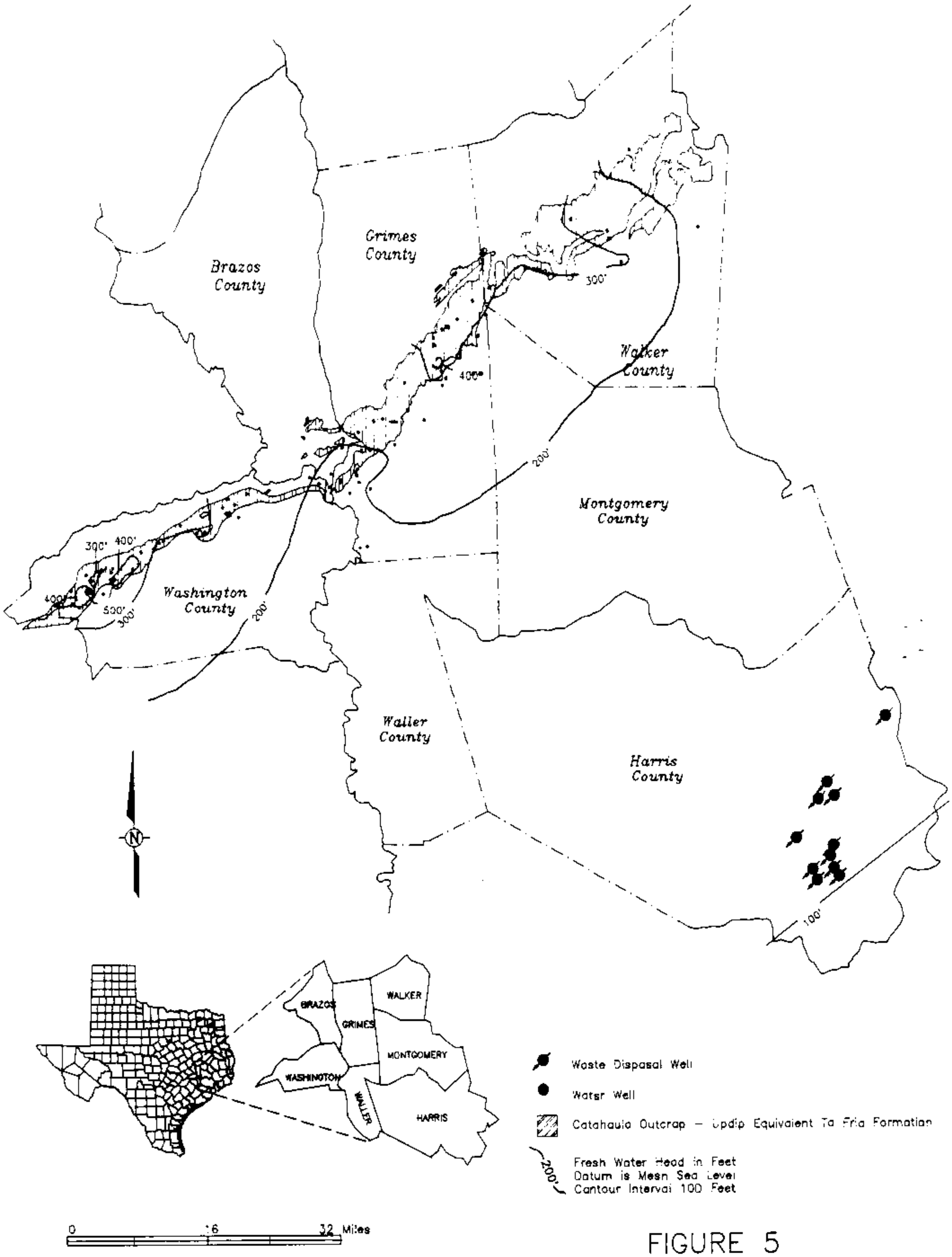

FIGURE 5
POTENTIOMETRIC MAP FOR THE
FRIO AQUIFER SYSTEM

flow. The average permeability for the Frio in this area is 800 md. The average downdip velocity flow rate is approximately 9 inches per year for the Frio formation at a depth of 6800 feet near Harris County, Texas. Groundwater flow in this area could reflect a static basin which is between geopressure and basinward flow. This static basin flow would be less, however, more data are needed on north Harris County to make this determination.

Our data indicated that basinward flow or static flow is still the dominant mechanism for the Frio formation near Harris County, Texas, whereas geopressure flow is not evident. This statement is supported in a study by Bethke et al. (1988). Bethke et al.'s analysis of the Gulf Coast sedimentary basin near Houston, Texas, showed that geopressured zones occur at depths >6400 to 9000 feet (2 to 3 km). The Tertiary sediments in offshore sections are clays that form thick, impermeable shale successions which are different from the near-shore sandy facies. Geopressures develop because the impermeable sediments cannot expel fluids quickly enough to compact fully during burial. Therefore, in the offshore sections of the Texas and Louisiana Gulf Coast, the geopressure zones occur at depths shallower than 6400 feet. See Figure 6 for calculated present-day distribution of geopressures in the Gulf basin. Pressure gradients >10 MPa/km (1 MPa = 10 atm) are overpressures, and those >16 MPa/km describe hard geopressures. Bethke et al. (1988) stated that groundwater flow rates in deep saline aquifers is probably on the order of centimeters per year in the Gulf Coastal Plain.

Preparing horizontal flow maps for deep saline aquifers can be difficult due to the limited database. This limitation is both in quantity of wells and quality of the reservoir pressure measurement. Pressure measurement errors associated with downhole pressure equipment do exist. For example, Figure 7 shows pressure measurement versus depth for waste disposal wells (WDW) 222 and 223 in Harris County, Texas. These wells are 500 feet apart were completed into the same zone at the same time. The original bottom hole pressure measurements show a head difference of 46 feet between the two wells, where the heads should have been equal. This difference is caused by the inaccuracy of the pressure measurement equipment.

A summary of the natural horizontal groundwater flow rates in deep saline aquifers is presented in Figure 8.

Flow Through Intact Confining Layers

Confining layers without defects provide assurance against vertical migration of fluids from the injection zone into overlying aquifers. Recent reports and test results have confirmed that the essential element for effective confinement of injected fluids is the impermeable nature of the confining layers. Vertical flow can be significant in confining layers with defects. These defects could include the following: 1) transmissive fractured or faulted confining layers, 2) improperly plugged abandoned wells, 3) discontinuous confining layers, and 4) confining layer dissolution by injected wastes. These potential defects are site specific, and migration of fluids through confining layer defects can only be addressed in the area of review study for a particular site.

Natural groundwater flow through shales, siltstones, and limestones will be through intergranular spaces and can be calculated by using Darcy's law (Warner et al., 1986, see Equation 1). Warner et al. (1986) state that shales are suitable confining layers where permeabilities are in the range of 0.001 to 0.000001 md. Sensitivity studies, conducted by Warner et al. (1986) for vertical flow

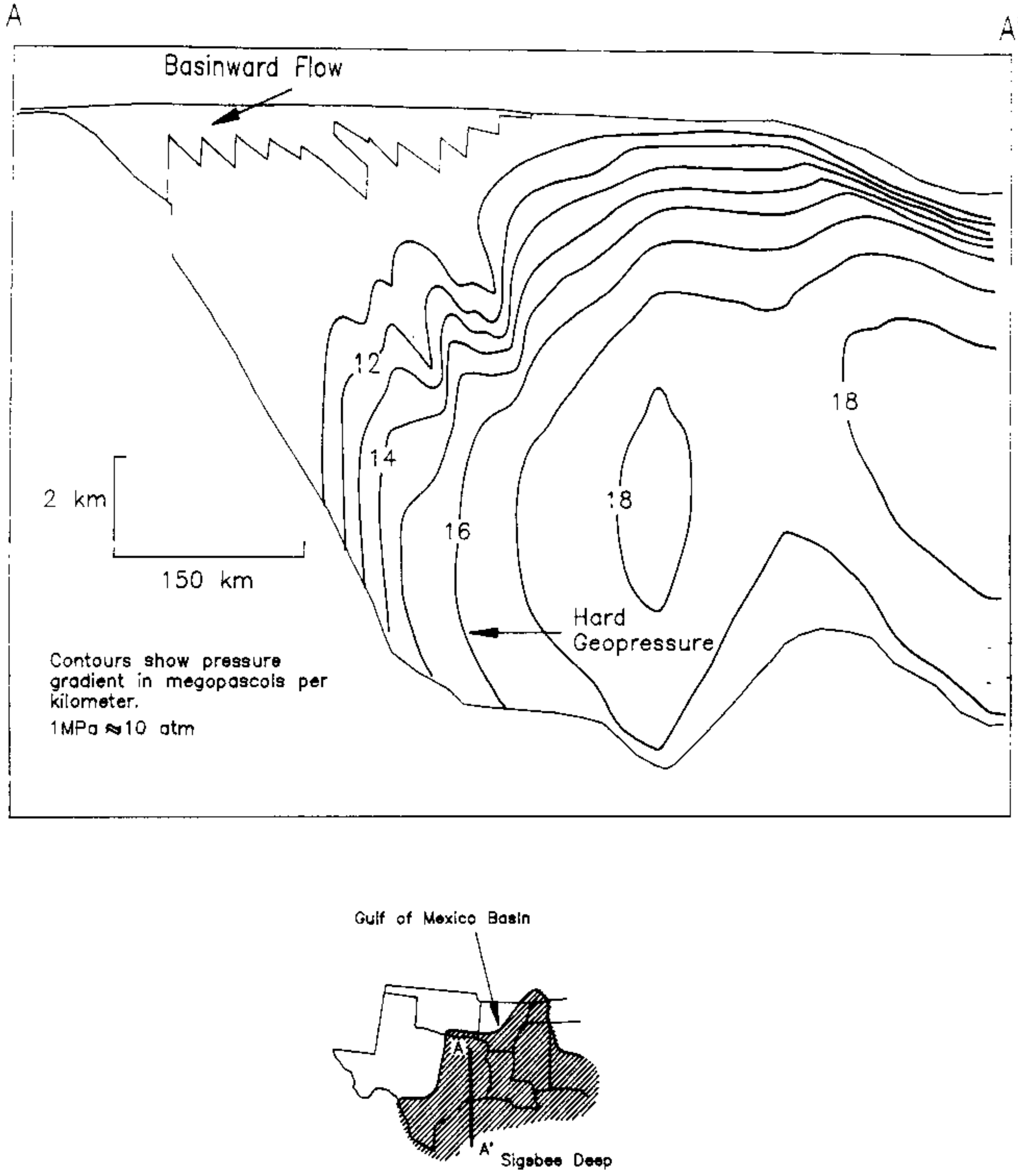

FIGURE 6

EXTENT OF BASINWARD FLOW DUE TO TOPOGRAPHIC RELIEF ON THE COASTAL PLAIN (BETHKE et al, 1988)

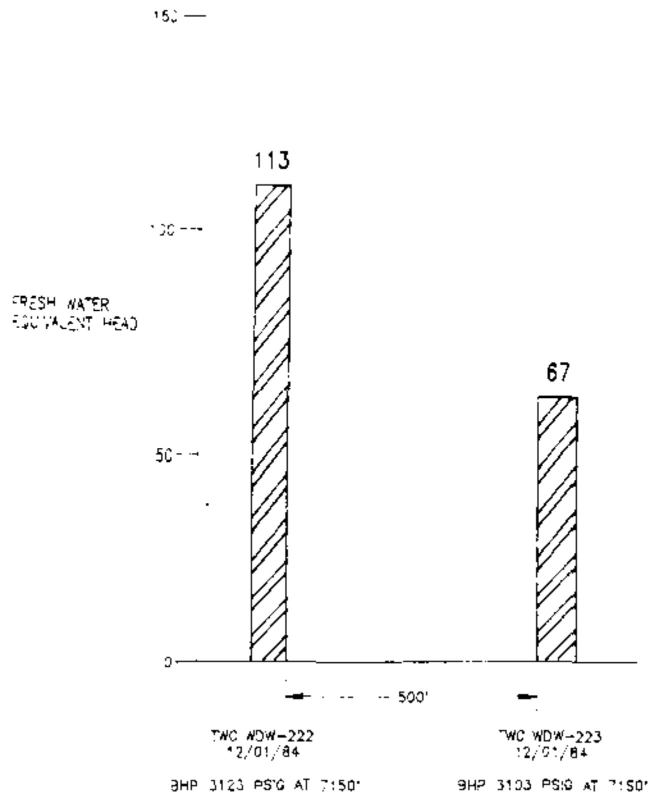

FIGURE 7
PRESSURE MEASUREMENT ERRORS
WITH DOWNHOLE EQUIPMENT

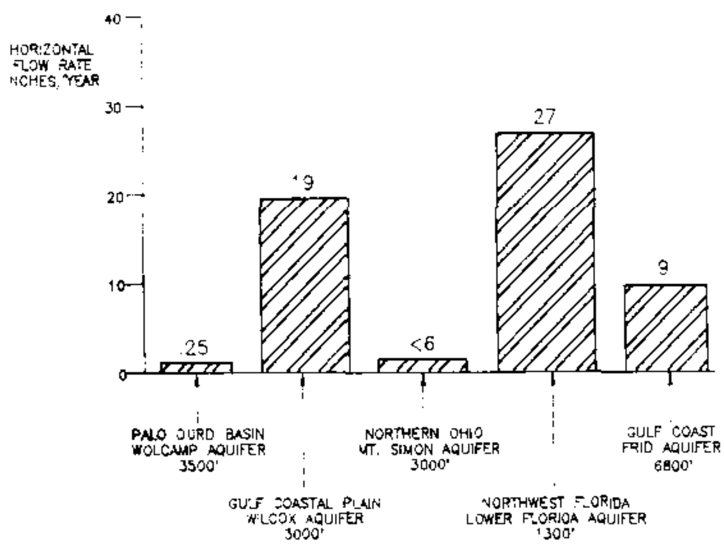

FIGURE 8
NATURAL HORIZONTAL GROUNDWATER FLOW RATES
IN DEEP SALINE AQUIFERS

calculations of injected wastewater through a 100 foot thick confining unit with various permeabilities and injection-induced pressure gradients, are tabulated below:

Table 2

	ΔP (psi)			
k (md)	500	1000	2000	5000
1.0	114 ft/yr	228 ft/yr	456 ft/yr	570 ft/yr
0.01	1.14	2.28	4.56	5.7
0.0001	1.14×10^{-2}	2.28×10^{-2}	4.56×10^{-2}	5.7×10^{-2}
0.000001	1.14×10^{-4}	2.28×10^{-4}	4.56×10^{-4}	5.7×10^{-4}

NOTE: Effective porosity was assumed to be 10 percent and viscosity to be one centipoise.

In summary, this sensitivity analysis indicates that, for a given permeability, even with large pressure gradient differentials, the flow through the confining layer does not increase significantly. This indicates that the permeability is the main factor in controlling vertical migration. In addition, even if the confining layer were reduced to a very thin zone, say 10 feet instead of 100 feet, the vertical flow would increase by only one order of magnitude. Because of the very low permeabilities of suitable confining layers, the potential upward migration rate is very low.

In a study by Conger (1986) on upper Miocene confining layers of the Geismar-St. Gabriel area, Iberville and Ascension Parishes, Louisiana, permeabilities of shale cores from 3600 feet indicate vertical permeabilities to liquids of 0.001 to 0.0001 md. Conger calculated that it would take more than 50,000 years for upward migration to penetrate even the thinnest confining clay.

Clark (1988) conducted a study on shale permeabilities versus injection pressure. Permeabilities ranging from 10^{-4} to 10^{-6} md were found. This study shows the importance of confining pressure or over-burden pressure in reducing the permeability of the shale material. The deeper the shale, the higher the confining pressure, and, therefore, the lower the permeability.

A special core analysis was conducted for Du Pont on cores from injection well No. 3 at Beaumont, Texas. Whole core samples were taken at various intervals with special emphasis on coring the shale units, particularly the shale units directly above permeable sand units (see Figure 9). Whole core samples were analyzed by Core Laboratories (1987a,b) for cap-rock vertical permeabilities under formation pressure, temperature, and salinity. The results indicated shale permeabilities on the order of 10^{-5} to 10^{-6} md.

These permeability values indicated that the shale is essentially impermeable. Such permeabilities are consistent with those for effective shale confining layers (Warner et al., 1986).

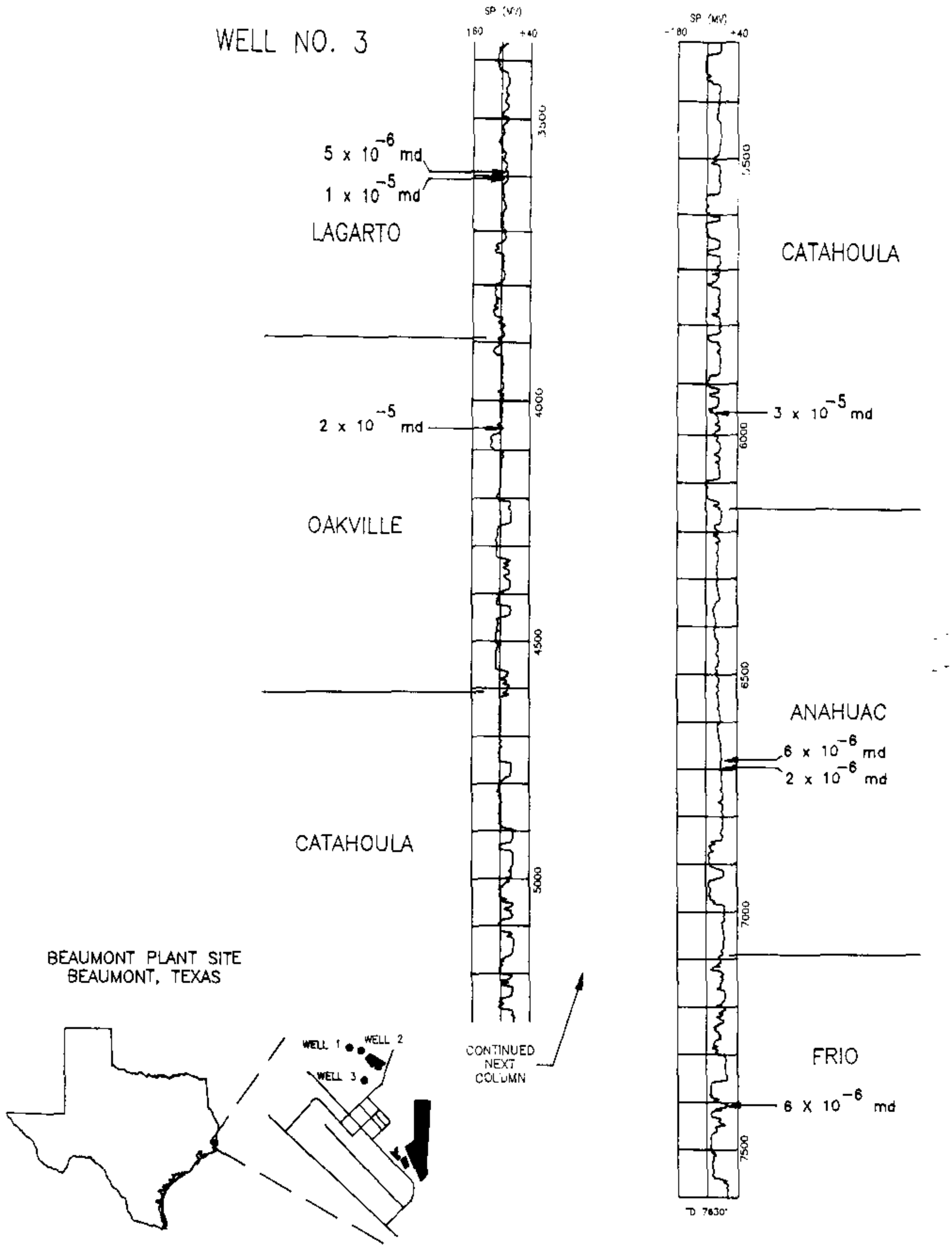

FIGURE 9

TYPICAL GULF COAST SHALE PERMEABILITIES

Using the sensitivity study of Warner et al. (1986), the vertical flow through the confining layers at the Beaumont site would be approximately 1 to 10 feet in 10,000 years. This study indicated the extremely low potential for vertical migration into intact confining layers (see Figure 10). In fact, this demonstrated that the vertical migration will be so minute, in a non-induced (natural) environment, that it probably cannot be measured in a 10,000-year time frame (on the order of 1 foot per 10,000 years).

In a study conducted by Buss et al. (1984) for the EPA, only three orders of magnitude (1000X) difference was used for modeling between the injection and confining zone permeabilities. The results of the study showed containment even at this small permeability differential. In reality, the injection reservoirs in the Gulf Coast region approach a permeability of 1000 md, and, as shown in the preceeding tabulation, the confining layer permeabilities are less than 0.00001 md. This difference in permeability is not three orders of magnitude (1000X), but eight orders of magnitude (100,000,000X).

Beaumont, Texas--Case History

Before construction of well No. 3, well No. 2 injected into the 4200-foot Oakville sand as shown in Figure 11. The electric logs show a 10-foot shale layer separating the injection unit from an upper sand. Injection well No. 3 was drilled using an experimental Du Pont polymer mud system to limit mud invasion and obtain representative fluid samples. Evidence from the microlog and sidewall cores confirmed the limited mud invasion into the permeable formations. By using Schlumberger's Repeat Formation Tester (RFT) with dual sample chambers, we recovered waste reaction products from the current 4200 foot injection zone. However, no waste or reaction products were recovered from the upper 4100 foot sand unit showing that even thin shale units are effective barriers to upward migration. Also notice that the spontaneous potential (SP) inversion confirms that injection fluids have moved horizontally in the injection interval with no evidence of upward migration through the 10 foot shale confining unit.

After protection casing was set, a temperature log was run in well No. 3. It also confirmed injection fluid is present from well No. 2 and shows no upward migration of fluids through the 10 foot shale unit (see Figure 11).

Sabine River Works, Texas--Case History

At the Sabine River Works, Orange, Texas, isolation of an injection zone by a low permeability confining zone was demonstrated in the field by measuring in situ physical properties of an overlying formation before and after a period of injection. This was shown by the geophysical logging of three injection wells at the above facility. Well Nos. 3 and 4 were drilled in 1969 and completed in a zone from 4880 to 5000 feet. The second zone, from 4630 to 4730 feet, was completed in 1981. Well No. 9 was drilled approximately 300 feet from well No. 4 through the same injection zones with their overlying shales or clays. Figure 12 shows the geophysical logs for all three wells in the 4400 to 5000-foot interval.

A key characteristic of the logs is the difference in resistivity shown by the three wells. The logs of Wells Nos. 3 and 4 show consistently low resistivity within the injection zone interval, which is characteristic of formations containing highly conductive brine. The logs of these two wells were run prior to injection and before the native brine was disturbed. The resistivity log of Well No. 9, shown in Figure 12, exhibited a remarkable change within the injection zone

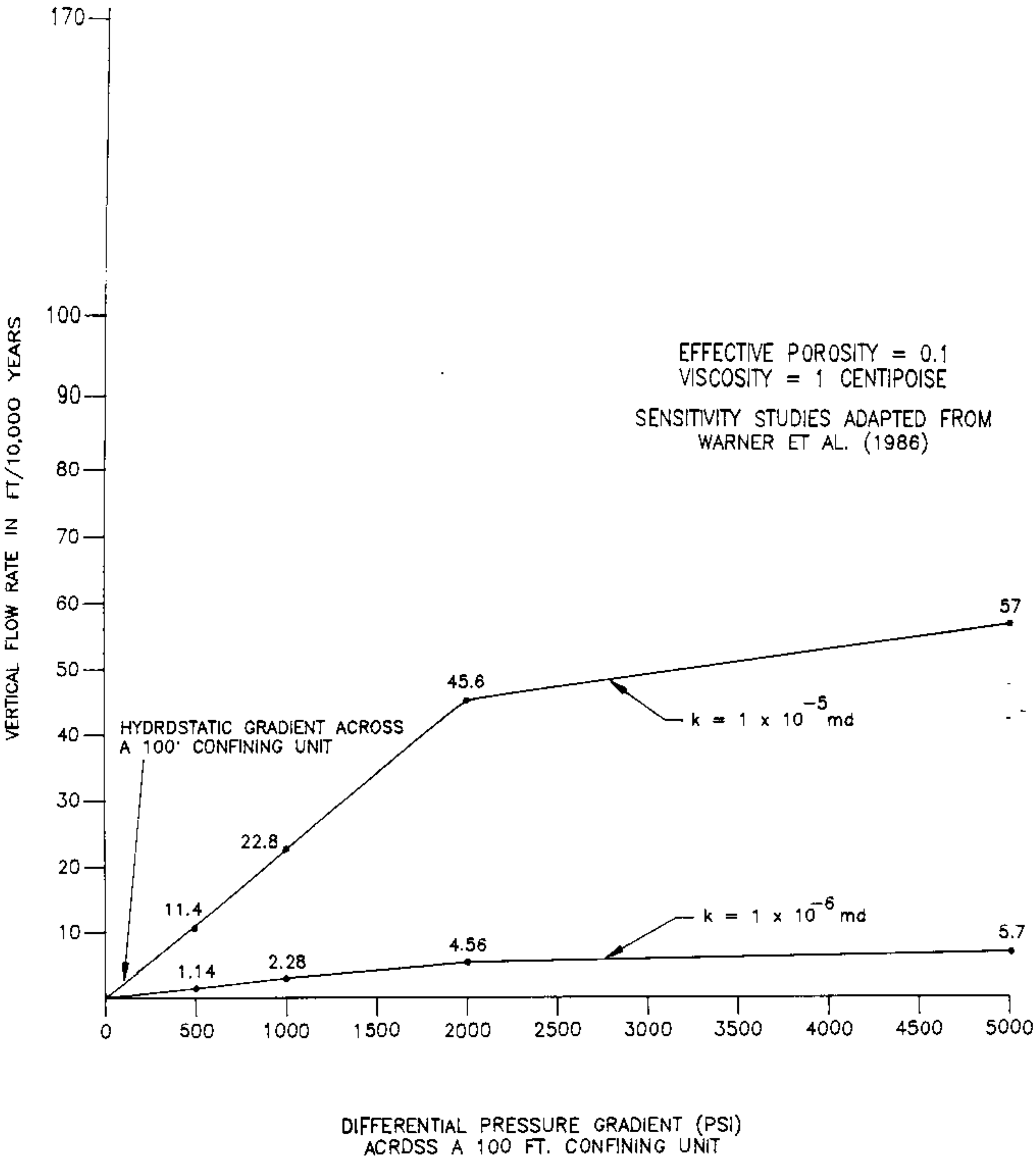

FIGURE 10

VERTICAL GROUNDWATER FLOW RATE
FOR A GULF COAST SHALE
UNDER INJECTION–INDUCED PRESSURE GRADIENTS

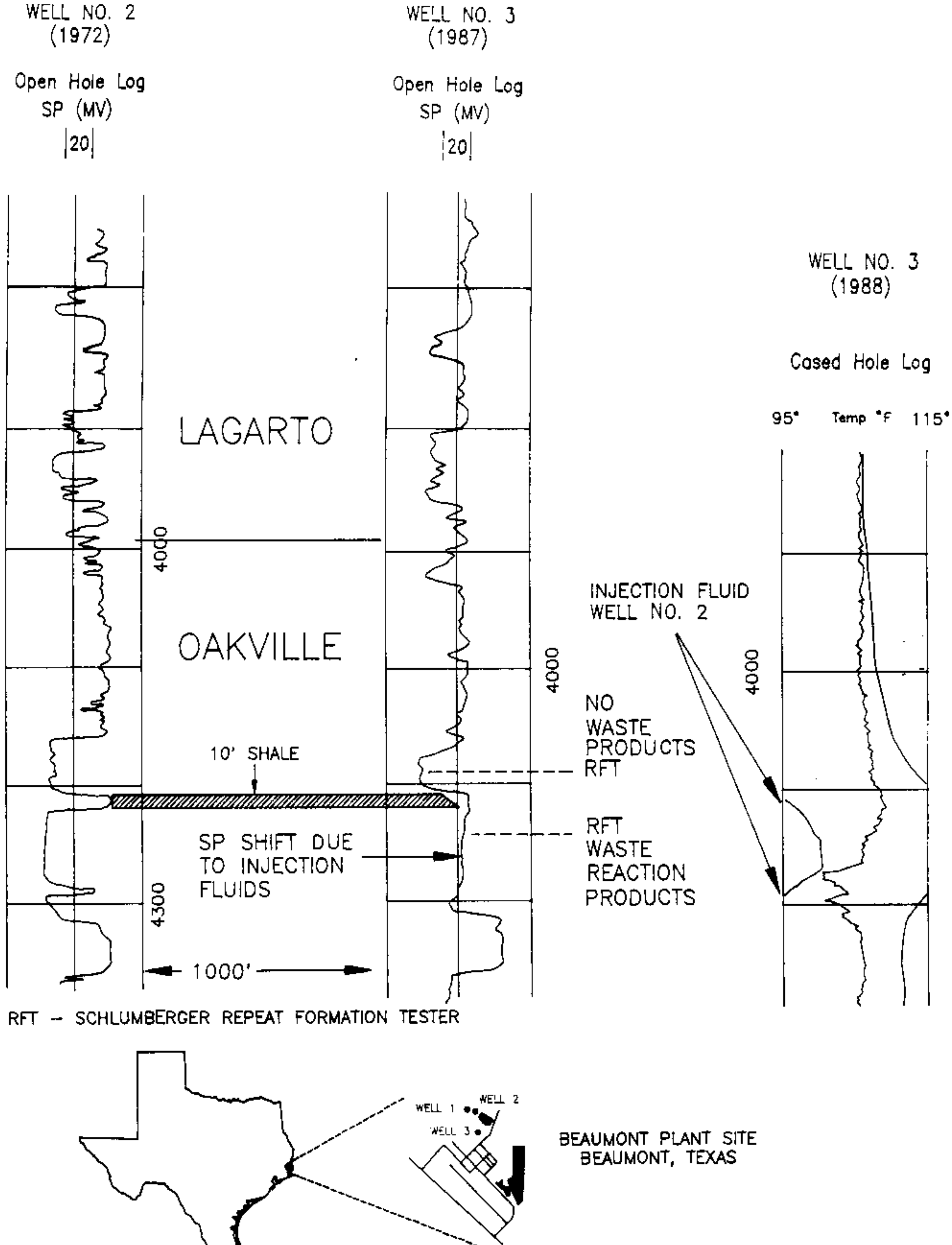

FIGURE 11

GEOPHYSICAL LOGS FOR BEAUMONT WELLS NO. 2 & 3
SHOWING EFFECTIVENESS OF A 10' SHALE CONFINING UNIT

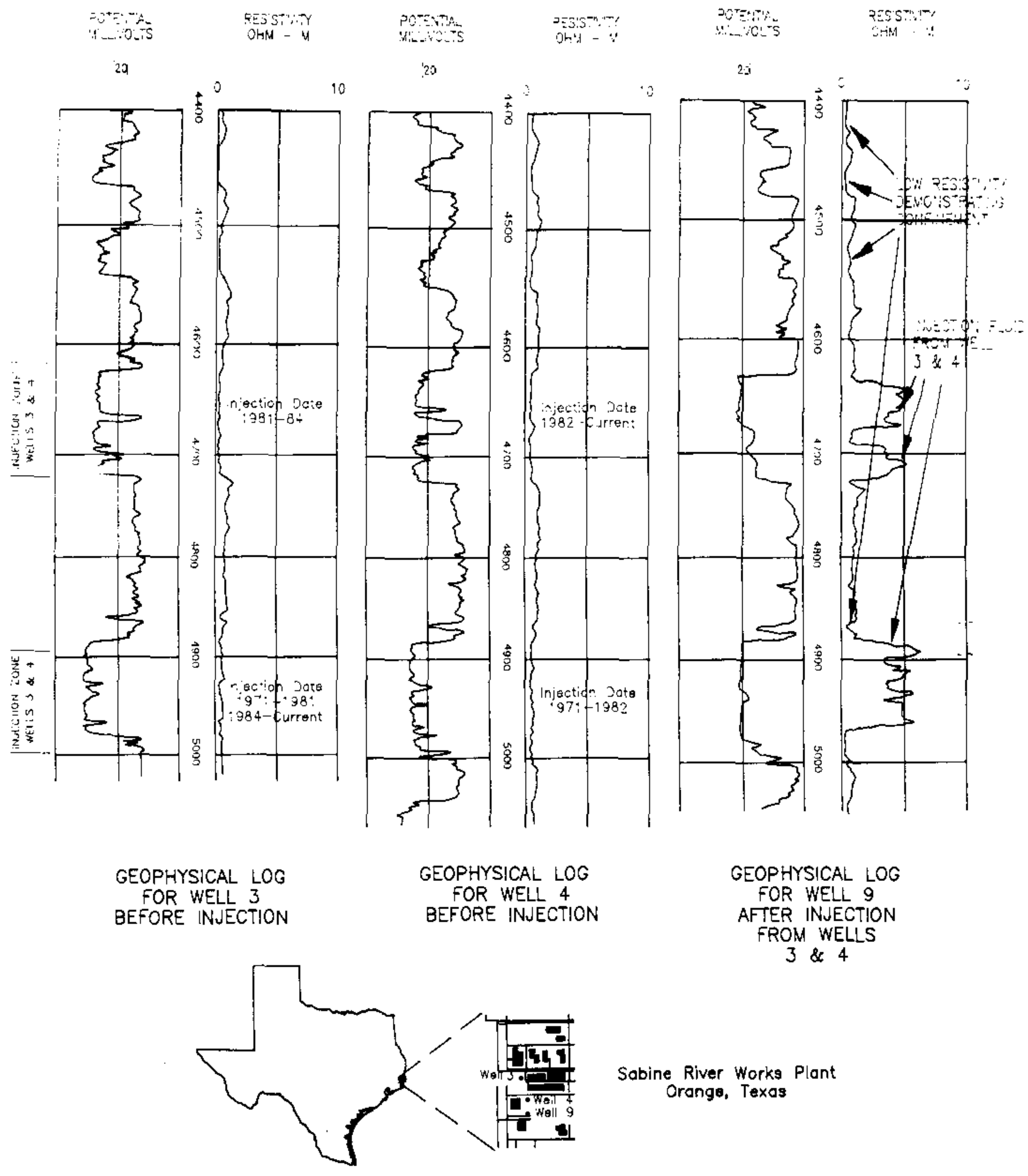

FIGURE 12

GEOPHYSICAL LOGS DEMONSTRATING INJECTION FLUID CONTAINMENT IN THE 4400 TO 5000 FOOT INTERVAL SABINE RIVER WORKS, ORANGE, TEXAS

15 years later. These two zones at 4630 to 4730 feet and 4880 to 5000 feet displayed resistivities that are more than twice the previously recorded values for Wells Nos. 3 and 4. This higher resistivity has resulted from the replacement of the native brine by the low-conductivity waste stream.

The most important observation was that the higher resistivity readings in the log for Well No. 9 were confined to the injection sand interval. Consequently, no detectable vertical migration of the waste stream has occurred. If significant vertical migration had occurred, higher resistivity readings would be recorded within the confining zones and/or the next overlying sands at 4450 to 4500 feet (see Figure 12). This demonstration provided a direct field example of the lack of significant migration across shales and clays at a site in the Gulf Coast.

Louisville, Kentucky--Case History

A third case study, demonstrating confinement of injected waste, involved our Louisville, Kentucky plant. This facility started injection of an acid waste into well No. 1 in 1973. Injection well No. 2 and the monitor well located in the downdip direction were used to monitor the waste reaction front while injection occurred only in well No. 1 (see Figure 13). The site injects into the Knox dolomite at a depth of ≈3100 feet. Water quality and well head pressures were monitored for both the monitor well at a depth of 2800 feet and injection well No. 2 at ≈3100 feet. The reaction products passed well No. 2 ≈460 days after well No. 1 injection startup. A wellhead pressure drop of several hundred feet below the surface in well No. 2 was the first indication that reaction products had passed and was due to the higher density of the reaction front.

When the waste front passed well No. 2, water quality parameters were sampled and substantiated that the reaction front indeed had reached well No. 2, passing below the monitor well (see Figure 14). Continued monitoring of the monitor well shows no pressure or water quality changes associated with the waste injection for over 15 years.

Local Structural Features Affecting Groundwater Flow

Structural features such as faults, folds, and salt domes can affect groundwater movement. Any potential local discharge of fluids from the injection zone caused by structural features can be identified in the area of review process.

Faulting is common in the Gulf Coastal Plain and is responsible for many of the hydrocarbon traps in Texas and Louisiana. Faults appear to act as complete or partial barriers to fluid migration. Evidence of sand-against-shale fault sealing tendency can be seen in numerous oil and gas fields associated with a fault trapping mechanism. There would not be large amounts of hydrocarbons in oil fields, which indicate millions of years of containment and accumulation, if the faults served as vertical pathways (Jones and Haimson, 1986).

In other instances faulting places sand against sand; either the same sands are just slightly offset or displacement is greater than the confining layers and places one sand unit against a different sand unit. A relatively deep injection zone with a sufficiently thick confinement zone is preferred and can usually be selected. Nevertheless, there are many examples where this type of faulting acts as an impermeable boundary where hydrocarbons have not migrated across the fault

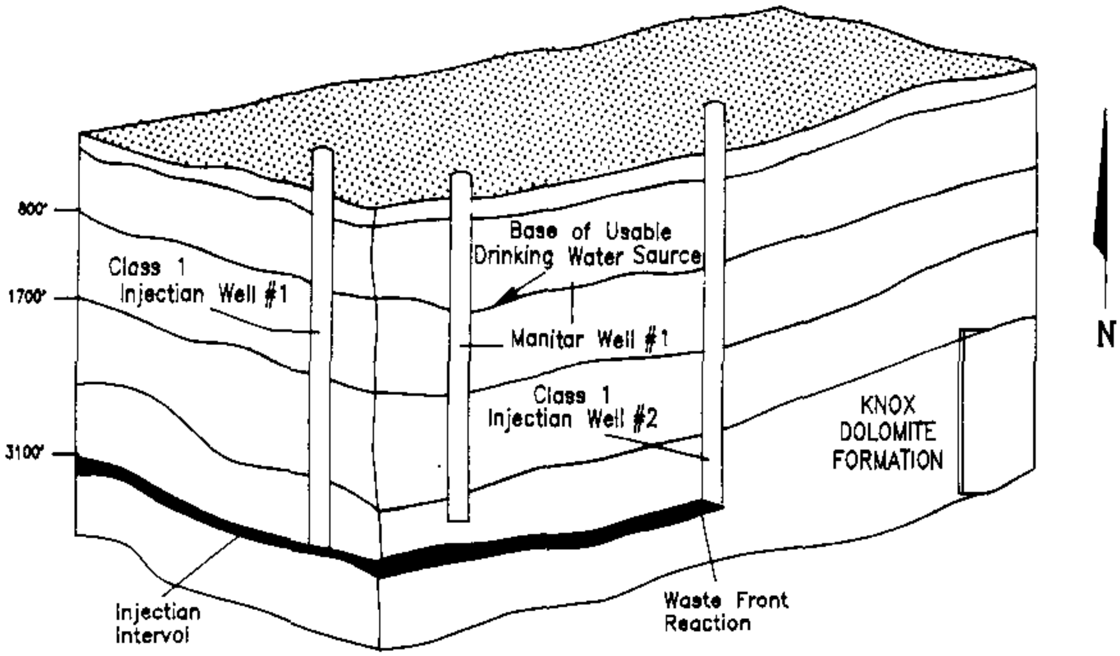

FIGURE 13
LOUISVILLE PLANT CROSS-SECTION

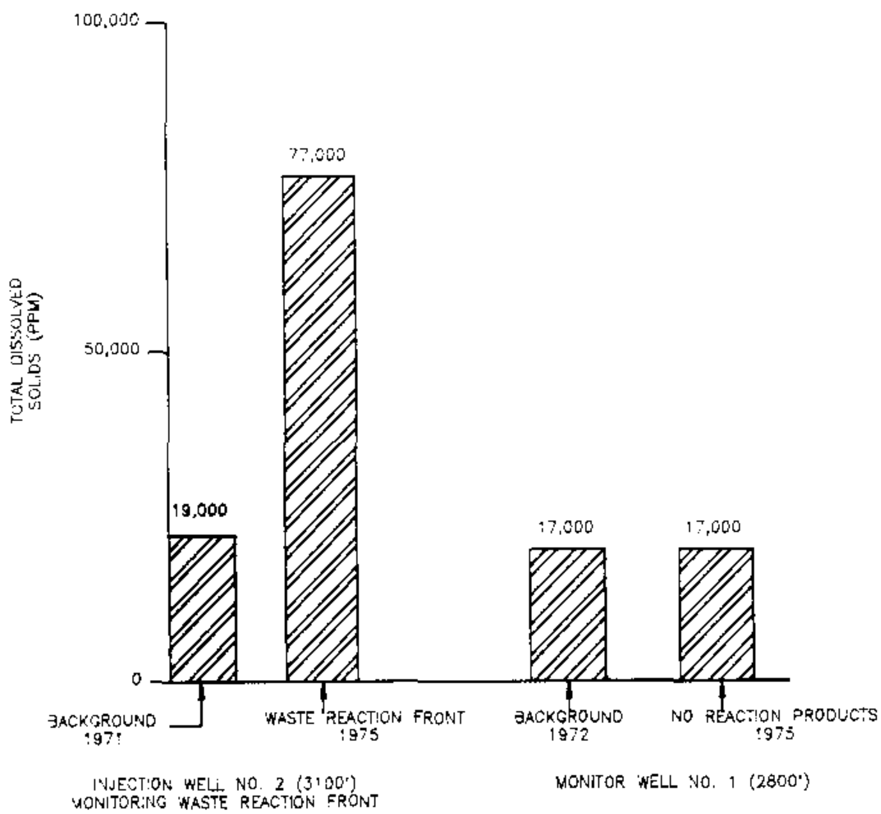

FIGURE 14
LOUISVILLE PLANT WATER QUALITY MONITORING

from one sand to another. Two important fault-sealing processes in this case are clay sheath (smear) and cementation.

Clay smear occurs when a soft shale is displaced past a sand unit during the fault movement and shale impregnates the face of the faulted zone. This acts as an impervious barrier to fluid flow. Weber and Daukoru (1975) concluded from field evidence in the Niger Delta that a fault is sealing at a given depth when passed by shale consisting of more than 25% shale on the downthrown side. Another fault sealing mechanism is cementation. Galloway (1982) reported on sealing of fault zones in the Oakville Formation by secondary minerals deposited from subsurface waters.

In another example of how faulted zones act as compartments or boundaries to fluid flow, Kreitler (1976) issued a report on the fault control of subsidence in the Houston-Galveston, Texas area. He observed pressure declines and differential subsidence across approximately 87 fault zones in areas where the faults acted as hydrologic barriers (impermeable boundary conditions).

Piercement salt domes can have an impact on the groundwater flow, and the area around the flanks of a dome should be studied in detail to verify that this condition does not serve as an area of local discharge. These domes were formed by diapiric intrusion of the Jurassic and Tertiary sediments. Intrusion of the salt stocks created complex geologic structures. Reservoirs may be truncated updip by the salt stock due to a pinching out of the units or thrust fault. In some places marine shale, due to its plastic nature, is dragged upward with the salt stock and makes an effective seal for hydrocarbons. This shale sheath generally seals the units that contain hydrocarbons and protects the dome from groundwater dissolution.

Artificial Hydraulic Gradients

No report on hydraulic gradients would be complete without discussion and recognition of the importance of man-made influences. Man can have an impact on groundwater flow in the production and abandonment of water, oil, injection, and gas wells. Figure 15 shows the increased groundwater flow or hydraulic gradient near the town of Columbia, Mississippi. This increase in hydraulic gradient in a reservoir 2300 feet below mean sea level is caused by injection of brine fluids from the cavern dissolution of Lampton Salt Dome. One needs to be aware of such types of activities that can alter the natural flow gradient.

In general, man-made activities are short lived, measured in years rather than thousands of years. This is favorable as it tends to minimize the impact on long-term natural groundwater flow. In addition, once production or injection has stopped the hydraulic gradient returns to a normal condition and, generally, recovery time is much less than the production or injection time. Class I injection wells also are not usually associated with other man-made activities, i.e., oil, gas, and Class II injection wells. Figure 16 shows how a Repeat Formation Tester tool run in open hole, before well construction, can indicate whether the reservoirs might be influenced by man-made activities (underpressure/overpressure) or are limited in extent.

Summary

Published literature and research show that deep saline aquifers have natural groundwater flow rates that are on the order of inches per year compared to the

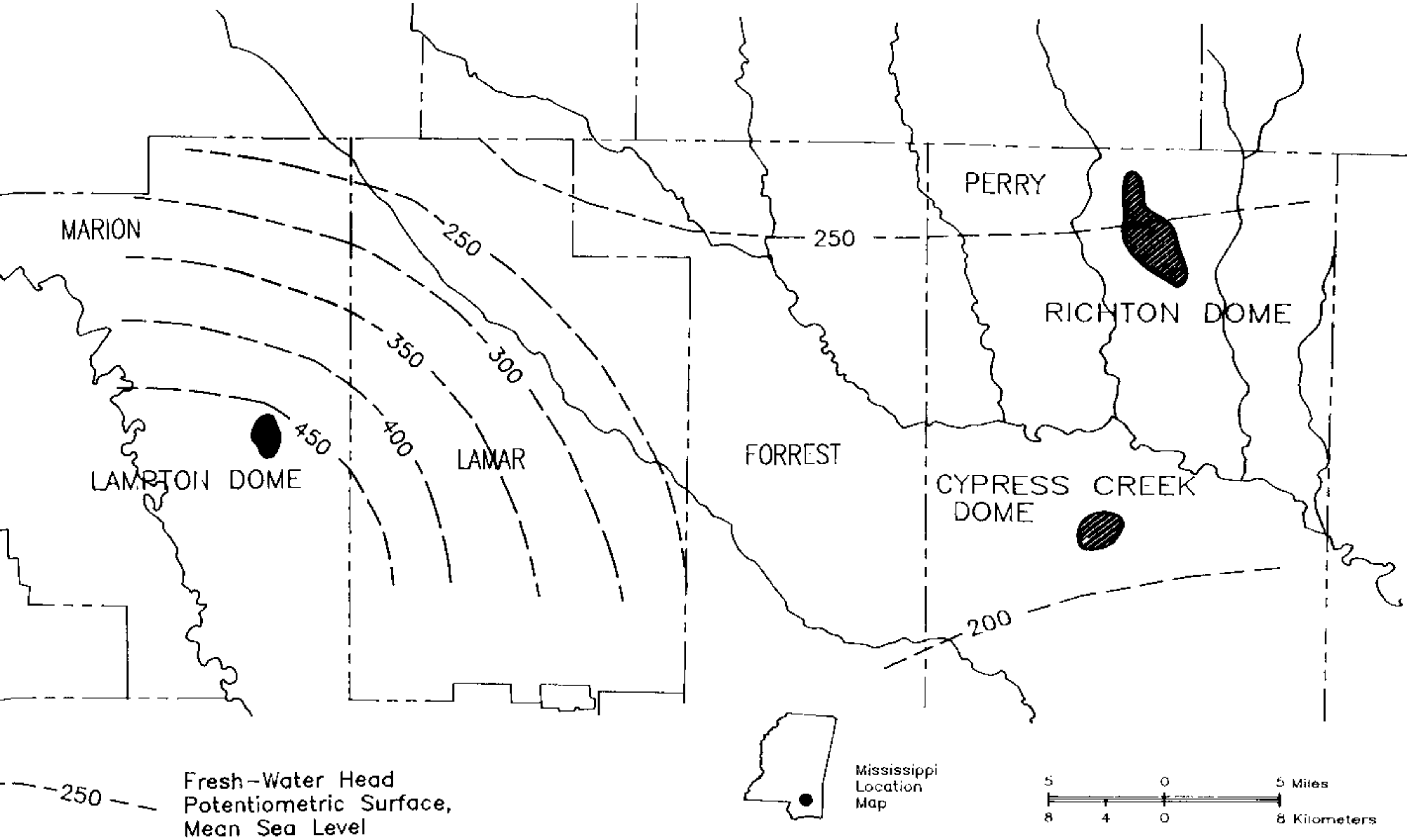

FIGURE 15

POTENTIOMETRIC SURFACE MAP
FOR ELEVATION (-2300 FEET MSL)
INTERIOR SALT DOMES, MISSISSIPPI (SLAUGHTER 1981)

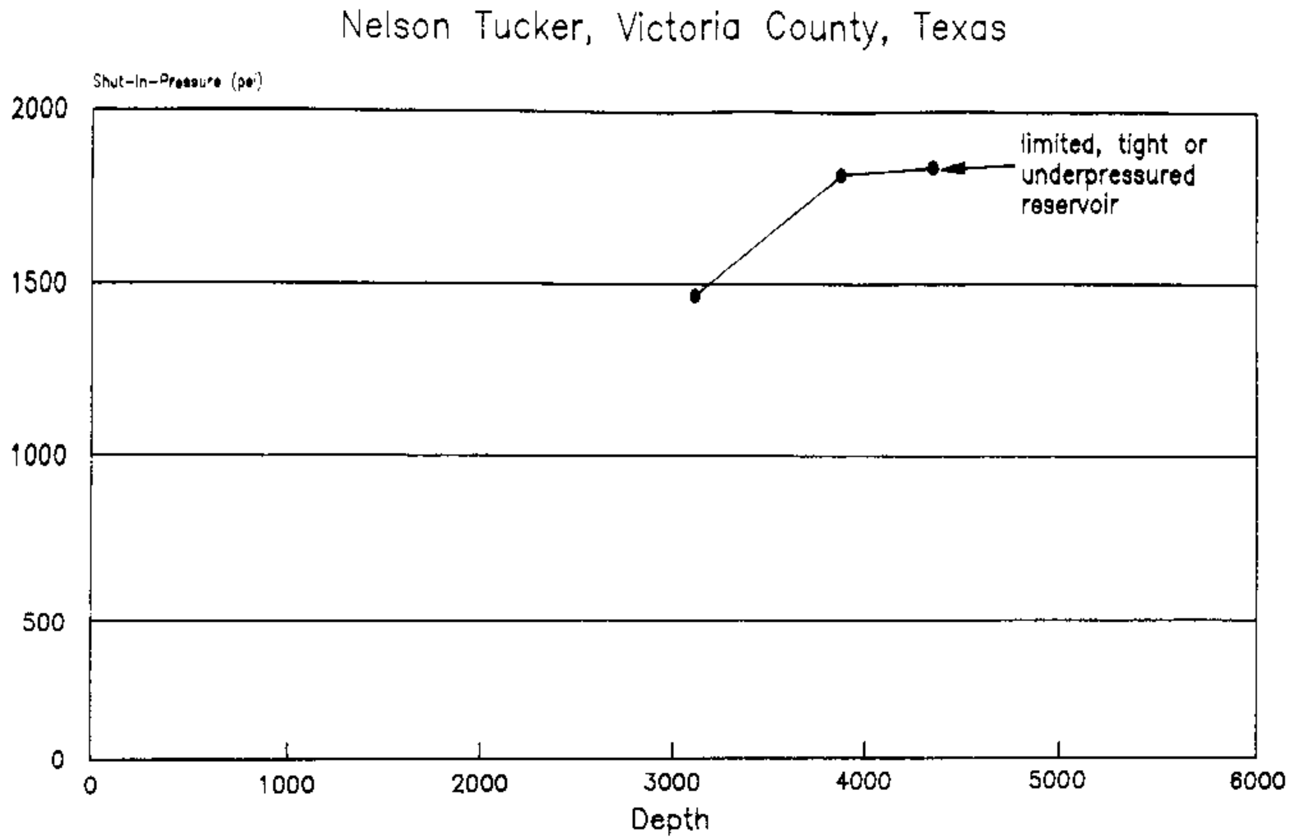

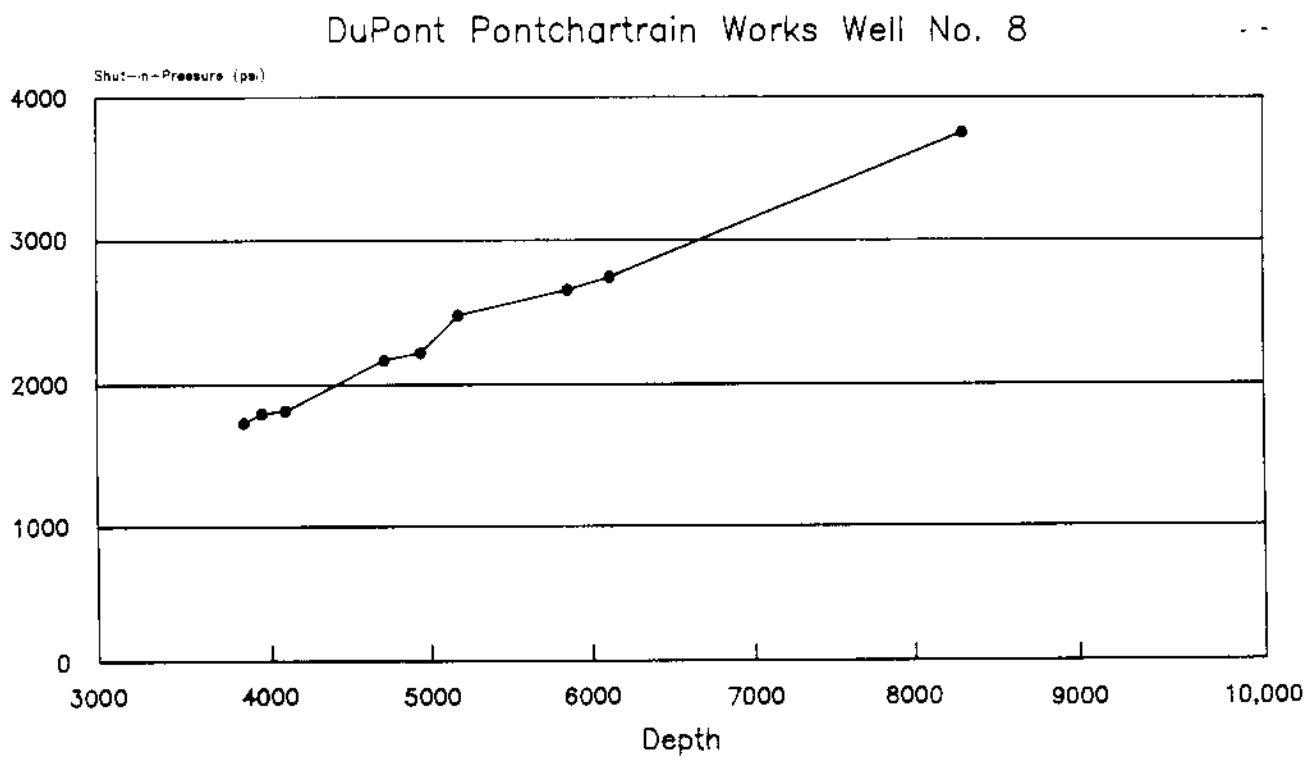

FIGURE 16

REPEAT FORMATION TESTER
SHUT-IN-PRESSURE VS. DEPTH

shallow freshwater aquifers of feet per year. In general, hydraulic gradient is not the dominant variable controlling groundwater flow in deep saline aquifers because the hydraulic gradient does not change by orders of magnitude for fresh water and saline water units. The dominant parameter controlling groundwater movement relates to the hydraulic conductivity of the sand units. Freshwater sands have a permeability of at least two orders of magnitude greater than the saline water units. Confining layer studies have shown that the vertical migration potential in Gulf Coastal Plain shales will be on the order of 1 foot in 10,000 years. Man-made influences may increase the natural low-flow gradient in deeper saline aquifers; however, this influence can only change the gradient for a time period of years and not thousands of years. Local discharge zones in the natural gradient are of utmost concern in the context of long-term confinement of hazardous wastes within the intended injection zone. Local discharge zones resulting from structural features can be identified in the Area of Review study for the injection site. Where head data is lacking, regional temperature maps are useful tools for locating potential changes in the regional gradients.

Acknowledgements

The author would like to express his appreciation for review of this paper by Diane K. Sparks, consulting geologist, Beaumont, TX, and Fred T. Fischer, consulting geologist, Nashville, TN. Also, I wish to mention the excellent typing services provided by Mary Ramirez, Du Pont ESD, Beaumont, TX, who prepared this report for publication.

References

Bassett, R. L., and M. E. Bently, 1983. "Deep Brine Aquifers in the Palo Duro Basin: Regional Flow and Geochemical Constraints", Report of Investigations No. 130, Texas Bureau of Economic Geology.

Bentley, C. B., 1983. "Preliminary Report of the Geohydrology Near Cypress Creek and Richton Salt Domes, Perry County, Mississippi", Water-Resources Investigations Report 83-4169, U.S.G.S., Jackson, MS.

Bentley, M. E., R. T. Kent, and G. R. Myers, 1986. "Site Suitability for Waste Injection" International Symposium on Subsurface Injection of Liquid Wastes, New Orleans, LA, published by UIPC, Oklahoma City, OK.

Bethke, C. M., W. J. Harrison, C. Upson, and S. P. Altaner, 1988. "Supercomputer Analysis of Sedimentary Basins", Science, Vol. 239, Washington, D.C.

Buss, D. R., B. H. Lester, G. C. Zalaskus, and J. W. Mercer, 1984. "A Numberical Simulation Study of Deep-Well Injection in Two Hydrogeologic Settings--Texas Gulf Coast, Great Lakes Basin", U.S. EPA, Washington, D.C.

Clark, D. A., 1988. "An Experimental Evaluation of Containment Properties for Shales Associated with Deep-Well Hazardous Waste Injection Zones", Thesis, University of Alabama.

Clifford, M. J., 1973. "Hydrodynamics of the Mt. Simon Sandstone, Ohio and Adjacent Areas, in Underground Waste Management and Artificial Recharge, Vol. 1", American Association of Petroleum Geologists, Tulsa, OK.

Clifford, M. J., 1975. "Subsurface Liquid-Waste Injection in Ohio", Ohio Geological Survey Information Circ., No. 43.

Conger, R. M., 1986. "Upper Miocene Injection Reservoirs of the Geismar-St. Gabriel Industrial Area, Iberville and Ascension Parishes, Louisiana", Journal of the Underground Injection Practices Council, Vol. 1.

Core Laboratories, 1987a. "Special Core Analysis Study for E. I. du Pont de Nemours & Co., Inc., Waste Disposal Tests".

Core Laboratories, 1987b. "Petrographic Study for Du Pont de Nemours & Company, Inc., Beaumont Waste Well No. 3".

Environmental Protection Agency, 1987. "Proposed Rule for Underground Injection Control Program: Hazardous Waste Disposal Injection Restrictions", 40 CFR Parts 124, 144, 146 and 148.

Everett, A. G., 1986. "Upward Vertical Migration of Warmer Saline Waters Along Fault Zones with Massive Sand Units", personal communication.

Freeze, R. A., and J. A. Cherry, 1979. Groundwater, Prentice Hall, Englewood Cliffs, NJ.

Galloway, W. E., T. E. Ewing, C. M. Garrett, N. Tyler, and D. G. Debout, 1983. Atlas of Major Texas Oil Reservoirs, Bureau of Economic Geology, Austin, TX.

Galloway, W. E., C. D. Henry, and G. E. Smith, 1982. "Depositional Framework, Hydrostratigraphy, and Uranium Mineralization of the Oakville Sandstone (Miocene), Texas Coastal Plain", Bureau of Economic Geology, University of Texas at Austin, Austin, TX.

Goolsby, D. A., 1972. "Geochemical Effects and Movement of Injected Industrial Waste in a Limestone Aquifer", In T. D. Cook, ed., Underground Waste Management and Environmental Implications. American Association of Petroleum Geologists Memoir 18, p. 355-368.

Jones, T. A., and J. S. Haimson, 1986. "Demonstration of Confinement: An Assessment of Class I Wells in the Great Lakes Regiona and Gulf Coast Regions", Journal of the Underground Injection Practices Council.

Kreitler, C. W., 1976. "Fault Control of Subsidence, Houston-Galveston Area, Texas", Bureau of Economic Geology, University of Texas at Austin, Austin, TX.

LeGrand, H. E., 1962. "Geology and Groundwater Hydrology of the Atlantic and Gulf Coastal Plain as Related to Disposal of Radioactive Wastes", USGS Report TEI-805.

Nealon, D. J., 1982. "A Hydrological Simulation of Hazardous Waste Injection in the Mt. Simon, Ohio", Master's Thesis, Ohio University.

Slaughter, G. M., 1981. "An Analysis of Ground Water Flow Times Near Seven Interior Salt Domes", Dept. of Energy for Battelle Memorial Institute Office of Nuclear Waste Isolation.

Smith, G. E., W. E. Galloway, and C. D. Henry, 1982. "Regional Hydrodynamics and Hydrochemistry of the Uranium-Bearing Oakville Aquifer of South Texas", Bureau of Economic Geology Report of Investigations No. 124.

Warner, D. L., and J. H. Lehr, 1981. Subsurface Wastewater Injection, Premier Press, Berkeley, CA.

Warner, D. L., T. Syed, and S. N. Davis, 1986. "Confining Layer Study", U.S. EPA Region V.

Weber, K. J., and E. Daukoru, 1975. "Petroleum Geology of the Niger Delta", Proceedings of the Nineth World Petroleum Conference, Vol. 2.

Biography

James E. Clark holds a B.S. in geology (1972) from Auburn University and an M.S. in geophysical sciences (1977) from Georgia Institute of Technology. He is a Registered Geologist in Georgia. From 1972 to 1976 Clark was Chief Geologist for the Georgia Department of Transportation, conducting geotechnical, geohydrological, environmental, and mineral studies/investigations. From 1977 to 1981, Clark was a geohydrologist with Law Engineering Testing Co., working on suitability studies of salt domes as repositories for high-level nuclear waste. He joined Du Pont in 1981 in the Solid Waste and Geological Engineering group and is active in evaluation and permitting of disposal wells.

APPENDIX 3-6
ROCK COMPRESSIBILITY

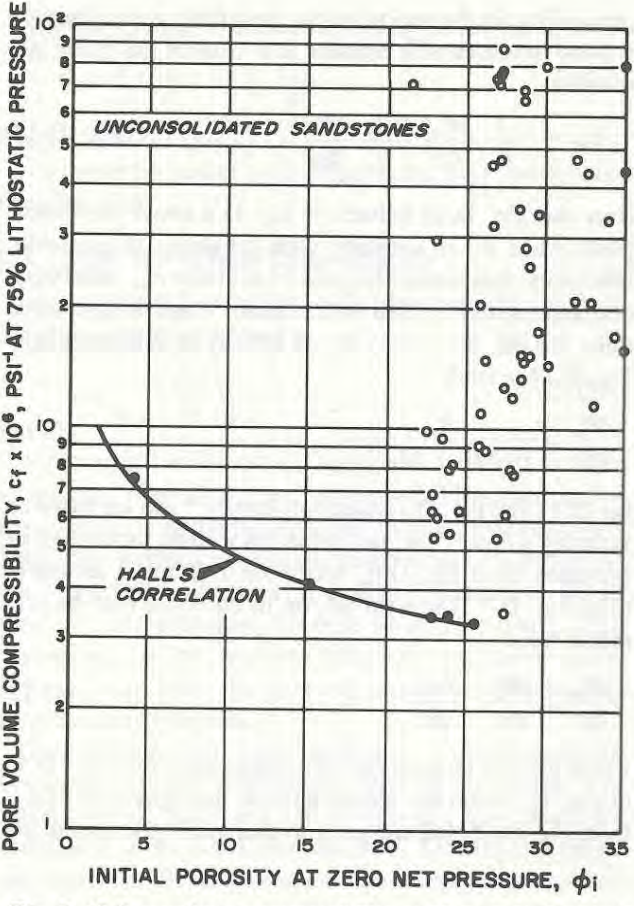

Fig. D.12 Pore-volume compressibility at 75-percent lithostatic pressure vs initial sample porosity for unconsolidated sandstones. After Newman.[9]

APPENDIX 3-7
DUPONT AND SWIFT MODEL COMPARATIVE ANALYSES

SWIFT Model Run **Chemours 700x1250v8**

Light Density Injection Fluid - (Washita-Fredericksburg Injection Interval)

Chemours 700x1250v8 considers injection of a light density injection fluid into the Washita-Fredericksburg Injection Interval. Model includes historical injection from October 1979 to December 31, 2015 and future injection at 2,200 gpm (into a single well) from January 1, 2016 to December 31, 2020. Chemours 700x1250v8.dat is the input file for the model run and Chemours 700x1250v8.out is the output file for the model run. The subject SWIFT model is a constant dip and uniform thickness model constructed to closely match the DuPont Basic Plume Model for light density fluid movement.

SWIFT Model Run **Chemours 10KL Lat**

Light Density Injection Fluid - (Washita-Fredericksburg Injection Interval)

Chemours 10KL Lat considers injection of a light density injection fluid into the Washita-Fredericksburg Injection Interval. Model includes historical injection from October 1979 to December 31, 2015 and future injection at 2,200 gpm (550 gpm into Wells 2, 3, 4 and 5) from January 1, 2016 to December 31, 2020. Chemours 10KL Lat.dat is the input file for the model run and Chemours 10KL Lat.out is the output file for the model run. The subject SWIFT is a variable thickness dip and variable structure model. All reservoir fluid and injection fluid parameters match the DuPont Basic Plume Model for light density fluid movement.

SWIFT Model Run **Chemours 700x1101**

High Density Injection Fluid - (Washita-Fredericksburg Injection Interval)

Chemours 700x1101 considers injection of a high density injection fluid into the Washita-Fredericksburg Injection Interval. Model includes historical injection from October 1979 to December 31, 2015 and future injection at 2,200 gpm (into a single well) from January 1, 2016 to December 31, 2020. Chemours 700x1101.dat is the input file for the model run and Chemours 700x1101.out is the output file for the model run. The subject SWIFT model is a constant dip and uniform thickness model constructed to closely match the DuPont Basic Plume Model for high density injection fluid movement.

SWIFT Model Run **Chemours 10KL Lat**

High Density Injection Fluid - (Washita-Fredericksburg Injection Interval)

Chemours WF-HD Lat R considers injection of a high density injection fluid into the Washita-Fredericksburg Injection Interval. Model includes historical injection from October 1979 to December 31, 2015 and future injection at 2,200 gpm (550 gpm into Wells 2, 3, 4 and 5) from January 1, 2016 to December 31, 2020. Chemours WF-HD Lat R.dat is the input file for the model run and

Chemours WF-HD Lat R.out is the output file for the model run. The subject SWIFT is a variable thickness dip and variable structure model. All reservoir fluid and injection fluid parameters match the DuPont Basic Plume Model for high density fluid movement.

APPENDIX 3-8
SWIFT MODELING (DATA FILES PROVIDED ON CD-ROM)

<u>Reservoir Pressurization (Washita-Fredericksburg Injection Interval)</u>SWIFT Model Run **Chemours WF Prs** – End of Operations Pressure Buildup

Chemours WF Prs models reservoir pressure buildup associated with the injection of an average density injection fluid into the Washita-Fredericksburg Injection Interval. Model includes historical injection from October 1979 to December 31, 2015 and future injection at 2,200 gpm (550 gpm into Well Nos. 2, 3, 4 and 5) from January 1, 2016 to December 31, 2050. Chemours WF Prs.dat is the input file for the model run and Chemours WF Prs.out is the output file for the model run.

SWIFT Model Run **Chemours WF Prs(2)** – End of Operations Pressure Buildup

Chemours WF Prs(2) models reservoir pressure buildup associated with the injection of an average density injection fluid into the Washita-Fredericksburg Injection Interval. Model includes historical injection from October 1979 to December 31, 2015 and future injection at 2,200 gpm (400 gpm into Well Nos. 2, 3 and 4 and 1,000 gpm into Well No. 5) from January 1, 2016 to December 31, 2050. Chemours WF Prs(2).dat is the input file for the model run and Chemours WF Prs(2).out is the output file for the model run.

SWIFT Model Run **Chemours WF Prs(3)** – End of Operations Pressure Buildup

Chemours WF Prs(3) models reservoir pressure buildup associated with the injection of an average density injection fluid into the Washita-Fredericksburg Injection Interval. Model includes historical injection from October 1979 to December 31, 2015 and future injection at 2,200 gpm (250 gpm into Well Nos. 2, 3, 4 and 5 and 1,200 gpm into Well No. 6) from January 1, 2016 to December 31, 2050. Chemours WF Prs(3).dat is the input file for the model run and Chemours WF Prs(3).out is the output file for the model run.

Reservoir Pressurization (Tuscaloosa Massive Sand)

SWIFT Model Run **Chemours TMS Prs** – End of Operations Pressure Buildup
Chemours TMS Prs models reservoir pressure buildup associated with the injection of an average density injection fluid into the Tuscaloosa Massive Sand. Model includes future injection at 2,200 gpm (550 gpm into Well Nos. 2, 3, 4 and 5) from January 1, 2020 to December 31, 2050. Chemours TMS Prs.dat is the input file for the model run and Chemours TMS Prs.out is the output file for the model run.

SWIFT Model Run **Chemours TMS Prs(2)** – End of Operations Pressure Buildup
Chemours TMS Prs(2) models reservoir pressure buildup associated with the injection of an average density injection fluid into the Tuscaloosa Massive Sand. Model includes future injection at 2,200 gpm (400 gpm into Well Nos. 2, 3 and 4 and 1,000 gpm into Well No. 5) from January 1, 2020 to December 31, 2050. Chemours TMS Prs(2).dat is the input file for the model run and Chemours TMS Prs(2).out is the output file for the model run.

SWIFT Model Run **Chemours TMS Prs(3)** – End of Operations Pressure Buildup
Chemours TMS Prs(3) models reservoir pressure buildup associated with the injection of an average density injection fluid into the Tuscaloosa Massive Sand. Model includes future injection at 2,200 gpm (250 gpm into Well Nos. 2, 3, 4 and 5 and 1,200 gpm into Well No. 6) from January 1, 2020 to December 31, 2050. Chemours TMS Prs(3).dat is the input file for the model run and Chemours TMS Prs(3).out is the output file for the model run.

Lateral Migration – Light Density Injection Fluid - (Washita-Fredericksburg Injection Interval)

Chemours WF-LD considers injection of a light density injection fluid into the Washita-Fredericksburg Injection Interval. Model includes historical injection from October 1979 to December 31, 2015 and future injection at 2,200 gpm (550 gpm into Well Nos. 2, 3, 4 and 5) from January 1, 2016 to December 31, 2050. Chemours WF-LD Lat.dat is the input file for the model run and Chemours WF-LD Lat.out is the output file for the model run.

Lateral Migration – Light Density Injection Fluid (Tuscaloosa Massive Sand)

Chemours TMS-LD considers injection of a light density injection fluid into the Tuscaloosa Massive Sand. Model includes future injection at 2,200 gpm (550 gpm into Well Nos. 2, 3, 4 and 5) from January 1, 2020 to December 31, 2050. Chemours TMS-LD Lat.dat is the input file for the model run and Chemours TMS-LD Lat.out is the output file for the model run.

Lateral Migration – High Density Injection Fluid - (Washita-Fredericksburg Injection Interval)

Chemours WF-HD considers injection of a high density injection fluid into the Washita-Fredericksburg Injection Interval. Model includes historical injection from October 1979 to December 31, 2015 and future injection at 2,200 gpm (550 gpm into Well Nos. 2, 3, 4 and 5) from January 1, 2016 to December 31, 2050. Chemours WF-HD Lat.dat is the input file for the model run and Chemours WF-HD Lat.out is the output file for the model run.

Lateral Migration – High Density Injection Fluid (Tuscaloosa Massive Sand)

Chemours TMS-HD considers injection of a high density injection fluid into the Tuscaloosa Massive Sand. Model includes future injection at 2,200 gpm (550 gpm into Well Nos. 2, 3, 4 and 5) from January 1, 2020 to December 31, 2050. Chemours TMS-HD Lat.dat is the input file for the model run and Chemours TMS-HD Lat.out is the output file